THE PARAMETRIC TRANSFORMER

by

EYUP SALIH TEZ, MSc

A Doctoral Thesis

Submitted in partial fulfilment of the requirements
for the award of the degree of Doctor of Philosophy
of the Loughborough University of Technology

September, 1977

Supervisor:—I.R. Smith, DSc, CEng, FIEE
Department of Electronic and Electrical Engineering

© by Eyup Salih Tez, 1977

"To my daughter

I M G E"

ACKNOWLEDGEMENTS

The author wishes to express his sincere gratitude to Professor I.R. Smith who supervised the project,for the help he provided by every possible means.

The author is indebted to his wife for her endurance throughout the project and her assistance with the drawings.

Finally, thanks are due to Mrs. J. Smith who patiently carried out the typing of the thesis.

SYNOPSIS

Although parametric devices have been known for many years, very little attention had been paid to the possibilities of exploiting the principles involved for low-frequency power conversion purposes, until the recent advent of the parametric transformer. The theory of this device is developed in the thesis, and the unusual performance characteristics are explained. Possible application areas are discussed, for an assessment of the future potential of the device as a power control element.

The operation of the parametric transformer is considered initially on the basis of the Mathieu-Hill equations. The stability chart for these equations is extensively used to permit graphical interpretation of the behaviour and characteristics. As no complete theory exists for non-linear systems with time-varying parameters, other analytical methods are also considered, although since all of these regard the device as a parametric oscillator they throw little light on the inherent transformer action.

By considering the parametric transformer as a conventional saturable reactor with a capacitor connected across the load winding and the control winding driven from an alternating source, it can be placed within the perspective of non-linear magnetic devices already known. Many possible magnetic constructions with parallel and/or orthogonal flux

interactions are investigated, with special attention paid to the bridged magnetic core analogue of the two-C-core construction. The illustration of parametric coupling as a result of flux interaction in saturable reactor devices leads to a derivation of the overall equations directly from the physical system.

The functions representing the magnetic structure of the parametric transformer are first evaluated graphically, and using various analytical representations of the B/H curve their explicit expressions are then formulated for different magnetic configurations. The introduction into the study of the concept of a relative magnetisation curve is invaluable in explaining the current waveforms and many other aspects of the device.

A mathematical model is established for the parametric transformer and the system equations are solved numerically by a digital computer. The voltage and current waveforms and performance characteristics are demonstrated, and the correctness of the theory is ascertained by comparison with experimental results.

Based on considerations of losses and efficiency, the advantages and disadvantages of parametric transformers are discussed. Possible applications in such areas as power supplies, inverters and converters are viewed and examples are given.

LIST OF PRINCIPAL SYMBOLS

Chapter II

F	:	magnetomotive force
ϕ	:	magnetic flux
R_m	:	reluctance
ϕ_1	:	primary flux
ϕ_{1m}	:	primary flux amplitude
R_{m2}	:	secondary reluctance
R_{m2av}	:	average value of secondary reluctance
R_{m2min}	:	minimum value of secondary reluctance
N_2	:	number of secondary winding turns
m	:	modulation index
L_0, L_{2av}	:	average value of secondary reluctance
ω	:	angular frequency of input signal
ϕ_s	:	saturation flux level
v_1, e_1	:	input (primary) voltage
v_2, e_2	:	output (secondary) voltage
i_1	:	primary current
i_2	:	secondary current
i_L	:	load current
Γ	:	coefficient introducing effect of primary flux on secondary reluctance

Chapter III

C	:	secondary circuit capacitance
ϕ_2	:	secondary flux

Chapter III continued

ϕ_{2m}	:	secondary flux amplitude
a, q	:	coefficients of the Mathieu equation
ω_0	:	angular resonant frequency of secondary circuit
z (= ωt)	:	independent variable, time converted into radians.
μ	:	characteristic exponent of solution of Mathieu equation
a_{c1}, a_{s1}	:	functions of q, giving boundary curves of the first unstable region
a_{c2}, a_{s2}	:	functions of q, giving boundary curves of the second unstable region
N_1	:	number of primary winding turns
R_{m1}	:	primary reluctance
R_{m1av}	:	average value of primary reluctance
R_{m1min}	:	minimum value of primary reluctance
Γ	:	coefficient introducing effect of secondary flux on primary reluctance
λ	:	coefficient introducing non-linearity to secondary reluctance
R_2	:	secondary winding resistance
ϕ'_{1m}	:	primary flux amplitude necessary to initiate oscillations
ϕ''_{1m}	:	primary flux amplitude corresponding to over-voltage protection
R_L	:	load resistance
R'_{Lmin}	:	minimum load resistance for threshold condition
R''_{Lmin}	:	minimum load resistance for over-load protection
ϕ'''_{1m}	:	primary flux amplitude at under-voltage protection

Chapter IV

B	:	magnetic flux density
H	:	magnetic field intensity
dcv source	:	direct constant voltage source
dcc source	:	direct constant current source
acv source	:	alternating constant voltage source
acc source	:	alternating constant current source
F_1	:	primary mmf
F_2	:	secondary mmf
H=f(B)) B=f(H))	:	magnetisation characteristic of core material
A_1, ℓ_1) A_2, ℓ_2) A_0, ℓ_0)	:	dimensions of the bridged core (see Figure 4.39)
ℓ_g	:	air-gap length
R_g	:	air-gap reluctance
μ	:	magnetic permeability

Chapter V

R_1	:	primary winding resistance
i_C	:	capacitor current
L_p, L_s	:	primary and secondary leakage inductances
R_{01}, R_{02}	:	resistors representing iron losses
R_L, C_L, L_L	:	resistive, capacitive and inductive components of load

Chapter VII

C_1, C_2, C_3 etc	:	coefficients in analytical expressions of magnetisation curve

Chapter VIII

ε	:	error
B_{0max}	:	saturation flux density
h	:	step-size
e_1, i_1, e_2, i_2	:	instantaneous values of input and output voltage and currents

Chapter IX

V_1'	:	input voltage (rms) to switch-on the parametric transformer
V_1''	:	input voltage at over-voltage protection
V_1'''	:	input voltage at under-voltage protection
P_L	:	load power
P_1	:	input power (apparent)
P_o	:	total loss at no-load operation
E	:	efficiency

TABLE OF CONTENTS

		Page No.
ACKNOWLEDGEMENT		i
SYNOPSIS		ii
LIST OF PRINCIPAL SYMBOLS		iv
CHAPTER I:	INTRODUCTION	1
1.1	Historical Background	1
1.2	Scope of the Project	9
CHAPTER II:	SIMPLIFIED EXPLANATION OF THE OPERATION AND CHARACTERISTICS OF THE PARAMETRIC TRANSFORMER	14
2.1	Operation of the Parametric Transformer	14
2.1.1	Modulation of the Secondary Reluctance at Twice Frequency	15
2.1.2	Parametrically Developed Voltage and Negative Resistance Property	19
2.2	Characteristics of the Parametric Transformer	24
2.2.1	Under- and Over-voltage Protection and Voltage Regulation	24
2.2.2	Load Regulation and Over-load Protection	26
2.2.3	Sinuscidal Output Voltage and Bilateral Filtering	27
2.2.4	Phase-Shift and Bistability of the Phase	29
CHAPTER III:	THEORY OF PARAMETRIC OSCILLATIONS AS APPLIED TO THE PARAMETRIC TRANSFORMER	36
3.1	Linear Case (Build-up of Oscillations)	36
3.1.1	General Solution of the Mathieu Equation in the First Unstable Region	43

Page No

3.1.2 Operation in the Second Unstable Region: Frequency Multiplication 49

3.1.3 The Hill Equation 57

3.1.4 The Hill-Meisner Equation, and Parametric Generation and Absorption of Energy 64

3.1.5 Mechanism of Energy Transfer 75

3.2 Non-linear Case 81

3.3 The Effect of Damping 94

3.3.1 Linear Case 94

3.3.2 Non-linear Case 103

3.4 The Effect of Detuning 109

3.5 The Effect of the Load 120

3.5.1 Linear Case 122

3.5.2 Non-linear Case 127

3.6 Complementary Remarks on the Characteristics of the Parametric Transformer 136

3.6.1 Under- and Over-voltage Protection, and Voltage Regulation 136

3.6.2 Filtering Ability and Sinusoidal Output Voltage 142

3.6.3 Bistability of the Phase 154

3.6.4 Frequency Multiplying/Dividing Operation 156

3.7 Other Methods of Mathematical Analysis 159

CHAPTER IV: PARAMETRIC TRANSFORMER AS A NON-LINEAR DEVICE 196

4.1 Saturable Reactors Used as Variable Inductors 198

4.1.1 The Classification of Saturable Reactor Devices 199

Page No

4.1.2 Various Forms of Saturable Reactors 201

4.2 Analogous Electric Circuits with Elimination of Mutual Flux Coupling 209

4.3 Mutual Parametric Coupling and Representation of Saturable Reactors 212

4.3.1 Parametric Coupling as a Result of Interaction in Non-linear Medium 216

4.3.1a Orthogonal Interaction 217

4.3.1b Parallel Interaction 218

4.3.2 Mathematical Representation of Saturable Reactors 221

4.4 Magnetic Structure of the Parametric Transformer 224

4.4.1 Equivalent Magnetic Structure and Analogous Electric Circuit 230

4.4.2 Mathematical Representation of the Bridged Magnetic Core 233

4.4.3 Inclusion of Air-gap 240

4.4.4 Primary and Secondary Inductances 245

4.5 Mathematical Representation of Other Saturable Reactors 246

4.5.1 A Parallel-Flux Saturable Reactor 247

4.5.2 An Orthogonal-Flux Saturable Reactor 250

CHAPTER V: THE MATHEMATICAL MODEL OF THE PARAMETRIC TRANSFORMER 275

5.1 The $F_1(\phi_1, \phi_2)$ and $F_2(\phi_1, \phi_2)$ Functions and Departures from the Ideal 275

5.2 The General Differential Equations with Winding Resistances and Resistive Load 283

5.3 Inclusion of Leakage Inductances into the Mathematical Model 289

5.4 Hysteresis and Eddy Current Losses 292

Page No

5.5 The General Equations with Reactive Loads 299

5.6 Simulation by Analogue Computer 305

CHAPTER VI: THE RELATIVE MAGNETISATION CURVES AND THE CURRENT WAVEFORMS 317

6.1 The Graphical Form of the $F_1(\phi_1, \phi_2)$ and $F_2(\phi_1, \phi_2)$ Functions 317

6.1.1 Reluctance Modulation at Twice Frequency 322

6.2 The Relative Magnetisation Curve 324

6.2.1 Relative Magnetisation Characteristics with both Windings Driven by Synchronous Sources 326

6.3 The Relative Magnetisation Characteristics and the Current Waveforms of the Parametric Transformer 330

6.3.1 The Primary and Secondary Current Waveforms 335

6.4 Prediction of the Best Condition for Parametric Transformer Operation 341

CHAPTER VII: APPLICATION OF ANALYTICAL APPROXIMATIONS OF THE B/H CURVE TO OBTAIN EXPLICIT EXPRESSIONS FOR THE $F_1(\phi_1, \phi_2)$ AND $F_2(\phi_1, \phi_2)$ FUNCTIONS 354

7.1 Analytical Representation of the B/H Curve 354

7.1.1 Requirements on the Form of Representation 354

7.1.2 Some Forms of Analytical Representation by Single Explicit Expressions 358

7.2 Application of Power Series Approximation to Two-C-Core Device 363

7.2.1 Differentiation of the Function $F_2(\phi_1, \phi_2)$ 367

		Page No
	7.3 Applications of Other Approximations of B/H Curve to the Two-C-Core Device	373
	7.3.1 Hyperbolic Sine Function	373
	7.3.2 Tangent Function	375
	7.4 Application of Power-Series Approximation to Hollow Toroidal Core	378
CHAPTER VIII:	DIGITAL COMPUTER SIMULATION	381
	8.1 Curve Fitting to the Magnetisation Characteristic of the Core Material	381
	8.1.1 The Method and Computer Program	385
	8.1.2 Discussion of Results	387
	8.2 Numerical Computation of Various System Functions	393
	8.3 Numerical Solution of the Differential Equations	404
	8.3.1 The Equations to be Solved	404
	8.3.2 Review of Basic Numerical Methods	405
	8.3.3 The Choice of Method	411
	8.3.4 The Computer Program	412
	8.4 Discussion of Results	419
CHAPTER IX:	EXPERIMENTAL INVESTIGATION	495
	9.1 Design	495
	9.2 Operational Characteristics	500
	9.3 Voltage and Current Waveforms	503
	9.4 Single to Three Phase Conversion	512
	9.5 Power and Efficiency Considerations	515
	9.6 Relation Between Relative Magnetisation Characteristics, Current Waveforms and Real Input Power	520
CHAPTER X:	APPLICATIONS OF THE PARAMETRIC TRANSFORMER	574

10.1 Applications as a Saturable Reactor 574

10.2 Applications of the Parametric Transformer 577

10.2.1 Power Conditioning (Voltage Regulator-Filters) 577

10.2.2 Power Conversion Applications 579

10.2.2.1 AC to DC Inverters (DC Power Supplies) 579

10.2.2.2 DC to AC Inverters 579

10.2.2.3 DC to DC Converters 581

10.2.2.4 Frequency Converters 583

10.2.3 Frequency Multiplier/Dividers 583

10.2.4 Parametric Filters 584

10.2.5 Phase Converters 585

10.3 Advantages and Disadvantages of the Parametric Transformer 586

CHAPTER XI: CONCLUSIONS 594

REFERENCES 599

APPENDIX I: Amplitude of the Fundamental Frequency Component 614

APPENDIX II: Harmonic Distortion in the Secondary Flux with Square-Wave Input Voltage 617

APPENDIX III: Non-uniform Flux Distribution in the Hollow Toroidal Core 620

APPENDIX IV: Application of Power-series Approximation to the two-C-core Device 623

APPENDIX V:	Program Listing: Curve Fitting	628
APPENDIX VI:	Data on the Experimental Device	630
APPENDIX VII:	Program Listing: Voltage/Current Characteristic	632
APPENDIX VIII:	Program Listing: Solution of Differential Equations Simulating Parametric Transformer	634

CHAPTER I

INTRODUCTION

1.1 Historical Background

The possibility of exciting a dynamic system by means of a periodic variation of one of the system parameters has been known for many years. The oscillations that are produced in the system are termed *parametric oscillations*, and the process is generally referred to as *parametric excitation*.

The history of parametric excitation dates back to the last century, with the experiments of Faraday (1831) on the vibrations in the surface level of a fluid resting on a vertically vibrating support[1]. In other early experiments by Melde (1859), one end of a stretched string was attached to a prong of a tuning fork vibrating in the direction of the string, and transverse oscillations at a frequency one-half those of the fork vibrations were observed along the string[2]. In 1868, Mathieu investigated the vibrations of a stretched membrane having an elliptical boundary[3], and in conducting the first analysis of the problem, he introduced the equation and functions subsequently named after him. In 1886, Hill investigated the mean motion of the lunar perigee[4], using an extended or generalised form of the Mathieu equation, later termed the Hill equation. In other important studies of parametric excitation, Lord Rayleigh (1887) investigated the classical Melde experiment and dealt also with the problem of wave propa-

gation in stratified media[5]. Amongst the names of those who later made important contributions to the theory of linear differential equations with periodic coefficients, required in a study of parametric oscillations, are Floquet[6], Whittaker[7], Ince[8], Meisner[9] and Strutt[10]. A detailed history of the development of the theory of Mathieu-Hill type equations is given elsewhere[11].

In addition to the examples given above, Froude's pendulum[12], Bethenod's experiment[13], a simple pendulum with vertically vibrating support[14], and subharmonic oscillations in loudspeaker diaphragms[15] are often quoted as classical examples of parametric oscillations.

The common principle which underlies all these experiments is that the energy of an oscillating system can be increased, by changing the value of an energy storage parameter of the system at a frequency different from (generally twice) the resonance frequency of the system. When the parameter variations are at twice the resonant frequency, a parametric resonance occurs, and self-excited parametric oscillations build up. The commonest example of this principle is a playground swing, where a child *pumps up* the amplitude of oscillations of the swing by changing the position of the centre of gravity at twice the oscillating frequency, lowering it on the down swing and raising it on the up swing.

In electrical circuits, the works of Brillouin[16] and Poincare[17] followed basically similar lines to the mechanical studies described above, while Kuhn[18], Zenneck[19], Alexenderson[20] and Hartley[21] were among the first contributors to the theory of parametric transducers. Since the chief interest was in the area of communications, parametric excitators found most application at radio frequencies, where the object was to modulate a continuous wave transmitter by means of a non-linear inductance or saturable reactance. Although Alexenderson had shown that, under certain conditions, instability and generation of self-excited oscillations can exist, it was not until 1930 that Peterson managed to make use of these effects in his negative resistance straight-through amplifier[22]. In later years, the techniques of variable reactance amplifiers and modulators were developed, and with the advent of varactor diodes, the range of applications were extended to the microwave region. Today, there exists much literature about parametric amplifiers, modulators and harmonic generators which operate at ultra high frequencies and employ such features as the variable capacitance of semiconductor diodes, the variable reactance of wave-guides, space-charged waves in an electron beam, ferromagnetic resonance and so on. A comprehensive list of references up to 1960 is available in the survey paper of Mumford[23].

Although considerable attention has been paid to the development of parametric circuits, this has mainly been confined to the high frequency range and related to communication

engineering. The idea of using parametric excitation for energy conversion has attracted very little attention except during the 1930s,when a number of scientists were involved in proving the basic theory of parametric oscillations by experiments with electrical circuits. A systematic study of the phenomenon was initiated by the experiments of Heegner[24] and Guenther-Winter[25] on the excitement of electrical oscillations of acoustic frequencies by alternately magnetising the iron core of a self-induction winding. The experiments of Guenther-Winter[26] and Y. Watanabe et al[27] were the first ones conducted on the excitation of electrical oscillations by mechanical periodic variation of the self-inductance of an electric oscillating system. In 1934, a report by Mandelstam, Papalexi et al[28] described the extensive research on non-linear oscillations performed in various institutions of the USSR. A large section of the report is devoted to parametric excitation and parametric coupling, and a comprehensive bibliography on non-linear oscillations is given. Mandelstam and Papalexi correlated the phenomena of parametric excitation and parametric resonance with the theory of subharmonic resonance. Using different devices from those used by Guenther-Winter and Watanabe, they constructed ingenious parametric generators, capable of delivering a considerable power output, in which the self-inductance[29] or the capacitance[30] of an oscillatory circuit was varied periodically by mechanical means to create the self-excited parametric oscillations. These

generators transformed the mechanical power absorbed in the process of a periodic variation of a system parameter (L or C) into the electrical energy of an alternating current at a certain frequency. Mandelstam and Papalexi also studied the effects of parametric coupling and indicated that, in contradistinction to linearly coupled systems, a phenomenon of *regeneration* was produced due to parametric coupling in parametrically coupled non-linear systems[28]. They dealt not only with energy conversion but also with power conversion by means of parametric oscillations, and reference 28 was the first scientific paper in which the concept of parametric power conversion appeared using the term *Parametric Transformer*. Quoting from page 131: *"A.Tscharakhtschian studied the action of a sinusoidal force on two circuits in parametric coupling forming a* "Parametric Transformer". *In this system, the variations of the current in the primary circuit causes the induction coil of the secondary circuit to vary by modifying the magnetisation of the iron core coils. This allows production of phenomena of parametric excitation. The related publication is in preparation"*. In Tscharakhtschian's article[31], the theory of the parametric transformer was developed for the first time, on the basis of non-linear differential equations with time-varying parameters, although attention was concentrated on the frequency-changing mode of operation. However, the concept of creating the parameter variations, not by an external, independent force, but by parametric coupling in which the changes in the system also influence the force producing the parameter varia-

tions, was appropriately expressed. Most aspects of the theory Tscharakhtschian developed, such as modulation of the secondary inductance by the primary current, reaction between the primary and secondary circuits, stabilization of the amplitude of the self-excited oscillations by the non-linearity of the magnetisation characteristics etc., remain true also for the devices investigated in this study. He also pointed out the possibility of using parametric transformers for voltage regulation purposes.

The wide interest on oscillatory systems with periodically varying parameters[28,32] inevitably lessened during World War II and no further investigation on the parametric transformer seems to have been carried out until recently, although during the 1950s, McLachlan[11,12], and Minorsky[33,34] dealt with parametric excitation in various other physical systems. When interest was renewed, the main application in electrical circuits was for parametric oscillators[35], but Neuman[36] and Goto[37] discovered independently in 1954 that parametric oscillations exhibited a phase ambiguity which could be utilized in logic circuits. The device, called the *Parametron*, made use of the phase relationship of the parametric oscillations which can be obtained in two opposite phases, each representing a binary digit. The parametron is exactly the same device as Tscharakhtschian's parametric transformer, operating as a frequency-divider. However, it was not intended for power conversion applications, although once used widely as a digital computing element especially in Japan[38].

During the 1960s, attention in the area of voltage stabilizing centred around constant voltage transformers[39], employing the phenomenon of ferro-resonance to produce operational characteristics somewhat similar to those of parametric transformers. However, the phenomenon involved is different from parametric resonance in respect of the energy introduction into the system. In ferro-resonance, the energy is introduced directly by the external source, while, in parametric resonance, the energy introduction is achieved indirectly, through a degree of freedom of the system, with the external source creating variations in an energy storage parameter of the system.

The idea of using parametric oscillations for electrical power conversion came into practice with Paraformers[40], first described in a patent by Wanlass[41]. The device proposed was for voltage regulation, and employed the new types of magnetic core configurations suggested previously by the same author[42,43]. Currently, the Paraformer devices are manufactured by the Tele-Dynamics/Wanlass Company in the USA, and are commercially available in the UK through T.I. Supply Limited.

The unique characteristics of the parametric transformer have attracted considerable interest, and its application in rapid transit railroads has been seriously suggested[44]. The fact that little was known on the operation principles prompted publication of several papers on the analytical treatment of the device. Burian[45] dealt mainly with a stability analysis,

but unfortunately his paper contains some serious errors. Fam and Verma[46] gave an analysis on the basis of the Mathieu equation, just before the commencement of the study described in this thesis. The parametric transformer was cited as an example of parametric devices in a paper[47] summarizing physical principles of parametric oscillators. A paper was published by Smith and the author[48], which explained concisely the principles and merits of the device. During the course of this project, other articles on the parametric transformer have been published,some of which overlap in some respects with the investigations carried out independently by the author. Meiksin[49-51] considered both orthogonal and parallel flux devices but assumed wrongly, although implicitly, that the two-C-core parametric transformer was an orthogonal flux system. In all the works mentioned, attention was focused on the secondary circuit of the device, which was considered a parametric oscillator. The device was then represented by a *single* differential equation, non-linear with time-varying coefficients, to which the analytical treatment was directed. The existence of parametric coupling between the primary and secondary circuits was generally completely overlooked. Although Fam and Bahl[52] represented the system by *two* simultaneous differential equations, and pointed out the correlation of the primary and secondary fluxes with the corresponding mmf's in the form of two 2-variable functions, they were unable to relate the form of these functions with the physical structure of the device.

The interest shown to the parametric transformer in Japan was confined to experimental investigations, rather than to full analytical considerations. Bessho et al[53] discovered the equivalence between the two-C-core and the bridged core devices, by which time the author's analytical treatment based on this equivalence was already complete. However, Bessho et al did not attempt an analytical treatment but, based on an analogy between the two-C-core and the bridged core devices, they took a further step in experimentation by investigating firstly a bridge-connected reactor circuit[53], and later a centre-tapped reactor circuit[54]. Phasor diagrams were used to explain the operations of these circuits, and the authors concluded that their characteristics, when employed as power converters, were similar to those of the parametric transformer. Finally, Power[55] applied the inverse Nyquist diagram technique to the secondary circuit equation of a parametric transformer and obtained results similar to those produced by considering the device as a parametric oscillator.

1.2 Scope of the Project

To date, it appears that a full analytical treatment has not yet been given to the parametric transformer, considering the device as a whole and including both the primary and the secondary circuits and the parametric coupling between them. In most recent work, an explanation of the operation of the

device has used only the single differential equation of the secondary circuit, with the damping present at no load either intentionally assumed non-existent or wrongly taken as constant. Although the theory of Mathieu-Hill type equations has been applied to some extent, the situation is far from complete for many aspects of the device. Consideration as a parametric oscillator has not allowed the inherent mechanism of energy transfer from the primary to the secondary circuit to be explained. Apart from no attention being paid to the primary circuit, no relation has been established between the system equations and the physical structure of the device, and in none of the recent work is any mention made of the unusual waveforms of the primary and the secondary currents. System equations derived from the physical structure, in which non-linear flux interaction produces parametric coupling, have not yet been established and solved by computer, so as to form a simulation of the device.

The project presented in this thesis aims at developing the theory of parametric transformers and explaining their unusual characteristics. For this purpose, experimental units with a two-C-core construction were designed, and their operational characteristics obtained. The basic differential equations of the transformer were established, and these formed the basis of a computer simulation of the device characteristics, which yielded results generally in good agreement with those obtained experimentally.

To present the work in a logical sequence, the thesis is divided into eleven chapters, with the scope of each of these discussed below.

Chapter I introduces the topic and traces the historical background of parametrical oscillations and related parametric devices.

Chapter II introduces the parametric transformer and its operational characteristics and explains how the necessary variation of a circuit parameter is achieved. The use of reluctance, rather than inductance, for this parameter makes a straightforward derivation of the system equations possible. Modulation of the secondary reluctance at twice supply frequency serves as the basis for the work in Chapter III.

In Chapter III, the theory of parametric oscillations is developed through the differential equation with periodic coefficients applying to the secondary circuit. Although this means the device is considered as a parametric oscillator, the mechanism of energy transfer through parametric coupling is also explained, to illustrate the operation as a transformer. Investigating the secondary circuit equation in linear and non-linear forms allows both the initiation of parametric oscillations and the steady state conditions to be studied separately, and effects such as damping, detuning and load are introduced in a gradual manner as the theory grows in complexity. If a mathematical analysis of the device will suffice, regardless of its

physical aspects, Chapter III, with Chapter II as an introduction, can be read independently of the rest of the thesis.

In Chapter IV, the parametric transformer is placed within the perspective of non-linear magnetic devices already known, by investigating the parametric coupling resulting from flux interaction in conventional saturable reactors. Mathematical representations of various magnetic devices by two 2-variable functions are obtained directly from their physical structure.

Chapter V describes the differential equations of the parametric transformer, independently on the form of the magnetic structure. A mathematical model is obtained for the device and an analog computer simulation given.

In Chapters IV and V, the magnetisation characteristic of the core material is given implicitly in the form H=f(B). Using a graphical representation of this characteristic, a mathematical model of the magnetic structure is evaluated graphically in Chapter VI. The same is achieved in Chapter VII by expressing the magnetisation characteristic analytically. A concept of a relative magnetisation curve is developed, to explain the primary and secondary current waveforms.

In Chapter VII, various analytical approximations to the B/H curve are applied to obtain models representing different saturable reactor devices. With a power-series approximation applied to the two-C-core construction, explicit expressions

for these functions are simplified, so as to establish a bridge between the mathematical theory of Chapter III and the physical considerations of Chapters IV to VII. After an approximate curve is fitted to the magnetisation characteristic, the differential equations simulating the parametric transformer are solved by digital computer, for different operational conditions, with the results given in Chapter VIII.

Chapter IX outlines the design of the experimental unit constructed,and gives the performance characteristics and the voltage and current waveforms recorded under different operational conditions. These are explained by reference to the theory developed in the previous chapters.

The possible application areas for the parametric transformer are discussed in Chapter X, and the advantages and disadvantages are viewed to establish the future potential of the device.

The final chapter of the thesis records the conclusions arising from the project and suggests how the work might be developed and extended in the future.

CHAPTER II

SIMPLIFIED EXPLANATION OF THE OPERATION AND CHARACTERISTICS OF THE PARAMETRIC TRANSFORMER

2.1 Operation of the Parametric Transformer

The parametric transformer is a passive, static power conversion device, which utilises the principles of parametric excitation to produce output power. It consists essentially of a variable inductor and a capacitor, which together form an oscillatory circuit. The variable inductor corresponds to the secondary winding of the parametric transformer, the inductance of which is varied periodically in time by the alternating current in the primary winding. A load to which power is delivered is connected across the capacitor.

The basic operation of the parametric transformer may be explained on the basis of the general principle of parametric resonance stated in the previous chapter. When the primary winding of the parametric transformer is fed with alternating current of frequency f, the inductance of the secondary winding is varied at twice this frequency through the non-linear magnetisation process in the iron core. Connecting a capacitor across the secondary winding to form a parallel resonant circuit at the frequency f, provides a parametric oscillator working at this frequency, and capable of delivering power to a load connected in parallel with the capacitor. Since the device is driven with the electrical energy required to vary the core reluctance, and also delivers electrical energy to the load, it forms an electrical

power converter which is termed rightly a *parametric transformer.*

2.1.1 Modulation of the Secondary Reluctance at Twice Frequency

Parametric transformers currently manufactured employ the two-C-core construction shown in Figure 2.1, where the capacitor is also shown connected across the secondary winding. The paths for the magnetic fluxes produced by each winding are completed through a portion of the magnetic circuit of the other winding, so that this portion is common to the two magnetic circuits. None of the flux produced by either winding links with the other winding, and there is no mutual coupling whatever the relative directions of the two fluxes.

Suppose, initially, that only a primary flux exists in the magnetic core. As this passes through the part of the core also associated with the secondary magnetic circuit, it causes a change in the inductance of this winding, provided only that the flux density is sufficient to take advantage of the non-linearity in the magnetic characteristic of the core material. When there is no primary flux, the reluctance of the secondary magnetic circuit is a minimum. If sufficient primary flux is now introduced to saturate the common magnetic region, the secondary reluctance is increased, irrespective of the relative direction of the primary flux, with the changes in secondary reluctance being in effect, a full-wave rectification of the primary flux variations. A sinusoidally varying primary flux with a frequency f will thus

produce periodic variation in the secondary reluctance at the double frequency 2f. A similar argument also applies if only secondary flux is assumed to exist in the core.

The above process can be further discussed by reference to Figure 2.2. When hysteresis of a magnetic core is neglected, the flux is a single-valued and odd symmetrical function of the applied magnetomotive force, as shown in Figure 2.2(a). In Figure 2.2(b), the dependence of the secondary reluctance R_{m2} on the primary flux ϕ_1, based on the foregoing discussion, is shown as an even symmetrical curve and the relationship may be termed a *trans-reluctance* characteristic. Figure 2.2b shows clearly the double frequency variation of the secondary reluctance, superimposed on an average value. This variation contains, in addition to the second harmonic component, a series of higher order even harmonics.

Drawing R_{m2} as a function of the primary current (or the mmf F_1 applied to the primary circuit) instead of the primary flux, results in Figure 2.3. With a magnetisation characteristic such as Figure 2.2(a), the reluctance of the iron core is constant before saturation and the current required to drive the core into saturation is small. Thus, the part of the curve, in Figure 2.3, where the reluctance is constant (minimum) is much shorter than that of Figure 2.2(b). However, it is not in practice zero, contrary to the assumption in the patents[1] by Wanlass, of a trans-inductance curve shown in Figure 2.4, where the secondary inductance falls immediately to very small values with a non-zero

primary current. Although the current to drive the core into saturation, shown as i_s in Figure 2.2(a), is small, the amplitude of the alternating voltage required to produce it is large (proportional to frequency, number of turns in the primary winding and the saturation flux level ϕ_s). This is a quite important fact, and when considered together with the under-voltage protection property of the parametric transformers (threshold effect), leads to the conclusion that some of the applications proposed by Wanlass[2] are in fact impossible to obtain in practice, as is explained later in Chapter X.

With the simplifying assumptions given above, the reluctance of the secondary magnetic circuit with respect to the primary flux, may most simply be expressed as:

$$R_{m2} = R_{m2min} + \Gamma \phi_1^2 \qquad \ldots\ldots \qquad (2.1)$$

where R_{m2min} and Γ are constants. R_{m2min} is the minimum constant value of the secondary reluctance, given by the inverse slope of the secondary magnetisation curve (ϕ_2/F_2) before saturation, and Γ is a coefficient introducing the effect of the primary flux.

It will be seen in Chapter VII that R_{m2min} and Γ are given as:

$$R_{m2min} = R_g + s_1 + r_1 \qquad \ldots\ldots \qquad (2.2)$$

$$\Gamma = 3\, r_3 \qquad \ldots\ldots \qquad (2.3)$$

where R_g, s_1, r_1 and r_3 are coefficients directly related to the physical dimensions and the B/H characteristic of the core. R_g is defined by equation (4.41), Section 4.4.3, and the definitions of s_1, r_1 and r_3 first appear in Section 6.3.1, as given by equations (6.17). To have a physical meaning strictly related to the physical construction of the two-C-core parametric transformers in the work described in the following chapters, R_{m2min} and Γ will be assumed, from the beginning, to be given by equations (2.2) and (2.3), and the dependence of the secondary reluctance on the primary flux to be expressed as:

$$R_{m2} = R_{m2min} + \Gamma\,\phi_1^2 = (R_g + s_1 + r_1) + 3r_3\,\phi_1^2 \quad \ldots \quad (2.4)$$

If the sinusoidally varying primary flux is of amplitude ϕ_{1m}, and is defined by

$$\phi_1 = \phi_{1m} \sin \omega t \quad \ldots\ldots \quad (2.5)$$

introducing equation (2.5) into (2.4) gives the time-variation of the secondary reluctance as:

$$R_{m2} = (R_g + s_1 + r_1 + \frac{3}{2} r_3\,\phi_{1m}^2) - (\frac{3}{2} r_3\,\phi_{1m}^2) \cos 2\omega t \quad (2.6)$$

This variation contains an average component

$$R_{m2av} = R_g + s_1 + r_1 + \frac{3}{2} r_3 \phi_{1m}^2 \qquad \ldots\ldots \qquad (2.7)$$

and a component varying sinusoidally at twice the frequency of the primary flux. The process may be seen as a modulation of the secondary reluctance by the primary flux, by writing

$$m = \frac{\frac{3}{2} r_3 \phi_{1m}^2}{R_{m2av}} \qquad \ldots\ldots \qquad (2.8)$$

when equation (2.6) becomes:

$$R_{m2} = R_{m2av} (1 - m \cos 2\omega t) \qquad \ldots\ldots \qquad (2.9)$$

where m is the modulation coefficient or modulation index.

2.1.2 Parametrically Developed Voltage and Negative Resistance Property

Having established a periodic variation in the reluctance (and therefore also the inductance) of the secondary circuit, the secondary circuit capacitance is adjusted to resonate at the frequency of the input voltage, with the mean value of the varying inductance. As shown in the next chapter (Section 3.3), if the amplitude of the secondary reluctance variations is sufficiently large, i.e. the modulation is sufficiently deep, the oscillatory circuit is parametrically excited, and oscillates at a frequency equal to the input frequency. Once oscillations

start, their amplitude increases, until they reach a stationary level determined by the saturation level in the magnetic core.

The flux in a magnetic circuit may be expressed as:

$$\phi = \frac{F}{R_m} \qquad \ldots\ldots \qquad (2.10)$$

where F, the magnetomotive force, is given in terms of the number of turns N and the current i, by

$$F = N.i \qquad \ldots\ldots \qquad (2.11)$$

Introducing equations (2.10) and (2.11) into the basic equation for the induced electromotive force

$$e = N \frac{d\phi}{dt} \qquad \ldots\ldots \qquad (2.12)$$

gives

$$e = \frac{N^2}{R_m} \frac{di}{dt} + i \frac{d}{dt} \left(\frac{N^2}{R_m}\right) \qquad \ldots\ldots \qquad (2.13)$$

The first term in equation (2.13) expresses the voltage due to changes in the exciting current i, and it represents flux-coupling term involved in the conventional transformer operation. The second term expresses the parametric coupling due to variations in the reluctance parameter, and the operation and energy transfer in the parametric transformer are achieved as a result of this term.

Since there is no flux coupling between the primary and secondary of a parametric transformer, the first term in equation (2.13) may be omitted, leaving

$$e = i \frac{d}{dt} \left(\frac{N^2}{R_m} \right) \qquad \ldots\ldots \qquad (2.14)$$

On substituting R_{m2} from equation (2.9) into equation (2.14) for R_m, the term to be differentiated becomes

$$\frac{N^2}{R_m} = \frac{N_2^{\,2}}{R_{m2av}\,(1 - m \cos 2\omega t)} \qquad \ldots\ldots \qquad (2.15)$$

which, by using the binomial expansion and neglecting higher-order terms, may be written as, approximately:

$$\frac{N_2^{\,2}}{R_{m2}} \simeq L_o\,(1 + m \cos 2\omega t) \qquad \ldots\ldots \qquad (2.16)$$

where L_o, the mean value of the secondary inductance, is

$$L_o = \frac{N_2^{\,2}}{R_{m2av}} \qquad \ldots\ldots \qquad (2.17)$$

Suppose now that a small initial current

$$i = I \cos (\omega t + \alpha) \qquad \ldots\ldots \qquad (2.18)$$

is present in the secondary circuit, with α being the phase difference from the primary flux. Introducing equations (2.16) and (2.18) into equation (2.14) gives the parametrically developed voltage as

$$e = L_o I \omega m [\sin(\omega t - \alpha) + \sin(3\omega t + \alpha)] \qquad (2.19)$$

The second term in equation (2.19) may be neglected since it is far from the resonant frequency of the secondary circuit. With only the fundamental frequency components considered, equations (2.18) and (2.19) may be written in the complex form as

$$\bar{i} = I e^{j\alpha} \qquad \ldots\ldots \qquad (2.20)$$

$$\bar{e} = L_o I \omega m j e^{-j\alpha} \qquad \ldots\ldots \qquad (2.21)$$

respectively. The complex impedance offered to the initial current is, therefore

$$Z = \frac{\bar{e}}{\bar{i}} = m L_o \omega j e^{-j2\alpha}$$

$$= m L_o \omega(\sin 2\alpha + j \cos 2\alpha) \quad \ldots\ldots \qquad (2.22)$$

Clearly, for $\alpha = -\frac{\pi}{4}$ or $+\frac{3\pi}{4}$, the secondary circuit has the maximum negative resistance

$$R_{-} = -m\, L_{o}\, \omega \qquad \ldots\ldots \qquad (2.23)$$

and if small oscillations exist in the secondary circuit, these will grow by virtue of the negative resistance effect arising as a consequence of the time-varying part of the secondary inductance. As the amplitude of the oscillations builds up, their phase changes, so that α finally becomes equal to either $-\frac{\pi}{4}$ or $+\frac{3\pi}{4}$, to obtain maximum negative resistance and to ensure maximum energy transfer. It is thus apparent that oscillations can be obtained with two different phases 180° apart, as is also the case in parametrons[3]. The energy transfer is a direct consequence of the variation of the secondary reluctance caused by the primary flux.

The energy stored in a magnetic circuit is

$$E_{m} = \frac{1}{2} F.\phi = \frac{1}{2} R_{m}.\phi^{2} \qquad \ldots\ldots \qquad (2.24)$$

where the mmf is given as

$$F = R_{m}.\phi \qquad \ldots\ldots \qquad (2.25)$$

Assume now that the reluctance of the magnetic circuit is instantaneously increased by a factor k, the flux (ideally) remaining constant. The new value of reluctance is $k.R_{m}$ and the corresponding energy stored

$$E_{m}' = k.\ (\frac{1}{2} R_{m}\ \phi^{2}) = k.E_{m} \qquad \ldots\ldots \qquad (2.26)$$

is increased by k times. Thus, if the secondary reluctance is increased at proper instants, energy is delivered parametrically into the secondary circuit to maintain the oscillations.

2.2 Characteristics of the Parametric Transformer

Since the secondary circuit of a parametric transformer operates as a parametric power oscillator, it offers very useful performance characteristics, such as line and load voltage regulation, over-voltage and over-load protection, filtering, phase-shift etc. not found in conventional transformers. These characteristics are closely related to the inherent features of parametric oscillators. Although some similar characteristics are provided by such non-linear magnetic control devices as ferro-resonant transformers, the phenomena involved are entirely different from those of parametric excitation. They rely on the properties of non-linear resonance to maintain the output voltage at a relatively constant level, but the power transfer from input to output circuits is achieved on the basis of flux coupling or mutual inductance.

2.2.1 Under- and Over-Voltage Protection and Voltage Regulation

As mentioned earlier, parametric excitation of the secondary circuit requires the variations of the secondary reluctance to have a sufficiently large amplitude. This requires a certain

amplitude of the primary flux in equation (2.6), which, in turn, means that the parametric transformer will not operate until the magnitude of the primary voltage is adequate to create sufficiently large variations in the secondary reluctance by saturating the common region of the core at certain instants. The parametric transformer does not operate at small values of the input voltage, and thereby exhibits an inherent under-voltage protection.

Parametric oscillations in the secondary circuit cease at very large input voltages. If an excessively large primary flux exists in the magnetic core, the common region of the core is driven far into saturation at almost all times, and the limitation on the amplitude of the flux causes the relative reluctance changes to become very small, which leads to the cessation of the parametric oscillations. This inherent action automatically protects both the device and any connected circuits from the effects of an excessive input voltage.

The increasing amplitude of the oscillations excited in the secondary circuit is limited by the saturation flux level of the magnetisation characteristic to a stationary value. At steady state operation, changes in the amplitude of the secondary flux are relatively small as long as the secondary operates in the saturation region of the magnetisation curve (above the knee of the curve), and this provides in the device an intrinsic voltage regulation characteristic.

An ideal operational characteristic for the output voltage as a function of the input voltage is shown in Figure 2.5, where the under- and over-voltage protection and voltage regulation

properties are clearly seen. However, the characteristic of a practical device will be more like that shown in Figure 2.6, since the device will exhibit the hysteresis or jump phenomenon encountered in all non-linear resonant circuits.

2.2.2 Load Regulation and Over-Load Protection

A load connected across the capacitor introduces both damping and detuning into the secondary oscillatory circuit. The power delivered to the load is only a portion of the total parametric power developed in the secondary circuit. As will be seen in Chapter III, the amplitude of oscillations in the secondary circuit is determined mainly by saturation (i.e. the non-linearity of the magnetisation characteristic) and is much less affected by the damping present in the circuit. Therefore, the changes in the load do not basically affect the amplitude of the secondary flux, and a good load regulation characteristic is obtained. However, there is a maximum value for the load at which the oscillations will cease, as is also the case in a conventional oscillator circuit which ceases to function if excessively loaded. The maximum load for the parametric transformer is determined by the maximum value of negative resistance (equation (2.23)) introduced into the secondary circuit through parametric excitation. If the damping in the circuit becomes equal to or greater than this value, the circuit ceases to oscillate, and the immediate fall in the output voltage is accompanied by a large reduction in the primary excitation current.

The output voltage is influenced by the power factor of the load, rather than its value. A reactive load modifies the effective value of inductance or capacitance in the secondary circuit and changes the resonant frequency by introducing detuning into the circuit.

The ideal and practical curves illustrating the load regulation and inherent over-load protection characteristics of the parametric transformer are shown in Figure 2.7.

2.2.3 Sinusoidal Output Voltage and Bilateral Filtering

Since the secondary circuit of a parametric transformer behaves like a tuned oscillator, the waveform of the oscillations is substantially independent of the input voltage waveform. This is also due to the fact that energy is not transferred by mutual flux coupling but by parametric excitation which is not directly dependent on the input waveform.

When the input voltage is not purely sinusoidal, the primary flux will contain harmonic components. Even if the input voltage is sinusoidal, the primary flux is not sinusoidal due to the winding resistance and non-linearity of the primary magnetic circuit. Moreover, the dependence of the secondary reluctance on the primary flux is not as simple as in equation (2.1) and may include terms of higher powers. Consequently, the time-variation of the secondary reluctance is not purely sinusoidal, as in equation (2.6), but contains higher frequency terms.

Nevertheless, the essential term which causes parametric excitation at the frequency f is the one at the frequency 2f. Although the other terms do not have a substantial effect on the parametric oscillations at the frequency f, they may excite the circuit if the resonant circuit is tuned to half the frequency of the particular term. Thus, while the waveform of parametric oscillations does not depend on the input voltage waveform, there arises a possibility for employing the parametric transformer as a frequency multiplier.

Apart from the filtering action introduced by the phenomenon itself, the secondary circuit is a tuned tank circuit which intrinsically exhibits a filtering ability by virtue of the Q-factor of the circuit. The particular magnetic core arrangement also reduces the effects of higher harmonics in the primary circuit, by minimising the flux coupling and providing a good isolation between the primary and secondary circuits. Thus, even with a square wave input voltage, the output voltage of a parametric transformer is quite sinusoidal.

This filtering ability of the parametric transformer is bilateral; harmonics in the input voltage are suppressed and any disturbances at the load side are not transferred to the supply side. The latter is due to the unilateral mechanism of operation of the parametric transformer, (i.e. if input voltage is applied to the secondary, no output voltage is obtained in the primary circuit where no resonating capacitor is employed). Furthermore, high-voltage spikes of short duration are also suppressed, since the primary magnetic circuit is driven further into saturation and the reluctance does not vary.

2.2.4 Phase-Shift and Bistability of the Phase

It is a characteristic feature of all parametric oscillators that there is a defined phase relationship between the output and the pump signals. To accomplish maximum energy transfer, the parameter variations must be properly timed in order that the parameter change increases the energy of the system. If this phase relationship is not satisfied, less energy is delivered and, for some phase difference values, energy may even be removed from the oscillating system. This is apparent in equation (2.22), where the resistive part of the impedance is positive for $0<\alpha<\frac{\pi}{2}$ and $\pi<\alpha<\frac{3\pi}{2}$, while it takes a maximum negative value at $\alpha = -\frac{\pi}{4}$ and $+\frac{3\pi}{4}$. Actually, the parametric oscillation adjusts itself, by changing its phase, so that the energy taken during each cycle of oscillation becomes a maximum. The parametric oscillation is thereby phase-locked with the variation of the parameter, and finally takes either of the phase angles $\alpha = -\frac{\pi}{4}$ or $+\frac{3\pi}{4}$, depending upon the phase of the initial oscillation. This emphasises the bistability of the phase of the oscillations, which may be obtained at two opposite phases, each in a defined relationship with the input signal.

The phase relationship between the input and output signals at steady state operation of the parametric transformer is that the output voltage is $\mp 90^{\circ}$ out of phase with the input voltage. As will be seen in Chapter III, the non-linearity in the secondary circuit not only sets a limit on the amplitude of the oscillations but also varies the phase of initial oscillations so that it is finally locked into one of these two values. It is apparent from

Figure 2.1 that in the different common regions of the magnetic core the resultant amplitude of the total flux which is the sum or the difference between the primary and secondary fluxes, is limited to the saturation flux level. When the primary flux is at its maximum, the secondary flux is forced to zero, and at the instant 90° later, when the primary flux is zero, the whole region is free for the secondary flux to attain the saturation level.

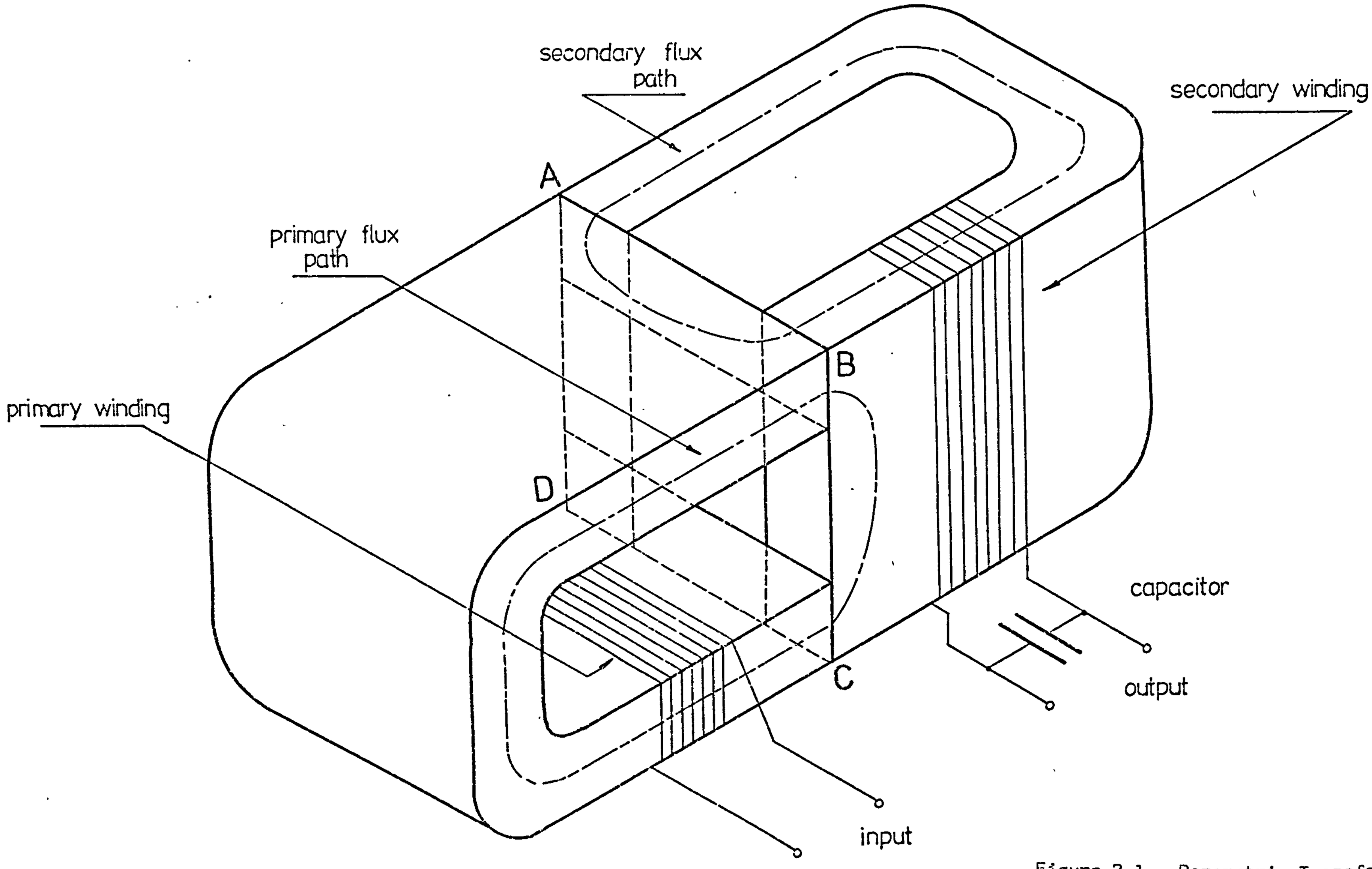

Figure 2.1 Parametric Transformer

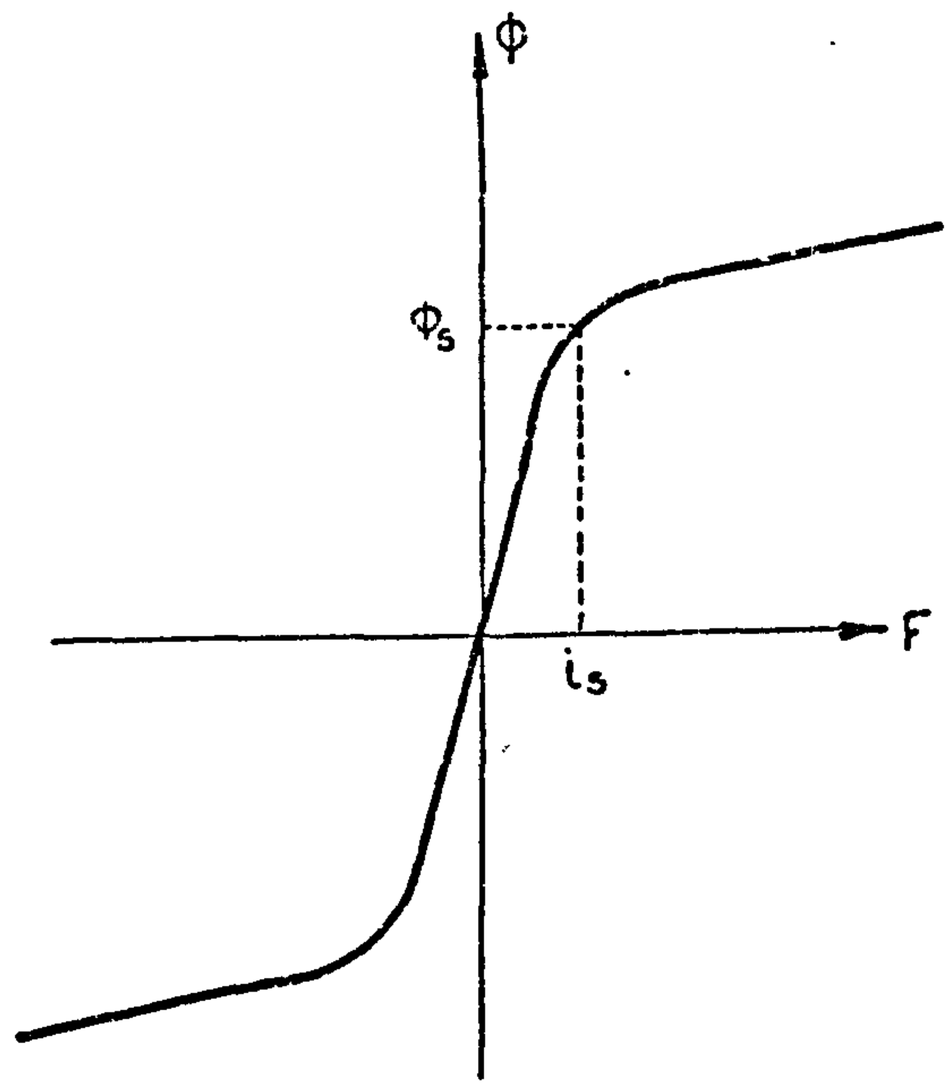

a _ Magnetisation characteristic

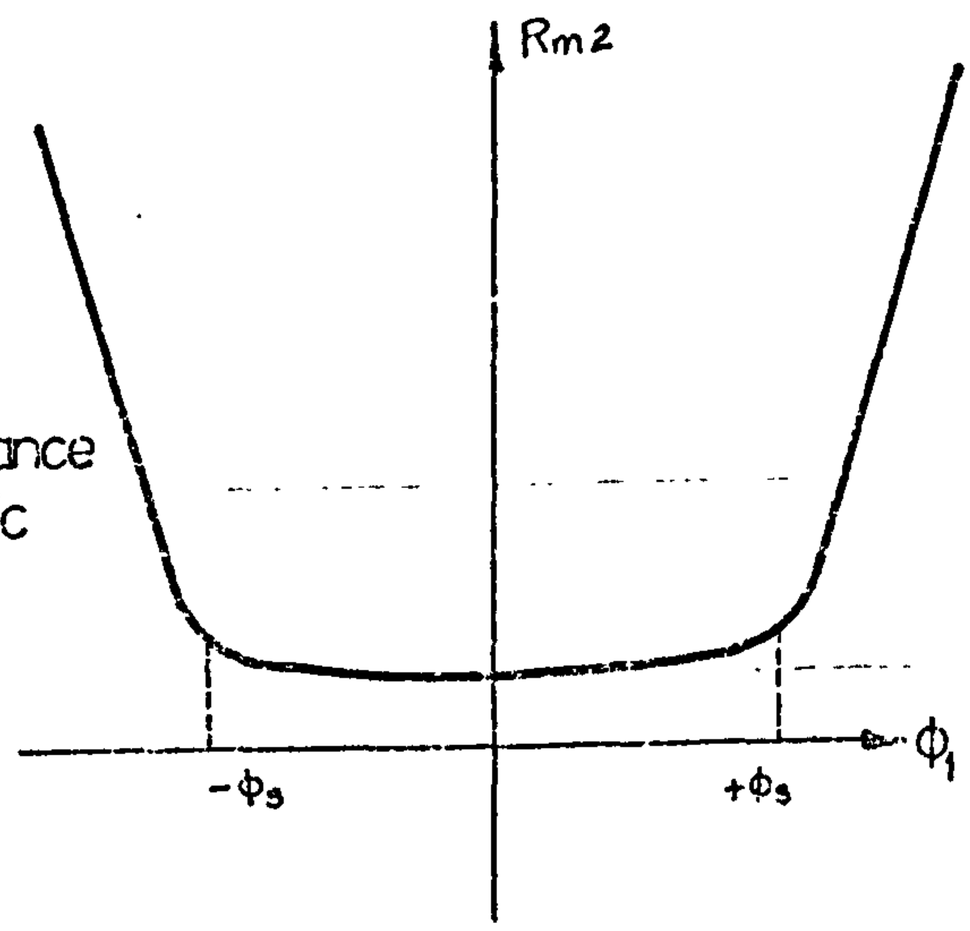

b _ Trans_reluctance characteristic

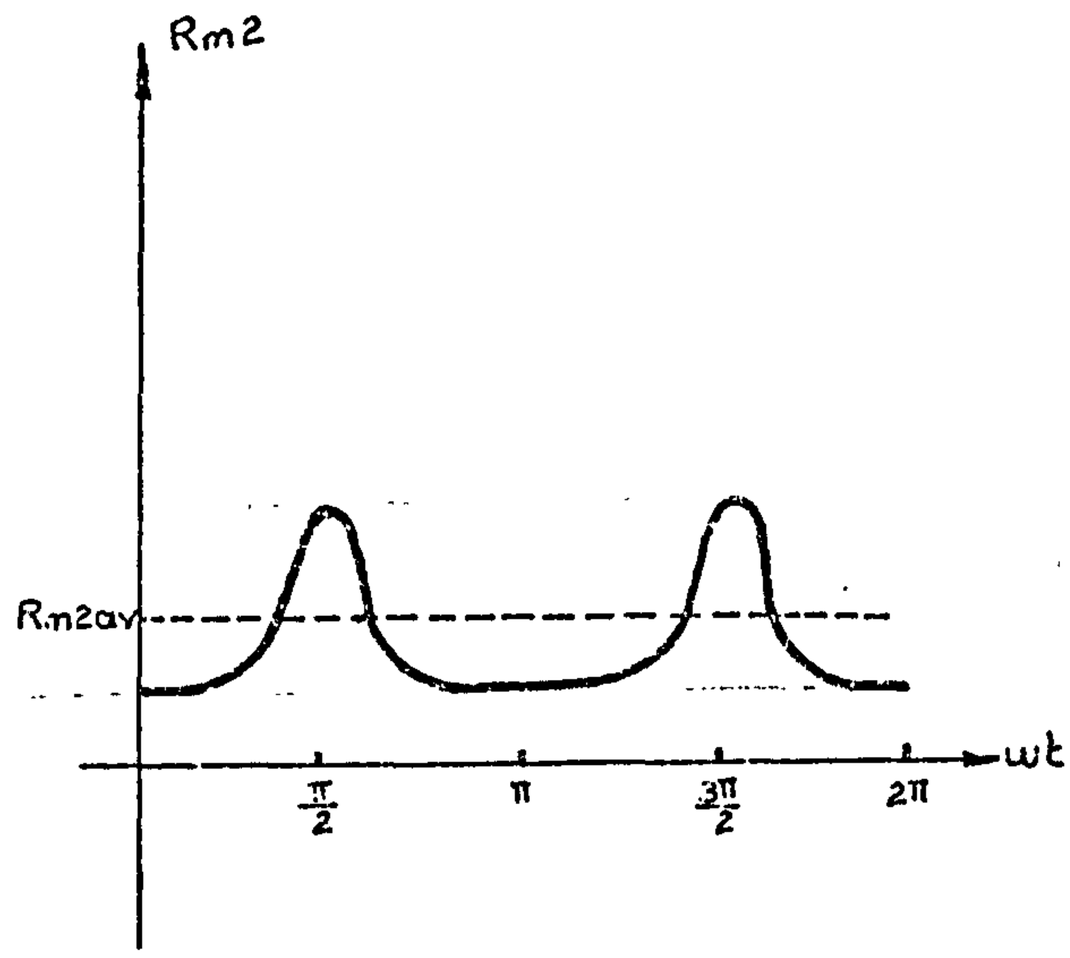

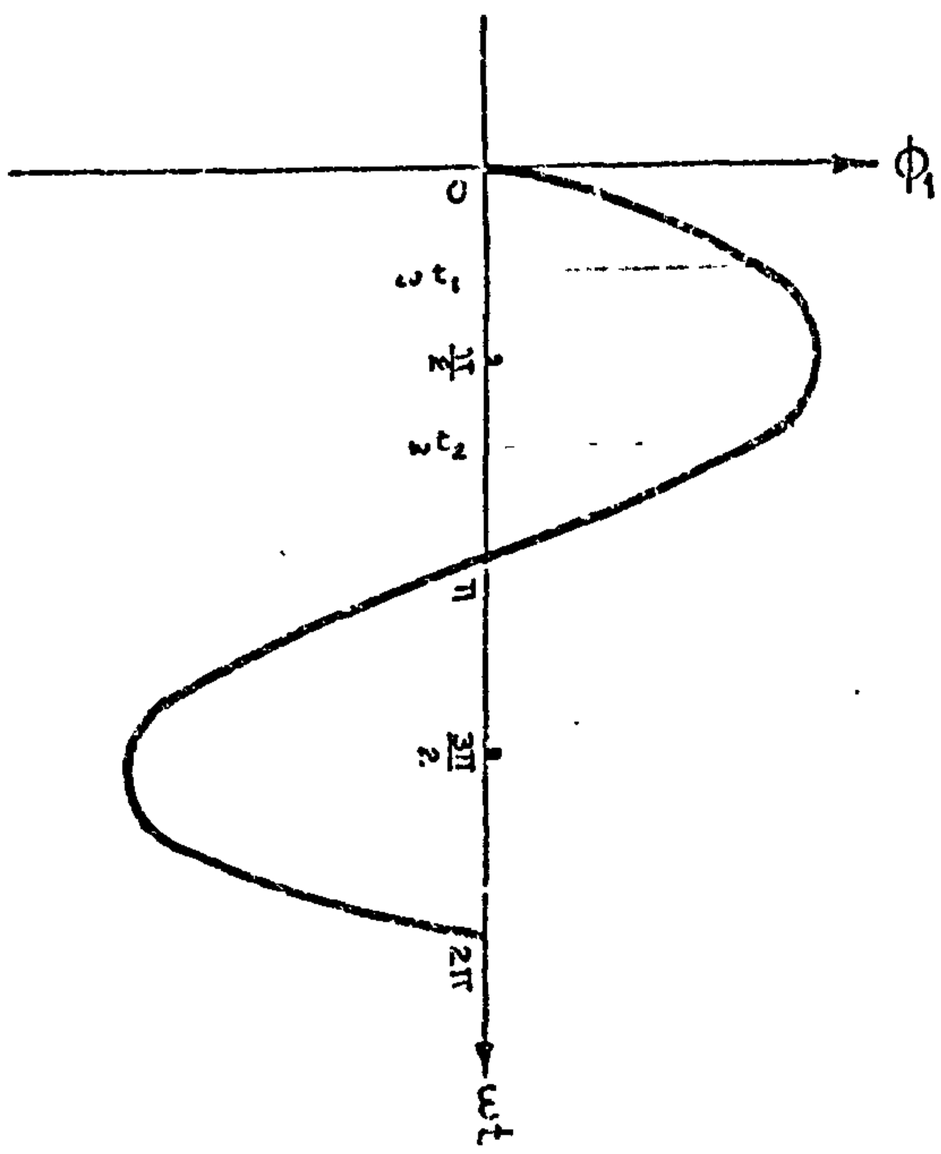

Figure 2.2 Process of Reluctance Modulation

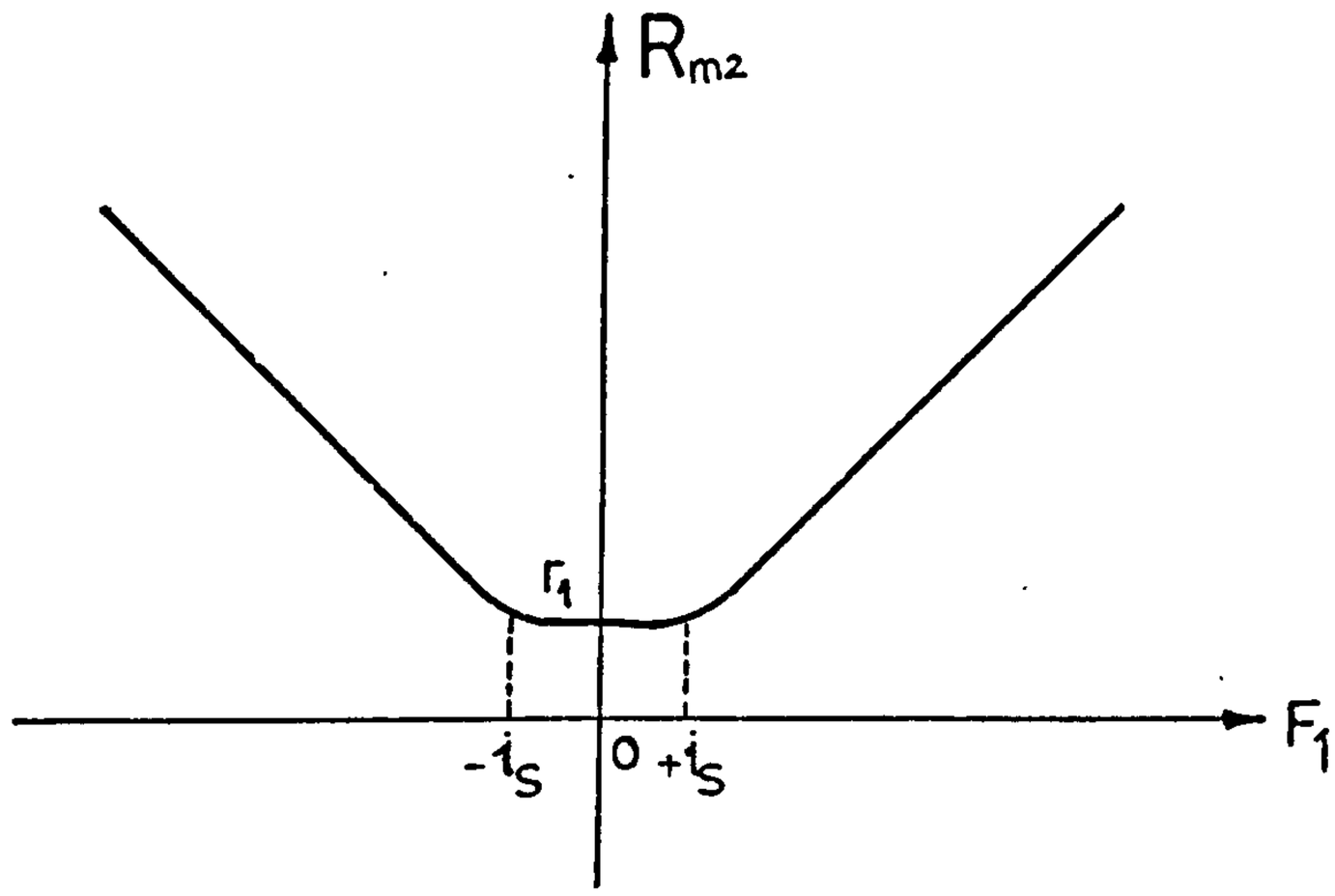

Figure 2.3 Dependence of secondary reluctance on primary mmf

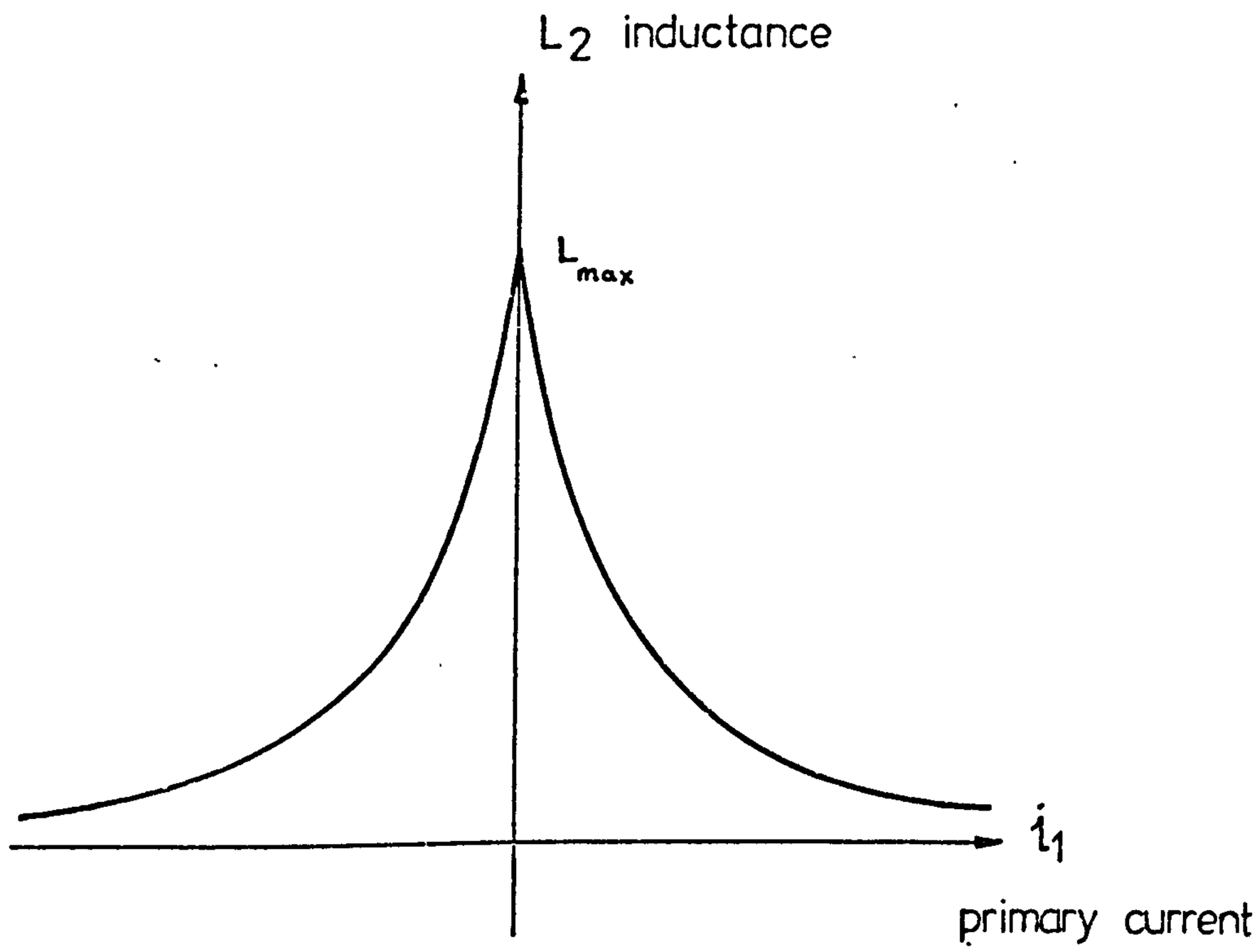

Figure 2.4 Trans-inductance curve assumed by Wanlass

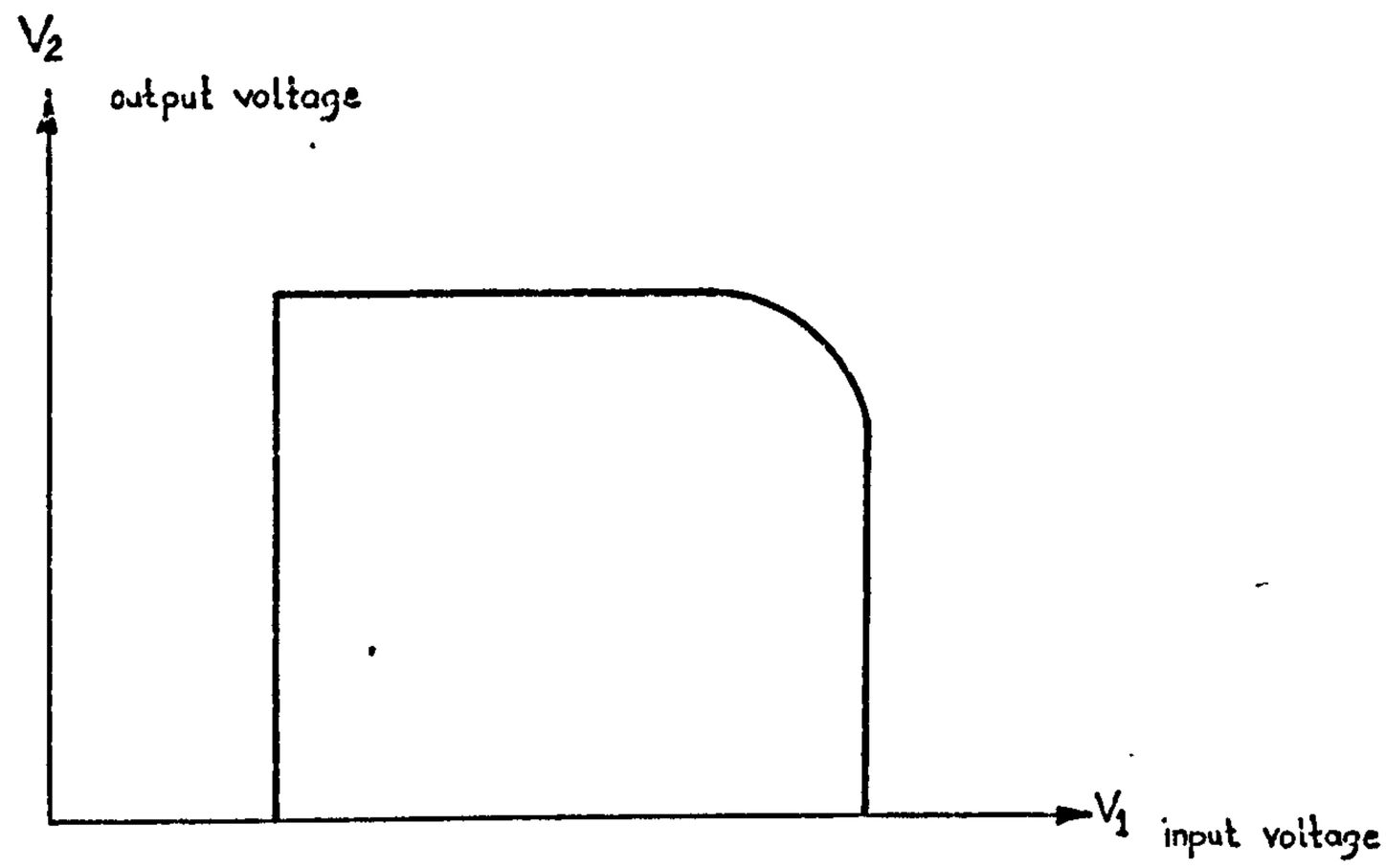

Figure 2.5 Ideal operational characteristic

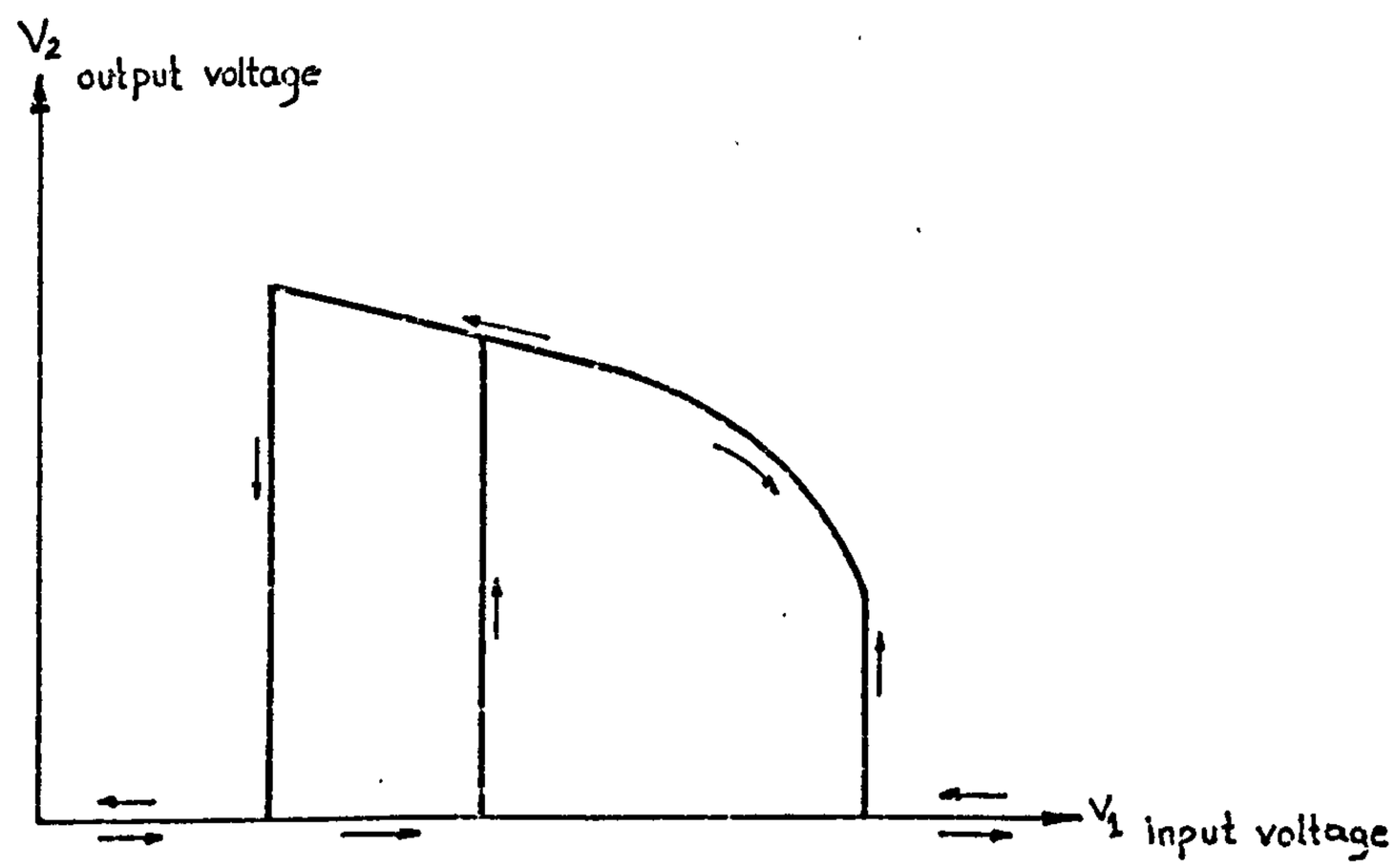

Figure 2.6 Practical operational characteristic

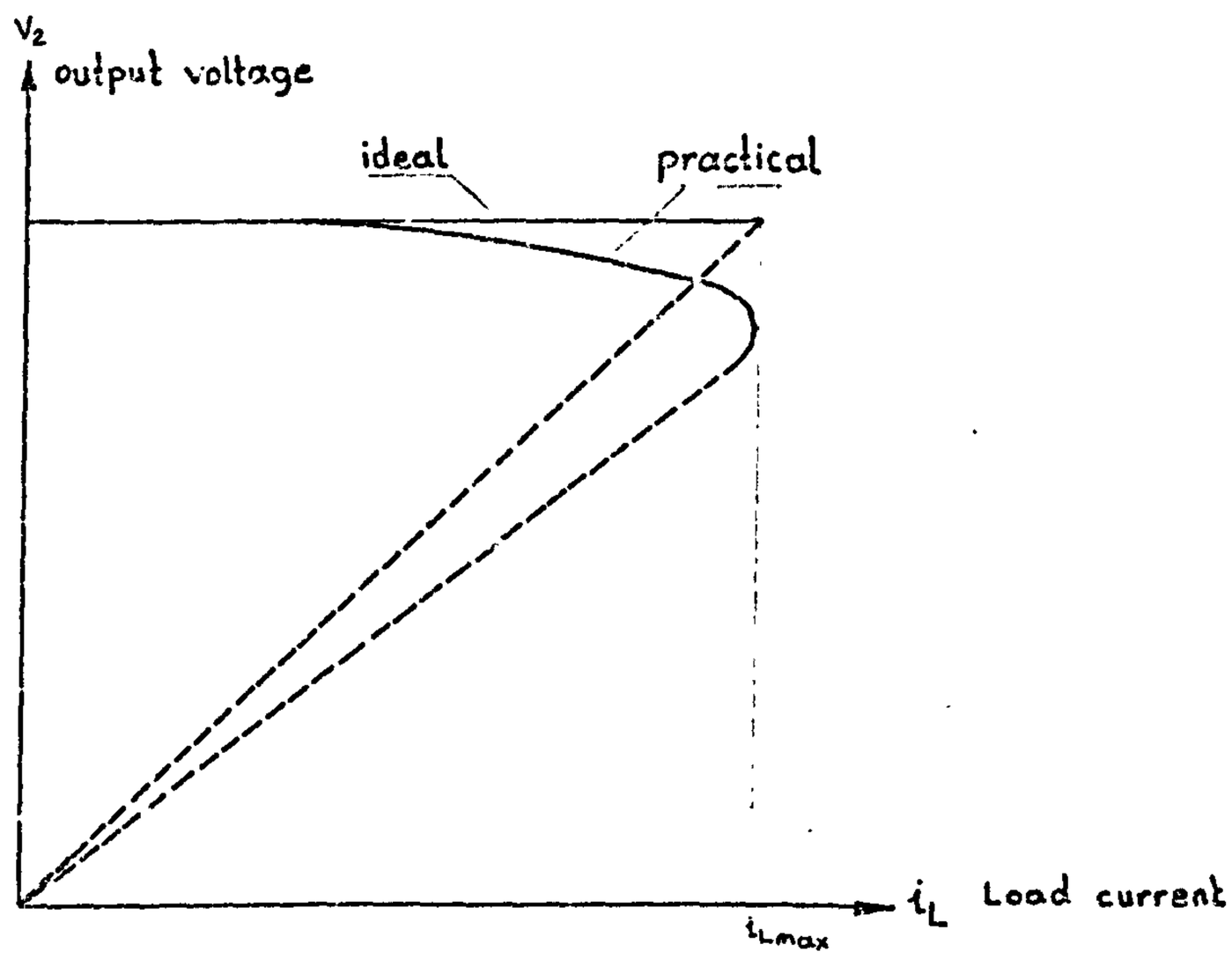

Figure 2.7 Load regulation and overload protection characteristics

CHAPTER III

THEORY OF PARAMETRIC OSCILLATIONS AS APPLIED TO THE PARAMETRIC TRANSFORMER

A study of the phenomenon of parametric excitation is obviously concerned with the solution of differential equations with periodically varying coefficients, a subject on which a considerable amount of literature exists. However, most of this deals with the stable solutions of these equations, in particular of the Mathieu and Hill type equations. Moreover, attention is directed mainly to the linear forms of these equations, in accordance with the emphasis towards considerations of linear systems. These linear forms are also encountered very frequently in investigating the stability of the periodic solutions of non-linear, second order oscillating systems, where the stability of the system depends on the stability of a 'variational equation' which always leads to a Hill equation.

In this chapter, the theory of the parametric transformer is developed on the basis of the Mathieu-Hill type equations; the secondary circuit is considered first as a linear circuit having a periodically varying parameter, and the effects of the non-linearity and the load are subsequently investigated.

3.1 Linear Case (Build-up of Oscillations)

Initially, the reluctance of the secondary magnetic circuit, as modulated by the primary flux, will be assumed to have the sinusoidal variation given by equation (2.9), and not to be a

function of the secondary flux. Furthermore, by neglecting both electrical and magnetical losses, the secondary circuit is assumed to be non-dissipative, although it is not conservative. On this basis, a simple equivalent circuit for the output side of the parametric transformer is shown in Figure 3.1. From this figure, it follows that

$$N_2 \frac{d\,\phi_2}{dt} + \frac{1}{C} \int i_2 \, dt = 0 \qquad \cdots\cdots \qquad (3.1)$$

where the current i_2 is, from equations (2.10) and (2.11),

$$i_2 = \frac{R_{m2} \cdot \phi_2}{N_2} \qquad \cdots\cdots \qquad (3.2)$$

Substituting equation (3.2) into equation (3.1) and differentiating gives

$$\frac{d^2\,\phi_2}{dt^2} + \frac{R_{m2}}{C\,N_2^{\,2}} \phi_2 = 0 \qquad \cdots\cdots \qquad (3.3)$$

a differential equation describing the circuit in terms of the secondary flux. On introducing into equation (3.3) the assumed variation of the secondary reluctance from equation (2.9), we obtain

$$\frac{d^2\,\phi_2}{dt^2} + \frac{R_{m2av}}{C\,N_2^{\,2}} (1 - m \cos 2\,\omega t)\, \phi_2 = 0 \quad .. \qquad (3.4)$$

which is a typical Mathieu equation. By putting

$$z = \omega t \qquad \cdots\cdots \qquad (3.5)$$

$$\omega_0^2 = \frac{R_{m_2 av}}{C\ N_2^2} \qquad \cdots\cdots \qquad (3.6)$$

$$a = \frac{\omega_0^2}{\omega^2} \qquad \cdots\cdots \qquad (3.7)$$

and $$q = \frac{m}{2}\, a \qquad \cdots\cdots \qquad (3.8)$$

equation (3.4) reduces to the standard form of the linear Mathieu equation:

$$\frac{d^2 \phi_2}{dz^2} + (a - 2q \cos 2z)\, \phi_2 = 0 \qquad \cdots\cdots \qquad (3.9)$$

The theory of this equation has been treated in detail elsewhere[1], where the general solutions are shown to be quite complicated. However, for the present purposes, only the forms of these solutions and their stability will be considered, since the essence of parametric excitation lies in the instability of the solution.

The particular form and stability of the solutions depend upon the values of the coefficients a and q. For some combinations of a and q, the solution for ϕ_2 grows without bound

as z increases, and it is, therefore, unstable. With other combinations, the solution is stable and remains bounded, for all values of z. The combinations of a and q corresponding to stable and unstable solutions are indicated on the 'stability chart'[1] for the Mathieu equation, shown in Figure 3.2. The (a;q) plane is divided into stable and unstable regions, and according to the values of the coefficients, the parametric point (a;q) may lie in either of these regions or on the boundary curves by which they are separated. The corresponding solutions are stable, unstable, or neutral.

The general theory of linear differential equations with periodic coefficients, developed by Flouqet,[2] establishes that the general solution of the Mathieu equation is of the form

$$\phi_2 = A\, e^{\mu z}\, \phi\,(z) + B\, e^{-\mu z}\, \psi\,(z) \qquad \cdots\cdots \qquad (3.10)$$

where A and B are arbitrary constants, μ is a constant depending solely on a and q, and ϕ and ψ are purely periodic functions of z.

Within an unstable region, the two linearly independent solutions in equation (3.10) take the non-periodic forms

$$\phi_2' = e^{\mu z} \sum_{r=0}^{\infty} \rho_n \cos(nz + \alpha_n) \qquad \cdots\cdots \qquad (3.11)$$

$$\phi_2'' = e^{-\mu z} \sum_{r=0}^{\infty} \rho_n \cos(nz - \alpha_n) \qquad \cdots\cdots \qquad (3.12)$$

where μ is a real and positive constant, and ρ_n and α_n are the amplitude and phase of the nth harmonic component, μ, ρ_n and α_n all depending on a and q. The harmonic order n is $2r$ or $2r + 1$, according as the parametric point lies, respectively within an even or odd numbered unstable region.

As $z \to +\infty$, $\phi_2' \to \mp\infty$ and $\phi_2'' \to 0$, because of the exponential term. Thus, although the ϕ_2'' solution is stable, the ϕ_2' solution and the complete solution

$$\phi_2 = \phi_2' + \phi_2'' \qquad \cdots\cdots \quad (3.13)$$

are both unstable.

Although most applications based on the phenomenon of parametric excitation make use of one of the stable regions in Figure 3.2, the parametric transformer functions only when the parametric point exists in one of the unstable regions. Together with equation (2.17), equation (3.6) shows ω_0 to be the resonant frequency of the secondary circuit; thus, for normal parametric transformer operation, with the output frequency the same as the input frequency, Figure 3.2 indicates that the parametric point must lie in the first unstable region. Hence the conditions for instability are

$$a = 1 \qquad \cdots\cdots \quad (3.14)$$

and

$$q > 0 \qquad \cdots\cdots \quad (3.15)$$

Once the capacitor is adjusted to the corresponding value of

$$C = \frac{R_{m2av}}{\omega^2 N_2^{\ 2}} \qquad \cdots\cdots \qquad (3.16)$$

the parametric point is driven into the first unstable region, since the modulation coefficient m is finite and q is, therefore, greater than zero. The solution of equation (3.9) is then unstable, and parametric oscillations are excited, with the amplitude of the secondary flux (and voltage) growing with time.

By considering only r=0 in equation (3.11),where now n=1(= 2r+1), a first-order approximation of the solution for ϕ_2 is obtained as

$$\phi_2 = e^{\mu z} . \rho . \cos(z + \alpha) \qquad \cdots\cdots \qquad (3.17)$$

with the second linearly-independent solution ϕ_2'' omitted as it vanishes with time.

If q is small, the exponent μ and the phase α in equation (3.17) may, approximately, be determined by using the 'variation of parameters' method.[3] With the coefficient values a=1, 0<q<<1, and with the initial conditions $\phi_2 = \phi_{20}$, $\frac{d\phi_2}{dt} = 0$, at t=0, the approximate solution of equation (3.9) is obtained by introducing a generating solution of the form

$$\phi_2 = \rho \cos(z + \alpha) \qquad \cdots\cdots \qquad (3.18)$$

into the equation, and expressing the average variations in ρ and α, as

$$\left(\frac{d\alpha}{dz}\right)_{av} = -\frac{q}{2} \cos 2\alpha \qquad \cdots\cdots \qquad (3.19)$$

$$\left(\frac{d\rho}{dz}\right)_{av} = \frac{1}{2} q \rho \qquad \cdots\cdots \qquad (3.20)$$

Equation (3.19) can be plotted in a kind of phase-plane diagram, as shown in Figure 3.3. Equilibrium points for α occur when it takes values that are odd multiples of $\frac{\pi}{4}$ radians. The variable z increases as shown by the arrows in the figure, and stable values evidently exist for $\alpha = \ldots, -\frac{\pi}{4}, +\frac{3\pi}{4}, \ldots$ while unstable values are $\alpha = \ldots, -\frac{3\pi}{4}, +\frac{\pi}{4}, \ldots$. Thus, as z increases, α will change from its initial value to one of the stable equilibrium values. The simplest equilibrium value is $\alpha = -\frac{\pi}{4}$, and this has been taken in the calculation of equation (3.20). Integration of equation (3.20) gives the change in the amplitude of the oscillation as

$$\rho = \phi_{20}\, e^{\frac{1}{2}qz} \qquad \cdots\cdots \qquad (3.21)$$

and the approximate solution is

$$\phi_2 = \phi_{20}\, e^{\frac{1}{2}qz} \cos\left(z - \frac{\pi}{4}\right) \qquad \cdots\cdots \qquad (3.22)$$

In this unstable solution, the exponential term shows that the rate of growth of the amplitude is proportional to m, and the larger the amplitude of the variations in the secondary reluctance, the more rapid is the growth of the amplitude of the parametric oscillations.

3.1.1 General Solution of the Mathieu Equation in the First Unstable Region

With q=0 in equation (3.9), this becomes

$$\frac{d^2 \phi_2}{dz^2} + a\,\phi_2 = 0 \qquad \cdots\cdots \qquad (3.23)$$

for which the solutions are $\mp \cos nz$, $\mp \sin nz$, where $n = a^{\frac{1}{2}}$. When $q \neq 0$, a and q must be interrelated for the periodic solution of equation (3.9) to have period π or 2π, so that a is necessarily a function of q. By writing

$$a = n^2 + c_1 q + c_2 q^2 + c_3 q^3 + \ldots \qquad \cdots \qquad (3.24)$$

the desired form $a=n^2$ is obtained when q=0, when the Mathieu equation reduces to equation (3.23).

The periodic solutions of the Mathieu equation, termed 'neutral' in the previous section (i.e. when the parametric point lies on the boundaries of the stability chart) must, therefore, reduce to cos nz and sin nz when $q \to 0$. These solutions, called

Mathieu functions, are sine-elliptic and cosine-elliptic functions, the Fourier series for which may be written in the form[4]

$$ce_{2n}(z,q) = \sum_{r=0}^{\infty} A_{2r}(q) \cos 2rz$$

$$ce_{2n+1}(z,q) = \sum_{r=0}^{\infty} A_{2r+1}(q) \cos(2r+1)z$$

$$\ldots\ldots (3.25)$$

$$se_{2n}(z,q) = \sum_{r=0}^{\infty} B_{2r}(q) \sin 2r\,z$$

$$se_{2n+1}(z,q) = \sum_{r=0}^{\infty} B_{2r+1}(q) \sin(2r+1)z$$

for positive and small values of q.

All Mathieu functions reduce either to cos nz or sin nz for $q \to 0$, because the coefficients A and B in the Fourier series are functions of q. For a given q, the value of a is definite for each Mathieu function and is given with a function of q in the form of equation (3.24).

The Mathieu functions associated with the first unstable region are $ce_1(z,q)$ and $se_1(z,q)$ which are the solutions for equation (3.9), when, respectively[5]

$$a = a_{c1} = 1 + q - \frac{1}{8} q^2 - \frac{1}{64} q^3 - \frac{1}{1536} q^4 + \ldots \qquad (3.36)$$

$$a = a_{s1} = 1 - q - \frac{1}{8} q^2 + \frac{1}{64} q^3 - \frac{1}{1536} q^4 + \ldots \qquad (3.37)$$

The functions $ce_1(z,q)$ and $se_1(z,q)$ are given by the series[5]

$$ce_1(z,q) = \cos z - \frac{1}{8} q \cos 3z + \frac{1}{64} q^2(-\cos 3z + \frac{1}{3} \cos 5z) - \frac{1}{512} q^3$$

$$(\frac{1}{3} \cos 3z - \frac{4}{9} \cos 5z + \frac{1}{18} \cos 7z) + \frac{1}{4096} q^4$$

$$(\frac{11}{9} \cos 3z + \frac{1}{6} \cos 5z - \frac{1}{12} \cos 7z + \frac{1}{180} \cos 9z) + \ldots$$

$$(3.28)$$

$$se_1(z,q) = \sin z - \frac{1}{8} q \sin 3z + \frac{1}{64} q^2(\sin 3z + \frac{1}{3} \sin 5z) - \frac{1}{512} q^3$$

$$(\frac{1}{3} \sin 3z + \frac{4}{9} \sin 5z + \frac{1}{18} \sin 7z) + \frac{1}{4096} q^4$$

$$(- \frac{11}{9} \sin 3z + \frac{1}{6} \sin 5z + \frac{1}{12} \sin 7z + \frac{1}{180} \sin 9z) + \ldots$$

$$(3.29)$$

To provide these functions as solutions of the Mathieu equation, the coefficient a, called the characteristic number of the Mathieu equation, must respectively take the values a_{c1} and a_{s1}, given by equations (3.26) and (3.27). Equation (3.26) and (3.27), when a is plotted as a function of q on the plane $(a;q)$, give the boundary curves of the first unstable region in the stability chart of Figure 3.2. When the parametric point is on the curve a_{c1}, the periodic solution of the Mathieu equation is $ce_1(z,q)$, and when the parametric point is on the curve a_{s1}, the solution is $se_1(z,q)$.

The solutions, given by equations (3.28) and (3.29), are of period 2π in z, and being neither stable nor unstable, they may be classed as neutral. However, as pointed out by Whittaker[6], they are in fact degenerate cases of a quasi-periodic solution of the Mathieu equation, having the form

$$\phi_2 = e^{\mu z}\ \phi(z,\sigma) \qquad \cdots\cdots \qquad (3.30)$$

with

$$\phi(z,\sigma) = \sin(z - \sigma) + c_3 \cos(3z - \sigma) + s_3 \sin(3z - \sigma) + c_5 \cos(5z - \sigma)$$

$$+ s_5 \sin(5z - \sigma) + \cdots\cdots \qquad \cdots\cdots \qquad (3.31)$$

where σ is a new parameter taking a value between 0 and $-\frac{\pi}{2}$ for the unstable solution. Hence, the Mathieu equations $se_1(z,q)$ and $ce_1(z,q)$ are simply particular cases of the solution, corresponding to $\sigma = 0$ and $\sigma = -\frac{\pi}{2}$, respectively. The unknown coefficients c_3, s_3, ... in equation (3.31) are determined in terms of q and σ as follows[7]

$$c_3 = \frac{3}{64} q^2 \sin 2\sigma - \frac{3}{512} q^3 \sin 4\sigma + \ldots.$$

$$s_3 = -\frac{1}{8} q + \frac{1}{64} q^2 \cos 2\sigma - \frac{1}{512} q^3 \left(-\frac{14}{3} + 5 \cos 4\sigma\right) + \ldots$$

$$c_5 = -\frac{7}{2304} q^3 \sin 2\sigma + \ldots \tag{3.32}$$

$$s_5 = \frac{1}{192} q^2 - \frac{1}{1152} q^3 \cos 2\sigma + \ldots$$

.....

and the characteristic exponent of the unstable solution is[7]

$$\mu = -\frac{1}{2} q \sin 2\sigma + \frac{3}{128} q^3 \sin 2\sigma - \frac{3}{1024} q^4 \sin 4\sigma + \ldots \tag{3.33}$$

The characteristic number a now becomes[7]

$$a = 1 - q \cos 2\sigma + \frac{1}{4} q^2 \left(-1 + \frac{1}{2} \cos 4\sigma\right) + \frac{1}{64} q^3 \cos 2\sigma + \ldots \qquad (3.34)$$

which gives a_{c1} and a_{s1} of equations (3.26) and (3.27) for $\sigma = -\frac{\pi}{2}$ and $\sigma = 0$, respectively.

From these results, the characteristic exponent μ is readily calculable, when the new parameter σ is known. In practice, however, when the Mathieu equation is to be solved, the parameters a and q are known, and it is difficult to find σ from given values of a and q by solving equation (3.34). To avoid this situation, a and μ are first calculated from equations (3.33) and (3.34) by varying q and σ, and the iso-μ and iso-σ curves are then plotted[8] in the $(a;q)$ plane. In Figure 3.4, these curves are shown for the unstable regions of the stability chart. The curves in the first unstable region are illustrated in more detail in Figure 3.5 which covers the area indicated in Figure 3.2.

When a Mathieu equation in the form of equation (3.9) is given, and the solution in the first unstable region is to be found, the iso-μ and iso-σ curves which intersect at the parametric point determined by the values of a and q give the values of μ and σ in the unstable solution of equation (3.30). In the first-order approximation, by taking only the fundamental frequency component in $\phi(z,\sigma)$ of equation (3.31), the unstable solution becomes

$$\phi_2 = \phi_{20}\, e^{\mu z} \sin(z - \sigma) \qquad \ldots\ldots \qquad (3.35)$$

where ϕ_{20} arises from the initial condition. For the coefficients $a=1$ and $0<q<<1$, it is clear from the iso-μ and iso-σ curves of Figure 3.5 that $\sigma = -45^{o}$, and μ is proportional to $\frac{q}{2}$. Inserting these values in equation (3.35) gives the approximate solution as

$$\phi_2 = \phi_{20}\, e^{\frac{qz}{2}} \sin(z + \frac{\pi}{4}) = \phi_{20} e^{\frac{1}{2} qz} \cos(z - \frac{\pi}{4}) \qquad (3.36)$$

the same as the solution found by the method of variation of parameters, and given in equation (3.22).

3.1.2 Operation in the Second Unstable Region: Frequency Multiplication

In the first unstable region, the periodic function $\phi(z,\sigma)$ has period 2π in z, indicating that parametric oscillations are obtained at the same frequency as the input frequency (which is normal operation of the parametric transformer). However, the periodic solutions of the Mathieu equation for the second unstable region, ce_2 and se_2 , have period π in z. Hence, if the parametric point is in the second unstable region, parametric oscillations are obtained at twice the input frequency and, in this way, the parametric transformer operates as a frequency multiplier.

The instability conditions are now

$$a = 4 \qquad \cdots\cdots \qquad (3.37)$$

and

$$q>0 \qquad \cdots\cdots \qquad (3.38)$$

to drive the parametric point into the second unstable region.

The first condition above corresponds to $\omega_o = 2\omega$, and, physically to tuning the secondary resonant circuit to twice the frequency of the input. The capacitor is thus adjusted to the value

$$C = \frac{R_{m2av}}{4\ \omega^2\ N_2^{\ 2}} \qquad \cdots\cdots \qquad (3.39)$$

and parametric oscillations are excited with any positive value of q, since no damping is assumed present in the circuit.

The general solution for the second unstable region will be outlined in a manner similar to that followed for the first unstable region. The unstable solution is again in the form of equation (3.30), where μ and $\phi(z,\sigma)$ are now[8]

$$\mu = -\frac{1}{16}\, q^2 \sin 2\sigma + \ldots. \qquad \cdots\cdots \qquad (3.40)$$

$$\phi(z,\sigma) = \sin(2z - \sigma) + c_4 \cos(4z - \sigma) + s_4 \sin(4z - \sigma)$$

$$+ c_6 \cos(6z - \sigma) + s_6 \sin(6z - \sigma) + \ldots. \qquad (3.41)$$

where the coefficients c_4, s_4, ... are determined by q and σ. The characteristic number a, in terms of q and σ, is[8]

$$a = 4 + \frac{1}{2} q^2 \left(\frac{1}{3} - \frac{1}{2} \cos 2\sigma\right) + \ldots. \qquad (3.42)$$

which reduces to

$$a_{c2} = 4 + \frac{5}{12} q^2 + \ldots \qquad (3.43)$$

$$a_{s2} = 4 - \frac{1}{12} q^2 + \ldots \qquad (3.44)$$

for $\sigma = -\frac{\pi}{2}$ and $\sigma = 0$, respectively.

Equations (3.43) and (3.44) give the boundary curves of the second unstable region, shown as a_{c2} and a_{s2} in Figure 3.2. The unstable solution $\phi_2 = e^{\mu z} \phi(z,\sigma)$, therefore, reduces to the Mathieu function $se_2(z,q)$ or $ce_2(z,q)$ depending on whether $\sigma = 0$ or $\sigma = -\frac{\pi}{2}$, respectively, i.e. whether the parametric point lies

on the boundary curve a_{s2} or a_{c2}. The Mathieu functions associated with the second unstable region are given by the series[8].

$$ce_2(z,q) = \cos 2z - \frac{1}{8} q(\frac{2}{3} \cos 4z - 2) + \frac{1}{384} q^2 \cos 6z - \frac{1}{512} q^3$$

$$(\frac{1}{45} \cos 8z + \frac{43}{27} \cos 4z + \frac{40}{3}) + \ldots. \qquad (3.45)$$

$$se_2(z,q) = \sin 2z - \frac{1}{12} q \sin 4z + \frac{1}{384} q^2 \sin 6z - \frac{1}{512} q^3$$

$$(\frac{1}{45} \sin 8z - \frac{5}{27} \sin 4z) + \ldots \qquad (3.46)$$

The iso-μ and iso-σ curves in the second unstable region are shown in Figure 3.6, which covers the indicated part of Figure 3.2. When a and q are given, the μ and σ of the unstable solution of the form $\phi_2 = e^{\mu z} \phi(z,\sigma)$ may immediately be evaluated by using these curves.

With the characteristic number a=4, and $0<q<<1$, σ is approximately $-\frac{\pi}{4}$, as seen from Figure 3.6, and the characteristic exponent μ is found from equation (3.40) as

$$\mu = \frac{1}{16} q^2 \qquad \ldots\ldots \qquad (3.47)$$

The first-order approximate solution in the second unstable region is, therefore

$$\phi_2 = \phi_{20}\, e^{\frac{1}{16} q^2 z} \sin(2z + \frac{\pi}{4}) = \phi_{20}\, e^{\frac{1}{16} q^2 z} \cos(2z - \frac{\pi}{4}) \qquad (3.48)$$

It should be noted that, for a given $q(<1)$, μ is much smaller in the second unstable region than in the first. This is clear from Figures 3.5 and 3.6, and also from a comparison of the characteristic exponents of equations (3.36) and (3.48).

In general, the stability chart of Figure 3.2 indicates that parametric oscillations may be obtained at any multiple of the input frequency when a is made equal to 4, 9, 16, ..., n^2, ... etc. (by adjusting the resonant circuit such that $\omega_o = 2\omega$, 3ω, 4ω, ..., $n\omega$, ..., respectively), and it follows that the parametric transformer may be used as a frequency multiplier by operating in different unstable regions.

Frequency multiplication by the parametric transformer can also arise due to the presence of harmonic components in the secondary reluctance variations, as mentioned in Section 2.2.3. Since the primary flux is non-sinusoidal, due to the resistance and non-linearity of the primary circuit, it may contain both even- and odd-harmonic components in its Fourier series expansion,

$$\phi_1 = \sum_{i=1}^{\infty} a_i \sin i\,\omega t \qquad \ldots\ldots \qquad (3.49)$$

There are no cosine terms in this expansion, since the time reference has been chosen to coincide with that of the primary flux.

Since the secondary reluctance is an even function of the primary flux, the trans-reluctance characteristic of Figure 2.2 may be expressed as a power series expansion in ϕ_1, as

$$R_{m2} = R_{m2min} + \sum_{j=1}^{\infty} \Gamma_j \ \phi_1^{2j} \qquad \cdots\cdots \qquad (3.50)$$

where $R_{m2min} = R_g + s_1 + r_1$ is the minimum constant value of R_{m2} for $\phi_1 = 0$, and Γ_j are constants. Now, substituting equation (3.49) into equation (3.50) gives the variation of the secondary reluctance

$$R_{m2} = R_{m2av} + \sum_{n=1}^{\infty} R_{2n} \cos 2n\,\omega t \qquad \cdots\cdots \qquad (3.51)$$

which is the Fourier series expansion of the secondary reluctance, and contains only even-order harmonics, whatever the harmonic content of the primary flux. The average value R_{m2av} is positive, but the coefficients R_2, R_4, ... may be positive or negative, depending on the form of the trans-reluctance curve and the sign of a_i in equation (3.49).

Introducing equation (3.51) into equation (3.3), the basic differential equation of the circuit leads to

$$\frac{d^2 \phi_2}{dz^2} + (\theta_o + 2 \sum_{n=1}^{\infty} \theta_n \cos 2n\, z)\phi_2 = 0 \qquad (3.52)$$

where $z = \omega t$, and

$$\theta_o = \frac{R_{m2av}}{\omega^2 C N_2^2} = \frac{\omega_o^2}{\omega^2} \qquad \cdots\cdots \qquad (3.53)$$

$$\theta_n = \frac{R_{2n}}{2\omega^2 C N_2^2} \qquad n = 1,2,3,\ldots. \qquad \cdots\cdots \qquad (3.54)$$

Equation (3.52) is known as the Hill equation, and is a general case of the Mathieu equation. The general solution of the Hill equation is more complicated than that of the Mathieu equation, but in the next section, a brief outline is given. At this point, it is sufficient to state that the instability of the Hill equation in the nth unstable region is a function not only of θ_n but also of the other coefficients θ.

To see the effect of higher harmonics in the secondary reluctance on the instability within the second unstable region, consider only the fourth harmonic term in equation (3.51) and suppose that the secondary reluctance is given simply by

$$R_{m2} = R_{m2av} + R_4 \cos 4\omega t \qquad \ldots\ldots \qquad (3.55)$$

Substituting this into equation (3.3) gives a Mathieu equation

$$\frac{d^2 \phi_2}{dz^2} + (a + 2q' \cos 4z)\, \phi_2 = 0 \qquad \ldots\ldots \qquad (3.56)$$

with the coefficients $a = (\frac{\omega_o}{\omega})^2$, as before, and $q' = \frac{R_4}{2 R_{m2av}}$ a. With the independent variable changed to $\tau = 2z + \frac{\pi}{2}$, equation (3.56) becomes

$$\frac{d^2 \phi_2}{d\tau^2} + (A - 2Q \operatorname{Cos} 2\tau)\, \phi_2 = 0 \qquad \ldots\ldots \qquad (3.57)$$

which is the standard form of the Mathieu equation with the coefficients $A = \frac{a}{4}$ and $Q = \frac{q'}{4}$. When A = 1, equation (3.57) is unstable in the first unstable region of the (A;Q) plane (i.e. the stability chart for equation (3.57)). This corresponds to

$$\frac{1}{4} (\frac{\omega_o}{\omega})^2 = 1$$

which gives $\omega_o = 2\omega$, the same conditions as for instability of equation (3.9) in the second unstable region of the (a;q) plane. Therefore, the fourth harmonic in the secondary reluctance

variation may excite the circuit by itself when ω_o is adjusted to 2ω, implying that the instability in the second unstable region is also a function of R_4 of equation (3.51). In general, when the secondary reluctance is given by equation (3.51), the instability of the system in different unstable regions will depend on all the R terms of equation (3.51).

3.1.3 The Hill Equation

In the Mathieu equation (3.9), the primary flux was assumed purely sinusoidal, by neglecting the resistance of the primary circuit. When the resistance is neglected, the primary flux is always sinusoidal, even with a highly non-linear magnetisation characteristic. On taking the resistance into account, the primary flux is given by a Fourier series as in equation (3.49). With the secondary circuit of the parametric transformer still considered linear and non-dissipative, the harmonic components in the primary flux and the assumed form of equation (3.50) for the trans-reluctance characteristic, lead to the differential equation of the circuit in the form of the Hill equation.

$$\frac{d^2 \phi_2}{dz^2} + (\theta_o + 2 \sum_{n=1}^{\infty} \theta_n \operatorname{Cos} 2nz)\, \phi_2 = 0 \qquad (3.58)$$

The coefficients θ of this equation are given in equations (3.53) and (3.54), and it is assumed that $\sum_{n=1}^{\infty} |\theta_n|$ converges.

Whittaker's "change of parameter" method has also been applied to the Hill equation[8]. By Flouqet's theory, a particular solution of equation (3.58) is given by

$$\phi_2 = e^{\mu z} \phi(z) \qquad \ldots\ldots \qquad (3.59)$$

Following Whittaker's method, the periodic function $\phi(z)$ is assumed to be

$$\begin{aligned}\phi(z,\sigma) = \sin(z-\sigma) &+ \theta_1 f_1(z,\sigma) + \theta_2 f_2(z,\sigma) + \ldots + \\ &+ \theta_1^2 g_1(z,\sigma) + \theta_2^2 g_2(z,\sigma) + \ldots + \\ &+ \theta_1\theta_2 g_{12}(z,\sigma) + \ldots + \qquad (3.60) \\ &+ \theta_1^3 h_1(z,\sigma) + \ldots + \\ &+ \ldots\ldots\end{aligned}$$

with the characteristic exponent

$$\mu = \theta_1 \psi_1(\sigma) + \theta_2 \psi_2(\sigma) + \theta_3 \psi_3(\sigma) + \ldots +$$

$$+ \theta_1^2 \varepsilon_1(\sigma) + \theta_2^2 \varepsilon_2(\sigma) + \ldots +$$

$$+ \theta_1 \theta_2 \varepsilon_{12}(\sigma) + \ldots + \qquad (3.61)$$

$$+ \theta_1^3 x_1(\sigma) + \ldots +$$

$$+ \ldots\ldots$$

where σ is a new parameter to be determined. In the first unstable region, where the periodic function $\phi(z)$ has period 2π, the new parameter σ is determined by the expression[8]

$$\theta_o = 1 - \frac{1}{4}\theta_1^2 - \frac{1}{6}\theta_2^2 - \frac{11}{192}\theta_1^2\theta_2 - \frac{13}{192}\theta_1\theta_2\theta_3 + \frac{1}{48}\theta_1^4 + \ldots +$$

$$+ \cos 2\sigma(\theta_1 + \frac{1}{4}\theta_1\theta_2 + \frac{1}{12}\theta_2\theta_3 - \frac{1}{64}\theta_1^3 + \frac{5}{192}\theta_1^2\theta_3 + \ldots) +$$

$$+ \cos 4\sigma(\frac{1}{8}\theta_1^2 + \frac{5}{64}\theta_1^2\theta_2 + \frac{13}{576}\theta_1\theta_2\theta_3 + \ldots) +$$

$$+ \cos 6\sigma(\frac{7}{512}\theta_1^3\theta_2 - \frac{13}{4096}\theta_1^5 + \ldots) + \qquad (3.62)$$

$$+ \ldots\ldots$$

and the characteristic exponent is[8]

$$\mu = \sin 2\sigma(\frac{1}{2}\theta_1 + \frac{1}{8}\theta_1\theta_2 + \frac{1}{24}\theta_2\theta_3 - \frac{3}{128}\theta_1^3 + \ldots) +$$

$$\sin 4\sigma(\frac{1}{128}\theta_1^2\theta_2 + \frac{1}{1152}\theta_1\theta_2\theta_3 + \ldots) + \qquad (3.63)$$

$$\sin 6\sigma(\frac{5}{1024}\theta_1^3\theta_2 + \ldots) +$$

$$+ \ldots\ldots$$

The periodic function $\phi(z,\sigma)$ takes the form[8]

$$\phi(z,\sigma) = \sin(z-\sigma) + \sin(3z-\sigma)[\frac{1}{8}\theta_1 + \frac{1}{64}\theta_1^2\cos 2\sigma + \theta_1\theta_2(\frac{1}{48} - \frac{1}{32}\operatorname{Cos} 2\sigma) + \ldots] +$$

$$+ \sin(3z+\sigma)[-\frac{1}{8}\theta_2 + \ldots] + \cos(3z-\sigma)[\frac{3}{64}\theta_1^2\sin 2\sigma - \frac{1}{32}\theta_1\theta_2\sin 4\sigma + \ldots]$$

$$+ \sin(5z-\sigma)[\frac{\theta_2}{24} + \frac{\theta_1^2}{192} - \frac{\theta_1\theta_2}{288}\sin 2\sigma + \ldots] + \sin(5z+\sigma)[-\frac{\theta_3}{24} + \ldots]$$

$$+ \cos(5z-\sigma)[\frac{1}{288}\theta_1\theta_2\sin 2\sigma + \ldots] + \sin(7z-\sigma)[\frac{1}{48}\theta_3 + \frac{1}{288}\theta_1\theta_2 + \ldots]$$

$$+ \sin(7z-\sigma)[-\frac{1}{48}\theta_4 + \ldots] + \sin(9z-\sigma)[\frac{1}{80}\theta_4 + \ldots] + \ldots$$

$$\ldots\ldots\ldots\ldots \qquad (3.64)$$

As is seen from equation (3.63), $\mu=0$ for $\sigma=0$ and $\mp\frac{\pi}{2}$, corresponding to neutral solutions of the Hill equation. The boundary curves of the first unstable region are thus obtained by putting $\sigma=0$ and $\sigma=-\frac{\pi}{2}$ in equation (3.62), as in the case of the Mathieu equation.

The solutions of equation (3.58) in the different unstable regions may be given in the same way, by determining the expressions for θ_0, μ and $\phi(z,\sigma)$, although all these results are very complicated.* However, since the θ coefficients are small, the periodic function $\phi(z,\sigma)$ in the nth unstable region may be assumed, to a first approximation, to have the form

$$\phi(z,\sigma) = \sin(nz-\sigma) \qquad n = 1,2,3.. \qquad (3.65)$$

Substituting equation (3.59), with $\phi(z,\sigma)$ from equation (3.65), into equation (3.58), and equating the coefficients of sin nz and cos nz separately to zero, leads to

$$\mu = \frac{\theta_n}{2n} \sin 2\sigma \qquad ..... \qquad (3.66)$$

and

$$\theta_0 = n^2 + \theta_n \cos 2\sigma - \left(\frac{\theta_n}{2n}\right)^2 \sin^2 2\sigma \qquad (3.67)$$

respectively. Eliminating σ between equations (3.66) and (3.67) gives μ in terms of θ as

$$\mu^2 = -(\theta_0 + n^2) + (4n^2\,\theta_0 + \theta_n{}^2)^{\frac{1}{2}} \qquad (3.68)$$

---

*The expressions only for θ_0 and μ in the second and third unstable regions are given by Hayashi in reference (8).

From equations (3.66) and (3.68), μ and σ may be determined for any given θ_0 and θ_n, so that the solution $\phi_2 = e^{\mu z}(z,\sigma) = e^{\mu z}\sin(nz-\sigma)$ is completely determined. The second independent solution, obtained by replacing z by $-z$ in equation (3.59), is not of much importance, as it is stable and vanishes with time. Since the characteristic exponent μ may be imaginary or real, according as the complete solution is stable or unstable, the condition for instability is

$$\mu^2 > 0 \qquad \ldots\ldots \qquad (3.69)$$

which, by use of equation (3.68) becomes

$$|\theta_n| > |\theta_0 - n^2| \qquad \ldots\ldots \qquad (3.70)$$

Since $\mu=0$ on the boundary between the stable and unstable regions, the boundary lines of the nth unstable region are given by

$$\theta_0 = n^2 \mp \theta_n \qquad \ldots\ldots \qquad (3.71)$$

which may also be derived directly by putting $\sigma=0$ and $\sigma= -\frac{\pi}{2}$ in equation (3.67).

In a more general case, the Hill equation may take the form[8]

$$\frac{d^2\phi_2}{dz^2} + (\theta_0 + 2\sum_{n=1}^{\infty}\theta_{nc}\cos 2nz + 2\sum_{n=1}^{\infty}\theta_{ns}\sin 2nz)\phi_2 = 0 \qquad (3.72)$$

known as the extended form of the Hill equation. Proceeding in the same way as above, the characteristic exponent is obtained as

$$\mu^2 = -(\theta_0 + n^2) + (4n^2\,\theta_0 + \theta_n{}^2)^{\frac{1}{2}} \qquad (3.73)$$

where now $\theta_n{}^2 = \theta_{ns}^2 + \theta_{nc}^2$

In the derivation of the above results, the coefficients θ of equation (3.58) are assumed to be small and only a first approximation is considered. The values of μ and σ in equations (3.66) and (3.67) are, therefore, determined only by θ_0 and θ_n, and not by any other coefficients. For the first unstable region, neglecting all the terms which involve θ_2, ... , θ_n, ... (other than θ_1), and all powers of θ_1 in equations (3.62) and (3.63), gives the approximate equations (3.66) and (3.67) with n=1.

Since μ is a function of all the coefficients θ in equation (3.58), the instability in the nth unstable region depends on all the harmonic components in the secondary reluctance variation, as mentioned in the explanation of frequency multiplication in the parametric transformer.

3.1.4 The Hill-Meisner Equation[9,10], and Parametric Generation and Absorption of Energy

Equation (3.3) may be written in the general form

$$\frac{d^2 \phi_2}{dz^2} + F(z)\, \phi_2 = 0 \qquad \ldots\ldots \qquad (3.74)$$

where F(z) represents the time-varying parameter, which is a periodic function of z with period π. If F(z) follows a sinusoidal variation around an average value, equation (3.74) becomes a Mathieu equation. If the variation is not sinusoidal, F(z), may be expanded as a Fourier series, when equation (3.74) becomes a Hill equation. A particular case of the Hill equation is the so-called Hill-Meisner equation in which the function F(z) is the rectangular ripple shown in Figure 3.7. The Fourier expansion in this case is

$$F(z) = a + \frac{4}{\pi} b \left(\cos 2z - \frac{1}{3} \cos 6z + \frac{1}{5} \cos 10z + \ldots\right) \qquad (3.75)$$

With the Hill-Meisner equation, it is assumed that the variation of secondary reluctance between the maximum and the minimum values is produced discontinuously at certain instants. For this reason, it is convenient to write equation (3.74) in the form

$$\frac{d^2 \phi_2}{dz^2} + (a \mp b)\, \phi_2 = 0 \qquad \ldots\ldots \qquad (3.76)$$

which means that the two linear differential equations

$$\frac{d^2 \phi_2}{dz^2} + (a + b)\, \phi_2 = 0 \,, \qquad \frac{d^2 \phi_2}{dz^2} + (a - b)\, \phi_2 = 0$$

should be considered, alternately, during each half period of the ripple, with the understanding that the solutions must be continuous, although not necessarily analytic at the points at which the change from (a + b) to (a - b), and vice versa, occurs. At these points, $a > b$, since the reluctance modulation is around an average value. If the secondary reluctance varies between the limits $R_{m2max} = R_{m2av} + \Delta R$ and $R_{m2min} = R_{m2av} - \Delta R$, as the rectangular ripple shown in Figure 3.8, the coefficients of equation (3.76) are

$$a = \frac{R_{m2av}}{\omega^2 N_2^{\,2} C} \,, \qquad b = \frac{\Delta R}{\omega^2 N_2^{\,2} C} \qquad \ldots\ldots \qquad (3.77)$$

If a certain flux ϕ_{20} exists initially in the magnetic core, and the secondary circuit is closed, an undamped oscillation is established in this circuit, with energy oscillating between the electromagnetic form $\frac{1}{2} R_{m2min}\, \phi_{20}^{\,2}$ (since $R_{m2} = R_{m2min}$ when there is no modulation), when the capacitor is discharged and the current is a maximum, and the electrostatic form $\frac{1}{2} C\, V_0^{\,2}$, when the current is zero.

Now, assume the reluctance of the secondary winding is increased by + $2\Delta R$ at the instant the energy is entirely electromagnetic (i.e. when ϕ_2 is a maximum and $V = \frac{d\phi}{dt}$ is zero, the point A at $z = \frac{\pi}{2}$ in Figure 3.8), which requires an impulse of work to overcome the electromagnetic forces. This work is provided, as explained in the next section, by the primary flux which increases the secondary reluctance. Since the secondary circuit is assumed to be conservative, an equivalent increment ΔE of electrical energy is added to the initial energy content $E_0 = \frac{1}{2} R_{m2min} \phi_{20}^2$ of the circuit. This increment is obtained as

$$\Delta E = \phi_{20}^2 \cdot \Delta R \qquad \ldots\ldots \qquad (3.78)$$

by differentiating equation (2.24) with respect to R_m and putting $dR_m = 2\,\Delta R$. After the sudden increase in the reluctance, the energy stored in the secondary winding is

$$E_1 = E_0 + \Delta E = \frac{1}{2}\ \phi_{20}^2\ (R_{m2min} + 2\,\Delta R)$$

A quarter of a period later, at the point B in Figure 3.8, the energy is purely electrostatic, with the flux zero and a maximum voltage across the capacitor. At this instant, we can re-establish the former value of the reluctance by a reduction of $-\,2\,\Delta R$, without doing any work, since the flux at this instant is zero. At the point C, when the energy is again purely electromagnetic, the

reluctance is increased by + 2 ΔR, so that it again takes the maximum value. This adds another increment of energy, and the new energy content is

$$E_2 = E_1 + \Delta E = \frac{1}{2} \phi_{20}^2 \, (R_{m2min} + 4 \, \Delta R)$$

At the time $z = 2\pi$ (i.e. the point D of Figure 3.8), we can again reduce the reluctance to its minimum value without doing any work, since the flux is again zero. Thus, increasing the reluctance at the instants $z = \frac{\pi}{2}, \frac{3\pi}{2}, \ldots\ldots, (2n+1)\frac{\pi}{2}, \ldots$ adds energy to the system, and after N periods the total energy becomes

$$E = \frac{1}{2} \phi_{20}^2 \, (R_{m2min} + 4 N \Delta R)$$

At the instants $z=0, \pi, 2\pi, \ldots\ldots, n\pi, \ldots\ldots$, the reluctance can be decreased, without requiring any impulsive work. Therefore, by correct timing of the discontinuous changes of reluctance, the energy stored in the system is gradually increased as the result of the operation of the ripple $\mp \Delta R$.

As seen from Figure 3.8, a certain phase relationship exists between the secondary flux and the discontinuous reluctance changes; that is the reluctance is increased when the flux is a maximum so that the decrease in the reluctance occurs when the flux is zero. Maximum energy is developed parametrically when this phase relationship is satisfied.

If the relative phase between the flux and the reluctance variation is as shown in Figure 3.9, the effect becomes reversed, with the ripple withdrawing, instead of adding, energy from the oscillation. Because the reluctance decreases by $-2\Delta R$ when the flux is at its maximum, the energy increment given by equation (3.78) is negative, which means that energy is not added to but is withdrawn from the system. When the reluctance increases by $+2\Delta R$, no energy is added, since at these instants the flux is zero.

In general, with the phase difference β between the secondary flux and the reluctance variations, as shown in Figure 3.10, the amount of energy added to the system by a positive jump in the reluctance is $\phi_2'.\Delta R$, and the energy withdrawn by a negative jump is $\phi_2''.\Delta R$. It is now clear that for $0 < \beta < \frac{\pi}{4}$, the net increase in energy to the system within a half period is positive, since $\phi_2' > \phi_2''$, and, for $\frac{\pi}{4} < \beta < \frac{\pi}{2}$, the energy content of the system decreases, as the energy withdrawn by a negative jump is greater than the energy added by a positive jump. When $\beta = 0$, as in Figure 3.8, maximum energy is supplied by parametric excitation for $\phi_2'' = 0$. However, when $\beta = \frac{\pi}{2}$, as in Figure 3.9, the reluctance variation works completely as an energy absorber, instead of exciting the system. For $\beta = \frac{\pi}{4}$, the amount of energy added by a positive jump is equal to that absorbed by a negative jump. The net increase in energy is, therefore, zero, and the undamped initial oscillation continues with a fixed amplitude.

In equation (3.76), a=1, since the capacitor in the secondary circuit is tuned to resonate with R_{m2av} at the frequency ω. Thus, the two alternate differential equations are in the form

$$\frac{d^2 \phi_2}{dz^2} + \alpha_1 \phi_2 = 0, \qquad \frac{d^2 \phi_2}{dz^2} + \alpha_2 \phi_2 = 0$$

where $\alpha_1 = 1+b$, $\alpha_2 = 1-b$, replacing each other at the frequency of the ripple $\mp \Delta R$. The solutions for each of these two differential equations can be represented in the phase plane i.e. the plane ($\frac{d\phi_2}{dz}$; ϕ_2), by the families L_1 and L_2 of concentric homotetic ellipses[11] shown in Figure 3.11, since α_1 and α_2 are not equal to unity. For b=0, and $\alpha_1 = \alpha_2 = 1$, the phase trajectories of the equations form a continuous family of concentric circles. The family L_1 corresponds to R_{m2max}, and the family L_2 to R_{m2min}, since $\alpha_1 > 1$ and $\alpha_2 < 1$. The motion of the representative point P on these phase trajectories gives the form of the solution for the Hill-Meisner equation.

Starting from the initial conditions $\phi_2 = \phi_{20}$ and $\frac{d\phi_2}{dz} = 0$, corresponding to the point A in Figures 3.8 and 3.11, the representative point follows the arc AB of the ellipse belonging to the family L_1, since the reluctance is R_{m2max} during this interval. A quarter of a period later, at the point B, the reluctance is reduced to R_{m2min}, and, the representative point passes onto the elliptic trajectory belonging to the family L_2 and passing through B, and continues to move along that trajectory until the next change to R_{m2max} occurs at the point C. At this

instant, the reluctance is again increased to R_{m2max}, which transfers the representative point to the ellipse of the family L_1 passing through C up to the point D, and so on. It is thus clear that the amplitude of the oscillation increases with time, with the radius vector r increasing continuously. As r^2 represents the total energy stored in the circuit, the energy of the system steadily increases, as a result of the variation in the reluctance.

However, with the phase difference $\beta = \frac{\pi}{2}$ between the oscillation and the reluctance variation, the phase trajectory starts from the point A in Figures 3.9 and 3.12, and the representative point moves on the arc AB' of the ellipse of the family L_2, since the reluctance is R_{m2min} during this interval. At the point B', when the reluctance is increased to R_{m2max}, the representative point is transferred onto the ellipse belonging to the family L_1, from when it follows the elliptic arc B'C', and so on. In this case, the phase trajectory shown in Figure 3.12 is a convergent spiral, which means that the oscillation is rapidly damped by the reluctance variation withdrawing energy from the system.

For $\beta = \frac{\pi}{4}$, the motion of the representative point is on a closed trajectory[10], as shown in Figure 3.13, indicating that the amplitude of the oscillations will not grow with time and that the net energy increase over a period is zero.

The cases explained above, for $\beta = 0$ and $\beta = \frac{\pi}{2}$, correspond to the stable and unstable equilibrium values of α, the phase of the approximate solution for the Mathieu equation determined by

Figure 3.3. It was also shown in Section 3.1.1 that the characteristic exponent μ is a maximum, for a given q, when $\sigma = -\frac{\pi}{4}$, and it is zero when $\sigma = 0$ or $-\frac{\pi}{2}$. These results may also be obtained by approaching the Mathieu equation through the Hill-Meisner equation.

Thus, by choosing the time reference in Figure 3.8 at $= \frac{\pi}{4}$ and by replacing the rectangular ripple with the proper sinusoidal variation shown by the dotted curve, the variations of the flux and of the reluctance may be written, respectively, as

$$\phi_2 = \phi_{20} \cos(z - \frac{\pi}{4}) \qquad \ldots\ldots \qquad (3.79)$$

$$R_{m2} = R_{m2av} - \Delta R \cos 2z \qquad \ldots\ldots \qquad (3.80)$$

Equation (3.80) is in the same form as equation (2.9) which led to the Mathieu equation, and equation (3.80) is in phase with the unstable solution of the Mathieu equation. Therefore, $\beta = 0$ corresponds to $\alpha = -\frac{\pi}{4}$, or to $\sigma = -\frac{\pi}{4}$ in the case of the Mathieu equation.

By taking $z = \frac{3\pi}{4}$ as the time reference in Figure 3.9, the reluctance variation is again expressed in the form of equation (3.80), but the flux is now

$$\phi_2 = \phi_{20} \cos (z + \frac{\pi}{4}) \qquad \ldots\ldots \qquad (3.81)$$

which gives the unstable equilibrium value of $\alpha = \frac{\pi}{4}$ as determined by equation (3.19). This case clearly corresponds to the reluctance variation completely withdrawing energy from the system.

For $\beta = \frac{\pi}{4}$, the same reluctance variation is obtained, by taking the time reference at $z = \frac{\pi}{2}$, with the flux variation

$$\phi_2 = \phi_{20} \cos z \qquad \ldots\ldots \qquad (3.82)$$

which corresponds to the case of the Mathieu equation with a neutral solution, when $\sigma = -\frac{\pi}{2}$ and $\mu = 0$.

The relative positions of the flux and the sinusoidal reluctance variation for these three cases are shown in Figure 3.14 a, b, and c, respectively, which correspond to maximum energy release, zero energy release, and maximum energy absorption by the reluctance variation.

If the Mathieu equation is written in the form

$$\frac{d^2 \phi_2}{dz^2} + a\, \phi_2 = (2q \cos 2z)\, \phi_2 \qquad \ldots\ldots \qquad (3.83)$$

the right-hand side can be considered as a forcing function, although it depends on ϕ_2. Taking only the first term of equation (3.31) and neglecting the increase in amplitude within a period, the solution of equation (3.83) may be assumed as

$$\phi_2 = \phi_{20} \sin(z - \sigma) \qquad \ldots\ldots \qquad (3.84)$$

to a first approximation.

Multiplying equation (3.83) throughout by $d\phi_2 = \phi_2'.dz$ (dots denote differentiation) and integrating over a period $(0, 2\pi)$, gives the energy equation of the system

$$\int_0^{2\pi} \phi_2'' . \phi_2' \, dz + a \int_0^{2\pi} \phi_2 . \phi_2' \, dz = 2q \int_0^{2\pi} \text{Cos } 2z \, \phi_2' . \phi_2 . dz \qquad (3.85)$$

where the left-hand side represents the energy consumed within a period, and the right-hand side represents the energy supplied to the system by the forcing function in the same period. Upon introducing ϕ_2 from equation (3.84) into equation (3.85), the energy equation becomes

$$0 = 2 \, q \, \phi_{20}^2 \int_0^{2\pi} \cos 2z . \cos(z - \sigma) . \sin(z - \sigma) \, dz \qquad (3.86)$$

The left-hand side of equation (3.86) is equal to zero, since there is no first derivative term in equation (3.83) and the other terms vanish on integration because of the orthogonality properties of circular functions. This result is obvious, because the secondary circuit is assumed to be non-dissipative, and thus

consumes zero energy. The energy supplied by the forcing function on the right-hand side of equation (3.83) is not identical to zero, and the circuit is, therefore, not conservative although it is non-dissipative.

Carrying out the integration, the energy supplied within a period is found to be

$$E = - q \phi_{20}^{2} \pi \sin 2\sigma \qquad \ldots\ldots \qquad (3.87)$$

It is clear from equation (3.87) that the energy supplied by the parameter variation is a maximum for $\sigma = -\frac{\pi}{4}$, and is zero for $\sigma=0$ and $\sigma= -\frac{\pi}{2}$. These results agree with the general theory of the Mathieu equation (and also with that of the Hill equation), where the characteristic exponent μ is found as zero for $\sigma=0$ and $\sigma= -\frac{\pi}{2}$, and is a maximum, for a given q, when $\sigma= -\frac{\pi}{4}$. With $\sigma= +\frac{\pi}{4}$, the energy supplied takes a maximum negative value, which means that the energy is not supplied but is withdrawn from the system.

These three cases, corresponding to $\sigma= -\frac{\pi}{4}$, $\sigma = -\frac{\pi}{2}$, and $\sigma = \frac{\pi}{4}$, have also been obtained before in this section by energy considerations of the Hill-Meisner equation with a rectangular ripple having a phase difference from the oscillation $\beta = 0$, $\beta = \frac{\pi}{4}$, and $\beta = \frac{\pi}{2}$, respectively. These are illustrated in Figures 3.14a, b, and c.

3.1.5 Mechanism of Energy Transfer

In practice, there is always some residual flux in the magnetic core, which is sufficient to establish a small initial oscillation in the secondary circuit. When the reluctance of the secondary circuit is modulated, as given by equation (2.9), these small oscillations increase as defined by equations (3.22) and (3.36), by virtue of the instability of equation (3.4). For a closer approximation to the increasing secondary flux, additional terms may be calculated in equations (3.32) and (3.33) by putting $\sigma = -\frac{\pi}{4}$. As shown by equation (3.19) and Figure 3.3, the secondary flux eventually takes a phase of $\sigma = -\frac{\pi}{4}$, whatever the phase of the initial oscillations; the oscillations thus change in phase until the energy supplied to the system by the reluctance variations becomes a maximum (i.e. μ becomes a maximum), as explained for the case of $\beta = 0$ in the previous section.

The energy is supplied by the variations in the secondary reluctance as explained for a particular case of a rectangular ripple in Section 3.1.4, and the secondary reluctance is varied by the primary flux, and the primary flux supplies energy to the secondary circuit. In what follows, the mechanism by which energy is transferred from the primary to the secondary circuit is explained, so that the operation of the device as a transformer may be clearly understood.

As is evident from Figure 2.1, a secondary flux existing in the magnetic core will also modulate the primary reluctance,

in a similar way to that explained in Section 2.1.1. As the symmetry of the core implies, the dependence of the primary reluctance on the secondary flux is assumed to have the same form as in equation (2.1), i.e.

$$R_{m1} = R_{m1min} + \Gamma \phi_2^{\,2} \qquad \ldots\ldots \qquad (3.88)$$

where R_{m1min} and Γ are assumed to be

$$R_{m1min} = R \;\; + p_1 + r_1 \qquad \ldots\ldots \qquad (3.89)$$

$$\Gamma = 3r_3 \qquad \ldots\ldots \qquad (3.90)$$

The correctness of the forms of equations (3.88) to (3.90) is ascertained in Chapter VII where the reluctance coefficients p_1, r_1 and r_3 are also defined from the physical dimensions and the magnetic properties of the core. With these assumptions, the initial oscillation of the secondary flux, given by $\phi_2 = \phi_{20} \cos(z - \frac{\pi}{4})$, modulates the primary reluctance as

$$R_{m1} = R_{m1av} + \Delta R_1 \sin 2z \qquad \ldots\ldots \qquad (3.91)$$

where $$R_{m1av} = R_g + p_1 + r_1 + \frac{3}{2} r_3 \phi_{20}^2 \qquad \ldots\ldots \qquad (3.92)$$

and $$\Delta R_1 = \frac{3}{2} r_3 \phi_{20}^2 \qquad \ldots\ldots \qquad (3.93)$$

The primary circuit, in which the primary flux of equation (2.5) exists, thus exhibits the time-varying reluctance of equation (3.91), and it is necessary to evaluate the relation between the primary flux and the reluctance variations on the basis of Section 3.1.4. The relative positions of the primary flux and the primary reluctance variation are shown in Figure 3.15a, from which it is seen that the disposition of the waveforms corresponds to the case, shown in Figure 3.14c, when the parameter variations completely withdraw energy from the oscillation.

The initial oscillations in the secondary circuit create variations in the primary reluctance, the phase of these ensuring that maximum energy is drawn from the primary flux, and thus from the primary voltage supply, the energy being absorbed by the primary reluctance variations. As seen from Figure 3.15a, the primary reluctance decreases while the primary flux is around a maximum value, (i.e. energy is absorbed), and increases while the primary flux is around zero (i.e. no energy is added). Since the primary flux is inexorably fixed by the supply voltage, as given by equation (2.5), the primary reluctance variations increase as energy is absorbed from the supply; this, in turn, means that the initial oscillation in the secondary circuit will increase, as this creates the primary reluctance variation.

The reluctances of the primary and secondary circuits increase with the absolute value of the secondary and primary

flux, respectively. In a half-period, as the primary flux increases from zero to its maximum value, the secondary reluctance is accordingly increased, and, since the secondary flux takes a maximum value during this interval, energy is added to the secondary flux variations by the increasing secondary reluctance. At the same time, as the secondary flux decreases from its maximum value to zero, the primary reluctance is accordingly decreased, and, since the primary flux is a maximum at this interval, energy is drawn from the primary flux variation by the decreasing primary reluctance. This process continues in each half cycle, and energy is transferred from the primary to the secondary flux by the properly phased variations in the primary and secondary fluxes.

As the secondary flux builds up from the initial oscillation, the amplitude of the variation in the primary reluctance, given in equation (3.93), increases, and more energy is drawn from the supply. The amplitude of the secondary flux thus increases more rapidly, in the form $\phi_{2m} = \phi_{20}\, e^{\mu z}$, and so on.

Energy transfer from the primary to the secondary circuits of the parametric transformer is a consequence of the modulation of the primary reluctance by the secondary flux, which may be considered as a reaction from the output to the input, and the process may be considered as a kind of super-regeneration. In this way, the primary side of the parametric transformer operates as a parametric energy absorber, whose time-varying parameter

withdraws energy from the supply. Correspondingly, the secondary side operates as a parametric oscillator, oscillating as a result of the variation in its own parameter, and maintaining the energy absorption from the supply by modulation of the primary circuit parameter.

The primary and secondary flux and reluctance variations are shown in Figure 3.15, where the intervals of energy absorption from the primary flux and energy delivery to the secondary flux by the reluctance variations are indicated by the shaded areas.

If the primary circuit is assumed non-dissipative and the supply voltage is

$$e = E \cos \omega t$$

the equations describing the circuit are

$$N_1 \omega \frac{d\phi_1}{dz} = E \cos z \qquad \ldots\ldots \qquad (3.94)$$

$$F_1 = R_{m1} . \phi_1 \qquad \ldots\ldots \qquad (3.95)$$

and the primary flux is found from equation (3.94) as

$$\phi_1 = \frac{E}{N_1 \omega} \sin z = \phi_{1m} \sin z \qquad \ldots\ldots \qquad (3.96)$$

as given by equation (2.5). The power drawn from the supply by the primary circuit is

$$P = e.i_1 = e \frac{F_1}{N_1} = e. \frac{R_{m1}.\phi_1}{N_1} \qquad ..... \qquad (3.97)$$

which, on substituting the expressions for e, R_{m1} and ϕ_1, becomes

$$P = \frac{E^2}{2 N_1^2 \omega} (R_{m1av} \sin 2z + \frac{1}{2}\Delta R_1 - \frac{1}{2} \Delta R_1 \text{ Cos } 4z)$$

where $R_{m1av} = R_g + p_1 + r_1 + \frac{3}{2} r_3 \phi_{2m}^2$ and $\Delta R_1 = \frac{3}{2} r_3 \phi_{2m}^2$, respectively, the average value and the amplitude of the variations of the primary reluctance. The average power of

$$P_{av} = \frac{E^2}{4 N_1^2 \omega} \Delta R_1 \qquad ..... \qquad (3.98)$$

is proportional to the amplitude of the secondary flux (because of ΔR_1), and is not zero. There is, therefore, always a non-zero average power drawn continuously from the supply, despite both the primary and secondary circuits being assumed non-dissipative. As the amplitude of the secondary flux increases, the average power drawn from the supply increases, until a limit is set on the secondary flux amplitude by the non-linearity of the secon-

dary circuit. The active power consumed in the primary circuit is, in fact, zero when there are no parametric oscillations, since the primary circuit is assumed non-dissipative. With the growth of the parametric oscillations, the active power drawn from the voltage supply increases, and the growth in the secondary flux and voltage is accompanied therefore, by a large increase in the primary current.

3.2 Non-Linear Case

As the amplitude of the secondary flux increases, so too does the active power drawn from the supply. However, on physical grounds, this increase cannot continue indefinitely, since a limit clearly exists on the amplitude of the secondary flux. Since the secondary flux is a non-linear function of the secondary current, this limit is set by the non-linearity of the secondary magnetisation characteristic. Before the secondary flux reaches the saturation flux level ϕ_s, the secondary magnetisation characteristic is linear. This assumption is valid for the initiation and growth of the parametric oscillations in the secondary circuit, and the considerations of Sections 3.1 to 3.1.5 were based on this assumption. As the secondary flux reaches ϕ_s, the effect of saturation in the magnetic core needs to be considered, as this has a very important influence on the steady-state operation.

Neglecting hysteresis, the magnetisation characteristic of the secondary circuit may simply be expressed as

$$F_2 = R_{m2min}\,\phi_2 + \lambda\,\phi_2^{\,3} \qquad \ldots\ldots \quad (3.99)$$

where R_{m2min} is given by equation (2.2), and λ is a positive constant introducing the non-linearity and is assumed $\ll R_{m2min}$. In Chapter VII, λ is defined as

$$\lambda = s_3 + r_3 \qquad \ldots\ldots \quad (3.100)$$

in terms of the coefficients s_3 and r_3 which are directly related to physical construction of the core. With these assumptions, the secondary reluctance is now

$$R_{m2} = \frac{F_2}{\phi_2} = (R_g + s_1 + r_1) + (s_3 + r_3)\,\phi_2^{\,2} \quad (3.101)$$

a function of the secondary flux. To express, in this case, the dependence of the secondary reluctance on the primary flux is rather a complex matter, and is attempted later in Chapter VII. For simplicity, it is assumed here that only the linear part of the secondary reluctance is modulated by the primary flux, in the manner described in Section 2.1.1. The modulated secondary reluctance is thus

$$R_{m2} = (R_{m2min} + \Gamma\,\phi_1^2) + \lambda\,\phi_2^{\,2}$$

$$\ldots\ldots \quad (3.102)$$

$$= [(R_g + s_1 + r_1) + 3\,r_3\,\phi_1^2] + (s_3 + r_3)\,\phi_2^{\,2}$$

which, on substituting for ϕ_1 from equation (3.96) becomes

$$R_{m2} = R_{m2av}(1 - m \cos 2z) + \lambda \phi_2^{\,2} \qquad (3.103)$$

where R_{m2av} and m are as given by equations (2.7) and (2.8). It is seen from equation (3.103) that the part of R_{m2} that is independent of the secondary flux becomes time-varying, with the rest remaining unaffected by ϕ_1, although varying with ϕ_2 because of non-linearity. Substituting R_{m2} from equation (3.103) into the basic differential equation for the secondary circuit, equation (3.3), gives

$$\frac{d^2 \phi_2}{dz^2} + (a - 2q \cos 2z)\, \phi_2 + g\, \phi_2^{\,3} = 0 \qquad (3.104)$$

where a, q and z are as given by equations (3.5) to (3.8), and

$$g = \frac{\lambda}{\omega^2 N_2^{\,2} C} = \frac{s_3 + r_3}{\omega^2 N_2^{\,2} C} \qquad \ldots\ldots \qquad (3.105)$$

There is no first derivative term in equation (3.104), since the secondary circuit is still assumed non-dissipative, and again a=1, as normal operation with $\omega_0 = \omega$ is concerned. Equation (3.104) may be written in the form

$$\frac{d^2 \phi_2}{dz^2} + [(a + g\, \phi_2^{\,2}) - 2q \cos 2z]\, \phi_2 = 0 \qquad (3.106)$$

where the non-linearity term may be considered as detuning, since it changes the value of a. When ϕ_2 is small, the term $g\,\phi_2^{\,2}$ in equation (3.106) is insignificant, since $g \ll 1$ ($\lambda \ll R_{m2av}$ assumed). Neglecting this term, equation (3.106) becomes a Mathieu equation, which has, in the first unstable region, the first-order approximate solution given by equation (3.36). As the secondary flux increases, its amplitude approaches the saturation flux level, from whereon the non-linearity term becomes significant and the equation describing the secondary circuit is either (3.104) or (3.106). The initial solution for this equation is, therefore,

$$\phi_2 = \phi_{2m} \sin(z-\sigma) \qquad \ldots\ldots \qquad (3.107)$$

where $\phi_{2m} = \phi_{20}\, e^{\mu z}$ is the exponentially increasing amplitude of the secondary flux. Substituting this solution for ϕ_2 in the non-linearity term of equation (3.106), gives the linear equation

$$\frac{d^2\phi_2}{dz^2} + \left\{ \left[a + g\,\phi_{2m}^{\,2} \sin^2(z-\sigma) \right] - 2q \cos 2z \right\} \phi_2 = 0$$

$$\ldots\ldots \qquad (3.108)$$

or

$$\frac{d^2\phi_2}{dz^2} + \left[\left(a + \frac{1}{2} g\,\phi_{2m}^{\,2} \right) - \left(4q^2 + 2q\,g\,\phi_{2m}^{\,2} \cos 2\sigma + \frac{1}{4} g^2 \phi_{2m}^{\,4} \right)^{\frac{1}{2}} \cos(2z-\gamma) \right] \phi_2 = 0 \qquad \ldots\ldots \qquad (3.109)$$

where $$\gamma = \tan^{-1} \frac{\frac{1}{2} g \ \phi_{2m}^{2} \sin 2\sigma}{2q + \frac{1}{2} g \ \phi_{2m}^{2} \cos 2\sigma}$$

It is seen that the non-linearity can only limit the amplitude of the secondary flux, by changing σ (the phase of the parametric oscillation) to a value at which the energy supplied to the oscillation by the reluctance variation decreases to zero, as in the case of Figure 3.14b. Since there is no first derivative term in equation (3.106), the circuit is non-dissipative, and the non-linearity cannot ensure the stability of the secondary flux amplitude by increasing the losses to be equal to the amount of energy supplied to the circuit. By multiplying equation (3.109) throughout by $d\phi_2 = \phi_{2m} \cos(z-\sigma).dz$, and integrating over a period, the corresponding energy supplied to the secondary circuit is

$$E = \frac{1}{2} \pi \ \phi_{2m}^{2} \ [4 \ q^2 + 2q \ g \ \phi_{2m}^{2} \cos 2\sigma + \frac{1}{4} g^2 \ \phi_{2m}^{4}]^{\frac{1}{2}}.\sin(\gamma - 2\sigma) \qquad \text{.....} \quad (3.110)$$

For this to be zero, decreasing from the initial maximum value given by equation (3.87), where $\sigma = -\frac{\pi}{4}$ and $\phi_{20} = \phi_{2m}$ now, the argument $\gamma - 2\sigma$ must tend to $\mp \pi$, giving

$$\sigma = \frac{1}{2} \tan^{-1} \frac{\sin 2\sigma}{\frac{4q}{g \ \phi_{2m}^{2}} + \cos 2\sigma} \mp \frac{\pi}{2} \qquad (3.111)$$

The value of σ found from equation (3.111) gives the phase of the secondary flux when no energy is added by the reluctance variation. The required solution is clearly $\sigma = \mp \frac{\pi}{2}$, and there is no increase in the amplitude of the secondary flux which continues with the constant amplitude determined when σ takes one of these values.

The stable solution of equation (3.106), with $\sigma = -\frac{\pi}{2}$, in equation (3.107), is

$$\phi_2 = -\phi_{2m} \cos z \qquad \ldots\ldots \qquad (3.112)$$

where ϕ_{2m} is now the final value of the amplitude when $\sigma = -\frac{\pi}{2}$. Substituting this solution into equation (3.106), and equating the coefficient of $\cos z$ to zero, gives the constant level of the secondary flux amplitude as

$$\phi_{2m}^{2} = \frac{4}{3g} (1 + q - a) \qquad \ldots\ldots \qquad (3.113)$$

from which it follows that the amplitude of the secondary flux is limited by virtue of the factor $\frac{1}{g}$.

When σ, being changed by the non-linearity, finally takes the value $\sigma = -\frac{\pi}{2}$, the characteristic exponent μ of equation (3.33) becomes zero, and the c coefficients of equations (3.32) all become zero. Therefore, for a closer approximation than equation (3.112), the secondary flux may be written from equation (3.31) as

$$\phi_2 = A \cos z + B \cos 3z \qquad \ldots\ldots \qquad (3.114)$$

since, in equation (3.31), $s_3 \neq 0$, although $c_3 = 0$. In Appendix I, it is shown that

$$A^2 \simeq \frac{4}{3g} \left[1+q-a+(a-1)\frac{(2q+a-1)}{3(2q-a-7)}\right] \ldots\ldots \qquad (3.115)$$

which is the dominant term in determining the amplitude of the secondary flux in equation (3.114). Equation (3.115) gives the amplitude of the fundamental frequency component in the secondary flux, which is inversely proportional to the non-linearity coefficient g, illustrating the amplitude limiting effect of the non-linearity.

Putting the value $\sigma = -\frac{\pi}{2}$ into equation (3.108) yields

$$\frac{d^2 \phi_2}{dz^2} + \left[\left(a + \frac{1}{2} g \phi_{2m}^2\right) - 2\left(q - \frac{1}{4} g \phi_{2m}^2\right)\cos 2z\right]\phi_2 = 0 \qquad \ldots\ldots \qquad (3.116)$$

which is a Mathieu equation with the parametric point of

$$A = a + \frac{1}{2} g \phi_{2m}^2 \; ; \qquad Q = q - \frac{1}{4} g \phi_{2m}^2 \; .$$

Before the secondary flux reaches the non-linear part of the secondary magnetisation characteristic, equation (3.116) (neglecting the non-linearity term $g \phi_{2m}^2$) provides the original

Mathieu equation of the secondary circuit, with the parametric point a=1, q>0, shown as P in Figure 3.16. As the secondary flux approaches the saturation flux level, the coefficient a is increased by $\frac{1}{2}$ g ϕ_{2m}^2, and q is decreased by $\frac{1}{4}$ g ϕ_{2m}^2, and the parametric point moves along the PP' line in Figure 3.16. Therefore, it seems probable that the parametric point of equation (3.116) lies on the curve a_{c1} in the figure. If q<<2, the curve a_{c1} may be expressed as

$$a = 1+q \qquad \ldots\ldots \qquad (3.117)$$

when higher powers of q than the first in equation (3.26) are neglected. If the parametric point of equation (3.116) satisfies equation (3.117), it lies on the curve a_{c1}. Putting A, Q values in equation (3.117) gives

$$a = 1+q - \frac{3}{4} g \ \phi_{2m}^2 \qquad \ldots\ldots \qquad (3.118)$$

As already seen, stabilization occurs when the amplitude of the secondary flux takes the value given by equation (3.113). Substituting this value of ϕ_{2m} into equation (3.118) shows that equation (3.117) is satisfied. As the amplitude of the secondary flux increases, the parametric point of equation (3.114) moves along the line PP' in Figure 3.16, until it finally reaches the point P' on the curve a_{c1} when the secondary flux amplitude has the stable value ϕ_{2m} of equation (3.113). Once the parametric point reaches this point, the transient operation of the

parametric transformer is completed and it operates in the steady state. Since the distance between the points P and P' is proportional to ϕ_{2m}, this is a measure of how far into saturation the secondary circuit is driven during steady state operation.

The movement of the parametric point from P to P' indicates what happens to the parametric oscillations during the transient state. Initially, the oscillation starts from the amplitude of the residual flux, whatever the phase may be. As the amplitude of the initial oscillation increases, the phase changes so that maximum energy is supplied to the oscillation, and it takes the value $\alpha = -\frac{\pi}{4}$ or $\frac{3\pi}{4}$, as determined by equation (3.19). The parametric point P corresponds to this case ($\alpha = -\frac{\pi}{4}$), with a=1 and q(>0) determined by the primary flux. The parametric point stays at P during the stage of maximum energy supply to the secondary flux by the secondary reluctance variation, until the secondary flux grows sufficiently for saturation to become effective. As soon as the secondary flux reaches the non-linear region of the secondary magnetisation characteristic, the parametric point moves to the right along the line PP' in Figure 3.16. This is accompanied by a change in phase of the secondary flux, and, correspondingly, the energy supplied to the secondary flux is reduced, and the rate of increase of the secondary flux amplitude diminishes.

This is easily seen by reference to the iso-μ and iso-σ curves in Figure 3.5. As the parametric point moves along the line PP', it intercepts these curves, so that σ changes from $-\frac{\pi}{4}$ to $-\frac{\pi}{2}$, while the characteristic exponent μ decreases from its initial (maximum) value to zero on the curve a_{c1}. The increase in the secondary flux amplitude continues, but at a diminishing rate, until the parametric point reaches P' on the curve a_{c1}, where $\sigma = -\frac{\pi}{2}$ and $\mu = 0$. At this point, the secondary flux becomes

$$\phi_2 = - \phi_{2m} \cos z$$

with the stable amplitude ϕ_{2m} given by equation (3.113). The changes in μ, σ and ϕ_{2m} with time are shown in Figure 3.17, where the arbitrary initial phase of the secondary flux is taken as $\sigma = -\frac{\pi}{4}$.

The energy drawn from the supply is determined as follows: on writing the secondary flux in equation (3.88) as $\phi_2 = \phi_{2m} \sin(z-\sigma)$, the primary reluctance is obtained as

$$R_{m1} = R_{m1av} - \Delta R_1 \cos 2(z-\sigma) \qquad \ldots\ldots \qquad (3.119)$$

which gives equation (3.91) for $\sigma = -\frac{\pi}{4}$. Substituting R_{m1} in equation (3.97) gives the power drawn from the supply by the primary circuit as

$$P = \frac{E^2}{2\,N_1^{\,2}\,\omega}\left[\,R_{m1av}\sin 2z - \frac{\Delta R_1}{2}\sin 2(2z-\sigma) - \frac{\Delta R_1}{2}\sin 2\sigma\,\right] \qquad \ldots\ldots \quad (3.120)$$

The average power

$$P_{av} = -\frac{E^2}{4\,N_1^{\,2}\,\omega}\,\Delta R_1 \sin 2\sigma \qquad \ldots\ldots \quad (3.121)$$

decreases from the maximum value, given by equation (3.98), at $\sigma = -\frac{\pi}{4}$ to zero at $\sigma = -\frac{\pi}{2}$. When the secondary flux takes the form of equation (3.112), no energy is added to increase its amplitude (since μ=0), and no energy is drawn from the supply, since the active power of equation (3.121) is zero.

The positions of the primary and secondary fluxes, in this case relative to their reluctance variations, are superimposed in Figure 3.18a and b, which both correspond to Figure 3.14b, with zero energy release or absorption.

The reluctances of the primary and secondary magnetic circuits of the parametric transformer are determined by the reluctance of the common magnetic region of the core, which is a function of the sum of the primary and secondary fluxes. In a simple form, the magnetisation characteristic of the common magnetic region is as shown in Figure 3.19. In Figure 3.20, the saturation flux level ϕ_s is represented by a circle of radius ϕ_s (since $|\phi_1 + \phi_2| \leqslant \phi_s$), and the primary flux and the

small initial oscillation of the secondary flux (of amplitude ϕ_{20} and arbitrary phase α) are shown by phasors. As the amplitude of the initial oscillation increases its phase immediately assumes the value $\alpha = \sigma = -\frac{\pi}{4}$, and the increase in the amplitude of the secondary flux continues exponentially with this phase, until the amplitude of the total flux reaches ϕ_s (the circle at the point C'). The amplitude of the total flux in the common region cannot increase beyond ϕ_s, despite maximum energy being supplied to the secondary flux. To allow a further increase in the secondary flux, requires a change in the phase so that the end-point of the total flux phasor moves on the circle, giving $|\vec{\phi}_1 + \vec{\phi}_2| = \phi_s$ at all time. The secondary and primary reluctance variations are also shown as phasors, although it must be noted that these have an angular frequency of 2ω and not ω. The secondary reluctance R_{m2} determined by the primary flux is of fixed phase, but R_{m1} changes in phase at a rate twice the change in the phase of the secondary flux. As the secondary flux increases along the line BC of Figure 3.20, maximum energy is supplied by the secondary reluctance variation, because the phase difference between ϕ_2 and R_{m2} corresponds to that in Figure 3.14a. At the same time, the phase difference between ϕ_1 and R_{m1}, determined by ϕ_2, is such that, corresponding to Figure 3.14c, maximum energy is withdrawn by R_{m1} from ϕ_1. As the secondary flux phasor moves on the curve CD, the phase difference between ϕ_2 and R_{m2} changes, and the energy supplied to ϕ_2 decreases and becomes zero when ϕ_2 reaches the point D. During this interval, the phase difference between ϕ_1 and R_{m1} also changes, as R_{m1} changes in phase in accordance with

ϕ_2, and the energy drawn from ϕ_1 from R_{m1} decreases and becomes zero when R_{m1} takes its final position on the vertical axis. At this instant, the phase differences between ϕ_1 and R_{m1}, and also ϕ_2 and R_{m2} both correspond to the case of Figure 3.14b, where no energy is released or absorbed by the reluctance variations.

Transient operation of the parametric transformer thus starts from the initial oscillation, and continues with the secondary flux phasor moving on the path ABCD, and finishes when the secondary flux phasor is OD in Figure 3.20. During steady state operation, the secondary flux is in quadrature with the primary flux, and has an amplitude determined by the saturation flux level in the common magnetic region and by the primary flux, as is also given by equation (3.113). The secondary flux phasor cannot pass to the left of the vertical axis in Figure 3.20 at any time and has to remain on that axis where $\sigma = -\frac{\pi}{2}$. Otherwise, since the phase of phasor R_{m2} is inexorably fixed by ϕ_1, the phase relationship between ϕ_2 and R_{m2} becomes such that the secondary reluctance variations withdraw energy from the secondary flux oscillations, and this would, in effect, force the secondary flux phasor back onto the vertical axis in Figure 3.20, which is a stable equilibrium state.

3.3 The Effect of Damping

In the preceding sections, the secondary circuit was assumed non-dissipative, and the conditions for parametric excitation were found to be a=1 and q>0, in normal parametric transformer operation. When damping exists, i.e. the secondary circuit is dissipative, the variation of the secondary reluctance needs to be sufficiently large in amplitude to excite the circuit, that is q will have to be greater than a certain value, giving a threshold condition. In an actual device, even when there is no load connected across the output, damping always exists in the secondary circuit, due to the resistance of the secondary winding and to other losses present. In the case of parametric circuits, where capacitance or elastance variations are used to excite the circuit, the damping effect is simple and autonomous (i.e. the independent variable z does not appear explicitly in the damping term). However, if the time-varying parameter is an inductance or reluctance, as in the case of the parametric transformer, the damping is non-autonomous and more complicated, since the current in the circuit is also a function of the parameter variation. The effect of damping is represented by a series resistance, and the dissipation in this resistance will be non-autonomous, since it is determined by the current (or the mmf) in the secondary circuit.

3.3.1 Linear Case

If a series resistance is inserted in the circuit of Figure 3.1, the voltage equation (3.1) becomes

$$N_2 \frac{d\phi_2}{dt} + R_2 i_2 + \frac{1}{C}\int i_2 \, dt = 0 \qquad \ldots\ldots \qquad (3.122)$$

where the current i_2 is given by equation (3.2), since, during initiation of the parametric oscillations, the secondary circuit may be assumed linear. Substituting equation (3.2) into equation (3.122), and differentiating gives

$$\frac{d^2\phi_2}{dt^2} + \frac{R_2}{N_2^{\,2}} \frac{d}{dt}(R_{m2}\,\phi_2) + \frac{1}{C\,N_2^{\,2}}(R_{m2}\,\phi_2) = 0 \qquad (3.123)$$

which becomes

$$\frac{d^2\phi_2}{dt^2} + \frac{R_2}{N_2^{\,2}} R_{m2} \frac{d\phi_2}{dt} + \left(\frac{1}{C\,N_2^{\,2}} R_{m2} + \frac{R_2}{N_2^{\,2}} \frac{d R_{m2}}{dt}\right)\phi_2 = 0$$

$$\ldots\ldots \qquad (3.124)$$

for a linear R_{m2} independent of ϕ_2.

The coefficient in the first derivative term in equation (3.124) is time-varying, because of R_{m2}, and the damping is, therefore, non-autonomous. Moreover, another term proportional to ϕ_2 appears, which must be considered since it changes the amplitude and phase of the variation in the coefficient of ϕ_2. On introducing R_{m2} from equation (2.9) into equation (3.124), the equation describing the dissipative secondary circuit is obtained as

$$\frac{d^2 \phi_2}{dz^2} + 2k\,(1 - m \cos 2z)\,\frac{d\,\phi_2}{dz} + (a - 2q \cos 2z + 4\,k\,m \sin 2z)\,\phi_2 = 0 \qquad \ldots\ldots \quad (3.125)$$

where m is the modulation index of equation (2.8), and

$$k = \frac{R_2}{2\,\omega\,N_2^{\,2}}\,R_{m2av} \qquad \ldots\ldots \quad (3.126)$$

and z, a and q are as given by equations (3.5) to (3.8).

The first derivative term in equation (3.125) may be removed by using the transformation of the dependent variable

$$\psi_2 = \phi_2 \exp\left[\int k(1 - m \cos 2z)dz\right] \qquad (3.127)$$

which, when applied to equation (3.125), gives

$$\frac{d^2 \psi_2}{dz^2} + (\theta_0 + \theta_{1c} \cos 2z + \phi_{1s} \sin 2z + \theta_{2c} \cos 4z)\psi_2 = 0 \qquad \ldots\ldots \quad (3.128)$$

where

$$\theta_0 = a - k^2\left(1 + \frac{m^2}{2}\right)$$

$$\theta_{1c} = -2(q - m\,k^2)$$

$$\theta_{1s} = 2\,km \qquad \ldots\ldots \quad (3.129)$$

$$\theta_{2c} = -\frac{k^2\,m^2}{2}$$

Equation (3.128) is an extended form of Hill's equation, having the form in equation (3.72), and has a solution

$$\psi_2 = e^{\mu' z} \cdot \phi(z,\sigma) \qquad \ldots\ldots \qquad (3.130)$$

in the form of equation (3.59). Once this solution is obtained, the solution of the basic equation, equation (3.125), is found by using the inverse transformation

$$\phi_2 = \psi_2 \exp\left[-\int k(1 - m\cos 2z)dz\right] \qquad (3.131)$$

The characteristic exponent of the solution of equation (3.125) is then

$$\mu = \mu' - k + \frac{m}{2}\sin 2z \qquad \ldots\ldots \qquad (3.132)$$

The sinusoidal term in the characteristic exponent does not account for any increase in the amplitude of oscillations, since its average value is zero. The instability condition for equation (3.125) is, therefore

$$\mu = \mu' - k > 0 \qquad \ldots\ldots \qquad (3.133)$$

To obtain the instability condition, μ' must be calculated in terms of the coefficients θ in equations (3.129), which depend on k and m, both of small magnitude. The modulation

index m(<1), given by equation (2.8) is small, since modulation around an average value is concerned. By putting $L_{2av} = \frac{N_2^2}{R_{m2av}}$, k is obtained as

$$k = \frac{1}{2Q} \qquad \ldots\ldots \qquad (3.134)$$

where

$$Q = \frac{L_{2av}.\omega}{R_2} \qquad \ldots\ldots \qquad (3.135)$$

is the quality factor of the secondary circuit. In an actual device, Q is of the order of 50, and k is, therefore, small. In the first instance, neglecting terms of the order of magnitude of k.m, or less, when compared with the other terms in equations (3.129), equation (3.128) reduces to

$$\frac{d^2 \psi_2}{dz^2} + (a - 2q \cos 2z)\, \psi_2 = 0 \qquad \ldots\ldots \qquad (3.136)$$

which has the approximate solution

$$\psi_2 = e^{\frac{1}{2}qz} \cos (2 - \frac{\pi}{4}) \quad \text{with} \quad \mu' = \tfrac{1}{2}\, q.$$

The condition for the instability of equation (3.125) is, therefore

$$\mu = \tfrac{1}{2}\, q - k > 0 \qquad \ldots\ldots \qquad (3.137)$$

which, on substituting for k from equation (3.134) becomes

$$q > \frac{1}{Q} \qquad \ldots\ldots \qquad (3.138)$$

For the given value of a=1, $q = \frac{m}{2}$ by equation (3.8), and this threshold condition gives

$$m > \frac{2}{Q} \qquad \ldots\ldots \qquad (3.139)$$

which means that the amplitude of the secondary reluctance variation is required to reach a certain value before the parametric excitation starts and that the higher the quality factor of the secondary circuit, the easier it is to start parametric oscillations.

Equation (3.136) has the same stability chart as shown in Figure 3.2. However, in the light of equation (3.133) and, neglecting terms of order k.m in equation (3.125), the stability chart for equation (3.125) is obtained from the stability chart for equation (3.136) as shown in Figure 3.21, where the boundary curves are now the iso-μ' curves on which $\mu'=k$. The lines also drawn in Figure 3.21 represent the relationship $q = \frac{m}{2}.a$ for different values of m. With the given value of a=1, the parametric point moves upwards on the dotted line AA', as the modulation index increases. The condition for parametric excitation is determined with the value of m when the parametric point is on the boundary curve. The slope of the line OM corresponding

to this situation is $\frac{\overline{AP}}{\overline{OA}} = \overline{AP}$ (see Figure 3.21). As can be seen from Figure 3.5, the minimum point of the boundary curve is, approximately, on the AA' line, at the level q = 2k. Therefore, $\overline{AP}$ = 2k, and the slope of the line OM is $\frac{m}{2}$ = 2k. The condition for parametric excitation is thus obtained as m > 4k, which gives the same condition as (3.139) when k is substituted from equation (3.134). If R_2 is increased, k increases proportionally, and the unstable region in Figure 3.21 moves upwards, as it is determined by the iso-μ' curve of μ'=k, and the slope of the q = $\frac{m}{2}$ a line necessary for the parametric point to be on the boundary curve, will be greater.

By putting the expressions for q and k into the condition of (3.137), the value of the primary flux amplitude to initiate parametric oscillations in the secondary circuit (i.e. to *switch-on* the parametric transformer) is found as

$$\phi'_{1m} > \left[\frac{4\, R_{m2min}\, R_2}{3r_3\, (\frac{1}{\omega C} - 2\, R_2)} \right]^{\frac{1}{2}} \qquad \ldots\ldots \qquad (3.140)$$

which gives the minimum primary voltage (the *switch-on* voltage) as

$$V'_1 = \frac{\omega\, N_1}{\sqrt{2}} \left[\frac{4\, R_{m2min}\, R_2}{3r_3\, (\frac{1}{\omega C} - 2\, R_2)} \right]^{\frac{1}{2}} \text{ (volts rms)}$$

$$\ldots\ldots \qquad (3.141)$$

Noting that $r_3 \ll R_{m2min}$, V_1' clearly has a considerable value, which explains the under-voltage protection feature of the parametric transformer.

A better approximation than equation (3.141) for V_1' may be obtained by calculating μ' from equation (3.73), and substituting in the instability condition of equation (3.133). With a=1

$$\mu'^2 = -[2-k^2(1 + \frac{m^2}{2})]+2[1 + k^2(\frac{1}{2} m^2-1)+(q - mk^2)^2]^{\frac{1}{2}}$$

..... (3.142)

and the instability condition $\mu'^2 > k^2$ gives

$$(\frac{k^2 m^2}{2} - 2) + 2 [1 + k^2(\frac{1}{2} m^2 - 1) + (q - mk^2)^2]^{\frac{1}{2}} > 0$$

..... (3.143)

which, upon substituting for k, m and q, finally becomes

$$\frac{9}{32} (\frac{R_2 r_3}{\omega N_2^2})^2 \phi_{1m}^4 -2+2 \{1 + \frac{9}{32} (\frac{R_2 r_3}{\omega N_2^2})^2 \phi_{1m}^4 - (\frac{R_2}{2 \omega N_2^2})^2$$

$$(R_{m2min} + \frac{3}{2} r_3 \phi_{1m}^2)^2 + [\frac{3r_3}{4 \omega^2 N_2^2 C} \phi_{1m}^2 - \frac{3}{8} (\frac{R_2}{\omega N_2^2})^2 r_3 \phi_{1m}^2$$

$$(R_{m2min} + \frac{3}{2} r_3 \phi_1^2)]^2\}^{\frac{1}{2}} \geqslant 0 \qquad \text{.....} \qquad (3.144)$$

In equation (3.144), ω, N_2, C, R_{m2min} (= $R_g + s_1 + r_1$) and r_3 are all constants; s_1, r_1 and r_3, are defined in Chapter VII, as earlier mentioned in Section 2.1.1. To find the amplitude of the primary flux which will initiate parametric oscillations, equation (3.144) is solved for a given R_2. Once this value of ϕ'_{1m} is found, the *'switch-on'* voltage of the parametric transformer is easily calculated from

$$V'_1 = \frac{\omega N_1}{\sqrt{2}} \phi'_{1m} \qquad \text{(volts rms)} \qquad (3.145)$$

If the primary voltage exceeds V'_1, the instability condition (3.133) is satisfied, the characteristic exponent of equation (3.125) becomes positive and the amplitude of oscillations increases exponentially.

The approximate solution for equation (3.125) is

$$\phi_2 = \phi_{2m} \sin(z-\sigma) \qquad \ldots\ldots \qquad (3.146)$$

where $\phi_{2m} = \phi_{20}\, e^{(\mu'-k)z}$. By multiplying equation (3.125) throughout by $d\phi_2 = \phi_{2m} \cos(z-\sigma)dz$, and integrating over a period (0, 2π), the energy equation of the system is found as

$$2\, k\pi\, \phi_{2m}^{\,2} = -q\, \phi_{2m}^{\,2}\, \pi \sin 2\sigma \qquad \ldots\ldots \qquad (3.147)$$

The left hand side of equation (3.147) gives the energy consumed by R_2 within a period, which is independent of σ. The right hand side gives the energy supplied by the reluctance variation, which is a maximum for $\sigma = -\frac{\pi}{4}$, as before. As the oscillation builds up, the energy dissipation in R_2 increases; however the energy supplied to the system also increases, and σ rapidly changes from its initial value to $\sigma = -\frac{\pi}{4}$. These changes continue steadily until σ begins to change from $\sigma = -\frac{\pi}{4}$ to $-\frac{\pi}{2}$ by virtue of the non-linearity.

3.3.2 Non-Linear Case

When the amplitude of the secondary flux approaches the knee of the secondary magnetisation curve, the non-linearity becomes effective, and the secondary reluctance is given by equation (3.101). On introducing the secondary reluctance from equation (3.103) into equation (3.123), the differential equation of the non-linear, dissipative secondary circuit is obtained as

$$\frac{d^2 \phi_2}{dz^2} + [2k(1-m \cos 2z) + d\,\phi_2^{\,2}]\,\frac{d\,\phi_2}{dz} + (a-2q \cos 2z + 4\,km \sin 2z)\phi_2$$

$$+ g\,\phi_2^{\,3} = 0 \qquad \ldots\ldots \qquad (3.148)$$

where $$d = \frac{3\,R_2\,\lambda}{\omega\,N_2^{\,2}} = \frac{3\,R_2}{\omega\,N_2^{\,2}}\,(s_3 + r_3) \qquad \ldots\ldots \qquad (3.149)$$

and k, g are given by equations (3.126) and (3.105) respectively. The damping term is now both time-varying and non-linear, and it cannot be removed by any transformation, since equation (3.148) is non-linear.

Equation (3.148) may be written in the alternative form

$$\frac{d^2\,\phi_2}{dz^2} + [2k(1-m\cos 2z) + d\,\phi_2^{\,2}]\,\frac{d\,\phi_2}{dz} + [(a+g\,\phi_2^{\,2}) - 2q\cos 2z + 4\,km\sin 2z]\phi_2 = 0 \qquad \ldots\ldots \qquad (3.150)$$

where the non-linearity may be considered as an increase in the damping term, and also as a detuning, since it changes the value of a. When $R_2 = 0$, equation (3.150) gives equation (3.106), and when d and g = 0, it becomes the same as equation (3.125). As the non-linearity becomes effective after the secondary flux has reached a certain amplitude, the solution for equation (3.150) is, initially, as given by equation (3.146). Substituting this initial solution for ϕ_2 in the coefficients of equation (3.150) gives

$$\frac{d^2\phi_2}{dz^2} + [2(k+h)-2(km+h\cos 2\sigma)\cos 2z-2h\sin 2\sigma\sin 2z]\frac{d\phi_2}{dz} +$$

$$+[(a+\frac{1}{2}g\phi_{2m}^2)-(2q+\frac{1}{2}g\phi_{2m}^2\cos 2\sigma)\cos 2z+(4km-\frac{1}{2}g\phi_{2m}^2\sin 2\sigma)\sin 2z]\phi_2 = 0$$

..... (3.151)

where $h = \frac{d}{2}\phi_{2m}^2$

By multiplying equation (3.151) throughout by $d\phi_2 = \phi_{2m}\cos(z-\sigma)dz$, and integrating over a period, the energy equation is obtained as

$$\phi_{2m}^2.\pi(2k+h+km\cos 2\sigma + q\sin 2\sigma) = 0 \quad ..... \quad (3.152)$$

When equation (3.152) is satisfied, the parametric transformer completes the transition to the steady state, with the phase of the parametric oscillations being determined by the equation. For $R_2 = 0$, equation (3.152) gives

$$q\sin 2\sigma = 0 \quad ..... \quad (3.153)$$

from where σ is found as $\mp \frac{\pi}{2}$ * as obtained by equation (3.111). When $R_2 \neq 0$, σ is less than $\frac{\pi}{2}$, to ensure that energy is still supplied by the reluctance variation to provide the energy dissipated in the secondary circuit resistance. Writing equation (3.152) as

$$\phi_{2m}^{2}.\pi \left(2k + \frac{d}{2}\phi_{2m}^{2}\right) = -(k\,m \cos 2\sigma + q \sin 2\sigma)\phi_{2m}^{2}.\pi \qquad \ldots\ldots \quad (3.154)$$

the left hand side represents the energy dissipated in R_2, which is independent of σ, but is a function of both ϕ_1 and ϕ_2. The right hand side gives the terms responsible for energy supply to the parametric oscillation, where the additional term $k\,m \cos 2\sigma$, which arises due to the non-autonomous damping, can be considered either as an extra effect or as a reaction from the primary to the secondary circuit of the parametric transformer.

The phase of the secondary flux during the steady state is calculated from equation (3.152), as

---

* σ=0 is also a possible solution of equation (3.153), but does not apply here. Since the non-linearity coefficient g is positive, the value of a is increased (by $\frac{1}{2}.g\,\phi_{2m}^{2}$), and the parametric point approaches the curve a_{c_1} in Figure 3.16, where $\sigma = -\frac{\pi}{2}$. If g was a negative constant, the value of a would be decreased, and the parametric point would move towards the curve a_{s_1} in the Figure, where σ=0.

$$\sigma = \frac{1}{2}\cos^{-1}\left(-\frac{2\,k+h}{\sqrt{k^2\,m^2+q^2}}\right)+\frac{1}{2}\tan^{-1}\left(\frac{q}{km}\right) \qquad (3.155)$$

Since both k and m are small, $q \gg km$, and if it is assumed that $\gg 2k+h$ (which is practically true since $R_2 \ll$), σ is approximately equal to $-\frac{\pi}{2}$, differing by only a very small amount since $\frac{2\,k+h}{\sqrt{k^2\,m^2+q^2}} \ll 1$.

The initial solution of equation (3.150), given by equation (3.146), may be written as

$$\phi_2 = A\cos z + B\sin z \qquad \ldots\ldots \qquad (3.156)$$

where $A = -\phi_{2m}\sin\sigma$ and $B = \phi_{2m}\cos\sigma$. To find the final amplitude of the secondary flux, ϕ_2 from equation (3.156) is substituted into equation (3.150), and when the coefficients of $\cos z$ and $\sin z$ are equated to zero

$$A\left[-1+a-q+\frac{3}{4}g\,\phi_{2m}^{\,2}\right] + B\left[2\,k+km+\frac{d}{4}\,\phi_{2m}^{\,2}\right] = 0 \qquad (3.157)$$

and $$A\left[-2k+km-\frac{d}{4}\,\phi_{2m}^{\,2}\right] + B\left[-1+a+q+\frac{3}{4}g\,\phi_{2m}^{\,2}\right] = 0 \qquad (3.158)$$

with $\phi_{2m}^{\,2} = A^2 + B^2$. For A and B to be non-zero, we must have,

from the determinant of the coefficients in the system of equations (3.157) and (3.158)

$$[-1+a+\frac{3}{4}\, g\, \phi_{2m}^{\;2}\,]^2 - q^2 - [k^2\, m^2 - (2k+\frac{d}{4}\, \phi_{2m}^{\;2})^2] = 0 \qquad (3.159)$$

or

$$\phi_{2m}^{\;4}\,(\frac{9\, g^2 + d^2}{16}) + \phi_{2m}^{\;2}\,[\frac{3}{2}\, g(a-1)+kd] - q^2 + 4k^2 - k^2\, m^2 + (a-1)^2 = 0$$

$$\ldots\ldots \qquad (3.160)$$

Solving equation (3.160) for ϕ_{2m}, the square of the ultimate amplitude of the secondary flux is

$$\phi_{2m}^{\;2} = \frac{8}{9\, g^2 + d^2}\left\{ \frac{3}{2}\, g(1-a) - kd + \left\{ [\, \frac{3}{2}\, g(a-1)+kd]^2 - \frac{9\, g^2 + d^2}{4}\, [4\, k^2 - k^2 m^2 + (a-1)^2 - q^2] \right\}^{\frac{1}{2}} \right\}$$

$$\ldots\ldots \qquad (3.161)$$

From equation (3.158), it follows that

$$\frac{A}{B} = \frac{a-1+q+\frac{3}{4}\, g\, \phi_{2m}^{\;2}}{2\, k - km + \frac{d}{4}\, \phi_{2m}^{\;2}} \qquad \ldots\ldots \qquad (3.162)$$

and since $\frac{A}{B} = -\tan\sigma$, σ follows from equation (3.162) as

$$\sigma = \tan^{-1}\left(\frac{a-1+q+\frac{3}{4}\,g\,\phi_{2m}^{2}}{km-2k-\frac{d}{4}\,\phi_{2m}^{2}}\right) \qquad \ldots\ldots \quad (3.163)$$

During steady-state operation of the parametric transformer, the amplitude and phase of the secondary flux are given by equations (3.161) and (3.163), respectively. For a higher accuracy than this first-order solution, higher frequency terms must be included in equation (3.156), when, by using the harmonic balance method, higher-order correction terms may be computed for the secondary flux. However, when $R_2 = 0$, k and d become zero, and equation (3.161) gives equation (3.113), while equation (3.163) gives σ as exactly $\mp\frac{\pi}{2}$. In practice, with no load connected to the output of the parametric transformer, R_2 consists only of the resistance of the secondary winding, and is very small. Therefore, at no load, the ultimate amplitude of the secondary flux is approximately given by equation (3.113), and the phase of the secondary flux is $\sigma = \mp\frac{\pi}{2}$.

3.4 The Effect of Detuning

On initiation of parametric oscillations in the non-dissipative secondary circuit, the system is described by equation (3.9), and a necessary condition is that the secondary

resonant circuit is tuned to the input frequency so that a=1. Instability then occurs in the first unstable region of the stability chart for the Mathieu equation. When a has the different values of 4, 9, 16 .... etc. the parametric transformer operates as a frequency multiplier in different unstable regions of the chart. The coefficient a is a measure of the tuning (or detuning).

To make a equal to 1, the capacitor is adjusted to the value given by equation (3.16). With no voltage applied to the primary circuit, the reluctance of the secondary circuit is $R_{m2} = R_{m2min} = R_g + s_1 + r_1$ (by putting $\phi_1 = 0$ in equation (2.4), and the resonant frequency of the secondary circuit is given by

$$(\omega_0')^2 = \frac{1}{C\dfrac{N_2^2}{(R_g + s_1 + r_1)}} = \frac{1}{CL'} \quad ..... \quad (3.164)$$

where L' is the linear inductance of the secondary winding. It will be noted that ω_0' given by this equation differs from the frequency to which the secondary circuit is adjusted for a=1. When a sinusoidal primary flux exists in the core, the average value of the inductance of the secondary winding is

$$L_0 = \frac{N_2^2}{R_{m2av}} = \frac{N_2^2}{R_g + s_1 + r_1 + \frac{3}{2} r_3 \phi_{1m}^2} \quad (3.165)$$

which is smaller than L'. It is also clear from Figure 2.2b that the average value of the secondary reluctance is greater than R_{m2min}. Therefore, to satisfy the instability condition a=1, the capacitor must have a greater value than is necessary to resonate the secondary circuit with no primary flux. Normally, when $\phi_1 = 0$, the value of the capacitor for a=1, is

$$C' = \frac{R_g + s_1 + r_1}{\omega^2 N_2^2} \qquad \ldots\ldots \qquad (3.166)$$

which may be determined by measuring L' from the actual device. However, as the primary flux amplitude increases, the inductance of the secondary winding decreases, as given by equation (3.165), and to maintain a=1, the capacitor must be given the value

$$C = \frac{R_{m2av}}{\omega^2 N_2^2} = \frac{R_g + s_1 + r_1 + \frac{3}{2} r_3 \phi_{1m}^2}{\omega^2 N_2^2} \qquad (3.167)$$

for a certain amplitude of the primary flux. The importance of this will now be explained. On substituting for R_{m2av}, a and q are obtained from equations (3.7) and (3.8) as

$$a = \frac{1}{\omega^2 N_2^2 C} (R_{m2min} + \frac{3}{2} r_3 \phi_{1m}^2) \qquad \ldots\ldots \qquad (3.168)$$

and

$$q = \frac{1}{\omega^2 N_2^2 C} \frac{3}{4} r_3 \phi_{1m}^2 \qquad \ldots\ldots \qquad (3.169)$$

respectively. If the capacitor has the value C' of equation (3.166), the coefficient a becomes

$$a = 1 + \frac{1}{\omega^2 N_2^{\ 2} C'} \frac{3}{2} r_3 \phi_{1m}^2 \qquad \ldots\ldots \qquad (3.170)$$

and a=1 only when $\phi_{1m} = 0$. Eliminating ϕ_{1m} between equations (3.169) and (3.170) gives

$$a = 1 + 2q \qquad \ldots\ldots \qquad (3.171)$$

which is shown by the line AA' in Figure 3.22. The parametric point (a,q) is the point A when $\phi_{1m} = 0$, and moves along AA' as ϕ_{1m} increases. Since this line lies completely within a stable region, parametric excitation does not occur. However, if the capacitor has the value given by equation (3.167), which requires adjustment for each ϕ_{1m}, the parametric point moves along AA" in Figure 3.22, and is in the unstable region for a non-zero q (or ϕ_{1m}). For any fixed value of C, the relation between a and q is

$$a = \frac{R_{m2min}}{\omega^2 N_2^{\ 2} C} + 2q \qquad \ldots\ldots \qquad (3.172)$$

which corresponds to the family of lines in Figure 3.23a. As C increases, the lines move to the left with constant slope, since the abcissa of the point of intersection with the a-axis is $\frac{R_{m2min}}{\omega^2 N_2^2 C}$. Solving for C from equation (3.169) and substituting in equation (3.168) gives

$$a = [2 + \frac{4 R_{m2min}}{3 r_3 \phi_{1m}^2}]q \qquad \ldots\ldots \qquad (3.173)$$

For different values of ϕ_{1m}, equation (3.173) represents another family of radial lines, shown in Figure 3.23b, where the representative line of the family turns upwards starting from the line q=0 (the a-axis), as ϕ_{1m} increases from zero. When $\phi_{1m} \to \infty$, the line finally becomes a=2q, that is when the modulation index m becomes 100%. When C is fixed, the parametric point is on the corresponding line in Figure 3.23a, and when ϕ_{1m} is fixed, the parametric point is on the corresponding radial line. When both C and ϕ_{1m} are fixed, the parametric point is at the intersection of these two lines.

With this representation, it is seen from Figure 3.24 that, for a given ϕ_{1m}, parametric excitation is possible for values of C between C_1 and C_3 ($C_3 > C_1$), which means that parametric oscillations can be excited despite a large detuning in the secondary circuit. With this value of ϕ_{1m}, a=1 only when the capacitor takes the value C_2 determined in the figure. The boundary curves of the unstable region in Figure 3.24 are drawn as lines, since $a_{s1} \simeq 1-q$ and $a_{c1} \simeq 1+q$ for q<<. The coordinates of the point A are found as

$$A\left(\frac{2+\dfrac{4\,R_{m2min}}{3\,r_3\,\phi_{1m}^2}}{3+\dfrac{4\,R_{m2min}}{3\,r_3\,\phi_{1m}^2}}\;;\;\frac{1}{3+\dfrac{4\,R_{m2min}}{3\,r_3\,\phi_{1m}^2}}\right) \qquad (3.174)$$

by the intersection of the lines $a=1-q$ and $a=\left(2+\dfrac{4\,R_{m2min}}{3\,r_3\,\phi_{1m}^2}\right)q$.

Putting the coordinates of A into the line of equation (3.172), the value C_3 is

$$C_3=\frac{R_{m2min}}{\omega^2\,N_2^{\,2}}\left(1+\frac{9\,r_3\,\phi_{1m}^2}{4\,R_{m2min}}\right)=\frac{1}{\omega^2\,N_2^{\,2}}\left(R_{m2av}+\frac{3}{4}\,r_3\,\phi_{1m}^2\right)$$

..... (3.175)

Proceeding in the same way, the coordinates of point C in the figure, which is the intersection point of the lines $a=1+q$ and $a=\left(2+\dfrac{4\,R_{m2min}}{3\,r_3\,\phi_{1m}^2}\right)q$, is substituted into equation (3.172), and the value C_1 is obtained as

$$C_1=\frac{R_{m2min}}{\omega^2\,N_2^{\,2}}\left(1+\frac{3\,r_3\,\phi_{1m}^2}{4\,R_{m2min}}\right)=\frac{1}{\omega^2\,N_2^{\,2}}\left(R_{m2av}-\frac{3}{4}\,r_3\,\phi_{1m}^2\right)$$

..... (3.176)

For a specified amplitude of primary flux, the characteristic number a is equal to unity, only when the capacitance takes the value

$$C_2 = \frac{R_{m2min}}{\omega^2 N_2^{\ 2}} \left(1 + \frac{3\ r_3\ \phi_{1m}^{\ 2}}{2\ R_{m2min}}\right) = \frac{1}{\omega^2 N_2^{\ 2}} \cdot R_{m2av} \qquad \ldots\ldots \quad (3.177)$$

which is the same as that given by equation (3.167).

Therefore, if the parametric point is initially at point B in Figure 3.24, i.e. the capacitor is given the value of equation (3.177), parametric oscillations will still be excited although the capacitance in the secondary circuit is varied between the limits

$$C_2 - \Delta C < C < C_2 + \Delta C$$

where

$$\Delta C = \frac{1}{\omega^2 N_2^{\ 2}} \ \frac{3}{4} r_3\ \phi_{1m}^{\ 2} \qquad \ldots\ldots \quad (3.178)$$

It is clear from equations (3.175) to (3.177) that C must take a value greater than that given by equation (3.166), and, as ϕ_{1m} is increased, the interval in which parametric excitation is possible, becomes wider.

Since $\phi(z)$, the periodic part of the unstable solution of the Mathieu (or Hill) equation, given by equations (3.31) and (3.60), has period 2π in z in the entire first unstable region, the parametric oscillations in the secondary circuit are always at a frequency equal to the input frequency, despite the resonant frequency of the secondary circuit being changed within the band

$$\omega^2 - \Delta\omega^2 < \omega_0{}^2 < \omega^2 + \Delta\omega^2$$

where $$\Delta\omega^2 = \omega^2 \frac{\frac{3}{4} r_3 \phi_{1m}^2}{R_{m2av}} \qquad \text{.....} \qquad (3.179)$$

If damping exists in the secondary circuit, the boundary of the first unstable region is an iso-μ curve, on which $\mu' = k$ as explained by Figure 3.21. For the parametric point to enter the unstable region, the line of the family in Figure 3.23b must, at least, be tangential to the boundary curve, as shown by the line OP in Figure 3.25. For this case, the value of C is determined by the line of the family in Figure 3.23a which passes through this tangential point, the point P in Figure 3.25. If ϕ_{1m} is made greater than the value corresponding to the line OP, the parametric point, which is at the intersection of the two lines given by equations (3.172) and (3.173), is in the unstable region, and the condition for parametric excitation is satisfied. With a value of ϕ_{1m} satisfying this condition, parametric excitation is possible when the capacitor takes any value between those corresponding to the lines C'B and C"D in Figure 3.25. Since the analytical expressions for the iso-μ curves are not known, only the graphical solution of Figure 3.25 may be made to find the interval of allowable detuning and the minimum amplitude of the primary flux to start oscillations.

The lines of Figure 3.23b are exactly the same as the $q=\frac{m}{2}$ a lines in Figure 3.21. The modulation coefficient m is always <1, and for the extreme case $m \to 1$ or $\phi_{1m} \to \infty$, equations

(3.8) and (3.173) both give the line a=2q, which cannot be reached practically.

In practice, the secondary circuit capacitor is given a constant value, shown by the line CD in Figure 3.26, and the primary voltage or ϕ_{1m} is variable. As ϕ_{1m} increases from zero, the parametric point moves on the line CD, starting from the point C. As seen from the figure, ϕ_{1m} must be increased until the line of equation (3.173) intersects the line CD at point P', that is the parametric point comes onto P' on the boundary before parametric oscillations start, giving the under-voltage protection feature of the parametric transformer. If ϕ_{1m} is further increased, parametric excitation occurs so long as the parametric point is between points P' and P" . As ϕ_{1m} increases, the value of a increases, as given by equation (3.168), and the detuning changes accordingly. The exact tuning condition* is a=1 for q<<. When the parametric point is, for instance, at the point P in the figure, parametric oscillations grow exponentially in amplitude until non-linearity becomes effective, when the parametric point moves on the PP_1 line.

---

* With this, the value of a which will start parametric oscillations for a minimum value of q (or ϕ_{1m}) is meant, when the damping coefficient k (equal to μ') determines the boundary of the unstable region. As can be seen from Figure 3.5, the minimum points of iso-μ curves are exactly on the iso-σ curve of $\sigma = -\frac{\pi}{4}$; however, this curve can be taken as the line a=1 when q<<1.

Stabilization of the amplitude is accomplished when the parametric point is P_1, on the boundary curve where the energy equation (3.154) is satisfied. Thus, increasing ϕ_{1m} moves the initial position of the parametric point on the line P'P" as the steady state position of the parametric point moves on the boundary curve towards the point P" in Figure 3.26. The point P" is a critical case, as is the point P', since the parametric point leaves the unstable region if ϕ_{1m} exceeds the value corresponding to the line OP". As the steady state position of the parametric point moves towards P", the amplitude of parametric oscillations (or secondary flux) gradually decreases, since the distance between the initial and final positions of the parametric point is a measure of ϕ_{2m}. At P" the secondary flux amplitude corresponds to a point on the linear part of the secondary magnetisation characteristic, and if ϕ_{1m} exceeds the value corresponding to the line OP", the amplitude of the secondary flux falls to zero, since the parametric point leaves the unstable region and parametric oscillations immediately cease, providing the over-voltage protection inherent in the parametric transformer.

Since a and q are as given by equations (3.168) and (3.169), the parametric transformer still provides under- and over-voltage protection, even when no secondary circuit damping exists, if C is kept constant, as it is in practice. However, as mentioned earlier, the capacitor value must exceed that given by equation (3.166); for such a value of C, the extreme values of

ϕ_{1m} are illustrated by lines OP' and OP" in Figure 3.27, where the boundary curves are the same as in Figure 3.24, since the secondary circuit is assumed to be non-dissipative and q<<.

Carrying out analytical calculations to find the intersection points of the lines in Figure 3.27, the values of the primary flux amplitude that switches on and off the parametric transformer, when the secondary circuit is non-dissipative and C is fixed, are obtained as

$$\phi'_{1m} = \frac{2}{3}\left[\frac{\omega^2 N_2^{\,2} C - R_{m2min}}{r_3}\right]^{\frac{1}{2}} \qquad \ldots\ldots \qquad (3.180)$$

$$\phi''_{1m} = \frac{2}{\sqrt{3}}\left[\frac{\omega^2 N_2^{\,2} C - R_{m2min}}{r_3}\right]^{\frac{1}{2}} \qquad \ldots\ldots \qquad (3.181)$$

respectively, and the parametric transformer functions as long as ϕ_{1m} is between these values, giving the inherent under-voltage and over-voltage protection feature of the device.

Increasing ϕ_{1m} to a value more than that corresponding to the OP" line in Figure 3.26 or 3.27, drives the parametric point into the stable region between the first and second unstable regions of the stability chart. If ϕ_{1m} is then further increased so that the parametric point moves along the line CD and reaches the point P''' in Figure 3.28, there arises the possibility of

parametric excitation in the second unstable region, although the capacitor still has the value required for operation in the first unstable region. When ϕ_{1m} exceeds the value corresponding to the line OP''' in Figure 3.28, the parametric transformer operates in the second unstable region, and gives an output at twice the input frequency. Normally, for frequency-doubler operation of the parametric transformer, C is given a value corresponding to the C'D' line in Figure 3.28, and the values of ϕ_{1m} necessary for the parametric point to be in the second unstable region are smaller than those when the value of the capacitor is given by the CD line.

The capacitor value for operation in the second unstable region is more critical than that for the first unstable region, since the iso-μ curves determining the boundaries of the unstable region moves more rapidly upwards with increasing damping coefficient.

3.5 The Effect of the Load

When a load is connected across the secondary capacitor, the output side of the parametric transformer becomes a two-loop circuit, as shown in Figure 3.29. With a load having a reactive component, this circuit can only be expressed by two simultaneous differential equations in terms of the two variables, i_2 and i_L, and these two equations (one for each loop) have to be solved simultaneously to determine the loop currents. However,

for a purely resistive load, the number of differential equations representing the secondary side can be reduced to one by combining the load resistance with the rest of the circuit, as the V/I relationship of a resistance does not involve integration or differentiation. The effect of the load then becomes decomposed into two different aspects: it alters the damping and also the detuning already existing in the circuit.

With the voltage and current directions in Figure 3.29, the equations describing this circuit are

$$i_2 = i_C + i_L$$

$$e_2 = R_L . i_L = \frac{1}{C} \int i_C \, dt = -(N_2 \frac{d\phi_2}{dt} + R_2 \, i_2) \qquad \text{.....} \quad (3.182)$$

By using equation (3.2), and eliminating i_C, i_L and e_2 from the equations above, the single differential equation representing the loaded secondary circuit is obtained as

$$\frac{d^2\phi_2}{dz^2} + \frac{1}{\omega R_L C} \frac{d\phi_2}{dz} + \frac{R_2}{\omega N_2^2} \frac{d}{dz}(R_{m2}\phi_2) + \frac{R_{m2}}{\omega^2 N_2^2 C}(1 + \frac{R_2}{R_L})\phi_2 = 0 \qquad \text{.....} \quad (3.183)$$

where $z = \omega t$.

3.5.1 Linear Case

During the initiation of oscillations, R_{m2} is assumed to be linear (i.e. independent of ϕ_2), though time-varying, and given by equation (2.9). For linear R_{m2}, equation (3.183) becomes

$$\frac{d^2 \phi_2}{dz^2} + \left(\frac{1}{\omega R_L C} + \frac{R_2}{\omega N_2^2} R_{m2}\right) \frac{d \phi_2}{dz} + \left[\frac{R_2}{\omega N_2^2} \frac{d R_{m2}}{dz} + \left(1 + \frac{R_2}{R_L}\right) \frac{R_{m2}}{\omega^2 N_2^2 C}\right] \phi_2 = 0 \qquad \ldots\ldots \quad (3.184)$$

which, with $R_L = \infty$, directly gives equation (3.124) for the unloaded secondary circuit where a time-varying damping is present. Thus, it is evident in equation (3.184) that a resistive load increases the damping coefficient by $\frac{1}{\omega R_L C}$ and also introduces some extra detuning by the term $\frac{R_2}{R_L}$ in the coefficient of ϕ_2. If the secondary winding is assumed to be resistanceless, the effect of the load is confined only to an increase in the damping since, for $R_2 = 0$, equation (3.184) becomes

$$\frac{d^2 \phi_2}{dz^2} + \frac{1}{\omega R_L C} \frac{d \phi_2}{dz} + \frac{1}{\omega^2 N_2^2 C} R_{m2} \phi_2 = 0 \qquad \ldots\ldots \quad (3.185)$$

where the damping is now autonomous, the non-autonomous part due to R_2 being absent.

Substituting R_{m2} from equation (2.9) into equation (3.184) gives

$$\frac{d^2 \phi_2}{dz^2} + 2[\eta + k(1-m \cos 2z)] \frac{d \phi_2}{dz} + [a' - 2q' \cos 2z + 4 k m \sin 2z] \phi_2 = 0 \qquad \ldots\ldots \quad (3.186)$$

where

$$\eta = \frac{1}{2 \omega R_L C} \qquad \ldots\ldots \quad (3.187)$$

$$a' = a(1 + \frac{R_2}{R_L})$$

$$q' = q(1 + \frac{R_2}{R_L})$$

and k and m are the same as given before (a and q in equations (3.187) are also the same as before). Comparing equation (3.186) with (3.125) shows that the load increases the average value of the coefficient of the first derivative term by η and also alters the values of a and q to a' and q'.

In order to determine the condition for the parametric transformer to *switch on* when loaded, the stability of equation (3.186) must be investigated in the same way as followed for equation (3.125). Applying the transformation

$$\phi_2 = \psi_2 \exp\{ - \int [\eta + k(1-m \cos 2z)] dz\}$$

to remove the first derivative term in equation (3.186), results in the extended form of Hill equation

$$\frac{d^2 \psi_2}{dz^2} + [\theta_0 + \theta_{1C} \cos 2z + \theta_{1S} \sin 2z + \theta_{2C} \cos 4z] \psi_2 = 0 \qquad \text{.....} \qquad (3.188)$$

where

$$\theta_0 = a' - k^2 (1 + \frac{m^2}{z}) - 2 k\eta - \eta^2$$

$$\theta_{1C} = -2 (q' - k m\eta - k^2 m)$$

$$\theta_{1S} = 2 k m \qquad \text{.....} \qquad (3.189)$$

$$\theta_{2C} = - \frac{1}{2} k^2 m^2$$

Carrying the necessary steps forward, the instability condition for equation (3.186) is obtained as

$$\mu = \mu' - (\eta + k) > 0$$

where μ' is the characteristic exponent of equation (3.188) and is determined by the θ coefficients in equations (3.189). In this case, the instability condition cannot be interpreted in such a simple way as that followed for equations (3.134) to (3.141), and the value of μ' has, therefore, to be calculated by means of equation (3.73). The instability condition then gives

$$-1 - a' + \frac{1}{2} k m + [a' - k^2 + \frac{7}{2} k^2 m^2 - 2 k\eta - \eta^2 + 4(q' - km\eta - k^2 m^2)]^{\frac{1}{2}} > 0 \qquad \ldots\ldots \qquad (3.190)$$

where a' is now different from unity. For a given ϕ_{1m}, k and m are definite, but η, a' and q' are all functions of R_L. Following substitution for all these parameters, R_L may be solved from equation (3.190) as R'_{Lmin}, when the instability condition becomes

$$R_L > R'_{Lmin} \qquad \ldots\ldots \qquad (3.191)$$

which means that parametric oscillations are not excited if the

load resistance is smaller than a given minimum value. Therefore, if the parametric transformer is loaded excessively, it will not *switch on* when the supply voltage is applied to the primary circuit. This is an important aspect of the intrinsic over-load protection ability of the device.

Based on the simplified representation of Figure 3.21, the overload protection may be explained graphically, if terms involving both k and m are neglected in equation (3.186). When $a=1$ and $q>0$, the parametric point is at P in Figure 3.30a, with no load connected, and the small resistance of the secondary winding changing the shape of the boundary curve by only a small amount. As R_L decreases from infinity, the boundary curve moves upwards, since it is the iso-μ curve on which $\mu' = k + \eta$, and the parametric point moves to the left along the line OA (corresponding to the fixed amplitude of the primary flux) since θ_0 and θ_{1C} of equations (3.189) (corresponding to a and $-2q$ respectively, when $R_2 = 0$ and $R_L = \infty$) tend to decrease with increasing η. This is shown in Figure 3.30b. The critical case is when R_L is so decreased that the parametric point is on the boundary curve of the unstable region, as shown in Figure 3.30c. A further decrease in R_L moves the parametric point out of the unstable region, and in this case, as shown in Figure 3.30d, the parametric transformer cannot start operating since the instability condition is not satisfied. The parametric transformer therefore protects itself from any harmful effects of an excessive load, by not *switching on* when the input voltage is applied.

However, this is only one aspect of the over-load protection. Once parametric oscillations have been initiated and the parametric

transformer has achieved the steady-state operation, the load resistance may be gradually reduced, while still drawing power from the device. When R_L becomes smaller than a minimum value (different from R''_{Lmin}), the parametric oscillations cease and the device is automatically *switched off* with the output voltage falling immediately to zero. To explain this, the stability of the differential equation governing the loaded secondary circuit during steady-state must be investigated.

3.5.2 Non-linear Case

Substituting R_{m_2} from equation (3.103) into equation (3.184), gives the equation for a loaded, dissipative and non-linear secondary circuit, as

$$\frac{d^2 \phi_2}{dz^2} + [2\eta + 2k(1-m \cos 2z) + d\, \phi_2^{\,2}] \frac{d\, \phi_2}{dz} + (a' - 2q' \cos 2z + 4\, km \sin 2z)\phi_2$$

$$+ g'\, \phi_2^{\,3} = 0 \qquad \ldots\ldots \qquad (3.192)$$

where $\quad g' = g\,(1 + \frac{R_2}{R_L})$

and all the other parameters are as defined previously. Defining two intermediate parameters

$$K = \eta + k$$

and $$M = \frac{k\ m}{\eta + k}$$

in order to make equation (3.192) of the same form as equation (3.148), the results obtained in Section 3.3.2 can readily be adapted to the case of the loaded secondary circuit. (Note that K.M = k.m). The stable amplitude and phase of the secondary flux during steady state are found from equations (3.161) and (3.163), but with a, q, k, m and g now replaced by a', q', K, M and g', respectively. In terms of the new parameters, equations (3.161) and (3.163) become very complicated to evaluate, and the case for $R_2 = 0$ (a resistanceless secondary winding) is considered in order to obtain a clearer picture of the load characteristics of the parametric transformer.

With $R_2 = 0$, k and d become zero, and $K = \eta$, $a' = a$, $q' = q$ and $g' = g$. Equation (3.161) is then simplified to

$$\phi_{2m}^{\ 2} = \frac{4}{3g}\ [1 - a + (q^2 - 4\,\eta^2 + \eta^2\ m^2)^{\frac{1}{2}}] \ \ldots\ldots \qquad (3.193)$$

which illustrates the load regulation characteristic of the device. For $R_L = \infty$, $\eta = 0$, and equation (3.193) becomes equation (3.113). When $\phi_{2m}^{\ 2}$ is plotted from equation (3.193) as a function of $\frac{\phi_{2m}}{R_L}$ (a measure of the load current), a curve in the shape of Figure 3.31 is obtained. However, at a certain value of the load resistance, the parametric transformer is *switched off*, and ϕ_{2m}

falls to zero, as indicated by the broken line in the figure.

With a finite R_L and $R_2 = 0$, equation (3.163) becomes

$$\sigma = \tan^{-1}\left(- \frac{a - 1 + q + \frac{3}{4} g \phi_{2m}^{2}}{2\eta}\right) \quad \ldots\ldots \qquad (3.194)$$

where ϕ_{2m}^{2} must be substituted from equation (3.193) to obtain the dependence of σ on the load. As is evident from Figure 3.31, ϕ_{2m}^{2} is fairly constant within the operating range, and the constant value of ϕ_{2m}^{2} from equation (3.113) may therefore be used in equation (3.194) as a reasonable approximation. Thus, the phase angle of the secondary flux is approximately

$$\sigma \simeq \tan^{-1}\left(- \frac{q}{\eta}\right) = \tan^{-1}(- 2q \ \omega C R_L) \quad \ldots\ldots \qquad (3.195)$$

With no load connected ($R_L = \infty$), $\sigma = - \frac{\pi}{2}$, but for a finite value of R_L ($< \infty$), $|\sigma| < \frac{\pi}{2}$ and the decrement from $- \frac{\pi}{2}$ is a function of R_L. This decrement in σ is also a measure of the energy supplied to the load, as equation (3.154) now becomes

$$\phi_{2m}^{2} \pi (2 \eta) = \phi_{2m}^{2} \pi (- q \sin 2 \sigma)$$

in which the left hand side represents the energy dissipated in R_L, and the right hand side is the parametrically supplied energy which is a positive value for $- \sigma < \frac{\pi}{2}$.

The approximate steady-state solution of equation (3.192) is then $\phi_2 = \phi_{2m} \sin(z-\sigma)$, the amplitude and phase of which are given by equations (3.193) and (3.194). This is the stable and periodic solution of the system. However, the stability of this periodic solution against any changes in the system parameters must be investigated, in order to determine the condition for the parametric transformer to switch itself off when excessively loaded.

The behaviour of a small disturbance ξ around the periodic solution determines the asymptotical stability of the periodic oscillations in the secondary circuit. If the secondary flux is assumed to be

$$\phi_2 = \phi_{2m} \sin(z-\sigma) + \xi \qquad \ldots\ldots \qquad (3.196)$$

with a small variation ξ from its stable value, then substituting equation (3.196) in equation (3.192) (in which the coefficient of the first derivative term is $[2K(1-M \cos 2z) + d\,\phi_2^{\,2}]$ with the intermediate parameters K and M) gives the variational equation

$$\frac{d^2 \xi}{dz^2} + 2K(1-M \cos 2z) \frac{d\xi}{dz} + [(a' + \frac{3}{2} g' \phi_{2m}^{\,2}) - (2q' + \frac{3}{2} g' \phi_{2m}^{\,2} \cos 2\sigma)\cos 2z$$

$$+ (4\,km - \frac{3}{2} g' \phi_{2m}^{\,2} \sin 2\sigma)\sin 2z\,]\,\xi = 0$$

$$\ldots\ldots \qquad (3.197)$$

when terms in ξ of higher order than the first are neglected (since ξ is assumed small). By using the transformation

$$\xi = \nu \exp[\int K(1-M \cos 2z)dz]$$

equation (3.197) changes to the Hill equation

$$\frac{d^2 \nu}{dz^2} + (\theta_0 + \theta_{1C} \cos 2z + \theta_{1S} \sin 2z + \theta_{2C} \cos 4z)\nu = 0 \qquad \ldots\ldots \quad (3.198)$$

where $\theta_0 = a' + \frac{3}{2} g' \phi_{2m}^2 - K^2(1 + \frac{M^2}{2})$

$$\theta_{1c} = -2q' - \frac{3}{2} g' \phi_{2m}^2 \cos 2\sigma + 2 K^2 M$$

$$\theta_{1s} = 2 KM - \frac{3}{2} g' \phi_{2m}^2 \sin 2\sigma$$

and $\theta_{2c} = - \frac{K^2 M^2}{2}$

Proceeding in a similar manner to that in Section 3.3.1, the instability condition for equation (3.197)

is*

$$\mu'^2 > K^2 = (k + \eta)^2$$

where μ' is the characteristic exponent of equation (3.198).

With μ'^2 calculated from equation (3.73), this instability condition gives

$$-(a' + \frac{3}{2} g' \phi_{2m}^2 - \frac{K^2M}{2} + 1) + 2 [\frac{3}{2} g' \phi_{2m}^2 (1 - kM \sin 2\sigma + q' \cos 2\sigma -$$

$$- K^2M \cos 2\sigma) + K^2(K^2M^2 + \frac{M^2}{2} - 2q' M - 1) + a' + q'^2]^{\frac{1}{2}} > 0$$

..... (3.199)

If the condition (3.199) is satisfied, the solution of equation (3.197) becomes unstable, that is ξ increases with time, and the solution of equation (3.192) diverts from the stable periodic solution $\phi_2 = \phi_{2m} \sin(z-\sigma)$. Since ϕ_{2m} cannot increase to more than

---

* For complete stability of equation (3.197), the instability of equation (3.198) must be considered in all unstable regions of the stability chart corresponding to equation (3.198). However, since the term of 2z is dominant in equation (3.195), it is sufficient to investigate its stability in only the first unstable region. Further information about generalized stability conditions of periodic oscillations in second-order systems may be obtained from reference 8.

the value determined by the saturation level of the magnetic core, the instability of ξ indicates that parametric oscillations will diminish in amplitude towards zero, as ξ increases (ξ is a periodic function of z having the same frequency as the secondary flux, but with exponentially increasing amplitude). Equation (3.199) is, therefore, the condition for switch-off of the oscillations in the secondary circuit of the parametric transformer operating in the steady state.

In condition (3.199), all the parameters are functions of the load resistance R_L. For $R_2 = 0$, the primed parameters cease to be so, and $K = \eta$, $M = 0$. However, ϕ_{2m} and σ remain functions of R_L. For a given ϕ_{1m} and R_L, they are substituted in equation (3.199) from equations (3.193) and (3.194) respectively. The instability condition is then obtained in terms of R_L and ϕ_{1m} only (apart from the other system parameters ω, N_2, C, R_2, s_1, r_1, s_3, r_3 etc). The value of R_L may now be solved for a specified ϕ_{1m} from this condition, which gives the condition for switch-off as

$$R_L < R''_{Lmin} \qquad \ldots\ldots \qquad (3.200)$$

where R''_{Lmin} is smaller than R'_{Lmin} of condition (3.191). If condition (3.200) is satisfied, with R_L decreased below a given minimum value, the voltage and current of the secondary circuit immediately fall to zero, and no power is delivered to the load, until parametric oscillations are re-started. For re-starting the

parametric transformer, R_L has to be increased to more than R'_{Lmin}, so that condition (3.191) can be satisfied. After oscillations are re-established, R_L may take values between R'_{Lmin} and R''_{Lmin}. In practice, this aspect of the over-load protection ability of the parametric transformer, expressed by condition (3.200), is more important than that considered by condition (3.191), as far as safety is concerned.

Finally, although two simultaneous equations are required when the load has a reactive component, some rough considerations can be given to the secondary circuit in the following manner. Considering the loaded secondary circuit as a high-Q tank circuit, with only signals of frequency ω existent, the impedance (in the frequency domain) seen at AA' of Figure 3.29 is the parallel combination of $Z_L(=R_L + j X_L)$ and $\frac{1}{j\omega C}$, together with the series secondary winding resistance R_2. The combined impedance Z, assumed to have been connected across the resistanceless secondary winding, is found as

$$Z = R_2 + \frac{R_L}{(\omega C R_L)^2 + (\omega C X_L - 1)^2} - j\,\frac{R_L^2 + X_L\,(X_L - \frac{1}{\omega C})}{\omega C\,[R_L^2 + (X_L - \frac{1}{\omega C})^2]}$$

which yields an equivalent series resistance of

$$R'_2 = R_2 + \frac{R_L}{(\omega C R_L)^2 + (\omega C X_L - 1)^2}$$

and an equivalent series capacitance of

$$C' = C\left(1 + \frac{\frac{1}{\omega C} - X_L}{\omega C R_L^2 + \omega C X_L^2 - X_L}\right)$$

forming the equivalent circuit shown in Figure 3.32. It is again evident that the effect of the load is decomposed into increases in both damping and detuning. Thus, considerations similar to those in Sections 3.3 and 3.4 may be applied to the circuit of Figure 3.32, using R_2' and C' to determine the new system parameters. Minimum values for the load not to initiate oscillations and to cause oscillations to cease may be obtained similarly. However, a study of the equations giving R_2' and C' shows that, when X_L is capacitive, the increase in the effective series resistance is smaller and the increase in the effective capacitance is larger, than when X_L is inductive. The increase in the effective capacitance affects the amplitude of the secondary flux more in a positive direction than it does in a negative direction. (Since the distance between P and P_1 in Figure 3.26 is a measure of the secondary flux amplitude at steady state, an increase in the capacitance moves the parametric point P to the left on the ϕ_{1m} = constant line, resulting in a longer distance from P_1, the point projected on the iso-μ curve. A decrease in the capacitance results in a shorter distance between P and P_1). From this discussion, it may be concluded that a better load regulation characteristic is obtained when the load has a capacitive reactance, and, conversely, that the load regulation characteristic with an inductive load is poorer than for a purely resistive load. Typical load regulation characteristics for the

loads of different power factors may therefore be anticipated as those shown in Figure 3.33.

3.6 Complementary Remarks on the Characteristics of the Parametric Transformer

The equations describing various aspects of the parametric transformer have been treated in Sections 3.1 to 3.5, and the behaviour and operation characteristics have been developed. In this section, some of these are collected together and summarised, and a few complementary remarks are added.

3.6.1 Under- and Over-Voltage Protection, and Voltage Regulation

In Section 3.3.1, it was demonstrated that a threshold condition exists for initiation of oscillations in the secondary circuit, due to the presence of damping. In obtaining those equations, the coefficient a was taken as unity and kept constant. However, as shown in Section 3.4, if the capacitor in the secondary circuit has a fixed value, the coefficient a is a function of ϕ_{1m}, and the parametric transformer provides under-voltage protection (and also over-voltage protection), even when the secondary circuit is non-dissipative. Hence, the under-voltage protection feature, is not only due to the damping in the secondary circuit, but also to the primary flux amplitude changing the average value of the secondary reluctance, thus introducing detuning into the circuit. Secondly, as is clear from the discussion of Section 2.1.1 with regard to Figures 2.2,

2.3 and 2.4, the primary flux amplitude has to be increased to the knee region of the primary magnetisation characteristic, before any variations in R_{m2} can occur and as a consequence, oscillations can be excited.

The steady-state amplitude of the secondary flux is given, to a first approximation, by equation (3.113), and to a closer approximation by equation (3.115), in the case of non-dissipative secondary circuit. The parameters in equation (3.113), are functions of ϕ_{1m} (C fixed). When the expressions for a, q and g are substituted in equation (3.113), the relationship between the amplitudes of the secondary and primary fluxes is as

$$\phi_{2m}^{2} = \frac{4}{3(s_3 + r_3)} [\omega^2 N_2^{\,2} C - R_{m2min}] - \frac{r_3}{s_3 + r_3} \phi_{1m}^{2} \qquad (3.201)$$

which gives a curve in the first quadrant of the ϕ_{2m} - ϕ_{1m} plane, as shown in Figure 3.34. Due to the existence of the threshold condition, this relationship becomes modified to that shown in Figure 3.35. This figure demonstrates clearly both the under- and over-voltage protection features of the parametric transformer, with the over-voltage protection being provided when the primary flux reaches the value

$$\phi_{1m}^{2} = \frac{4}{3\, r_3} [\omega^2 N_2^{\,2} C - R_{m2min}] = (\phi_{1m}'')^2 \qquad (3.202)$$

Equation (3.113) was obtained by the harmonic balance method, and it agrees well with the considerations made from the simplified stability chart of Figure 3.27. The primary flux amplitude at switch off (ϕ''_{1m}) was obtained from this figure as given by equation (3.181) which is exactly the same as equation (3.202). Equation (3.201) may be written in the form

$$A^2 \phi_{2m}^2 + \phi_{1m}^2 = (\phi''_{1m})^2 \qquad \ldots\ldots \qquad (3.203)$$

where

$$A^2 = \frac{s_3 + r_3}{r_3} \quad \text{and} \quad \phi''_{1m} \; .$$

given by equation (3.202), are constants. This form indicates that the curve in Figure 3.34 is a quarter section of a compressed circle in which the compression has been made in the direction of the ϕ_{2m} axis by the factor A. If A is assumed to equal unity, this relationship corresponds to the magnetisation characteristic of Figure 3.19 with $\phi_s = \phi''_{1m}$, which resulted in a circular relationship between the amplitudes of the primary and the secondary flux phasors in Figure 3.20. Therefore, for an accurate representation of Figure 3.20, all the dimensions in the vertical direction must be divided by A, producing a vertical compression of the whole phasor diagram. (This point is brought up here, because the object of Figure 3.20 was to explain different steps in the growth of the secondary flux amplitude). Equation (3.203) also throws light on how the primary and the secondary fluxes are

limited in the common region of the magnetic core.

When damping exists in the secondary circuit, the amplitude of the secondary flux is given, to a first-order approximation, by equation (3.161) from which the ϕ_{2m}/ϕ_{1m} characteristic may be derived with a load connected at the output, the form of the equation involved becomes even more complicated, and the secondary winding resistance is, therefore, neglected in obtaining equation (3.193). For a given R_L (or η), a ϕ_{2m}/ϕ_{1m} characteristic can be obtained from equation (3.193), although it will not be as simple as equation (3.201). Nevertheless, the similarity between the forms of equations (3.193) and (3.113) implies that the ϕ_{2m}/ϕ_{1m} characteristic is obtained in a similar shape to that of Figure 3.34.

Once the parametric transformer is operating in the steady-state, parametric oscillations are sustained in the secondary circuit even when ϕ_{1m} is decreased below ϕ_{1m}', the primary flux amplitude corresponding to the threshold condition. The reason for this is that the secondary flux also modulates the primary reluctance, and energy transfer still continues, in the way explained in Section 3.1.5, until ϕ_{1m} is so decreased that the energy transferred to the secondary circuit is insufficient to overcome the secondary circuit damping. The ϕ_{2m}/ϕ_{1m} characteristic therefore exhibits the operational hysteresis indicated in Figure 3.36. The minimum value of ϕ_{1m} to switch off the parametric transformer is obtained from the instability condition (3.199). For a fixed value of the load resistance satisfying the condition $R_L > R''_{Lmin}$,

ϕ_{1m} may be solved from equation (3.199), though this is difficult since ϕ_{2m} and σ are also dependent on ϕ_{1m}, and the condition for switch-off takes the form

$$\phi_{1m} < \phi'''_{1m} \qquad \ldots\ldots \qquad (3.204)$$

where ϕ'''_{1m} is smaller than ϕ'_{1m}, the threshold condition. The switch-off condition (3.204) means that oscillations immediately cease if the primary flux amplitude is decreased below ϕ'''_{1m}, and that the secondary flux amplitude falls instantaneously to zero, just as in the case of over-load protection.

It is apparent from Figure 3.36 that, for a good voltage regulation, the parametric transformer must operate between the points A and B. As explained in the next section, the output voltage becomes distorted in the region between B and C, as well as having poor regulation with variations in ϕ_{1m}. The necessity for the operating point to lie within the region AB introduces some impracticalities, since the parametric oscillations are self-starting only when the primary flux amplitude is between ϕ'_{1m} and ϕ''_{1m}, i.e. the region BC. If the operating point is chosen within the region AB, parametric oscillations are not restored even when the excessive load that has already switched off the parametric transformer is removed. To restore secondary oscillations, the primary flux amplitude needs to be increased temporarily to satisfy the threshold condition $\phi_{1m} > \phi'_{1m}$. Since the operating point is

determined by the input or supply voltage, and the supply voltage is constant, a special starter circuit is therefore required to drive the operating point into the region BC of Figure 3.36, for a short time interval sufficient for oscillations to build up, and then to let it return to the normal operating location. It is necessary, therefore, to use this starter circuit whenever the parametric transformer provides over-load or under-voltage protection, and switches itself off. However, when the parametric transformer provides an over-voltage protection, the secondary flux (and therefore the output voltage) gradually decrease in amplitude in the BC region of Figure 3.36, and finally becomes zero for $\phi_{1m} > \phi''_{1m}$ but the oscillations are not switched off. If the primary flux (or the input voltage) amplitude is decreased below the point C, the secondary flux is again restored and the parametric transformer continues operating.

If equation (3.104) is written in the form

$$\frac{d^2 \phi_2}{dz^2} + a\,\phi_2 + g\,\phi_2^{\,3} = (2q \cos 2z)\,\phi_2$$

it resembles a standard Duffing's equation[39], when the left-hand side is regarded as an independent driving force. Duffing's equation has been used to explain the phenomenon of ferroresonance in non-linear resonant circuits driven by an external source. In such systems, discontinuous jumps occur in the amplitude of oscillation when the frequency of the external driving function is varied, with its amplitude kept constant. This unexpected result

is due to the shape of the non-linear resonance curve, and a similar phenomenon of discontinuous jumps also occurs if the driving frequency is held constant but the amplitude of the driving force is varied. In the case of Duffing's equation, it is not difficult to derive the relationship between the amplitudes of the oscillation and the driving force, which explains these discontinuous jumps. But, the left-hand side of the equation above is not independent of the system as it involves ϕ_2. The primary flux amplitude ϕ_{1m} enters into the equation through the parameter q, and the amplitude of the left-hand side cannot be varied independently. However, by analogy with such externally driven non-linear resonance circuits[40], the existence of different values of ϕ_{1m} to switch on and off the oscillations suggests that the relationship between ϕ_{2m} and ϕ_{1m} is as shown in Figure 3.37. This curve explains the discontinuous jumps, i.e. the operational hysteresis in the under-voltage protection feature of the parametric transformer, since the part of the curve between A and D is unstable and cannot be observed in the experiments.

3.6.2 Filtering Ability and Sinusoidal Output Voltage

In general, the secondary circuit of a parametric transformer is described by a non-linear equation, for which it is quite difficult to obtain an analytical solution. The existence of damping makes this even more difficult, by introducing a first

derivative term with time-varying coefficients. However, when the secondary circuit resistance is neglected, the effect of non-linearity may be considered as a change in the parameter σ in the solution for the linear Hill equation, which at steady-state becomes equal to $-\frac{\pi}{2}$ and causes the characteristic exponent to be zero (the limiting action of the non-linearity on the amplitude of the secondary flux variations). The effect of damping is taken into account by the ultimate value of σ, given approximately by equation (3.163), which is now smaller than 90°, so that parametric energy still develops to overcome the dissipation. Under these considerations, the output waveform of the parametric transformer may be investigated by examining $\phi(z,\sigma)$, the stable part of the solution for the linear Hill equation.

The periodic function $\phi(z,\sigma)$ is given by equation (3.64), and its harmonic content depends upon the coefficients θ in the Hill equation, equation (3.58). These coefficients arise directly from the Fourier series expansion of the secondary reluctance variation, as given by equations (3.53) and (3.54). The waveform of this variation, as explained through equations (3.49) to (3.51), is determined both by the amplitude and the waveform of the primary flux, and by the shape of the transreluctance curve.

The shape of the transreluctance curve, shown in Figure 2.2b, is the most important factor in determining the waveform of the secondary reluctance variation. As can be seen from Figure 2.2,

when the amplitude of the primary flux is smaller than ϕ_s, the amplitude of the secondary reluctance variation is small, and when the primary flux amplitude is around ϕ_s, the secondary reluctance variation may be considered sinusoidal. However, if the primary flux amplitude exceeds ϕ_s, the secondary flux variation becomes distorted with high peaks, and contains a large number of harmonic components in its Fourier expansion. Consequently, the θ coefficients of the higher frequency terms in the Hill equation are not negligible.

In the power-series expansion of the transreluctance characteristic, equation (3.50), $R_{m2min}(= R_g + s_1 + r_1)$ is a small quantity, because of the high permeability of the magnetic core, and the coefficients Γ are even smaller than this, due to the shape of the transreluctance curve. If the amplitude of the primary flux is not much greater than ϕ_s, it is sufficient to neglect the $\Gamma_j \phi_1^{2j}$ terms in equation (3.50), for $j>1$, and to take the transreluctance characteristic as

$$R_{m2} = R_{m2min} + \Gamma_1 \phi_1^2 \qquad (R_{m2min} > 0,\ \Gamma_1 > 0) \tag{3.205}$$

Equation (3.205) leads to the Mathieu equation, the solution of which for steady-state operation of the parametric transformer ($\sigma = -\frac{\pi}{2}$), is the function $ce_1(z,q)$, given by equation (3.28). Since, in this case, $|\Gamma_1 \phi_1^2| \ll R_{m2min}$, and therefore $q \ll a$ ($a \simeq 1$), equation (3.28) indicates that the higher frequency components in the secondary flux are of very small amplitude, and thus that the secondary flux has a substantially sinusoidal waveform.

As long as the amplitude of the primary flux is not greatly in excess of ϕ_s, the secondary flux variation is not much influenced by the primary flux waveform, since the transreluctance curve is almost horizontal below ϕ_s. If the primary flux is non-sinusoidal, but the fundamental frequency component is dominant, the coefficients in the corresponding Hill equation with the comparatively greater magnitudes are θ_0 and θ_1, and with no damping in the secondary circuit $(\sigma = -\frac{\pi}{2})$, $\phi(z,\sigma)$ of equation (3.64) becomes

$$\phi(z) = \cos z + \cos 3z \left(\frac{1}{8}\theta_1 + \frac{1}{8}\theta_2 - \frac{1}{64}\theta_1^2 + \frac{5}{96}\theta_1\theta_2\right) + \cos 5z \left(\frac{\theta_2}{24} + \frac{\theta_3}{24} + \frac{\theta_1^2}{182}\right) + \cos 7z \left(\frac{1}{48}\theta_3 + \frac{1}{288}\theta_1\theta_2\right) \quad \ldots\ldots \quad (3.206)$$

when the terms with magnitudes smaller than $|\theta_1.\theta_2|$ are neglected.* The fact that $|\theta_1| >> |\theta_2| >> |\theta_3|$ etc. and $|\theta_1| << |\theta_0|$ ($\theta_0 \simeq 1$, from the tuning of the secondary resonant circuit) indicates that the higher harmonic components in $\phi(z)$ are of very small amplitudes, and that the secondary flux is almost purely sinusoidal, giving

---

* If the terms other than those involving only θ_1 are omitted, $\phi(z)$ gives the cosine-elliptic function $ce_1(z,\theta_1)$.

a sinusoidal output voltage waveform. Therefore, unless the amplitude of the primary voltage is so large as to saturate the common magnetic region of the core, the secondary voltage is independent of the input voltage waveform, providing the inherent filtering ability of the parametric transformer.

If the amplitude of the primary flux exceeds ϕ_s, the higher power terms in the power series expansion of the transreluctance characteristic need to be taken into account. With the transreluctance characteristic given by

$$R_{m2} = R_{m2min} + \Gamma_1 \phi_1^{\,2} + \Gamma_2 \phi_1^{\,4} + \Gamma_3 \phi_1^{\,6}$$

$$(R_{m2min}, \Gamma_1, \Gamma_2, \Gamma_3 > 0) \qquad \ldots\ldots \qquad (3.207)$$

a sinusoidal primary flux $\phi_1 = \phi_{1m} \sin z$, leads to the equation of the linear, non-dissipative secondary circuit as

$$\frac{d^2 \phi_2}{dz^2} + (\theta_0 + 2\theta_1 \cos 2z + 2\theta_2 \cos 4z + 2\theta_3 \cos 6z)\, \phi_2 = 0$$

$$\ldots\ldots \qquad (3.208)$$

where

$$\theta_0 = \frac{1}{\omega^2 N_2^2 C}\left(R_{m2min} + \frac{1}{2}\Gamma_1 \phi_{1m}^2 + \frac{3}{8}\Gamma_2 \phi_{1m}^4 + \frac{5}{16}\Gamma_3 \phi_{1m}^6\right) > 0$$

$$\theta_1 = \frac{1}{2\omega^2 N_2^2 C}\left(-\frac{1}{2}\Gamma_1 \phi_{1m}^2 - \frac{1}{2}\Gamma_2 \phi_{1m}^4 - \frac{15}{32}\Gamma_3 \phi_{1m}^6\right) < 0$$

$$\theta_2 = \frac{1}{2\omega^2 N_2^2 C}\left(\frac{1}{8}\Gamma_2 \phi_{1m}^4 + \frac{3}{16}\Gamma_3 \phi_{1m}^6\right) > 0$$

and $$\theta_3 = \frac{1}{2\omega^2 N_2^2 C}\left(-\frac{1}{32}\Gamma_3 \phi_{1m}^6\right) < 0$$

..... (3.209)

Since, now, $\phi_{1m} > \phi_s$ and $\Gamma_1 \phi_{1m}^2$, $\Gamma_2 \phi_{1m}^4$, $\Gamma_3 \phi_{1m}^6$ are not negligible, the higher frequency components in $\phi(z)$ become significant. Using the θ coefficients from equations (3.209), the periodic function $\phi(z)$ takes the form

$$\phi(z) = \cos z - A_1 \cos 3z + A_2 \cos 5z - A_3 \cos 7z + \ldots$$

$$(A_1, A_2, A_3 > 0) \qquad \ldots\ldots \qquad (3.210)$$

which gives a rather square shaped waveform to the secondary flux, as shown in Figure 3.38a, with the secondary voltage taking the waveform shown in Figure 3.38b. Even when the

primary flux is sinusoidal (with sinusoidal input voltage and the resistance of the primary winding neglected), but of sufficient amplitude to drive the common magnetic region far into saturation, the waveforms of the secondary flux and the output voltage become distorted as their amplitude decreases due to the shape of the ϕ_{2m}/ϕ_{1m} characteristic shown in Figure 3.35.

On initiation of parametric oscillations, the amplitude of the primary flux needs to be increased beyond ϕ_s (in Figure 2.2b), to obtain a sufficiently large variation in the secondary reluctance to satisfy the threshold condition. However, if the primary flux is maintained at this level, corresponding to some point in the region BC of Figure 3.36, the voltage regulation is poor and the output voltage has the waveform shown by Figure 3.38b. Therefore, the operational point in the input voltage/output voltage characteristic is chosen to be in the region AB of Figure 3.36, as mentioned in the previous section.

To sum up, the waveform of the output voltage depends on the maximum value of the primary flux (or input voltage) and is essentially independent of the input waveform. Irregularities in the primary flux waveform can only affect the secondary reluctance variation if they occur between the instants t_1 and t_2 in Figure 2.2b. Since, in normal operation, ϕ_{1m} is not greatly in excess of ϕ_s, for the reasons explained above, this interval is short, and the secondary flux, being a good sinusoid,does not reflect these irregularities. It is important that the parametric transformer provides this filtering ability against any disturbances in the primary flux, because the primary flux is

always non-sinusoidal due to the non-linearity and the resistance of the primary circuit. Furthermore, as shown later in Chapter VI, the primary current is quite non-sinusoidal because of both the magnetic non-linearity and the reaction from the secondary to the primary circuit.

The filtering property of the parametric transformer arises since the primary flux has no direct effect on the secondary flux. The effect of the primary flux on the secondary flux waveform is only through the θ coefficients, which, apart from θ_0, are quite small, and even the effect of the θ coefficients on the harmonic content of $\phi(z)$ is insignificant, because of the form of $\phi(z)$ given by equation (3.206). For instance, with a square-wave input voltage, and primary resistance neglected, the primary flux has the triangular waveform shown in Figure 3.39, which, in the Fourier series expansion, takes the form

$$\phi_1 = \phi_{1m} \frac{8}{\pi^2} (\sin z + \frac{1}{9} \sin 3z + \frac{1}{25} \sin 5z + \ldots.) \quad (3.211)$$

It is shown in Appendix II that, for such a primary flux and $\phi_{1m} < \phi_s$, the ratio of the amplitudes of the third harmonic to the fundamental frequency term in the secondary flux is of the order of 1.25%. Therefore, even with a square wave input voltage, a quite good sinusoidal output voltage is obtained.

With this inherent filtering property, the parametric transformer is able to suppress not only harmonic distortion

but also such disturbances in the mains voltage as superimposed high-frequency fluctuations, distortion due to large cyclic load variations, transients or high-voltage spikes that may be caused by the switching action of thyristors, mercury arc rectifiers, etc. The filtering property is strictly related to the mechanism by which energy is transferred from the input to the output. There is no direct relation between the input and output waveforms as the energy transfer is not achieved on the basis of mutual flux coupling, and, in the actual device, mutual flux coupling is completely eliminated. In conventional transformers, high-voltage short duration spikes on the input voltage cause discontinuous jumps in the primary flux (flux is the integral of voltage, and the integral of an impulse function is a step function) and, since the whole primary flux links the secondary winding (full mutual coupling), these spikes are reproduced in the output voltage on the derivation of secondary flux, $e_2 = -N_2 \frac{d\phi_2}{dt}$, the discontinuous jumps in the flux result again in spikes on the output voltage. However, in the parametric transformer, a primary flux with discontinuous jumps does not basically affect the secondary reluctance variation, as can be deduced from Figure 2.2, Chapter 2. Furthermore, as already seen, the waveform of the secondary flux (and consequently, of the output voltage) is essentially independent of the θ coefficients or the harmonic content of the secondary flux variation. The parametric transformer can, therefore, easily suppress high-voltage spikes on the input voltage of the order of kilovolts, subject to the strength of insulation. This filtering ability acts in

bilateral manner, and any disturbances caused by the load at the secondary side are not transferred to the supply side because of the absence of mutual flux coupling between the primary and secondary circuits.

The influence of the load on the output waveform may be summarized in the following manner. At no load, neglecting the secondary winding resistance, σ is taken as exactly $-\frac{\pi}{2}$, and equation (3.206) is obtained for the output waveform, and the output waveform remains a good sinusoidal as long as ϕ_{1m} is kept below ϕ_s. When the secondary circuit is loaded, σ decreases in magnitude from 90^0 as the load resistance decreases from infinity. Nevertheless, this decrease in σ is small for large load resistances, as evident from equation (3.195). Rearranging the terms, $\phi(z,\sigma)$ of equation (3.64) may be written as

$$\phi(z,\sigma) = \sin(z-\sigma)$$

$$+ \cos 3z \left[\left(-\frac{1}{8}\theta_1 - \frac{1}{8}\theta_2 + \frac{1}{32}\theta_1^2 - \frac{7}{192}\theta_1\theta_2\right)\sin\sigma + \right.$$

$$\left. + \frac{1}{64}\theta_1^2 \sin 3\sigma - \frac{1}{64}\theta_1\theta_2 \sin 5\sigma\right] +$$

$$+ \sin 3z \left[\left(\frac{1}{8}\theta_1 - \frac{1}{8}\theta_2 + \frac{1}{32}\theta_1^2 + \frac{1}{192}\theta_1\theta_2\right)\cos\sigma + \right.$$

$$\left. + \left(-\frac{1}{32}\theta_1\theta_2 - \frac{1}{64}\theta_1^2\right)\cos 3\sigma + \frac{1}{64}\theta_1\theta_2 \cos 5\sigma\right]$$

$$+ \cos 5z \left[\left(-\frac{\theta_2}{24} - \frac{\theta_3}{24} - \frac{\theta_1^2}{192} + \frac{\theta_1\theta_2}{576}\right)\sin\sigma + \frac{\theta_1\theta_2}{576}\sin 3\sigma + \right.$$

$$\left. + \frac{\theta_1\theta_2}{576}(\cos\sigma - \cos 3\sigma)\right]$$

$$+ \sin 5z \left[\left(\frac{\theta_2}{24} - \frac{\theta_3}{24} + \frac{\theta_1^2}{192} + \frac{\theta_1\theta_2}{576}\right)\cos\sigma - \frac{\theta_1\theta_2}{576}\cos 3\sigma - \right.$$

$$\left. - \frac{\theta_1\theta_2}{576}(\sin\sigma + \sin 3\sigma)\right]$$

$$+ \ldots\ldots\ldots \qquad \ldots\ldots \qquad (3.212)$$

which still gives equation (3.206) for $\sigma = -\frac{\pi}{2}$. For a finite load resistance, the parameter σ of equation (3.194) is smaller than 90° by a small amount, and the coefficients of sin 3z, sin 5z, sin 7z, etc. in equation (3.212) do not become equal to zero. Thus, both sine and cosine terms exist in the Fourier expansion of the secondary flux. The simultaneous existence of sine and cosine terms indicates that the secondary flux waveform is asymmetrical within a half-period with respect to the vertical axis passing through the maximum point in this half-period, as shown in Figure 3.40. A load connected at the output, therefore, not only changes the phase difference between the input and output voltages but also distorts the waveforms of the secondary flux and output voltage. The phase difference between the primary and secondary fluxes is closely equal to

σ^*, and the change in σ is small when $R_L >> R_{Lmin}$. The output waveform remains as a good sinusoid for large load resistances. As the load resistance is decreased towards the minimum value where oscillations cease as a result of the built-in over-load protection, the amplitudes of the sine terms in equation (3.212) increase, and the distortion in the output waveform becomes more apparent.

From the considerations at the end of Section 3.5 concerning the changes of R_2' and C' with loads of different power factors, it may be deduced that the output waveform distortion due to loading is less when the load is capacitive, and that an inductive load causes more distortion than a purely resistive one. Nevertheless, this distortion only becomes significant during operation with large load currents near to i_{Lmax} in Figure 3.33, and the nominal load current is chosen at a fraction of i_{Lmax} where the load regulation characteristic is good.

The phase difference here, means the time interval between the zero-crossing instants of the primary and secondary fluxes, since the secondary flux is now non-sinusoidal although the primary flux is sinusoidal. Taking only the fundamental component in the secondary flux, this phase difference is exactly σ.

3.6.3 Bistability of the Phase

It has been shown by Figure 3.3 that the solution of the Mathieu equation has different stable and unstable phase values and that the phase of the solution eventually takes one of the stable equilibrium values where the characteristic exponent becomes maximum and positive. The stable phase value $\alpha = -\frac{\pi}{4}$ has been taken in equations(3.20) to (3.22), however, $\alpha = +\frac{3\pi}{4}$ is also a stable equilibrium value which gives

$$\phi_2 = \phi_{20}\, e^{\frac{1}{2}qz} \cos(z + \frac{3\pi}{4})$$

as another unstable solution of the Mathieu equation.

Parametric oscillations may, therefore, build up in two distinct and opposite phases. In which of these the oscillations grow up, is determined by the amplitude and the phase of the initial oscillation. It is mainly the initial phase of the small oscillation before parametric excitation, which fixes the phase of oscillations growing in amplitude with parametric excitation. As seen from Figure 3.3, if the phase of initial oscillations is in the range $-\frac{3\pi}{4} < \alpha < \frac{\pi}{4}$, parametric oscillations take the stable phase $\alpha = -\frac{\pi}{4}$ as they build up, and if the initial phase is between $\frac{\pi}{4}$ and $\frac{5\pi}{4}$, oscillations grow with the stable phase $\alpha = \frac{3\pi}{4}$ (until the non-linearity becomes effective).

In a general equation of the form of equation (3.74), the independent variable z can be replaced by $z+\pi$ with no change. If $\phi_2'(z)$ and $\phi_2''(z)$ are the linearly indepedent solutions, then

$\phi_2'(z+\pi)$ and $\phi_2''(z+\pi)$ are also solutions. With Floquet's theory, a constant factor ε, depending on the initial conditions, can be found such that the relationship between $\phi_2(z)$ and $\phi_2(z+\pi)$ becomes[12]

$$\phi_2(z+\pi) = \varepsilon\,\phi_2(z)$$

In the case of the Mathieu equation, the boundaries between the stable and unstable solutions occur for $|\varepsilon|=1$ (reference 13) and for a periodic solution with period 2π (stable solution on the boundary curve a_{c1} corresponding to the steady state operation of the parametric transformer), $\varepsilon = -1$ (reference 13), which indicates bistability of the phase at the steady-state. This situation arises since the time-varying coefficient has a period of π radians whereas the solution is periodic with 2π radians.

It is also evident in Section 3.1.5 that the relative positions of the secondary flux and the secondary reluctance variations remain unchanged if the secondary flux is shifted in phase by $\mp\pi$ radians. The same amount of energy is supplied to or removed from the secondary flux both when it changes as $\sin(z-\sigma)$ or $-\sin(z-\sigma)$. Maximum energy is supplied when $\sigma = -\frac{\pi}{4}$, and parametric oscillations may build up in one of the following two forms

$$\phi_2 = \phi_{20} e^{\mu z} \sin\left(z + \frac{\pi}{4}\right)$$

$$\phi_2 = -\phi_{20} e^{\mu z} \sin\left(z + \frac{\pi}{4}\right)$$

Since the effect of non-linearity is considered as the change in the value of σ from $-\frac{\pi}{4}$ to $-\frac{\pi}{2}$, the secondary flux, depending on which of these two forms it has taken, finally becomes at steady-state either

$$\phi_2 = \phi_{2m} \cos z$$

or

$$\phi_2 = -\phi_{2m} \cos z$$

differing in phase by $\mp \frac{\pi}{2}$ radians from the primary flux. Equation (3.111) also gives the phase of the solution at the steady-state as $\sigma = \mp \frac{\pi}{2}$ for when no energy added to the secondary flux. For both of these values ($\sigma = \mp \frac{\pi}{2}$), the characteristic exponent μ of equation (3.33) becomes zero, while the characteristic number a of equation (3.34) remains the same.

3.6.4 Frequency Multiplying/Dividing Operation

The main concern in this Chapter has been the normal operation of the parametric transformer, i.e. output frequency equal to input frequency, except for Section 3.1.2 where attention was drawn to the possibility of employing the device as a frequency multiplier. In fact, most of the work in the later sections of this Chapter can be applied to the second unstable region (even the third etc.) of the stability chart in a similar manner. By using the concepts of the parametric point

moving on the chart due to non-linearity, and boundary curves moving upwards with increasing dissipation, and with the aid of the iso-μ and iso-σ curves of Figure 3.6, the operation in the second unstable region can be fully explained and the operation characteristics derived. It may be shown that the device still provides, while working as a frequency multiplier, the characteristics of under-voltage and over-voltage protection, overload protection etc. However, instead of repeating the whole work for the second unstable region, drawing conclusions similar to those for the first unstable region is considered sufficient. The most important difference is that the iso-μ curves in the second unstable region move upwards with increasing dissipation much more rapidly than in the first unstable region. This means that the parametric oscillations of twice the input frequency are both more difficult to start and more sensitive to the load changes. The first property necessitates greater depth of modulation in the secondary reluctance, requiring higher primary flux amplitude and higher input currents, while the latter indicates that the maximum load which can be connected before the oscillations are automatically switched off, is much smaller than in normal operation. Both these arguments lead to the conclusion that the device has far less power efficiency when operating as a frequency doubler in comparison with its normal transformer operation.

The possibility of obtaining parametric oscillations at the sub-multiples of the input frequency should also be mentioned. The secondary reluctance variations can be made to have a

fundamental frequency equal to (not twice) the input frequency by supplying into the magnetic circuit an additional d.c. bias current of a sufficiently large and constant amplitude, which results in operating at only one side of the transreluctance curve. Then, the reluctance variation in the form

$$R_{m2} = R_{m2av} - R_0 \cos \omega t$$

where ω is the input frequency, leads to a similar Mathieu equation

$$\frac{d^2 \phi_2}{dz^2} + (a - 2q \cos z) \phi_2 = 0$$

with $a = (\frac{\omega_0}{\omega})^2$ and $q = \frac{R_0 . a}{2 R_{m2av}}$. The transformation of the independent variable $\tau = \frac{1}{2} z$, results in the standard form of the Mathieu equation

$$\frac{d^2 \phi_2}{d\tau^2} + (A - 2Q \cos 2) \phi_2 = 0$$

with the coefficients A = 4.a and Q = 4.q. The conditions for the initiation of the oscillations with the frequency $\frac{\omega}{2}$ are

$$A = 1 \qquad \text{and} \quad Q > 0$$

The first one gives

$$4\left(\frac{\omega_0}{\omega}\right)^2 = 1 \qquad \text{or} \qquad \omega_0 = \frac{1}{2}\,\omega$$

Thus, if ω_0, the resonant frequency of the secondary circuit, is adjusted to half the input frequency, parametric oscillations are excited with this frequency when the threshold condition is satisfied.

The arguments made above for frequency multiplying operation also apply to frequency dividing operation of the parametric transformer. The difference in the physical set-ups is that, in the latter, proper adjustment of the secondary circuit capacitor alone is not sufficient to excite the sub-harmonic oscillations, and a high unidirectional biasing mmf must be injected into the magnetic circuit to obtain the required frequency of the secondary reluctance variation.

3.7 Other Methods of Mathematical Analysis

In this Chapter, attention was mainly centred around the secondary circuit of the parametric transformer, and the device is represented as a system, by a second-order, non-linear differential equation with time-varying parameters. The primary circuit is assumed resistanceless and to be driven by an alternating voltage source. The explanation of the process of reluctance

modulation was restricted only to the argument associated with transreluctance curve of Figure 2.2, Chapter 2, and attention was only paid to the waveform of the reluctance variation, not to how this variation is physically achieved. The primary circuit was only concerned in Section 3.1.5 for an explanation of the energy transfer mechanism, and the primary reluctance was assumed to be modulated through the same process characterized by a similar transreluctance curve. By what physical means the variation in the primary reluctance is achieved, is also left unclarified.

Disregarding how the variation in the secondary reluctance is created (which might well be by an external, independent electrical or mechanical driving force) means that the systemis considered as a parametric generator, like a simple pendulum with vertically moving support, which results in a single differential equation (second-order, non-linear, with periodic coefficients). The oscillations of the pendulum does not cause any reaction on the external periodic force moving the support vertically. However, in Bethenod's experiment[14], the oscillations of the pendulum reacts on the electromagnetic force of the electromagnet coil placed under the pendulum, by varying the reluctance of its magnetic circuit. Such a system has, therefore, to be represented by two simultaneous differential equations both having periodic coefficients. However, it is to be noted that both the pendulum with a vertically moving support and the Bethenod's pendulum have only one degree of freedom, although the number of differential equations required is different, as in the latter the external electrical source driving the electromagnet enters into the right-

hand side of one of the differential equations. In the case of an elastic pendulum or the experiment of Gorelik and Witt[15], the system has two degrees of freedom as no external source exists, and it is represented by two simultaneous second-order differential equations with zero right hand sides.* The common property of the systems of Bethenod and Gorelik is that the two variables of the system enter into both the differential equations, and therefore, a parametric coupling exists between these two variables. With this angle of view, the parametric transformer as a mathematical system corresponds to the Bethenod's pendulum, and has to be given by two simultaneous non-linear differential equations, in each of which both the system variables should exist, though one of them might be implicit.

When the secondary circuit only is considered as a parametric oscillator, the resulting differential equation most generally is equation (3.192), given for the loaded, dissipative and non-linear parametric resonant circuit. This equation can be treated using various analytical methods of the theory of differential equations, such as perturbation method, methods of averaging, equivalent linearization.[16] All of these attempts to find an approximate

---

* By analogy, Bethenod's system might be made to have two degrees of freeom, if the external source of electrical energy is replaced by an initially charged capacitor which resonates with the inductance of the electromagnet.

solution based on the assumption that the degree of non-linearity is not too large. As the equation considered, apart from being non-linear, does have periodic coefficients, a second necessary assumption follows so that the magnitudes of the time-varying coefficients are only permitted to small values. Furthermore, none of these methods can give all the information that may be desired about the problem. For instance, the perturbation method may be used to obtain information about the steady-state operation of oscillatory systems, but is of little use in determining how the oscillation builds up to the steady-state. Various averaging methods allow the growth period to be studied but gives steady-state information only to the first order approximation.

The method used in this Chapter has been a step-by-step approach on the basis of the classical theory of Mathieu-Hill type equations, starting from the standard Mathieu equation and growing in complexity up to equation (3.192). This approach has been preferred, because it gives more information on different aspects of the behaviour of the system, and non-linearity, damping, detuning and loading can be independently studied as well as being interrelated between themselves and also with the changes in the amplitude and phase of the oscillation. In this way, more physical insight is obtained, the phase relationships between the primary and secondary flux and reluctance variations are more readily understood and the operation characteristics of the device are obtained with comparatively less complexity. Yet, the study is

mainly confined to the fundamental frequency term in the output (i.e. a first-order approximation) and the two pre-requisite assumptions, that non-linearity is small (i.e. g<<) and that the time-varying coefficients are of small magnitudes (i.e. m<<, k<<, q<<, etc), are made anywhere necessary. One essential advantage of this method is that it permits extensive use of the boundary curves, and iso-μ and iso-σ curves on the stability chart of Mathieu equation. By this, direct graphical interpretation of the characteristics of the parametric transformer has been possible to a certain extent.

However, to obtain an overall view of the build-up of oscillations in the secondary circuit, the best is to apply one of the averaging methods (slowly varying parameters, or variation of parameters methods) to the most general equation of the secondary, equation (3.192). There are two basic averaging methods: the Van der Pol approximation method[17,20] and the asymptotic method of Krylov-Bogoliubov-Mitropolsky.[18-20] In the first method, a first-order approximate solution is assumed to be of the form

$$\phi(z) = X(z) \cos z + Y(z) \sin z \qquad \ldots\ldots \qquad (3.213)$$

where $z = \omega t$, and the functions $X(z)$ and $Y(z)$ are assumed to be slowly varying (i.e. variation within a period of 2π is assumed to be small). Substituting this solution into the differential equation and averaging by the assumption that X and Y are constant within an interval of 2π, an approximate set of differential equations

may be derived in the form

$$\frac{dX}{dz} = \mu\ f_1(X,Y)$$

$$\frac{dY}{dz} = \mu\ f_2(X,Y) \qquad \ldots\ldots \quad (3.214)$$

where μ is a small and positive constant. In this way, the difficult problem of seeking a general solution for a non-autonomous system such as equation (3.192) may be reduced to the much easier one of the analysis of an autonomous system. Thus, the behaviour of the system may be described in terms of a phase-portrait, and the steady-state periodic solutions may be identified as the singular points of equations (3.214). The stability of these periodic solutions may then be determined in terms of the stability of the associated singular point.

The 'stroboscopic method' of Minorsky[21] is of the same basic form as the Van der Pol method, although the resulting autonomous set of equations are expressed in terms of $\rho = r^2 = X^2 + Y^2$ and $\psi = \tan^{-1}(\frac{Y}{X})$.

The asymptotic method of Bogoliubov and Mitropolsky assumes the solution in the form

$$\phi(z) = R(z) \cos [z + \psi(z)]$$

to a first approximation, where R and ψ are *slowly varying* amplitude and phase of the oscillation. The *averaged* differential equations are

$$\frac{dR}{dz} = \mu . u_1 (R,\psi)$$

$$\frac{d\psi}{dz} = \mu . u_2 (R,\psi)$$

to which the same techniques of geometric and graphical analysis may be applied. This method has been carried further by Bogoliubov and Mitropolsky to higher approximations than the first, and for the first-order approximation, it is, in effect, the polar coordinate equivalent of the Van der Pol method. The two methods of approximation actually complement one another, for the former is most convenient in the autonomous case, while the latter is particularly well suited to the study of non-autonomous systems.

Since equation (3.192) is both non-linear and non-autonomous, the Van der Pol approximation method has been preferred to the asymptotic method, and it has been applied in its basic form to equation (3.192). In order to obtain more information on the amplitude and phase of oscillations, the stroboscopic method of Minorsky has also been applied to equation (3.192), as a version of the Van der Pol method. The sets of averaged differential equations have been obtained in the form of equations (3.214), but with such complex f_1 and f_2 functions that no further evaluation

of the analysis has been practicable. The complexity of the functions f_1 and f_2 in terms of X and Y and other system parameters has not permitted the obtaining of the singular points from the equations

$$f_1(X,Y) = 0$$

$$f_2(X,Y) = 0$$

and the drawing of the phase-portrait (X-Y plane) of the system, which would give information on the bistability of oscillations and the final values of their amplitude and phase.

The complexity of these functions arises mainly because the coefficient of the first derivative term in equation (3.192) is both non-linear and time-varying. The dependence of a', q' and g' on R_2 and R_L by the factor $(1 + \frac{R_2}{R_L})$ makes derivation of analytical relationships in terms of actual physical quantities even more complicated and tedious than ever. Although the dissipative term in equation (3.192) is created by both the load resistance and the resistance of the secondary winding, it is to be noted that only R_2, the secondary winding resistance is responsible for it being non-linear and time-varying. When energy dissipation in the secondary winding is neglected by assuming $R_2 = 0$, not only do k and d become zero but also a'=a, q'=q and g'=g. Equation (3.192) then reduces to

$$\frac{d^2 \phi_2}{dz^2} + 2\eta \frac{d \phi_2}{dz} + (a - 2q \cos 2z)\phi_2 + g\phi_2^{\,3} = 0 \qquad (3.215)$$

with the first derivative term now having a constant coëfficient, and the additional sin 2z term having vanished from the coefficient of ϕ_2.

In the literature, averaging methods have been applied to the differential equations of the exact form of equation (3.215), and the results thereby obtained will be directly adopted here. Although E. Goto[22] gives a similar treatment to this kind of equation and obtains the phase-portrait of a bistable parametron, T. Stern[23] applies the Van der Pol approximation method to obtain the singular points and the phase-portrait of bistable parametron, as shown in Figure 3.41. There are three singular points: one unstable saddle point at the origin, and two stable nodal or spiral points symmetrically located on the X-Y plane. These two symmetrical points are asymptotically stable, giving the desired pair of stable phase of oscillation. The global stability of the system has been investigated by Willoughby[24] by using the direct method of Lyapunov and later presented by Stern[23] in the form of the seperatrix shown in Figure 3.41; all the solutions in the shaded area approach the upper singular point, and all those in the unshaded area approach the lower singular point. The location of the nodal singular points on the X-Y plane determines the steady-state amplitude and phase of the oscillations.

The differential equation studied by Goto[22] for the case of the parametron in which the non-dissipative inductance is assumed

to be varying as $L(t) = L_0(1 + 2\Gamma \sin 2\tau - \beta I^2)$, is[24]

$$\frac{d^2I}{d\tau^2} + \delta \frac{dI}{d\tau} + (1 + \alpha)(1 - 2\Gamma \sin 2\tau + \beta I^2)\, I = 0 \qquad (3.216)$$

where $\tau = \omega t, \omega_0 = (L_0 C)^{-\frac{1}{2}}, \alpha = (\frac{\omega_0}{\omega})^2 - 1, \delta = \frac{1}{\omega CR}$ and $I = \frac{L}{L_0} i$ (see Figure 3.42).

The square of the steady-state amplitude of oscillations is found[24] to be

$$u_0^{\,2} = \frac{4\Gamma}{3\beta}(\sqrt{1 - a^2} + b) \qquad \ldots\ldots \qquad (3.217)$$

where $a = \frac{\delta}{\Gamma(1 + \alpha)}$ and $b = -\frac{\alpha}{\Gamma(1 + \alpha)}$. Comparing equations (3.215) and (3.216), one may note the correspondence between the parameters of the two equations, with the transformation $z = \tau + \frac{\pi}{4}$ which does not change the nature of the differential equation. The parameters of equation (3.215) may be expressed in terms of those of equation (3.216) as

$$\begin{aligned} 2\eta &= \delta \\ a &= 1 + \alpha \\ q &= \Gamma(1 + \alpha) \\ \text{and} \quad g &= \beta(1 + \alpha) \end{aligned} \qquad \ldots\ldots \qquad (3.218)$$

When these are substituted into equation (3.217), this takes the form

$$u_0^{\,2} = \frac{4}{3g}\left(1 - a + \sqrt{q^2 - 4\eta^2}\right) \qquad \ldots\ldots \qquad (3.219)$$

and comparing equation (3.219) with equation (3.193) shows that the result obtained by the averaging method is almost exactly the same as that obtained in Section 3.5. The final phase of the steady-state oscillations, θ_0, is found[24] to be given by

$$\sin 2\,\theta_0 = \sqrt{1 - a^2}$$

and $$\cos 2\,\theta_0 = -a$$

where $a = \frac{\delta}{\Gamma(1 + \alpha)}$. By making use of equations (3.218), the steady-state phase is obtained in terms of the parameters of equations (3.215) as

$$\tan 2\,\theta_0 = -\frac{1}{2\eta}\sqrt{q^2 - 4\eta^2} \qquad \ldots\ldots \qquad (3.220)$$

It follows from equation (3.219) that $\sqrt{q^2 - 4\eta^2} = \frac{3}{4} g\, u_0^{\,2} + a - 1$, and when this is substituted in equation (3.220), the steady-state phase is given by

$$2\theta_0 = \tan^{-1}\left(-\frac{a - 1 + \frac{3g}{4}u_0^2}{2\eta}\right) \qquad \ldots\ldots \qquad (3.221)$$

which is almost the same as equation (3.194). In fact, the results obtained in Section 3.5 are more accurate than those obtained by the averaging method, as equations (3.193) and (3.194) contain additional terms which are absent in equations (3.219) and (3.221).

For no load, $\eta = 0$, and the steady-state phase from equation (3.221) is $\theta_0 = -\frac{\pi}{4}$. This is almost evident in the phase-portrait of Figure 3.41. However, σ of equation (3.194) is equal to $\theta_0 + \frac{\pi}{4}$, because of the transformation of the independent variable, $z = \tau + \frac{\pi}{4}$, made to have equations (3.215) and (3.216) appearing similar. Since $\theta_0 \simeq \frac{\pi}{4}$, σ of equation (3.194) is approximately equal to $2\theta_0$ of equation (3.221).

Minorsky[21] studies the differential equation

$$\frac{d^2x}{dz^2} + b\frac{dx}{dz} + (1 + a\cos 2z)x + c\,x^3 = 0$$

by his stroboscopic method, and gives results similar to those already obtained. The square of the stationary amplitude is

$$\rho_0 = \frac{2}{3C}\sqrt{A^2 - 4B^2}$$

and the steady-state phase is

$$\sin 2\theta_0 = -\frac{2B}{A} \qquad \text{and} \qquad \cos 2\theta_0 = -\frac{3}{2}\frac{C\rho_0}{A}$$

where $A = \frac{a}{\mu}$, $B = \frac{b}{\mu}$, $C = \frac{c}{\mu}$ and μ is the small, positive constant of equations (3.214). The results Minorsky obtained do not allow detuning to be considered, since in all the Mathieu type equations he studied the characteristic number (the constant part of the coefficient of x) is taken as unity. However, he also gives the results of the asymptotic method (Krylov-Bogoliubov-Mitropolsky) applied to the differential equation[25].

$$\frac{d^2x}{dt^2} + 2\delta \frac{dx}{dt} + \omega^2(1 - h \cos \nu t)x + \gamma x^3 = 0 \qquad (3.222)$$

which assumes the first-order approximate solution of the form

$$x = a \cos \left(\frac{\nu}{2} t + \theta\right)$$

The square of the amplitude is found to be

$$a^2 = \frac{4}{3\gamma} \left[\left(\frac{\nu}{2}\right)^2 - \omega^2 \mp \frac{1}{2} \sqrt{h^2 \omega^4 - 4 \nu^2 \delta^2} \right] \qquad (3.223)$$

With the transformation $\nu t = 2z$, and $\frac{\nu}{2} = \omega$ (the frequency of oscillation), the parameters of equation (3.222) are expressed in terms of those of equation (3.215) as

$\omega \to \omega_0$ the resonant frequency

$$\frac{\delta}{\omega} = \eta$$

$$\frac{\omega_0^{\ 2}}{\omega^2} = a$$

$$\frac{\omega_0^{\ 2}}{\omega^2} h = 2q \qquad \ldots\ldots \quad (3.224)$$

$$\frac{\gamma}{\omega^2} = g$$

which make equation (3.222) exactly the same as equation (3.215). When parameter conversions of equations (3.224) are entered into equation (3.223), this becomes exactly the same as equation (3.219). Thus, the asymptotic method of Krylov-Bogoliubov-Mitropolsky also gives the same value for the steady-state amplitude of oscillations.

A frequency domain approach based on the method of equivalent linearization[16] may be considered to be of interest, as it enables valuable tools of the linear system theory to be used. This kind of approach also permits use of the well-known frequency-power relations formulated by Manley and Rowe,[26-28] and later generalized by Penfield.[29] Instead of representing the system under investigation by a differential equation, a linear matrix equation of the form $V = Z.I$ is used, where Z is the conversion impedance matrix.

This method is rather suitable for frequency converting networks, parametric amplifiers, modulators etc. where signals are present at several different frequencies and network equations are generally of higher order. A considerable amount of literature exists on this subject, especially on the devices operating at very high frequencies. However, an application of this linearization method to the parametron and to magnetic amplifiers has also been given in a paper by Oshima et al.[30] Since the output waveform of the parametric transformer is almost sinusoidal, and the non-linearity present is quite large, linearization techniques in the frequency domain are not treated here. They are found to be not particularly suitable for the case of the parametric transformer, as they give very little insight to the modes of operation and to the physical behaviour of the device.

All the analytical methods reviewed in this section, and also the classical method used throughout this Chapter, require the system under consideration to be nearly-linear, that is the non-linearity present in the system is assumed small. Nevertheless, a new method which has recently been developed by Samoilo[31-33] does not impose such restrictions on the degree of non-linearity and the amplitude of the parameter variations. The method, termed the *phase-pulse method*[31], is basically an averaging method in which the averaged set of (autonomous) equations is in the form[35]

$$2\frac{dR}{d\tau} = V(R,\phi)$$

$$2\frac{d\phi}{d\tau} = H(R,\phi)$$

where R and ϕ are the amplitude and phase of the oscillation, but the independent variable τ is not ordinary time. τ is called *non-linear time*, and the relationship between the *non-linear time* τ and the ordinary time t is given by[34]

$$\frac{d\,t_0}{d\tau} = B_0 + B_1 \cos \tau + B \cos 2\tau + \ldots. \qquad (3.225)$$

where B_i are constants, $t_0 = \omega_0 t$ and $\omega_0 = \frac{1}{\sqrt{LC}}$, the resonant frequency of the circuit with the values L and C when there are no oscillations in the circuit.

This method has been very successfully applied to free and forced oscillations in oscillatory circuits using non-linear capacitance or non-linear inductance[34,36,37], and the behaviour of oscillations and the resonance characteristics are obtained. Application of the method to parametric circuits employing non-linear capacitance or non-linear inductance has also been made[35,37,38], and the threshold condition for parametric excitation, the amplitude/frequency characteristic of the parametric resonance, and the phase characteristics of the parametric oscillator are derived comparatively simply and with higher accuracy.

It is thought that it may prove quite interesting and well worth the effort to apply the phase-pulse method to equation (3.192), where the concept of reluctance rather than inductance is used. The complexity and difficulty in the analysis arising due to the non-linear and time-varying dissipation in R_2 may well be counteracted by the non-linear coordinate transformation of equation (3.225),

together with the fewer imposed restrictions on the magnitude of coefficients and on the degree of non-linearity.

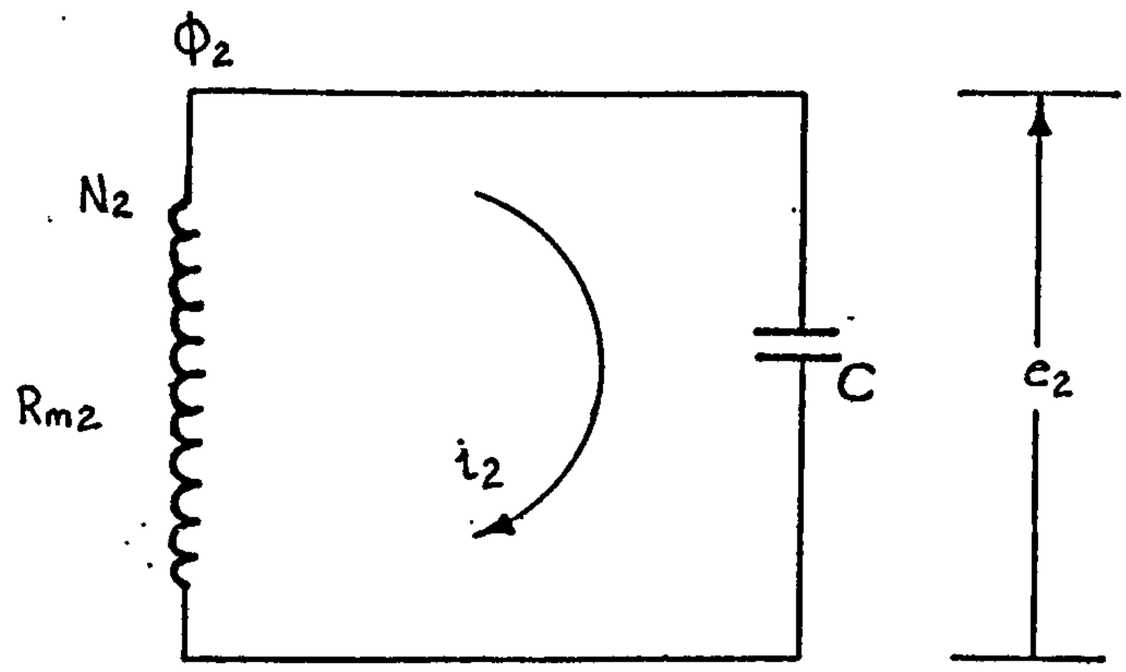

Figure 3.1 Equivalent circuit for the output side of the parametric transformer

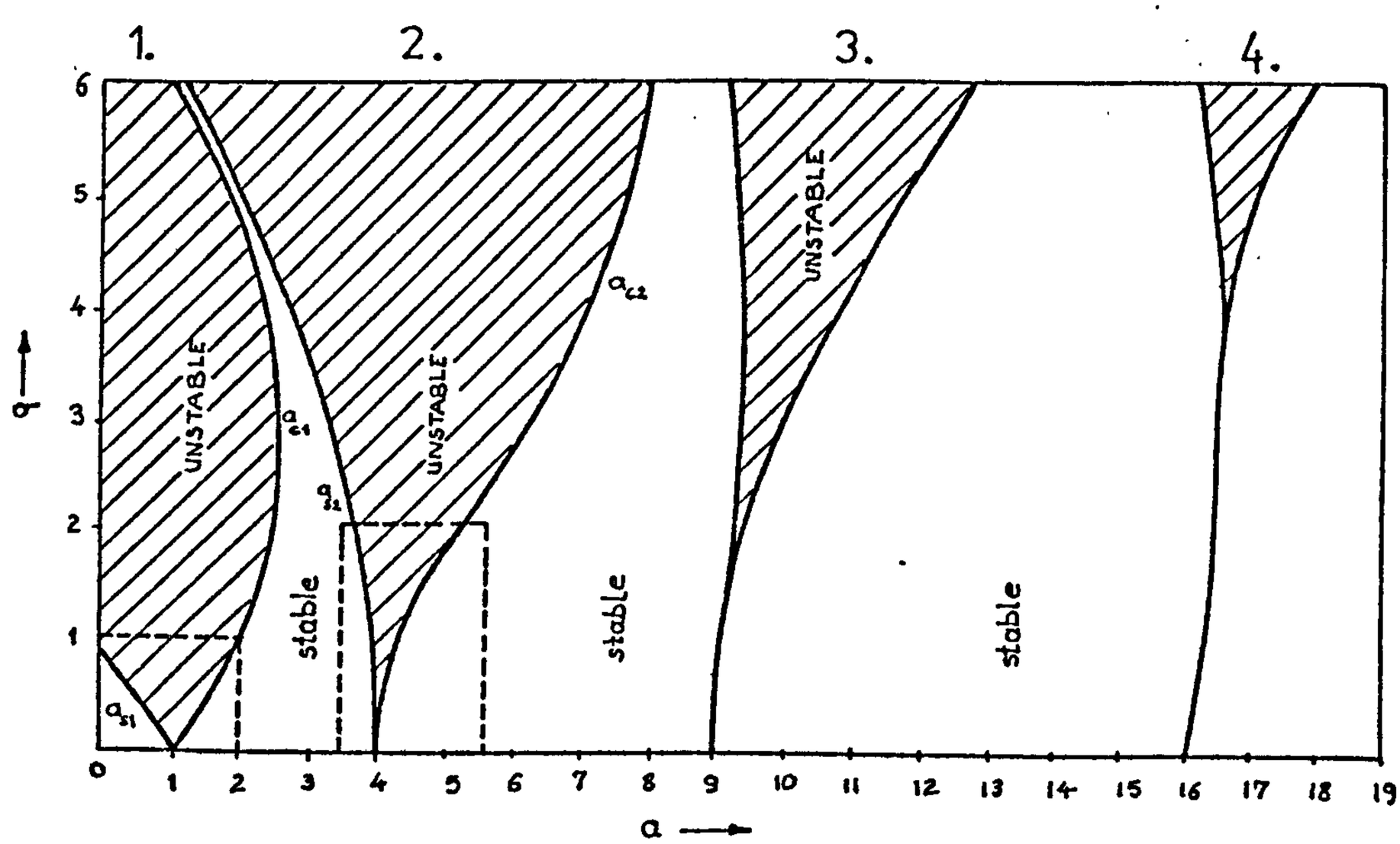

Figure 3.2 Stability chart for the Mathieu equation

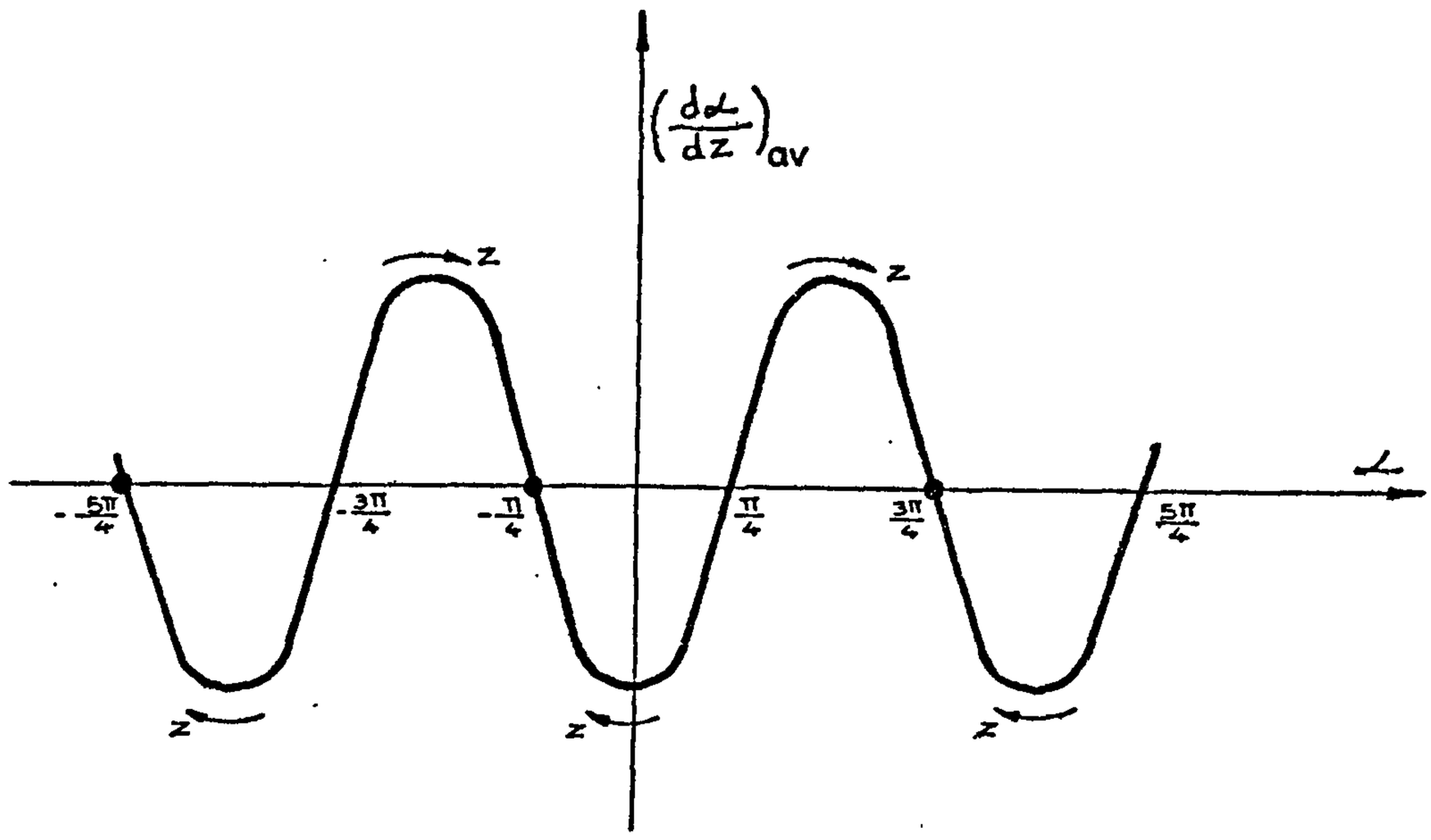

Figure 3.3 Phase-plane diagram for equation (3.19)

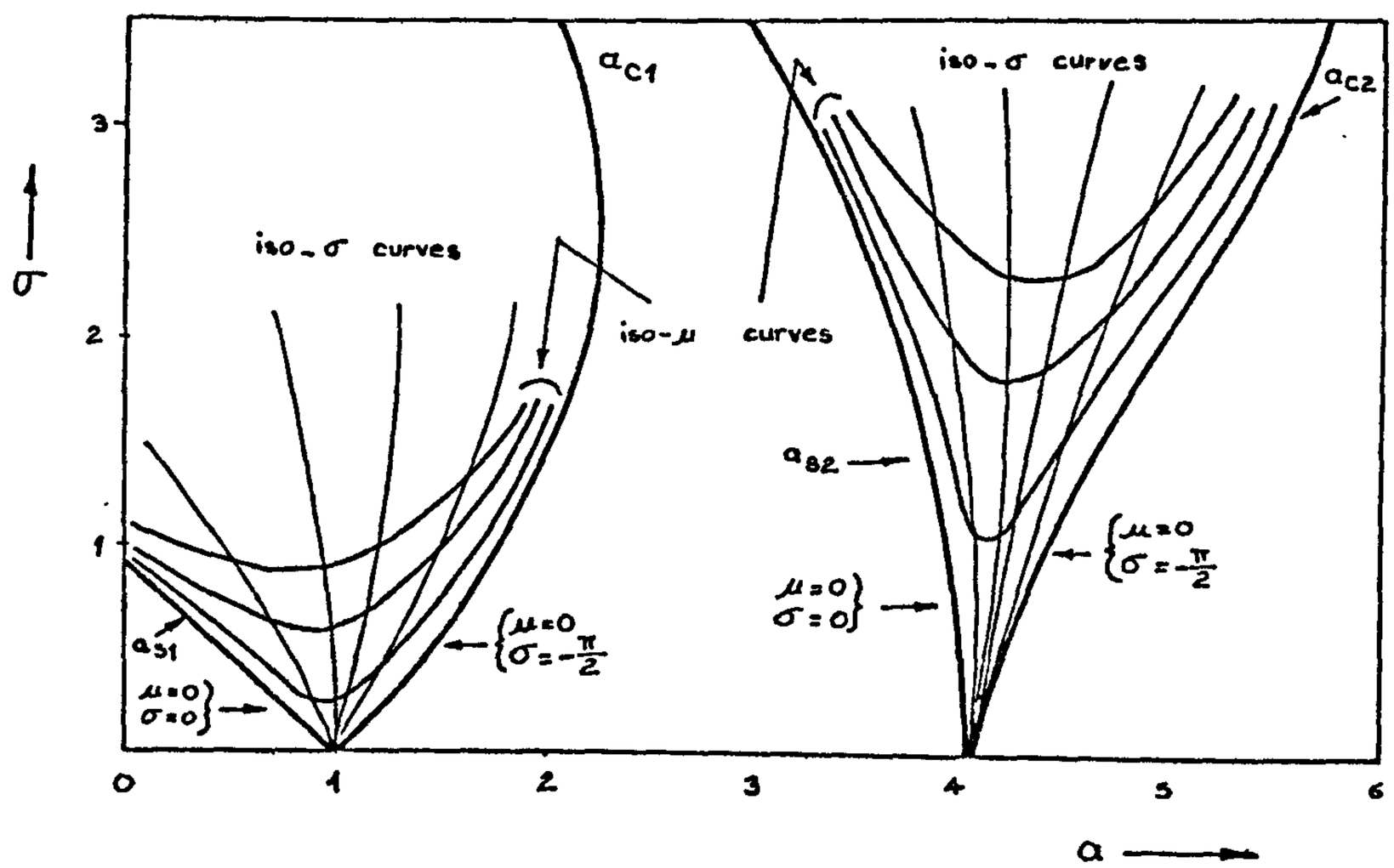

Figure 3.4 Iso-μ and Iso-σ curves in the unstable regions

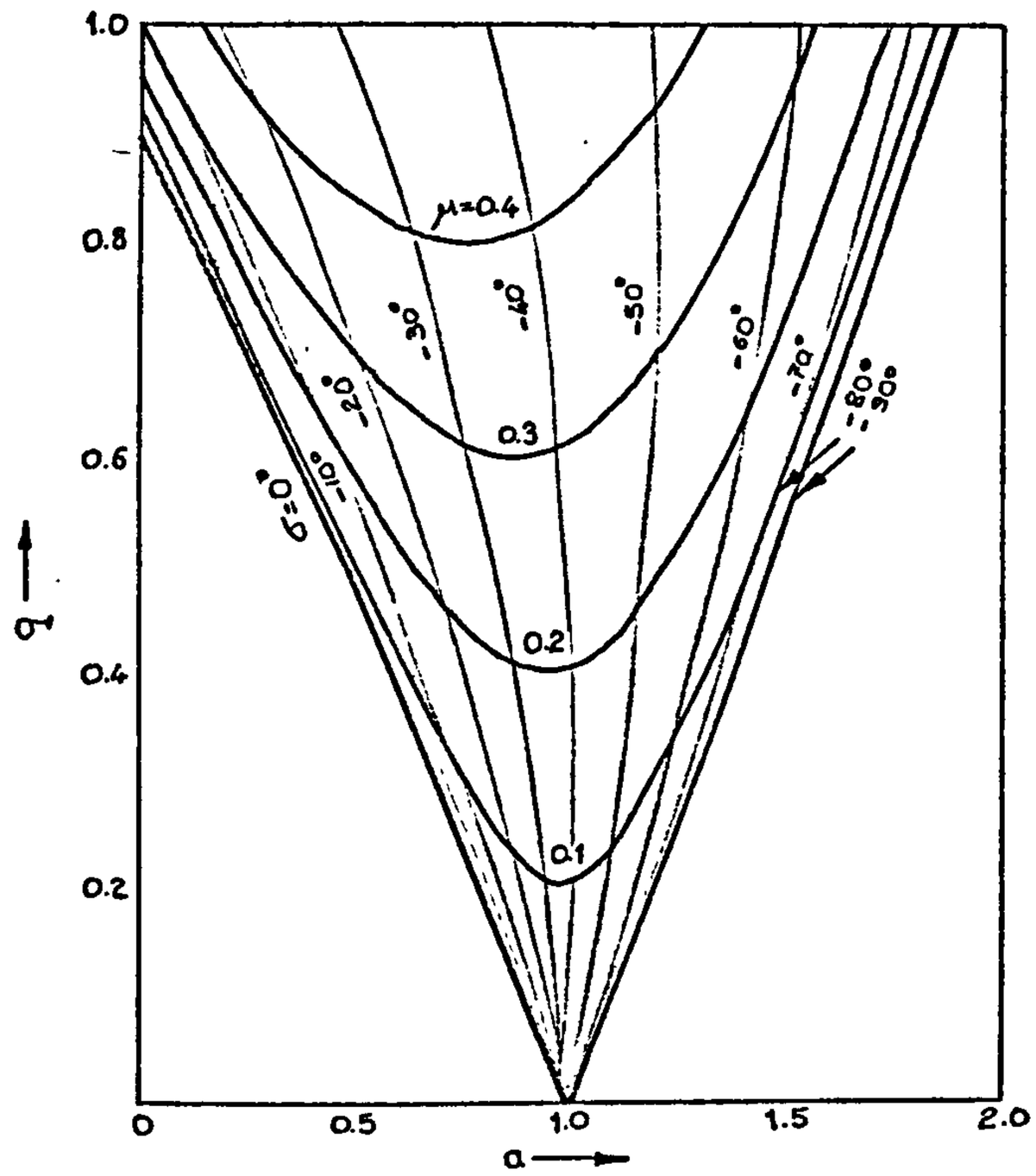

Figure 3.5 Iso-μ and Iso-σ curves in the first unstable region

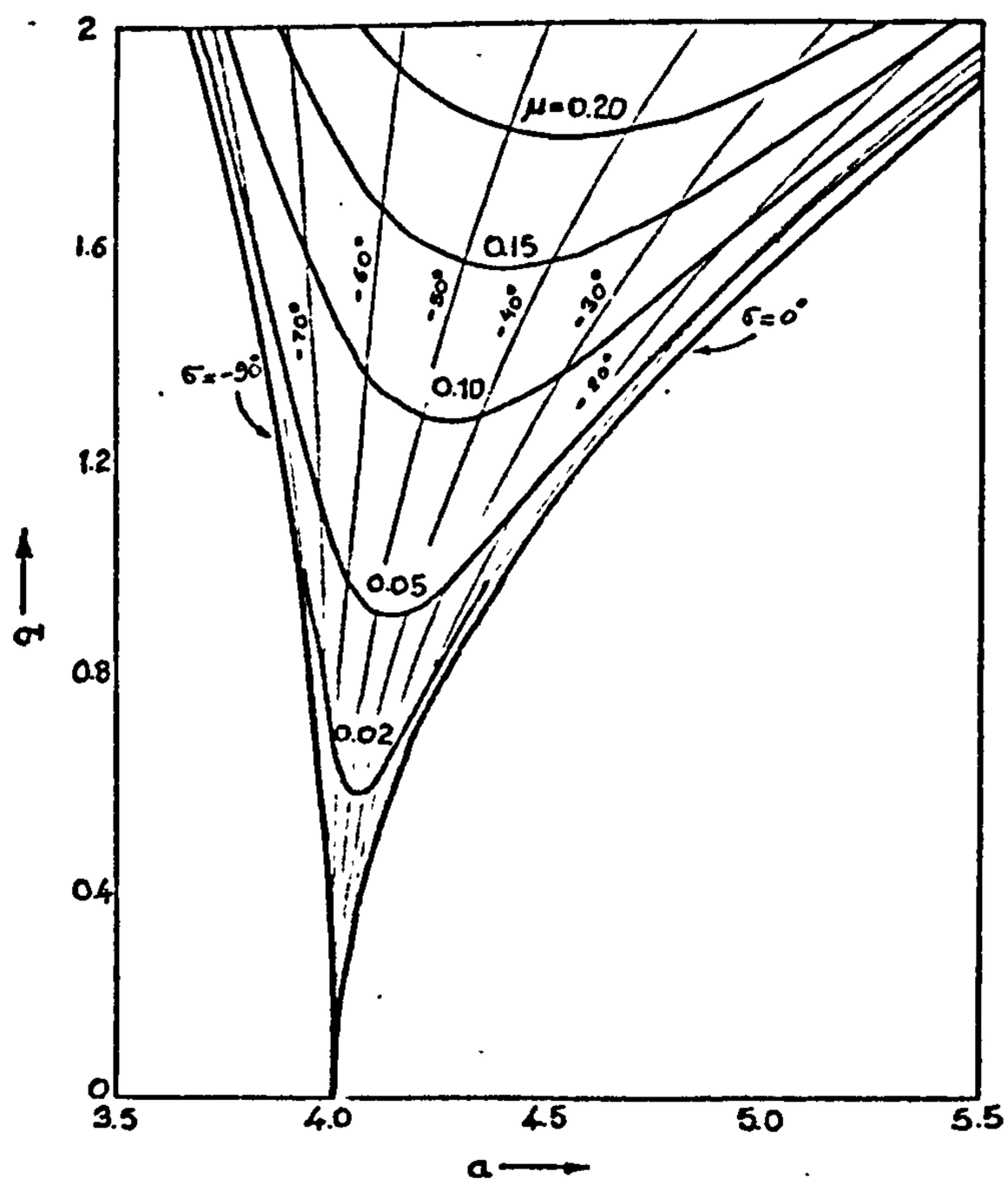

Figure 3.6 Iso-μ and Iso-σ curves in the second unstable region

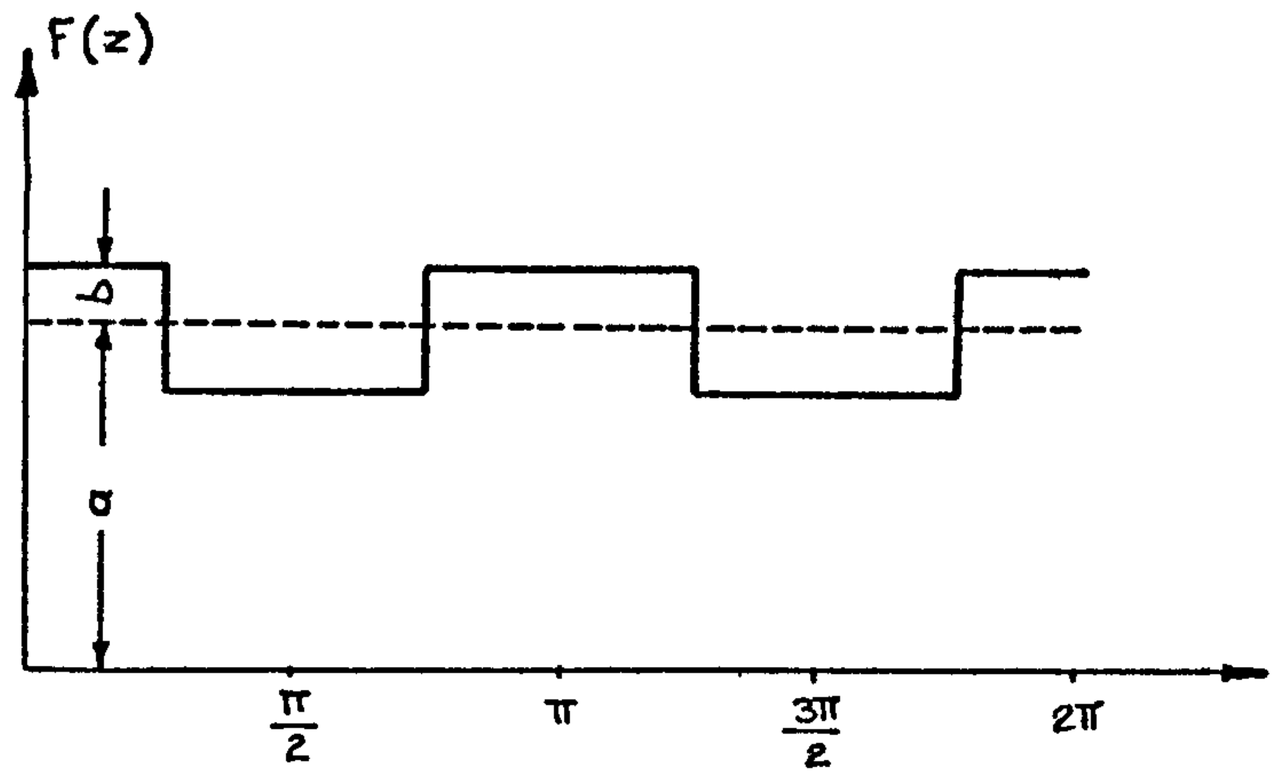

Figure 3.7 Rectangular ripple of the Hill-Meisner equation

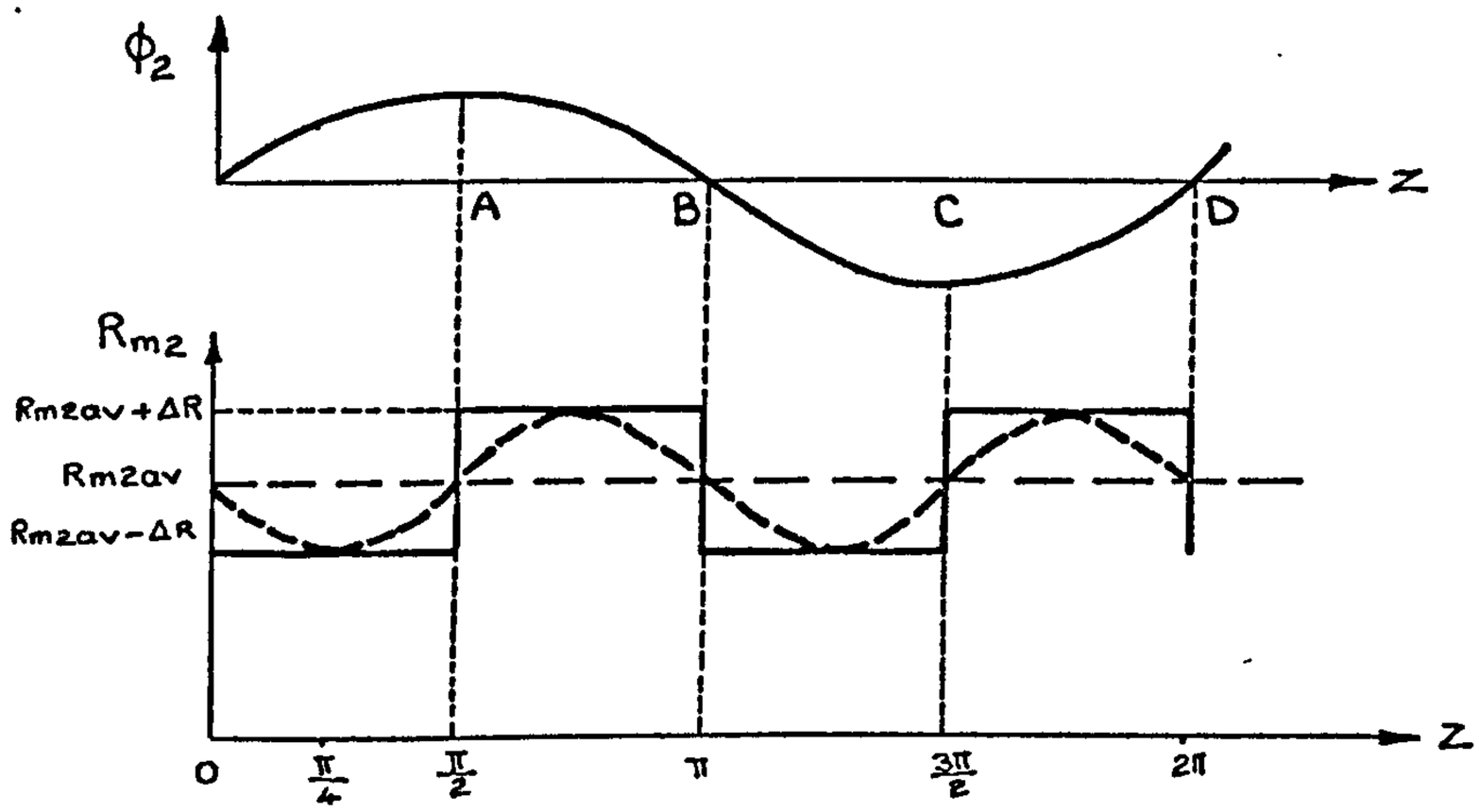

Figure 3.8 Relative positions of ϕ_2 and R_{m2}, for $\beta = 0$

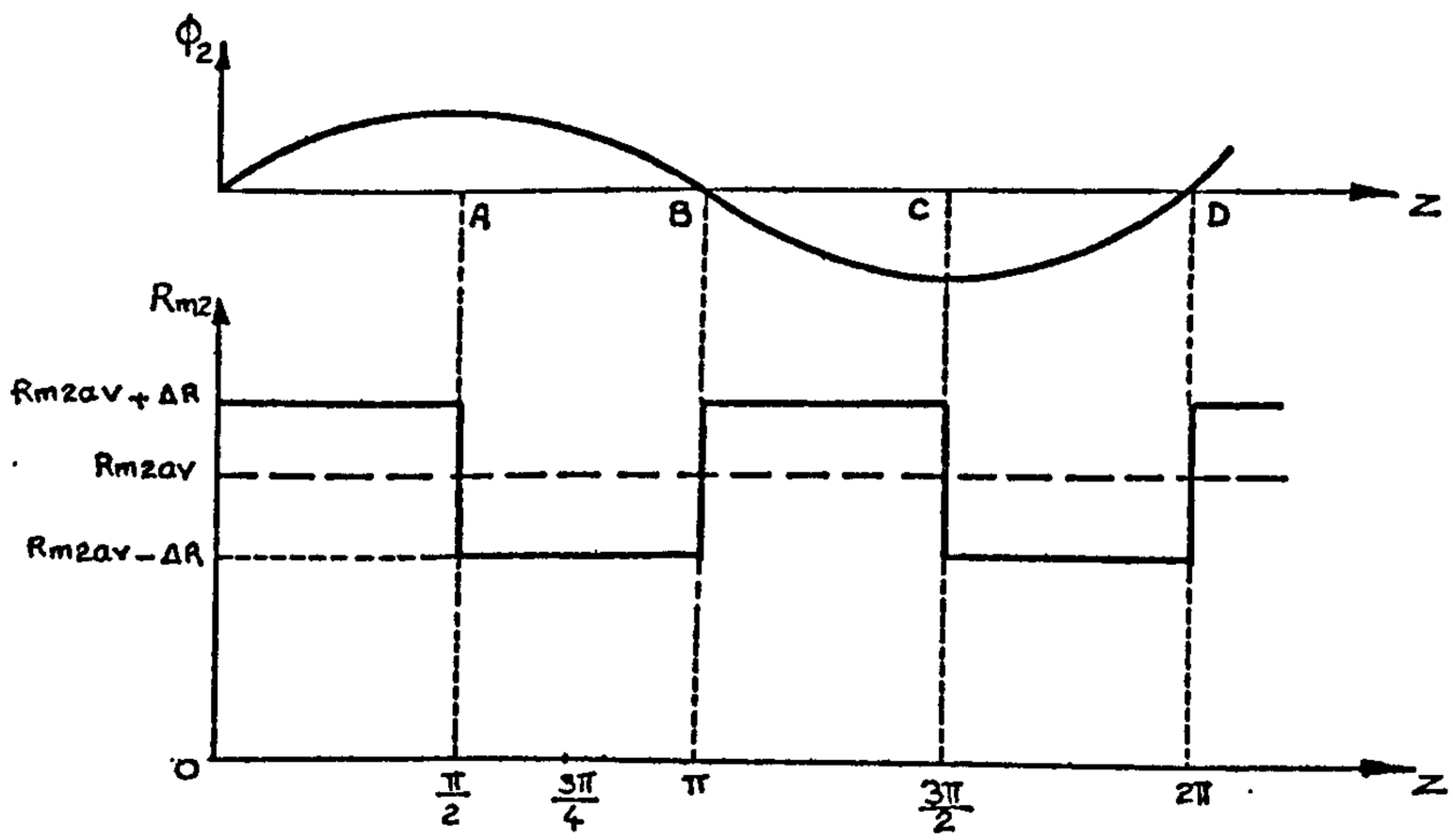

Figure 3.9 Relative positions of ϕ_2 and R_{m_2}, for $\beta = \frac{\pi}{2}$

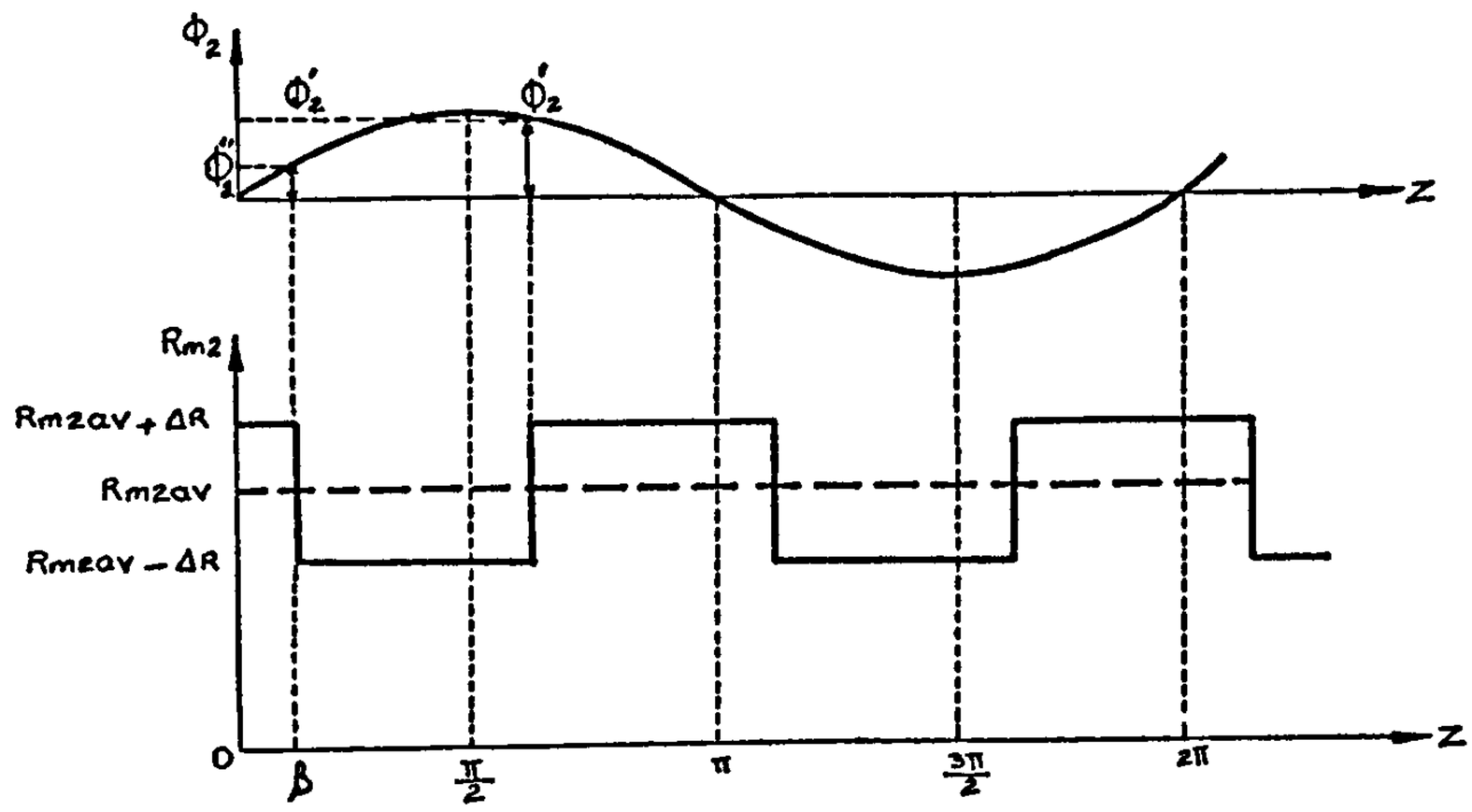

Figure 3.10 Relative positions of ϕ_2 and R_{m2}, for $0 < \beta < \frac{\pi}{2}$

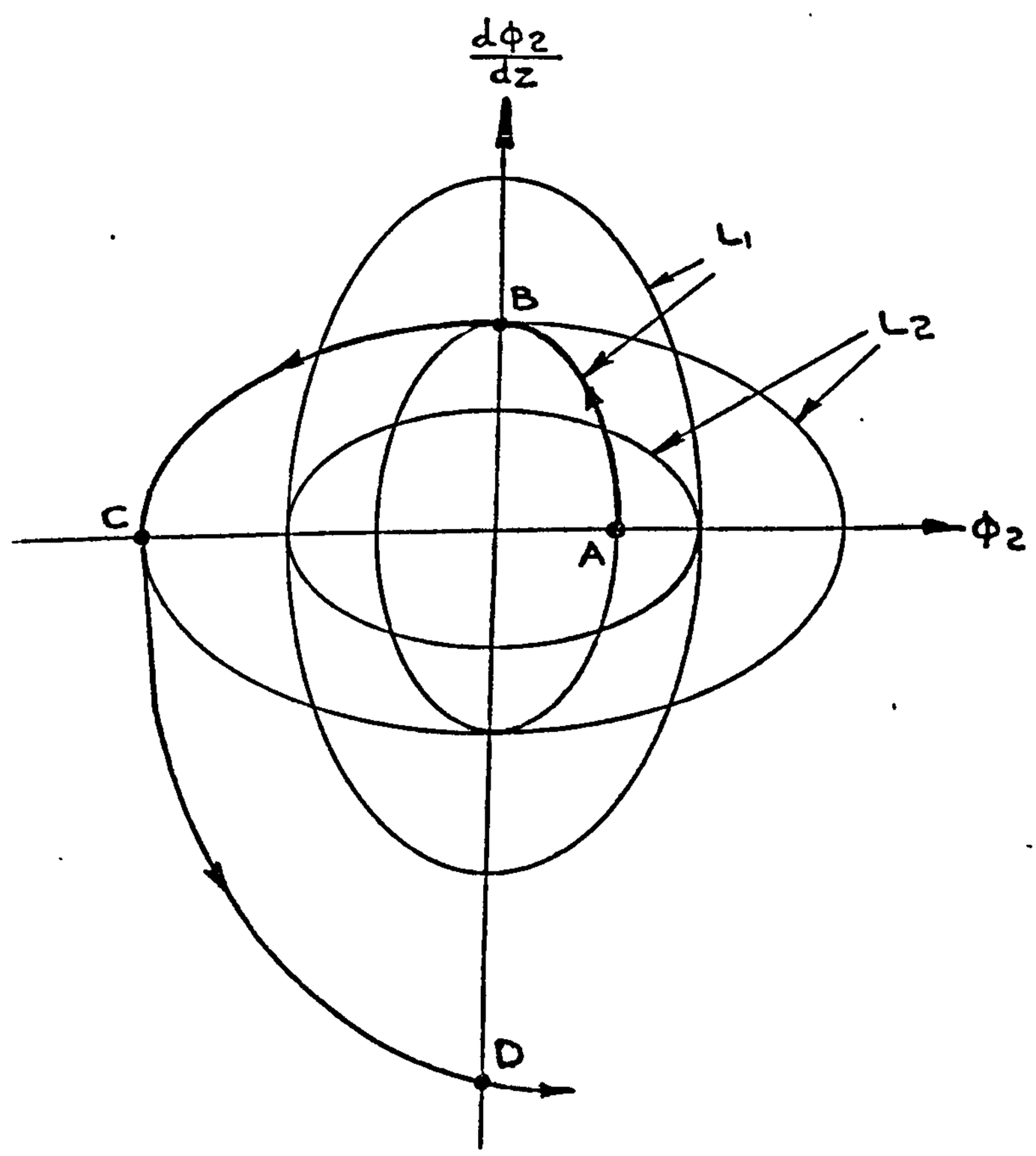

Figure 3.11 Phase-Plane Diagram for Hill-Meisner Equation with the Phase Trajectory for $\beta = 0$.

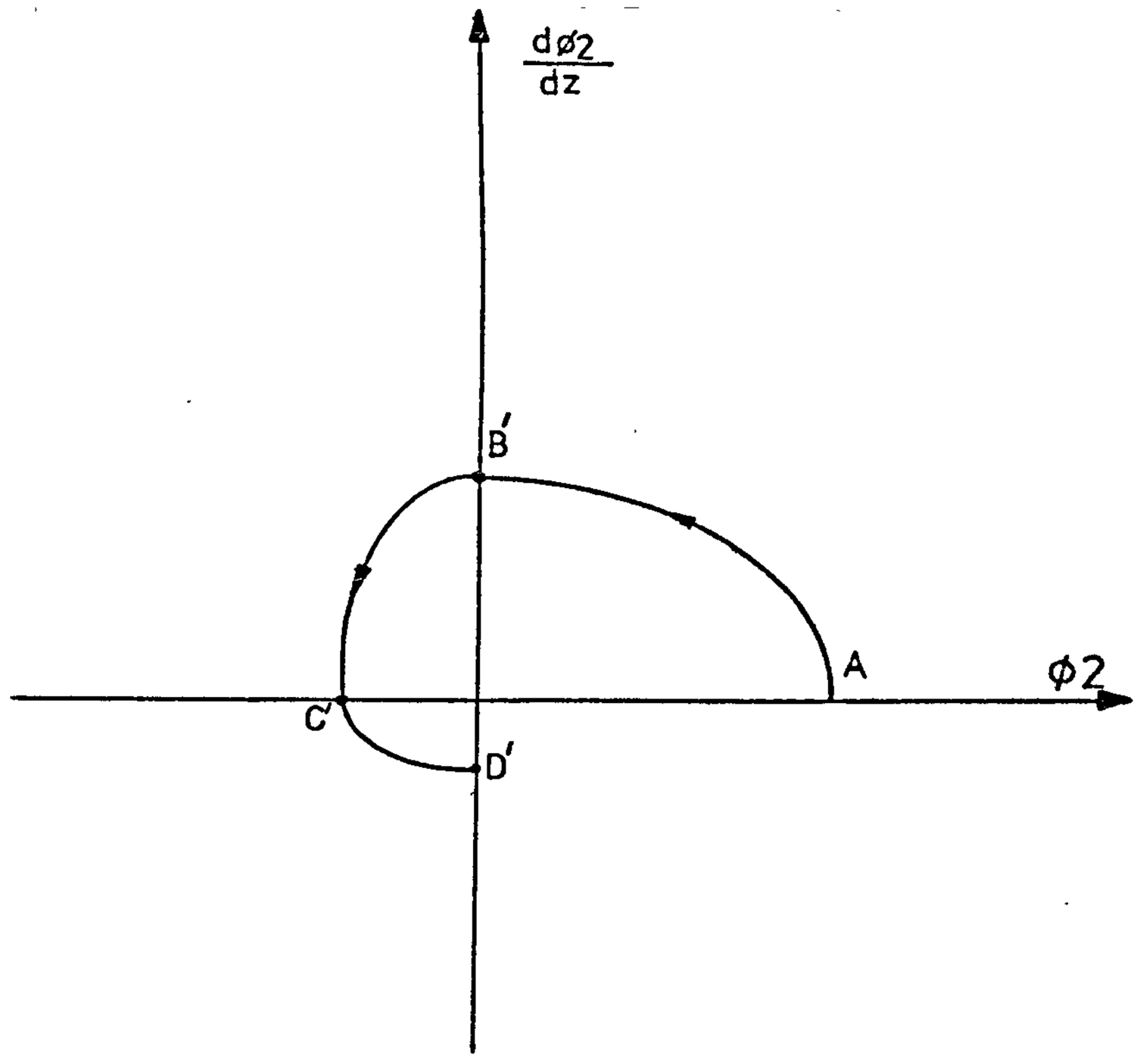

Figure 3.12 Phase Trajectory for $\beta = \pi/2$

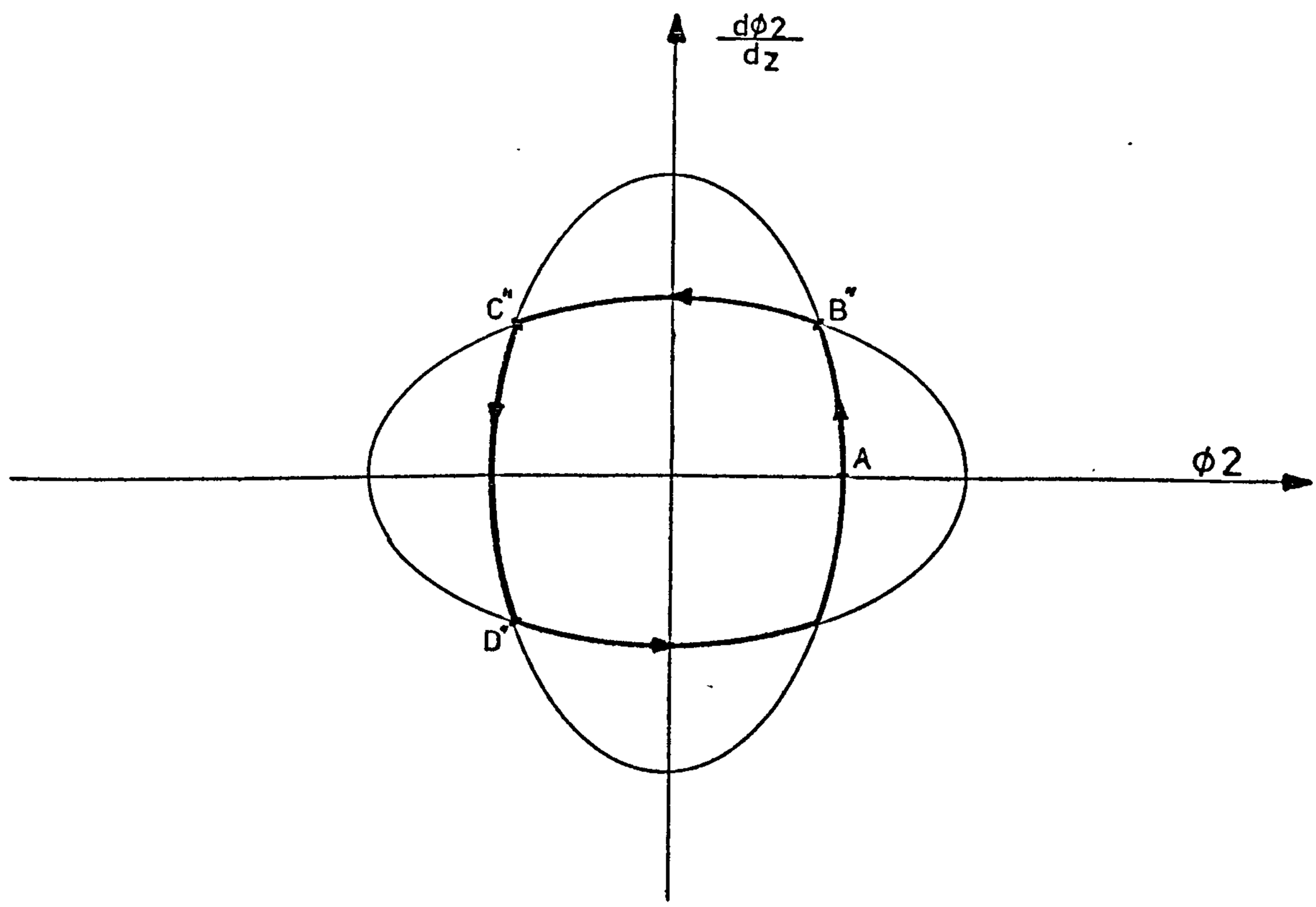

Figure 3.13 Phase Trajectory for $\beta = \pi/4$

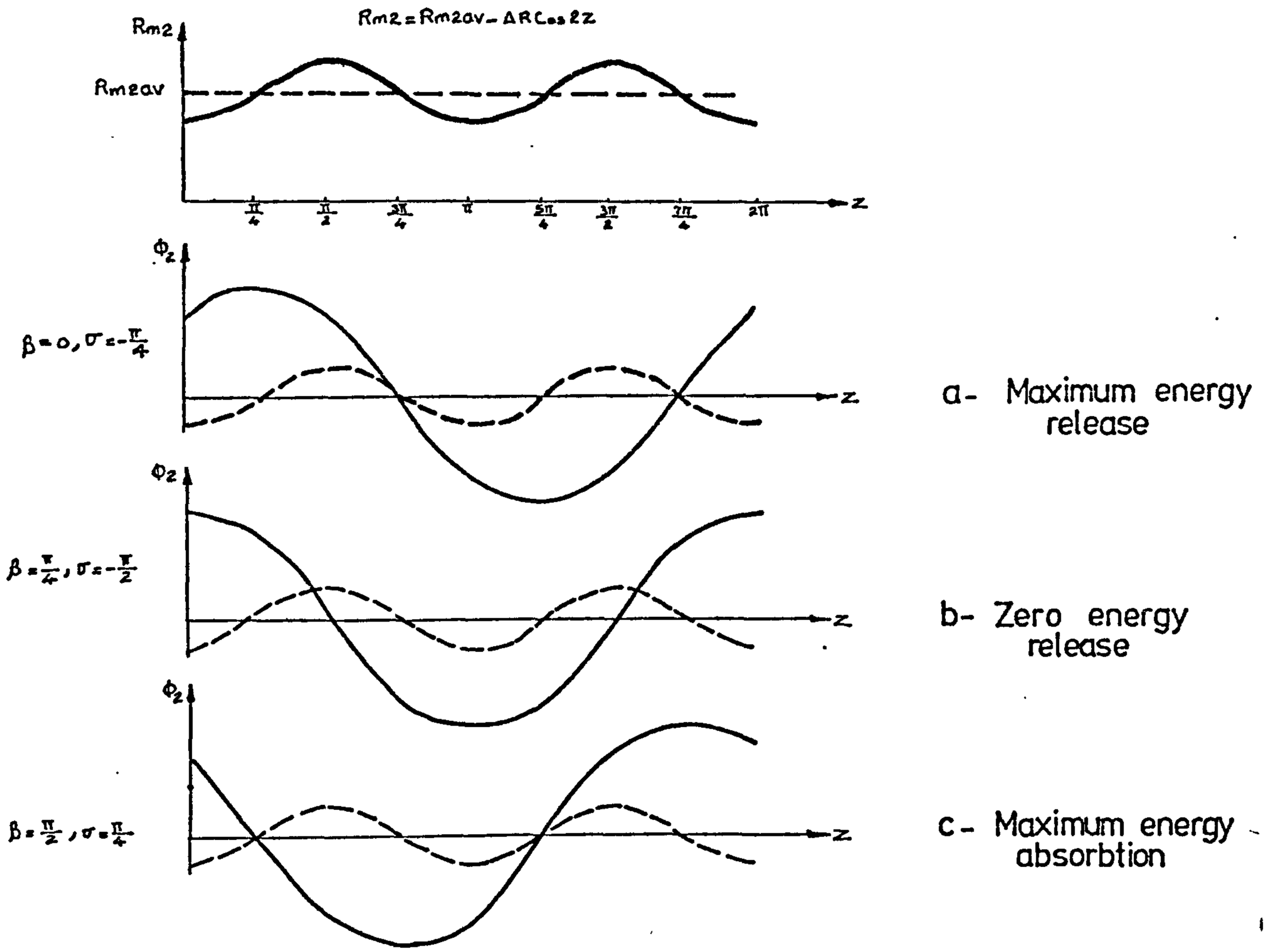

Figure 3.14 Relative positions of ϕ_2 and R_{m2} for different values of σ

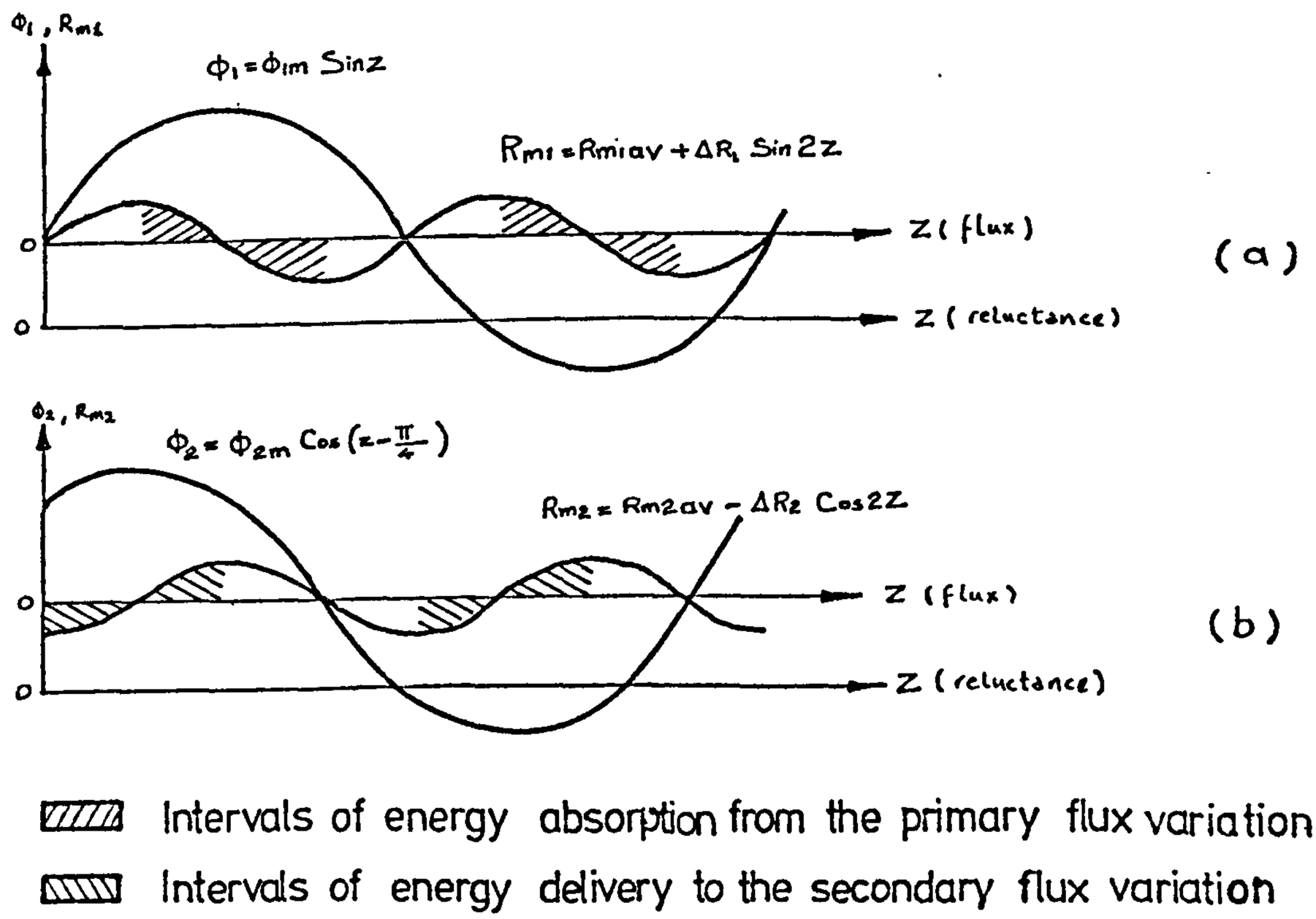

Figure 3.15 Primary and secondary flux and reluctance variations during the growth of oscillations

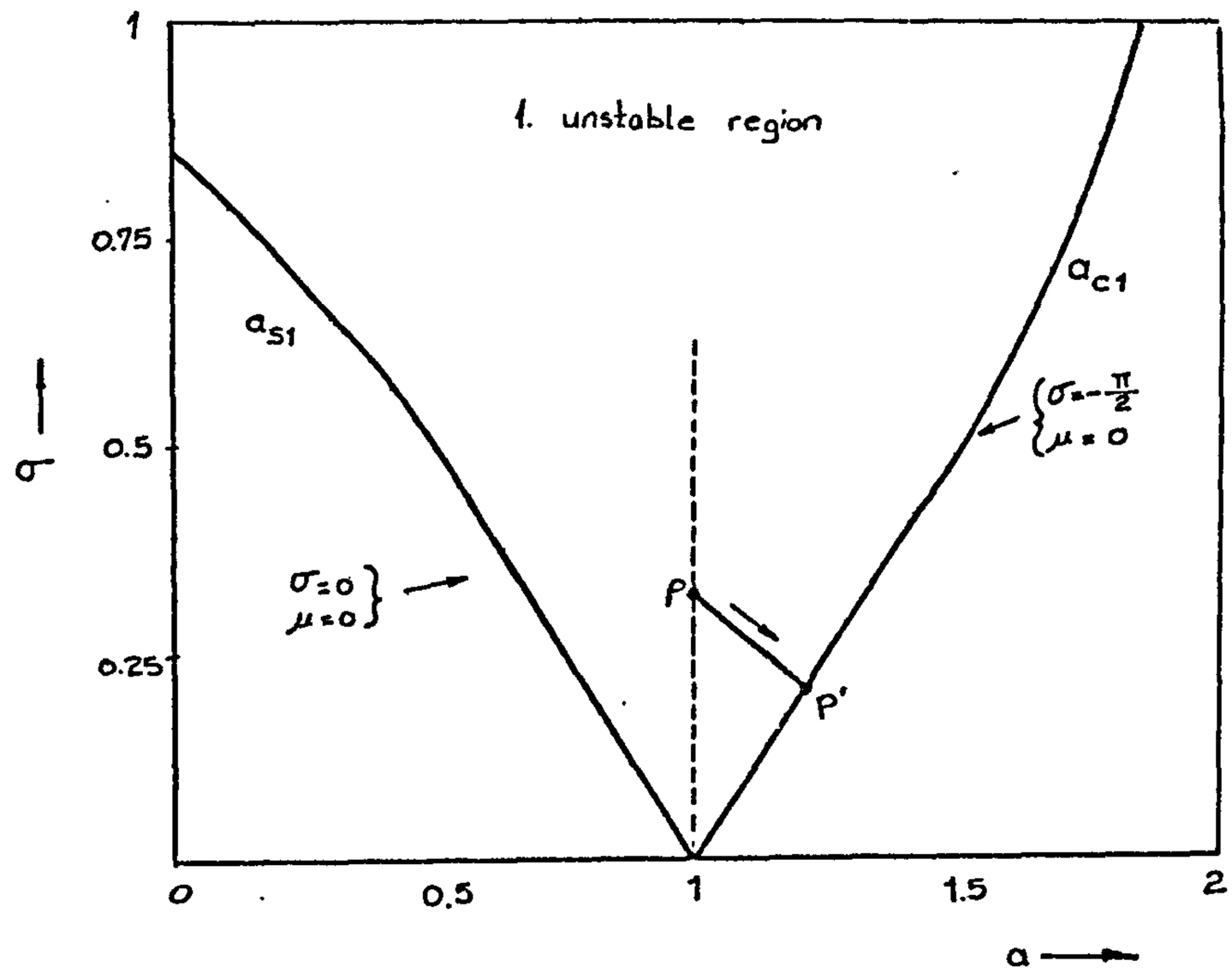

Figure 3.16 Movement of the parametric point due to non-linearity

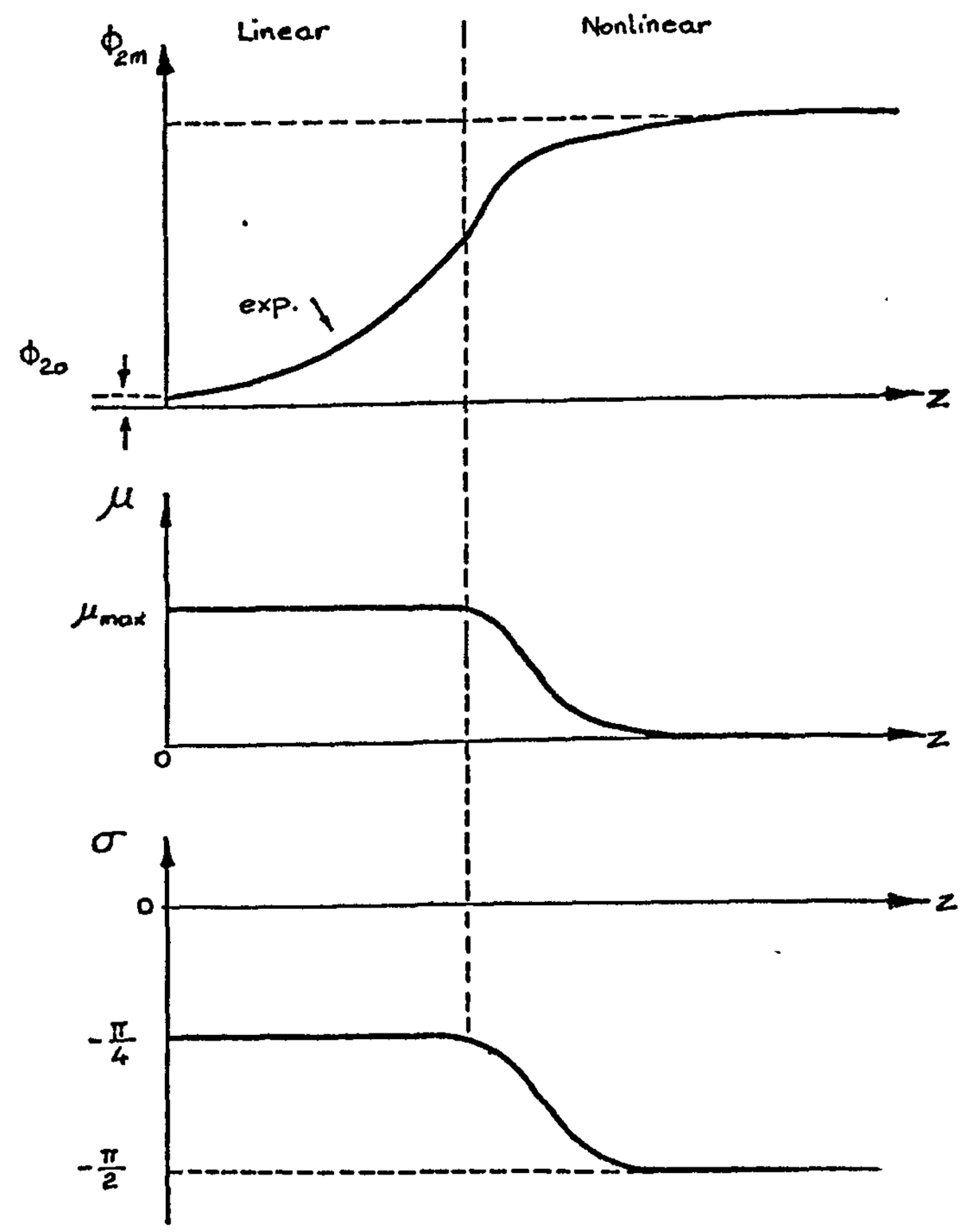

Figure 3.17 Changes in ϕ_{2m}, μ and σ during transient state

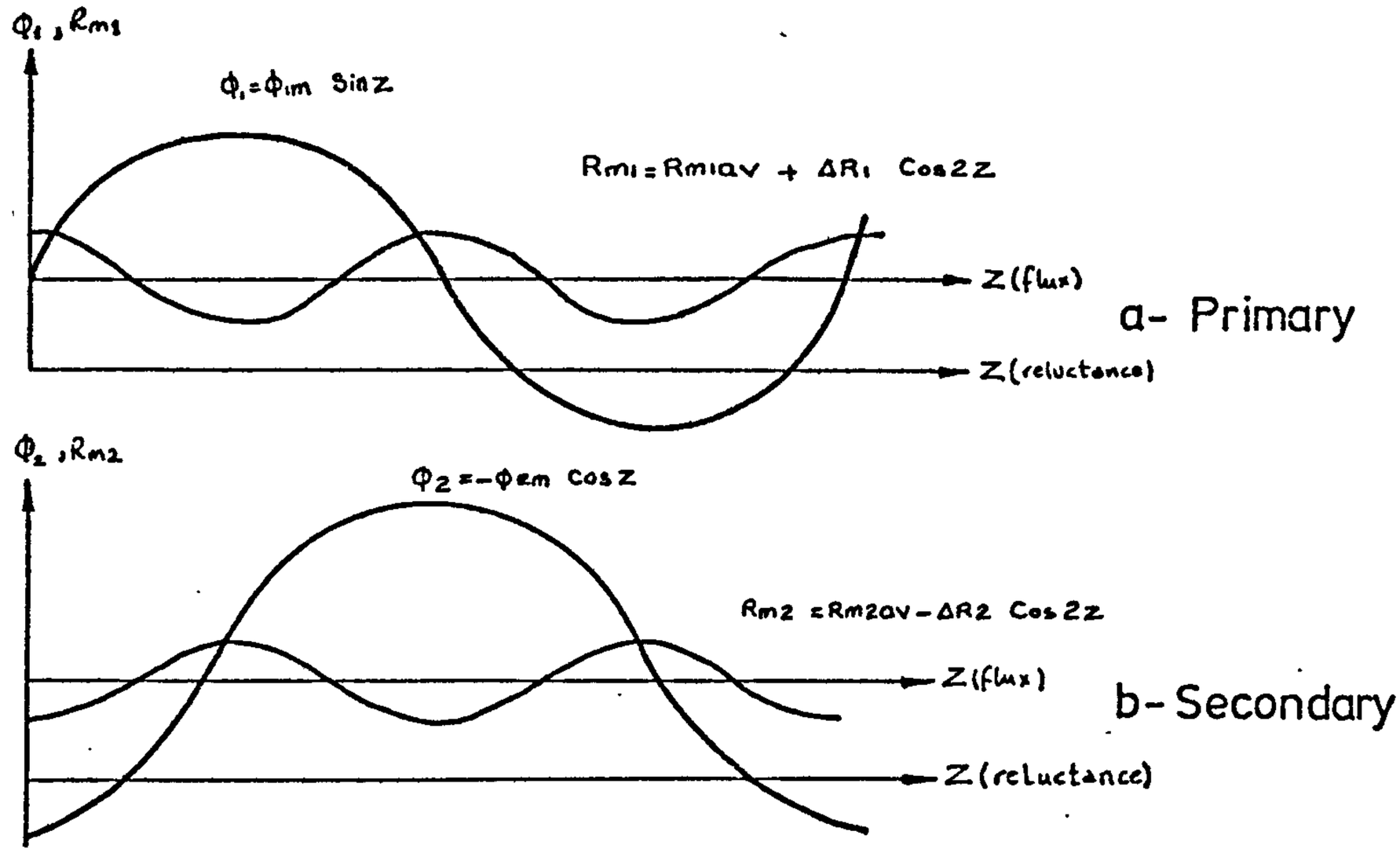

Figure 3.18 Primary and secondary flux and reluctance variations at steady state

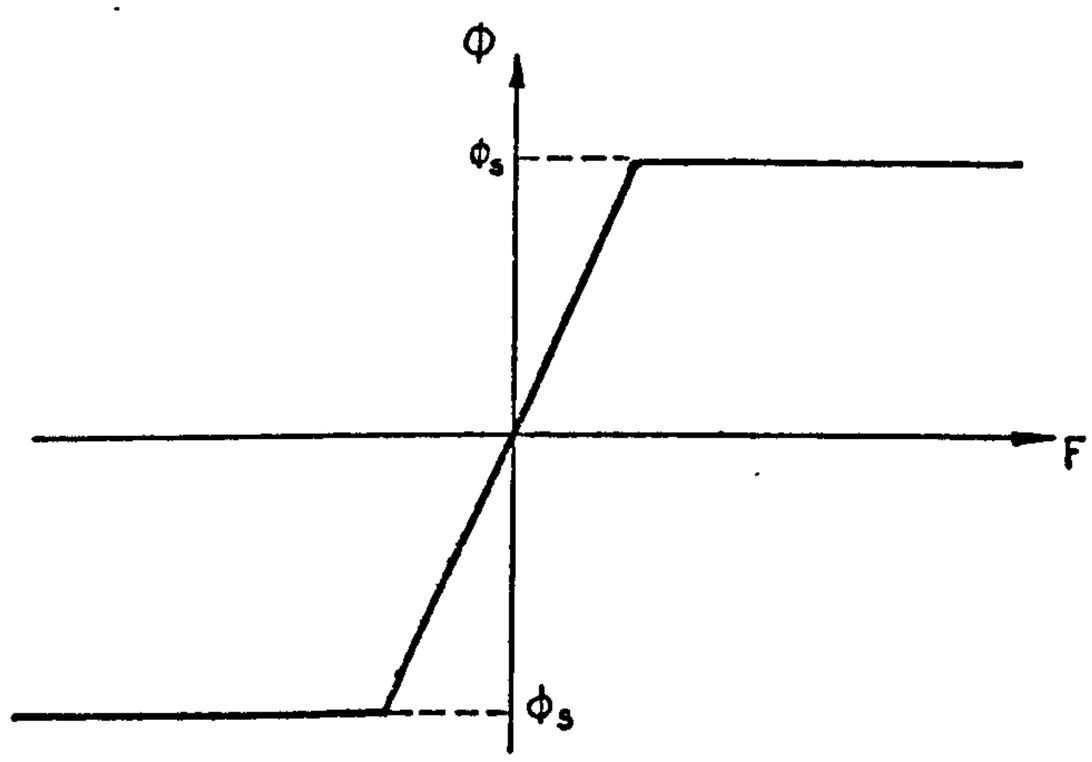

Figure 3.19 Idealized magnetisation characteristic

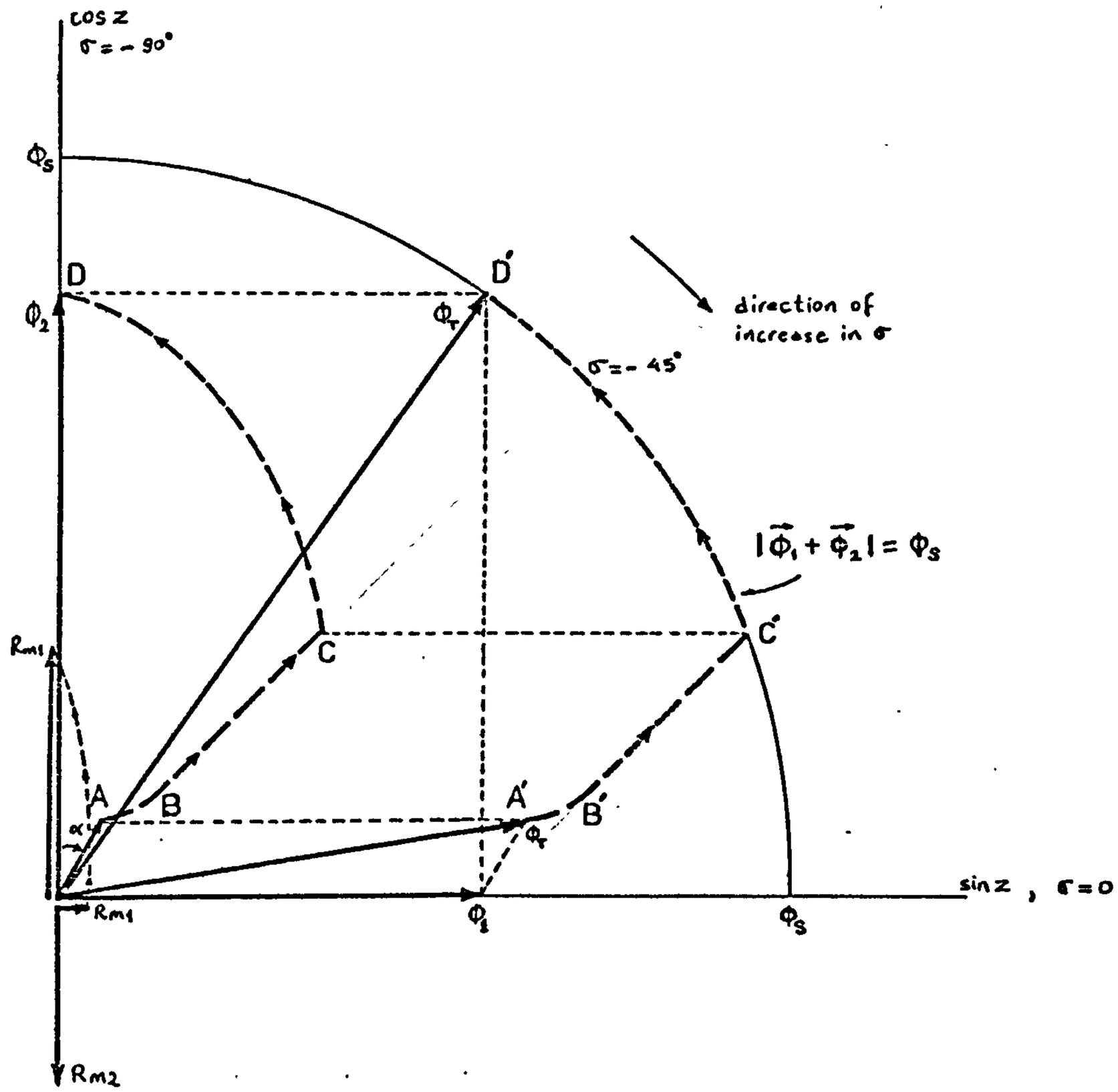

ABCD : path for secondary flux phasor

A' B' C' D': path for total flux phasor

Stages followed:

AB : Transition from initial to parametrically excited oscillation

BC : Maximum energy supply

CD : Change of secondary flux phase due to non-linearity

D : Final position of secondary flux phasor (steady-state)

Figure 3.20 Explanatory phasor diagram

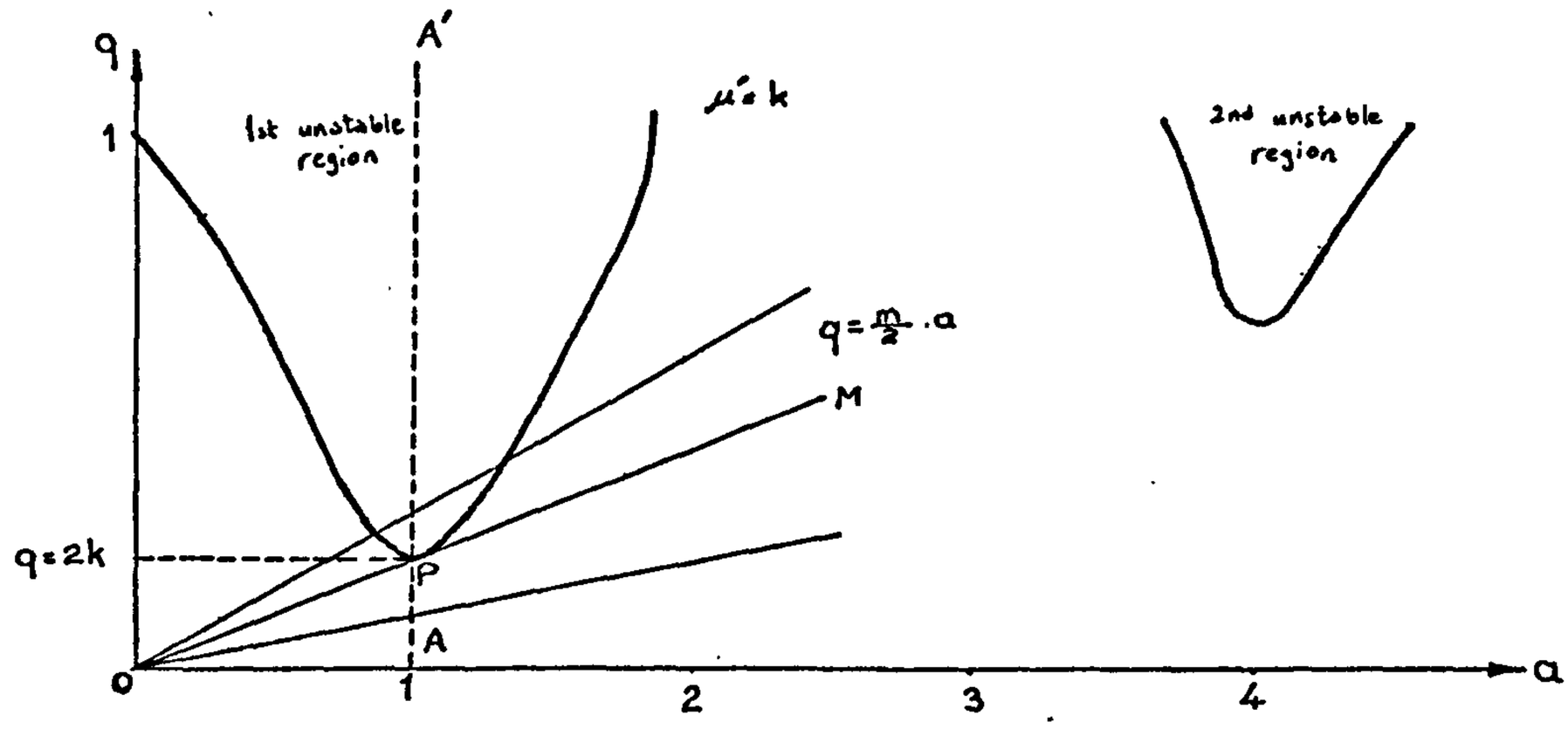

Figure 3.21 Stability chart for Equation (3.125)

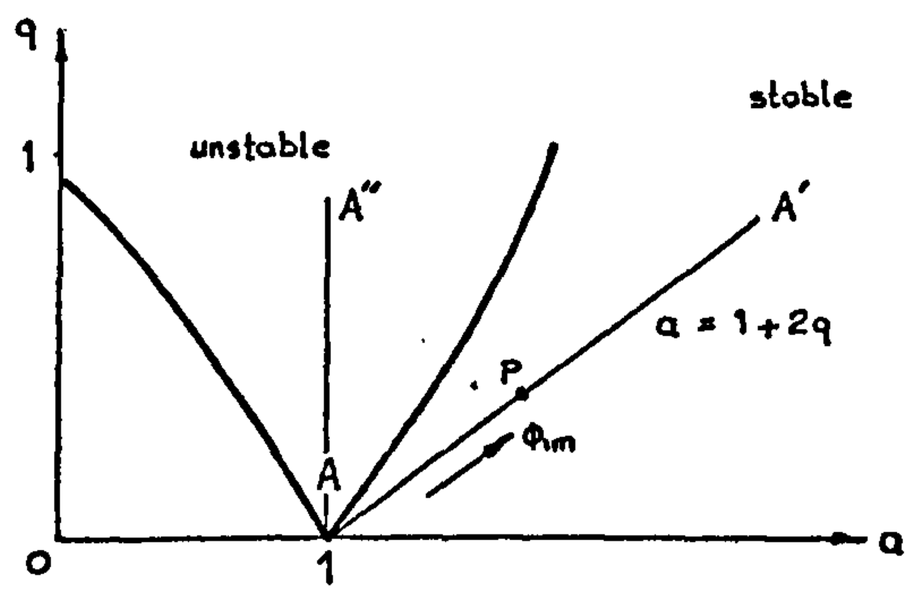

Figure 3.22 Stability chart with incorrect value of C

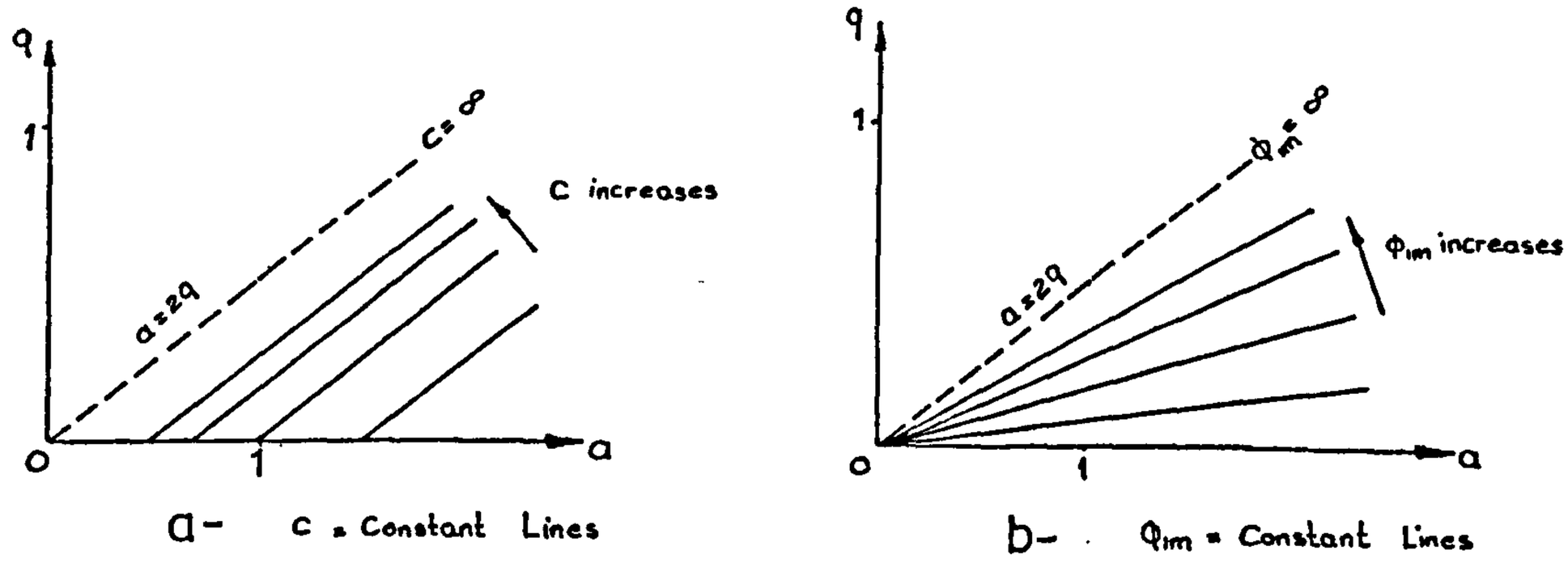

Figure 3.23 Families of constant-C and constant-ϕ_{1m} lines

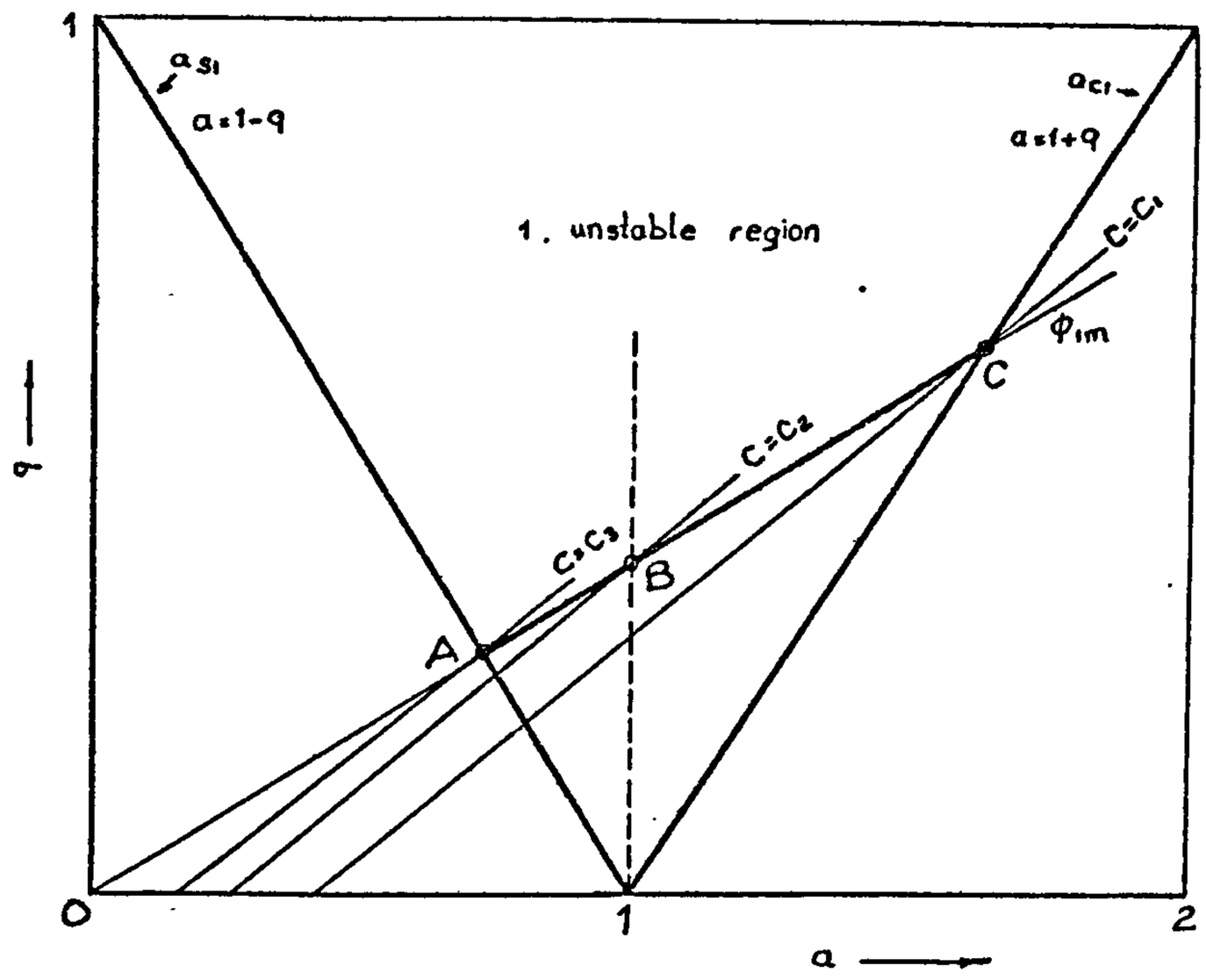

Figure 3.24 Range of tuning, non-dissipative case

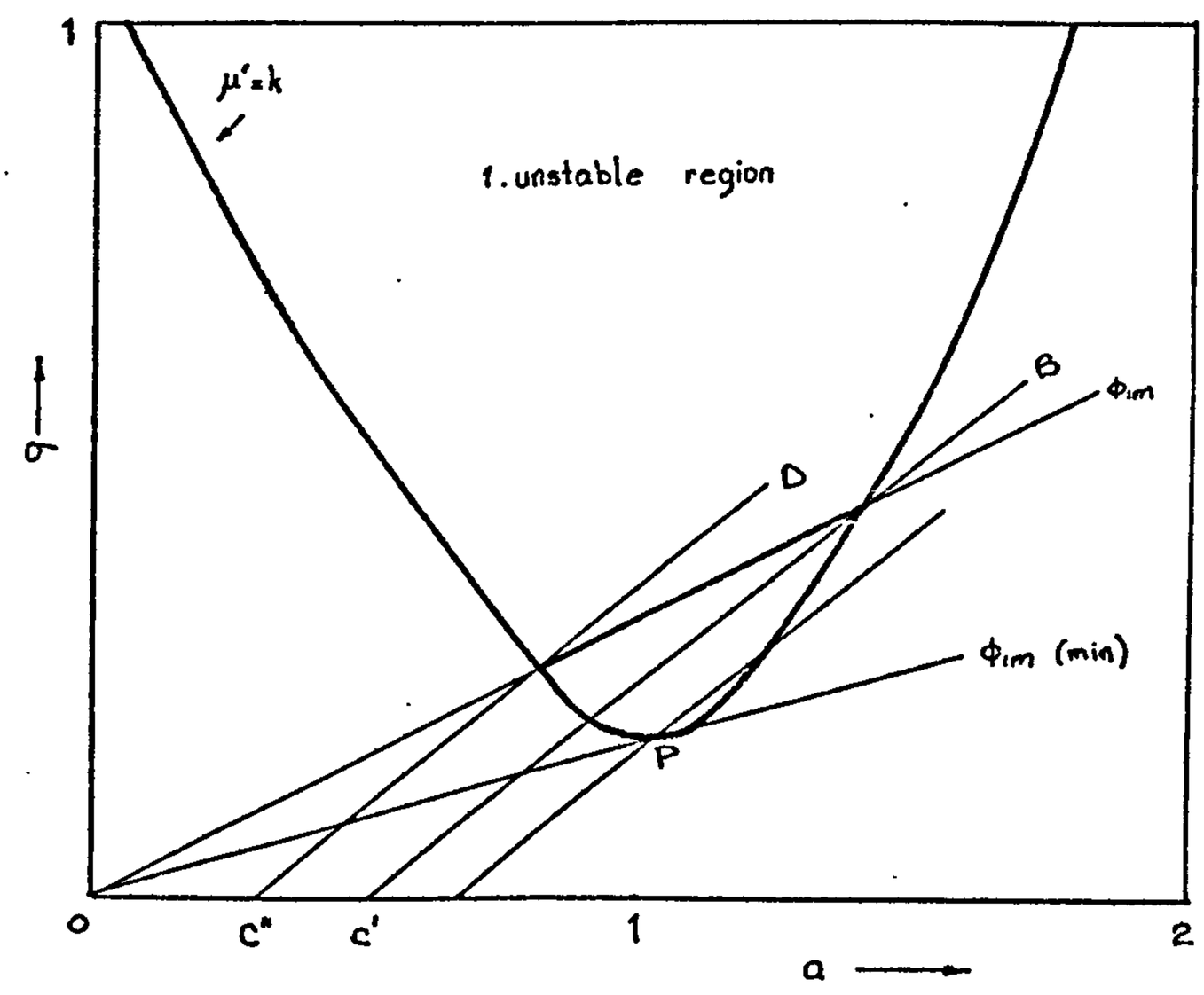

Figure 3.25 Range of tuning, dissipative case

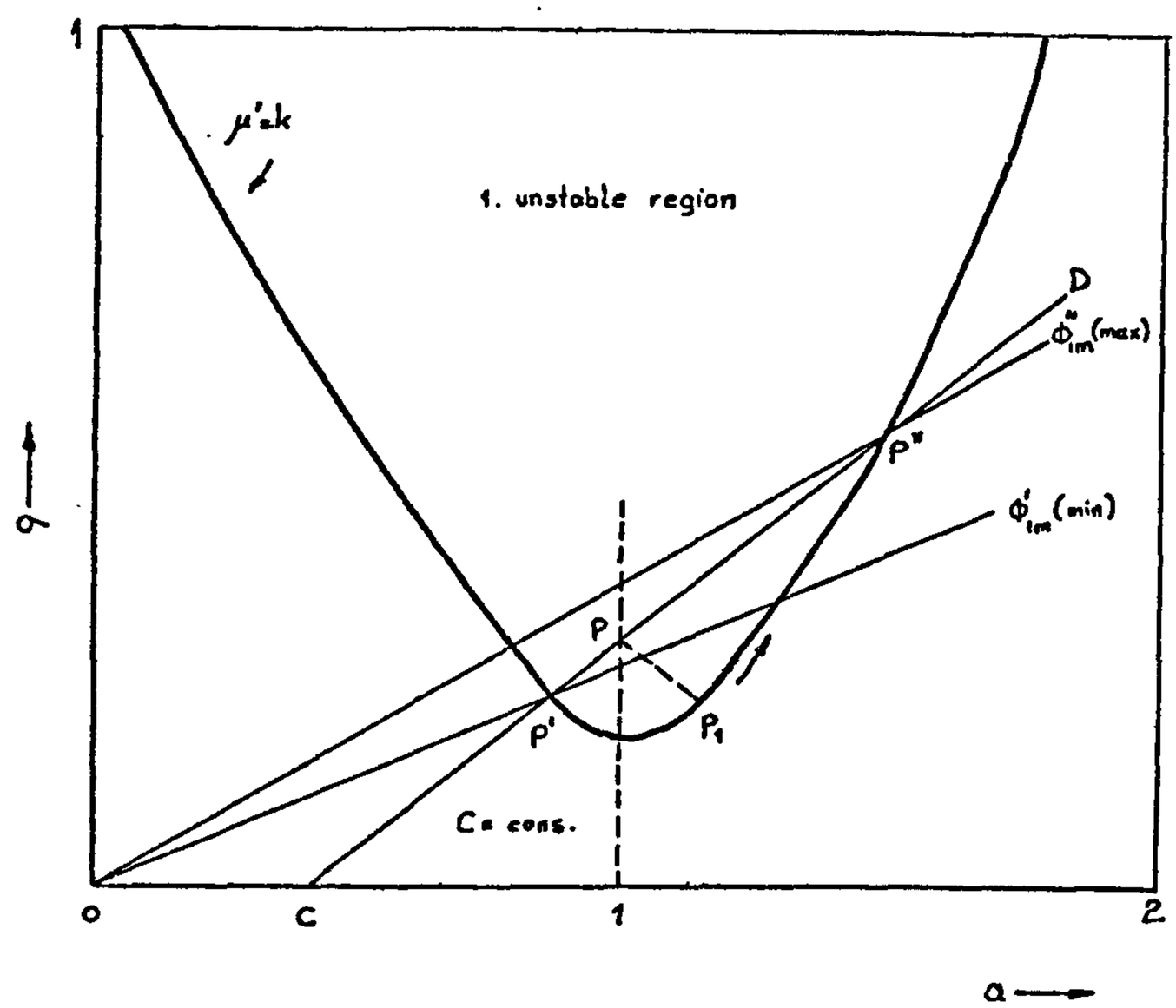

Figure 3.26 Range of ϕ_{1m} allowing parametric excitation for a fixed C, dissipative case

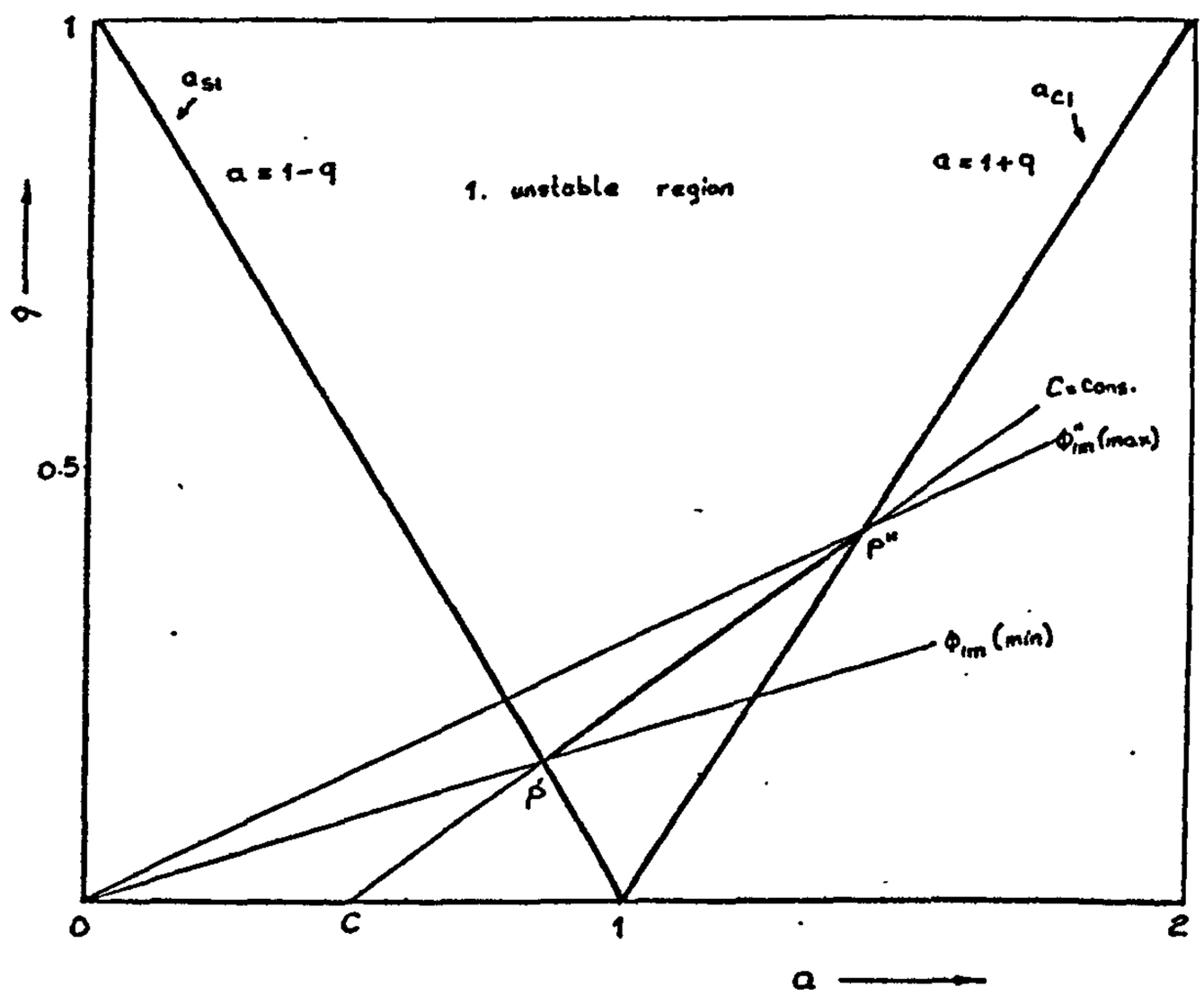

Figure 3.27 Range of ϕ_{1m} allowing parametric excitation for a fixed C, non-dissipative case

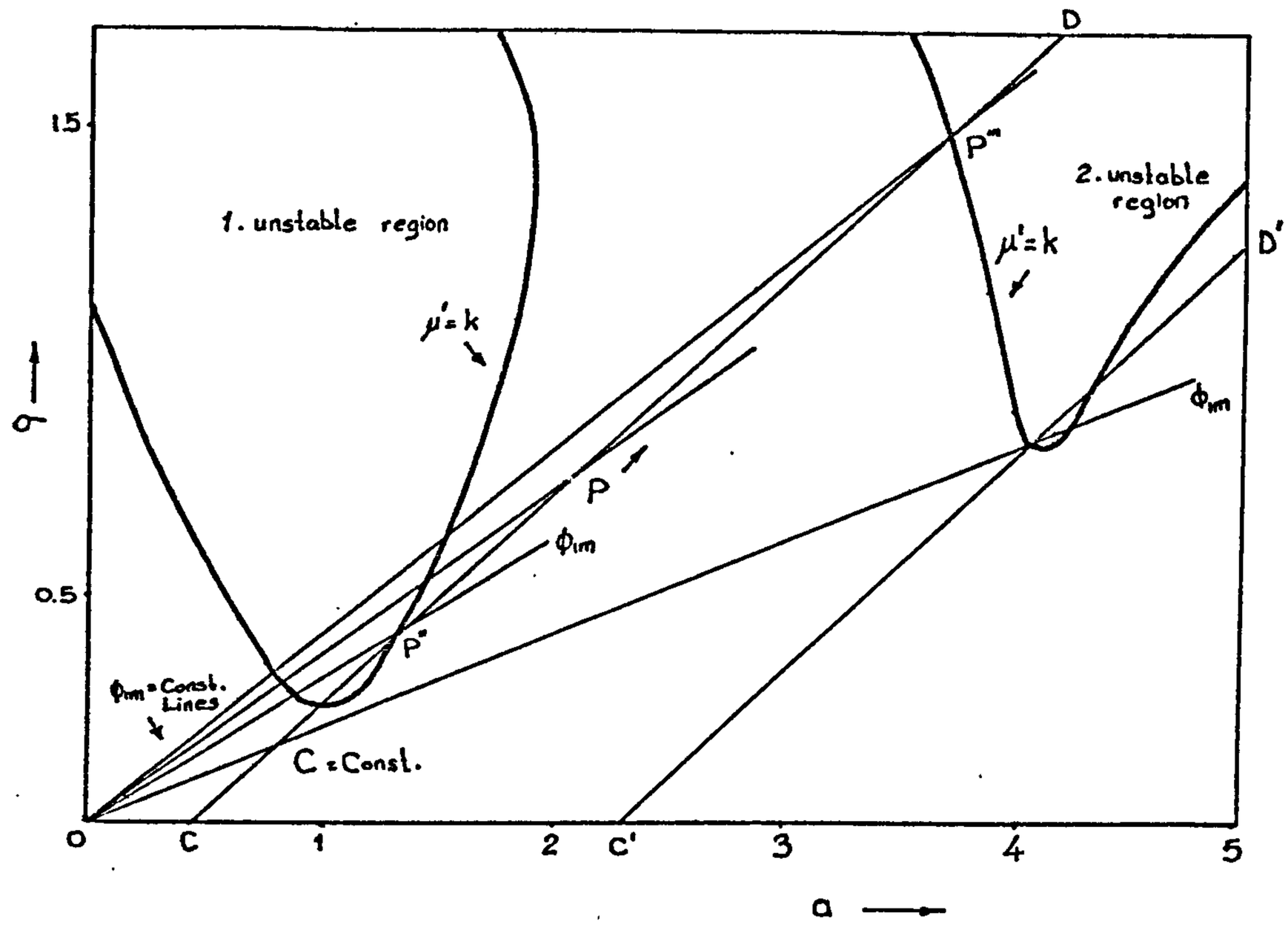

Figure 3.28 Parametric excitation in the second unstable region for two different C values

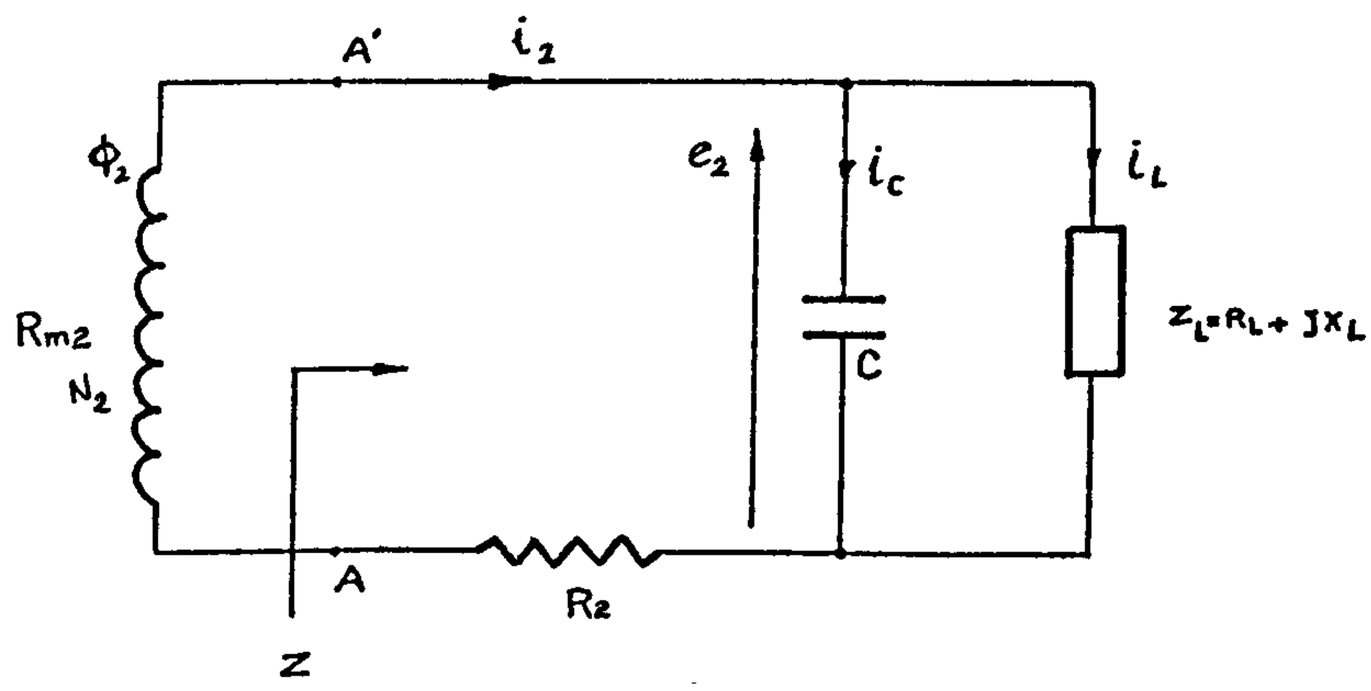

Figure 3.29 Loaded secondary circuit

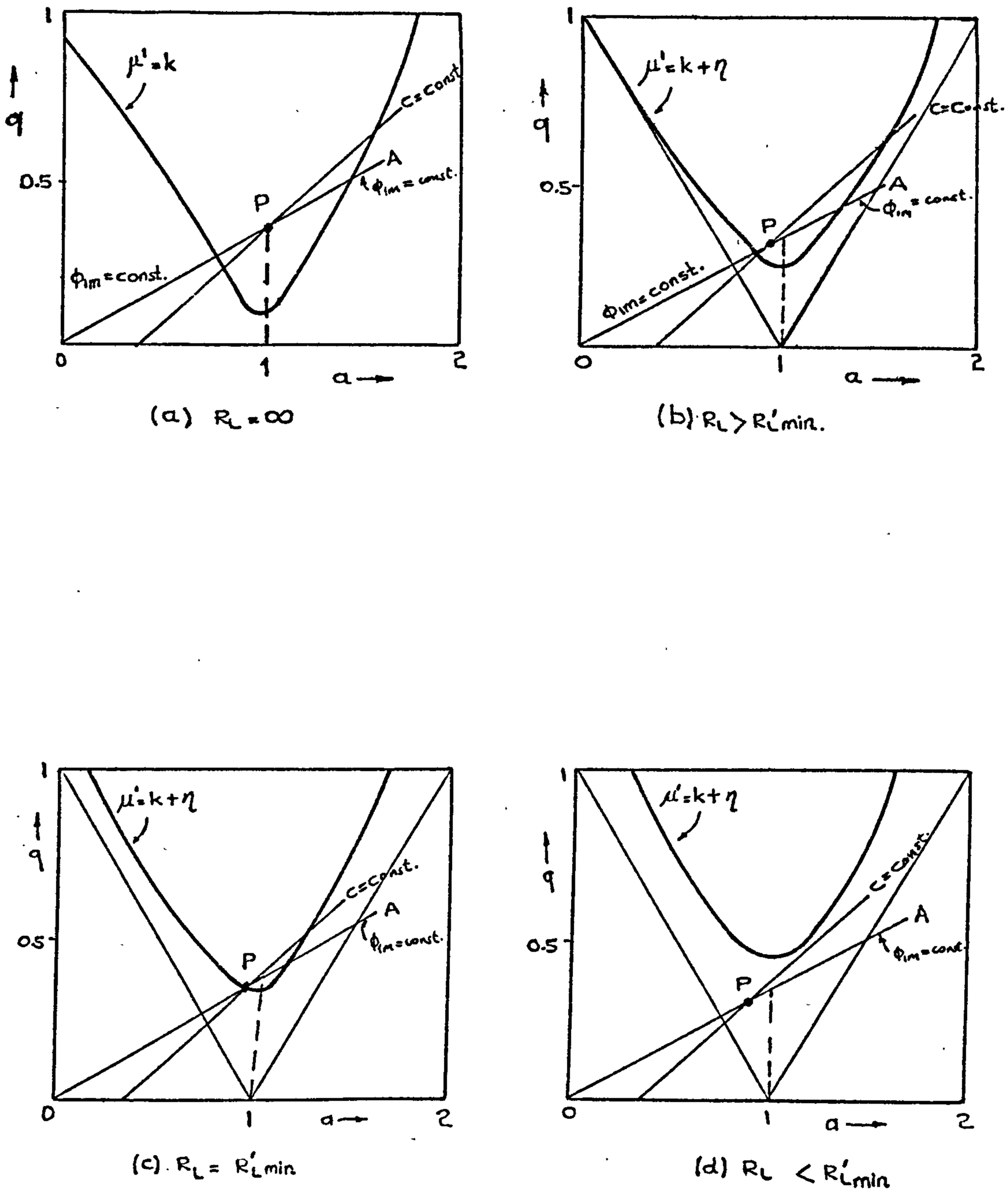

Figure 3.30 Effect of the load on the threshold condition

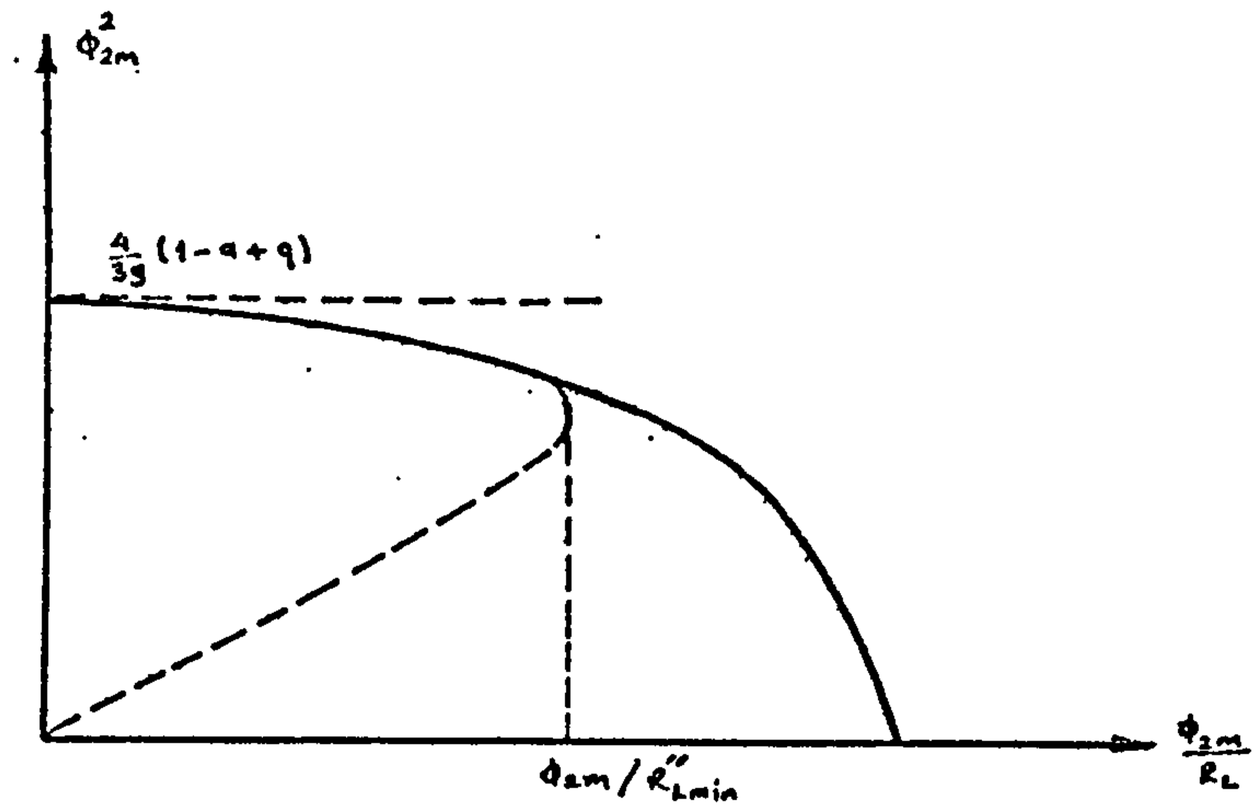

Figure 3.31 Load regulation characteristic

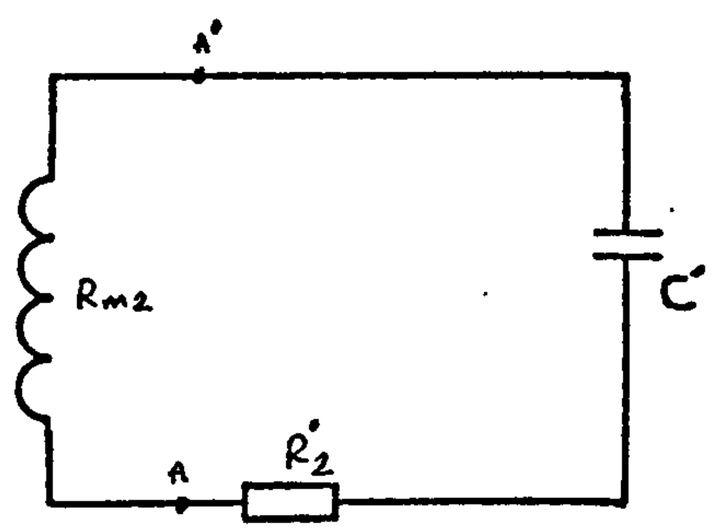

Figure 3.32 Equivalent circuit when Z_L is combined with R_2 and C

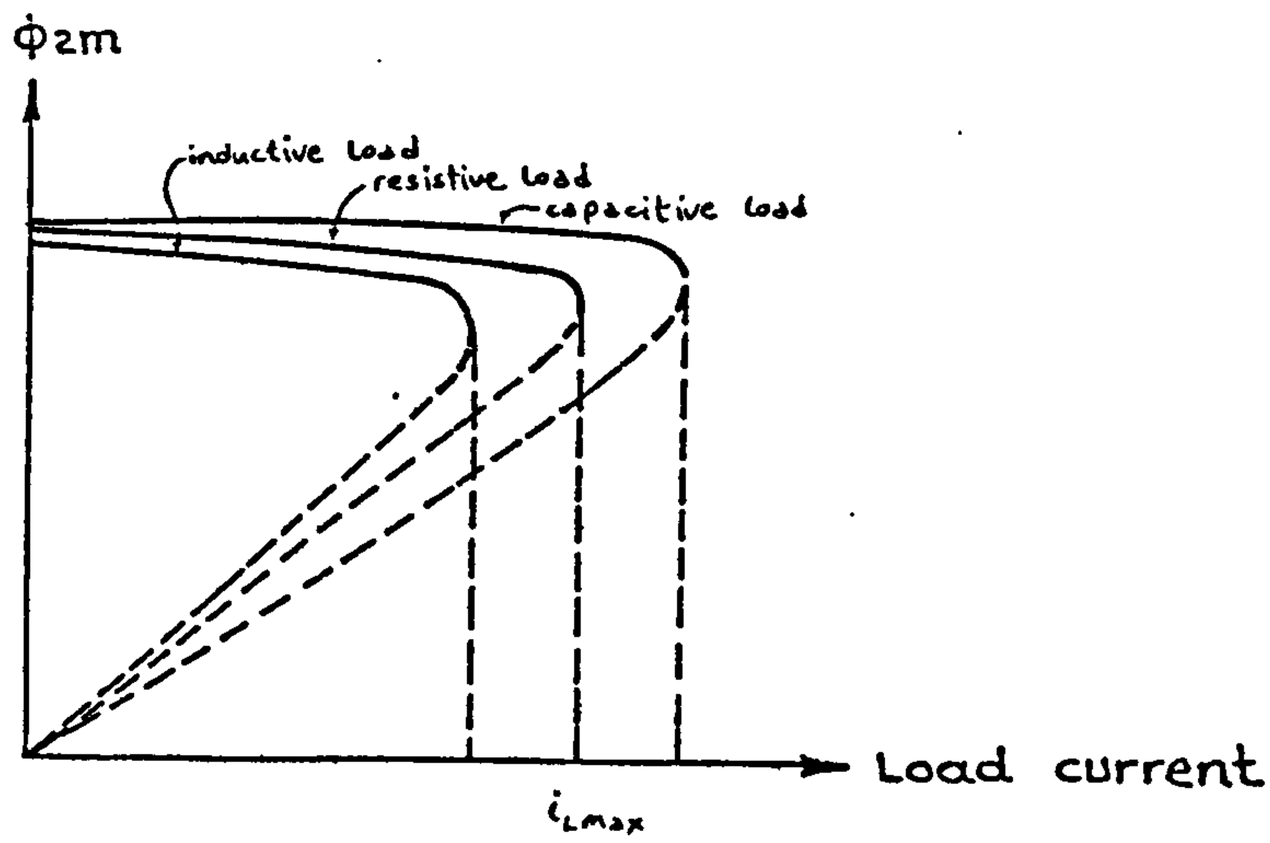

Figure 3.33 Load regulation characteristics for loads with different power factors

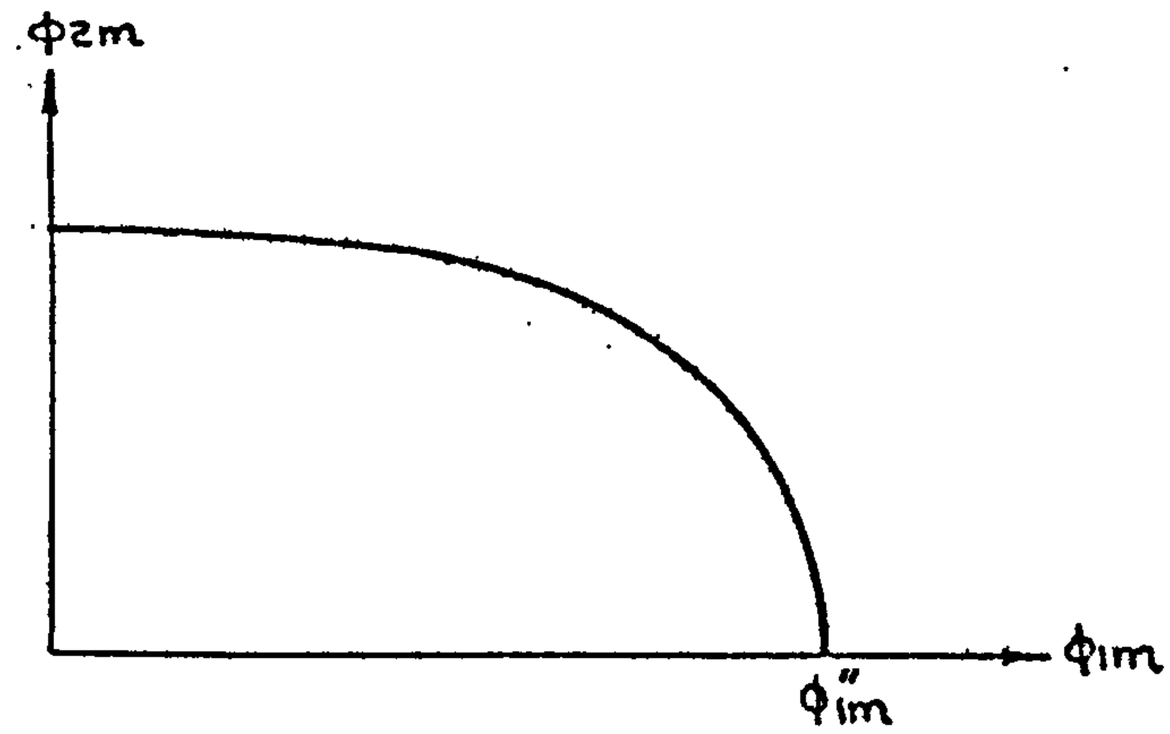

Figure 3.34 ϕ_{2m}/ϕ_{1m} relationship for non-dissipative secondary circuit

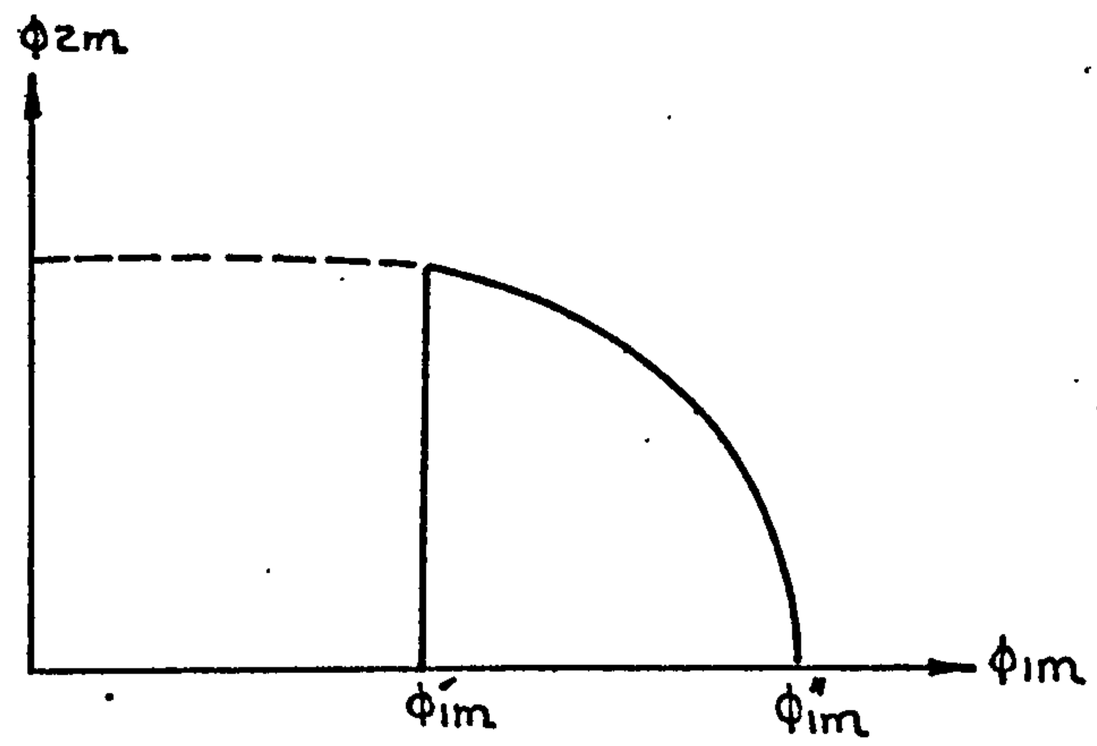

Figure 3.35 ϕ_{2m}/ϕ_{1m} relationship with threshold .

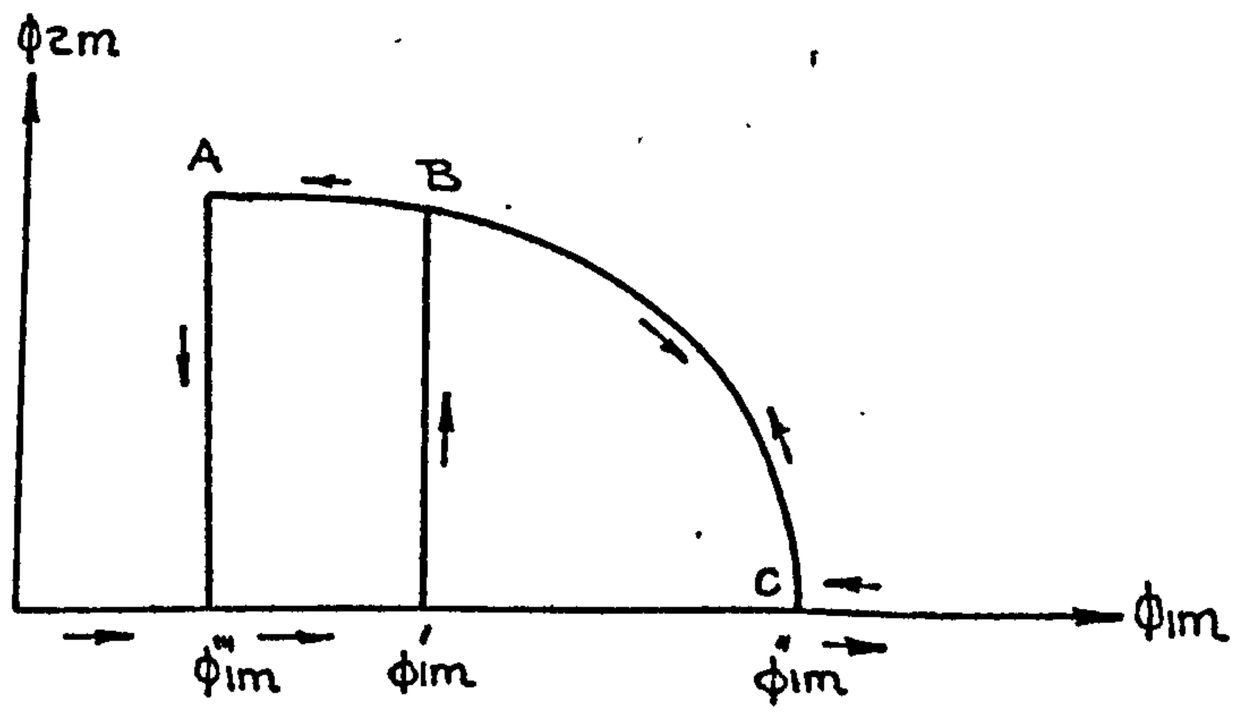

Figure 3.36 Actual characteristic with operational hysteresis

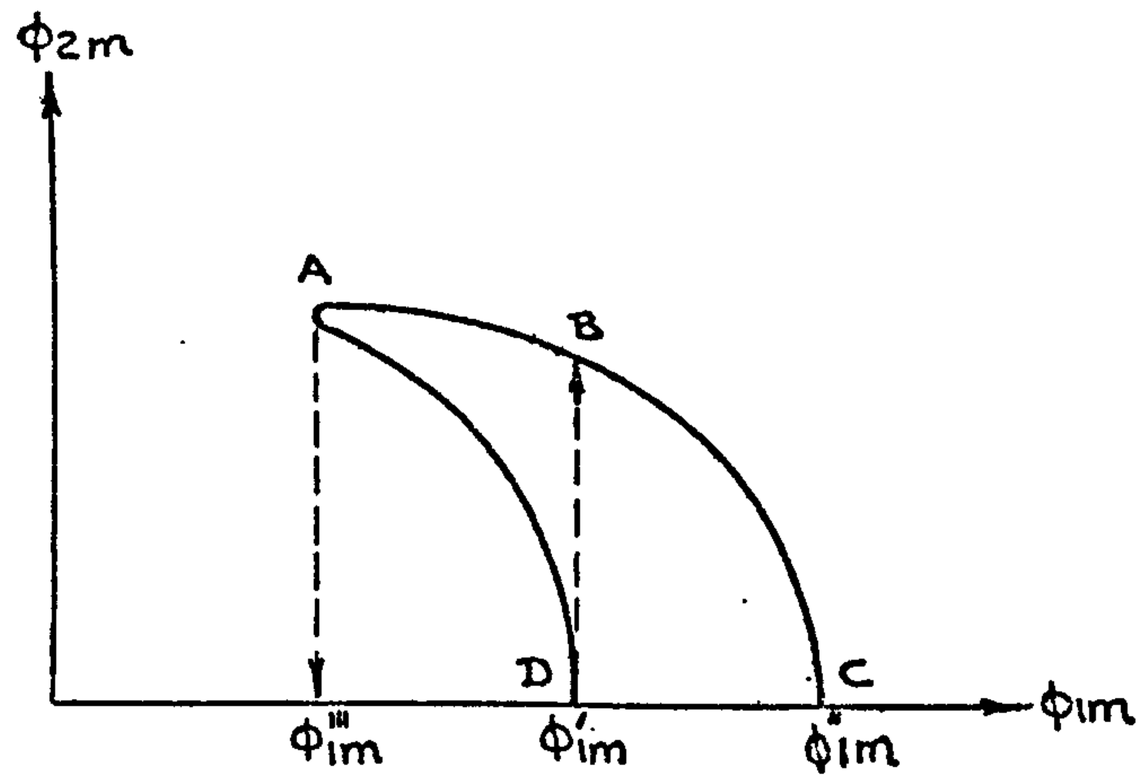

Figure 3.37 Operational hysteresis by analogy to non-linear resonance

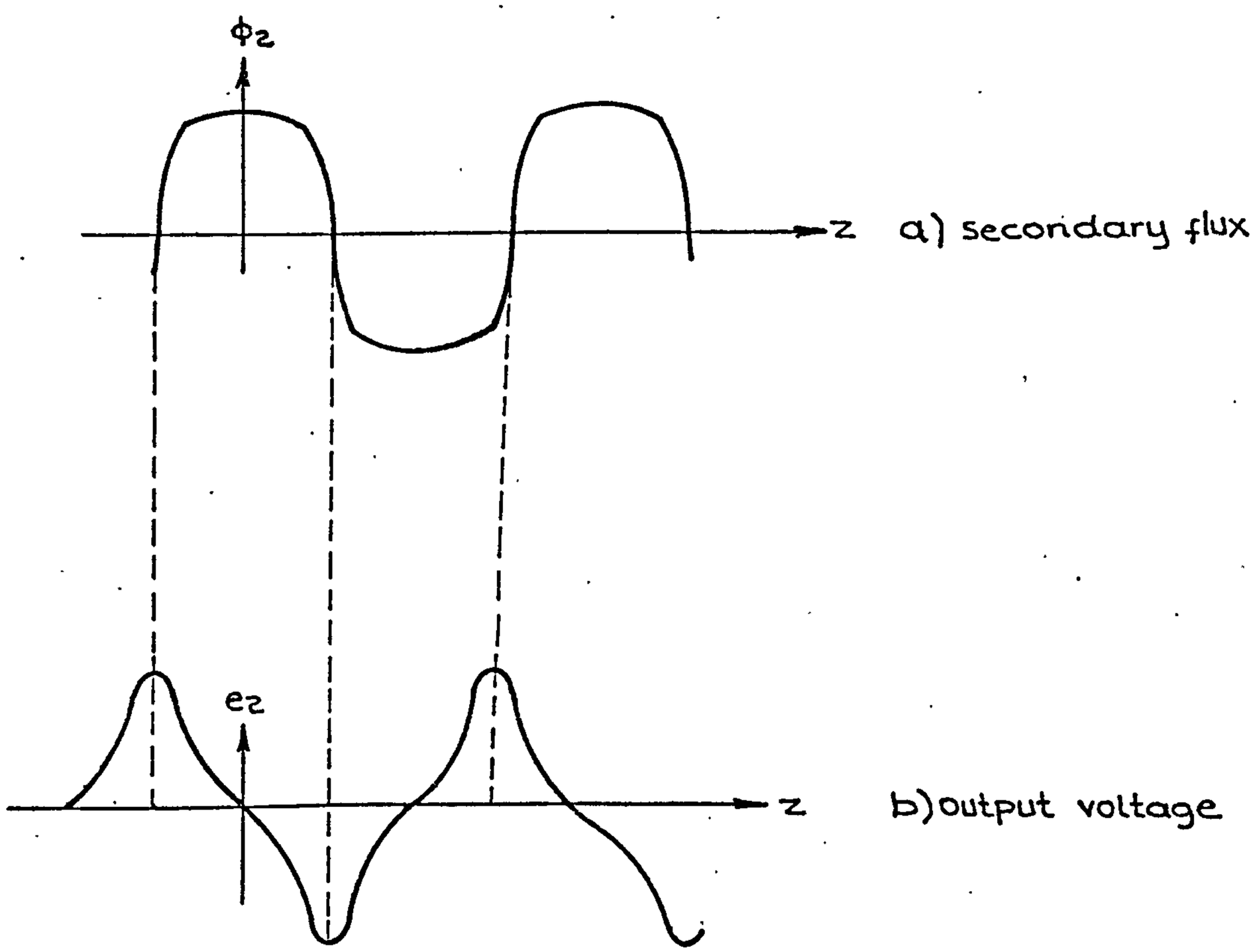

Figure 3.38 Waveforms of the secondary flux and voltage when $\phi'_{1m} < \phi_{1m} < \phi''_{1m}$

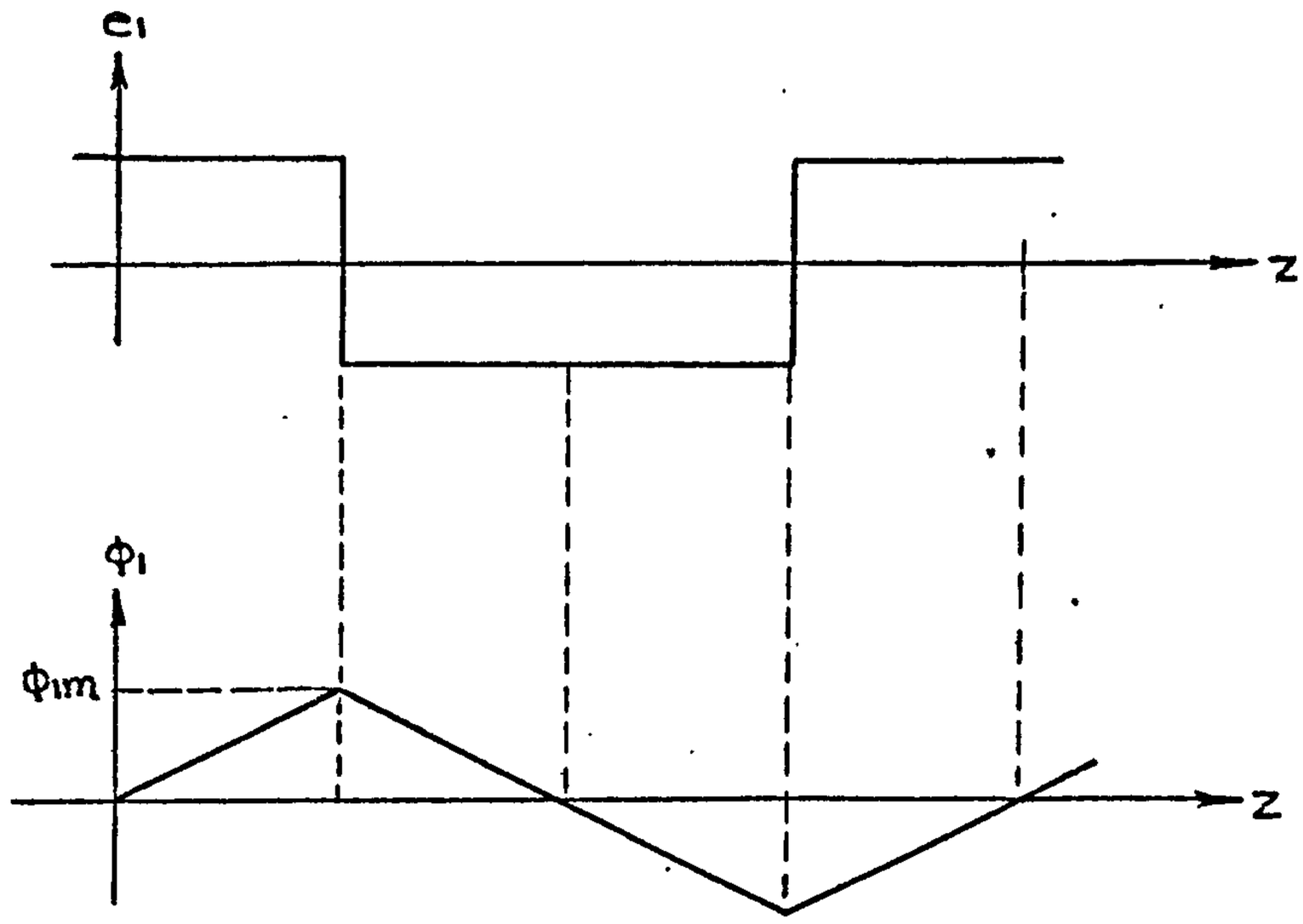

Figure 3.39 Square-wave input voltage and corresponding primary flux (no primary circuit resistance)

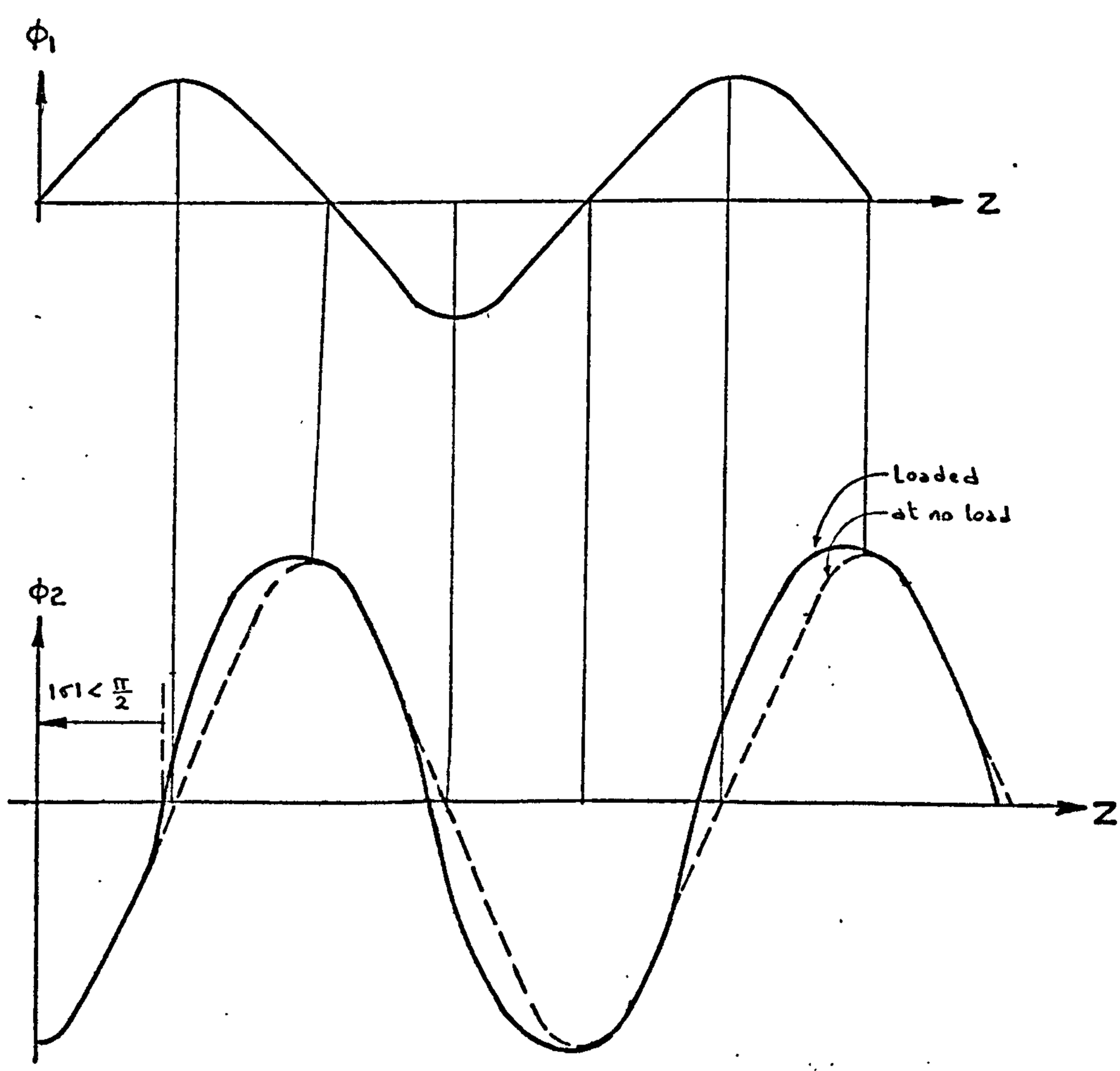

Figure 3.40 Effect of load on secondary flux waveform

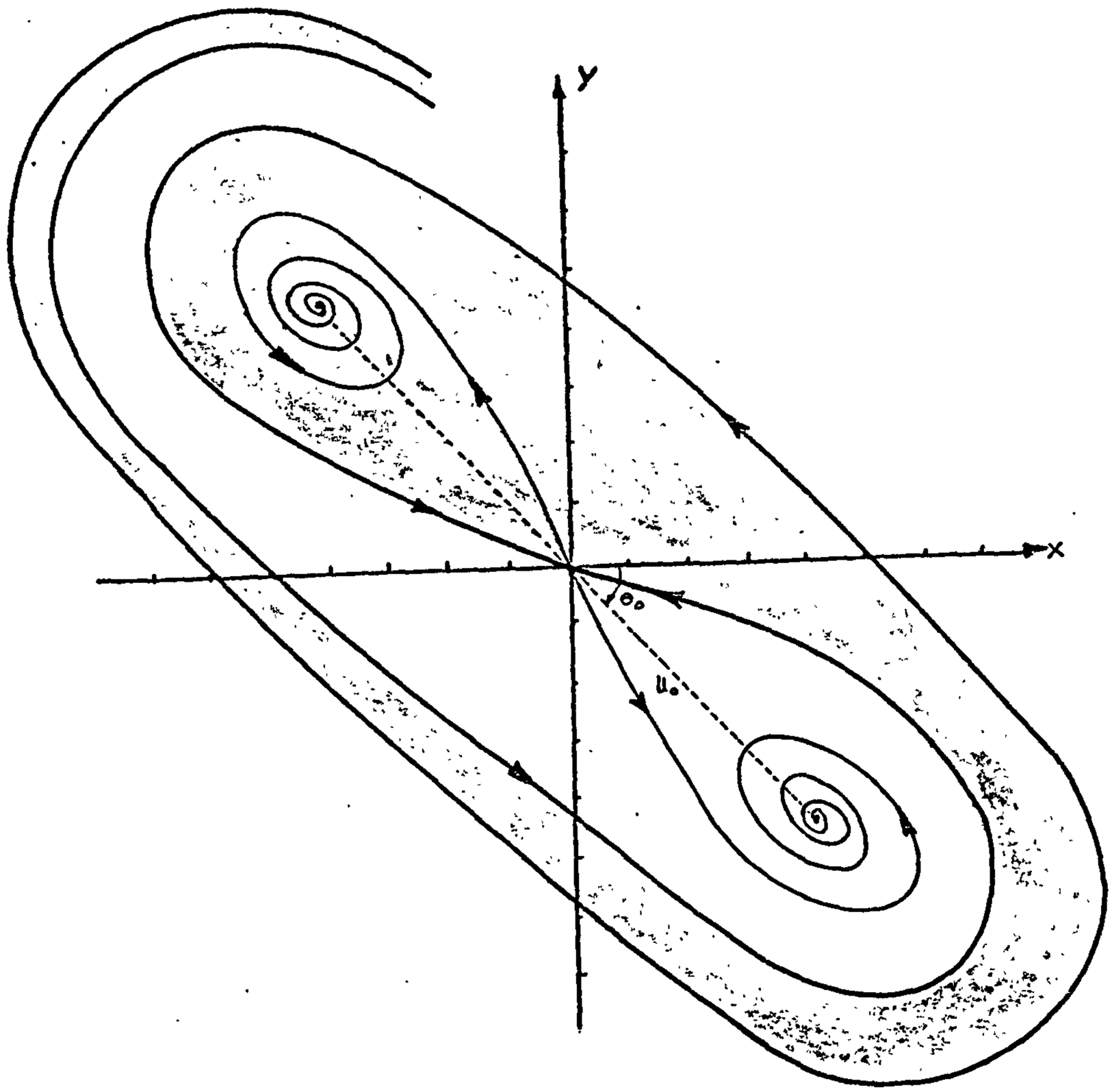

Figure 3.41 Phase-portrait for a bistable parametron

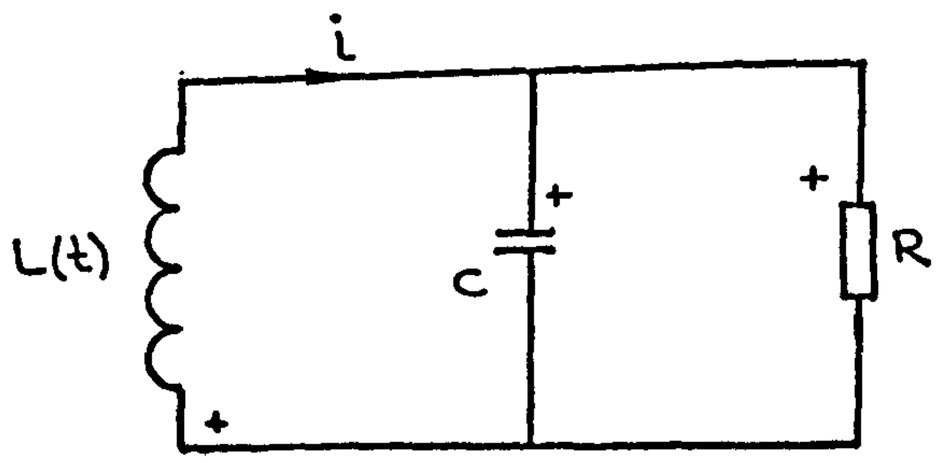

Figure 3.42 Basic circuit of parametron

CHAPTER IV

PARAMETRIC TRANSFORMER AS A NONLINEAR MAGNETIC DEVICE

When the inductance (or capacitance) of a parametric resonant circuit is varied at twice the resonance frequency, by using energy other than electrical energy, the system becomes a parametric *energy* converter, just as in the case of the parametric generators of Mandelstam and Papalexi[1], which converted mechanical energy into electrical energy. For parametric *transformer* action, the inductance has to be varied electrically so that, instead of energy conversion, the system accomplishes electrical power conversion and becomes a static, passive power converter, with the electrical input power required to vary the inductance of the resonant circuit and the output power obtained by parametric excitation in this circuit. So, the problem of constructing a parametric transformer is simply that of obtaining an electrically-varied inductance and connecting it in parallel with a capacitor to form a resonant circuit.

For an electrically-varied inductance, any practical form of dc-controlled saturable reactor may be used. However, since the inductance is now required to vary periodically (at twice the resonant frequency), it has to be controlled by alternating current instead of the direct current normally used, when the aim is to *regulate* the inductance in a gradual manner. The variation in the inductance of the load winding of a dc-controlled saturable reactor is independent of the direction of the direct control current, and

therefore, if the control current is alternating at a frequency f, the inductance of the load winding is varied at the frequency 2f, as required for parametric transformer operation. The control winding of the saturable reactor, used now as an ac-controlled variable inductor, needs to be modified to accept alternating current, and clearly, the number of turns needs to be different from that for a dc-control current, to create a sufficiently large control-mmf in the magnetic core.

Approaching the parametric transformer concept by replacing the time-varying inductance in a parametric resonant circuit by an electrically-varied inductance, makes possible the generalization of this concept, and is also of importance when investigating possible practical realizations of parametric transformers. Using this approach, a parametric transformer may be considered as comprising a saturable reactor, the control winding of which is driven by an alternating source, together with a capacitor connected across the load winding and tuned to resonate at a frequency equal to that of the control source. This is illustrated diagrammatically in Figure 4.1. It is now clear that the input or primary winding of a parametric transformer corresponds to the control winding of a saturable reactor, modified so as to accept an alternating voltage source, with the output or secondary winding corresponding to the load winding of the saturable reactor.

As the relation of saturable reactor devices to parametric transformers becomes evident, a closer look at such devices seems appropriate.

4.1 Saturable Reactors Used as Variable Inductors

Throughout this study, the term *saturable reactor* is used in the same sense as the commonly used term *ordinary saturable reactor*[2] or the German-originated term *transductor*[3], referring to the simplest form of magnetic amplifier[4] with no external components (diodes, resistors, capacitors etc) and no feedback arrangements. Thus, a saturable reactor is a magnetic device having two windings (the control and load windings) with the undesired transformer action between them eliminated by some arrangement.

It is also important to discriminate saturable reactors from *saturating* reactors (or ac-saturated nonlinear inductors[5]), in which saturation of the magnetic core is produced without dc magnetisation, solely by applying a sufficiently high alternating voltage to the excitation winding. In contradistinction to such *saturating* reactors, the various types of *saturable* reactor generally use an alternating excitation voltage of moderate amplitude (not causing saturation by itself) applied to the load winding in series with the load, together with a dc magnetisation produced in the control winding, which causes saturation phenomena in the core material. Operation of a great number of magnetic voltage or current stabilizing devices, such as ferro-resonant transformers, is based on the characteristics of such *saturating reactors*, and those devices are essentially different from parametric transformers making use of *saturable reactors* in their magnetic construction.

The history of dc-controlled saturable reactors begins with the early work of Burgess and Frankenfield[6,7] who were responsible for the first practical applications of the long-known principle of regulating the self-inductance of iron-cored coils through the non-linearity in the magnetisation characteristic of the core material. Their disclosures carry the significance that they included almost all the practical forms of saturable reactors used today.

4.1.1 The Classification of Saturable Reactor Devices

In several textbooks covering magnetic amplifiers[8-10], ordinary saturable reactor devices are classified with regard to their magnetic-core structure (2-core devices, 3-legged core devices, etc), their output-circuit configuration (series - or parallel-connected output windings) and their mode of operation in respect of even harmonics (natural or forced magnetisation conditions). However, another kind of classification will be attempted here, which is useful in evaluating the new magnetic-core configurations proposed by Wanlass[11], forming the basis of parametric transformers described by the same author in a later patent.[12]

The classification of saturable reactor devices is here based on:

a) How the undesired transformer action or the effects of the mutual coupling between the control and load windings are eliminated.

b) The relative positions of the control flux (dc-magnetisation) and the load flux (ac-magnetisation) in the magnetic core.

In most types of practical saturable reactors, undesired transformer action is eliminated by means of three different methods:

1. FORCED SUPPRESSION of the alternating current in the control winding induced by the mutual flux coupling existing between the control and load windings.

2. CANCELLATION of the effects of the mutual flux coupling, either by;

   a) summing the two equal portions of the same *flux*, which link either of the windings in opposite directions

   or b) summing the two equal but antiphase *voltages* which are induced in the two separate halves of the same winding.

3. ELIMINATION of magnetic coupling between the control and load windings by special configurations of the windings and the magnetic core

   a) using a magnetic short circuit to reduce the coupling,

   or b) having two separate magnetic paths for the control and the load circuits, with the whole or a part of the core common to these two magnetic circuits.

With regard to the second kind of classification, ordinary saturable reactor devices may be divided into two main groups:

1. PARALLEL-FLUX saturable reactors, in which superimposition of the control and load fluxes takes place in the whole or a part of the core, with the two fluxes being parallel to each other.

2. ORTHOGONAL-FLUX saturable reactors, in which superimposition of the control and load fluxes takes place in the whole or a part of the core, with the two fluxes being at right angles.

In any particular construction of the saturable reactor, more than one of the above means of elimination may be present in the device, and parallel- and orthogonal-flux interaction may co-exist in the same magnetic core. Thus, a particular saturable reactor device may belong simultaneously to a number of the above groups. However, in these cases the dominant factor will be emphasized as the practical forms of the saturable reactors are reviewed in the next section from the viewpoint of the classification made here.

4.1.2 Various Forms of Saturable Reactors

The simplest way of realizing a saturable reactor[13] is shown in Figure 4.2, which illustrates the *forced suppression of the effects of mutual flux coupling*. The control and load windings have full mutual coupling, and a large alternating voltage is induced across the load winding. For this not to produce excessively large currents in the low-impedance control circuit loop, a high impedance choke coil is connected in series with the control winding. In respect of the second kind of classification, it is obvious that *parallel-flux* interaction occurs in the *whole* of the magnetic core. This elementary form of saturable reactor is not used widely, except for the simple dc-instrument

transformers in which the bus-bar forms a single-turn control winding.

Traditional saturable reactor devices use mostly the second method of eliminating transformer action, based on the *cancellation effect* . Figure 4.3 shows such a device built on a single, three-legged, laminated transformer core (the centre leg having twice the cross-sectional area of the outer legs) with one dc control winding on the centre leg and two equal half-sections of the ac load winding on the outer legs. Again, full mutual flux coupling exists between the control winding and each section of the load winding. However, when both sections of the load winding are energized the alterating flux components created flow effectively through the centre leg in opposite directions, cancelling each other and producing no alternating voltage across the control winding. Since only unidirectional (dc) flux flows through the centre leg, unwanted hysteresis effects may arise, and to avoid this, the centre leg is split lengthwise, with a narrow gap provided between the two parts of the core to prevent the alternating flux from following the circumference path (Figure 4.4). The cancellation of the ac flux components can more readily be seen in this configuration. Both the devices in Figures 4.3 and 4.4 are parallel-flux systems; parallel interaction of the dc and ac fluxes occurs in a part (the circumference path) of the core in the first one, and in the whole core of the latter.

The other method (2(b) in the previous section) of cancelling the effect of mutual flux coupling in a saturable reactor employs

two separate and equally-rated units, as shown in Figure 4.5. The two load windings are connected in a series-aiding sense, whereas the two control windings are connected in series-opposing sense, or vice versa. This ensures the voltage across the full control winding is zero, as it is the sum of the two anti-phased components induced in the individual control windings. It is apparent that, in this method, cancellation of voltages rather than cancellation of fluxes takes place, and also that parallel flux interaction occurs in the whole of each of the cores. It is worth noting that, if the functions of the windings of the devices in Figures 4.3 and 4.4 are reversed, as shown in Figure 4.6, the method employed becomes *cancellation of voltages* rather than fluxes, as across each control winding now appears a large induced ac voltage.

The effects of mutual flux coupling can be reduced to a negligible level by either flux or voltage cancellation in a properly designed device, although this will only apply at the fundamental frequency of the alternating voltage supply. Because of the non-linear and hysteretic magnetisation characteristic, the voltages induced in the control winding from the two load windings will contain a large number of harmonics, and these will not necessarily cancel out at all harmonic frequencies. This is, in turn, due to the fact that full mutual coupling exists, between the control and load windings and its effects are cancelled rather than its presence being removed.

The last method of eliminating undesired transformer action (3 in Section 4.1.1) aims at removing the mutual flux coupling between the control and load windings, which can be partly achieved by a magnetic short circuit, as shown[14] in Figure 4.7a. The control and load windings are now placed on the outer legs of a three-legged core, with the centre leg acting as a magnetic short circuit to prevent a significant portion of the alternating flux from linking the control winding. The portion of this flux which links the control winding is proportional to the ratio of the reluctance of the centre leg (magnetic path AD in the figure) to that of the outer leg (magnetic path ABCD), and this ratio can be reduced by using the magnetic core[14] shown in Figure 4.7b or by inserting a narrow air gap into the magnetic circuit of the control winding as shown in Figure 4.7c. The form of the saturable device in the last figure has been employed in a kind of parametric transformer named *SW Transformer* by its manufacturer[15,16]. If the flux interaction occurring in the outer legs of the device in Figure 4.7a is neglected, the centre leg may be considered as a region, common to the principal magnetic paths of the control and load circuits, in which parallel interaction of the fluxes takes place.

Many magnetic control devices used in areas such as computer magnetics, magnetic modulators, magnetic frequency changers etc. rely on method 3(b), to eliminate directly the existence (not the effects) of mutual flux coupling, while using a magnetic core

configuration having a region common to both flux paths. Because of the special configurations of the core, orthogonal flux interaction is often used in these devices, giving rise to *multi-apertured* cores, the earliest example[17] of which is shown in Figure 4.8a. The interaction of the unidirectional and alternating fluxes takes place around the apertures and, as is evident in Figure 4.8b, parallel flux interaction is predominant, although some orthogonal interaction occurs in the marked regions. No alternating flux links the dc control windings and mutual flux coupling is eliminated but only unilaterally. The same magnetic configuration is employed in saturation-controlled transformers[18], magnetic modulators[19] and many other devices of computer magnetics[20,21]. Three-aperture transfluxors[22] have basically the same magnetic circuit structure, although most devices used in computer magnetics use the hysteresis property of square-loop ferrite materials.

Orthogonal flux interaction occurring in the whole of the core is best illustrated by means of a hollow toroidal core. One winding is placed within the annular hollow, and the second is wound on the core, as shown in Figure 4.9a. The two separate and closed flux paths associated with the windings are mutually perpendicular everywhere in the core (R>>r is assumed in Figure 4.9b), and no mutual coupling exists between the windings. The whole core acts as a region common to these flux paths. Although this configuration was first proposed[7] for saturable reactor power control applications its practical construction is only possible

with ferrite core materials[23], because of the lack of practical laminations effective in two perpendicular directions and the otherwise excessive eddy-current losses. The arrangement is, therefore, employed in magnetic modulators[23,24], magnetic memories[25] and other devices[26].

Operation of a different but large family of magnetic memory devices[27-30] is based upon orthogonal flux interactions within massive ferrite bodies of high-retentivity, having perpendicular apertures through which passes a single conductor, as shown in Figure 4.10a. The theory of magnetisation processes in such structures is given elsewhere[31]. The significance of these devices is that they have undergone the transfiguration illustrated by Figures 4.10a, b and c, with many devices[32-35] having the form of Figure 4.10b appearing before the magnetic configuration in Figure 4.10c were used in magnetic devices for computers[37,38].

A clear example of this method (3(b) in Section 4.1.1) is provided by the device in Figure 4.11, which has two separate magnetic circuits with a common region where orthogonal flux interaction occurs. No flux produced by either coil can link the other, and mutual flux coupling is completely absent. However, the unidirectional control flux changes the level of saturation in the common region, varying the reluctance of the magnetic circuit associated with the load. The only part of the core where flux interaction takes place is where the two core loops are common. This type of construction was first proposed[39,40]

with the two coils superimposed at right angle and wound on the cross-shaped common region, as shown in Figure 4.12. Since a portion of the flux created by each coil links each core loop, the parallel flux interaction in the core loops predominates over the orthogonal flux interaction taking place where the loops are common. However, unlike the arrangement in Figure 4.11, the whole core acts as a region common to both flux paths. The particular orientation of the windings, however, practically eliminates mutual coupling and this device was considered as one basic form of magnetic cross valve[39-41].

Magnetic cross valves[39-50] have the structure shown in Figure 4.13, and are constructed as in Figure 4.14. No mutual coupling exists between the orthogonal windings, and in the central region of the core (marked by a square in Figure 4.15) the fluxes undergo orthogonal interaction. However, in the remainder of the core, parallel flux interaction occurs as can be seen from the figure. Under ideal conditions (no winding resistances, and ideal voltage sources) and with complete symmetry, the net flux in each branch of the core is shown in Figure 4.16, where the fluxes ϕ_1 and ϕ_2 are established in the coils 1 and 2 respectively. Only at the centre point do the two fluxes cross orthogonally, in the directions indicated in the figure. The flux components in the directions of the inner branches of the core are additive or subtractive, and flux interaction takes place only in the inner, cross-shaped branches of the core, including the central region where interaction is orthogonal.

Magnetic cross valves, although extensively developed by Mc Creary[39-50], were proposed much earlier[51], with the winding arrangement shown in Figure 4.17. Under the foregoing considerations, the flux in the branches of the core is given in Figure 4.18, where it will be noted that the direction of the orthogonal interaction in the central region is different from that in the previous arrangement. As distinct from that arrangement, flux interaction takes place in a parallel manner in the circumferential branches of the core, and in an orthogonal manner in the central region. When the volume where parallel flux interaction occurs is compared with that where fluxes interact orthogonally, it is seen that parallel flux interaction predominates overall in both devices in Figures 4.13 and 4.17. The elimination of mutual flux coupling in the latter is achieved by the flux cancellation method, as the flux from one set of windings tends not to flow through the branches of the core where the other windings are situated. This is better understood if the core is temporarily imagined to be as in Figure 4.19.

The significance of magnetic cross-valve devices to the subject of parameter transformers is not only that they have been employed in similar areas, but also that they have a magnetic circuit structure very similar to that of two-C-core constructed parametric transformers, as will be clear shortly.

4.2 Analogous Electric Circuits with Elimination of Mutual Flux Coupling

In some cases where the magnetic circuit configuration permits an interpretation, it is useful to derive an electrical circuit analog to the magnetic circuit, using the magnetic equivalent of Ohm's Law:

$$\phi = \frac{F}{R_m} \qquad \ldots\ldots \qquad (4.1)$$

where $F = N.i$ is the magnetomotive force, $R_m = \ell/\mu A$ is the reluctance and ϕ is the flux. Analogous circuits for the simplest magnetic circuit driven by an ideal voltage or current source are shown in Figure 4.20. Although the equivalent reluctances of parallel or series branches of a magnetic core can be calculated, just as can series or parallel connected resistors in electrical circuits, it must always be borne in mind that, unlike resistors, these do not form linear elements, and further that they are functions of the corresponding fluxes.

An analogous circuit for the saturable reactor in Figure 4.3, with the windings on the outer legs driven by an acv source (see list of symbols) is shown in Figure 4.21. Although the reluctances R'_1, R''_1 and R_2 are flux dependent, R'_1 and R''_1 are always equal because of the symmetry in the magnetic circuit, and the alternating voltage source can be represented by two equal sources of flux. Considerations of the symmetry show that no flux flows through R_2 and hence, physically, that no voltage is induced across the corresponding winding.

A similar analogous circuit for the device in Figure 4.17 is given in Figure 4.22, when only one of the windings is driven by an acv source and the orthogonal flux interaction in the central region is neglected. The symmetry of the magnetic circuit leads to four equal reluctances (R_2) in the circumferential branches, and to two equal reluctances (R_1) in the branches where the winding is driven by an acv source. Without any further analysis, application of Kirchhoffs *current law* to the point O' in Figure 4.22b shows that no flux flows between the points O' and O", and hence that the connection between these two points may be disregarded. This immediately results in equal values for R_3 and R_4, as the fluxes through them are the same. Furthermore, the bridge circuit consisting of four R_1 reluctances is balanced, and no flux will therefore flow through R_3 and R_4, showing that mutual coupling is absent. Although the reluctances are flux dependent, the balance condition always exists, for the values of each of the R_2, though varying, are always the same, since equal fluxes flow in each. If the winding were driven by an acc source (see list of symbols) rather than an acv source, the flux sources in Figure 4.22a would be replaced by mmf sources of N.i(t). The previous results, i.e. that the bridge is always balanced, that no flux flows through R_3 and R_4, and that the connection between O' and O" may be disregarded, can be obtained, though not at a glance, by applying a circuit analysis technique such as the mesh current method.

All the considerations so far given to the elimination of mutual flux coupling are valid only when one of the windings of a saturable reactor is solely driven by an alternating source, and the other winding is observed as to whether or not a voltage at supply frequency is induced. During normal saturable reactor operation, when both windings are driven, the situation is totally different, as the superimposition of ac and dc magnetisation is always associated with the generation of even-harmonic flux components. This should not be confused with the harmonic components which do not cancel in the devices, such as those in Figures 4.3 and 4.5. With the two sources existing in the system at the same time, the net flux in various branches of the core will be different, causing different reluctance values for symmetrical branches of the core, and hence distorting the symmetry and the balance in the analogous electric circuit. If this circuit was linear, the total solution would be found as the superposition of the two solutions corresponding to the cases when either of the sources existed independently. It would, therefore, be anticipated that a component of voltage at supply frequency would appear across the dc control winding, and that the dc bias current would contain an ac component at the same frequency. However, linear superposition is not valid and consequently, mutual flux coupling cannot account for the generation of even-harmonic flux components in the core. Generation of a double-frequency alternating component in the dc control winding, despite the absence of mutual flux coupling, indicates therefore that another kind of coupling - namely parametric coupling - exists between the windings.

4.3 Mutual Parametric Coupling and Representation of Saturable Reactors

Mutual flux coupling is accounted for by the concept of Mutual Inductance, which is defined as the common property of two associated electric circuits which determines, for a given rate-of-change of current in one of the circuits, the emf induced in the other. In the linear system of Figure 4.23, this is formulated as

$$e_1 = L_1 \frac{di_1}{dt} + M \frac{di_2}{dt}$$

$$e_2 = M \frac{di_1}{dt} + L_2 \frac{di_2}{dt} \qquad \ldots\ldots \quad (4.2)$$

where L_1 and L_2 are the self inductances and M the corresponding mutual inductance.

Regarding the windings 1 and 2 of Figure 4.23 as the control and load windings of a saturable reactor, elimination of the effects of mutual flux coupling in the device of Figure 4.5 is accomplished in such a way that M_1 and M_2 in

$$e_1 = L_1 \frac{di_1}{dt} + M_1 \frac{di_2}{dt} - M_2 \frac{di_2}{dt} \qquad \ldots\ldots \quad (4.3)$$

are made equal. The same result is achieved in the saturable reactor of Figure 4.4 by equating M_1 and M_2 in

$$e_1 = L_1 \frac{di_1}{dt} + \frac{d}{dt}(M_1 i_2 - M_2 i_2) \qquad \ldots\ldots \qquad (4.4)$$

where $M_1.i_2$ and $M_2.i_2$ show the flux components created by each half of the ac load winding and linking the control winding in opposite directions. Equations 4.3 and 4.4 summarize the methods 2(a) and 2(b) in Section 4.1.1. All the saturable reactor devices seen under the method 3 aim at making the mutual inductance M directly equal to zero by special magnetic arrangements. With M equal to zero, the system of equations (4.2) reduces to

$$e_1 = L_1 \frac{di_1}{dt} \qquad \ldots\ldots \qquad (4.5)$$

$$e_2 = L_2 \frac{di_2}{dt} \qquad \ldots\ldots \qquad (4.6)$$

regardless of the method employed to eliminate mutual coupling. When the control winding is driven by a dcc source (see list of symbols), i.e. i_1 = constant, no voltage will appear across the winding, in accordance with equation (4.5). Since a double-frequency voltage is observed across the control winding with the application of an alternating current i_2 to the load winding, the only element in equation (4.5) to account for this is the self-inductance L_1, and L_1 should not therefore be constant but rather a function of time. If so, equation (4.5) can only be written in the form

$$e_1 = \frac{d}{dt}\,[L_1(t).I_1] \qquad \ldots\ldots \qquad (4.7)$$

where $L_1(t)$ is time-varying and I_1 is constant, and only this equation can explain that $e_1 = e_1(t) \neq 0$ when $i_2 = i_2(t)$ is present. The inductance L_1 is, therefore, a function of i_2. Furthermore, it is an even function of i_2, so that when i_2 is of a sinusoidal form, $e_1(t)$ does contain even-harmonic components.

It is clear that a circuit variable (i_2) in one of the two associated electric circuits causes a circuit parameter (L_1) to vary in the other. This is defined as the parametric coupling from the first circuit to the second. The same is also true for the load circuit whose inductance (L_2) is a function of I_1, the dc control current, as evident from the normal operation of saturable reactors. This indicates the parametric coupling from the second circuit to the first. Parametric coupling in saturable reactors, exists therefore in both directions between the load and control circuits. In this way, a saturable reactor can be represented by the two equations

$$e_1 = \frac{d}{dt}\{L_1[i_2(t)].i_1(t)\} \qquad \ldots\ldots \qquad (4.8)$$

$$e_2 = \frac{d}{dt}\{L_2[i_1(t)].i_2(t)\} \qquad \ldots\ldots \qquad (4.9)$$

Only during operation with the even-harmonics in the control current suppressed (forced magnetisation conditions), can the current i_1 be assumed constant. The equations then become

$$e_1 = \frac{d}{dt} \{ L_1[i_2(t)] . I_1 \} \qquad ..... \qquad (4.10)$$

$$e_2 = L_2(I_1) \frac{d}{dt} i_2(t) \qquad ..... \qquad (4.11)$$

still showing parametric coupling between the two circuits. With free (unsuppressed) harmonic components in the control current (natural magnetisation), i_1 is a function of time and the equations have therefore to be written in the form of equations (4.8) and (4.9).

In general, parametric coupling, represented by the functions $L_1(i_2)$ and $L_2(i_1)$ in equations (4.8) and (4.9), may be symmetrical or asymmetrical, and linear or non-linear. If these two functions are of the same form, the parametric coupling existing between the two circuits is symmetrical, and if they are non-linear with respect to their own independent variables, parametric coupling is non-linear, as generally encountered in practical cases. However, this non-linearity of parametric coupling, although parametric coupling is a result of non-linear media, should not be confused with the non-linearity of the system itself. The equations

$$e_1 = \frac{d}{dt} [L_1(i_2) i_1] \qquad ..... \qquad (4.12)$$

$$e_2 = \frac{d}{dt} [L_2(i_1) i_2] \qquad ..... \qquad (4.13)$$

represent two parametrically coupled linear inductances, the coupling between which is generally non-linear. As, in fact, the

self-inductances are also functions of the currents in the windings, a saturable reactor has to be represented by the equations

$$e_1 = \frac{d}{dt}\,[L_1(i_1,\ i_2).i_1] \qquad \ldots\ldots \qquad (4.14)$$

$$e_2 = \frac{d}{dt}\,[L_2(i_1,\ i_2).i_2] \qquad \ldots\ldots \qquad (4.15)$$

indicating non-linear parametric coupling between two non-linear inductors. The variables i_2 in the first equation and i_1 in the second are implicit variables, since they enter into the equations as explicit functions of time. The inductances L_1 and L_2 are, therefore, both non-linear and time-varying. It is worth emphasizing that, in the system represented finally by the set of equations (4.14) and (4.15), the parametric coupling between the two inductances is mutual, i.e. it exists in both directions between the control and the load circuits.

4.3.1 Parametric Coupling as a Result of Interaction in Non-Linear Medium

For parametric coupling to exist between two inductors, regardless of their linearity or otherwise, the magnetic fields created by each should interact in a non-linear medium. Flux interaction in various saturable reactor devices has already been seen in Section 4.1.2 in connection with the classification made

in Section 4.1.1. Parametric coupling arises due to the fact that linear superposition does not apply in the non-linear medium where the fluxes interact. This is true regardless of whether the flux interaction is parallel or orthogonal.

4.3.1a Orthogonal Interaction

Let the core material of Figure 4.11 be isotropic, with a non-linear characteristic of $B = f(H)$, and let the resistance-less windings be driven by ideal current sources, with initially one of the windings, and then the other, and then finally both windings driven. At any particular point in the common region of the magnetic core, when only one of the windings is driven, the flux densities $\vec{B}_1$ and $\vec{B}_2$, created separately by the magnetic field intensities $\vec{H}_1$ and $\vec{H}_2$, are $\vec{B}_1 = f(\vec{H}_1)$ and $\vec{B}_2 = f(\vec{H}_2)$, Figure 4.24. When both the current sources are simultaneously present, the total magnetic field intensity is $\vec{H} = \vec{H}_1 + \vec{H}_2$, which creates a resultant flux density $\vec{B}$ in this direction, given by $\vec{B} = f(\vec{H}) = f(\vec{H}_1 + \vec{H}_2)$. As the function $B = f(H)$ is of the non-linear form of Figure 4.24, the resultant flux density $\vec{B}$ is not equal to the vector sum $\vec{B}_1 + \vec{B}_2$, but is smaller in magnitude than this. The flux density $\vec{B}$ can be resolved into two components $\vec{B}'_1$ and $\vec{B}'_2$ in the direction of the magnetic field intensities $\vec{H}_1$ and $\vec{H}_2$, as shown in Figure 4.24, and clearly $|\vec{B}'_1| < |\vec{B}_1|$ and $|\vec{B}'_2| < |\vec{B}_2|$. Introduction of $\vec{H}_2$ when only $\vec{H}_1$ is originally present thus causes a reduction in $\vec{B}_1$ to $\vec{B}'_1$, indicating that the two circuits are coupled. As is clear in the figure, the vectors $\vec{H}_1 + \vec{H}_2$ and $\vec{B}_1 + \vec{B}_2$ do not satisfy the magnetisation curve, neither in respect of their magnitudes nor their different directions.

Let one of the sources creating the sinusoidal magnetic field intensity H_2 in Figure 4.25a be an acc source while a dcc source creates the constant field intensity H_1. As a result of orthogonal interaction between the magnetic fields, the flux density B_1 varies between the values B_1 when $H_2 = 0$ and B_1' when H_2 is a maximum. Since the interaction is symmetrical during the time H_2 is negative, B_1, varies with a double frequency between these two values, as shown in Figure 4.25b. Hence, an even-harmonic voltage is induced in the dc winding when an alternating source is applied to the other winding, although the current through the first winding is constant and uni-directional. Induction of a double frequency voltage in the dc control winding, despite the absence of mutual coupling, thus clearly illustrates the parametric coupling between the two windings of the saturable reactor in Figure 4.11.

A similar conclusion may be drawn by representing the magnetisation characteristic in the form of $H = f(B)$, if the windings are driven by ideal voltage sources rather than current sources. It may be shown that, although the control winding is driven by a dcv source, the current through this winding when an acv source is applied to the load winding, will have a double-frequency variation.

4.3.1b Parallel Interaction

Parametric coupling occurs not only as a result of orthogonal interaction but also due to parallel interaction of magnetic fields, as in the device of Figure 4.5 redrawn in Figure 4.26.

Let the magnetisation characteristic of the core material be given by $B = f(H)$ and the cores a and b be identical, with equal cross-sectional area A and equal mean flux-path length ℓ. Two resistanceless windings with N_1 and N_2 turns are wound on both cores and connected as shown in the figure. The control winding, consisting of the two windings with N_1 turns, is driven by a dcc source, whereas the load winding is driven by an acv source. The flux densities in the cores a and b are given by

$$B_a = f(H_2 + H_1) = f_1(H_2) \qquad \ldots\ldots \qquad (4.16)$$

and

$$B_b = f(H_2 - H_1) = f_2(H_2) \qquad \ldots\ldots \qquad (4.17)$$

respectively, where

$$H_1 = \frac{N_1 . I_1}{\ell} \qquad \ldots\ldots \qquad (4.18)$$

and

$$H_2 = \frac{N_2 . i_2}{\ell} \qquad \ldots\ldots \qquad (4.19)$$

H_1 is constant and completely determined by the acc source, H_2 is alternating and to be determined. With a constant H_1, equations (4.16) and (4.17) show that the curves illustrating the dependence of B_a and B_b on H_2 have the same shape as the original magnetisation curve, but are shifted to the right and left along the axis of the abcissae by $\mp H_1$, as shown in Figure 4.27a. The alternating voltage applied to the load winding is equal to the sum of the self-induced emf's in the two halves of the winding:

$$V_2 = N_2 A \frac{d B_a}{dt} + N_2 A \frac{d B_b}{dt} = N_2 A \frac{d (B_a + B_b)}{dt} \qquad (4.20)$$

i.e. $B_a + B_b$ is determined by the alternating voltage V_2 and should vary sinusoidally as in Figure 4.27b. In Figure 4.27c, the curve $B_a + B_b = F_1(H_2)$ is constructed from the two curves in Figure 4.27a. By taking definite instants of time (e.g. $t=t_1$), it is possible to carry over the values of $B_a + B_b$ to the curve of Figure 4.27c (from point 1 to point 2), and then H_2 is obtained as in Figure 4.27d. H_2 and consequently i_2 contain no even harmonics, as the curve of $B_a + B_b$ in Figure 4.27c is odd-symmetrical.

In a similar manner, the voltage induced in the control winding is found as

$$V_1 = N_1 A \frac{d (B_b - B_a)}{dt} \qquad \ldots\ldots \qquad (4.21)$$

meaning that the waveform of the voltage V_1 is determined by $B_b - B_a$. The curve $B_b - B_a = F_2(H_2)$ is also constructed from the curves in Figure 4.27a and drawn in Figure 4.27c. It is important to emphasize that this curve is even-symmetrical about the vertical axis. Since the variation of H_2 with time is now known (Figure 4.27d), the variation of $B_b - B_a$ in time is determined by this curve, and is given in Figure 4.27e (point 4 is found from point 3 , and from there point 5 is obtained). As seen from Figure 4.27e, $B_b - B_a$ and, consequently, the voltage induced in the control winding vary with twice the frequency of the alternating voltage supply. Induction of a double frequency

voltage in the control winding, despite the fact that mutual flux coupling is cancelled by the symmetry of the system, simply verifies the existence of parametric coupling for the case of parallel interaction of magnetic fields. In the absence of bias ($I_1 = 0$, and $H_1 = 0$), the curves B_a and B_b in Figure 4.27a coincide, their differences vanish, and accordingly the emf induced in the control winding becomes equal to zero (no mutual coupling). Parametric coupling therefore comes into action only when both the control and load magnetisations exist simultaneously in the core. This is also true for orthogonal interaction of magnetic fields.

If the sources are not ideal and the winding resistances are not neglected in the examples above, the situation is much more complex, as all the flux densities and field intensities are variable. They will therefore influence each other, due to the existence of parametric coupling in both directions between the load and control circuits, as well as to the non-linearity in each individual circuit. Such a system can only be represented by two simultaneous non-linear differential equations if the magnetisation characteristic is given by an analytical expression in the form of $B = f(H)$ or $H = f(B)$.

4.3.2 Mathematical Representation of Saturable Reactors

In common practice, a saturable reactor used as a control device to control the ac power delivered to a load is considered

rather like a current-controlled inductance, which changes in value with the dc control current or, in other words, with the dc control mmf. This is shown in Figure 4.28, as the electrical circuit with no winding resistances and the generation of even harmonics in the control circuit neglected. The control winding acts as a short circuit to the dcc control source and the inductance of the load winding is a function of both i_1 (controller effect) and i_2 (non-linearity effect). As far as the controlling action of a saturable reactor is concerned, only the influence of the control circuit on the load circuit is considered. In magnetic terms, such a saturable reactor, with no winding and load resistances and with the control winding driven by a dcc source and the loading winding by an acv source, may be represented by a mmf-dependent mmf source, which is also a function of the flux passing through it, as shown in Figure 4.29a. The alternative representation in Figure 4.29b takes the input variable as the flux, rather than the mmf in the control circuit, which is readily calculable from the B/H curve once the mmf (or current) is known. The form of the function, $F_2(\phi_1, \phi_2)$ mainly depends on three facts: the shape and size of the magnetic core, the way the control flux ϕ_1 affects the load circuit, and finally the B/H characteristic of the magnetic material.

However, as already seen, parametric coupling exists mutually between the control and load circuits of a saturable reactor, and a saturable reactor can therefore be fully represented only by two flux-dependent mmf sources as shown in Figure 4.30a. This representation is convenient when both the windings are driven by

voltage sources. If the windings are driven by current sources, the alternative representation will have two mmf-dependent flux sources, as in Figure 4.30b. Depending on the types of the sources which actually drive the windings, two of the four magnetic variables F_1, F_2, ϕ_1 and ϕ_2 are dependent on the other two. So, with voltage sources driving both the windings, the representation of a saturable reactor as a magnetic system is given by the two functions

$$F_1 = F_1 (\phi_1, \phi_2)$$
$$F_2 = F_2 (\phi_1, \phi_2) \qquad \text{.....} \qquad (4.21)$$

The form of these functions depends on the configuration and physical dimensions of the magnetic core, on the magnetisation characteristic of the core material, and on the manner in which fluxes interact in the core.

Simply integrating both sides of equations 4.14 and 4.15, which together form an electrical representation of a saturable reactor, and taking the number of turns of the windings into account by the transformations $N_1.i_1 = F_1$ and $N_2.i_2 = F_2$ shows that it is possible to obtain the magnetic representation in the form

$$\phi_1 = \phi_1 (F_1, F_2)$$
$$\phi_2 = \phi_2 (F_1, F_2) \qquad \text{.....} \qquad (4.22)$$

which corresponds to Figure 4.30b.

4.4 Magnetic Structure of the Parametric Transformer

The new magnetic-core configurations proposed by Wanlass[11] for variable inductor devices may now be investigated in the light of the general review in the previous sections. Although the commercially available parametric transformers (Paraformer) employ the saturable reactor constructed from two C-cores, Figure 4.31a, saturable reactors with the same magnetic structure may be realized with the magnetic-core configurations[11] illustrated in Figures 4.31b and c. The common property of all those configurations is that the two main portions of the core are joined together by portions comprising four spaced zones (legs in the last figure) which are common to the magnetic circuits of both windings. Hence, the spaced zones (legs) act as the common regions where the fluxes produced by each winding undergo an interaction.

Although an exact view of three-dimensional flux distribution in such a magnetic core as Figure 4.31a is difficult to obtain, the basic form of flux distribution when only one of the windings is driven, may be illustrated as in Figure 4.32. The basic flux-path is then as in Figure 4.33. When the other winding is independently driven, the flux generated has a distribution symmetrical to that in Figure 4.32, which is characterized by the flux-path of Figure 4.34. It is now clear that the flux of one winding does not link the other, and that the flux density in the core is highest at the plane where the two halves of the core are in contact with

each other. These two points are also true for the other configurations of Figure 4.31: the highest flux density occurring within the four spaced zones (the four legs in the case of Figure 4.31c), and the basic flux-path of one winding not linking the other winding. The method used to eliminate mutual flux coupling is, therefore, the method 3(b) explained in Section 4.1.1. However, when one winding, for example winding 2 of Figure 4.32, is driven by a source of sufficiently large amplitude, a portion of the flux created may follow the alternative path shown in Figure 4.35, in addition to the portion following the basic flux-path in Figure 4.34. The flux following the path in Figure 4.35 links winding 1 by two separate paths, with directions such that the net flux through winding 1 is zero. Mutual coupling for this portion of flux is cancelled through method 2(a) in Section 4.1.1. The linking path of Figure 4.35 is longer and flux will normally prefer to flow through the shorter and lower-reluctance path in Figure 4.34. However, the C cores are ordinary transformer cores and the core material is anisotropic. In cold-rolled, silicon-iron transformer laminations, the flux paths of Figure 4.35 follow the directions of relatively easy magnetisation when compared with that of Figure 4.34. Therefore, if the flux density in the core is high, the portion of the flux which links winding 1 may not be negligible. Nevertheless, no effects of mutual coupling are observed as the net flux through this winding is zero. Finally, although it is not a necessary condition to prevent mutual coupling, orthogonal positioning of the windings (i.e. with their axes transverse) aids to eliminate the coupling through leakage flux by minimising pick-up of stray flux.

When both windings are driven simultaneously, the control and load fluxes following the basic flux-paths in Figures 4.33 and 4.34 respectively interact in the core both in parallel and in orthogonal manners. The zones where parallel or orthogonal flux interaction takes place is shown in Figure 4.36. For flux interaction to occur at any point in the core, the flux density at that particular point should be so high as to saturate the core material therein. As the highest flux density occurs where the two C-cores join, this is where the parallel interaction of fluxes takes place, and parallel interaction is predominant over orthogonal interaction. This is also true for all the other devices in Figure 4.31. Orthogonal flux interaction is negligible, because the total flux density at a point where the control and load fluxes cross at right angles, is much lower than that in the spaced zones (or legs), due to both the larger volume (or cross-sectional area) and to the vector summation of fluxes. This flux density cannot be increased to the saturation level, as the flux density in the zones where parallel interaction occurs will attain the saturation level much earlier. It may, therefore, be considered as orthogonal *intersection*, rather than interaction of fluxes, and its effect is negligible compared with the parallel flux interaction in the core. Parametric coupling is then achieved only through the parallel interaction of fluxes in the corresponding zones shown in Figure 4.36. Contrary to the thoughts of some authors[52], who have evaluated the parametric transformers as orthogonal flux systems, it is now seen clearly that orthogonal interaction is not

essential to the operation of the devices in Figure 4.31, and that they are all basically parallel-flux systems. This was also the case for the magnetic cross-valve devices in Figures 4.13 and 4.17. Although it may appear confusing at first sight, orthogonal positioning of the C-cores and the windings does not contribute significantly to the operation as a saturable reactor, apart from being a particular means of eliminating mutual coupling.

In Figure 4.37, a cross-sectional view at the plane where the two C-cores contact each other is shown. With the flux directions in Figures 4.33 and 4.34, for both windings driven, the control and load (or the primary and secondary) fluxes, ϕ_1 and ϕ_2, cut this plane in the directions shown in Figure 4.37. It is seen that the fluxes are additive in two of the four interaction zones and subtractive in the other two. This remains true if either one or both fluxes change their direction. If, for example, ϕ_1 is reversed (Figure 4.37), the fluxes are additive in zones 2 and 3 and subtractive in zones 1 and 4. If the directions of both fluxes are changed, one diagonal pair of zones (1 and 4) will still have additive fluxes and the other diagonal pair (2 and 3) subtractive fluxes. When the windings are driven by dcc sources of moderate magnitude, the first pair of zones is driven into saturation, whereas the latter remains far from saturation. If one of the sources is an acc source, the pair of zones in saturation will alternately be on the diagonals 1-4 and 2-3. Alternation of the saturated zones twice within a period of the

acc source immediately suggests the double-frequency modulation of the reluctances of the associated magnetic circuits. This is obvious because, when both windings are driven, flux interaction occurs and the fluxes are no longer independent of each other. Although one of the windings is driven by a dcc source, the flux created by this source, though unidirectional, is no longer constant but has a double frequency component as a result of parametric coupling. This is not due to the particular configuration of the device but is inherent in flux interaction and parametric coupling.

In a later and more comprehensive patent by Wanlass[53], operation of the devices in Figure 4.31 as saturable reactors is explained on the basis of what is termed *cross-over flux phenomena*. Cross-over flux is simply the portion of the alternating load flux which follows the path in Figure 4.35, and which links the control winding. In the case of no dc bias applied to the control winding, no voltage appears across the control winding as the linking fluxes balance out. When a direct current is applied to the control winding, creating a flux in the direction shown in Figure 4.33, zones 1 and 4 in Figure 4.35 are driven into saturation, resulting in a distortion of the balance condition for the *linking* flux portions. The net flux linking the control winding will no longer be zero, and a net alternating voltage will be induced in this winding. During the next half period of the alternating load current the load flux changes to the opposite direction, the saturated pair of zones will switch from 1-4 to 2-3, and a net alternating flux will link the control winding in the direction opposite

to that of the net flux which linked the control winding in the previous half period. Consequently, a double-frequency voltage will appear across the dc-fed control winding. This is called in the patent the *frequency-doubling operation mode of the variable transformer* the output from which is taken across an additional winding coupled to the control winding, as shown in Figure 4.38. It is said to be a *variable* transformer because the amplitude of the generated double-frequency component varies with the level of dc-bias in the core.

This is a rather mechanical explanation of the phenomenon of the generation of even harmonic components, which gives the wrong impression that this generation is due to the particular configuration of the core. In fact, as explained earlier, generation of even harmonic components can only be attributed to the parametric coupling occurring through flux interaction in non-linear medium. This explanation by Wanlass falls short, because the even harmonics are observed as soon as both windings are driven simultaneously, even with a small alternating source which does not cause the load flux to fringe out from the normal path in Figure 4.34 and to link the control winding with the paths in Figure 4.35. Furthermore, cross-over flux in the sense used by Wanlass means direct mutual flux coupling between the load and control windings, and this is what a saturable reactor is intended to avoid. In this study, the behaviour of the device, will, therefore, be explained on the basis of the normal flux distribution in the core, characterized by the flux-paths in Figures 4.33 and 4.34, and the flux portions which may follow the path in Figure 4.35 will be completely neglected.

4.4.1 Equivalent Magnetic Structure and Analogous Electric Circuit

Two basic assumptions have so far been made on the magnetic structure of the two C-core parametric transformer: Firstly, it is essentially a parallel-flux system and secondly the normal flux distribution in the core is characterized by the pair of flux-paths shown in Figures 4.33 and 4.34. When orthogonal flux interaction and flux linkages which may link the other winding in opposite directions are neglected, a magnetic core structure equivalent to all those in Figure 4.31 is given in Figure 4.39, without reference to the exact physical dimensions of any of the cores in Figure 4.31. The equivalence can be more readily understood if this structure is compared with the normal flux-paths in Figures 4.33 and 4.34, for a two C-core device. Almost the same structure is obtained by cutting the marked sections out of the core of the device in Figure 4.31c, as shown in Figure 4.40. This equivalent structure establishes the magnetic model for the two C-core parametric transformers, a model on which whole analyses in this study are based.

From the magnetic model in Figure 4.39, it can be seen directly that no flux produced by one winding can link the other when only one of the windings is energized, and therefore that mutual flux coupling is absent. When both windings are energized, the fluxes created by them undergo parallel interaction in the branches which connect the main branches where the windings are placed.

The whole question of this magnetic model being exactly equivalent to any of those cores in Figure 4.31 lies simply in choosing proper values for ℓ_1, A_1, ℓ_2, A_2, ℓ_0, and A_0, the lengths and cross-sectional areas of the core branches, shown in Figure 4.39, by considering the flux distribution in the particular core concerned.

An analogous electrical circuit for the magnetic model of Figure 4.39 is given in Figure 4.41, when both the resistance-less windings are driven by voltage sources. The values of the reluctances in each branch depend on the total flux flowing through the corresponding branch of the magnetic model (i.e. the bridged magnetic core). When the secondary winding is unexcited ($\phi_2 = 0$), all four reluctances in the bridge become equal $[R'(\phi_1) = R''(\phi_1)]$, and the bridge is balanced, and none of the flux ϕ_1 flows through R_2.

However, when both flux sources exist simultaneously, the bridge is not balanced, as in different branches of the bridge different total flux values are present $[R'(\phi_1 - \phi_2) \neq R''(\phi_1 + \phi_2)]$. The value of the flux in one main branch is completely determined by the flux source in that branch, i.e. in one main branch only the flux created by the source of that branch can be present. This requirement arises since no mutual flux coupling exists between the windings of the bridged magnetic core. However, on introduction of the flux source ϕ_2, the mmf difference between the points A and B departs from zero. If the flux ϕ_1 is created by a dcv source and the flux ϕ_2 by an acv source of frequency f, a non-zero mmf difference will exist between A and B (or C and D) at the frequency f, if the circuit is linear. In fact, since the bridge

becomes out of balance twice in a period, due to the flux interaction in the non-linear reluctances R' and R", the mmf across AB (or CD) has also an alternating component of the frequency 2f.

The analogy between the bridged core and the magnetic cross-valve of Figure 4.17 is obvious, and if the connection between the points O' and O" in Figure 4.22 is removed, the two circuits become identical. Disconnecting O' from O" corresponds to neglecting orthogonal flux interaction in the central region of the device in Figure 4.17, and results in the assumption that the device is a completely parallel-flux system, just as the assumption already made when deriving the bridged magnetic core as a magnetic model for the devices in Figure 4.31. Analyses developed on the bridged magnetic core therefore apply also to the magnetic cross-valve utilising the winding arrangement in Figure 4.17. The equivalence of the magnetic cross-valve with orthogonally placed windings, Figure 4.13, to the magnetic model of the bridged core may also be obtained by using a different winding arrangement in Figure 4.39. Instead of being on the main magnetic branches, the windings may be placed on the branches of the bridge, in two equal halves of each winding, as indicated in Figure 4.42. Parallel interaction of the fluxes then takes place only in the main branches of the core, as is also evident from Figures 4.15 and 4.16. The magnetic cross-valves have a magnetic structure basically equivalent to that of the core configurations in Figure 4.31. Actually, the frequency changing devices of Mc. Creary[41-47], employing magnetic cross-valves of this type are essentially parametric transformers, operating as frequency mult-

ipliers or dividers. The *unusual* characteristics of magnetic cross-valve devices[39,40] such as the voltage regulation, load regulation, over-load protection, energy transfer without mutual inductance, etc., are only inherent in the phenomenon of parametric excitation and resonance.

4.4.2 Mathematical Representation of the Bridged Magnetic Core

When the bridged magnetic core device of Figure 4.39 is considered as a saturable reactor, it should be represented by a set of two functions in the form of either equation (4.21) or (4.22). These functions will now be derived directly from the structure of the bridged magnetic core, and will then be used in the analysis of parametric transformers, as this core provides the assumed magnetic model.

In normal parametric transformer operation, the primary winding is driven by an acv source. Since the output voltage obtained is of constant amplitude and constant frequency, and is also a good sinusoid, the secondary winding may be considered to be also driven by an acv source, with the secondary capacitor replaced by an equivalent acv source. In this case, the functions representing the magnetic system are more conveniently written as

$$F_1 = F_1(\phi_1, \phi_2) \qquad \ldots\ldots \qquad (4.23)$$

$$F_2 = F_2(\phi_1, \phi_2)$$

and to obtain the required form of these functions, the magnetisation characteristic of the core material must be given in the form

$$H = f(B) \qquad \ldots\ldots \qquad (4.24)$$

Since the cores of the two-C-core parametric transformer are made of the same magnetic material, the function (4.24) relates the field intensity to the flux density at any particular point in the bridged magnetic core.

The electrical analogue of the magnetic model is redrawn in Figure 4.43, where the mmf drops across each reluctance, and the fluxes flowing in each branch in terms of the three mesh fluxes ϕ_1, ϕ_2 and ϕ_0 are shown. Application of Kirchhoff's second law to each closed loop indicated in the figure gives the circuit equations

$$F_1 = F_a + F_e + F_f$$

$$F_2 = F_b + F_d - F_e \qquad \ldots\ldots \qquad (4.25)$$

$$F_c + F_d - F_e - F_f = 0$$

where the mmf drops F_a to F_f are defined by

$$F_a = R_a.\phi_1$$

$$F_b = R_b.\phi_2$$

$$F_c = R_c.\phi_0$$

$$F_d = R_d.(\phi_2 + \phi_0) \qquad \ldots\ldots \qquad (4.26)$$

$$F_e = R_e.(\phi_1 - \phi_0 - \phi_2)$$

$$F_f = R_f.(\phi_1 - \phi_0)$$

The reluctances R_a to R_f are functions of flux, and their magnetic circuits have the cross-sectional areas and flux-path lengths: A_1 and ℓ_1 for R_a; A_2 and ℓ_2 for R_b; and A_0 and $\frac{1}{2}\ell_0$ for R_c to R_f, as shown in Figure 4.39. By using the general relationships

$$F = H.\ell$$

$$H = f(B) \qquad \ldots\ldots \qquad (4.27)$$

and $$B = \frac{\phi}{A}$$

the mmf drops F_a to F_f can be expressed as

$$F_a = \ell_1 . f(\frac{\phi_1}{A_1})$$

$$F_b = \ell_2 . f(\frac{\phi_2}{A_2})$$

$$F_c = \frac{1}{2} \ell_0 . f(\frac{\phi_0}{A_0})$$

$$F_d = \frac{1}{2} \ell_0 . f(\frac{\phi_2 + \phi_0}{A_0}) \qquad \ldots\ldots \qquad (4.28)$$

$$F_e = \frac{1}{2} \ell_0 . f(\frac{\phi_1 - \phi_0 - \phi_2}{A_0})$$

$$F_f = \frac{1}{2} \ell_0 . f(\frac{\phi_1 - \phi_0}{A_0})$$

When these are substituted in equations (4.25), the circuit equations become:

$$F_1 = \ell_1 . f(\frac{\phi_1}{A_1}) + \frac{1}{2} \ell_0 [f(\frac{\phi_1 - \phi_0}{A_0}) + f(\frac{\phi_1 - \phi_0 - \phi_2}{A_0})] \qquad (4.29)$$

$$F_2 = \ell_2 . f(\frac{\phi_2}{A_2}) + \frac{1}{2} \ell_0 [f(\frac{\phi_2 + \phi_0}{A_0}) - f(\frac{\phi_1 - \phi_0 - \phi_2}{A_0})] \qquad (4.30)$$

$$f(\frac{\phi_0}{A_0}) + f(\frac{\phi_2 + \phi_0}{A_0}) - f(\frac{\phi_1 - \phi_0 - \phi_2}{A_0}) - f(\frac{\phi_1 - \phi_0}{A_0}) = 0 \qquad (4.31)$$

In order to obtain the functions (4.23), the variable ϕ_0 must be eliminated in equations (4.29) to (4.31). However, these equations are nonlinear because of the nonlinear function H = f(B), and the magnetisation characteristic H = f(B) must be given analytically to enable ϕ_0 to be eliminated. Neglecting hysteresis and the

curvature around the origin, the magnetisation characteristic of the core material can be represented by the power series

$$H = f(B) = c_1 B + c_3 B^3 + c_5 B^5 + \ldots \ldots \qquad (4.32)$$

where the c terms are constants. Using this form of the function f(B) in equation (4.31), results in the condition

$$\frac{c_1}{A_0}[\phi_0 + (\phi_0 + \phi_2) - (\phi_1 - \phi_0 - \phi_2) - (\phi_1 - \phi_0)] +$$

$$\frac{c_3}{A_0^3}[\phi_0^3 + (\phi_0 + \phi_2)^3 - (\phi_1 - \phi_0 - \phi_2)^3 - (\phi_1 - \phi_0)^3] +$$

$$\frac{c_5}{A_0^5}[\phi_0^5 + (\phi_0 + \phi_2)^5 - (\phi_1 - \phi_0 - \phi_2)^5 - (\phi_1 - \phi_0)^5] + \ldots = 0$$

$$\ldots\ldots \qquad (4.33)$$

For this to be equal to zero, each term within the square brackets must simultaneously be zero. In fact, if the linear term equals to zero, all the other terms immediately become equal to zero because of the identity

$$(a^n + b^n + c^n + d^n) \equiv (a + b + c + d)\ (\ldots\ldots.)$$

valid for all n=integer. Equating the linear term to zero, ϕ_0, the non-zero flux circulating around the bridge is found as

$$\phi_0 = \frac{\phi_1 - \phi_2}{2}$$

so that the fluxes in each branch of the bridge in Figure 4.43, are

$$\phi_1 - \phi_0 = \frac{\phi_1 + \phi_2}{2}$$

$$\phi_1 - \phi_0 - \phi_2 = \frac{\phi_1 - \phi_2}{2} \qquad \ldots\ldots \qquad (4.34)$$

$$\phi_0 + \phi_2 = \frac{\phi_1 + \phi_2}{2}$$

$$\phi_0 = \frac{\phi_1 - \phi_2}{2}$$

and the two circuit equations (4.29) and (4.30) become

$$F_1 = F_1(\phi_1, \phi_2) = \ell_1 . f(\frac{\phi_1}{A_1}) + \frac{1}{2}\ell_0 [f(\frac{\phi_1 + \phi_2}{2A_0}) + f(\frac{\phi_1 - \phi_2}{2A_0})] \qquad (4.35)$$

$$F_2 = F_2(\phi_1, \phi_2) = \ell_2 \; f(\frac{\phi_2}{A_2}) + \frac{1}{2}\ell_0 [f(\frac{\phi_1 + \phi_2}{2A_0}) - f(\frac{\phi_1 - \phi_2}{2A_0})] \qquad (4.36)$$

The functions (4.35) and (4.36) together constitute the exact mathematical representation of the bridged magnetic core and of the two-C-core device when A_1, ℓ_1, A_2, ℓ_2, A_0 and ℓ_0 are properly chosen. Corresponding to the representation in Figure 4.30a, these

two functions relate ϕ_1 and ϕ_2 to F_1 and F_2, and express the parametric coupling between the primary and secondary circuits (as each of F_1 and F_2 is a function of both ϕ_1 and ϕ_2). Their forms depend on (i) the form of the magnetisation characteristic whose nonlinearity, without any restriction on its degree, can now be fully expressed, (ii) the configuration and the dimensions of the magnetic core, (iii) the manner of flux interaction in the core. The parallel interaction of the fluxes ϕ_1 and ϕ_2 is demonstrated by equations (4.34) and by the fact that, in equations (4.35) and (4.36), $f(\frac{\phi_1 \mp \phi_2}{2A_0}) \neq f(\frac{\phi_1}{2A_0}) \mp f(\frac{\phi_2}{2A_0})$.

Another point on the forms of the function (4.35) and (4.36) is that, when the bridged magnetic core is symmetrical, i.e. $\ell_1 = \ell_2$ and $A_1 = A_2$, there is interchangeability between ϕ_1 and ϕ_2 in order to obtain F_1 from equation (4.36) and F_2 from equation (4.35). With $\ell_1 = \ell_2$ and $A_1 = A_2$, interchanging ϕ_1 and ϕ_2 in equation (4.35) produces equation (4.36), and similarly, interchanging ϕ_1 and ϕ_2 in equation (4.36) results in equation (4.35). This is clearly because, in addition to the physical symmetry of the core, the magnetisation characteristic $H = f(B)$ is odd symmetrical, and $f(\frac{\phi_1 - \phi_2}{2A_0}) = -f(\frac{\phi_2 - \phi_1}{2A_0})$.

Once the magnetisation characteristic is known, the functions $F_1(\phi_1, \phi_2)$ and $F_2(\phi_1, \phi_2)$ completely explain the behaviour of the device when the resistanceless primary and secondary windings are driven by ideal voltage sources. If resistances exist in the system, the equations describing the system, both electrically and

magnetically, will become differential equations.

4.4.3 Inclusion of Air-Gap

In the two-C-core device, an air-gap, however small, is inevitably present where the two C cores join, although special care is taken to minimise this by matching two cores with properly machined faces. Since even a small air-gap results in large changes in the total reluctance or inductance values, the presence of an air-gap must also be included in the magnetic model of the two-C-core device.

Air-gaps in the two-C-core device exist on the four rectangular areas shown by heavy lines in Figure 4.37 (the contacting portions of the faces of the C cores). Since these unintentional gaps are very small, it is firstly assumed that no fringing occurs and that the area of the gaps is equal to A_0, the cross-sectional area of the bridged-branches of the magnetic model. Secondly, all of the four air-gaps are assumed to have equal lengths, ℓ_g, as well as equal areas A_0.*

---

* These assumptions are made in order to simplify the way the air-gap reluctance enter into the equations. The air is a linear medium for magnetism and no flux interaction occurs in the air-gap, but, because of the core configuration with four air-gaps through which both ϕ_1 and ϕ_2 pass, four completely different gaps result in an effect somewhat similar to flux interaction. In that case, the condition (4.42), is not satisfied, and consequently, non-autonomous terms having ℓ_g appear in the primary and secondary reluctances.

This results in four equal air-gap reluctances in the bridge-branches of Figure 4.44, where the same variables (as in Figure 4.43) are assigned. From this figure, the loop equations are

$$F_1 = F_a + F_e + F_f + F_{g_3} + F_{g_4} \qquad \ldots\ldots \qquad (4.37)$$

$$F_2 = F_b + F_a - F_e + F_{g_2} - F_{g_3} \qquad \ldots\ldots \qquad (4.38)$$

$$(F_c + F_d - F_e - F_f) + (F_{g_1} + F_{g_2} - F_{g_3} - F_{g_4}) = 0 \qquad (4.39)$$

where F_a to F_f are the same as those given by equations (4.26) and

$$F_{g_1} = R_g . \phi_0$$

$$F_{g_2} = R_g . (\phi_2 + \phi_0) \qquad \ldots\ldots \qquad (4.40)$$

$$F_{g_3} = R_g . (\phi_1 - \phi_0 - \phi_2)$$

$$F_{g_4} = R_g . (\phi_1 - \phi_0)$$

The linear (constant) reluctance of one air-gap is given by

$$R_g = \frac{\ell_g}{\mu_0 A_0} \qquad \ldots\ldots \qquad (4.41)$$

Substituting for F_c to F_{g_4} in equation (4.39) and proceeding in the same manner as before, using the magnetisation characteristic given by equation (4.32), the condition to eliminate ϕ_0 becomes

$$\left(\frac{C_1}{A_0} + R_g\right).\left[\phi_0 + (\phi_2 + \phi_0) - (\phi_1 - \phi_0 - \phi_2) - (\phi_1 - \phi_0)\right] +$$

$$\frac{C_3}{A_0^3}\left[\phi_0^{\,3} + (\phi_2 + \phi_0)^3 - (\phi_1 - \phi_0 - \phi_2)^3 - (\phi_1 - \phi_0)^3\right] +$$

$$\frac{C_5}{A_0^5}\left[\phi_0^{\,5} + (\phi_2 + \phi_0)^5 - (\phi_1 - \phi_0 - \phi_2)^5 - (\phi_1 - \phi_0)^5\right] + \ldots\ldots = 0$$

$$\ldots\ldots \qquad (4.42)$$

Evidently, this condition is satisfied when $\phi_0 = \frac{1}{2}(\phi_1 - \phi_2)$, and the branch fluxes are as given by equations (4.34). Substituting equations (4.34) into (4.40), and the result obtained into (4.37) and (4.38) gives*

---

* Although equations (4.43) and (4.44) are obtained on the assumption that all the air-gaps are equal, it is noticeable that with four different air-gap reluctances, the simplification made therein does not apply, and hence F_1 and F_2 will have extra non-autonomous terms which are functions of the air-gaps.

$$F_1 = F_a + F_e + F_f + R_g.\frac{1}{2}(\phi_1 - \phi_2) + R_g.\frac{1}{2}(\phi_1 + \phi_2) = F_a + F_e + F_f + R_g\ \phi_1$$

..... (4.43)

$$F_2 = F_b + F_d - F_e + R_g.\frac{1}{2}(\phi_1 + \phi_2) - R_g.\frac{1}{2}(\phi_1 - \phi_2) = F_b + F_d - F_e + R_g\ \phi_2$$

..... (4.44)

and finally, the two functions representing the bridged magnetic core with equal air-gaps are obtained as

$$F_1 = F_1(\phi_1, \phi_2) = R_g.\ \phi_1 + \ell_1\ .f(\frac{\phi_1}{A_1}) + \frac{1}{2}.\ \ell_0\ [f(\frac{\phi_1 + \phi_2}{2A_0}) + f(\frac{\phi_1 - \phi_2}{2A_0})]$$

..... (4.45)

$$F_2 = F_2(\phi_1, \phi_2) = R_g.\phi_2 + \ell_2\ .f(\frac{\phi_2}{A_2}) + \frac{1}{2}.\ \ell_0\ [f(\frac{\phi_1 + \phi_2}{2A_0}) - f(\frac{\phi_1 - \phi_2}{2A_0})]$$

..... (4.46)

Obviously, all the remarks made for the functions (4.35) and (4.36) are valid also for the functions (4.45) and (4.46). In addition, it is understood that the necessary condition to obtain the analytic representation of the bridged core magnetic model (as given by equations (4.45) and (4.46) or by (4.35) and (4.36))is that the bridge-branches of the core in Figure 4.39 have equal

linear reluctances, that is, each bridge-branch has the same cross-sectional area A_0, and the same flux-path length $\frac{\ell_0}{2}$, and that the air-gaps present are also of the same length, ℓ_g. (The core is assumed to be made of the same magnetic material uniformly throughout its structure). Without this symmetry, it is not possible to obtain a mathematical representation with only the two functions, $F_1(\phi_1, \phi_2)$ and $F_2(\phi_1, \phi_2)$, but there will be at least a third variable and a third constraint equation similar to equation (4.31).

However, this gives rise to the possibility of exercising an external influence on the flux interaction in the core, as the differences between the linear reluctances of the bridge-branches changes the form of the relationships between F_1, F_2 and ϕ_1, ϕ_2. By introducing intentional air-gaps into one or more of the four rectangular areas in Figure 4.37, the $F_1(\phi_1, \phi_2)$ and $F_2(\phi_1, \phi_2)$ functions of a two-C-core device can be altered to a certain extent, and this may prove useful in obtaining improvements in some of the operational characteristics of parametric transformers.

For the purpose of tailoring the operational characteristics of the two-C-core parametric transformers, changing the proportion of A_1, A_2 and A_0 may also be considered, since the forms of the functions (4.45) and (4.46) depend significantly on their values.

4.4.4 The Primary and Secondary Inductances

With $\phi_2 = 0$, equation (4.45), gives

$$F_1 = F_1(\phi_1) = R_g\,\phi_1 + \ell_1 . f(\frac{\phi_1}{A_1}) + \ell_0 \quad .f(\frac{\phi_1}{2A_0}) \quad \cdots \qquad (4.47)$$

For values of the primary flux density far below the saturation level, the magnetisation characteristic may be expressed by the linear function

$$H = f(B) = \frac{1}{\mu} B \qquad \ldots\ldots \qquad (4.48)$$

where $\mu = \mu_0 . \mu_r$ is the absolute permeability, and the relative permeability μ_r has a maximum and constant value. (The curvature near the origin is neglected). Using equation (4.48) in (4.47), the primary mmf is found as

$$F_1 = F_1(\phi_1) = R_g\,\phi_1 + \frac{\ell_1}{\mu\,A_1} . \phi_1 + \frac{\ell_0}{\mu\,2A_0}\,\phi_1$$

and the minimum constant value of the primary reluctance is

$$R_{m1min} = \frac{F_1(\phi_1)}{\phi_1} = R_g + \frac{\ell_1}{\mu\,A_1} + \frac{\ell_0}{\mu\,2A_0} = \frac{\ell_g}{\mu_0\,A_0} + \frac{\ell_1}{\mu\,A_1} + \frac{\ell_0}{\mu\,2A_0} \qquad (4.49)$$

The primary inductance is then calculated from

$$L_{1max} = \frac{N_1^{\,2}}{R_{m1min}} = \frac{N_1^{\,2}}{\dfrac{\ell_g}{\mu_0 A_0} + \dfrac{\ell_1}{\mu A_1} + \dfrac{\ell_0}{\mu 2A_0}} \qquad \ldots\ldots \qquad (4.50)$$

which is a maximum for $\phi_2 = 0$ and $\phi_1 << \phi_s$.

Similarly, the minimum and constant value of the secondary reluctance is obtained from equation (4.46) for $\phi_1 = 0$ and $\phi_2 << \phi_s$, as

$$R_{m2min} = R_g + \frac{\ell_2}{\mu A_2} + \frac{\ell_0}{\mu 2A_0} \qquad \ldots\ldots \qquad (4.51)$$

and the maximum value of the secondary inductance is

$$L_{2max} = \frac{N_2^{\,2}}{R_{m2min}} = \frac{N_2^{\,2}}{\dfrac{\ell_g}{\mu_0 A_0} + \dfrac{\ell_2}{\mu A_2} + \dfrac{\ell_0}{\mu 2A_0}} \qquad \ldots\ldots \qquad (4.52)$$

These are the values of the primary and secondary inductances which would be measured when no biasing flux existed in the core with a B/H characteristic not exhibiting a curvature near the origin.

4.5 Mathematical Representation of Other Saturable Reactors

As a parametric transformer may be constructed by using any form of saturable reactor, the exact mathematical representations for two other forms of saturable reactors with parallel and orthogonal flux interaction, will be given in order to complete

the general treatment of saturable reactors. These representations are in the form of equations (4.21) corresponding to Figure 4.30a. However, the representation in the form of equations (4.22) can be obtained in a similar way by using the magnetisation characteristic in the form B = f(H) and by considering that the (resistanceless) primary and secondary windings are driven by (ideal) current sources.

4.5.1 A Parallel-Flux Saturable Reactor

The device in Figure 4.5 is redrawn in Figure 4.45, with the assumption that the primary and the secondary windings are resistanceless and driven by ideal voltage sources. Half the number of turns of each winding are on each core, with the relative directions shown. Both cores have the same cross-sectional area A, and the same mean flux-path length ℓ. The voltage equations for the two cores are

$$v_1 = v_{a1} + v_{b1} = \frac{N_1}{2}\frac{d\phi_a}{dt} + \frac{N_1}{2}\frac{d\phi_b}{dt} = N_1\frac{d}{dt}\left(\frac{\phi_a + \phi_b}{2}\right) \qquad (4.53)$$

$$v_2 = v_{a2} + v_{b2} = \frac{N_2}{2}\frac{d\phi_a}{dt} - \frac{N_2}{2}\frac{d\phi_b}{dt} = N_2\frac{d}{dt}\left(\frac{\phi_a - \phi_b}{2}\right) \qquad (4.54)$$

where ϕ_a and ϕ_b are the total fluxes created in the cores a and b, respectively, with the directions shown. Because of the two separate cores and two separate halves for each winding, a single

primary or secondary flux is not distinctly identifiable directly from the magnetic structure of Figure 4.45. However, a primary flux may be defined as

$$\phi_1 = \frac{\phi_a + \phi_b}{2} \qquad \ldots\ldots \qquad (4.55)$$

giving a primary voltage of

$$v_1 = N_1 \frac{d\,\phi_1}{dt}$$

from equation (4.53). Similarly, a secondary flux, defined as

$$\phi_2 = \frac{\phi_a - \phi_b}{2} \qquad \ldots\ldots \qquad (4.56)$$

gives a secondary voltage, from equation (4.54) as

$$v_2 = N_2 \frac{d\,\phi_2}{dt}$$

The primary and secondary mmf's are, by definition,

$$F_1 = N_1 . i_1$$

$$F_2 = N_2 . i_2$$

and the total mmf's creating the flux ϕ_a in core a, and flux ϕ_b in core b are, respectively

$$F_a = \frac{F_1}{2} + \frac{F_2}{2} \qquad \ldots\ldots \qquad (4.57)$$

$$F_b = \frac{F_1}{2} - \frac{F_2}{2} \qquad \ldots\ldots \qquad (4.58)$$

as is evident from the figure. F_1 and F_2 are obtained from equations (4.57) and (4.58) as

$$F_1 = F_a + F_b$$

$$F_2 = F_a - F_b$$

and F_a and F_b are related to ϕ_a and ϕ_b through the general relationships (4.27) as

$$F_a = \ell . f(\frac{\phi_a}{A})$$

$$F_b = \ell . f(\frac{\phi_b}{A})$$

Hence,

$$F_1 = \ell . \ [f(\frac{\phi_a}{A}) + f(\frac{\phi_b}{A})] \qquad ..... \qquad (4.59)$$

and

$$F_2 = \ell . \ [f(\frac{\phi_a}{A}) - f(\frac{\phi_b}{A})] \qquad ..... \qquad (4.60)$$

Solving equations (4.55) and (4.56) for ϕ_a and ϕ_b, gives

$$\phi_a = \phi_1 + \phi_2$$

$$\phi_b = \phi_1 - \phi_2$$

and when these are substituted into equations (4.59) and (4.60), the resulting functions are

$$F_1 = F_1(\phi_1, \phi_2) = \ell\ [f(\frac{\phi_1 + \phi_2}{A}) + f(\frac{\phi_1 - \phi_2}{A})] \quad \ldots \qquad (4.61)$$

$$F_2 = F_2(\phi_1, \phi_2) = \ell\ [f(\frac{\phi_1 + \phi_2}{A}) - f(\frac{\phi_1 - \phi_2}{A})] \quad \ldots \qquad (4.62)$$

which constitute an exact representation of the device. Most of the remarks made for equations (4.35) and (4.36) are also valid for equations (4.61) and (4.62). There is a striking similarity between the forms of both sets of equations, which is natural since both the bridged magnetic core and the device of Figure 4.5 are parallel-flux saturable reactors in which parametric coupling is achieved through parallel flux interaction. The parametric coupling term resulting from flux interaction is the second term in equations (4.35) and (4.36), where the first term is non-parametric, and there is no such non-parametric term in equations (4.61) and (4.62), where the whole function is a consequence of flux interaction. This is obviously because parallel flux interaction takes place only in a part of the bridged magnetic core (the bridge-branches), whereas the whole volume of the cores in Figure 4.5 is available for flux interaction.

4.5.2 An Orthogonal-Flux Saturable Reactor

The cross-sectional view of a hollow toroidal core is shown in Figure 4.46. The primary winding of N_1 turns is on the outside of the toroidal core, and the N_2 turns of the secondary winding

are within the annular hollow. The mean flux-path lengths for the primary and the secondary magnetic circuits are

$$\ell_1 = 2\pi R$$

and $$\ell_2 = 2\pi \left(\frac{R_1 + R_2}{2}\right) = \pi (R_1 + R_2)$$

respectively. Although ϕ_1 and ϕ_2 are orthogonal everywhere in the core, the flux distribution is such that the primary flux is uniformly distributed within the area

$$A_1 = \pi (R_2^2 - R_1^2)$$

but the secondary flux is not so distributed, as the area orthogonal to the closed flux-path of ϕ_2 is not constant along this flux-path with mean length ℓ_2. The area associated with ϕ_2 varies along its closed flux-path in the form

$$A_2(\alpha) = 2\pi R (R_2 - R_1) - \pi (R_2^2 - R_1^2)\cos\alpha \qquad (4.63)$$

where α is the angle shown in Figure 4.46a, and takes the maximum and minimum values

$$A_2' = 2\pi R (R_2 - R_1) + \pi (R_2^2 - R_1^2)$$

$$A_2''' = 2\pi R (R_2 - R_1) - \pi (R_2^2 - R_1^2)$$

for $\alpha = 180^0$ and 0^0, respectively, The mean value of A_2, for $\alpha = 90^0$, is

$$A_2'' = 2\pi R\ (R_2 - R_1)$$

The secondary flux created by the voltage source v_2 is fixed, but, since

$$B_2 = \frac{\phi_2}{A_2(\alpha)}$$

the secondary flux density B_2 is not constant everywhere in the core. Hence, the interaction between ϕ_1 and ϕ_2 is also a function of the angle α. Since the functions $F_1(\phi_1, \phi_2)$ and $F_2(\phi_1, \phi_2)$ are obtained through flux interaction, the dependence of the flux interaction on the coordinates of the point where interaction occurs, makes deriving F_1 and F_2 as functions of both ϕ_1 and ϕ_2 so complex that it is not practicable. It is shown in Appendix III that, even when only the secondary flux exists in the core, the function $F_2(\phi_2)$ has a quite complex form, because of the dependence of A_2 on α. Therefore, to neglect this effect resulting from the shape of the toroid core, and to assume a large slice of the toroidal core to be a straight cylinder, R is considered as much greater than R_1 and R_2. Consequently, A_2 is the same everywhere along the secondary magnetic path, with the constant (mean) value

$$A_2 = A_2'' = 2\pi R\ (R_2 - R_1)$$

and then the secondary flux density is constant everywhere in the core resulting in a uniform distribution of ϕ_2.

When only the secondary winding is driven by a voltage source, the secondary flux density $\vec{B}_2$ creates a field strength $\vec{H}'_2$, and driving only the primary winding by a voltage source results in $\vec{B}_1$ which creates $\vec{H}'_1$, as shown in Figure 4.47. When both windings are driven simultaneously, the total flux density at any point in the core is $\vec{B} = \vec{B}_1 + \vec{B}_2$ which produces a total field strength $\vec{H}$ as shown in the figure, (magnetic permeability of the core material is assumed isotropic and not tensoral). Clearly, $\vec{H} \neq \vec{H}'$ and $|\vec{H}| > |\vec{H}'|$, because of the nonlinearity of the medium. The components of the magnetic field strength $\vec{H}$ in the directions of $\vec{B}_1$ and $\vec{B}_2$ are

$$|\vec{H}_1| = |\vec{H}| \cos \gamma$$

$$|\vec{H}_2| = |\vec{H}| \sin \gamma$$

where $\cos \gamma = \dfrac{|\vec{B}_1|}{|\vec{B}|}$

and $\sin \gamma = \dfrac{|\vec{B}_2|}{|\vec{B}|}$, as apparent from Figure 4.47.

Hence,

$$H_1 = \frac{B_1}{(B_1^{\,2} + B_2^{\,2})^{\frac{1}{2}}} H \qquad \ldots\ldots \qquad (4.63)$$

$$H_2 = \frac{B_2}{(B_1^{\,2} + B_2^{\,2})^{\frac{1}{2}}} H \qquad \ldots\ldots \qquad (4.64)$$

The resultant field strength H is inexorably fixed by $\vec{B} = \vec{B}_1 + \vec{B}_2$, and is given by the magnetisation characteristic as

$$H = f(B) = f[(B_1^{\,2} + B_2^{\,2})^{\frac{1}{2}}]$$

Then, equations (4.63) and (4.64) become

$$H_1 = \frac{B_1}{(B_1^{\,2} + B_2^{\,2})^{\frac{1}{2}}} \cdot f\,[(B_1^{\,2} + B_2^{\,2})^{\frac{1}{2}}] \quad \ldots\ldots \qquad (4.65)$$

$$H_2 = \frac{B_2}{(B_1^{\,2} + B_2^{\,2})^{\frac{1}{2}}} \cdot f\,[(B_1^{\,2} + B_2^{\,2})^{\frac{1}{2}}] \quad \ldots\ldots \qquad (4.66)$$

Since the primary flux distribution is uniform, and the secondary flux distribution is assumed uniform,

$$B_1 = \frac{\phi_1}{A_1}$$

$$B_2 = \frac{\phi_2}{A_2}$$

and $\qquad F_1 = H_1 . \ell_1$

$$F_2 = H_2 . \ell_2$$

Consequently, the two functions representing the hollow toroid core saturable reactor (when both windings are driven by voltage

sources) are

$$F_1 = F_1(\phi_1, \phi_2) = \frac{\ell_1}{A_1}\phi_1 \cdot \frac{f\left[\left(\frac{\phi_1^2}{A_1^2} + \frac{\phi_2^2}{A_2^2}\right)^{\frac{1}{2}}\right]}{\left(\frac{\phi_1^2}{A_1^2} + \frac{\phi_2^2}{A_2^2}\right)^{\frac{1}{2}}} \quad \ldots\ldots \quad (4.67)$$

$$F_2 = F_2(\phi_1, \phi_2) = \frac{\ell_2}{A_2}\phi_2 \cdot \frac{f\left[\left(\frac{\phi_1^2}{A_1^2} + \frac{\phi_2^2}{A_2^2}\right)^{\frac{1}{2}}\right]}{\left(\frac{\phi_1^2}{A_1^2} + \frac{\phi_2^2}{A_2^2}\right)^{\frac{1}{2}}} \quad \ldots\ldots \quad (4.68)$$

Again, there is only one term in equations (4.67) and (4.68) which results from flux interaction, because orthogonal flux interaction occurs in the whole of the core. With such a device as in Figure 4.11, where orthogonal flux interaction takes place only in a part of the core, additional non-parametric terms would appear in the functions $F_1(\phi_1, \phi_2)$ and $F_2(\phi_1, \phi_2)$ to account for mmf drops across the reluctances of branches where only one of the fluxes exists. The remarks made for the functions (4.35) and (4.36) are also valid for the functions (4.67) and (4.68), except that the manner of flux interaction is now orthogonal.

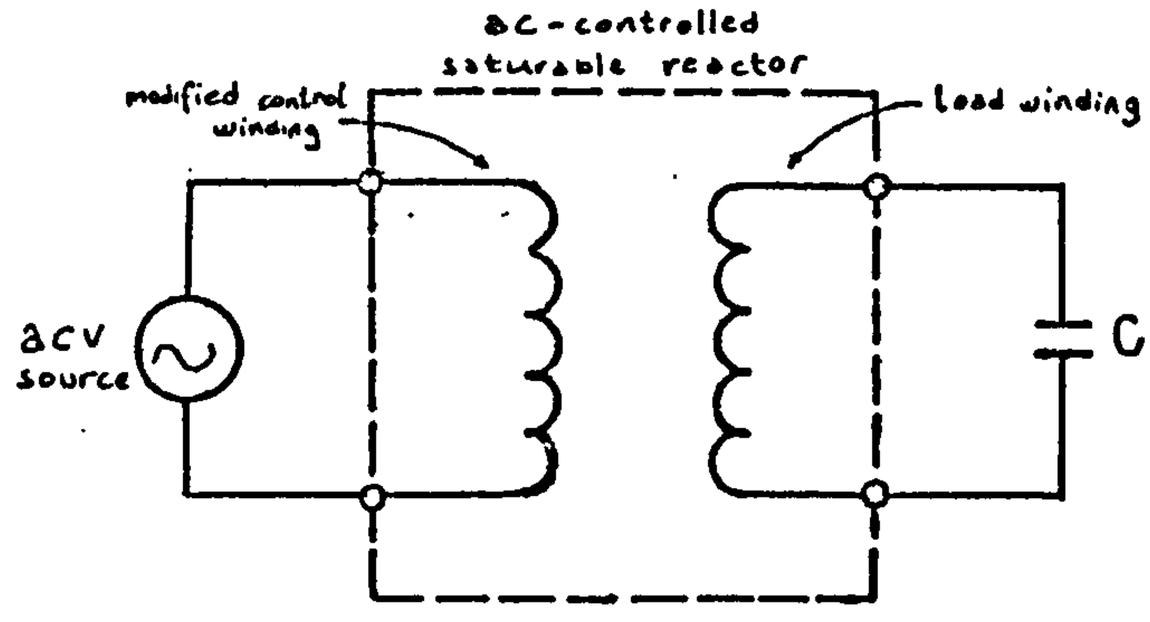

Figure 4.1 Parametric transformer comprising a saturable reactor and a capacitor

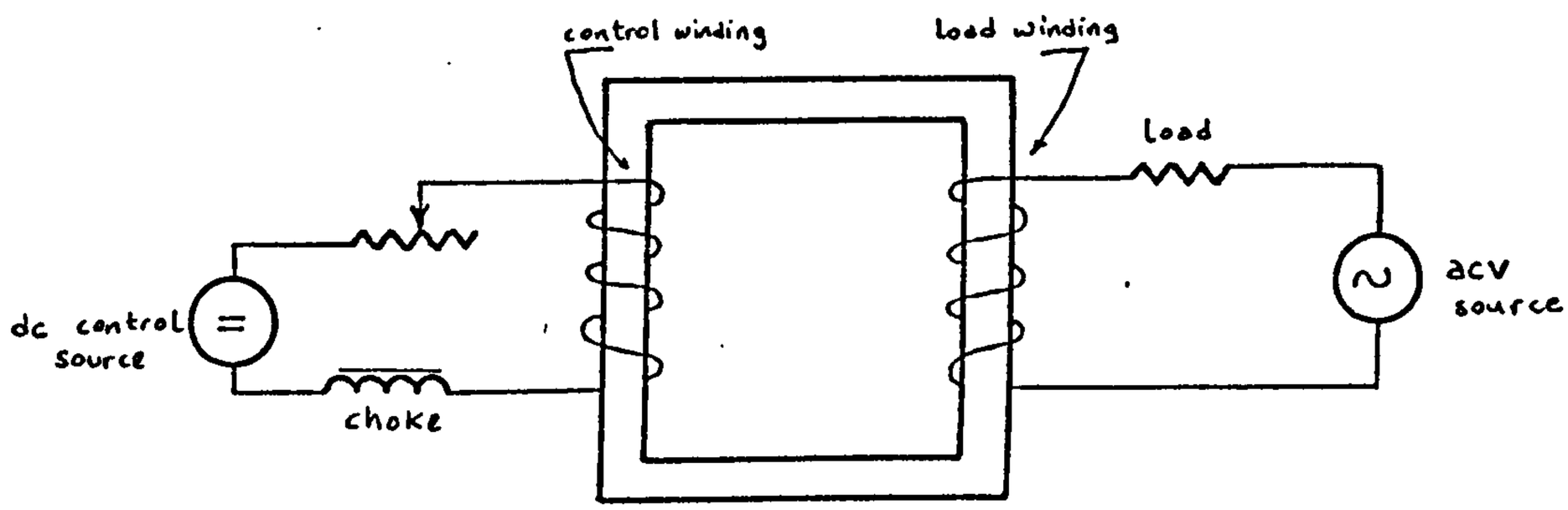

Figure 4.2 Suppression of effects of mutual coupling by a choke coil

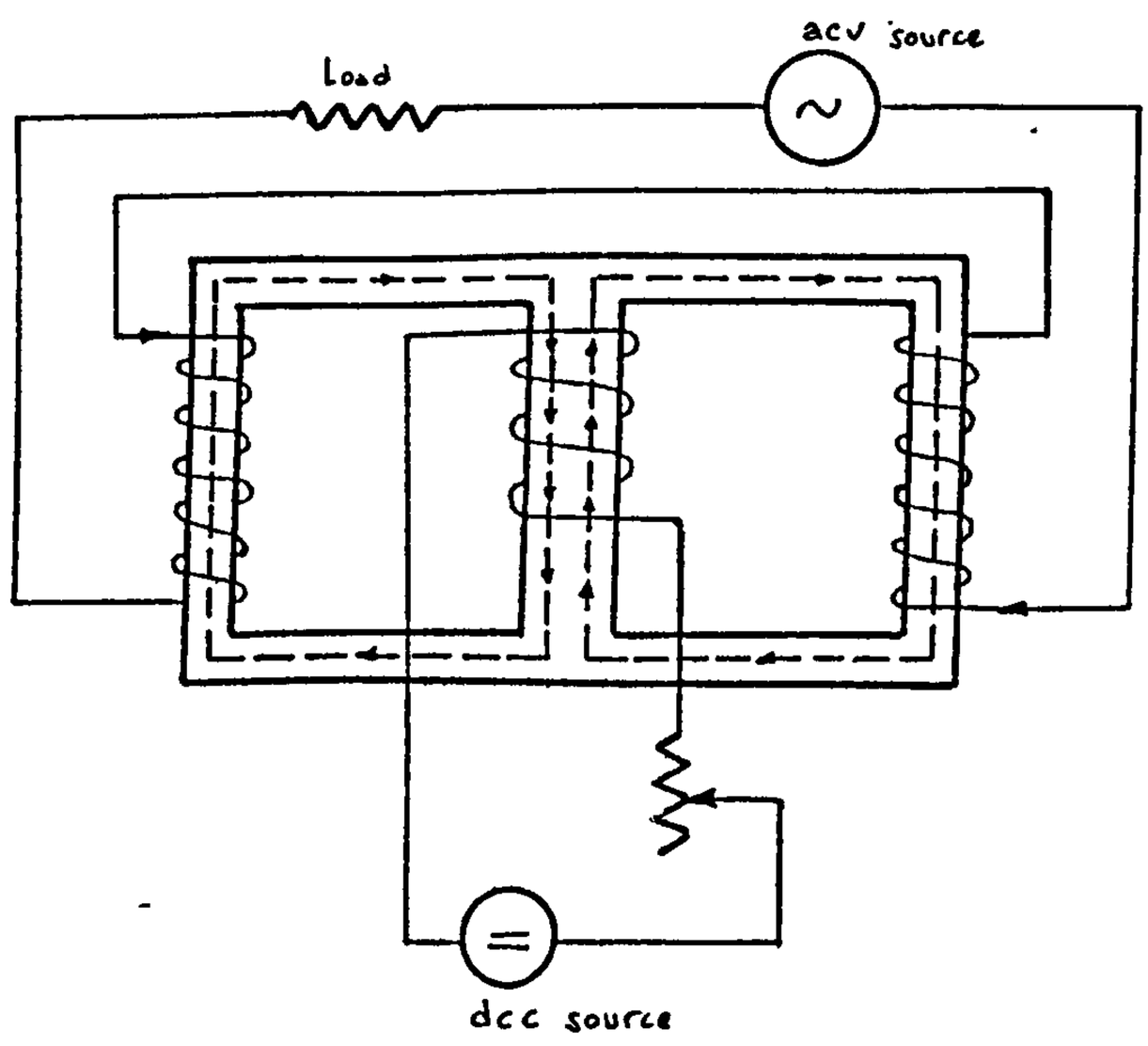

Figure 4.3 Saturable reactor with flux cancellation

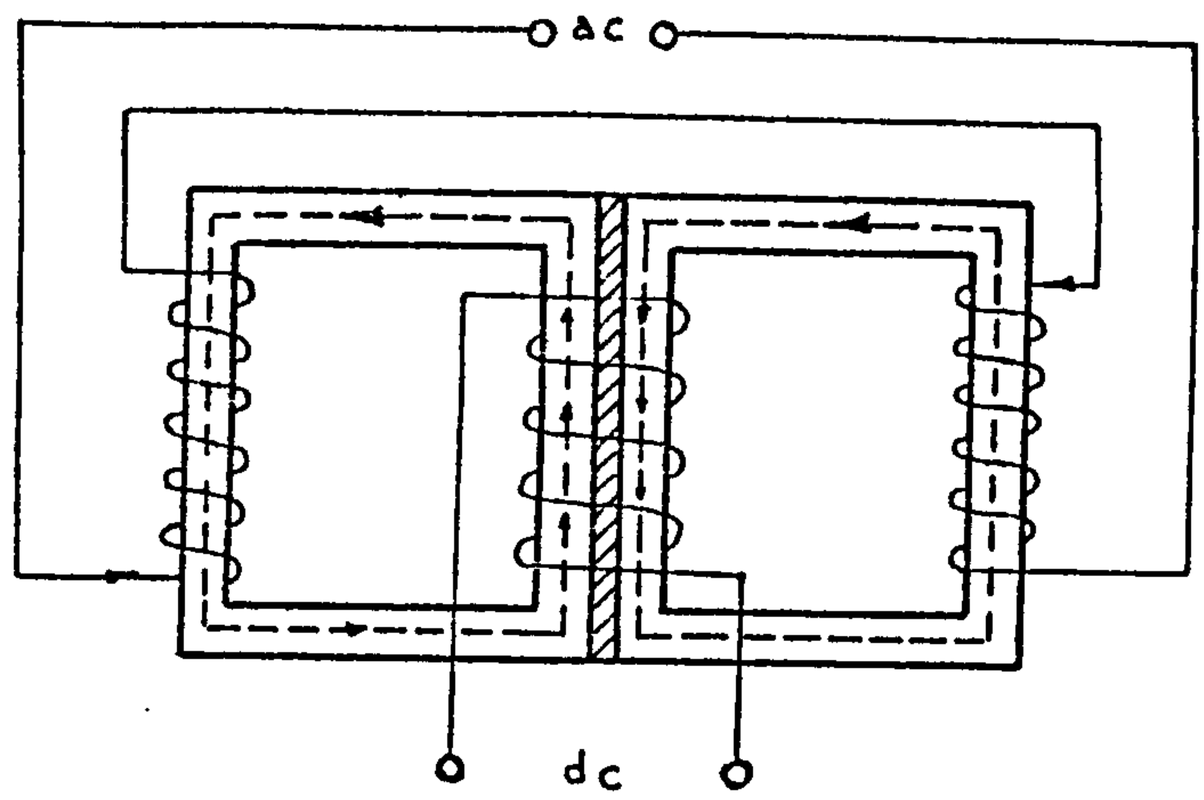

Figure 4.4 Another form of the device in Figure 4.3

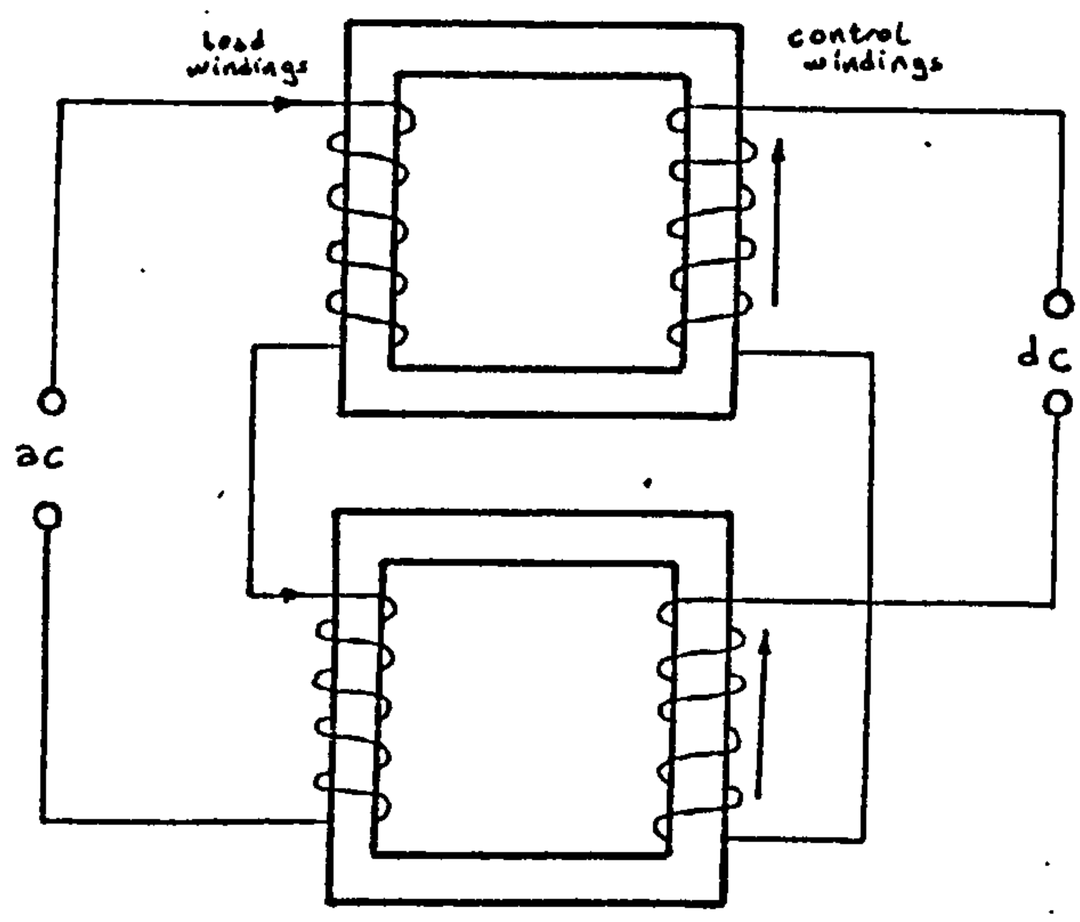

Figure 4.5 Saturable reactor with voltage cancellation

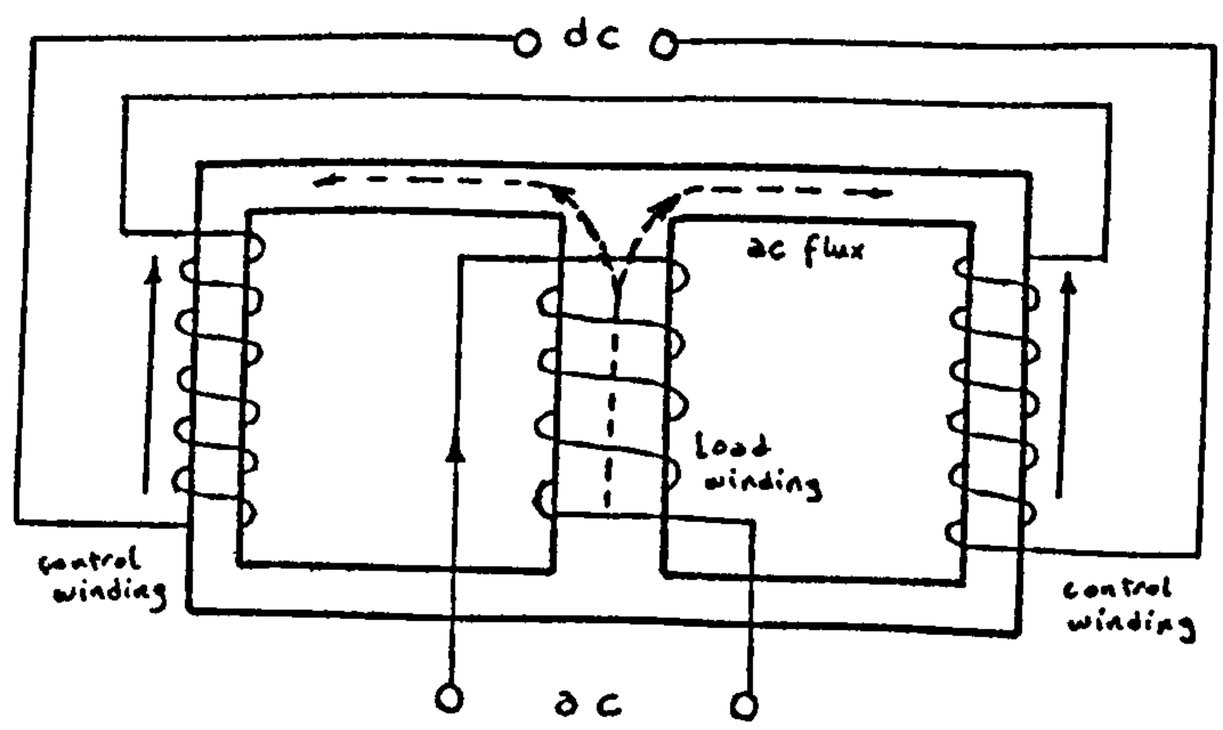

Figure 4.6 Saturable reactor of Figure 4.3, with functions of windings reversed

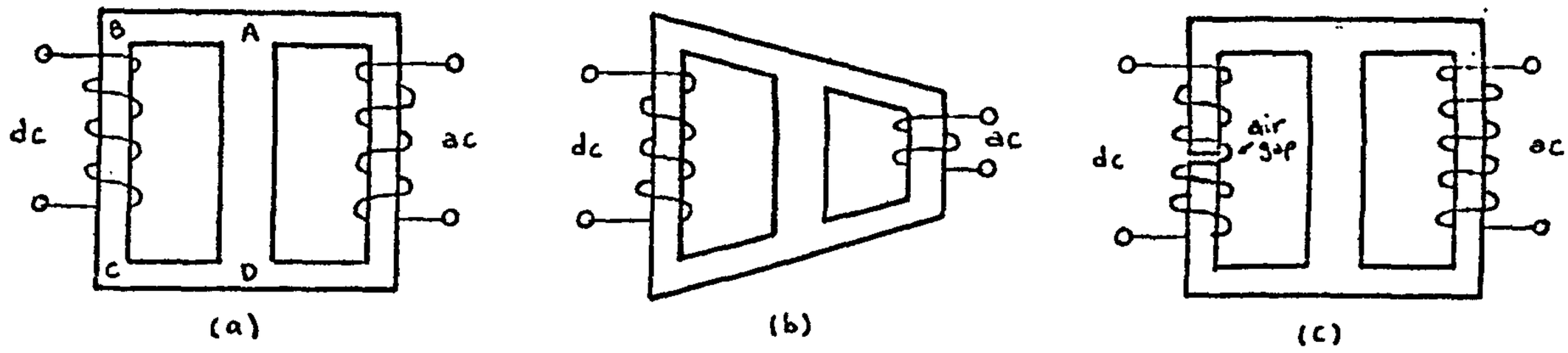

Figure 4.7 Part elimination of flux coupling by a magnetic short circuit

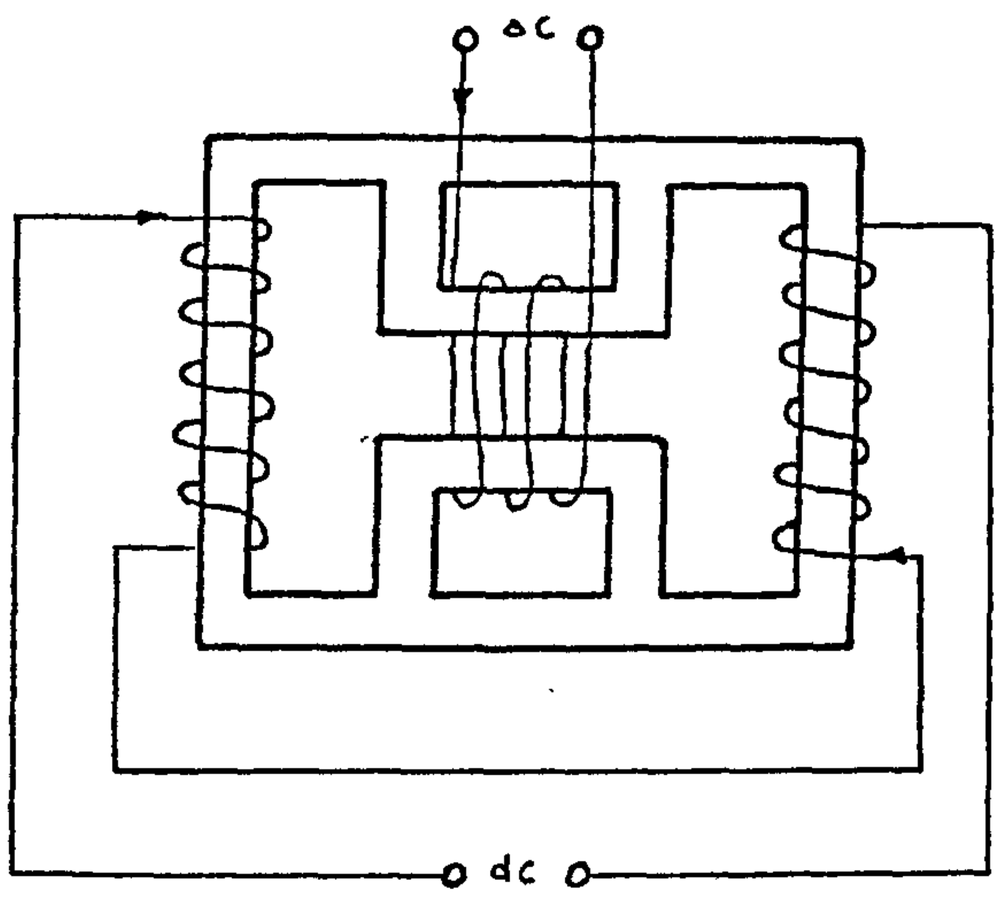

(a) Structure

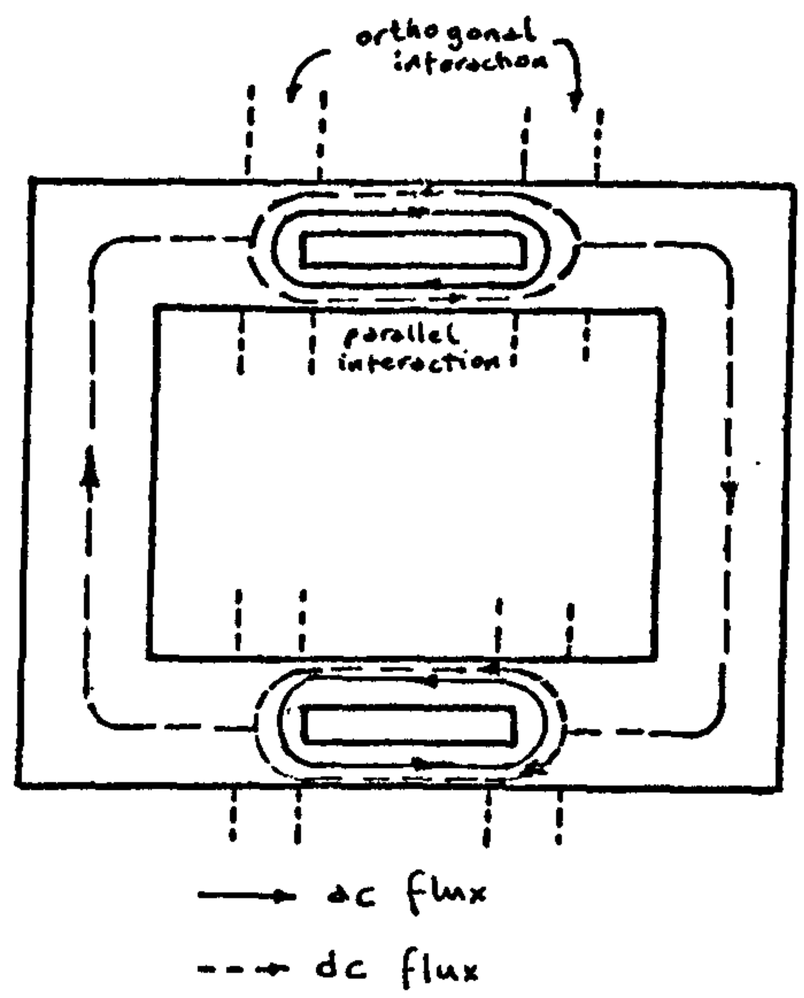

(b) Zones of interaction

Figure 4.8 A multi-apertured saturable reactor

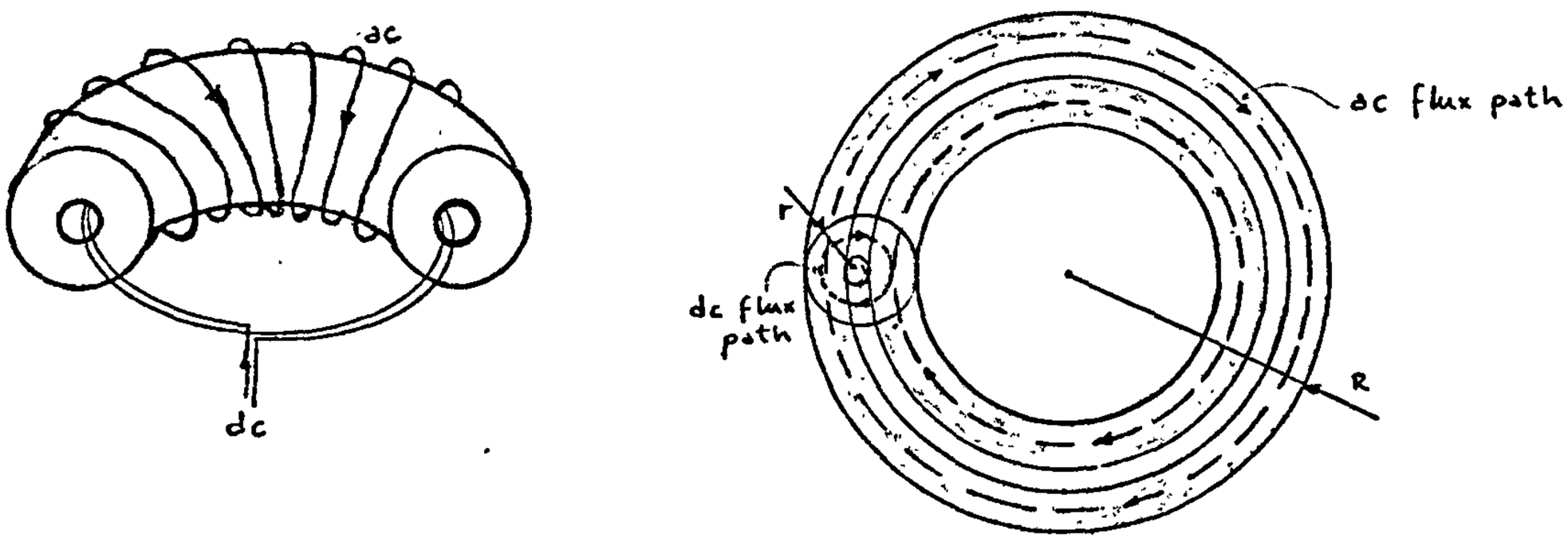

Figure 4.9 Orthogonal flux interaction saturable reactor

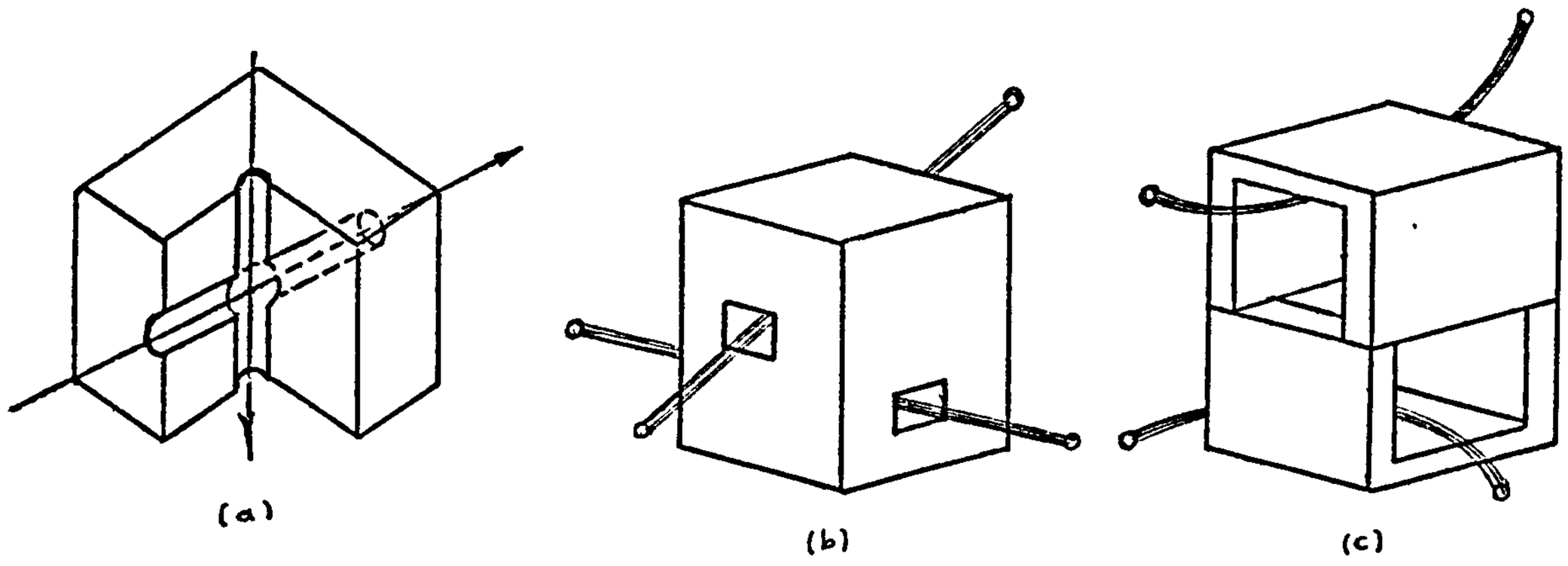

Figure 4.10 Development of orthogonal flux devices

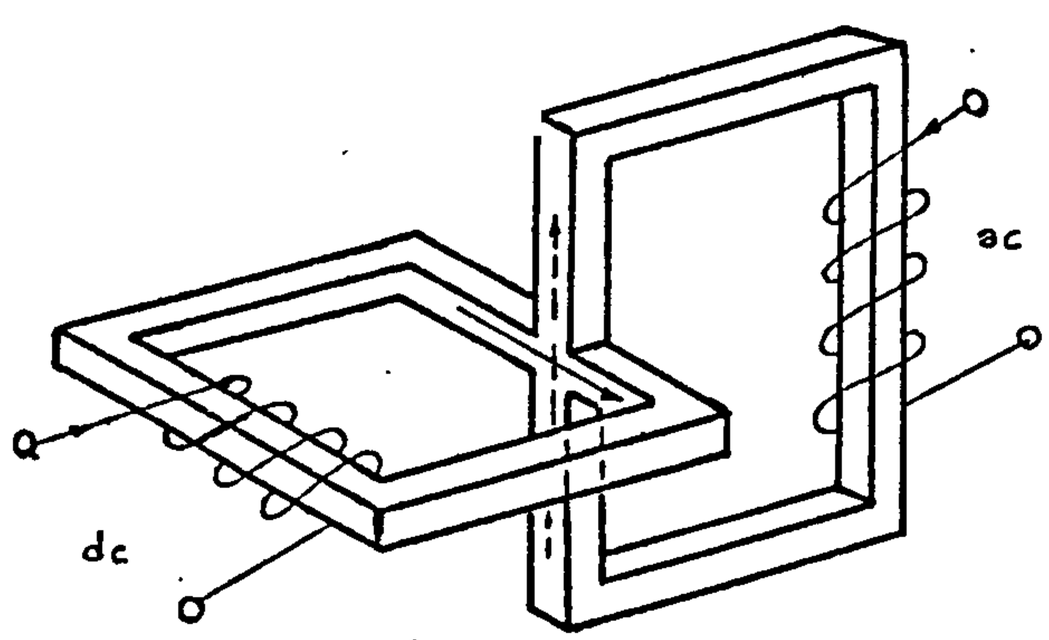

Figure 4.11 One basic form of magnetic cross valve

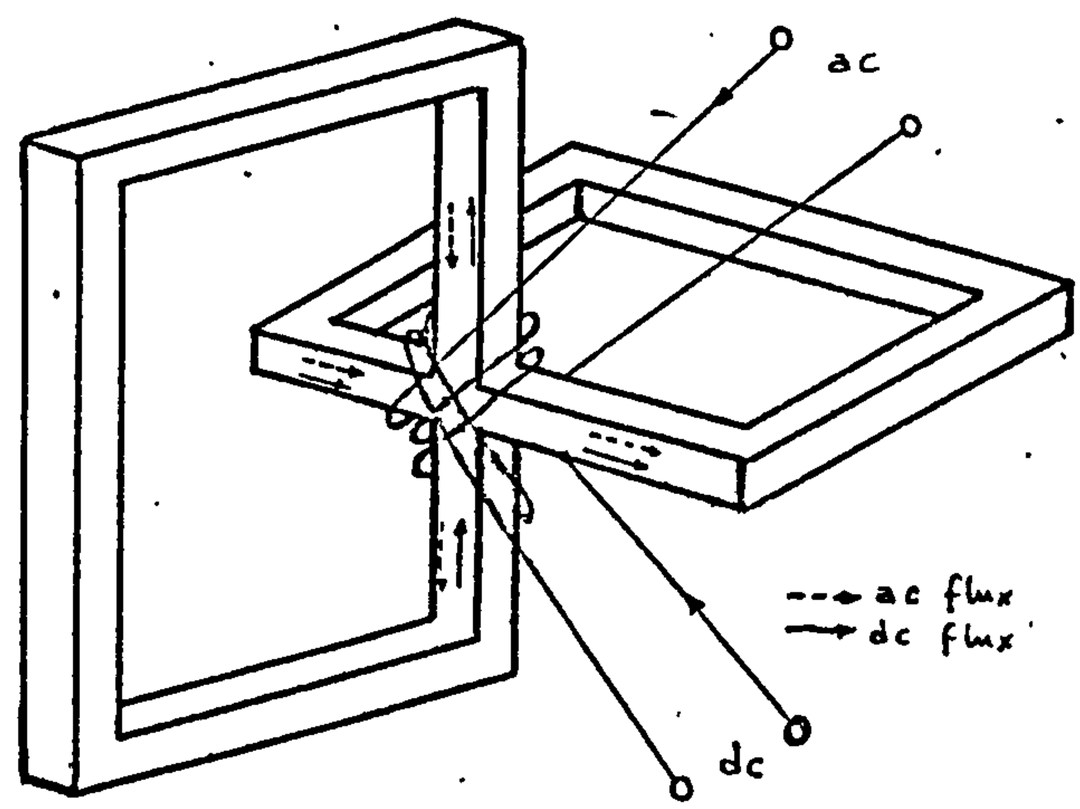

Figure 4.12 Another basic form of magnetic cross valve

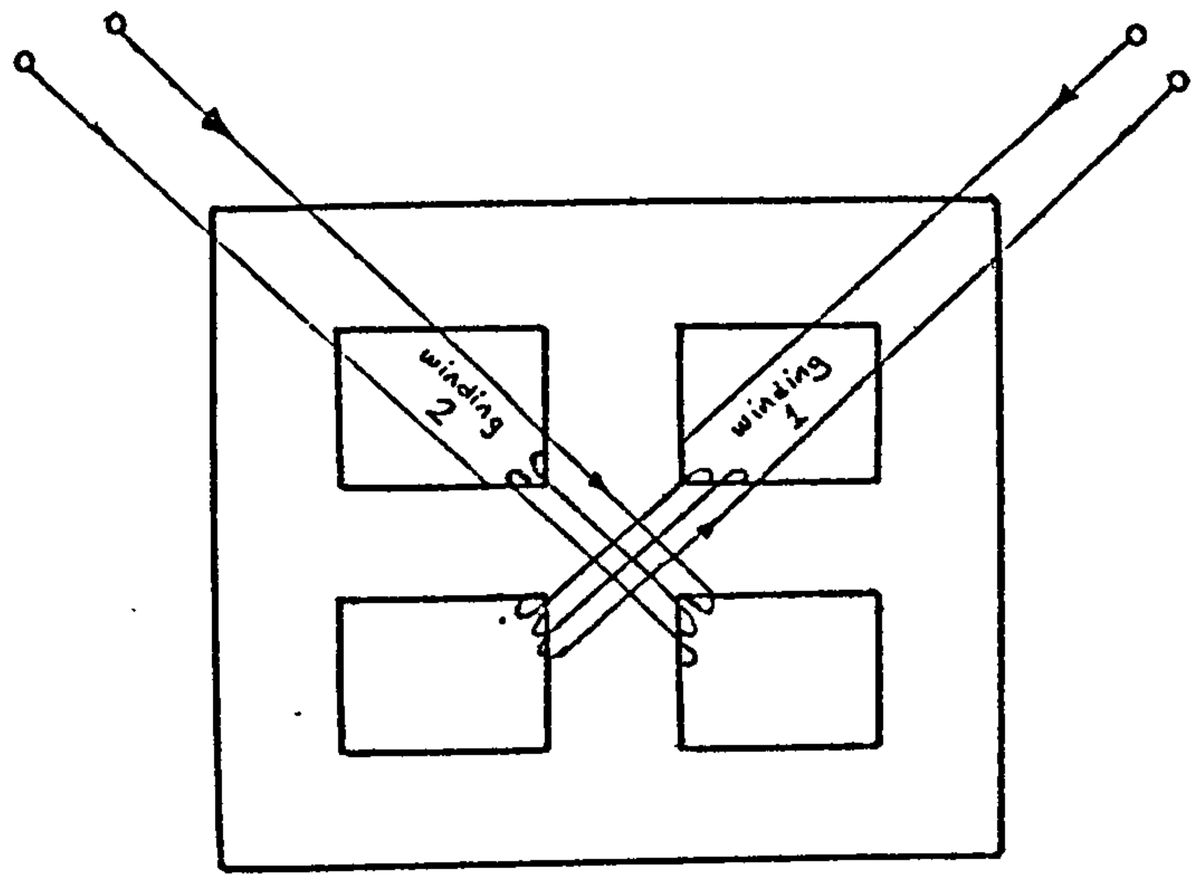

Figure 4.13 Magnetic Cross-Valve

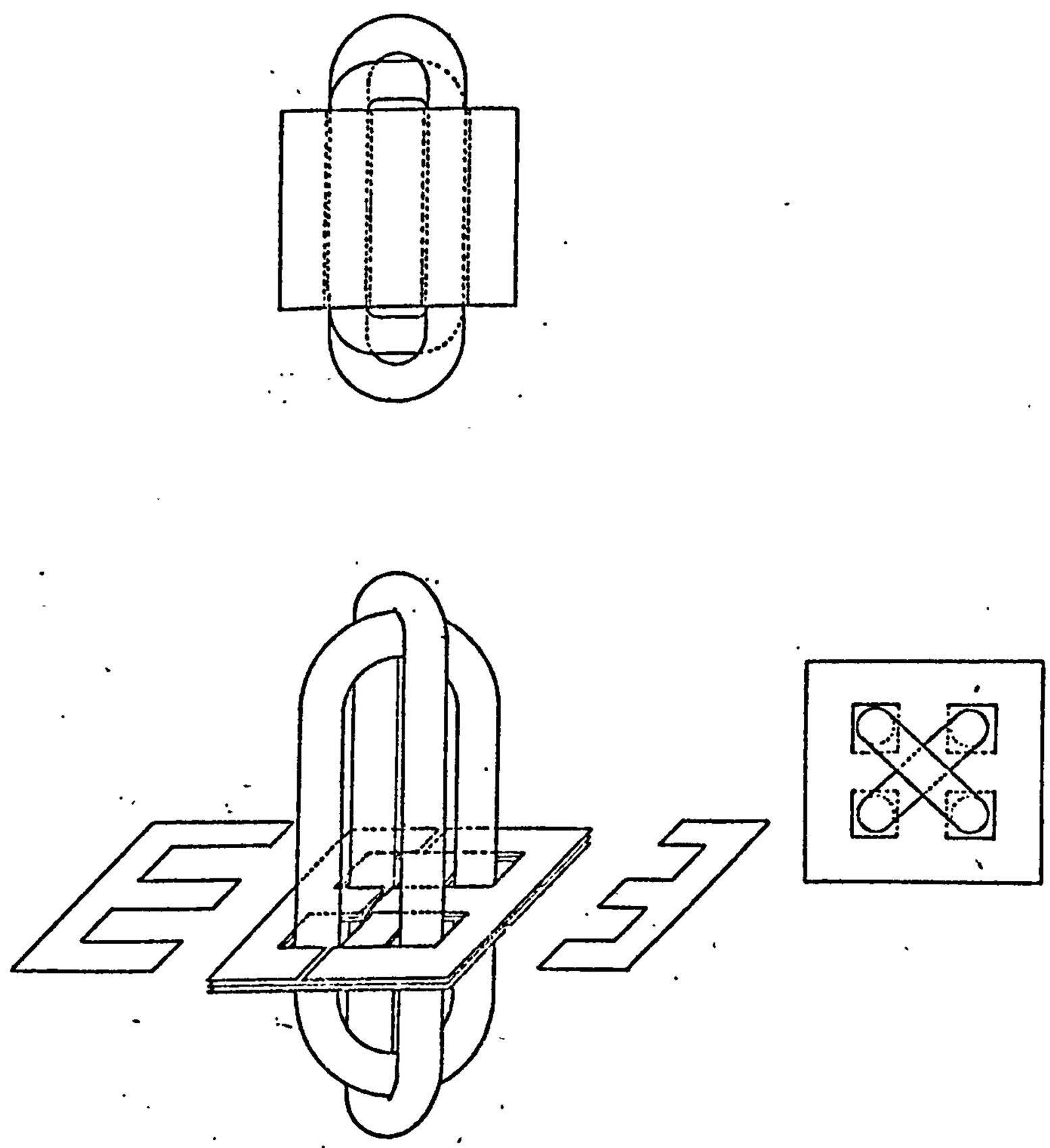

Figure 4.14 Construction of Magnetic Cross-Valves

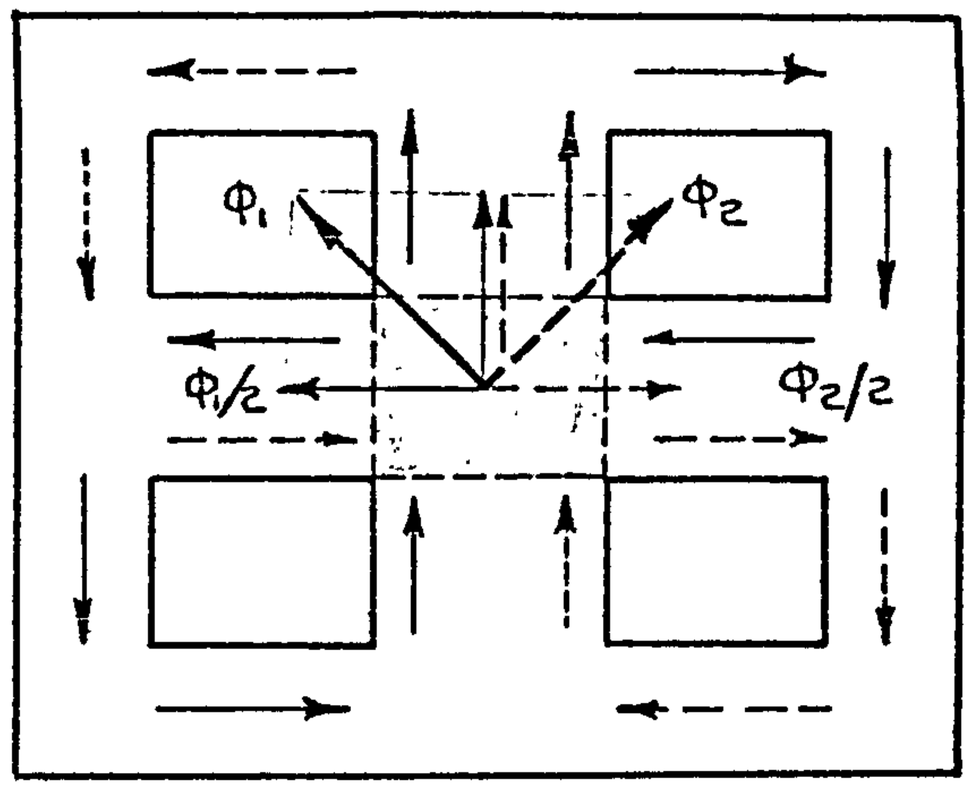

Figure 4.15 Flux distribution in the device of Figure 4.13

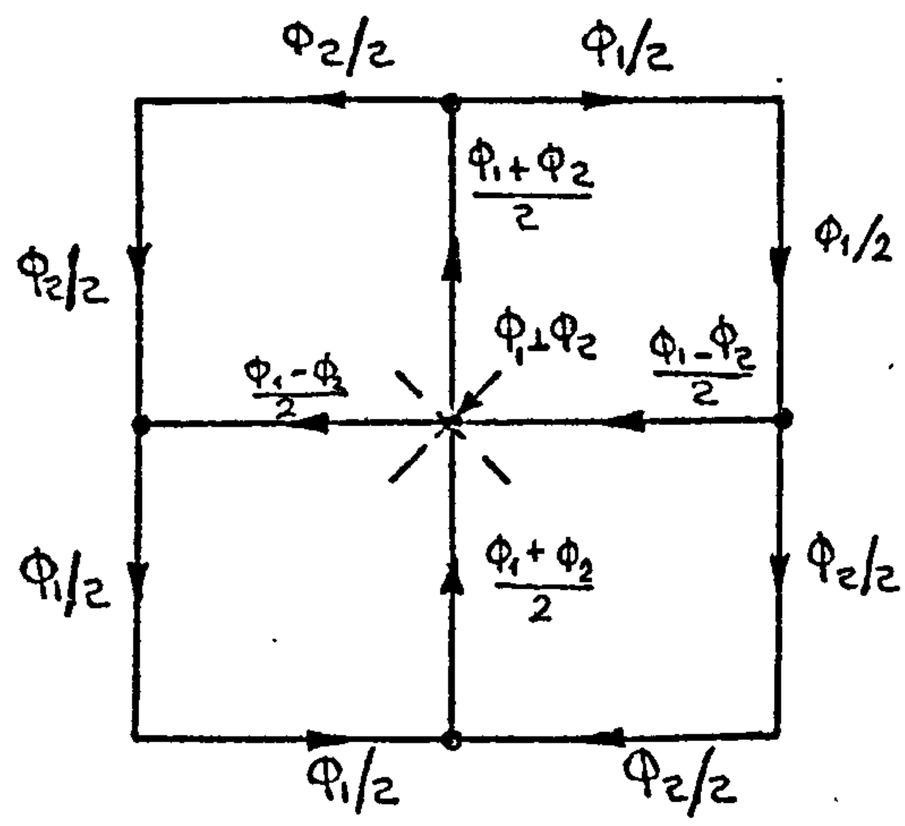

Figure 4.16 Pertaining to Figure 4.15

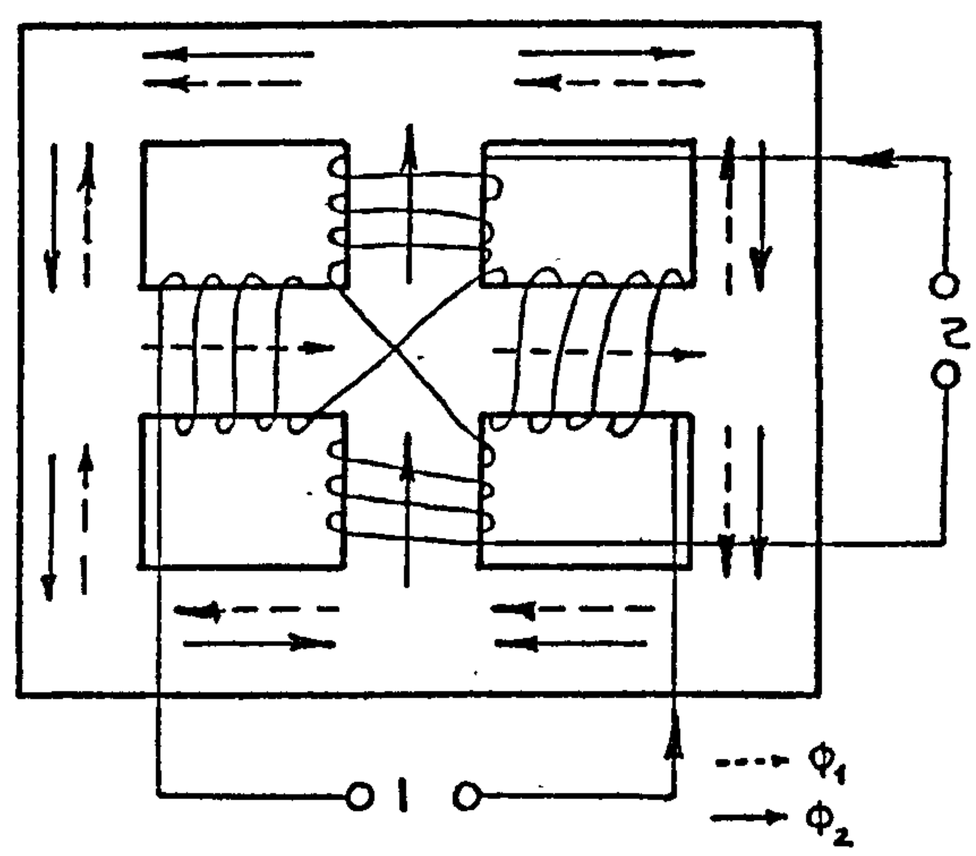

Figure 4.17 Magnetic X-valve with different winding arrangement

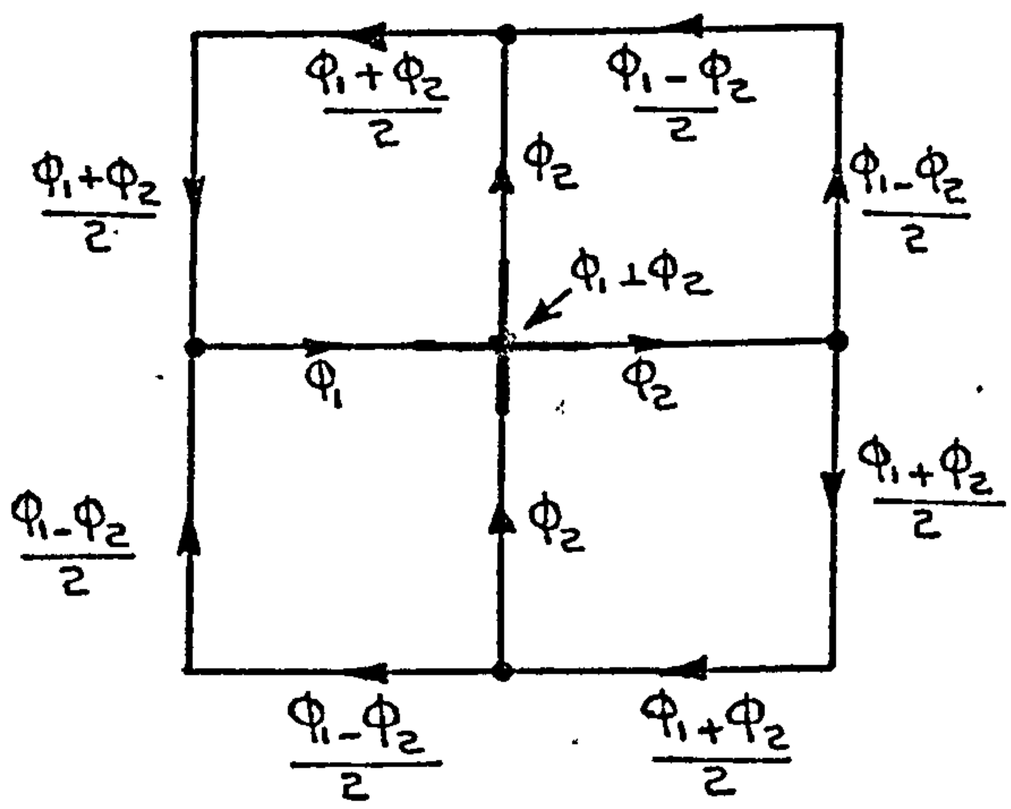

Figure 4.18 Pertaining to Figure 4.17

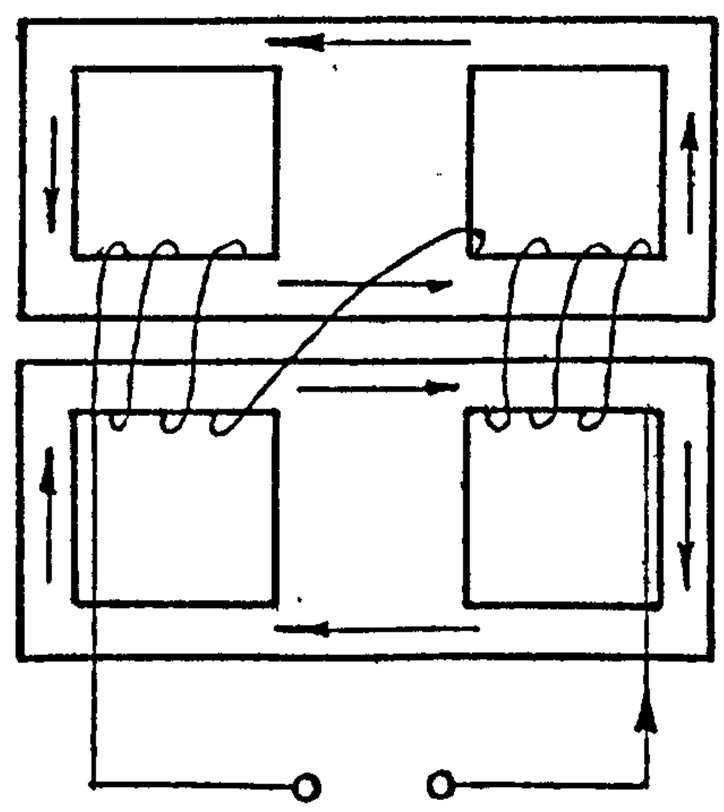

Figure 4.19 Flux cancellations for magnetic X-valve

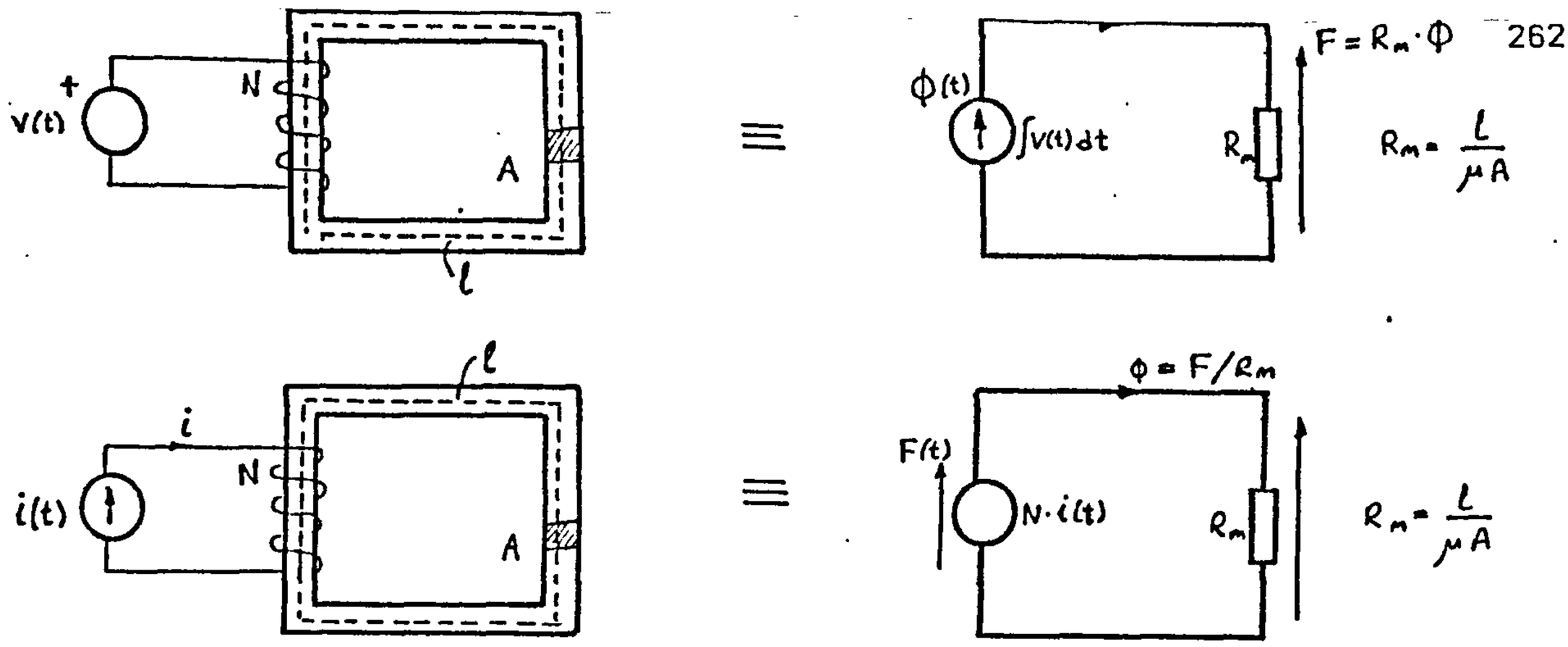

Figure 4.20 Derivation of analogous electric circuits

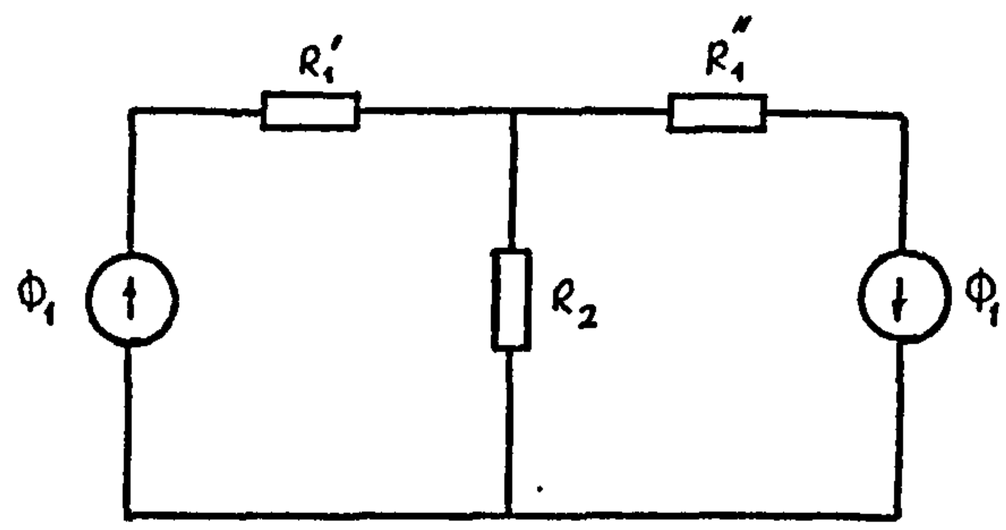

Figure 4.21 Analogous circuit for the saturable reactor of Figure 4.3

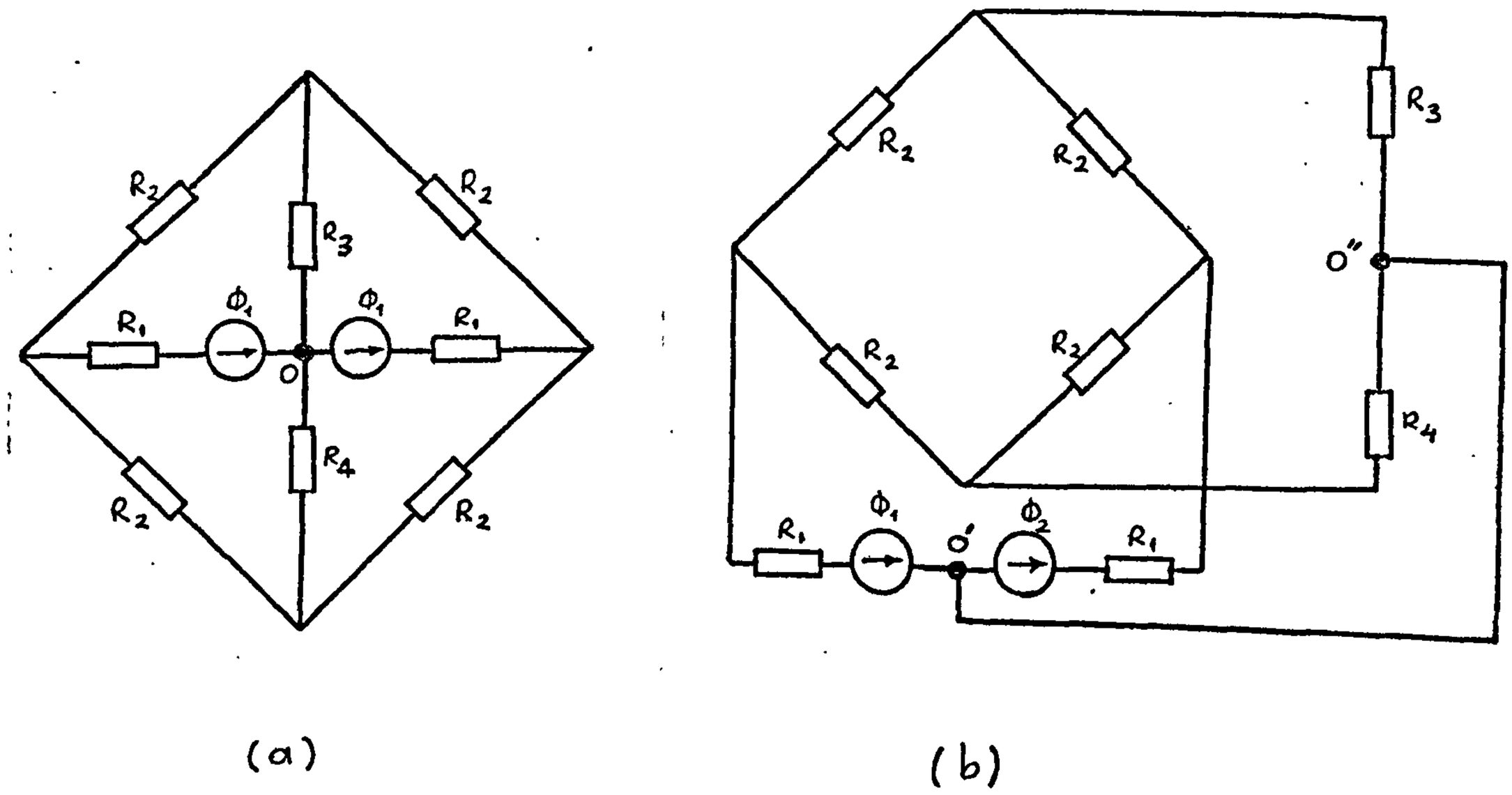

Figure 4.22 Analogous circuits for the magnetic X-valve of Figure 4.17

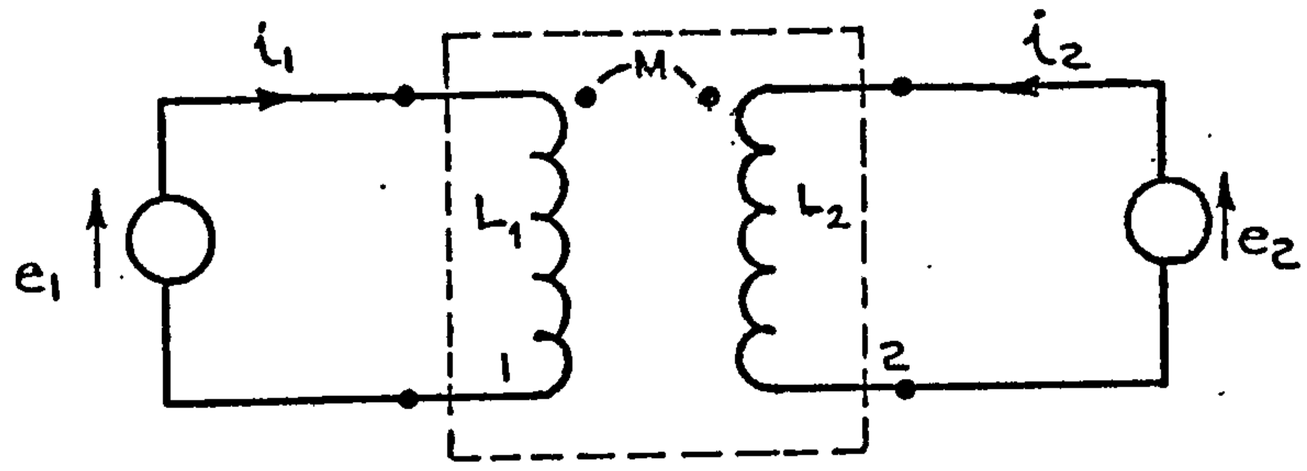

Figure 4.23 Two mutually flux-coupled inductors

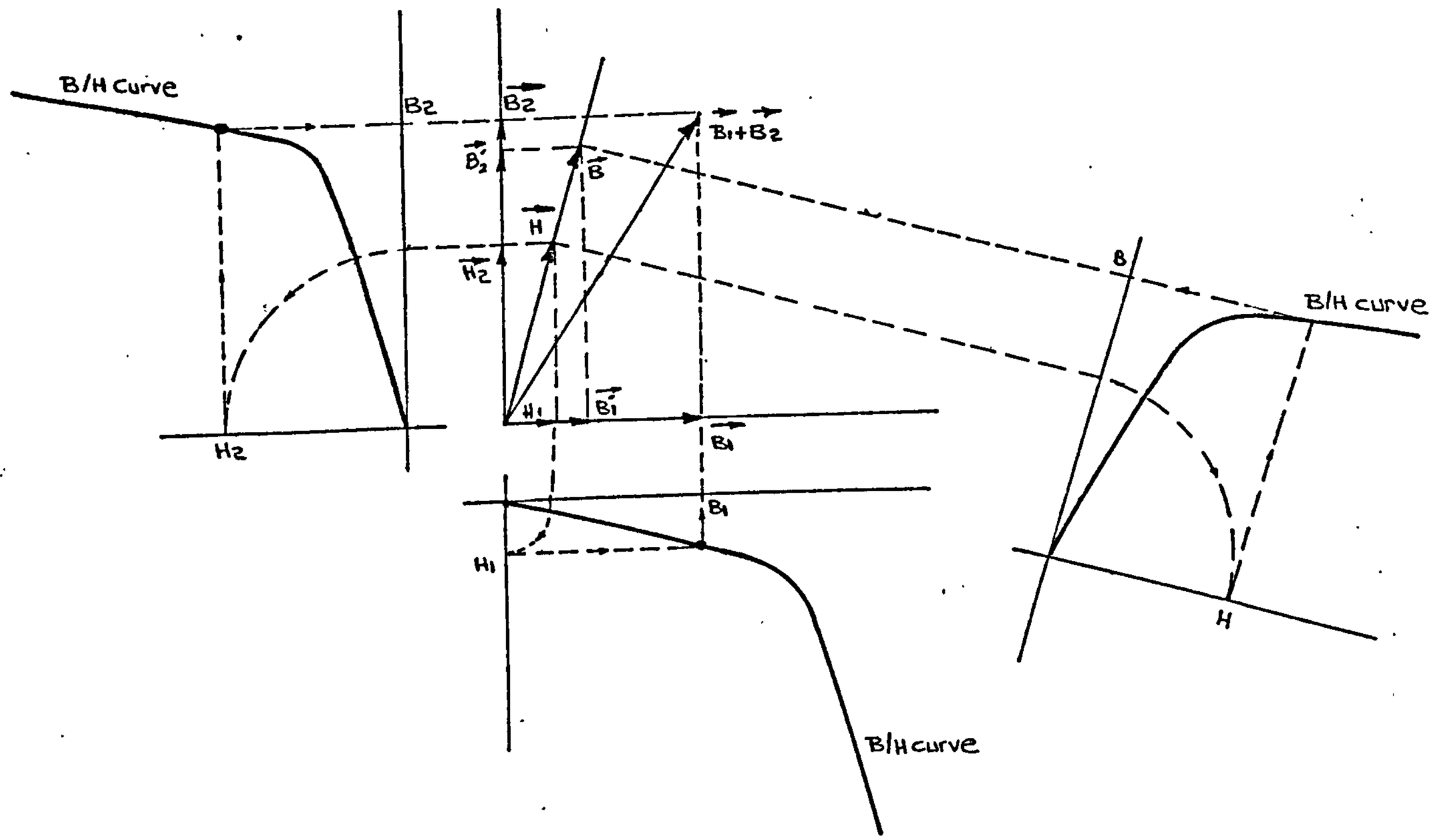

Figure 4.24 Orthogonal flux interaction

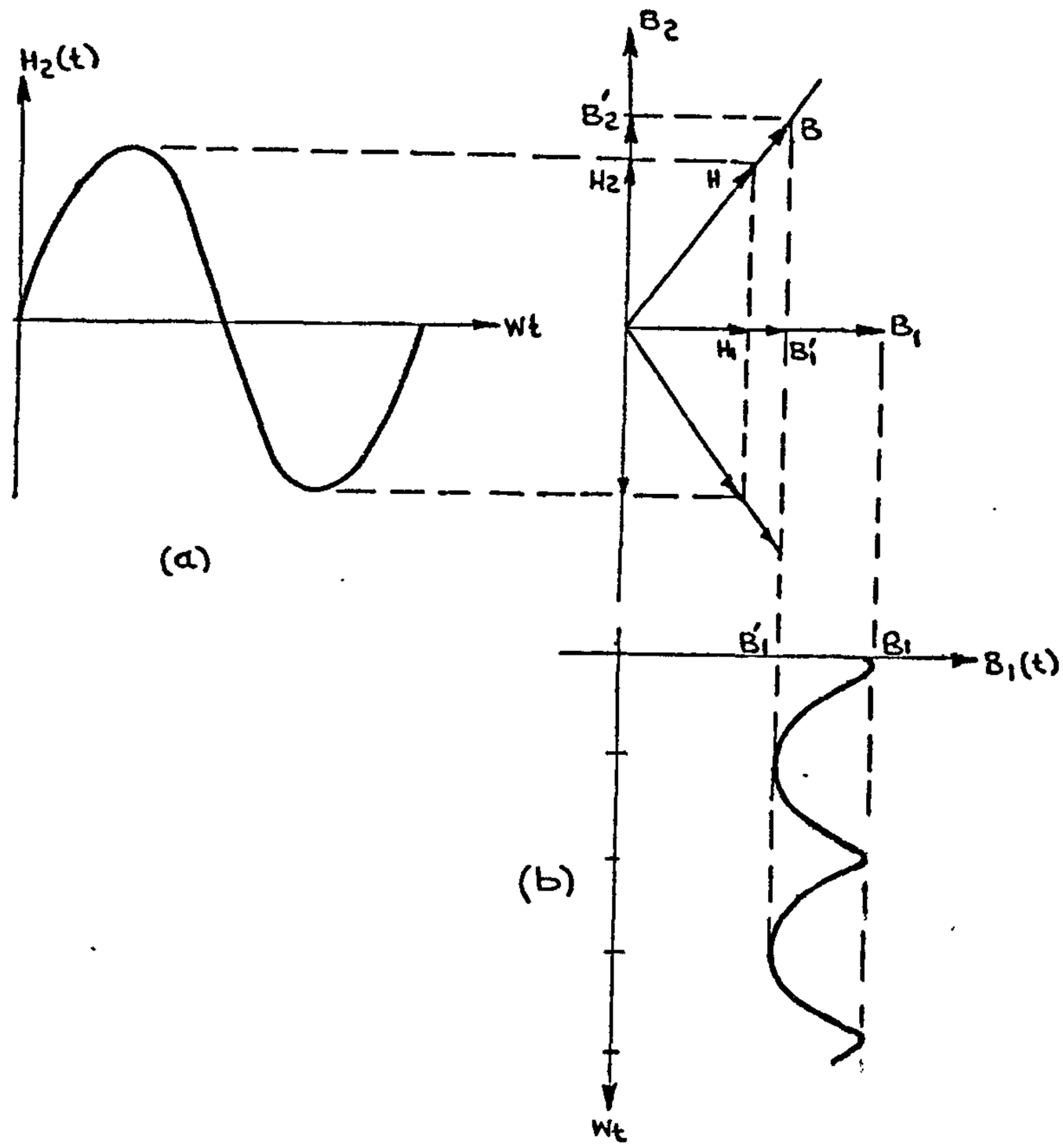

Figure 4.25 Generation of even harmonics in orthogonal flux interaction

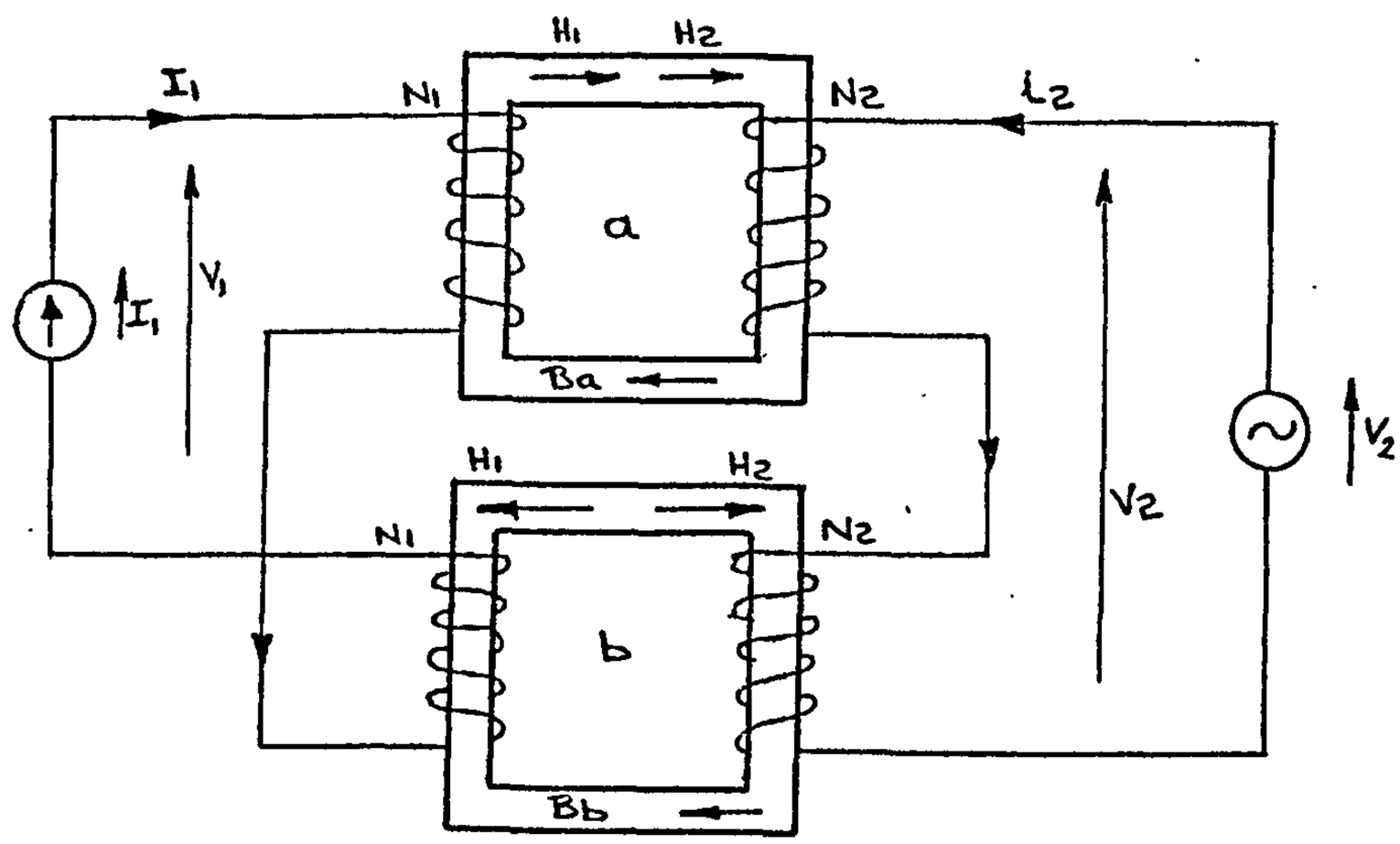

Figure 4.26 Saturable reactor of Figure 4.5

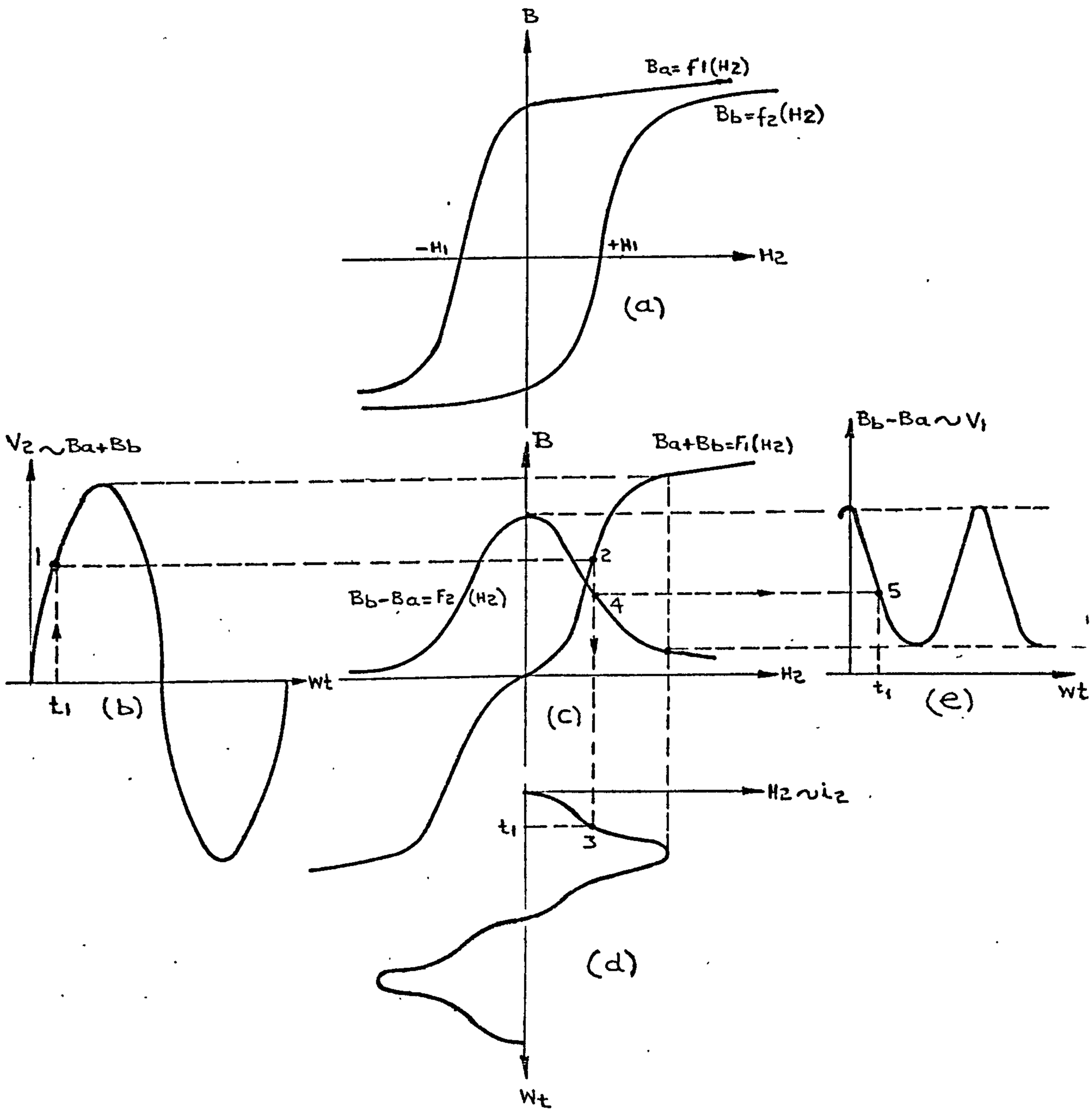

Figure 4.27 Parallel flux interaction

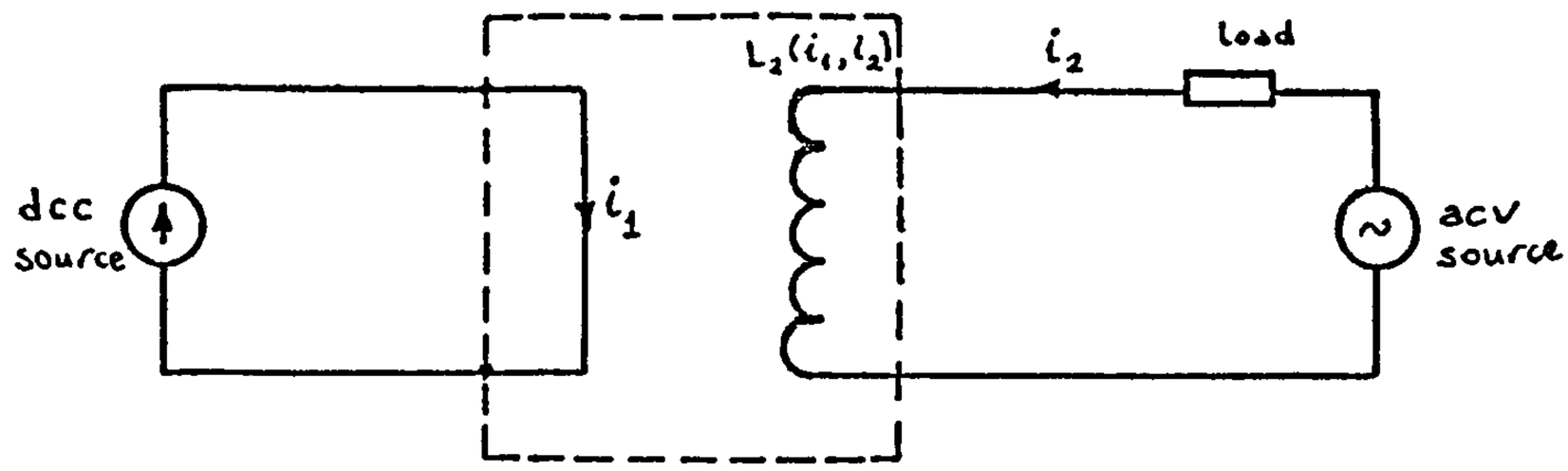

Figure 4.28 Saturable reactor as current-controlled, non-linear inductance (electrical representation)

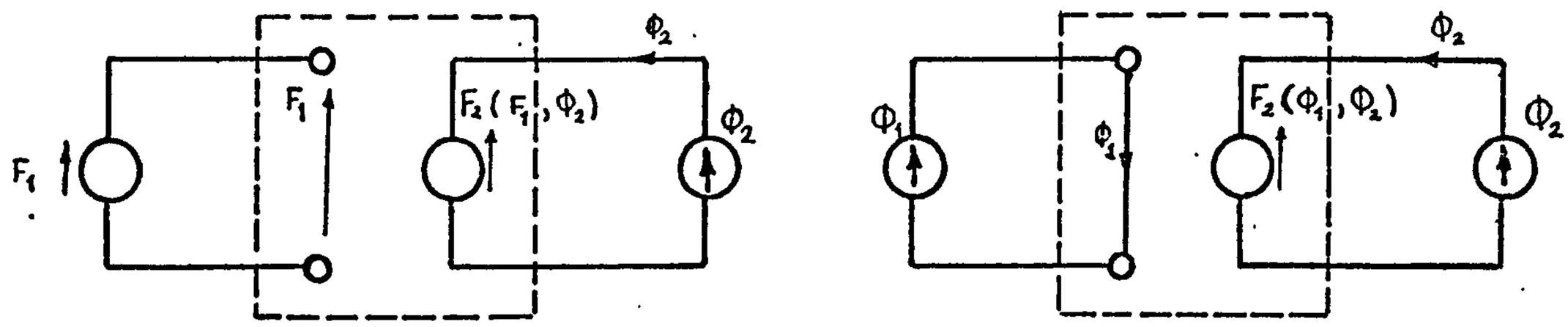

(a) Control winding driven by current course

(a) Control winding driven by voltage source

Figure 4.29 Analog magnetic representation of a saturable reactor as current-controlled, non-linear inductance

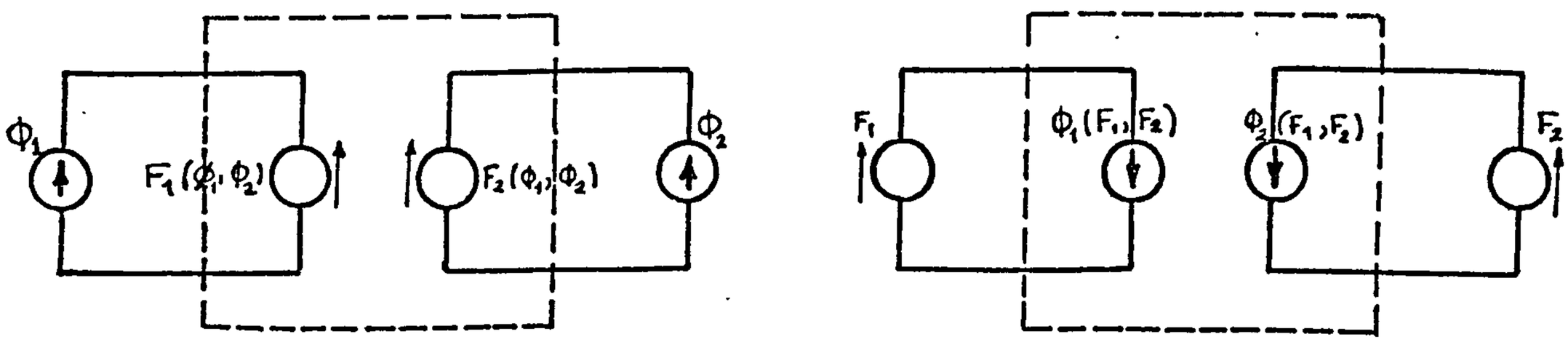

(a) Both windings driven by voltage sources

(a) Both windings driven by current sources

Figurr 4.30 Analog magnetic representation of two parametrically-coupled, non-linear inductors

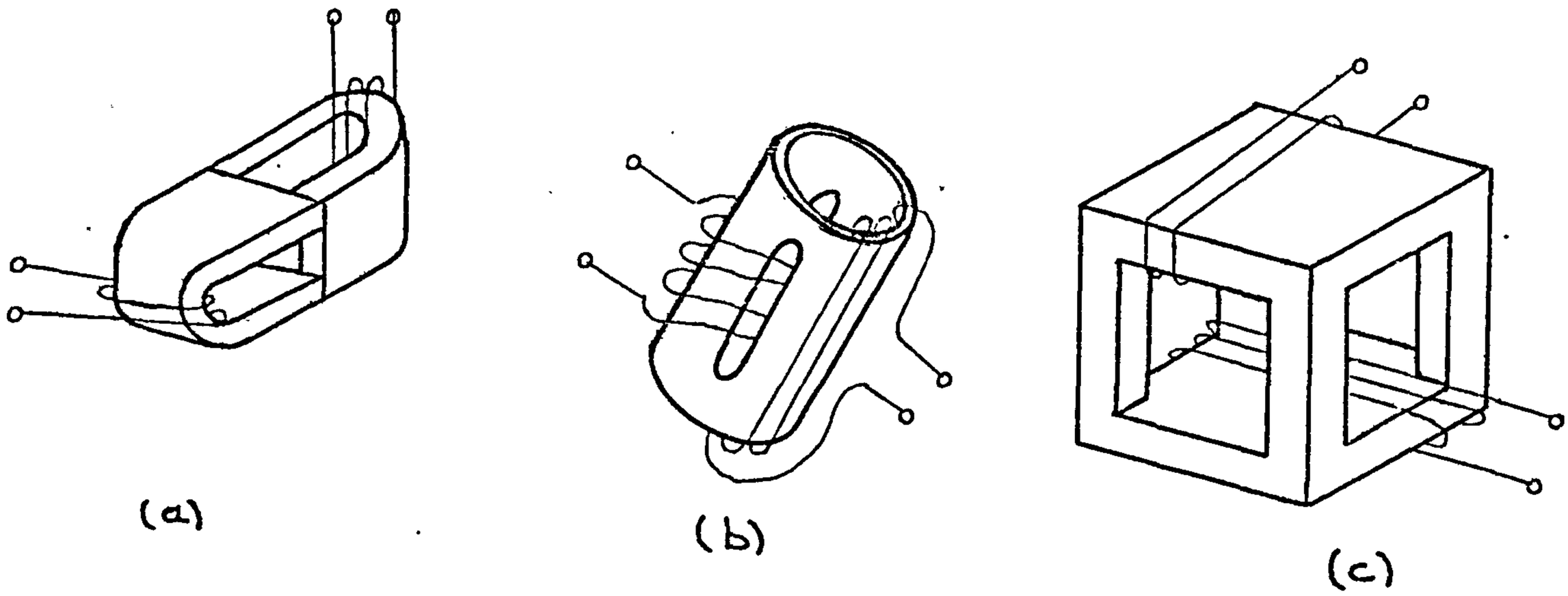

Figure 4.31 Magnetic core configurations proposed by Wanlass

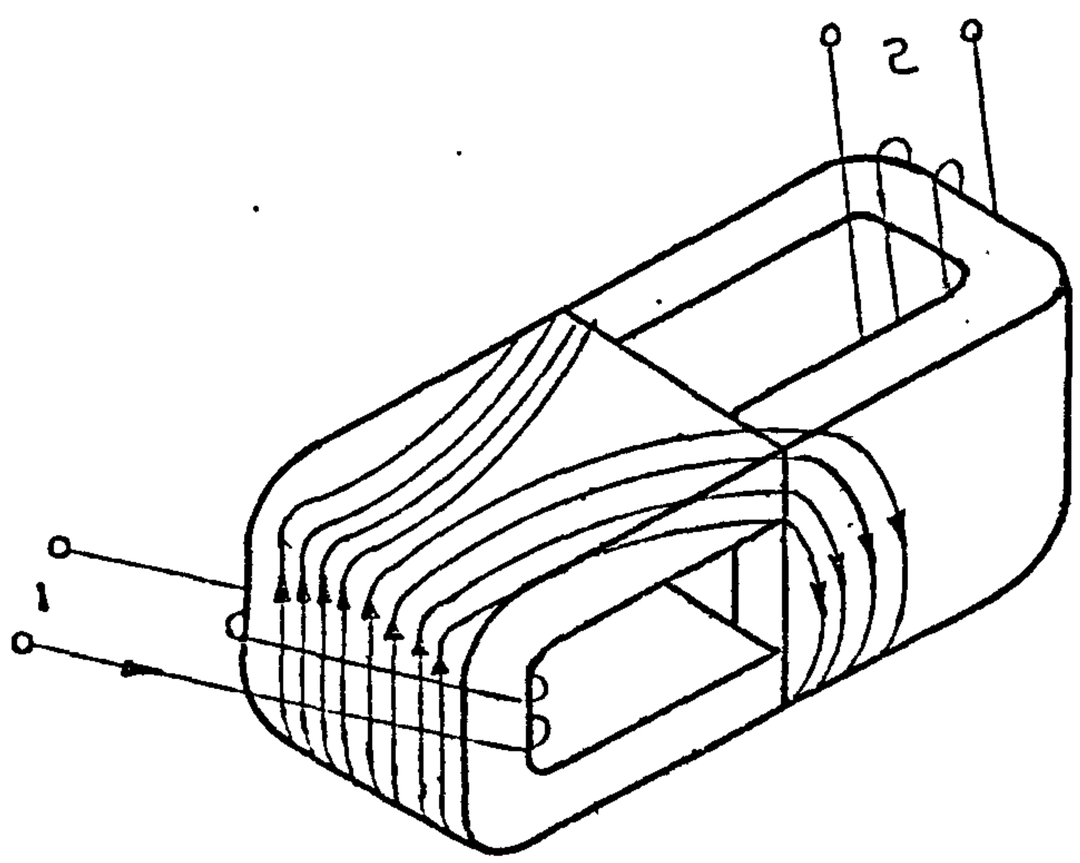

Figure 4.32 Flux distribution in the two-C-core device

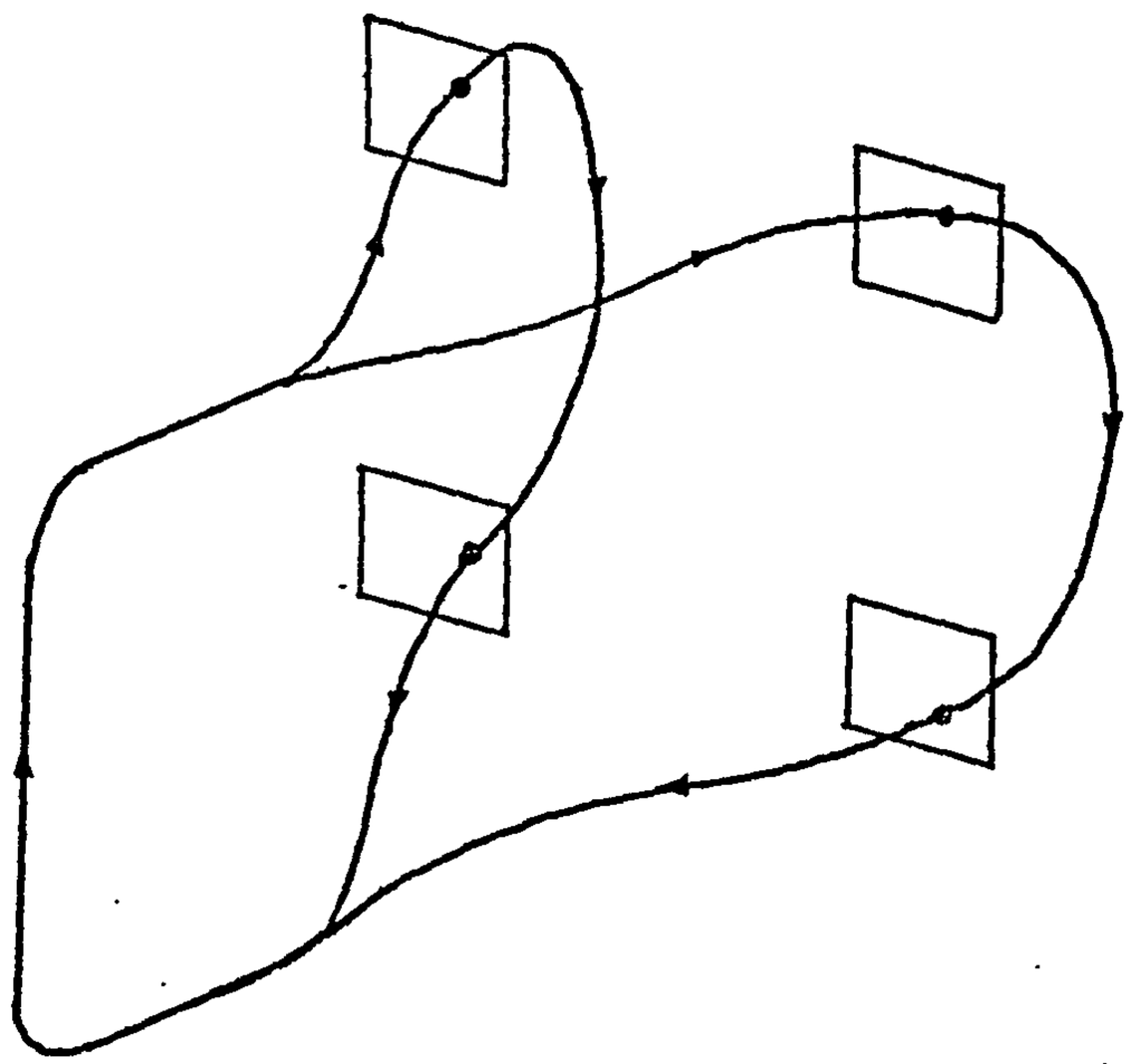

Figure 4.33 Basic primary flux-path

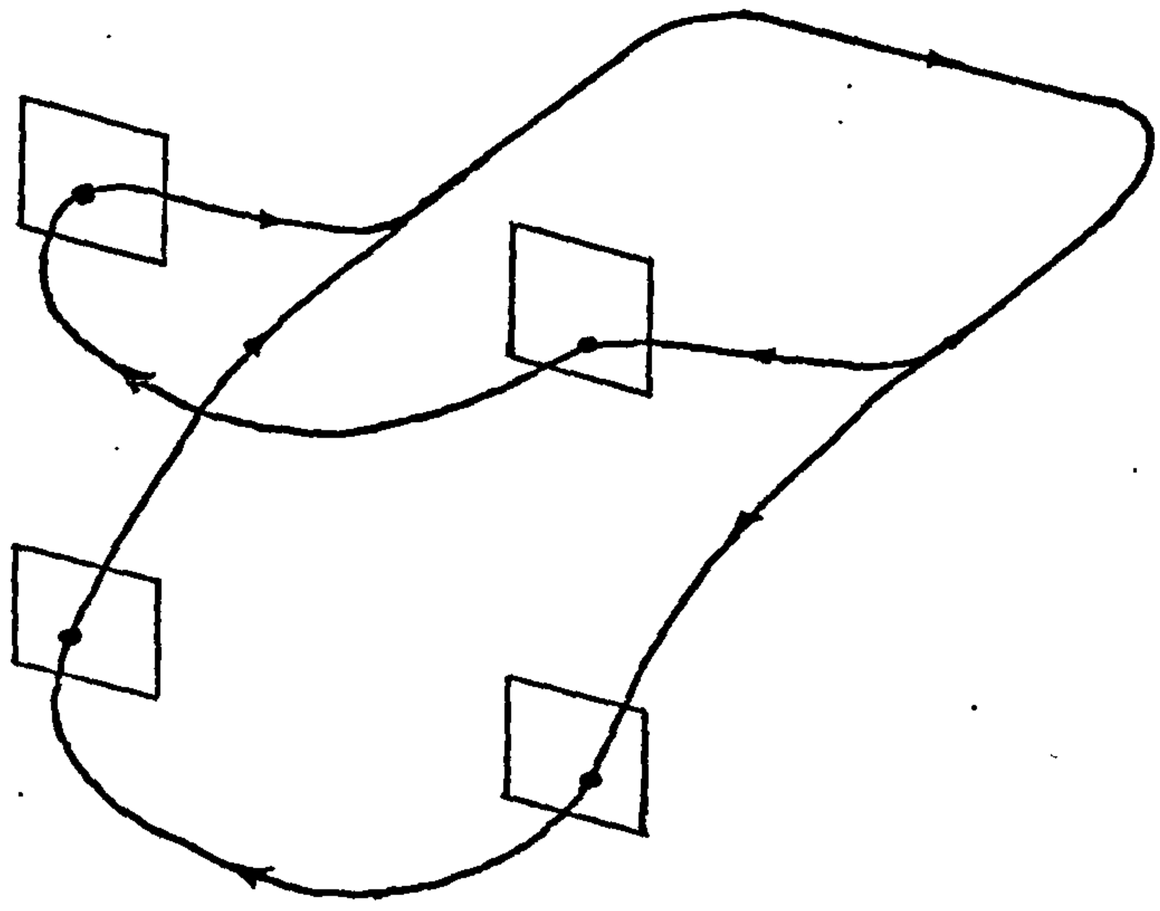

Figure 4.34 Basic secondary flux-path

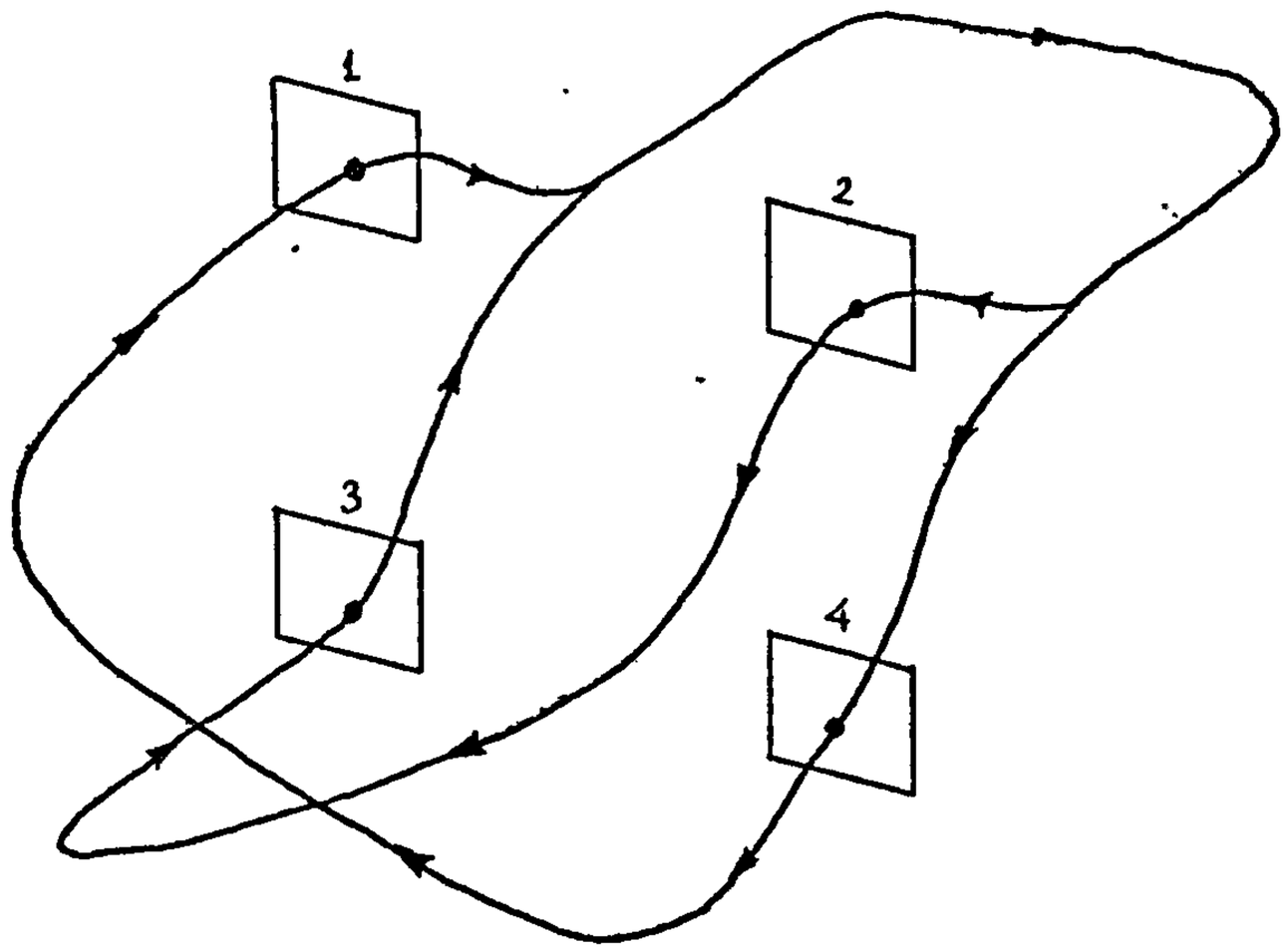

Figure 4.35 The linking flux-path

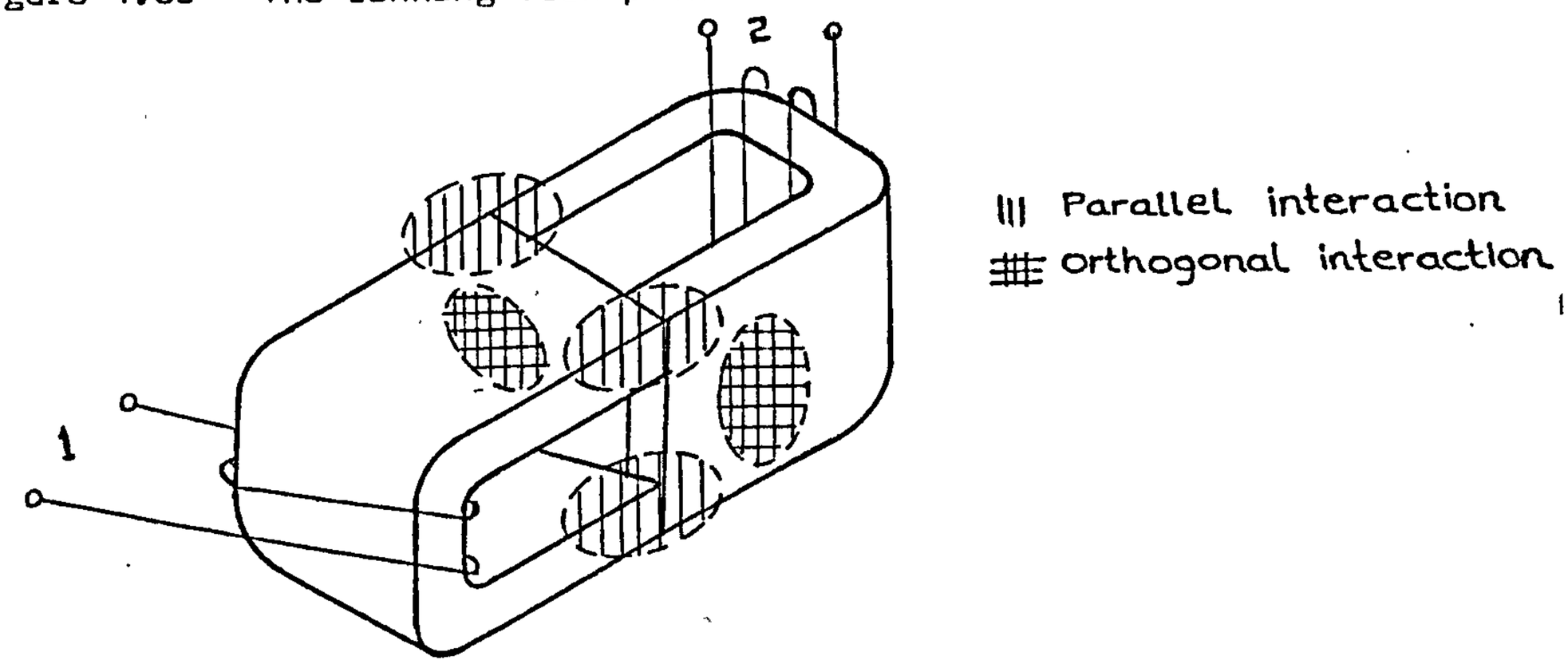

Figure 4.36 Zones of parallel and orthogonal interaction

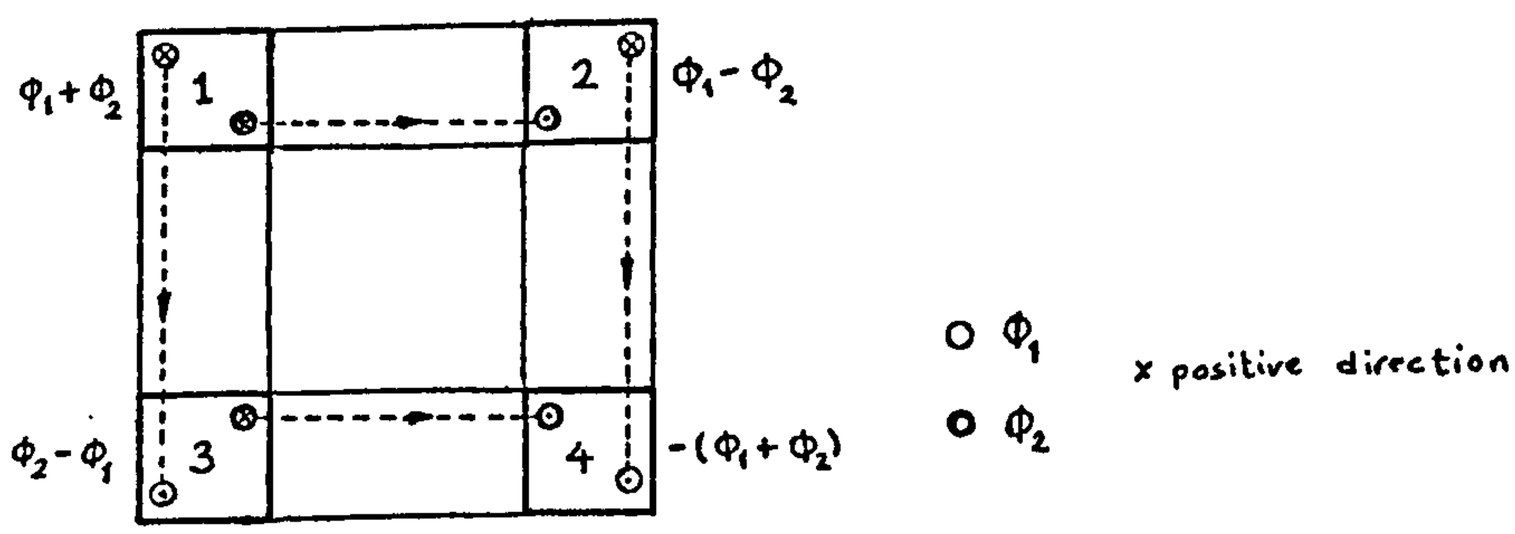

Figure 4.37 Flux positions in the common region

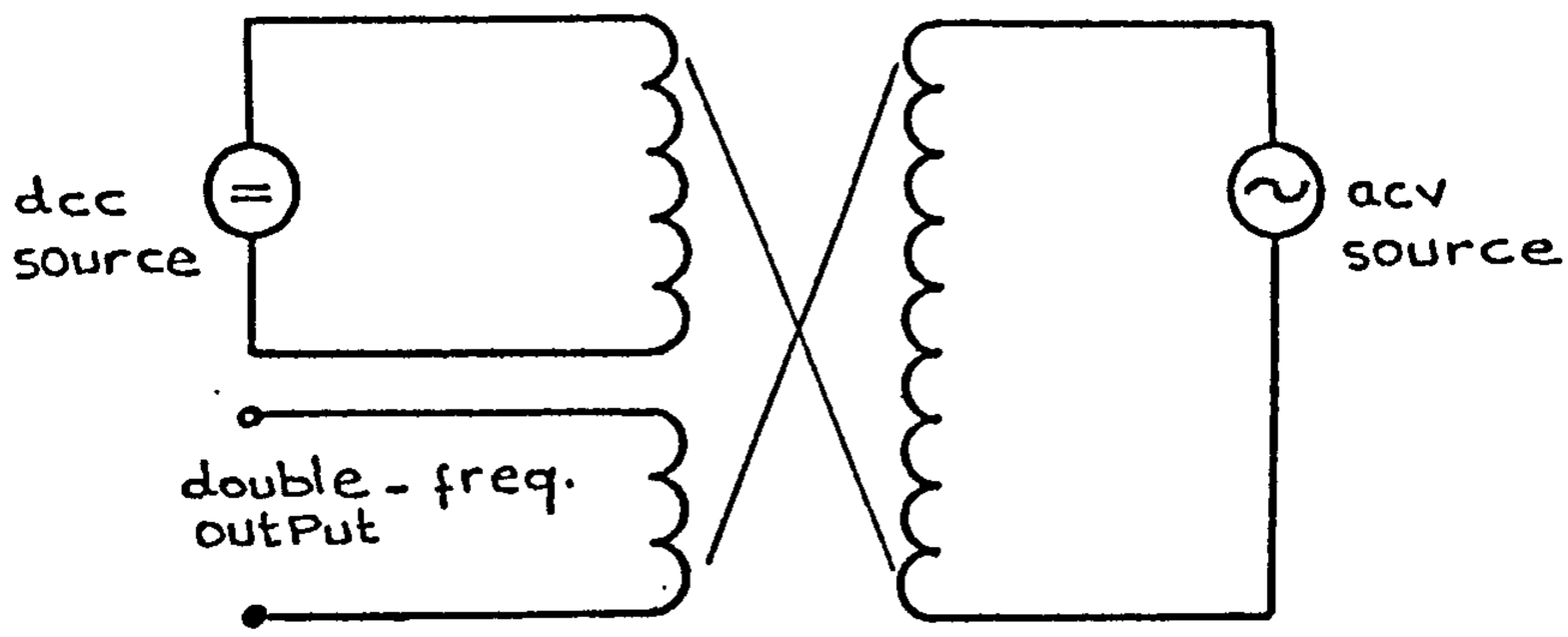

Figure 4.38 Variable transformer of Wanlass

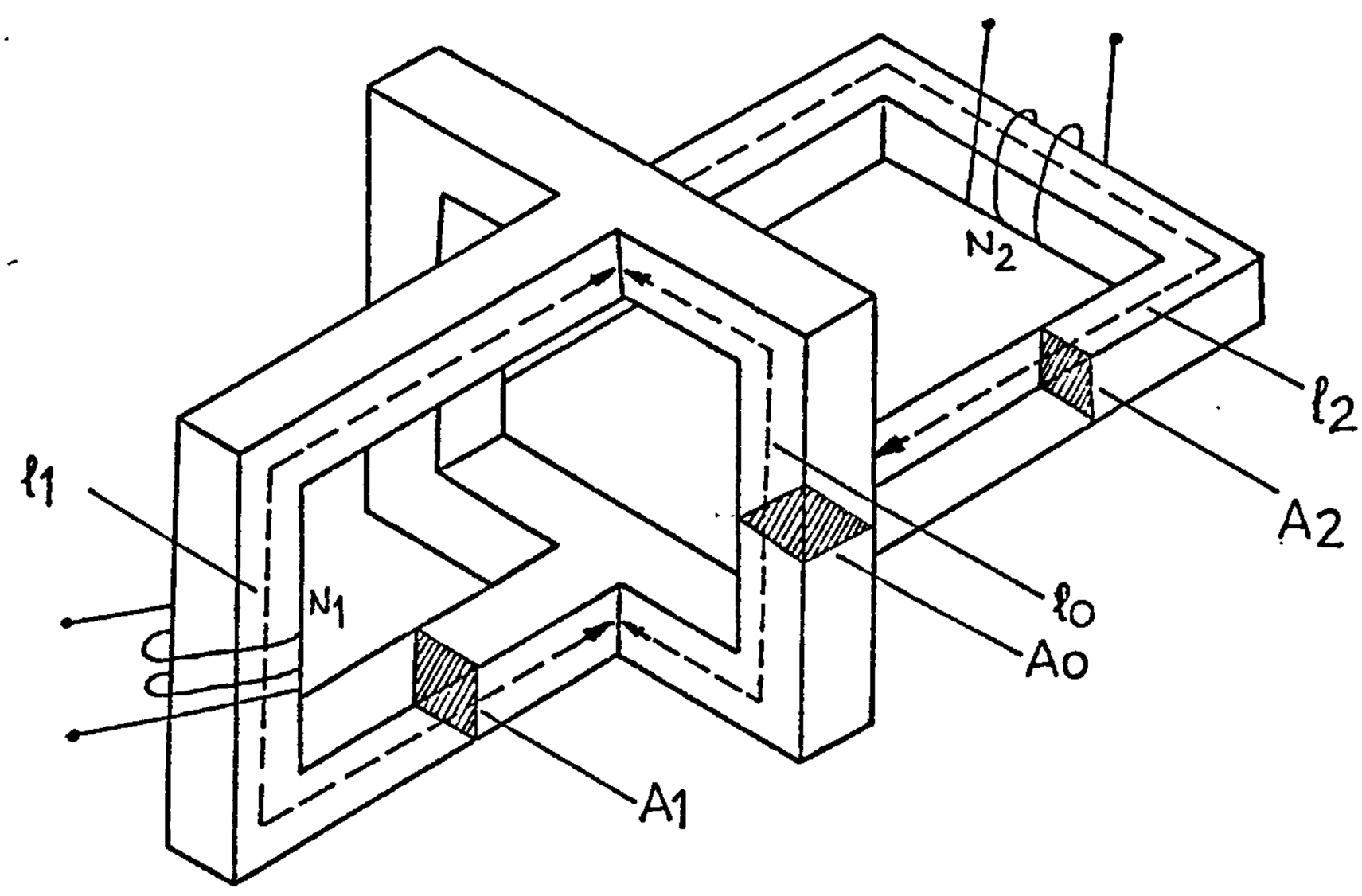

Figure 4.39 Equivalent magnetic model for the cores in Figure 4.31

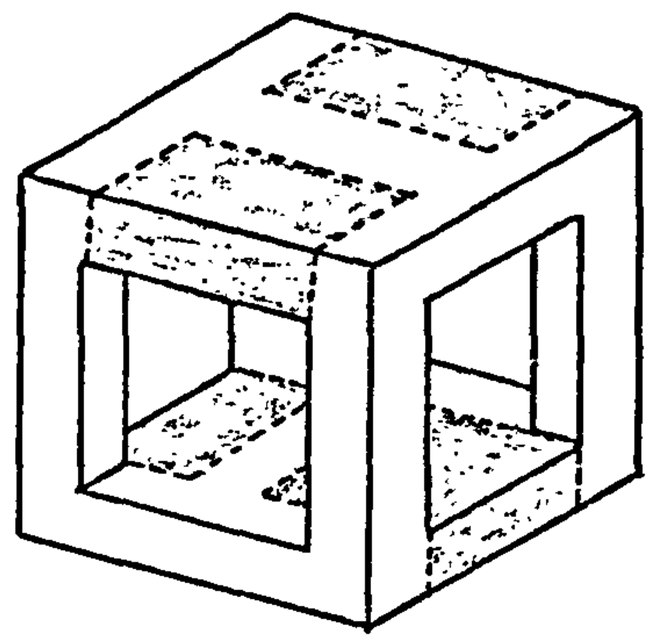

Figure 4.40 Derivation of equivalent structure from Figure 4.31c

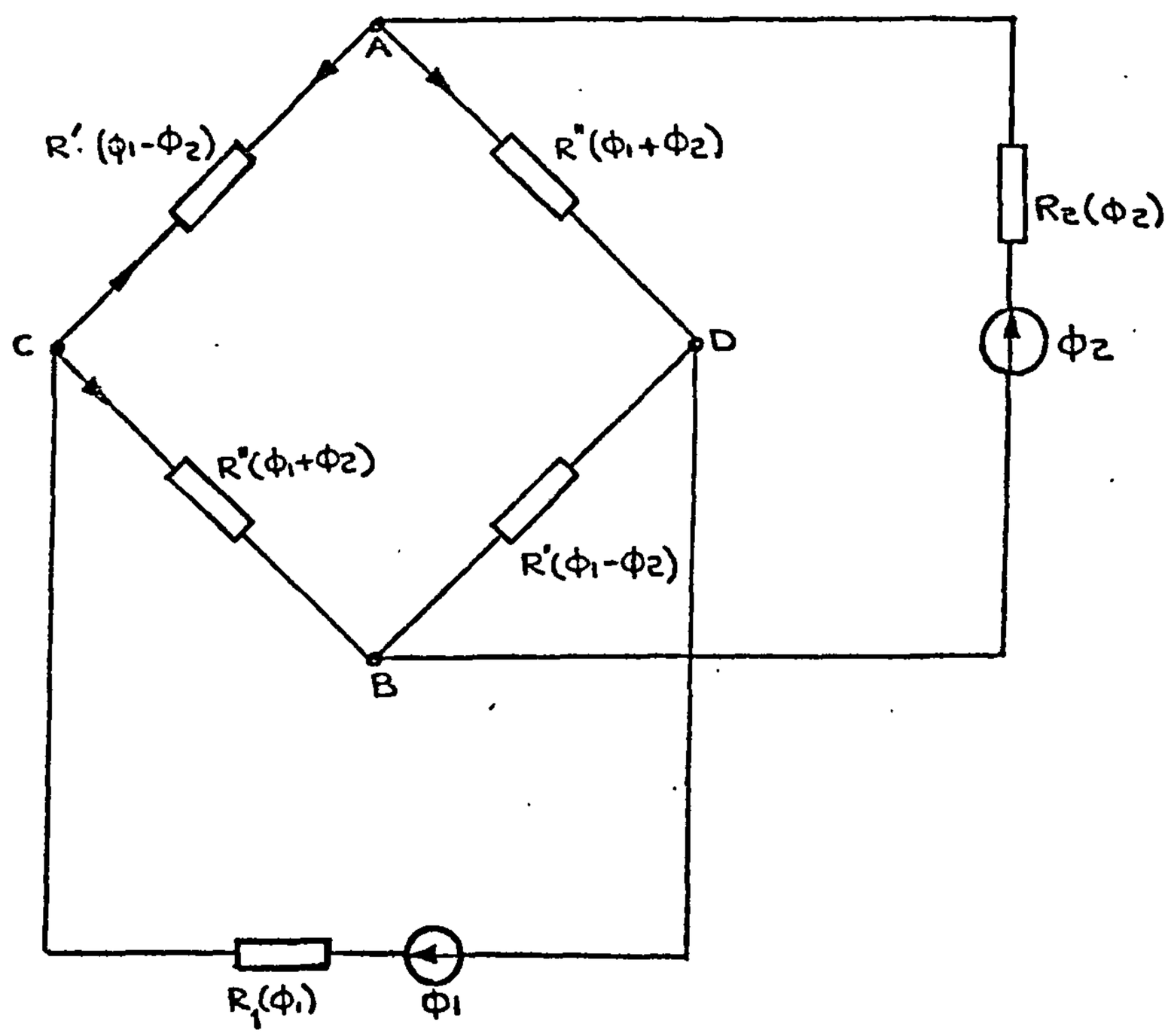

Figure 4.41 Analogous circuit for bridged magnetic core

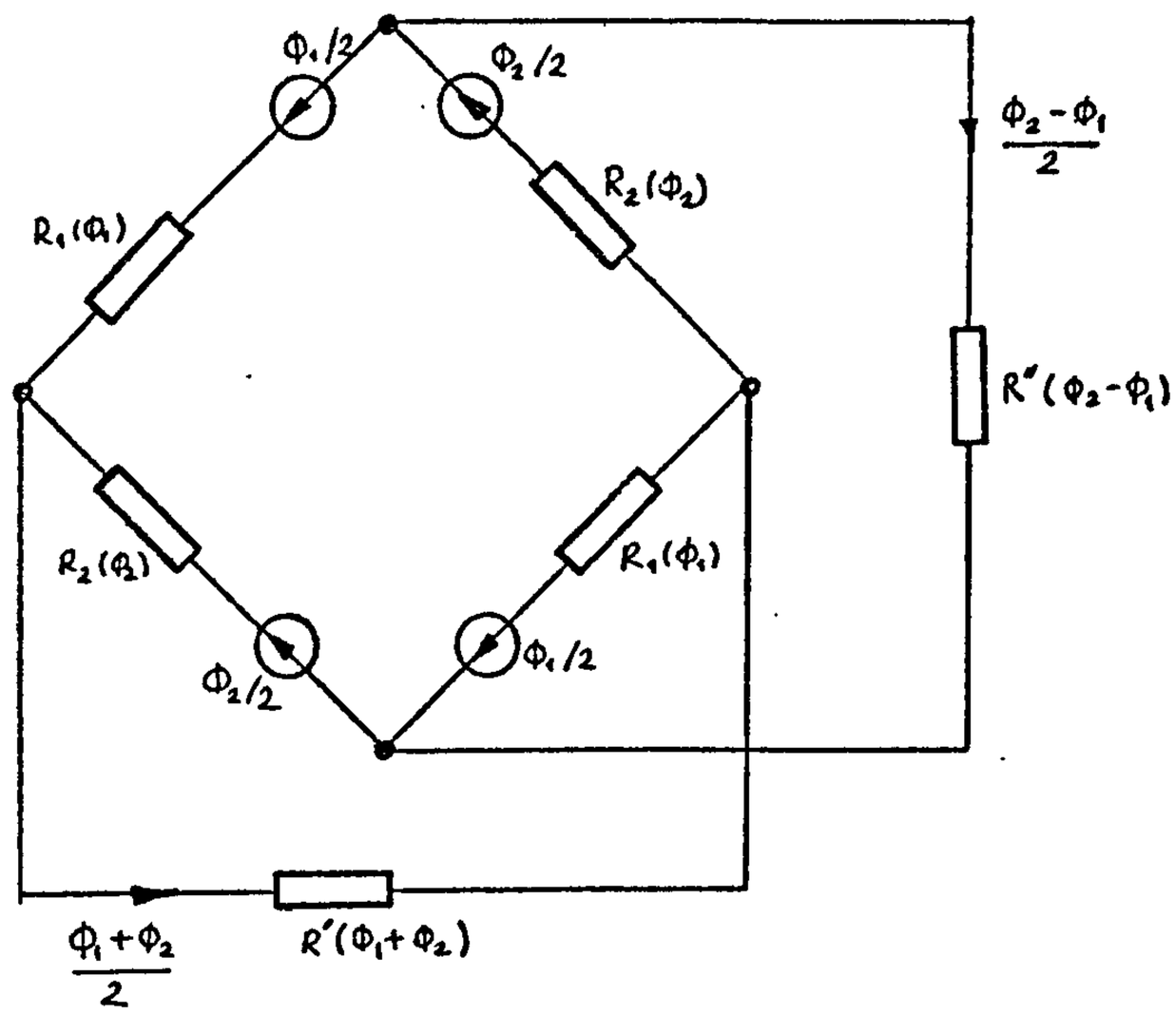

Figure 4.42 Analogous circuit for magnetic X-valve of Figure 4.13

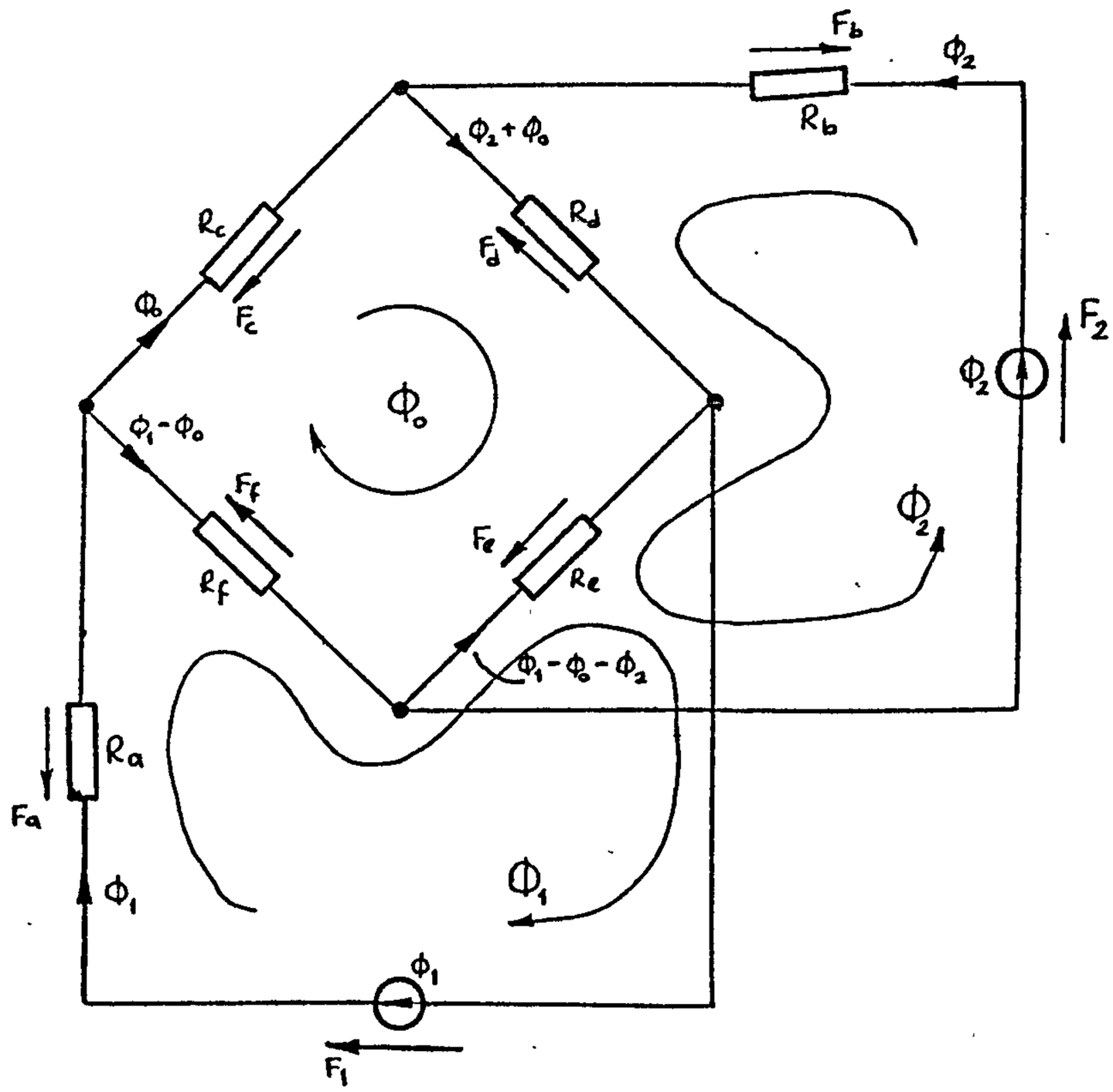

Figure 4.43 Analogous circuit for bridged magnetic core

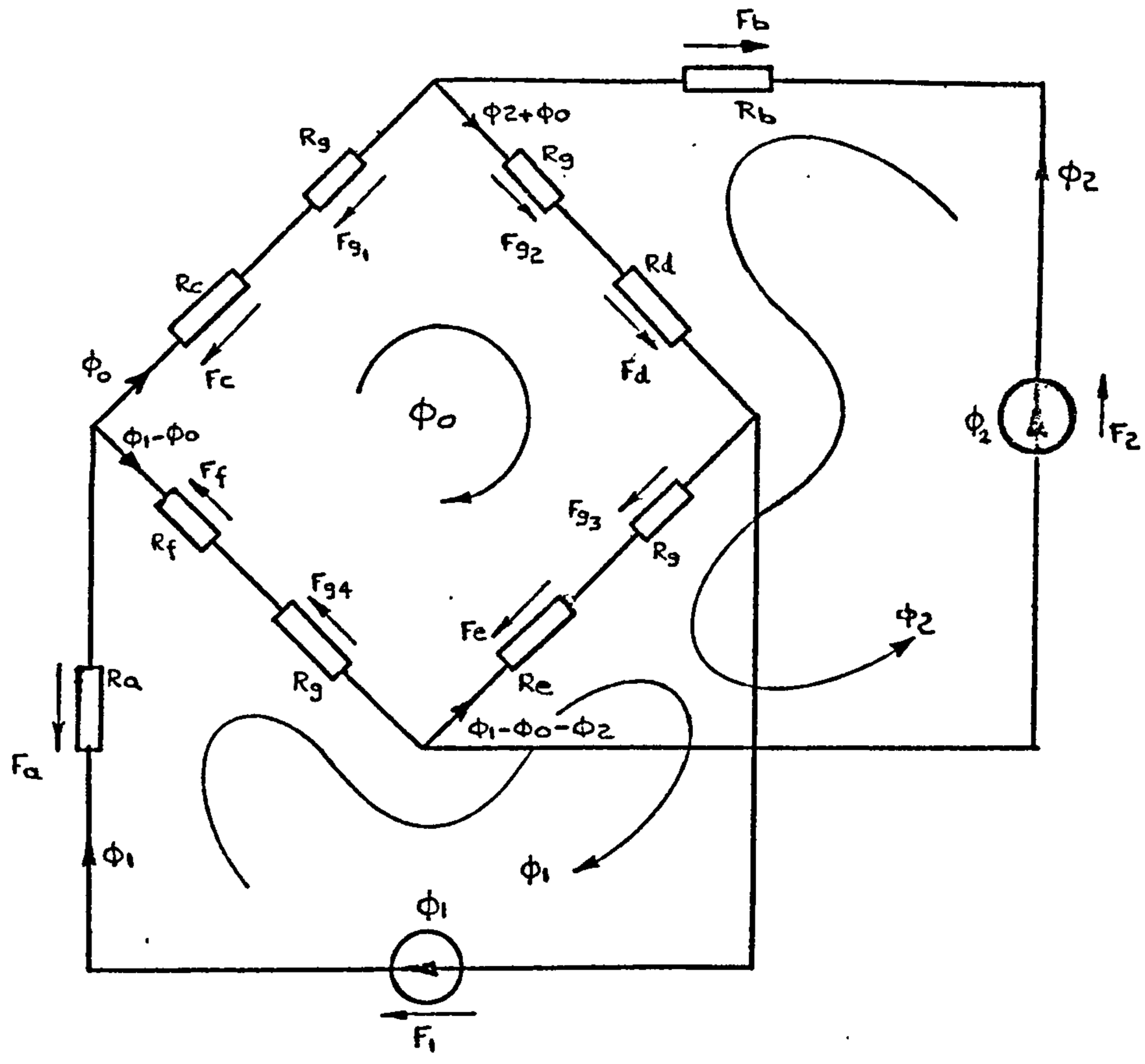

Figure 4.44 Analogous circuit for bridged magnetic core with four equal air-gaps

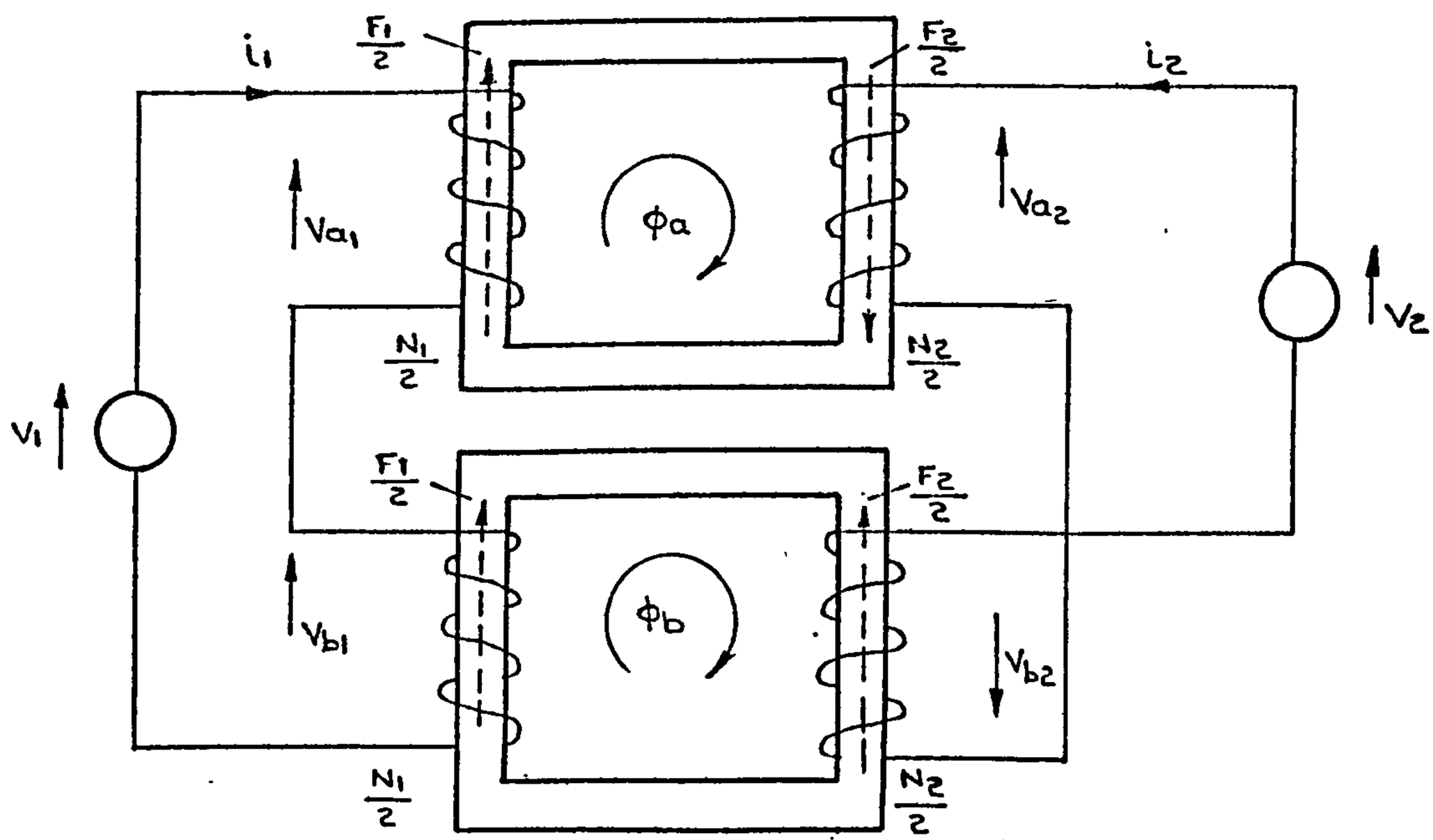

Figure 4.45 Pertaining to Section 4.5.1

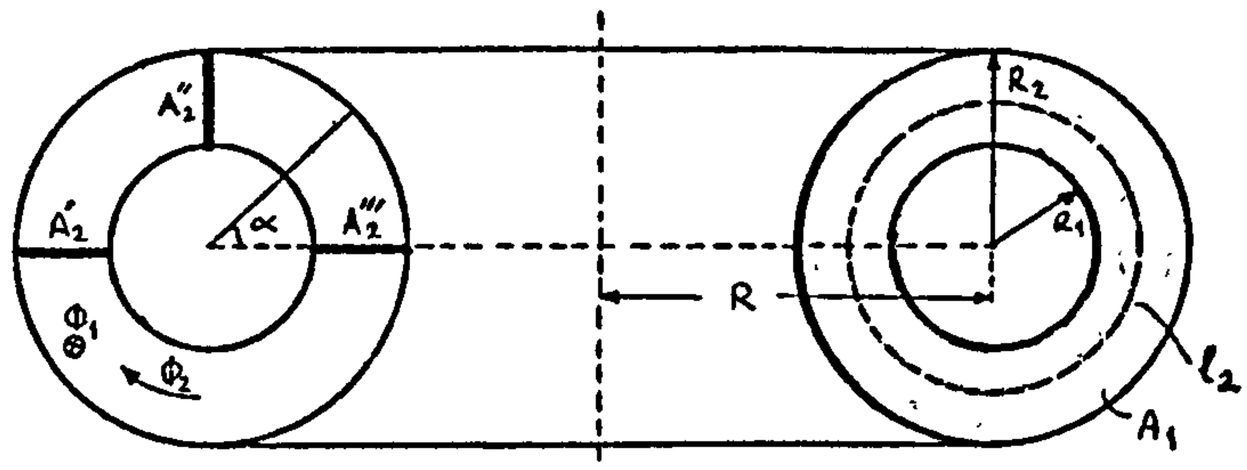

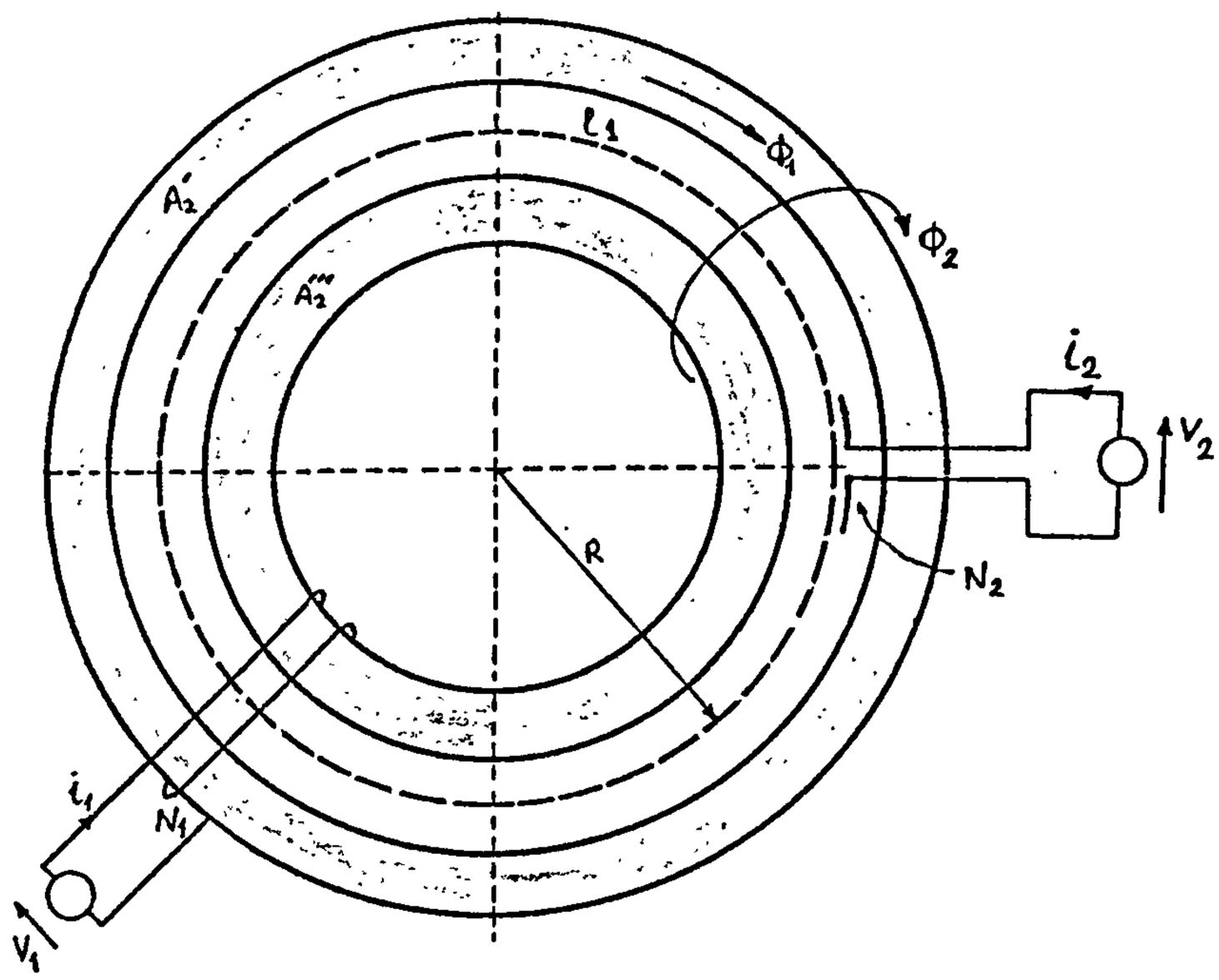

Figure 4.46 Cross-sectional views of hollow toroidal core

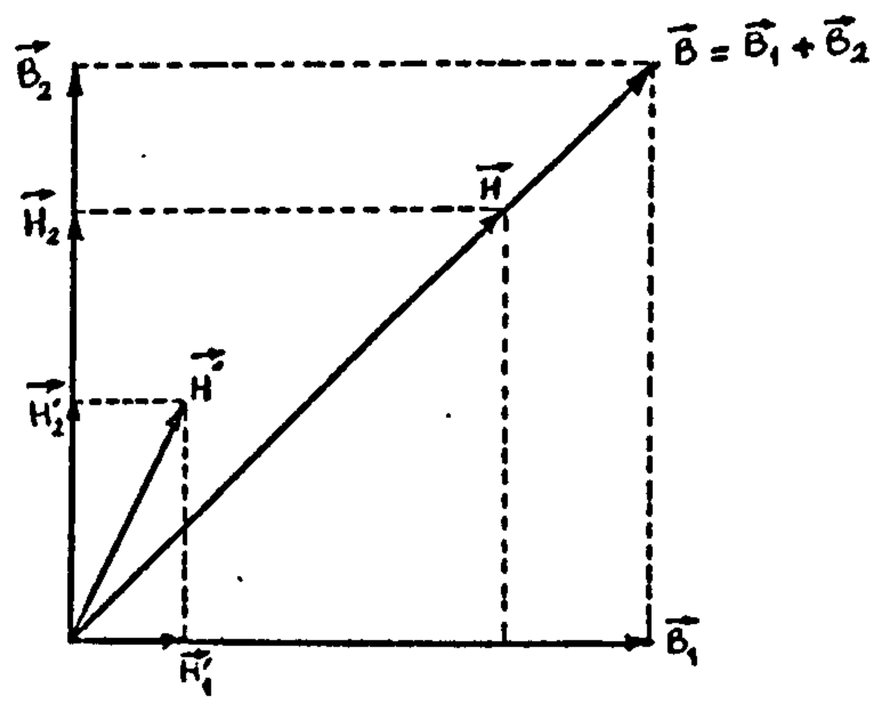

Figure 4.47 Orthogonal flux interaction, $\vec{B}_1$ and $\vec{B}_2$ fixed by voltage sources

CHAPTER V

THE MATHEMATICAL MODEL OF THE PARAMETRIC TRANSFORMER

5.1 The $F_1(\phi_1, \phi_2)$ and $F_2(\phi_1, \phi_2)$ functions and Departures from the Ideal

The functions $F_1(\phi_1, \phi_2)$ and $F_2(\phi_1, \phi_2)$ constitute, in general, the mathematical representation of a two-port electromagnetic device in which both parametric coupling and flux coupling may exist. Depending on the manner in which ϕ_1 and ϕ_2 are related to F_1 and F_2, these functions will also reflect the kinds of coupling existing between the two sides. Generally, in the explicit expressions of these functions, the terms containing the product of the variables ϕ_1 and ϕ_2 result from the parametric coupling, whereas the flux coupling gives rise to the terms independent of ϕ_1 in the function $F_1(\phi_1, \phi_2)$, and in the function $F_2(\phi_1, \phi_2)$ to the terms which are functions of only ϕ_1. However, in the devices concerned, flux coupling is deliberately eliminated.

The relationships between the magnetic quantities F_1, F_2, ϕ_1, ϕ_2 and the electrical quantities i_1, i_2, e_1, e_2 at the ports of the two-port device shown in Figure 5.1, are defined by

$$
\begin{aligned}
F_1 &= N_1 . i_1 \\
F_2 &= N_2 . i_2 \\
\phi_1 &= \frac{1}{N_1} \int e_1 \, dt \\
\phi_2 &= \frac{1}{N_2} \int e_2 \, dt
\end{aligned}
\qquad \ldots\ldots \qquad (5.1)
$$

where N_1 and N_2 are the number of turns in the windings if the device comprises two windings directly connected at the ports. If it is a multi-winding device such as shown in Figure 4.45, the way the windings are connected (e.g. series or parallel) will be accounted for by the parameters N_1 and N_2 in equations (5.1).

In fact, the functions $F_1(\phi_1, \phi_2)$ and $F_2(\phi_1, \phi_2)$ have been obtained in a way that takes the definitions of equations (5.1) as axiomatic. The variables F_1, F_2, ϕ_1 and ϕ_2 may not therefore necessarily correspond to actual physical quantities in the device represented. For example, in the device of Figure 4.45, the actual physical quantities are ϕ_a, ϕ_b and F_a, F_b, although ϕ_1, ϕ_2, F_1 and F_2 are defined in Section 4.5.1 to comply with equations (5.1).

The last two equations above, together with the way the variables ϕ_1 and ϕ_2 are used in the functions F_1 and F_2, indicate that the entire flux created by one of the voltage sources (e_1 or e_2) is assumed to be confined within the iron core. Actually, a small portion of the flux created by either of the voltage sources completes its magnetic circuit through the air and is termed as leakage flux. Therefore, these equations are more correctly written

$$\frac{1}{N_1} \int e_1 \, dt = \phi_{1total} = \phi_1 + \phi_{1L}$$

$$\frac{1}{N_2} \int e_2 \, dt = \phi_{2total} = \phi_2 + \phi_{2L} \qquad \ldots \qquad (5.2)$$

where ϕ_{1L} and ϕ_{2L} are the primary and the secondary leakage fluxes. However, in the functions $F_1(\phi_1, \phi_2)$ and $F_2(\phi_1, \phi_2)$, only portions of the total fluxes, i.e. ϕ_1 and ϕ_2, are taken into account. Apart from leakage fluxes, no such physical phenomena as hysteresis, eddy currents, winding resistances, winding capacitances etc. actually existing in the physical device have been included in these functions. For a more complete modelling of a saturable reactor device, these phenomena must also be considered.

The physical imperfections mentioned may be divided into two groups: (1) those of an electrical nature: winding resistances, winding capacitances; (2) those of a magnetic nature: leakage fluxes, hysteresis, eddy currents. The effect of the air-gaps have already been accounted by the functions $F_1(\phi_1, \phi_2)$ and $F_2(\phi_1, \phi_2)$. The distributed capacitances of the windings are negligible in the frequency range used (50 Hz) and will not therefore be considered. The distributed resistances of the windings can be simulated by lumped resistive components in an equivalent circuit, distinct from the magnetic model. Since the electrical equations of the system are derived from such an equivalent circuit, it becomes significant when the windings are connected to their associated circuits.

Since they correspond to the magnetic model of the device represented, the $F_1(\phi_1, \phi_2)$ and $F_2(\phi_1, \phi_2)$ functions must embody the magnetic imperfections. However, not only are the phenomena involved very complicated to describe mathematically, but the

complexity of deriving the magnetic model from the core structure and the assumptions made therewith prevent the magnetic imperfections being included in the functions $F_1(\phi_1, \phi_2)$ and $F_2(\phi_1, \phi_2)$. The magnetic imperfections are, therefore, treated as external imperfections and are represented by lumped electrical components in the equivalent circuit, separate from the magnetic aspects of the device. This is also the common practice in the theory of conventional transformers.

In the case of conventional transformers, departures from the ideal are considered at two different levels of abstraction: (a) ideal transformer, (b) perfect transformer. The ideal transformer, which has infinitely high winding inductances, is defined by the equations:

$$e_1 = n\, e_2$$
$$i_1 = \frac{1}{n}\, i_2 \qquad \ldots\ldots \qquad (5.3)$$

and draws no current from the primary voltage source at no-load operation. The perfect transformer has finite values of winding inductances and is defined by

$$e_1 = L_1 \frac{di_1}{dt} + M \frac{di_2}{dt}$$
$$\ldots\ldots \qquad (5.4)$$
$$e_2 = M \frac{di_1}{dt} + L_2 \frac{di_2}{dt}$$

where the mutual inductance M satisfies the condition.

$$M^2 = L_1 . L_2 \qquad \ldots\ldots \qquad (5.5)$$

for complete coupling. The imperfection of flux coupling due to the existence of leakage flux is accounted for by the coefficient

$$k = \frac{M}{\sqrt{L_1 . L_2}} \qquad \ldots\ldots \qquad (5.6)$$

which is smaller than unity for an actual (imperfect) transformer.

It is obvious from Sections 4.2 and 4.3 that the $F_1(\phi_1, \phi_2)$ and $F_2(\phi_1, \phi_2)$ functions or in other words, the magnetic model of two parametrically coupled windings, correspond to the second level of abstraction, where magnetisation current (reactive) drawn by the windings flows in their finite inductances. Nevertheless, no such definition as perfect parametric coupling can be made in the same sense as for mutual flux coupling. The leakage fluxes in equations (5.2) are defined to conform with the idea that *each winding has a certain degree of coupling with the core itself.* None of ϕ_{1total} or ϕ_{2total} links the other windings as mutual flux coupling is eliminated in the devices concerned. However, only ϕ_1 and ϕ_2 undergo flux interaction in the iron core, and no flux interaction of any kind occurs between ϕ_{1L} and ϕ_{2L}, as they complete their magnetic circuits through the linear magnetic medium of air. The property of *perfect* parametric coupling depends on the core structure and the manner of the flux interaction. In this respect, the following qualitative remarks

may be made:

1. In general, all ϕ_1 and all ϕ_2 experiences flux interaction in the core. However, if the whole core experiences flux interaction, the parametric coupling between the two windings may be assumed *perfect*.

2. Flux interaction depends on the relative directions of ϕ_1 and ϕ_2 in the core. As already seen, parallel flux interaction is more efficient than orthogonal flux interaction. Hence, the parametric coupling may be assumed *perfect* if the type of flux interaction is parallel.

3. The magnetic material of the cores used generally exhibits magnetic unisotropy. Hence, if flux interaction takes place in the direction of easy magnetisation, the parametric coupling may be assumed *perfect*. Note that both ϕ_1 and ϕ_2 should lie in the direction of easy magnetisation for *perfect* parametric coupling, that is the flux interaction must be of the parallel type.

The functions $F_1(\phi_1, \phi_2)$ and $F_2(\phi_1, \phi_2)$ already account for the facts in 1 and 2 above, but the magnetic material used has been assumed to be isotropic for the sake of simplicity. If the material is unisotropic, it will be quite difficult, although possible, to obtain these functions by using different B/H curves for different parts of the core, where the fluxes take specific directions. It is much more difficult to do this in the case of orthogonal flux interaction.

The ideal transformer defined by equations (5.3) is an impedance multiplying device. This property is used in the theory of conventional transformers to represent actual (imperfect) transformers by equivalent electrical circuits. The common practice is to represent the perfect transformer by the equivalent circuit, employing an ideal transformer whose impedance changing ratio is L_1/L_2, as shown in Figure 5.2. If $k<1$, the leakage fluxes can be accounted for by two separate series linear inductances, L_p and L_s, as shown in Figure 5.3. Common practice is to represent the transformer with finite inductances and imperfect coupling in Figure 5.3a by the equivalent circuit of Figure 5.3b, employing an ideal transformer to refer the impedances on the secondary side to the primary side, or vice versa. Assigning impedances to one side only of the equivalent circuits is a very convenient tool, and makes possible the production of phasor diagrams for practical transformers.

Hysteresis and eddy-current losses are considered together as the total core loss, represented in the equivalent circuit of Figure 5.4, by a resistor in parallel with the primary inductance. The equivalent circuit in this figure also includes the winding resistances R_1 and R_2. The secondary leakage inductance and winding resistance can both be referred to the primary side, through the impedance conversion ratio of the ideal transformer. However, before doing this, it is common practice to take R_o and L_1 in front of R_1 and L_p as shown in Figure 5.5, with

the argument that R_1 and $L_p << R_o$ and L_1. L_s and R_2 are then referred to the primary side, and the equivalent circuit of a practical transformer becomes as simple as that shown in Figure 5.6. With this equivalent circuit, it is now quite easy to determine the referred values of the various elements by no-load and short-circuit tests.

The above arguments of the theory of conventional transformers are not valid for the case of two parametrically-coupled windings, and since mutual flux coupling is completely eliminated, the concept of referring impedances is not appropriate. Furthermore, since parametric coupling is a non linear phenomenon, the principles of linear circuit theory as applied to the conventional transformers cannot be exploited in the case of two parametrically-coupled windings. In contradistinction to conventional transformers, open- or short-circuiting one of these two windings has no influence on the other winding, and it is not possible to measure referred values of leakage inductances and core loss by no-load or short-circuit tests. Neither is it possible to separate the hysteresis and eddy-current components of the total core loss from a no-load test, although by viewing the device as two independent windings, each winding may be associated with its own iron losses. The imperfections must therefore be considered for each winding separately.

The equivalent circuit for two parametrically-coupled windings with winding resistances, leakage inductances and core loss is shown in Figure 5.7, where the imperfections are represented by lumped elements in the circuits of the individual

windings. The $F_1(\phi_1, \phi_2)$ and $F_2(\phi_1, \phi_2)$ functions represent only the boxed part of the equivalent circuit, and once this is obtained the corresponding equivalent circuit may be established, simply by connecting terminals C and D (Figure 5.7) to a resonating capacitor in parallel with the load, and the input terminals A and B to the alternating voltage source. The differential equations constituting the mathematical model of the parametric transformer can then be derived, although their forms are quite complex. Hence, imperfections will be introduced one at a time.

5.2 The General Differential Equations with Winding Resistances and Resistive Load

The winding resistances are easy to determine. They can either be calculated from the characteristics of the wire used, or be directly measured from the actual device. Since the operating frequency is low, dc measurement will be of sufficient accuracy.

In Figure 5.8, the equivalent circuit for the parametric transformer is shown with the winding resistances R_1 and R_2 and the resistive load R_L connected across the output. The resistance R_1 might include the internal resistance, if any, of the alternating voltage source driving the primary winding, and the leakage resistance of the capacitor C might be included in R_L. The equations for the secondary circuit are

$$i_2 = \frac{F_2(\phi_1, \phi_2)}{N_2}$$

$$i_2 = i_C + i_L \qquad \ldots\ldots \qquad (5.7)$$

$$e_2 = R_L . i_L = \frac{1}{C} \int i_C \, dt = - N_2 \frac{d\phi_2}{dt} - R_2 \, i_2$$

which, upon elimination of i_C, i_L and e_2, result in the differential equation

$$\frac{d^2 \phi_2}{dz^2} + \frac{1}{\omega R_L C} \frac{d\phi_2}{dz} + \frac{R_2}{\omega N_2^2} \frac{d}{dz} F_2(\phi_1, \phi_2) + \frac{1}{\omega^2 N_2^2 C}$$

$$(1 + \frac{R_2}{R_L}) F_2(\phi_1, \phi_2) = 0 \qquad \ldots\ldots \qquad (5.8)$$

where $z = \omega . t$. This equation is exactly the same as equation (3.183). The differential equation for the primary circuit can be similarly derived as

$$\frac{d\phi_1}{dz} + \frac{R_1}{\omega N_1^2} F_1(\phi_1, \phi_2) = \frac{e_1(z)}{\omega N_1} = \frac{E_1}{\omega N_1} \cos(z + \pi) \quad (5.9)$$

which needs to be solved simultaneously with equation (5.8) to determine ϕ_1 and ϕ_2. Because of the form of the $F_1(\phi_1, \phi_2)$ and $F_2(\phi_1, \phi_2)$ functions, each of the above equations contains both variables ϕ_1 and ϕ_2, and this establishes the parametric coupling

between the primary and the secondary circuits. However, if $R_1 = 0$, the second term in equation (5.9) disappears, leaving

$$\frac{d\,\phi_1}{dz} = \frac{E_1}{\omega\,N_1}\cos\,(z + \pi) \qquad \ldots\ldots \qquad (5.10)$$

from which the primary flux is found as

$$\phi_1 = \frac{E_1}{\omega\,N_1}\sin z = \phi_{1m}\,\sin z \qquad \ldots\ldots \qquad (5.11)$$

This does not mean that the parametric coupling from the secondary circuit to the primary circuit disappears when $R_1 = 0$. The primary circuit is still determined by the function $F_1(\phi_1, \phi_2)$ and hence, is non-sinusoidal. The second term in equation (5.9) represents both the autonomous and the non-autonomous losses in the primary circuit. The non-autonomous losses can be considered as an extra effect, a (parametric) reaction from the secondary to the primary circuit. A similar but reciprocal reaction can also be said for the third term in equation (5.8).

As the third term in equation (5.8) dictates, the function $F_2(\phi_1, \phi_2)$ must be differentiable to the first order. (Differentiation is with respect to z, but ϕ_1 and ϕ_2 are both functions of z). This, in turn, requires the function $H = f(B)$ to be continuously differentiable and, therefore, to be analytic. This is an important factor when the mathematical representation

of the magnetisation curve of the core material is concerned. Full differentiation of the function $F_2(\phi_1, \phi_2)$ gives

$$\frac{d\,F_2(\phi_1, \phi_2)}{dz} = \frac{\partial}{\partial\,\phi_1} F_2(\phi_1, \phi_2)\,\frac{d\,\phi_1}{dz} + \frac{\partial}{\partial\,\phi_2} F_2(\phi_1, \phi_2).\frac{d\,\phi_2}{dz}$$

..... (5.12)

As can be deduced from the forms of $F_2(\phi_1, \phi_2)$ in Sections (4.4) and (4.5), the partial derivations $\frac{\partial F_2}{\partial\,\phi_1}$ and $\frac{\partial F_2}{\partial\,\phi_2}$ are obtainable if the function $H = f(B)$ is analytic and continuously differentiable. On substituting equation (5.12) and denoting

$$\frac{\partial\,F_2}{\partial\,\phi_2} = f_1(\phi_1, \phi_2)$$

$$\frac{\partial\,F_2}{\partial\,\phi_1} = f_2(\phi_1, \phi_2)$$

$$\varepsilon = \frac{E_1}{\omega\,N_1}$$

..... (5.13)

$$a = \frac{R_1}{\omega\,N_1^{\,2}}$$

$$b = \frac{1}{\omega\,R_L\,C}$$

$$c = \frac{R_2}{\omega\,N_2^{\,2}}$$

and $g = \dfrac{1}{\omega^2 N_2^{\,2} C} \left(1 + \dfrac{R_2}{R_L}\right)$

equations (5.8) and (5.9) become

$$\frac{d\phi_1}{dz} + a F_1(\phi_1, \phi_2) = e \cos(z + \pi)$$

$$\frac{d^2 \phi_2}{dz^2} + b \frac{d\phi_2}{dz} + c \left[f_1(\phi_1, \phi_2)\frac{d\phi_2}{dz} + f_2(\phi_1, \phi_2)\frac{d\phi_1}{dz}\right]$$

$$+ g F_2(\phi_1, \phi_2) = 0 \qquad \ldots\ldots \qquad (5.14)$$

With the transformation

$$\phi_1 = Y_1$$

$$\phi_2 = Y_2 \qquad \ldots\ldots \qquad (5.15)$$

$$\frac{d\phi_2}{dz} = Y_3$$

Equations (5.14) take the form

$$Y_1' = e \cos(z + \pi) - a F_1(Y_1, Y_2)$$

$$Y_2' = Y_3 \qquad \ldots\ldots \qquad (5.16)$$

$$Y_3' = -b Y_3 - c[f_1(Y_1, Y_2).Y_3 + f_2(Y_1, Y_2).Y_1'] - g.F_2(Y_1, Y_2)$$

where dots denote differentiation with respect to z. The term with Y' in the third equation above is a part of the (parametric) reaction from the primary to the secondary circuit. In order for these equations to be written with the normal representation[1]

$$\vec{Y}' = \vec{f}(z,\vec{Y})$$

where $\vec{Y}'$, $\vec{Y}$ and $\vec{f}$ are column vectors, Y_1' must be eliminated from the third equation. The three first-order differential equations defining the behaviour of the system in Figure 5.8 then become

$$Y_1' = e \cos (z + \pi) - a F_1(Y_1, Y_2)$$

$$Y_2' = Y_3 \qquad \ldots\ldots \qquad (5.17)$$

$$Y_3' = -b Y_3 - c \{f_1(Y_1,Y_2) . Y_3 + f_2(Y_1,Y_2).[e \cos (z + \pi) -$$

$$- a F_1(Y_1, Y_2)]\} - g F_2(Y_1, Y_2)$$

which are the system equations for the mathematical model established by the equivalent circuit in Figure 5.8, where the two parametrically-coupled inductors are represented by the $F_1(\phi_1, \phi_2)$ and $F_2(\phi_1, \phi_2)$ functions. These two functions (equations (4.45) and (4.46)) were obtained by simulating the

two-C-core device by the bridged magnetic core, and the system in Figure 5.8 or equations (5.17) is only an approximate mathematical model of the real device. Neither is it complete, since, apart from the winding resistances and the resistive load, other magnetic imperfections such as leakage inductances and core losses have not yet been included. However, even in this case, the complexity arising from both non-linearity and parametric coupling is evident from equations (5.17). Although the variable z appears explicitly only because of the driving function (acv source), it will be noted that both Y_1 and Y_2, everywhere in the equations are functions of time.

5.3 Inclusion of Leakage Inductances into the Mathematical Model

In general, leakage inductances depend on (a) size of cores and coils, (b) shape of cores and coils, (c) number of turns in coils, (d) disposition of windings etc. There is no exact way for calculating leakage inductances for a given magnetic device, although an estimate can be made based on practical experience and with some simplifying assumptions when certain core-winding arrangements are considered. In conventional transformers, the (referred) values of leakage inductances can be measured by short-circuit tests, but such measurements are not possible for devices in which mutual flux coupling is non-existent.

The following qualitative remarks may be made in respect of leakage fluxes when the two-C-core device or the bridged-core device investigated in Section 4.4, is compared with conventional transformers. In the two-C-core device:

1. the flux-path followed by the primary or the secondary flux is uneven with sharp changes of direction;
2. the effective cross-sectional area of the core changes suddenly at the joint of the two halves of the core where an air-gap is likely to exist;
3. the flux density is not the same everywhere in the core, but is highest where the two cores join, that is where the maximum possibility for flux leakage occurs;
4. the primary or the secondary winding is not encircled by an even, closed magnetic medium of high permeability (iron core) unlike the modern designs of conventional transformers.

Because of these factors, flux leakage from the primary and the secondary magnetic circuits of the two-C-core parametric transformer is higher than in conventional transformers. No interaction occurs between the primary and the secondary leakage fluxes even though they intersect each other mostly around the joining faces of the two-C-cores. This is accounted for by the fact that the leakage fluxes can be represented by two separate, linear inductances in the equivalent circuit.

The equivalent circuit for the parametric transformer with winding resistances, resistive load and with leakage inductances

of L_p and L_s is shown in Figure 5.9, from which the system equations are obtained as:

$$\frac{d\,\phi_1}{dz} + \frac{R_1}{\omega\, N_1^{\,2}} F_1(\phi_1, \phi_2) + \frac{L_p}{\omega\, N_1^{\,2}} \frac{d}{dz} F_1(\phi_1, \phi_2) = \frac{e_1(z)}{\omega\, N_1}$$

$$\frac{d^2\,\phi_2}{dz^2} + \frac{1}{\omega\, R_L\, C} \frac{d\,\phi_2}{dz} + \frac{(1 + R_2/R_L)}{\omega^2\, N_2^{\,2}\, C} F_2(\phi_1, \phi_2) + \frac{(R_2 C + L_s/R_L)}{\omega\, N_2^{\,2} C}$$

$$\frac{d\, F_2(\phi_1, \phi_2)}{dz} + \frac{L_s}{\omega\, N_2^{\,2}} \frac{d^2\, F_2(\phi_1, \phi_2)}{dz} = 0$$

..... (5.18)

Comparing these with equations (5.8) and (5.9) it is seen that the leakage inductances give rise to additional terms which require $\frac{d}{dz} F_1(\phi_1, \phi_2)$, $\frac{d}{dz} F_2(\phi_1, \phi_2)$ and $\frac{d^2}{dz^2} F_2(\phi_1, \phi_2)$. Recalling from equations (4.45) and (4.46), the complexity of the dependence of F_1 and F_2 on ϕ_1 and ϕ_2, it is not difficult to realise how much extra complexity these terms will add to the set of already very complex differential equations. This is justified at least by the fact that

$$\frac{d^2}{dz^2} F_2(\phi_1, \phi_2) = \frac{\partial f_2(\phi_1, \phi_2)}{d\ \phi_1} \left(\frac{d\ \phi_1}{dz}\right)^2 + f_2(\phi_1, \phi_2) \frac{d^2\ \phi_1}{dz^2}$$

$$+ \frac{\partial f_1(\phi_1, \phi_2)}{\partial\ \phi_2} \left(\frac{d\ \phi_2}{dz}\right)^2 + f_2(\phi_1, \phi_2) \frac{d^2\ \phi_2}{dz^2} \qquad (5.19)$$

where the functions $f_1(\phi_1, \phi_2)$ and $f_2(\phi_1, \phi_2)$ are as given by the first two equations in equations (5.13). However if the effects of leakage fluxes are neglected (by assuming ϕ_{1L} and ϕ_{2L} in equations (5.2) to be zero, equations (5.18) reduce directly to equations (5.8) and (5.9) for L_p and $L_s = 0$.

5.4 Hysteresis and Eddy Current Losses

Although considerable research has been devoted to investigating the hysteresis and eddy-current properties of iron-cored devices, these properties have yet not been formulated in a unique and general way which covers all their aspects and applies in all cases. Various methods are used to explore different aspects of the hysteresis and eddy-current effects which are generally accounted for by approximate empirical formulae.

Under cyclic magnetic conditions, energy is expended as the hysteresis loss, and the area of the hysteresis loop shown in Figure 5.10 is a measure of the energy expended per cycle. For the *static* hysteresis loop, the hysteresis loss per unit volume is empirically given by[2]

$$P_h = k_h . f . B_m^{\,x} \quad W/m^3 \qquad \ldots\ldots \qquad (5.20)$$

where k_h is a constant, f is the frequency and x is the Steinmetz index between 1.6 and 1.8 for common magnetic materials. If the loop is obtained *dynamically*, eddy-current losses are added and the loop area is increased, as shown in Figure 5.10.

Eddy currents are induced in the iron mass due to rapid flux changes. The flux produced by these currents are in opposition with the main magnetic flux and tends to reduce it. The energy loss due to the eddy-currents causes heating and is not recoverable. As an accurate calculation of eddy-current losses is difficult, an elementary appreciation is generally given by the formula[2]

$$P_e = k_e . f^2 \, B_m^{\,2} \quad W/m^3 \qquad \ldots\ldots \qquad (5.21)$$

where k_e is a constant. Since the eddy-current loss is proportional to the square of the frequency, the area of the *dynamic* hysteresis loop expands with an increase in the frequency.

A general trend is to represent the effects of eddy-currents by an imaginary equivalent circuit, consisting of a transformer with a short circuited secondary.[3,4] This concept has been used by Hindmarsh[3] in the case of the field winding of a

machine, and by Bean et al[4], for the eddy currents induced in the solid parts of transformers. The eddy-current losses are represented by a single short-circuited loop coupled to the transformer winding, which leads to the conclusion that the effect of the eddy current is to increase the effective resistance but to decrease the effective reactance of the transformer.

A well-known concept used for representing the hysteresis losses, is to regard permeability as a complex or vector quantity of the form

$$\mu = \mu' - j\,\mu'' \qquad \text{or} \qquad \underline{\mu} = \mu\, e^{-j\theta} \qquad \ldots\ldots \quad (5.22)$$

where the imaginary part of the complex permeability accounts for the hysteresis losses.* The real and imaginary components (or the modulus and the argument) of the complex permeability can be calculated with the aid of elliptical loops on the B/H plane, with areas equal to those of the actual hysteresis loops.[5]

---

* The negative signs in equations (5.22) are due to the fact that magnetic hysteresis always causes the fundamental component of B to lag behind that of H.

This complex notation method is convenient, as it enables permeability and loss to be expressed on an equal footing and represented in mathematical analyses by a single symbol. However, its application is restricted to the cases where B and H can be regarded as complex vectors when working in the frequency domain. As well as this, most of the other methods are concerned only with the steady-state performance, and cannot bring out information applicable to the transient operation.

As mentioned earlier, it is common practice to regard hysteresis and eddy current effects together as the total core loss. Notwithstanding this, their effects are not confined only to introducing damping into the associated circuits, since they also change the reactive parameters of the circuits by introducing phase shifts between voltages and currents. Most important of all, they cause the B-H relationship to become a multi-valued function and bring distortion into the voltage and current waveforms. In conventional transformers, it is relatively easy to determine the waveform distortion due to hysteresis when the time-variation of either B or H is completely known, but this waveform distortion is considered separate from other aspects of the hysteresis and is generally neglected. It has yet not been possible to express numerically or analytically the magnetisation curves of magnetic materials, with multi-valued functions giving simultaneous representation of both non-linearity and hysteresis property.

Since the construction of the $F_2(\phi_1, \phi_2)$ and $F_2(\phi_1, \phi_2)$ functions in Chapter IV was based on the assumption that the magnetisation characteristic is a single-valued function, we are restricted to the use of the equivalent circuit in Figure 5.7 where the total core loss is represented by the resistive elements R_{01} and R_{02}. This means that only one aspect - the loss - of the hysteresis and eddy current effects is concerned. The equivalent circuit for the parametric transformer is then shown in Figure 5.11, from which the differential equations are to be derived. However, before these equations can be written, the values of R_{01} and R_{02} must be calculated by using equations (5.20) and (5.21). Firstly, as the flux density is not constant everywhere in the two-C-core parametric transformer, different losses will occur at different parts of the magnetic circuit. Secondly, these empirical formulas require the maximum value of B to be known in order to calculate the losses. If only one of the windings is driven by a voltage source, it may be possible to find B_m in the core. But, if the two windings are driven simultaneously (or after the onset of parametric oscillations), B_m cannot be known before the differential equations are solved. Additionally, B_m will be changing during the transient state, until it settles down to a permanent value. Thirdly, with k_h and k_e known in equations (5.20) and (5.21), they are only valid for a sinusoidal waveform of flux density. It is therefore virtually impossible to determine the exact values of R_{01} and R_{02} in Figure 5.11.

As both ϕ_1 and ϕ_2 exist in the core during parametric transformer operation, the core losses and therefore R_{01} and R_{02} are functions of both ϕ_1 and ϕ_2, so that the resistive elements R_{01} and R_{02} are not simple linear resistors, but are non-linear and time-varying elements. Due to the complication of parametric coupling, it is not practically possible to express R_{01} and R_{02} as functions of ϕ_1 and ϕ_2. If the core losses could be obtained in the form of the two functions $R_{01}(\phi_1, \phi_2)$ and $R_{02}(\phi_1, \phi_2)$, the effects of hysteresis and eddy current losses on the parametric transformer operation would be more accurately represented in the system equations. However, disregarding the dependence of the total core losses on parametric coupling (or flux interaction) and simply assuming that R_{01} and R_{02} are linear, constant resistors enables the system equations to be written from Figure 5.11.

Unlike conventional transformer practice, R_{01} and R_{02} cannot be taken from their existing places to the terminals AB and CD in the equivalent circuit of Figure 5.11. Even with no load at the output of the parametric transformer, a high current flows in the secondary circuit after the parametric oscillations have built up, and a high primary current is drawn from the supply. The voltage drops across the series elements R_1, L_p and R_2, L_s have an important influence on no-load operation and are not negligible.

With the assumption that the values of the linear, constant resistors R_{01} and R_{02} are known, the differential equations then derived from Figure 5.11 will be more complex than equations (5.18). But, if the leakage inductances L_p and L_s are neglected, the equivalent circuit becomes simpler and yields the differential equation for the primary circuit

$$\frac{d\phi_1}{dz} + \frac{R_1 . R_{01}}{R_1 + R_{01}} \frac{1}{\omega N_1^2} F_1(\phi_1, \phi_2) = \frac{R_{01}}{R_{01} + R_1} \cdot \frac{e_1(z)}{\omega N_1} \qquad (5.23)$$

and for the secondary circuit

$$\frac{d^2\phi_2}{dz^2} + \frac{1}{\omega C}\left[\frac{1}{R_L(1 + \frac{R_2}{R_{02}})} + \frac{1 + \frac{R_2}{R_L}}{R_{02} + R_L}\right]\frac{d\phi_2}{dz} + \frac{R}{\omega N_2^2} \cdot \frac{1}{1 + \frac{R_2}{R_{02}}} \frac{d}{dz} F_2(\phi_1, \phi_2)$$

$$+ \frac{1 + R_2/R_L}{\omega C N_2^2} \cdot \frac{1}{1 + R_2/R_{02}} F_2(\phi_1, \phi_2) = 0$$

$$\ldots\ldots \qquad (5.24)$$

Apart from the appropriate changes in the coefficient of each term in these equations, their form is basically the same as equations (5.8) and (5.9). In fact, when the core losses are neglected by taking R_{01}, $R_{02} = \infty$, equations (5.23) and (5.24) directly reduce to equations (5.8) and (5.9).

As is evident from Sections 5.2 to 5.4, the equations constituting the mathematical model of the parametric transformer are quite complex, even when magnetic imperfections such as leakage fluxes and core losses are neglected. For this reason, investigations on the operation of the parametric transformer will be based on the equivalent circuit of Figure 5.8, or equations (5.8) and (5.9), and leakage fluxes and core losses will not be included in the system equations, even though they are comparatively higher than in conventional transformers. As can be seen from the coefficients of equations (5.23) and (5.24), the core losses increase damping and also introduce detuning into the system. Therefore, the effects of the core loss can be studied under the general guidelines of Sections 3.3 and 3.4, Chapter III.

5.5 The General Equations with Reactive Loads

As mentioned in Section 3.5, a single second-order differential equations is not sufficient to describe the secondary circuit if the power factor of the load is different from unity. Because the load current i_L cannot be eliminated amongst equations (5.7) when the load is reactive, it remains as another system variable to be determined in addition to ϕ_1 and ϕ_2.

The load to be connected across the output may in general, contain all resistance, capacitance and inductance components.

If such a load is given in impedance dimensions, it may be represented by a series RLC circuit as shown in Figure 5.12. The equation for the primary circuit remains unchanged as equation (5.9), while from this figure the secondary circuit equations are

$$e_2 = - N_2 \frac{d\phi_2}{dt} - R_2 i_2$$

$$e_2 = \frac{1}{C} \int i_C \, dt$$

$$e_2 = R_L i_L + \frac{1}{C_L} \int i_L \, dt + L_L \frac{d i_L}{dt} \qquad \ldots\ldots \qquad (5.25)$$

$$i_2 = i_C + i_L$$

which finally lead to the two second-order differential equations

$$\frac{d^2 \phi_2}{dz^2} + \frac{R_2}{\omega N_2^2} \frac{d F_2(\phi_1, \phi_2)}{dz} + \frac{F_2(\phi_1, \phi_2)}{\omega^2 N_2^2 C} - \frac{1}{\omega^2 N_2 C} i_L = 0 \qquad \ldots\ldots \qquad (5.26)$$

$$L_L C \frac{d^2 i_L}{dz^2} + \frac{C R_L}{\omega} \frac{d i_L}{dz} + \frac{1}{\omega^2} (1 + \frac{C}{C_L}) i_L - \frac{F_2(\phi_1, \phi_2)}{\omega^2 N_2} = 0 \qquad \ldots\ldots \qquad (5.27)$$

where $z = \omega t$. The system variables are ϕ_1, ϕ_2 and i_L, and these are to be solved from the three simultaneous differential equations given by equations (5.9), (5.26) and (5.27).

If inductive and capacitive components are not simultaneously present in the load, then a load with a negative power factor can be represented by a series RC circuit, and a load with a positive power factor by a series RL circuit. Both types of load are shown in Figures 5.13 and 5.14 at the output of the parametric transformer.

The first two of the three system equations for Figure 5.13 are found to be the same as equations (5.9) and (5.26), and the third equation is obtained as

$$\frac{d\, i_L}{dz} + \frac{1}{\omega R_L}\left(\frac{1}{C} + \frac{1}{C_L}\right) i_L - \frac{F_2(\phi_1, \phi_2)}{\omega N_2 R_L C} = 0 \qquad (5.28)$$

For Figure 5.14, the set of three system equations is given by equations (5.9), (5.26) and the third equation is

$$\frac{d^2 i_L}{dz^2} + \frac{R_L}{\omega L_L}\frac{d\, i_L}{dz} + \frac{1}{\omega^2 L_L C} i_L - \frac{F_2(\phi_1, \phi_2)}{\omega^2 L_L C N_2} = 0 \qquad (5.29)$$

Equation (5.29) may be obtained from equation (5.27), by substituting the hypothetic value $C_L = \infty$, representing a short circuit in place of C_L. Similarly, for $L_L = 0$, equation (5.27) reduces to equation (5.28).

If the load with the general RLC form is given in admittance dimensions it may be represented by the parallel RLC circuit shown at the output in Figure 5.15. With such a load in the secondary circuit, it can immediately be said that C and C_L can be combined, yielding the total capacitance in the secondary as $C_T = C + C_L$. The equation for the primary circuit of Figure 5.15 is still unchanged and is given by equation (5.9). The secondary circuit equations are

$$i_2 = \frac{F_2}{N_2} = C\frac{d\,e_2}{dt} + \frac{e_2}{R_L} + \frac{1}{L_L}\int e_2\,dt + C_L\frac{d\,e_2}{dt} \qquad (5.30)$$

$$e_2 = -N_2\frac{d\,\phi_2}{dt} - R_2\,i_2$$

which lead to the single but third-order differential equation

$$\frac{d^3\phi_2}{dz^3} + \frac{1}{\omega C_T R_L}\frac{d^2\phi_2}{dz^2} + \frac{1}{\omega^2 C_T L_L}\frac{d\,\phi_2}{dz} + \frac{R_2}{\omega N_2^{\,2}}\frac{d^2F_2}{dz^2} +$$

$$\frac{(1 + \frac{R_2}{R_L})}{\omega^2 C_T N_2^{\,2}}\frac{d\,F_2}{dz} + \frac{R_2}{\omega^3 L_L C_T N_2^{\,2}}F_2 = 0 \qquad (5.31)$$

where $C_T = C + C_L$. If, for a parallel RC-type load, the value $L_L = \infty$ is substituted in equation (5.31) and the resulting equation is integrated with respect to z, the equation finally obtained becomes the same as equation (5.8), but with C replaced

by C_T. Hence, a parallel RC-type load does not change the basic nature of the resistively loaded secondary circuit, apart from increasing the total value of the secondary circuit capacitance. But, in the case of a parallel RL-type load, the secondary circuit equation remains the same as equation (5.31), where C_T now equals C only. Like equations (5.18), this equation involves also the first and the second derivatives of the function $F_2(\phi_1, \phi_2)$, and the statement made in Section 5.3 on the overall complexity of the equations can also be repeated here.

As can be noticed from the form of the differential equations for different loads, an inductive load causes the secondary circuit differential equation to be more complex in form than does a capacitive load. This is also an indication of the poorer behaviour of the parametric transformer on inductive loads than on capacitive loads.

The equations obtained for the reactively loaded parametric transformer may also be represented in the normal form by a set of first-order differential equations. This is relatively easy for series RLC, RL and RC type loads, where the total number of equations is five, resulting from the five system variables, $Y_1 = \phi_1$, $Y_2 = \phi_2$, $Y_3 = \frac{d\phi_2}{dz}$, $Y_4 = i_L$ and $Y_5 = \frac{di_L}{dz}$. In the case of the series RC-type load, this number is four as the fifth variable is not needed.

The parametric transformer loaded with parallel RLC or RL type loads (equations (5.9) and (5.31) together) may be represented by a set of four first-order differential equations with the system variables $Y_1 = \phi_1$, $Y_2 = \phi_2$, $Y_3 = \frac{d\phi_2}{dz}$ and $Y_4 = \frac{d^2\phi_2}{dz^2}$. However, the last equation in the set,

$Y_4 = f(z, Y_1, Y_2, Y_3, Y_4)$, will be quite lengthy and complicated because of the involvement of the first and the second derivatives of the function $F_2(\phi_1, \phi_2)$, as given by equations (5.12) and (5.19). In the case of a parallel RC-type load, the number of equations in the normal form is only three, since equation (5.31) reduces to a second-order differential equation.

To avoid the extra complexity and the increased number of equations arising because of reactive loading, an approach similar to that followed in relation to Figure 3.32 at the end of Section 3.5 may also be considered, although this will not fully reflect the effects of the reactive load, especially on the voltage and current waveforms. Assuming signals exist only at the single frequency ω in the secondary circuit, the parallel combination of the resonating capacitor C and a general type load Z_L may be converted to an equivalent circuit consisting of C' and R_L', as shown in Figure 5.16, by using the concept of complex impedance. When this equivalent circuit is connected at the output terminals, the equivalent circuit for the parametric becomes as in Figure 5.8. Thus, equations (5.8) and (5.9) but with the new effective values C' and R_L' may be somewhat used to investigate the operation with reactive loads.

5.6 Simulation by Analogue Computer

Taking the equivalent circuit in Figure 5.8, together with equations (5.8) and (5.9), as the basic mathematical model of the parametric transformer, a block diagram for analogue simulation purposes may be obtained as in Figure 5.18. In this diagram, the differential equations of the primary and the secondary circuits, equations (5.8) and (5.9), are simulated by the computing elements whose symbols are defined in Figure 5.17. Normally, an analogue computer solution of ordinary differential equations does not require a differentiator unit, as differentiation may be eliminated from the equations, and integrator units suffice to establish the simulation. However, the term with $\frac{d}{dz} F_2(\phi_1, \phi_2)$ in equation (5.8) cannot be eliminated through integration or any other process, and the differentiator device remains necessary for the analogue simulation of the parametric transformer. If leakage inductances or some forms of reactive loads were also considered, more than one differentiator would be needed. Such a diagram as in Figure 5.18 is very troublesome to establish on an analogue computer, because of the difficulties arising from the use of a differentiating network.[6] The need for a differentiator may be avoided only if the explicit analytical expression of $F_2(\phi_1, \phi_2)$ in terms of ϕ_1 and ϕ_2 is known, so that the differentiation in equation (5.12) can be done manually. Extra function generators are then needed to produce the functions $f_1(\phi_1, \phi_2)$ and $f_2(\phi_1, \phi_2)$, which are the partial derivatives of $F_2(\phi_1, \phi_2)$ defined in equations (5.13).

The two-input, two-output block in the centre of the diagram designates the mathematical model of the magnetic structure of the parametric transformer, and is where the functions $F_1(\phi_1, \phi_2)$ and $F_2(\phi_1, \phi_2)$ are produced. The upper and lower parts of the diagram correspond to the primary and secondary circuit equations. Since these are simultaneous, the corresponding parts of the diagram have to be interconnected, and this takes place within the square block which represents two parametrically coupled windings. For different core-winding arrangements, such as the two-C-core, the hollow toroidal core, etc.employed to construct a parametric transformer, different diagrams generating the functions $F_1(\phi_1, \phi_2)$ and $F_2(\phi_1, \phi_2)$ are inserted in this block.

For the model of the two-C-core device simulated by the bridged core, equations (4.45) and (4.46) are simulated by the diagram in Figure 5.19, where four function generators producing the function $H = f(B)$ are required. When the diagram in this figure is inserted in the square block in Figure 5.18, the complete simulation diagram for the two-C-core parametric transformer is obtained. Equations (4.61) and (4.62) for the saturable reactor of Figure 4.45, are simulated by the similar but simpler diagram of Figure 5.20. In the case of orthogonal flux interaction, simulation of the $F_1(\phi_1, \phi_2)$ and $F_2(\phi_1, \phi_2)$ functions requires square-root and division circuits, which also introduce many practical difficulties into the realization of the simulation on a computer.[7] Nevertheless, equations (4.67) and

(4.68) representing the hollow toroidal core device may be simulated by the diagram in Figure 5.21, where *quarter squares multipliers*[8] are employed to obtain $\frac{\phi_1^2}{A_1^2} + \frac{\phi_2^2}{A_2^2}$.

Various methods may be applied to realize the function generators which simulate the magnetisation characteristic $H = f(B)$. The use of general purpose diode function generators on the basis of piecewise linear approximation to the magnetisation curve may not be permissible, as the derivative of $F_2(\phi_1, \phi_2)$ is required and this will contain discontinuities due to differentiation at the junctions of straight line segments in the approximated function.

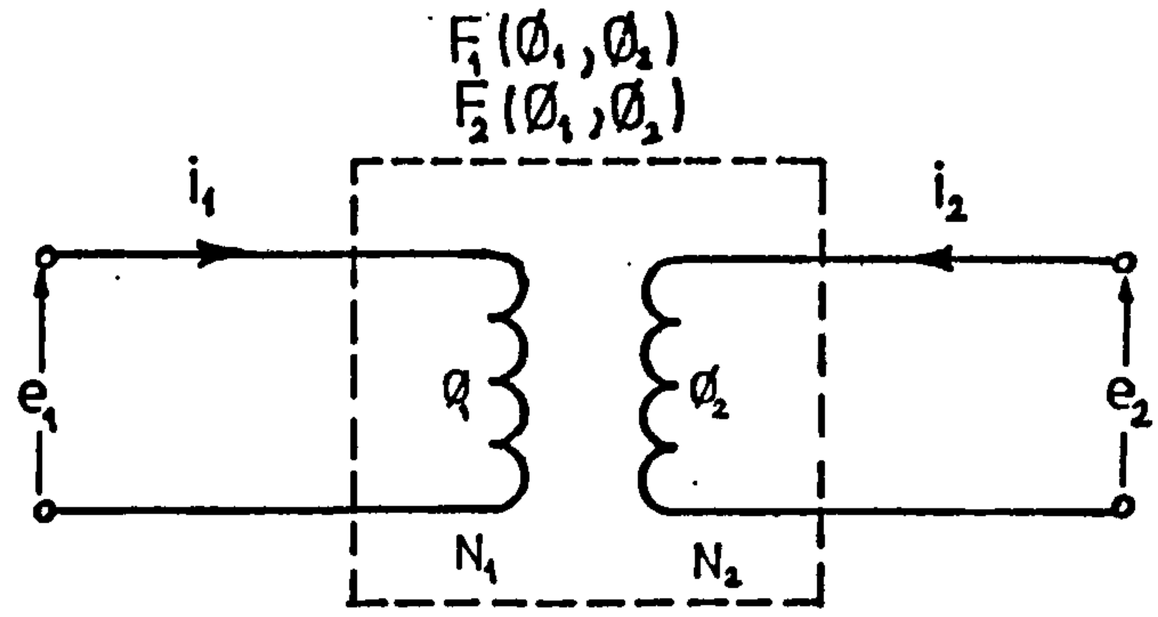

Figure 5.1 Two Parametrically Coupled Windings

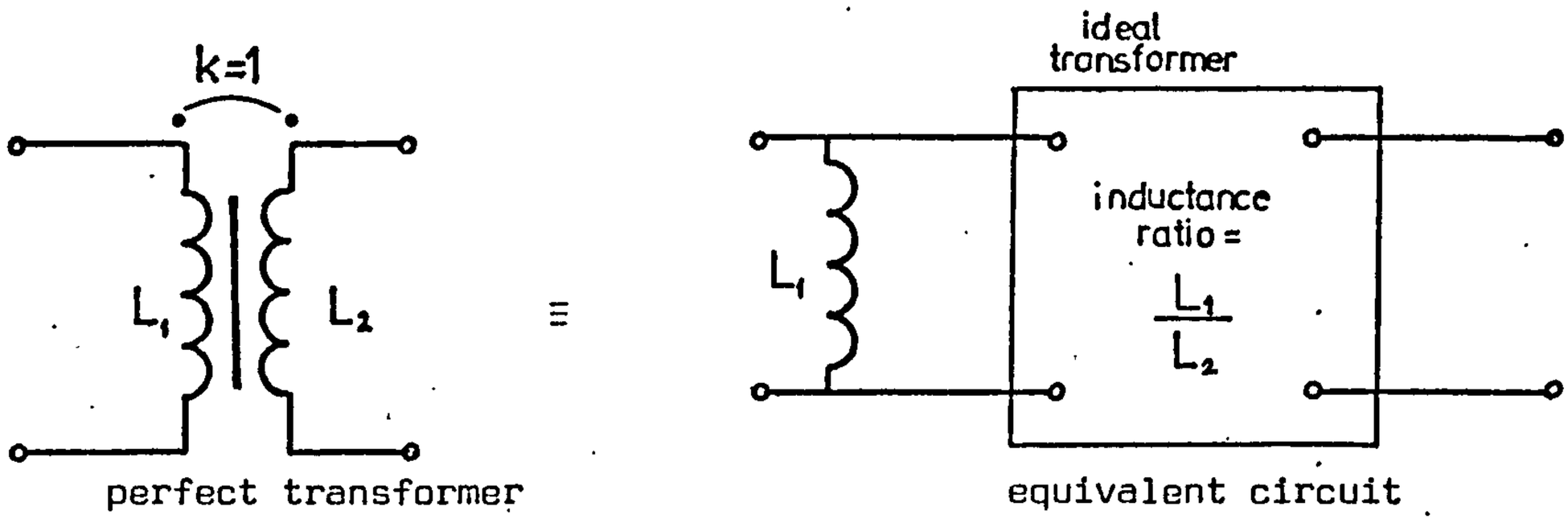

Figure 5.2 The Perfect Transformer and its Equivalent Circuit

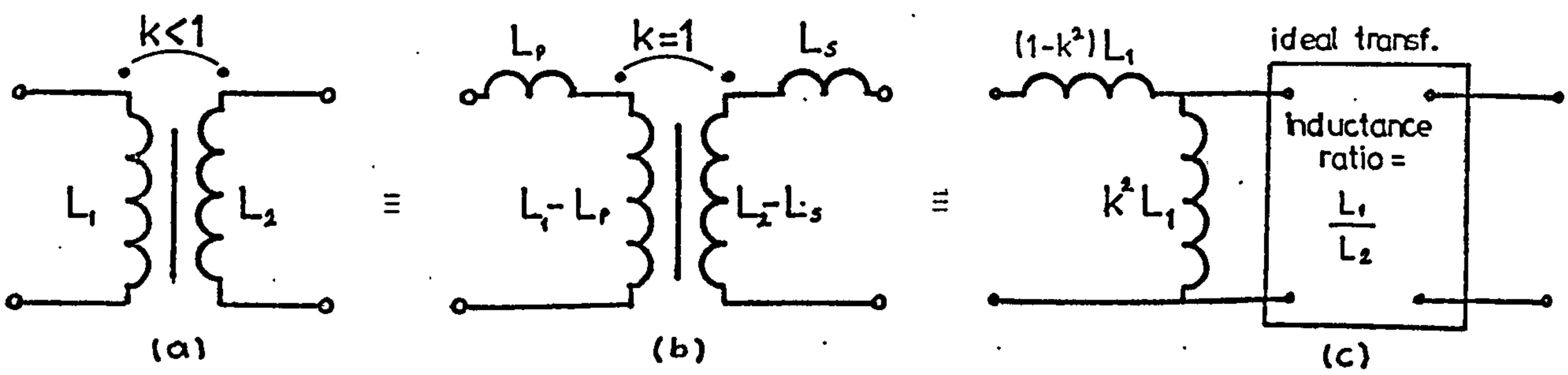

Figure 5.3 Transformer with Finite Inductances and Imperfect Coupling

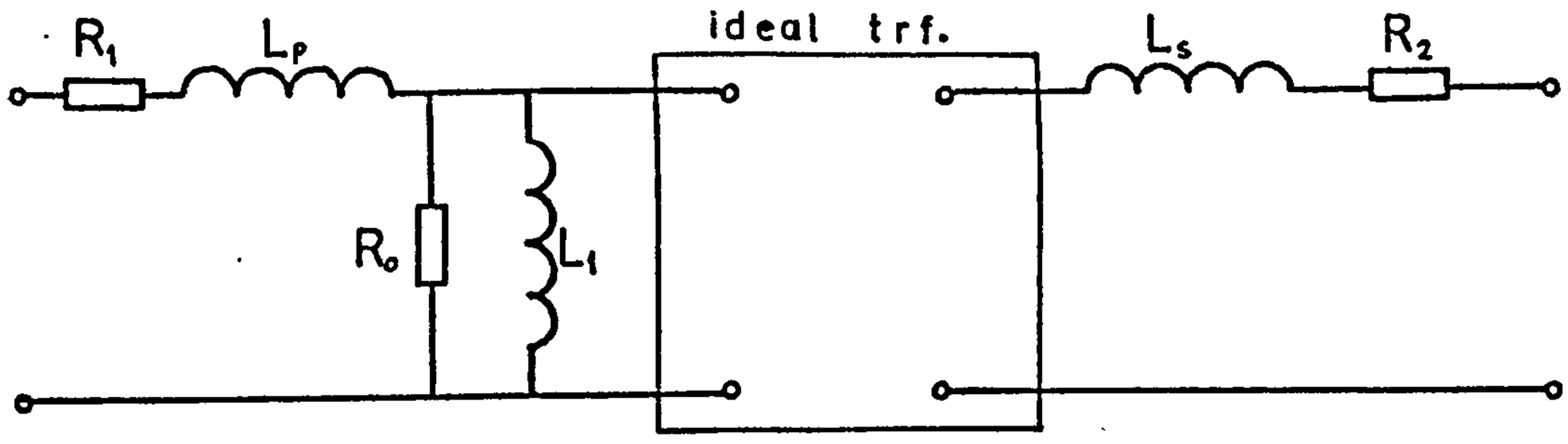

Figure 5.4 Equivalent Circuit for a Practical Transformer having Finite Inductances, Imperfect Coupling, Winding Resistances, and core loss.

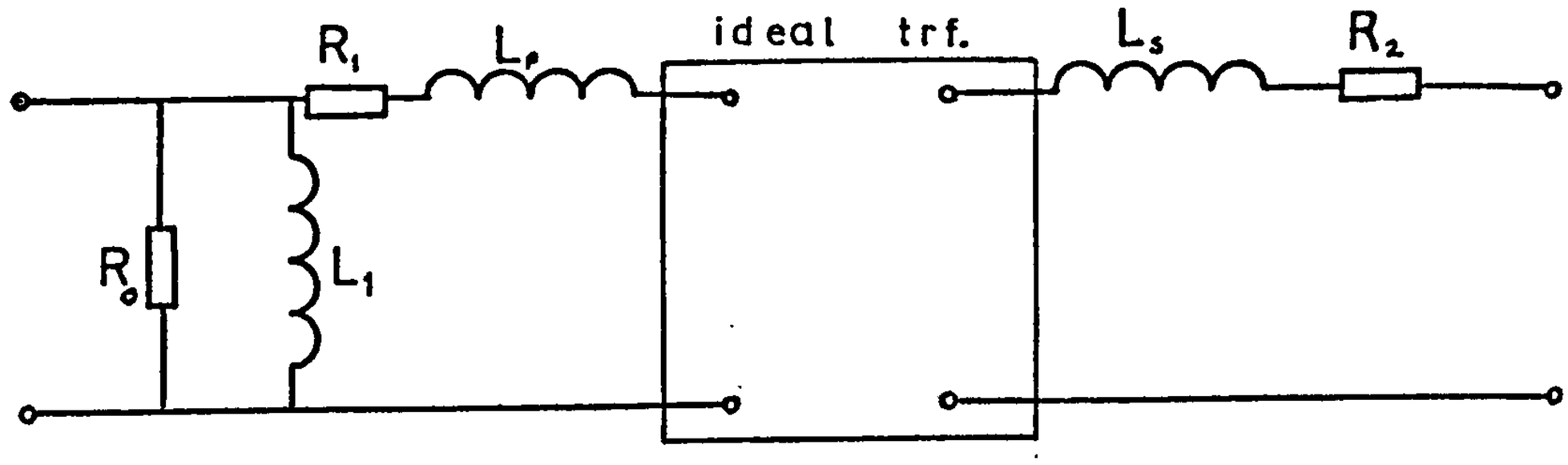

Figure 5.5 Equivalent Circuit as Figure 5.4 but with R_0 and L_1 Connected at the Supply Terminals

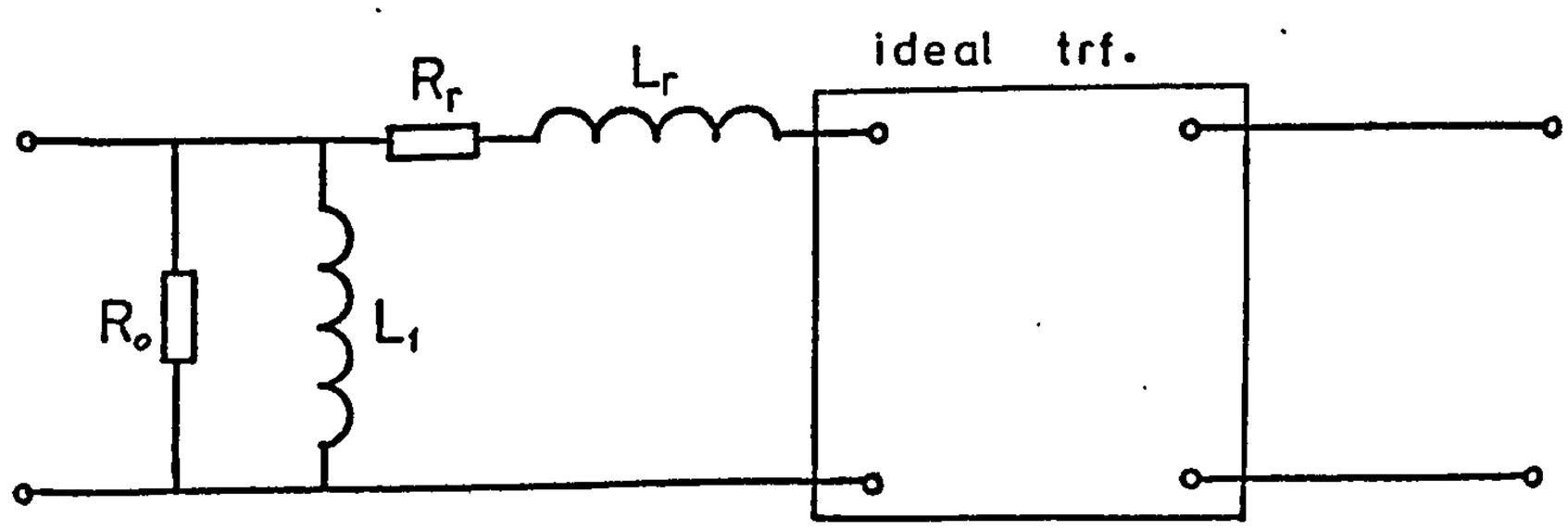

Figure 5.6 Equivalent Circuit as Figure 5.5 but with L_s and R_2 referred to the Primary Side.

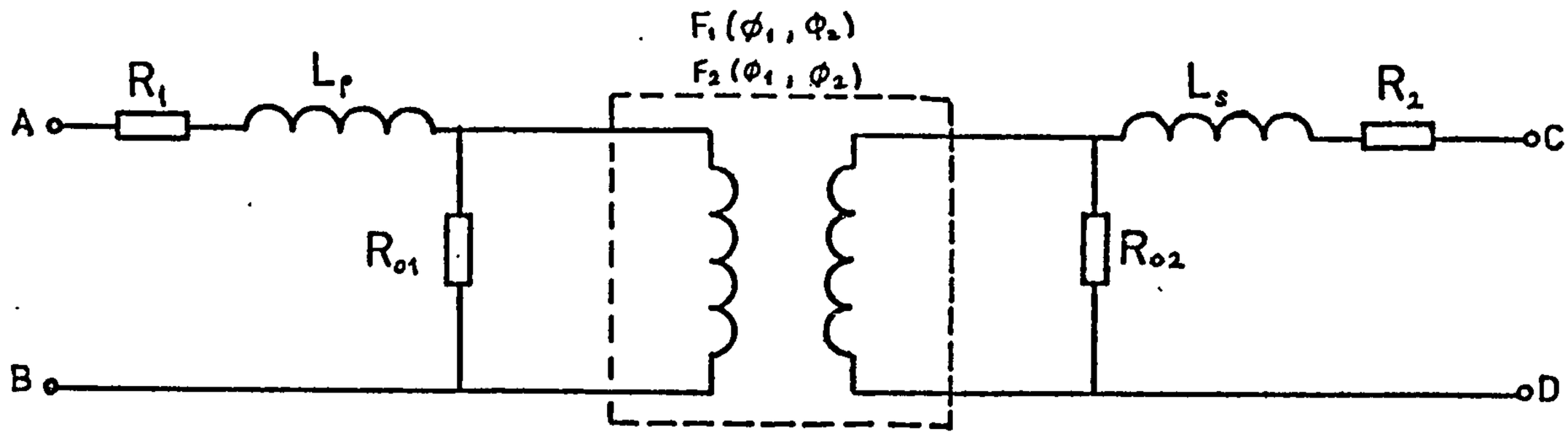

Figure 5.7 Equivalent Circuit for Two Parametrically Coupled Windings with Imperfections

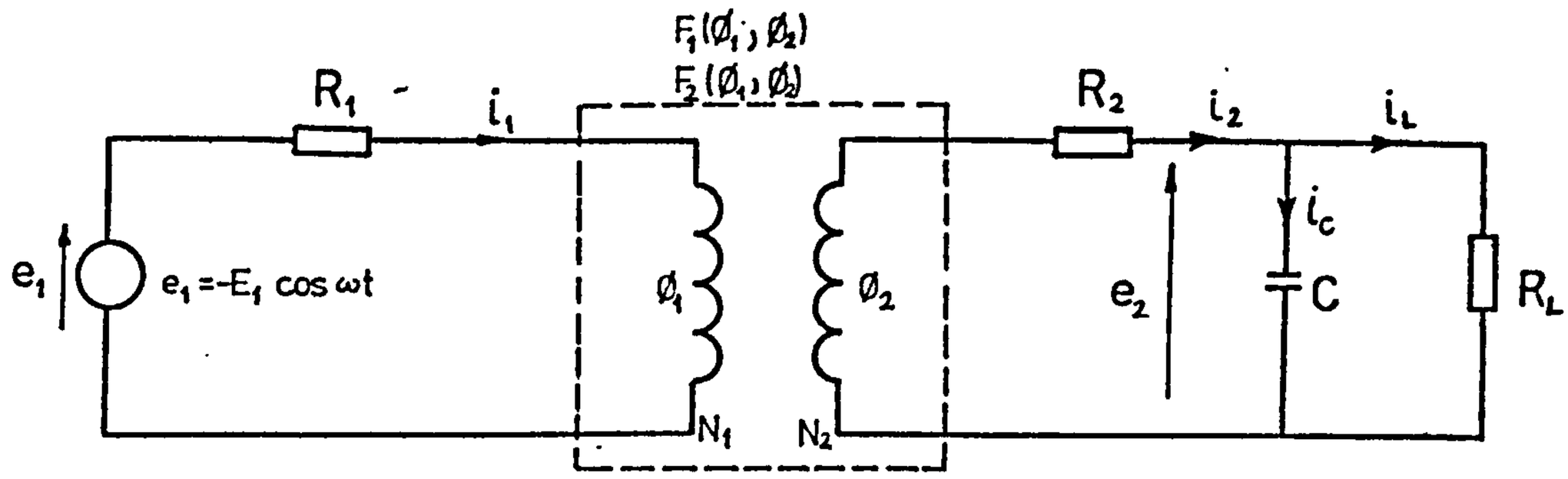

Figure 5.8 Equivalent Circuit for the Parametric Transformer with Winding Resistances and Resistive Load

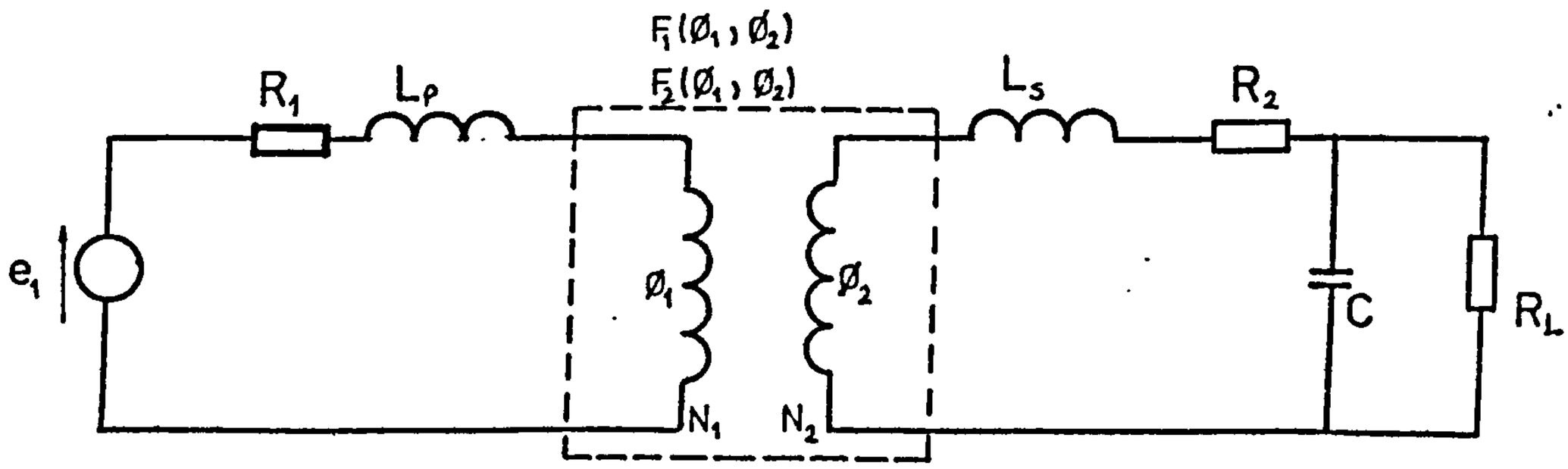

Figure 5.9 Equivalent Circuit for the Parametric Transformer with Winding Resistances, Leakage Inductances and Resistive Load

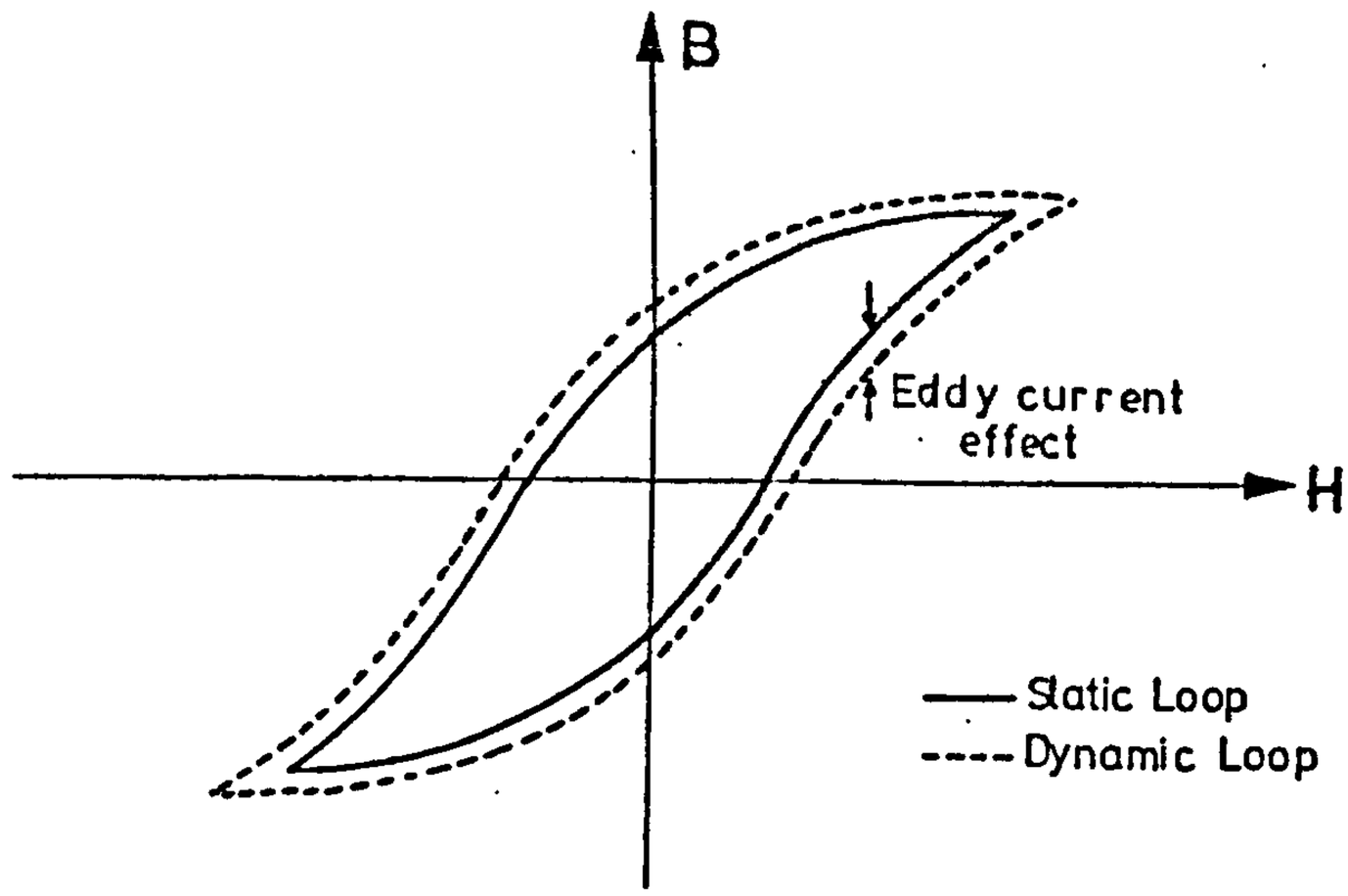

Figure 5.10 Static and Dynamic Hysteresis Loops

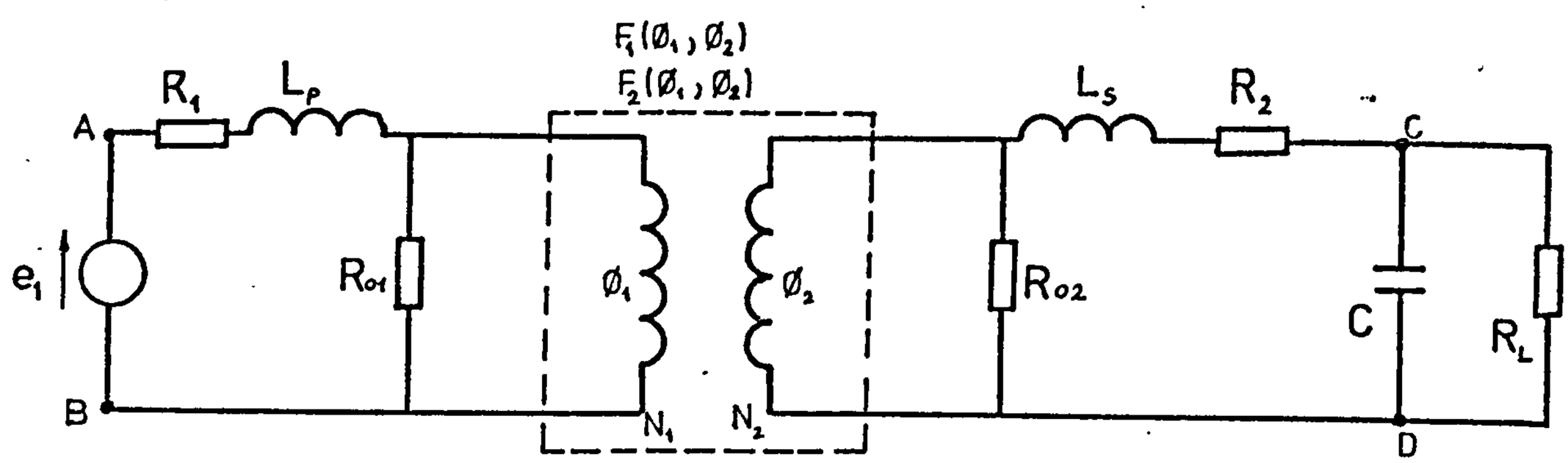

Figure 5.11 Equivalent Circuit for the Parametric Transformer with all the Imperfections and Resistive Load

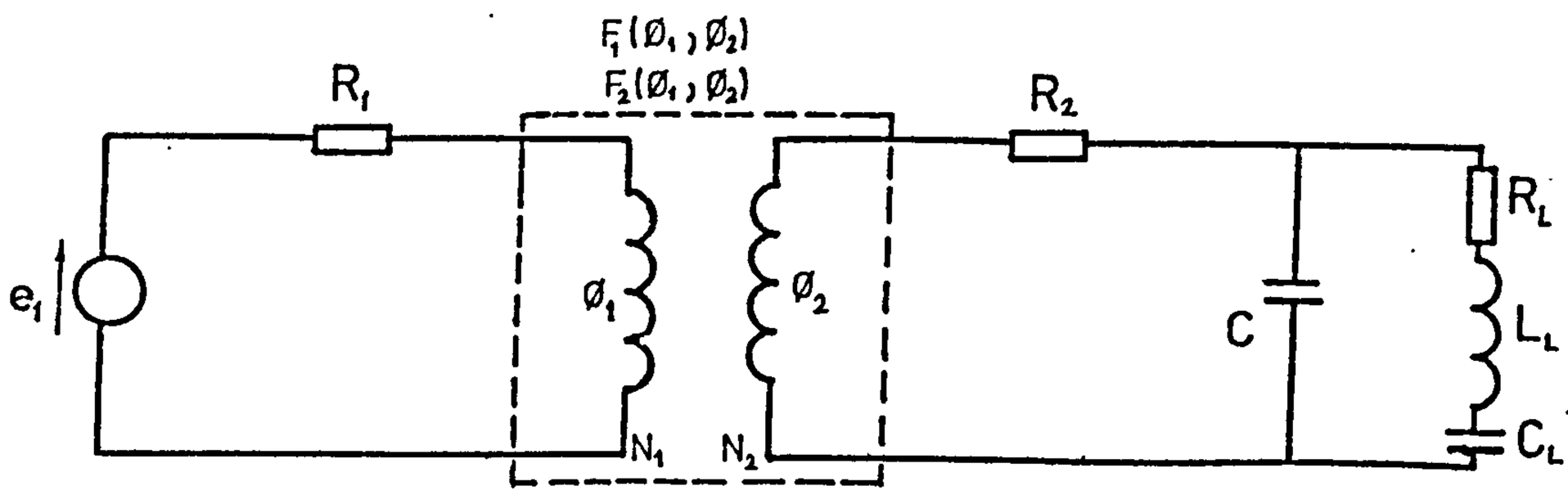

Figure 5.12 The Parametric Transformer with Series RLC-type Load.

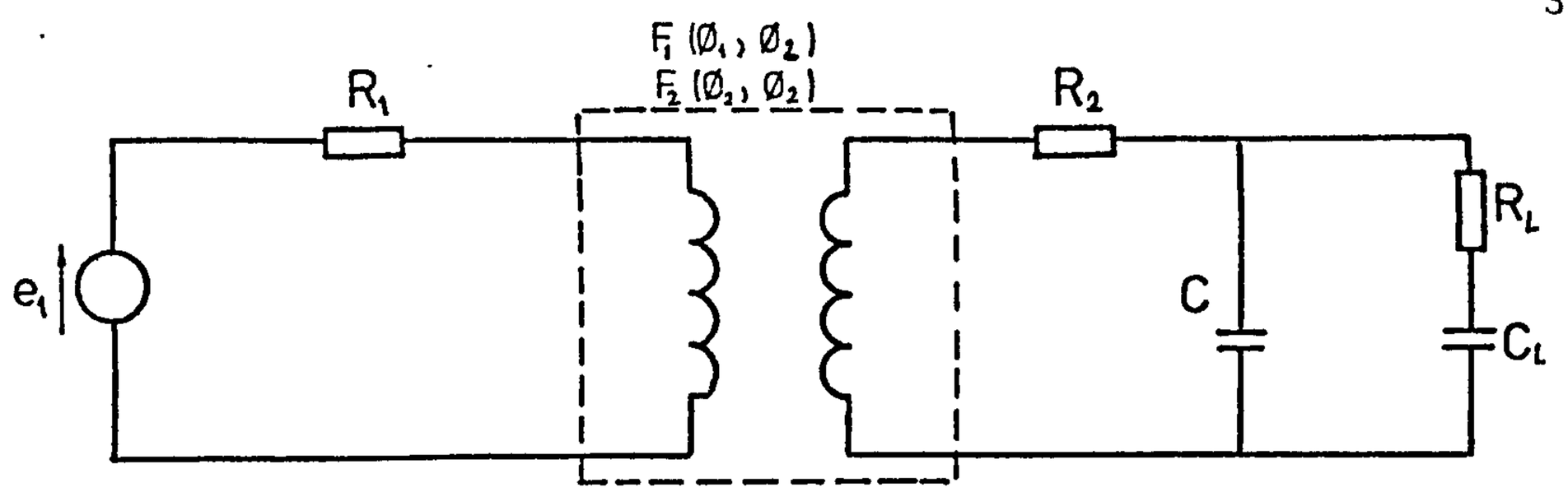

Figure 5.13 The Parametric Transformer with Series RC-type Load

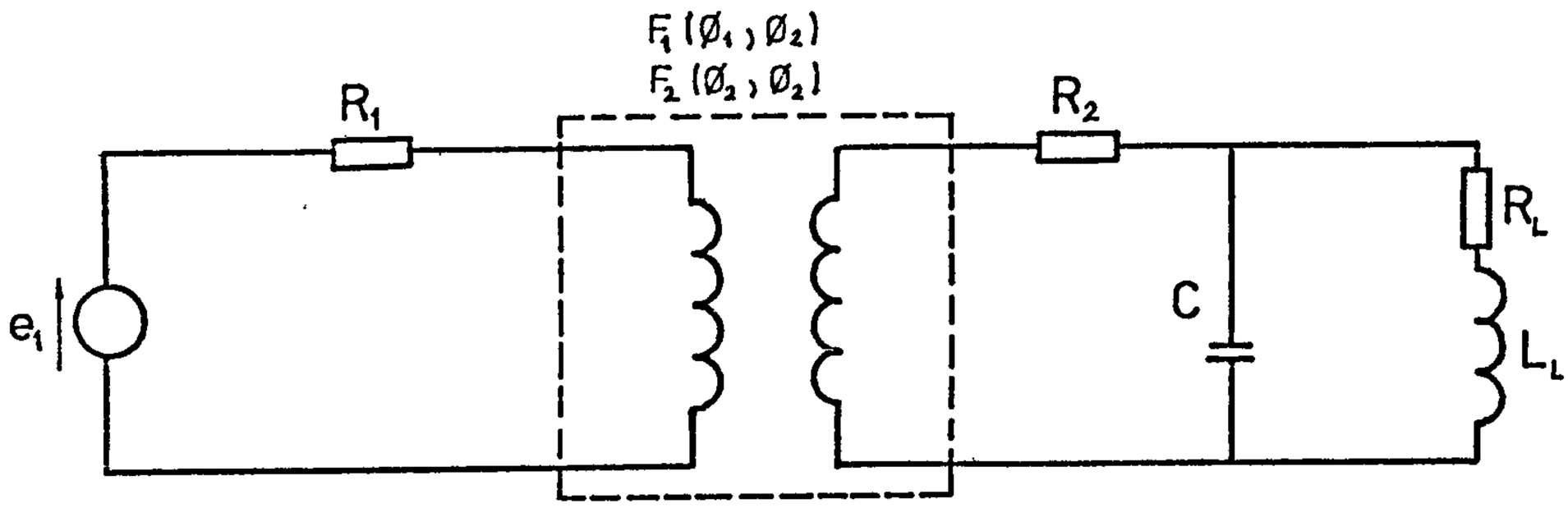

Figure 5.14 The Parametric Transformer with Series RL-type Load

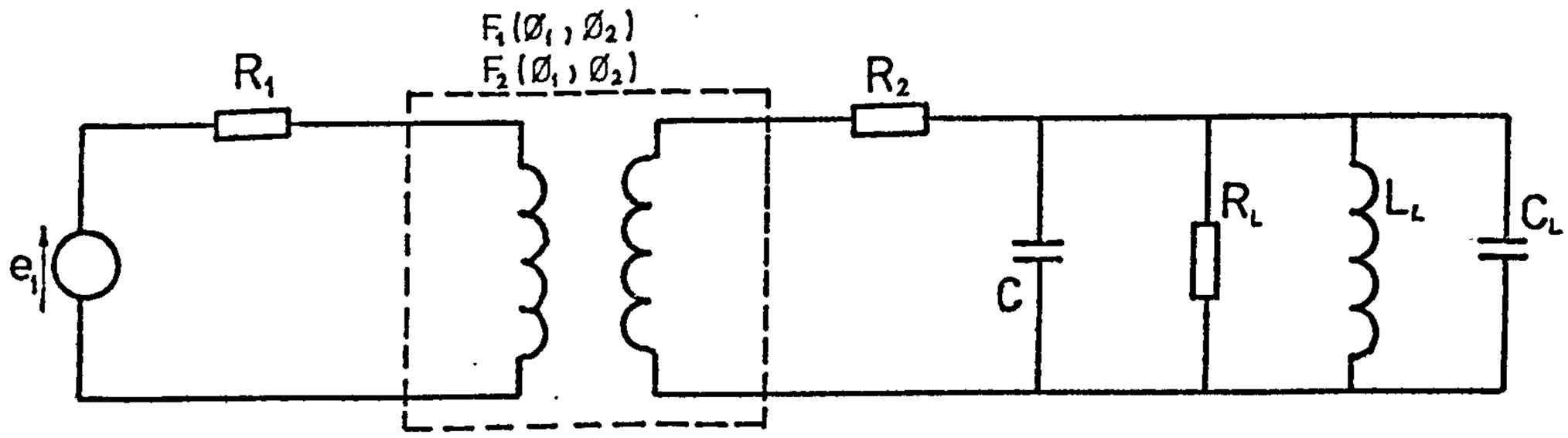

Figure 5.15 The Parametric Transformer with Parallel RLC-type Load

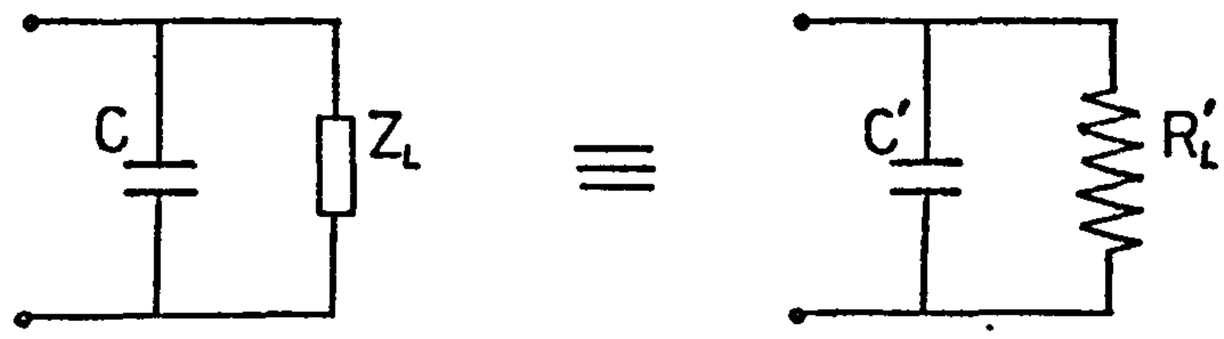

Figure 5.16 Combination of the Secondary Capacitor with a General Type Load, using the Concept of Complex Impedance

Coefficient multiplier

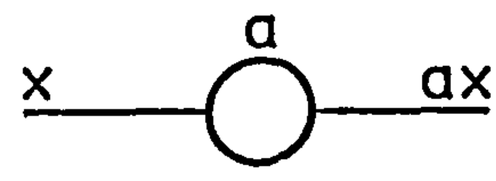

Sign changer

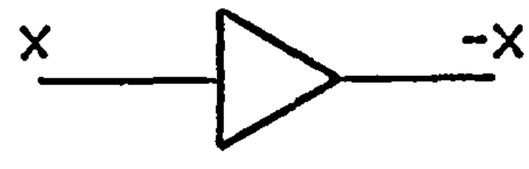

Summer

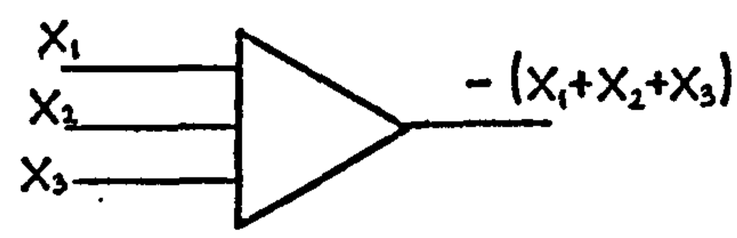

Integrator

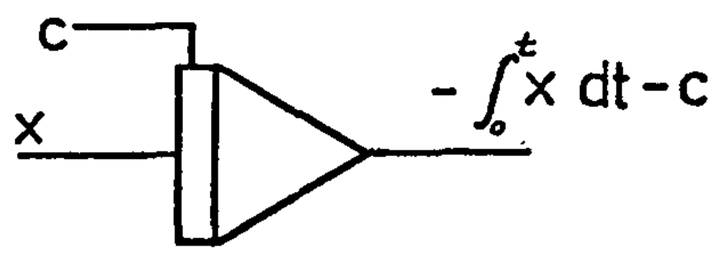

Differentiator

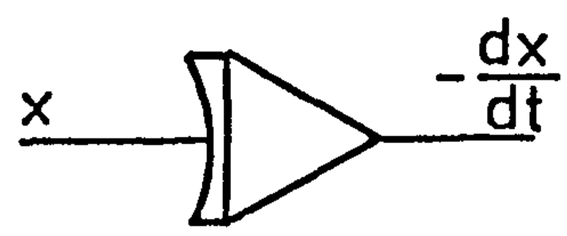

Function generator

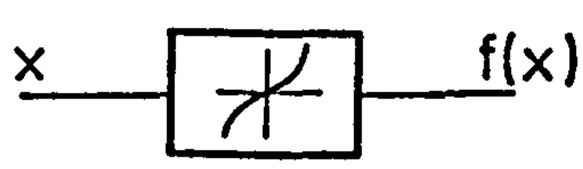

Multiplier

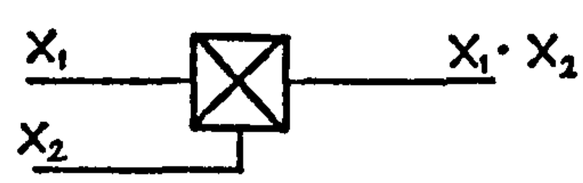

Divider

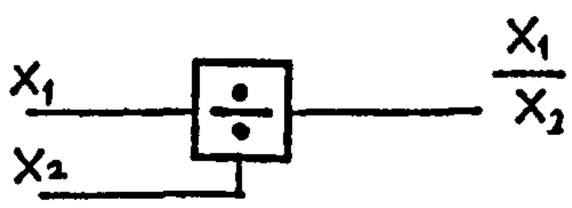

Quarter squares multiplier

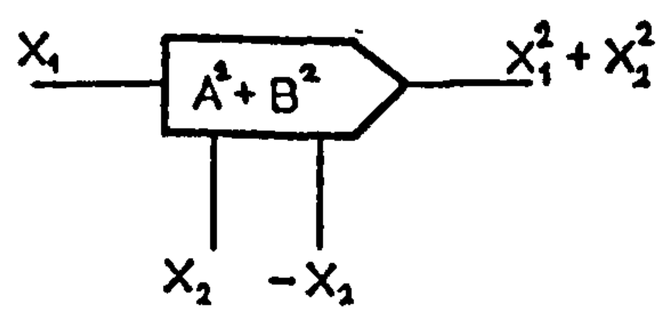

Figure 5.17 Symbols for the Computing Elements used in Analogue Simulation

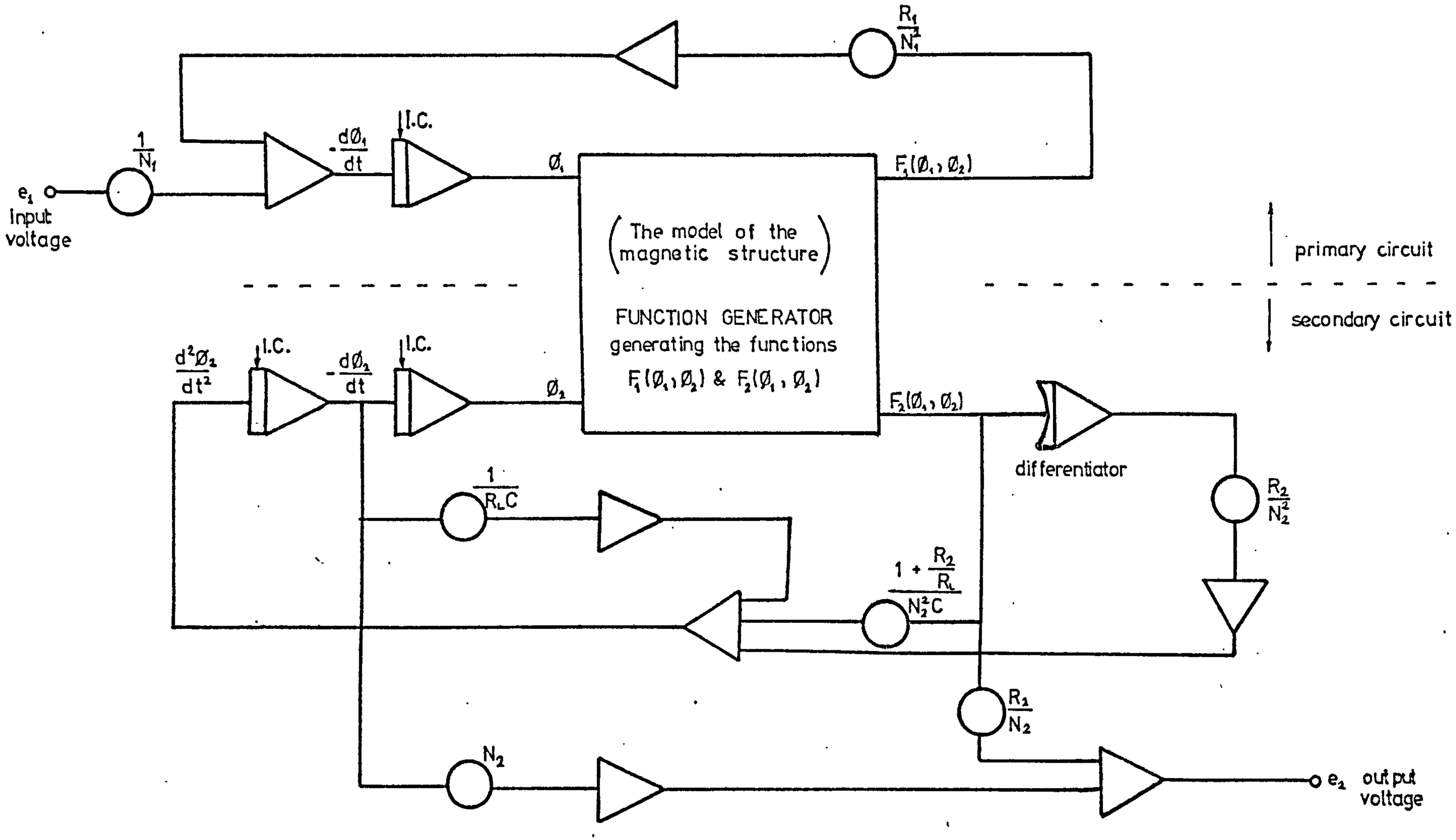

Figure 5.18 Analogue Computer Simulation of a Parametric Transformer

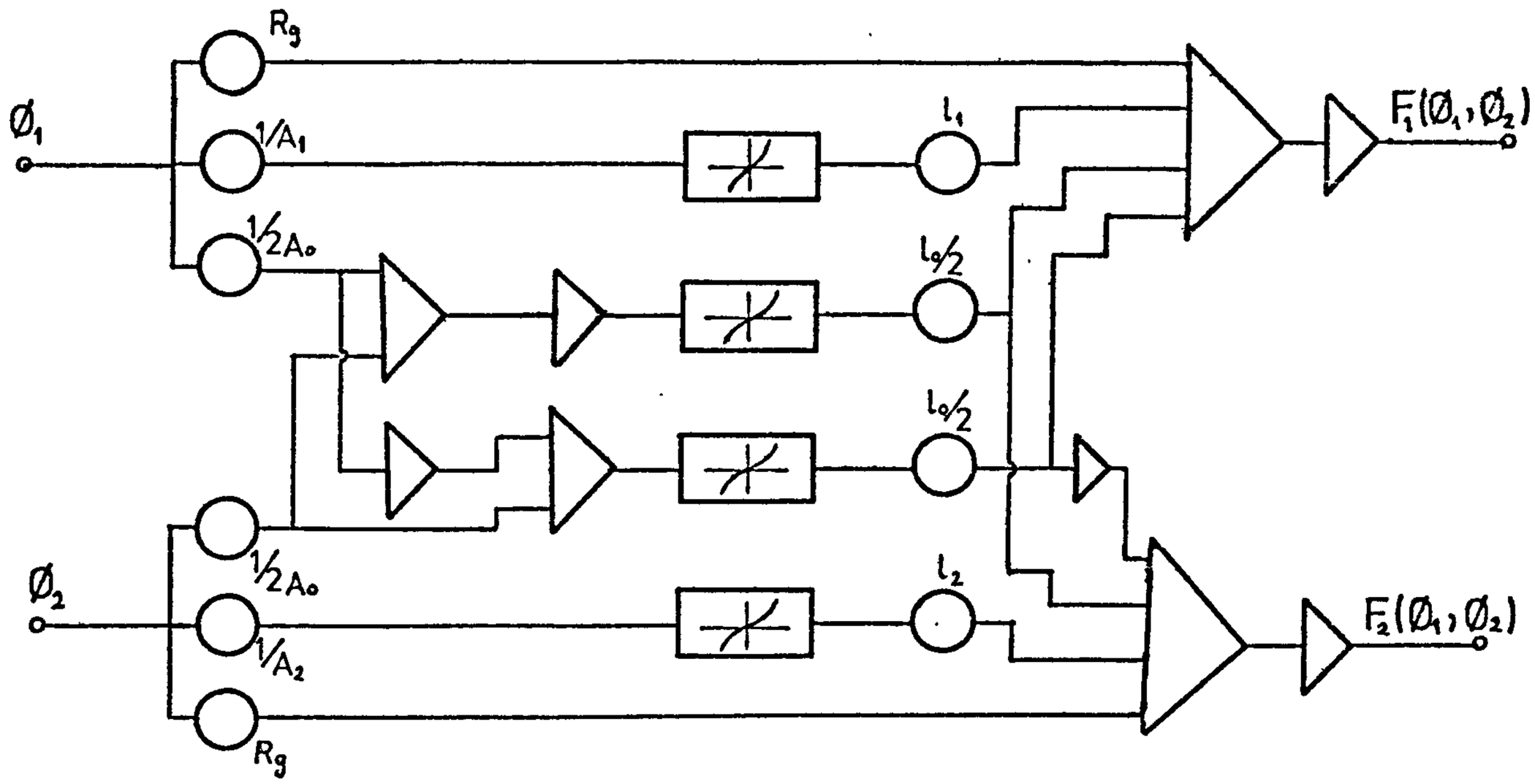

Figure 5.19 Analogue Simulation of the Magnetic Model for the Bridged Core Device or two-C-core Device

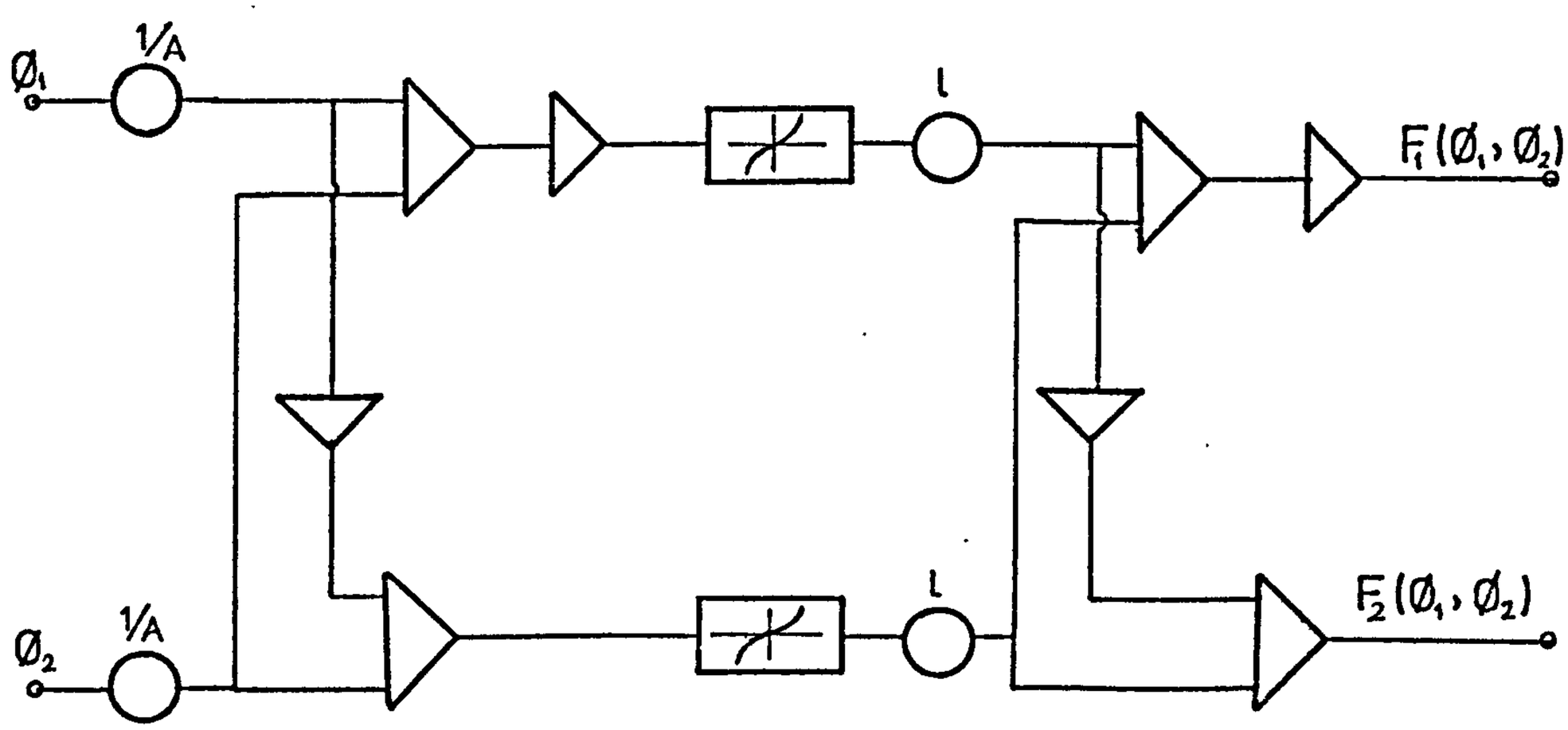

Figure 5.20 Simulation of the Magnetic Model for the Device of Figure 4.45.

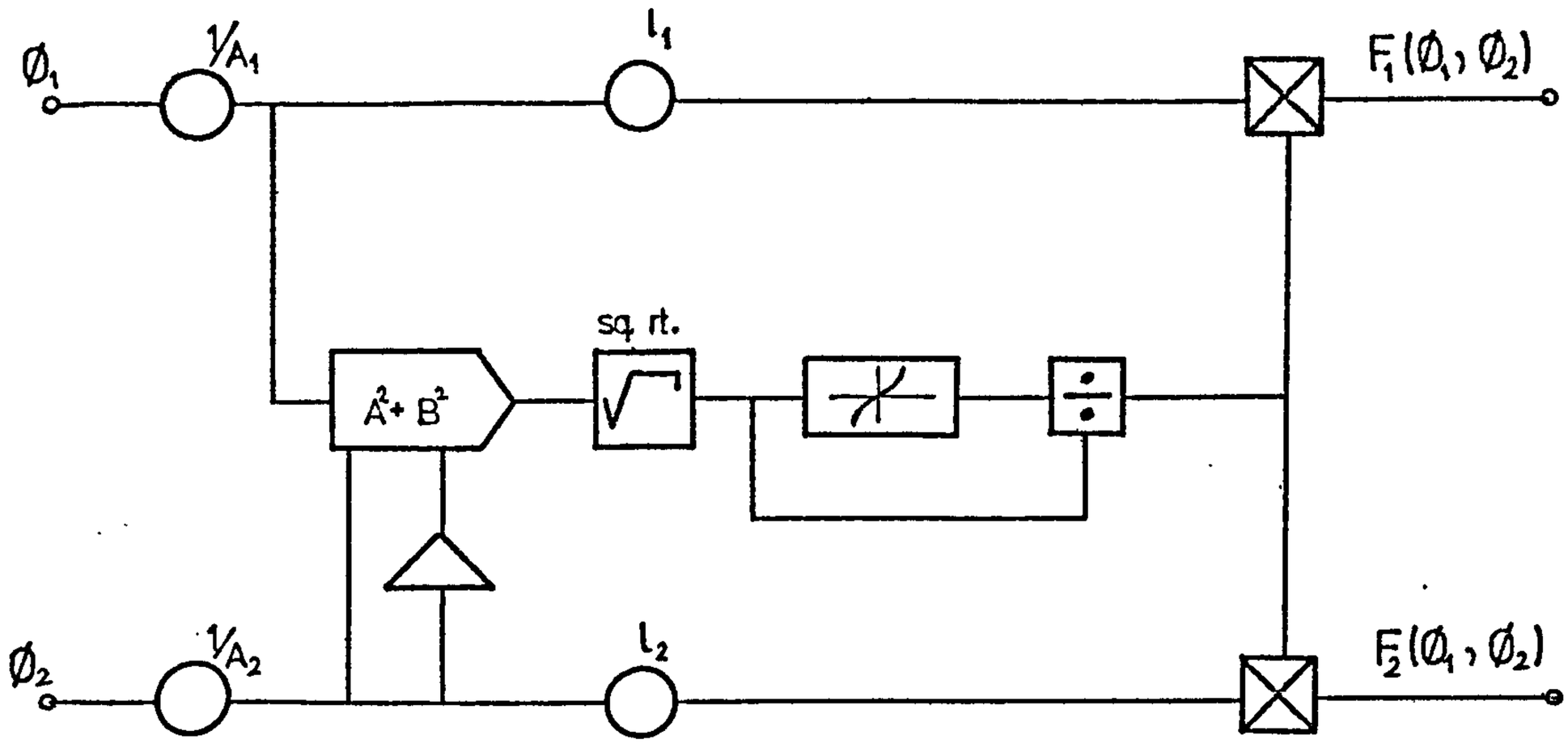

Figure 5.21 Simulation of the Magnetic Model for the Hollow Toroidal Core Device

CHAPTER VI

THE RELATIVE MAGNETISATION CURVES AND THE CURRENT WAVEFORMS

6.1 The Graphical Form of the $F_1(\phi_1, \phi_2)$ and $F_2(\phi_1, \phi_2)$ functions

When obtaining the functions $F_1(\phi_1, \phi_2)$ and $F_2(\phi_1, \phi_2)$ in Chapter IV, the only assumption made on the form of the magnetisation characteristic was that hysteresis could be neglected, so that $H = f(B)$ could be taken as a single-valued function. No restriction whatsoever was put on the degree of the non-linearity possessed by the magnetisation characteristic. It is therefore possible, once the magnetisation curve $(H = f(B))$ is given, as in Figure 6.1, graphically to construct the functions given by equations (4.45) and (4.46), for the bridgedmagnetic core including an air-gap.

The first two terms in equation (4.46) representing the secondary magnetic circuit are autonomous (non-parametric) and can be obtained by a simple linear scale conversion of the H/B curve. The linear term $R_g.\phi_2$ is a straight line in the F_2/ϕ_2 plane, with a slope $R_g = \frac{\ell_g}{\mu_o A_o}$. To obtain the term $\ell_2.f\left(\frac{\phi_2}{A_2}\right)$, the scale on the horizontal axis of Figure 6.1 is multiplied by the factor A_2, and the scale on the vertical axis by the factor ℓ_2. The curve resulting from

$$F_2' = F_2'(\phi_2) = R_g\,\phi_2 + \ell_2\, f\left(\frac{\phi_2}{A_2}\right) \quad \ldots\ldots \qquad (6.1)$$

is shown in Figure 6.2a, where the linear term $R_g\,\phi_2$ is shown by

the broken line.

The non-autonomous (parametric) term in equation (4.46) is the sum of two terms

$$F_2'' = \frac{1}{2}\,\ell_o.f\left(\frac{\phi_2}{2\,A_o} + \frac{\phi_1}{2\,A_o}\right) + \frac{1}{2}\,\ell_o.f\left(\frac{\phi_2}{2\,A_o} - \frac{\phi_1}{2\,A_o}\right) \qquad (6.2)$$

The curve for $\frac{1}{2}\,\ell_o.f\left(\frac{\phi_2}{2\,A_o}\right)$ may be obtained from Figure 6.1 in the same way as that outlined above, with multiplication factors for the horizontal and vertical axes of $2\,A_o$ and $\frac{1}{2}\,\ell_o$ respectively. However, the function $f\left(\frac{\phi_2}{2\,A_o} + \frac{\phi_1}{2\,A_o}\right)$ requires that, for a given ϕ_1, this curve, while retaining its shape, is shifted to the left by ϕ_1 in the F_2''/ϕ_2 plane. The curve representing the first term of equation (6.2) is thus given as the curve a in Figure 6.2b. Similarly the curve for the second term of equation (6.2) is given by the curve b in Figure 6.2b, shifted to the right by ϕ_1. The curve for the whole expression in equation (6.2) is then the sum of these two curves, that is the curve c in the same figure.

The curve of F_2/ϕ_2, for a given ϕ_1, for the secondary magnetic circuit of the bridged core is obtained by summing the curve in Figure 6.2a with the curve c in Figure 6.2b, i.e. at each point on the abcissae the corresponding ordinates are summed (e.g. $\overline{EF} = \overline{AB} + \overline{CD}$ in the figure). The resulting curve shown in Figure 6.2c is the graphical illustration of the function

$$F_2 = F_2(\phi_2)\Big|_{\phi_1=\phi_1} = F_2' + F_2'' = R_g\,\phi_2 + \ell_2\, f\left(\frac{\phi_2}{A_2}\right) + \frac{1}{2}\,\ell_0 \left[f\left(\frac{\phi_2+\phi_1}{2A_0}\right) + f\left(\frac{\phi_2-\phi_1}{2A_0}\right)\right] \quad \ldots\ldots \quad (6.3)$$

and demonstrates how F_2 varies with ϕ_2 for a given constant value of ϕ_1.

It is evident from Figure 6.2 that the parametric term in equation (6.3), illustrated by the curve c in Figure 6.2b, is overwhelmingly dominant over the non-parametric terms in determining the level of saturation (i.e. the value of ϕ_2 in Figure 6.2c for very rapidly increasing F_2). Around the origin, the slope of the linear portion of the F_2/ϕ_2 curve is not affected significantly by the variations in a small value of ϕ_1. However, if the given value of ϕ_1 is large, as is the case in the figure, the slope around the origin of the curve in Figure 6.2c, is much larger than when $\phi_1 = 0$. It is also noticeable that if the given value of ϕ_1 changes sign, the shifting curves a and b in Figure 6.2b interchange their places, although the resultant curve in Figure 6.2c remains the same.

By giving different but constant values to ϕ_1, a family of F_2/ϕ_2 curves can be obtained for the secondary magnetic circuit of the bridged core. Deriving such a family of curves establishes the graphical illustration, in the $F_2 - \phi_2$ plane, of the two-

variable function $F_2(\phi_2, \phi_1)$, in which ϕ_1 is considered a parameter rather than a variable. The family of curves obtained for different positive values of ϕ_1 with equal increments is shown in Figure 6.3, where equal increments in ϕ_1 are used to illustrate more precisely how the variation of F_2 depends on ϕ_1. A change in the sign but not the magnitude of ϕ_1 result in the same family of curves, because the change in the sign does not alter the nature of Figure 6.2b. It can, therefore, be stated that $F_2(\phi_1, \phi_2)$ is an odd function of ϕ_2 but an even function of ϕ_1.

Through the same graphical procedure outlined above, the primary magnetic circuit of the bridged core can be represented by equation (4.45), namely

$$F_1(\phi_1, \phi_2) = R_g \phi_1 + \ell_1 f\left(\frac{\phi_1}{A_1}\right) + \frac{1}{2} \ell_o \left[f\left(\frac{\phi_1 + \phi_2}{2 A_o}\right) + f\left(\frac{\phi_1 - \phi_2}{2 A_o}\right) \right] \qquad \ldots\ldots \quad (6.4)$$

and a family of curves similar to that in Figure 6.3 may be obtained in the $F_1 - \phi_1$ plane when ϕ_2 is considered a parameter. The graphical illustration of this two-variable function is given in Figure 6.4. In contrast to $F_2(\phi_1, \phi_2)$, it is clear that $F_1(\phi_1, \phi_2)$ is an odd function of ϕ_1 but an even function of ϕ_2.

An exact analytical representation of the bridged magnetic core as a saturable reactor is complete only when both Figures 6.3 and 6.4 are considered simultaneously, since the mathematical model

for a saturable reactor consists of a set of two simultaneous functions of two variables, as explained in Section 4.3.2. It is clear from the figures that the primary flux changes the characteristics of the secondary magnetic circuit, as well as the secondary flux affecting the primary magnetic circuit in a corresponding manner. Parametric coupling between the primary and secondary magnetic circuits therefore exists mutually, explaining both the even-harmonic generation and the controller action of the device.

The parallel-flux saturable reactor investigated in Section 4.5.1 may also be represented by two families of curves similar in form to Figures 6.3 and 6.4. As there are no autonomous terms in equations (4.61) and (4.62), and the whole of the expressions are parametric, the influence of ϕ_1 on the F_2/ϕ_2 characteristic, or of ϕ_2 on the F_1/ϕ_1 characteristic, is more direct than in the bridged magnetic core. In this way, the parametric coupling in the device of Figure 4.45 may be considered more effective than that in the bridged magnetic core.

A similar kind of graphical representation, although with only one family of curves, is used in the literature[1,2] to obtain the control characteristic of the dc-controlled saturable reactor, where the primary winding is assumed to be driven by a direct current source. These curves are shown in the first quadrant only in Figure 6.5a, with the derived F_2/F_1 (control) characteristic in Figure 6.5b. Obviously, the function of interest is $F_2(\phi_2, F_1)$, where F_1, the control ampere-turns, is taken as a parameter. No interest is shown to the function $\phi_1(F_1, \phi_2)$ (or $\phi_1(F_1, F_2)$) which

would represent the magnetic circuit associated with the control winding of a saturable reactor. However, in the case of the parametric transformer, the form of equation (4.23) must be used, and it is necessary to consider both of the families of curves in Figures 6.3 and 6.4.

6.1.1 Reluctance Modulation at Twice Frequency

When no primary flux exists in the bridged magnetic core, the secondary magnetisation is given by the outmost curve of Figure 6.3. From the slope of the linear portion of this curve around the origin, the minimum (initial) value of the secondary reluctance can be calculated, as given by equation (4.51). With the introduction of primary flux into the core, the initial reluctance of the secondary magnetic circuit increases. This is clearly illustrated in Figure 6.6a, where the initial portions of each curve of Figure 6.3 are shown by straight lines, the gradients of which give the secondary reluctance values for different values of ϕ_1. By carrying the corresponding values of R_{m2} and ϕ_1 into a new $R_{m2} - \phi_1$ plane, the variation of R_{m2} with ϕ_1 may be obtained from this figure, as in Figure 6.6b. The curve here is precisely the *trans-reluctance* characteristic of Figure 2.2, Chapter II, which was assumed on the basis of the qualitative discussions in Section 2.1.1. However, this characteristic has now been derived directly from the exact mathematical representation of the bridged magnetic core.

Since the gradients of the straight lines in Figure 6.6a, are proportional with the absolute value of the primary flux, the

other half of the trans-reluctance characteristic for $\phi_1 < 0$ is even symmetrical with that in Figure 6.6b. This leads immediately to the conclusion of Section 2.1.1, that if ϕ_1 varies sinusoidally with a frequency f, the variation in R_{m2} is of twice this frequency, or 2f.

The fact that the secondary flux ϕ_2 also modulates the primary reluctance R_{m1} is evident from Figure 6.4, where the gradient of the portion of each curve near the origin is dependent on ϕ_2. Following the same procedure as above, a trans-reluctance characteristic exhibiting how R_{m1} varies with ϕ_2 may be obtained in the R_{m1} - ϕ_2 plane, as shown in Figure 6.7. Like the curve in Figure 6.6b, this trans-reluctance curve is even symmetrical, justifying the assumption of a double-frequency modulation of the primary reluctance by a sinusoidally-varying secondary flux, made in Section 3.1.5.

The trans-reluctance characteristics of Figures 6.6b and 6.7 are only valid when ϕ_1 and ϕ_2 are zero or of small magnitude, since R_{m1} and R_{m2} are functions of both ϕ_1 and ϕ_2. A complete graphical illustration of the functions $R_{m1}(\phi_1, \phi_2)$ and $R_{m2}(\phi_1, \phi_2)$ must, therefore, be given by the families of curves shown in Figures 6.8 and 6.9, respectively. From these figures, it can be stated that both $R_{m1}(\phi_1, \phi_2)$ and $R_{m2}(\phi_1, \phi_2)$ are even functions of both ϕ_1 and ϕ_2, and further that the values R_{m1min} and R_{m2min} used in Chapters III and IV are the (minimum) values of the primary and the secondary reactances when both ϕ_1 and ϕ_2 equal zero. The variations of $R_{m1}(\phi_1, \phi_2)$ and $R_{m2}(\phi_1, \phi_2)$ can be precisely derived, though laboriously, from Figures 6.3 and 6.4, which together provide the exact representation of the bridged-magnetic-core saturable reactor device.

6.2 The Relative Magnetisation Curve

Since they provide an exact representation, Figures 6.3 and 6.4 can fully explain the operation of the bridged magnetic core device as a saturable reactor. For the sake of convenience, only the first quadrants of these figures are re-drawn in Figures 6.10 and 6.11, where the variables of the vertical and horizontal axes are interchanged. Suppose, initially, that the resistanceless secondary winding is driven by an alternating voltage source, creating the alternating flux shown in Figure 6.11. If the primary winding is not energized, $\phi_1 = 0$, and the magnetisation characteristic for the secondary magnetic circuit is the outmost curve in the figure. The current flowing through the secondary winding is thus that shown by the intermittent curve. Suppose now that a constant level of primary flux is somehow introduced into the core, so that the *relative* magnetisation characteristic of the secondary magnetic circuit becomes the thick curve, shown amongst the family of curves, corresponding to this constant value of the primary flux. On introduction of the primary flux, the secondary current immediately switches to the saturated waveform shown in the figure, showing that the amplitude of the alternating current in the secondary winding is controlled by the level of the primary flux in the core.

It is not physically practicable to generate a constant flux in a magnetic core by a voltage source, and therefore the control winding of a saturable reactor is generally driven by a direct current source, producing a constant level of mmf in the

core. The portions of the curves in Figure 6.10 near the origin are redrawn in Figure 6.12, where the constant level of primary flux created by the direct current source when $\phi_2 = 0$ is shown by the broken line. As the sinusoidally varying secondary flux increases from zero to its maximum value, the magnetisation characteristic of the primary circuit moves from the left most line to the right most line. During the next quarter period of ϕ_2, the primary magnetisation characteristic moves back to its original position, where it arrives when ϕ_2 becomes zero. In accordance with this movement of the primary magnetisation characteristic, the primary flux level in the core varies as shown in the figure. It is clear, therefore, that a twice-frequency alternating voltage appears across the primary winding when the secondary winding is driven by an alternating source, despite the fact that the primary winding is fed by a direct current source.

In many magnetic amplifier arrangements, a portion of the alternating load current, after full rectification, is fed back to the control circuit, in order to aid the direct control current. The feedback current has to be rectified to create an mmf in the same direction as the direct control current. Most magnetic amplifiers employing feedback techniques in this sense are based on the saturable reactor device of Figure 4.45, in which all the windings on one core are completely coupled. However, for a saturable reactor device such as the bridged magnetic core, in which mutual flux coupling is eliminated by method 3b of Section 4.1.2, there is also the possibility of using unrectified alter-

nating current as part of or the whole of the control current. In power control applications, it is inefficient to use an alternating source on the control circuit, because of the high alternating power required to achieve the same controlling action. Nevertheless, it is possible for saturable reactors with complete elimination of mutual flux coupling to have the control winding driven by an alternating supply of the same (synchronous) frequency as that used for the load circuit.

It is therefore interesting to investigate the use of alternating current in the primary winding of the two-C-core saturable reactor device to achieve control of the alternating current in the secondary winding, although this achievement is at the expense of high power consumption in the primary circuit.

6.2.1 Relative Magnetisation Characteristics with Both Windings Driven by Synchronous Sources

Suppose that the resistanceless windings on the core of the bridged magnetic device are driven by synchronous alternating voltage sources of moderate amplitudes. When only the secondary winding is driven, the magnetisation characteristic for the secondary magnetic circuit is the curve numbered 1 in Figure 6.13, where the half cycle of the secondary flux created by the voltage source is also shown. To find the alternating current in the secondary winding, each point on the secondary flux waveform is projected onto this curve (e.g. from point D, point D' is found), and the corresponding mmf values are transferred onto the F_2 - time plane (e.g. point D" is obtained from point D'). The secondary

current waveform is thus obtained as shown by the dotted curve in the figure. Clearly, the secondary current is of small amplitude, since ϕ_{2m} is below the saturation level.

However, when a sinusoidally varying primary flux is also present in the core, the secondary magnetisation characteristic moves so that each time it takes one of the curves among the family, depending on the value of the primary flux present at that particular instant. Suppose, that, at the instants z_1, z_2 and z_3 (when the secondary flux has the values at the points A B and C), the primary flux takes values such that the function $F_2(\phi_1, \phi_2)$ is expressed by the curves numbered 2, 3 and 4, respectively. (The corresponding primary flux values are shown by points E, F and G in Figure 6.14; the appearance of ϕ_{2m} and ϕ_{1m} as equal in Figures 6.13 and 6.14 is just coincidental).
At $z = \frac{\pi}{2}$, $\phi_2 = \phi_{2m}$ and also $\phi_1 = \phi_{1m}$ since the voltage sources driving the primary and the secondary windings are synchronous. At this instant, the secondary magnetisation characteristic becomes the curve numbered 5, and it can move no further down from this final position. Because of this movement of the secondary magnetisation characteristic, point A on the secondary flux waveform has to be projected onto curve number 2, point B onto curve number 3, point C onto curve number 4, and finally point D onto curve number 5. The corresponding mmf values at points a, b, c and d are then carried over to the F_2 - z plane, and the secondary current waveform is obtained as shown in the figure. From $z = \frac{\pi}{2}$ to $z = \pi$, when both ϕ_2 and ϕ_1 are decreasing, the secondary magnetisation characteristic moves upwards, taking curves numbered

5, 4, 3, 2 and 1, in reverse order, with the projected point again passing through the same points d, c, b, a and O. During the next (negative) half cycle of the secondary flux, the same process is repeated, but in the third quadrant of the $\phi_2 - F_2$ plane. Evidently, the secondary current is now very high and distorted because of the saturation effect brought into action by the primary flux.

At these operational conditions for a given ϕ_{1m} and ϕ_{2m}, the magnetic performance of the secondary circuit is determined completely by the imaginary curve passing through the points O, a, b, c and d in Figure 6.13. This curve is defined as the *relative* magnetisation characteristic of the secondary circuit, and is unique for given amplitudes of the primary and secondary fluxes. For each set of ϕ_{1m} and ϕ_{2m}, a different relative magnetisation characteristic is obtained, whence the magnetic performance of the secondary circuit can be fully determined and the secondary current waveform immediately and easily established.

The analytic equivalent of the concept of relative magnetisation characteristic is as follows. The primary and secondary fluxes, as determined by the voltage sources, are given by the time functions

$$\phi_1 = \phi_1(z) = \phi_{1m} . \sin z \qquad \ldots\ldots \qquad (6.5)$$

$$\phi_2 = \phi_2(z) = \phi_{2m} . \sin z \qquad \ldots\ldots \qquad (6.6)$$

and the family of secondary magnetisation curves, when drawn in the manner of Figures 6.11 and 6.13, is expressed by the function

$$\phi_2 = \phi_2(F_2, \phi_1) \qquad \ldots\ldots \qquad (6.7)$$

When equation (6.5) is substituted for ϕ_1 in the function above, this becomes

$$\phi_2 = \phi_2(F_2, z, \phi_{1m}) \qquad \ldots\ldots \qquad (6.8)$$

Now, the variable z can be eliminated between equations (6.6) and (6.8), leaving

$$\phi_2 = \phi_2(F_2, \phi_{1m}, \phi_{2m}) \qquad \ldots\ldots \qquad (6.9)$$

For given constant values of ϕ_{1m} and ϕ_{2m}, equation (6.9) reduces to the function of one variable

$$\phi_2 = \phi_2(F_2) \qquad \ldots\ldots \qquad (6.10)$$

which gives a direct relationship between the secondary flux and the secondary mmf. This function, although valid only for a given set of values of ϕ_{1m} and ϕ_{2m}, is useful as it gives a direct insight into the magnetic operation of the system, which is otherwise quite complex to investigate because of the time-varying property of all the fluxes, mmf's and reluctances in the system.

When derived graphically, the function represents what has been defined previously as the *relative* magnetisation characteristic of the secondary circuit.

Following the same procedure, through the movement of the primary magnetisation characteristics in accordance with the variation of the secondary flux, the relative magnetisation characteristic for the primary circuit can be obtained as shown in Figure 6.14. The primary relative magnetisation characteristic is the curve passing through the points 0, e, f, g and h, and it is only valid for the given values of the primary and secondary flux amplitudes. The waveforms of the primary current when ϕ_2 is non-existent and when an alternating ϕ_2 exists in the core are also derived in the same manner and shown in the figure. The relative magnetisation characteristic is given now by the function $\phi_1 = \phi_1(F_1)$, obtainable in the same way as followed from equation (6.5) to (6.10). Once this relative characteristic is drawn, it is very easy to produce the primary current waveform from the given primary flux variation.

6.3 The Relative Magnetisation Characteristics and the Current Waveforms of the Parametric Transformer

With resistanceless windings and at no-load operation, the primary and secondary fluxes of the parametric transformer, are given by

$$\phi_1 = \phi_{1m} \sin z \qquad \ldots\ldots \qquad (6.11)$$

$$\phi_2 \simeq \phi_{2m} \cos z \qquad \ldots\ldots \qquad (6.12)$$

when the primary winding is driven by an alternating voltage source of $e_1 = -E \cos z$. The variation of ϕ_2 is phase-locked with ϕ_1 at the same frequency, and the phase difference between ϕ_1 and ϕ_2 is exactly $\frac{\pi}{2}$. Furthermore, ϕ_2 is considered a very good sinusoidal, as explained in Section 3.6.2. The relationship between ϕ_{1m} and ϕ_{2m} is given approximately by Figure 3.34 or by equation (3.203), i.e. by

$$\phi_{2m}^{2} = \frac{1}{A^2} (\phi_s^2 - \phi_{1m}^{2}) \qquad \ldots\ldots \qquad (6.13)$$

where ϕ_s is the same as ϕ''_{1m} given by equation (3.202), and $A^2 = \frac{s_3 + r_3}{s_3}$.

Under these conditions, operation of the parameteric transformer may be simulated by the bridged magnetic core device whose primary winding is driven by the same voltage source $e_1 = -E_1 \cos z$ but with the secondary winding connected, instead of to a capacitor, to an alternating voltage source $e_2 = -E_2 \sin z \; (= N_2 \frac{d\phi_2}{dz})$ where E_2 is such that the secondary flux amplitude ϕ_{2m} created by it always complies with equation (6.13).

Since ϕ_{2m} is a function of ϕ_{1m} in parametric transformer operation, the relative magnetisation characteristic of the secondary circuit, as given by equation (6.9), needs only ϕ_{1m} to be specified. Therefore, for each value of the primary voltage amplitude E_2, there is a unique relative magnetisation characteristic for the secondary circuit.

The relative magnetisation curve of the secondary circuit can be obtained by the same procedure as followed for Figure 6.13. However, the $\frac{\pi}{2}$ phase difference between ϕ_1 and ϕ_2 brings about a substantial change in the shape of the resulting relative magnetisation curve. At $z = 0$, $\phi_2 = \phi_{2m}$ but $\phi_1 = 0$, as shown in Figures 6.15 and 6.16. Therefore point A on the secondary flux waveform in Figure 6.15 has to be projected onto the curve number 1, corresponding to $\phi_1 = 0$. As ϕ_1 increases from zero, points B, C and D on the secondary flux waveform are in turn projected onto the magnetisation curves 2, 3 and 4, respectively, yielding the points b, c and d. At $z = \frac{\pi}{2}$, $\phi_2 = 0$, but $\phi_1 = \phi_{1m}$, and the corresponding magnetisation curve is curve number 5, which determines the point O. The curve passing through the points a, b, c, d and O in Figure 6.15 is thus the secondary relative magnetisation characteristic corresponding to the present values of ϕ_{1m} and ϕ_{2m} (or rather of ϕ_{1m} only, as ϕ_{2m} is determined by ϕ_{1m}). During the next quarter period from $z = \frac{\pi}{2}$ to $z = \pi$, in accordance with the variations of ϕ_1 and ϕ_2, the other half of the secondary relative magnetisation characteristic, which is odd symmetrical to that shown in the figure, is traced similarly in the third quadrant of the ϕ_2/F_2 plane.

The resulting mmf waveform is also shown in Figure 6.15. Because of the unusual, convex shape of the relative magnetisation characteristic, the secondary current has a distorted waveform containing a large harmonic content.

The primary relative magnetisation characteristic is derived similarly in Figure 6.16, where it should be noted that ϕ_{1m} is greater than ϕ_{2m}. Mainly because of this, and through the corresponding movement of the magnetisation curve within the family of curves, the primary relative magnetisation characteristic takes the shape shown. The primary current waveform is also determined in the figure.

If the primary and secondary fluxes are in the same phase, it can be deduced that, with the large amplitudes ϕ_{1m} and ϕ_{2m} in Figures 6.15 and 6.16, the resulting primary and secondary currents become almost infinitely high.

In conclusion, a unique pair of relative magnetisation characteristics (primary and secondary), valid only for one given value of ϕ_{1m} (or the input voltage amplitude), determines the primary and secondary current waveforms under that operating condition. If the amplitude of the input voltage is altered, the shapes of the primary and secondary relative magnetisation characteristics change accordingly, and the waveforms of the primary and secondary currents also change, taking different forms at different values of E_1.

As can be noted from Figure 6.15, the secondary relative magnetisation characteristic starts from point 0 and ends at a point on the magnetisation curve number 1 which corresponds to $\phi_1 = 0$ and is fixed at all times. This is also true for the primary relative magnetisation characteristic, one of the end

points of which is the origin of the $F_1 - \phi_1$ plane while the other lies on the fixed magnetisation curve corresponding to $\phi_2 = 0$.

Equation (6.13) and Figure 3.34 show that if ϕ_{1m} is increased, the amplitude of the parametrically excited and maintained secondary flux oscillations decreases. Taking this relationship between ϕ_{1m} and ϕ_{2m} into account, different shapes of the secondary and the primary relative magnetisation characteristics are shown in Figures 6.17a and 6.17b, respectively, for different values of ϕ_{1m}. (The curves with the same number correspond to the same value of ϕ_{1m}). From the curves in Figure 6.17, the primary and secondary current waveforms during operation with any given amplitude of input voltage can be determined. As ϕ_{1m} is increased, the pair of relative magnetisation characteristics undergoes a change in shape, becoming successively the pair of curves numbered 1, 2, 3, 4 and 5. At a certain value of ϕ_{1m}, the primary relative magnetisation characteristic becomes an almost straight line (curve number 4 in Figure 6.17b), when the primary and secondary current waveforms are as shown in Figure 6.18a. At a smaller value of ϕ_{1m} (which yields a higher ϕ_{2m}), the secondary relative magnetisation characteristic becomes almost linear (curve number 2 in Figure 6.17a), when the corresponding current waveforms are as shown in Figure 6.18b.

The concept of a relative magnetisation characteristic is very helpful in explaining the magnetic operation and in determining the current waveforms of the device, although in practice, the situation is more complex than has been indicated. Firstly,

the secondary flux is created intrinsically by parametric excitation within the secondary circuit itself, and is not produced by an external voltage source. With the simulation of the secondary voltage of the parametric transformer by an external voltage source, only the amplitude of the secondary flux was assumed to be dependent on ϕ_{1m}. In fact, the waveform of the secondary flux also varies with the changes in the primary flux amplitude, and especially near the extremes of the operating range, the non-sinusoidal waveform of the secondary flux directly affects the shape of the relative magnetisation characteristics of both the primary and the secondary circuits. Secondly, the B/H characteristic of the core material was assumed to be a single-valued function. In fact, because of the existence of hysteresis, different branches of the B/H loops are followed, depending on whether the flux density is increasing or decreasing. Apart from influencing the shape of the relative magnetisation characteristics, hysteresis means that these are not unique at all times, (i.e. the variable z cannot be eliminated between equations (6.6) and (6.8)).

6.3.1 The Primary and the Secondary Current Waveforms

The variations of the primary and the secondary current waveforms can be derived from the $F_1(\phi_1, \phi_2)$ and $F_2(\phi_1, \phi_2)$ functions, if the secondary voltage is simulated by the correct external voltage source (i.e. the secondary flux is assumed always sinusoidal but with an amplitude dependent on ϕ_{1m}).

The secondary mmf, as given by equation (4.46), is

$$F_2(\phi_1, \phi_2) = R_g \phi_2 + \ell_2 f(\frac{\phi_2}{A_2}) + \frac{\ell_o}{2} [f(\frac{\phi_1 + \phi_2}{2 A_o}) + f(\frac{\phi_2 - \phi_1}{2 A_o})] \qquad \ldots\ldots \quad (6.14)$$

The B/H curve can be most simply expressed by

$$H = f(B) = c_1 B + c_3 B^3 \qquad \ldots\ldots \quad (6.15)$$

and using this function in equation (6.14) gives

$$F_2(\phi_1, \phi_2) = R_{m2min} \frac{1}{2} [(\phi_1 + \phi_2) + (\phi_2 - \phi_1)] + \frac{r_3}{2} [(\phi_1 + \phi_2)^3 + (\phi_2 - \phi_1)^3] + s_3 \phi_2^{\,3} \qquad \ldots\ldots \quad (6.16)$$

where $R_{m2min} = R_g + s_1 + r_1$

$$s_1 = c_1 \frac{\ell_2}{A_2}$$

$$r_1 = c_1 \frac{\ell_o}{(2 A_o)} \qquad \ldots\ldots \quad (6.17)$$

$$s_3 = c_3 \frac{\ell_2}{A_2^{\,3}}$$

and $r_3 = c_3 \dfrac{\ell_o}{(2 A_o)^3}$

From equations (6.11) and (6.12), it follows that

$$\phi_1 + \phi_2 = (\phi_{1m}^2 + \phi_{2m}^2)^{\frac{1}{2}} \cos (z - \alpha)$$

$$\phi_2 - \phi_1 = (\phi_{1m}^2 + \phi_{2m}^2)^{\frac{1}{2}} \cos (z + \alpha) \qquad \ldots\ldots \qquad (6.18)$$

where $$\alpha = \tan^{-1} \frac{\phi_{1m}}{\phi_{2m}} \qquad \ldots\ldots \qquad (6.19)$$

Before substituting equations (6.18) into equation (6.16), it should be noted that $s_3 \ll r_3$ ($s_3 \approx \frac{1}{8} r_3$, since $A_2 \approx 2.$ ($2 A_o$) in the bridged magnetic core equivalent of the two-C-core device). Although at the expense of a slight error, $s_3 \phi_2^3$ in equation (6.16) may therefore be neglected in comparison to the second term of that equation.* Since $s_3 \ll r_3$, A in equation (6.13) can be taken as unity

---

* This corresponds to neglecting the autonomous saturation effects in the branch of the bridged magnetic core where only ϕ_2 is present. Actually, the bridge-branches of the equivalent magnetic structure are driven into saturation much earlier than the main branches. In the saturable reactor of Figure 4.45, whose $F_2(\phi_1, \phi_2)$ function consists only of a single non-autonomous term, no problem of this kind arises. This is because flux interaction takes place in the whole of the cores in the latter device, but in a part of the core in the first.

which results in the circular relationship between ϕ_{1m} and ϕ_{2m}

$$\phi_{1m}^{2} + \phi_{2m}^{2} = (\phi_{1}'')^{2} = \phi_{s}^{2} \qquad \ldots\ldots \qquad (6.20)$$

where ϕ_s $(=\phi_{1m}'')$ is a constant as given by equation (3.202). This unity value of A makes the ϕ_{2m}/ϕ_{1m} characteristic of Figure 3.34 a quarter circle as shown in Figure 6.19, and thereby simplifies the relationship between ϕ_{1m} and ϕ_{2m}.*

The relationship in equation (6.20) may now be used in equations (6.18), and when those are substituted in equation (6.16), the secondary mmf is obtained as a function of time ($z = \omega t$) and α. The variable α is a measure of ϕ_{1m} since

$$\alpha = \tan^{-1} \frac{\phi_{1m}}{(\phi_s^{2} - \phi_{1m}^{2})^{\frac{1}{2}}}, \qquad \ldots\ldots \qquad (6.21)$$

---

* ϕ_s is the saturation flux level, if F/ϕ curve is assumed to be of the form in Figure 3.19. With A = 1, no vertical scale compression as mentioned in Section 3.6.1 is needed in Figure 3.20. Furthermore, for the device of Figure 4.45, equation (6.20) is exactly valid without any approximation, and the ϕ_{2m}/ϕ_{1m} characteristic of this device is always a circle. This is for the same reason stated in the footnote to the previous page.

where ϕ_s is constant, and its effect to determine the operational point on the ϕ_{2m}/ϕ_{1m} curve (i.e. α determines ϕ_{2m} for a given ϕ_{1m}) is shown in Figure 6.19. The secondary mmf is then obtained as

$$F_2(\phi_1, \phi_2) = F_2(z, \alpha) = \cos\alpha\,(R_{m2min}\,\phi_s + \frac{3}{4}\,r_3\,\phi_s^{\,3})\cos z +$$

$$\cos 3\alpha\,(\frac{1}{4}\,r_3\,\phi_s^{\,3})\cos 3z \qquad \ldots\ldots \qquad (6.22)$$

As α is changed by the amplitude of the input voltage, the amplitudes of the fundamental and the third harmonic in the secondary current also change. The secondary current waveform is thus dependent on the position of the operational point P on the ϕ_{2m}/ϕ_{1m} characteristic of Figure 6.19, and the amplitudes of the fundamental and the third harmonic are shown in Figure 6.20 as a function of α. It is evident from this figure that, for $\alpha = \alpha_2$, F_2 takes the waveform shown in Figure 6.18a, and for $\alpha = \alpha_1$, that shown in Figure 6.18b. The point where $\alpha = \alpha_1$ in Figure 6.19, therefore, corresponds to the value of ϕ_{1m} for which the secondary relative magnetisation characteristic is (almost) linear, as the curve 2 in Figure 6.17a.

Since the B/H characteristic of the magnetic material is, in fact, not so simple as given by equation (6.15), F_2 contains a number of odd harmonics higher than the third. If only the third harmonic is assumed present, $\alpha_1 = \frac{\pi}{6}$ and $\alpha_2 = \frac{\pi}{3}$. However, with a number of higher harmonics, α_1 and α_2 are difficult to determine exactly, as the amplitude of the sum of all harmonic components is

to be expressed as a function of α, which would obviously be more complex. Nevertheless, the same conclusion on how the waveform of F_2 varies with α, would still be reached.

The waveform of the primary current may be investigated in the same manner. The primary mmf up to the fifth harmonic is finally found as

$$F_1(\phi_1, \phi_2) = F_1(z, \alpha) = \sin\alpha\,(R_{m1min}\ \phi_s + \frac{3}{4} r_3\ \phi_s^{\ 3} + \frac{5}{8} r_5\ \phi_s^{\ 5})\ \sin z +$$

$$\sin 3\alpha(\frac{1}{4} r_3\ \phi_s^{\ 3} + \frac{5}{16} r_5\ \phi_s^{\ 5})\ \sin 3z +$$

$$\sin 5\alpha(\frac{1}{16} r_5\ \phi_s^{\ 5})\ \sin 5z \qquad \ldots. \qquad (6.23)$$

where $R_{m1min} = R_g + p_1 + r_1$

$$p_1 = c_1 \frac{\ell_1}{A_1} \qquad \ldots.. \qquad (6.24)$$

$$r_5 = c_5 \frac{\ell_o}{(2\ A_o)^5}$$

where c_5 is the coefficient of the additional fifth power term in the B/H curve. In equation (6.23), the terms coming from

$$p_3 = c_3 \frac{\ell_1}{A_1^{\ 3}}$$

$$\ldots.. \qquad (6.25)$$

$$p_5 = c_5 \frac{\ell_1}{A_1^{\ 5}}$$

have been neglected to make use of the circular ϕ_{2m}/ϕ_{1m} characteristic. From the expression in equation (6.23), the variation in the amplitudes of the higher harmonic components in F_1 with α can be evaluated, together with the changes in the primary current waveform depending on the position of the operational point on the ϕ_{2m}/ϕ_{1m} characteristic.

6.4 Prediction of the Best Condition for Parametric Transformer Operation

The secondary circuit of the parametric transformer operates as a parametrically pumped oscillator. The inherently generated secondary flux depends on the characteristics of the oscillatory circuit, as well as of the pumping action, and both of these features are combined in the relative magnetisation characteristic. It is not therefore erroneous to say that the shape of the relative magnetisation characteristic depends on the secondary flux, as well as the waveform of the secondary flux depending on the shape of the relative magnetisation characteristic.

In general, most physical oscillators produce the best waveform of the oscillation when the oscillatory system is linear. Accordingly, it may be predicted that the secondary flux will have the most sinusoidal waveform when the relative magnetisation characteristic of the oscillating secondary circuit is linear. As already seen, the secondary current is then also sinusoidal. The value of ϕ_{1m} (or the location of the operational point P on the ϕ_{2m}/ϕ_{1m} characteristic of Figure 6.21), which makes the secondary

relative magnetisation characteristic almost linear is thus defined as the best condition of parametric transformer operation. With this value of ϕ_{1m} (or with the corresponding amplitude of the input voltage), the secondary circuit operates like an apparently (almost) linear oscillatory circuit, although magnetic saturation is exercised within the iron core. As shown by point P in Figure 6.21, this value of ϕ_{1m} (corresponding to the curve 2 in Figure 6.17a) is, in practice, smaller than ϕ'_{1m}, the value necessary to start the oscillations in the secondary. This is because, even with an unloaded secondary circuit, a small winding resistance will require larger variations in the secondary reluctance to be produced by a higher ϕ_{1m}. Therefore, ϕ_{1m} is at first increased beyond ϕ'_{1m}, in order to initiate the oscillations, but then, is decreased below ϕ'_{1m} to a point where the secondary flux has the best waveform.

As mentioned in Section 3.6.1, the voltage regulation is poor if the operational point is chosen somewhere between the points B and C in Figure 6.21. The constraint that ϕ_{1m} must be between the values ϕ'_{1m} and ϕ'''_{1m} for good voltage regulation is also satisfied by the best condition of operation, the point P in the figure.

The moving end of the secondary relative magnetisation characteristic in Figure 6.17a is always on the intermittent curve (corresponding to $\phi_1 = 0$). The variations in ϕ_{1m} shift this end-point to the right or to the left on the intermittent curve. If ϕ_{1m} is chosen such that the secondary relative magnetisation characteristic is curve 2, the variations in ϕ_{1m} will be

only very slightly reflected onto ϕ_{2m}, because of the almost horizontal slope at this portion of the intermittent curve. Furthermore, since ϕ_{2m} is determined by the intermittent curve, the almost horizontal slope at beyond-the-knee portion of this curve means that ϕ_{2m} is quite constant within this range of operation. However, if the secondary relative magnetisation characteristic is, for instance, curve 5, the variations in ϕ_{1m} are fully reflected onto ϕ_{2m}, resulting in poor voltage regulation.

The relation between the secondary flux waveform and the shape of the secondary relative magnetisation characteristic may be deduced as follows. If ϕ_{1m} is near ϕ'''_{1m}, where the voltage regulation is still very good, the relative magnetisation characteristic has a shape like curve 1 in Figure 6.17a. With this kind of non-linearity on the ϕ_2/F_2 plane, the secondary flux, has the rather triangular-shaped waveform shown in Figure 6.22a, and the resulting output voltage becomes rather square-shaped, as in Figure 6.22b. The best condition of operation is, therefore, nearer to ϕ'_1 than to ϕ'''_1. However, when $\phi'_{1m} < \phi_{1m} < \phi''_{1m}$, the secondary relative magnetisation characteristic exhibits a convex curvature similar to that of curve 5 in Figure 6.17a. (Note that curve 5 was obtained for a secondary flux of purely sinusoidal waveform). This kind of non-linearity on the ϕ_2/F_2 plane results in the generation of the secondary flux in the waveform shown in Figure 3.38a, Chapter 1. The reason for this has also been justified by equation (3.210), Section 3.6.2.

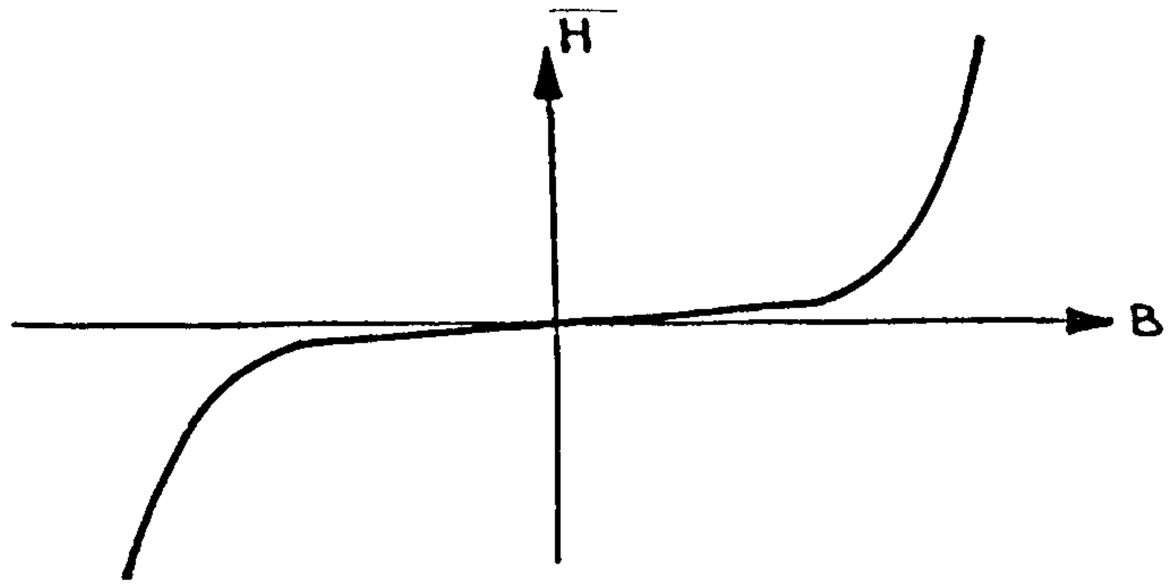

Figure 6.1 The Magnetisation Characteristic

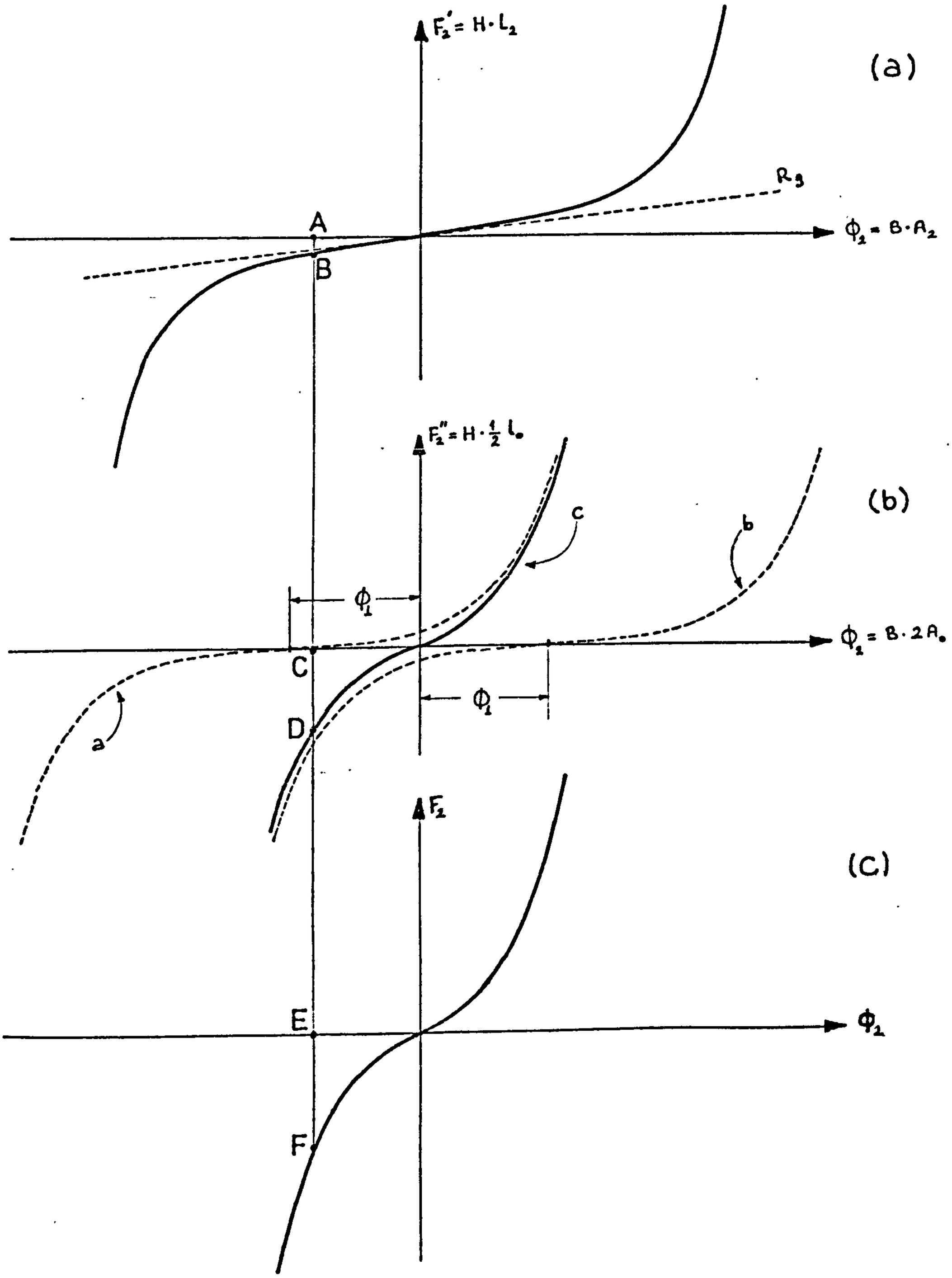

Figure 6.2 Graphical construction of the function $F_2(\phi_1, \phi_2)$

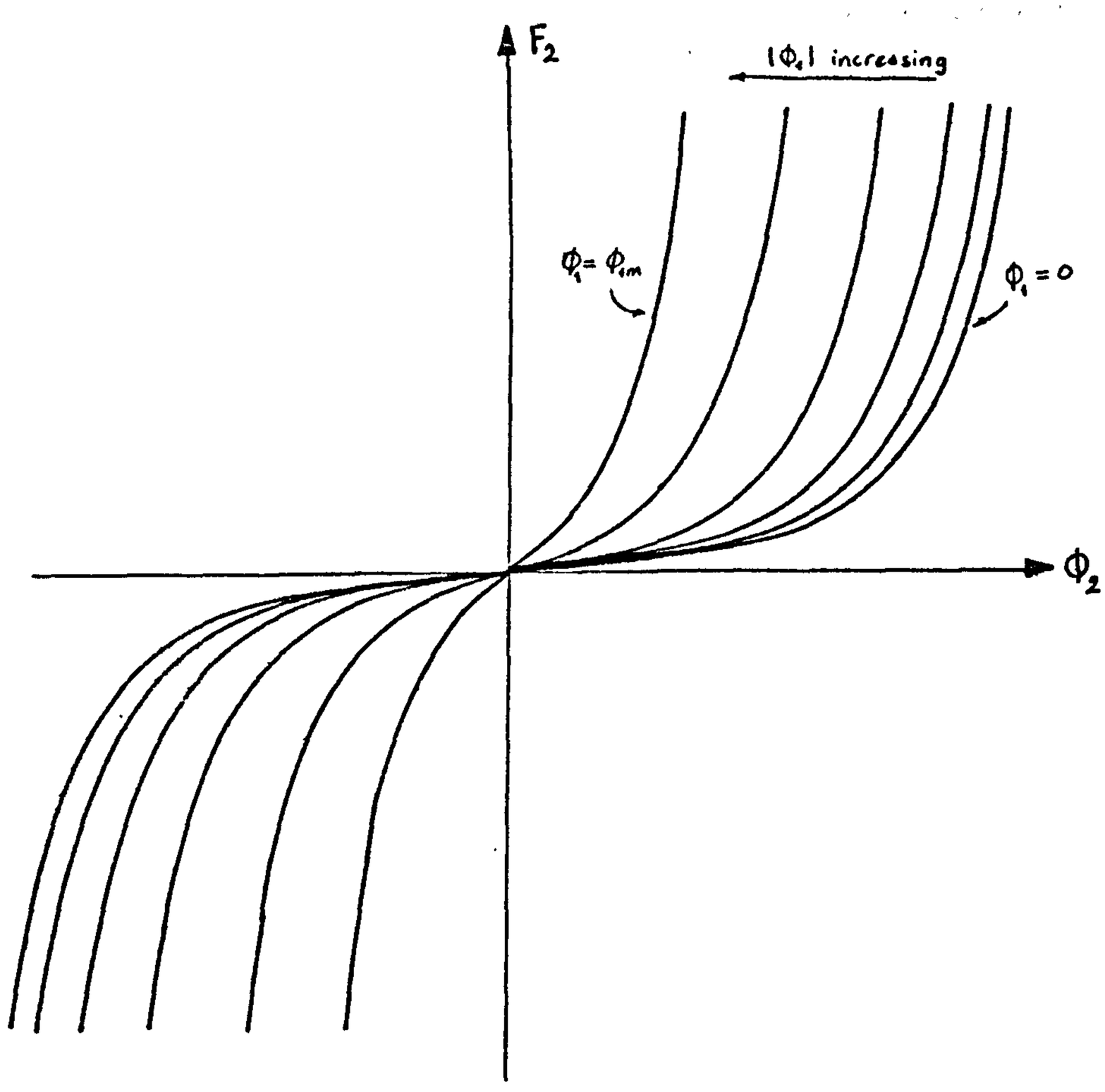

Figure 6.3 Family of secondary magnetisation curves representing $F_2\ (\phi_1, \phi_2)$

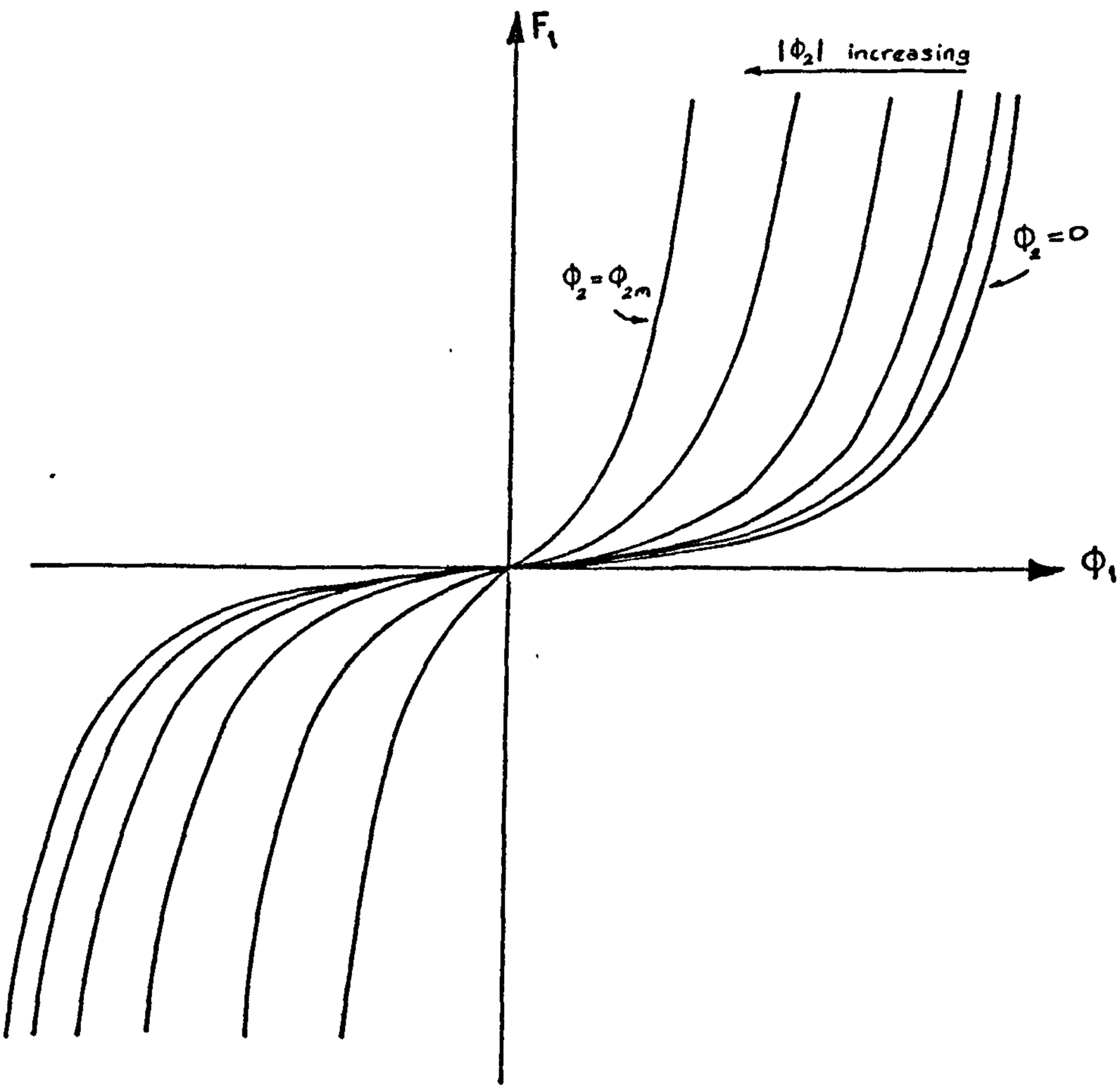

Figure 6.4 Family of primary magnetisation curves representing $F_1\ (\phi_1, \phi_2)$

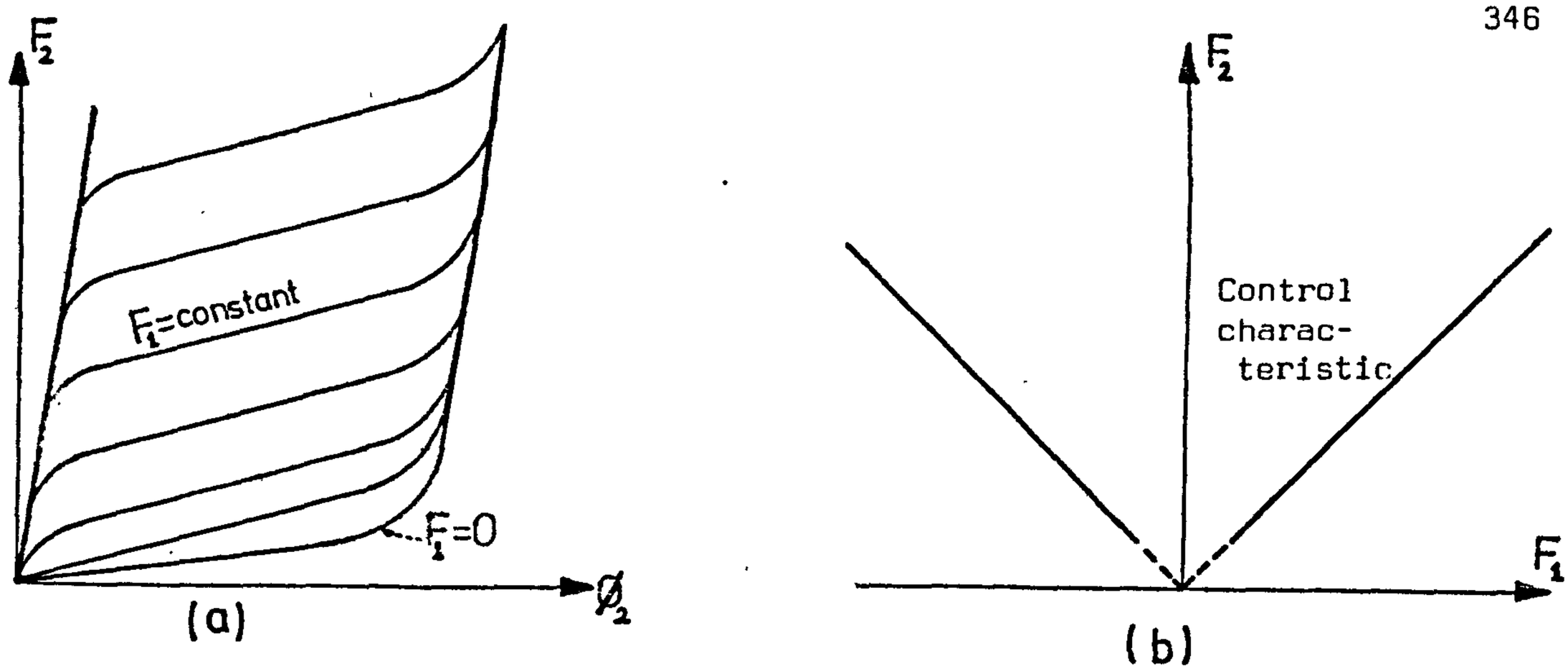

Figure 6.5 Family of curves used to obtain control characteristics of magnetic amplifiers

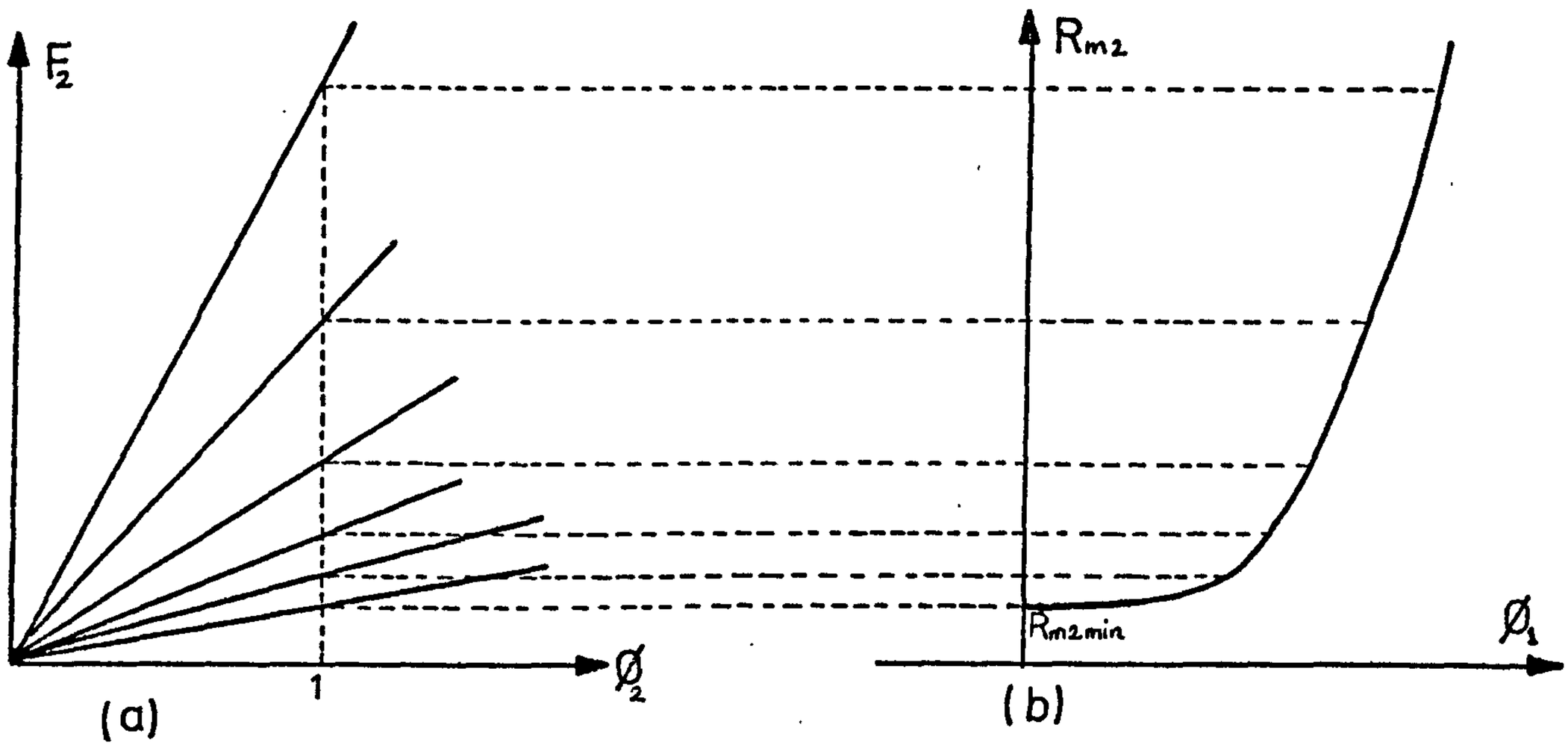

Figure 6.6 Construction of the secondary trans-reluctance characteristic

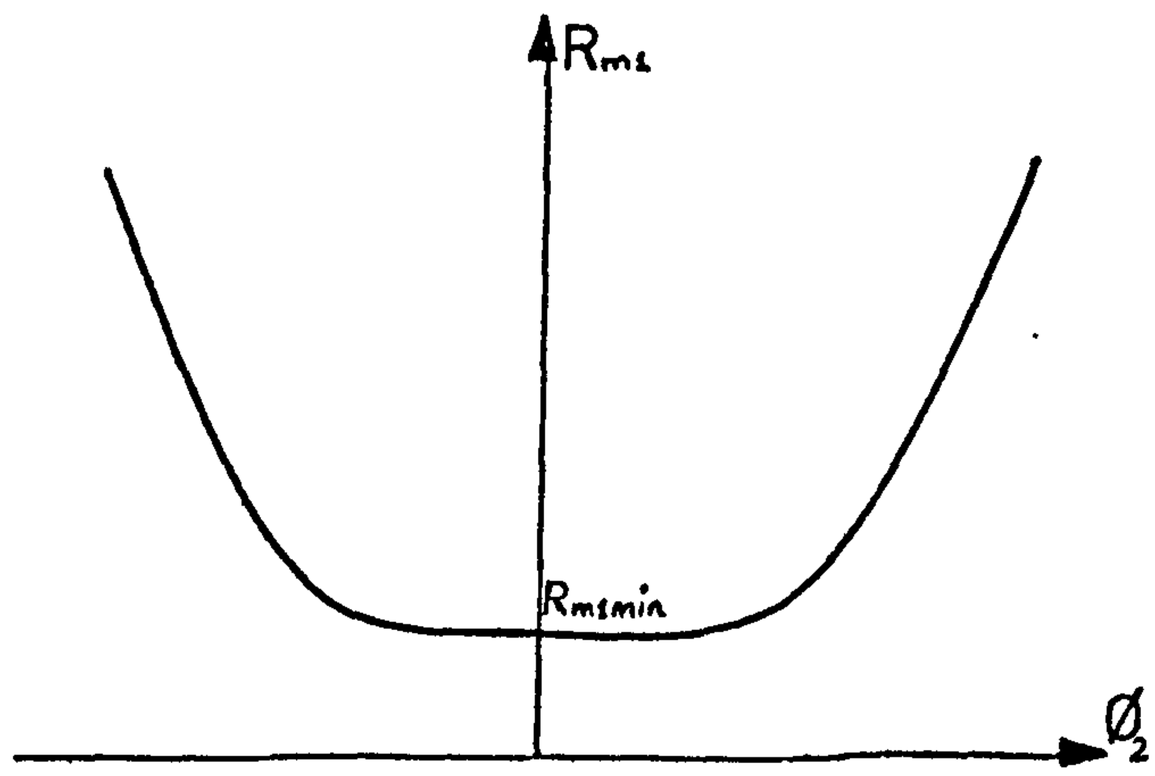

Figure 6.7 Primary trans-reluctance characteristic

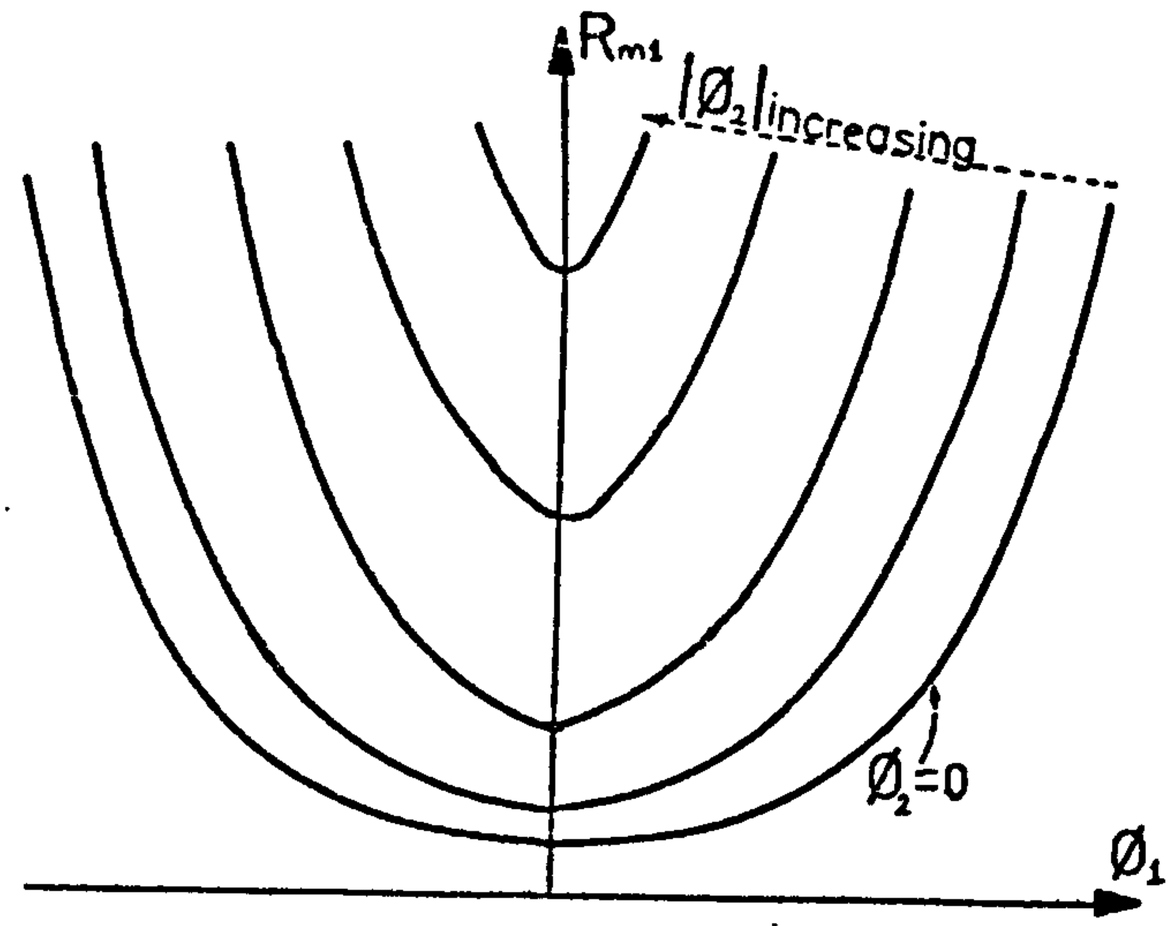

Figure 6.8 Family of curves representing the function $Rm_1(\phi_1, \phi_2)$

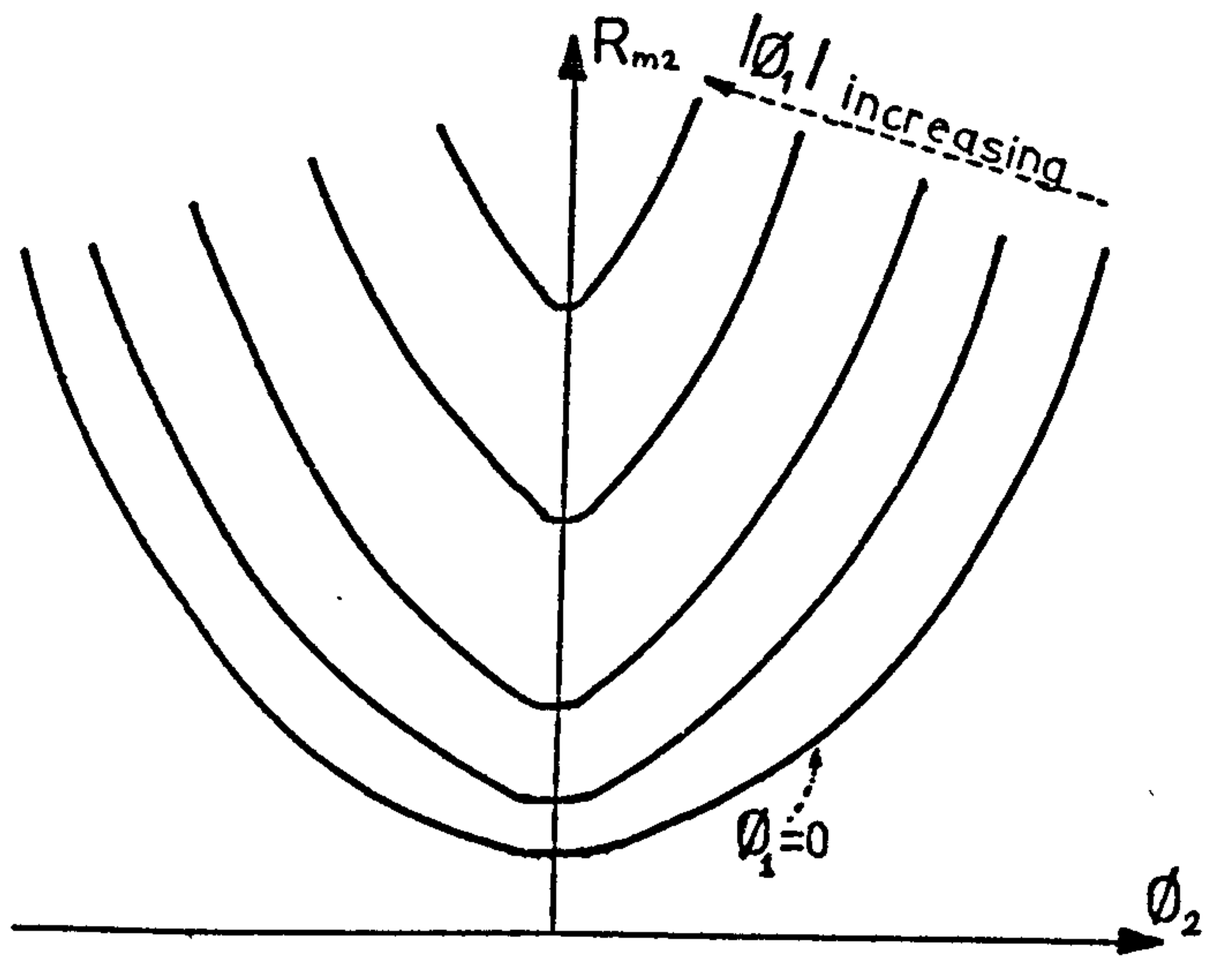

Figure 6.9 Family of curves representing the function $Rm_2(\phi_1, \phi_2)$

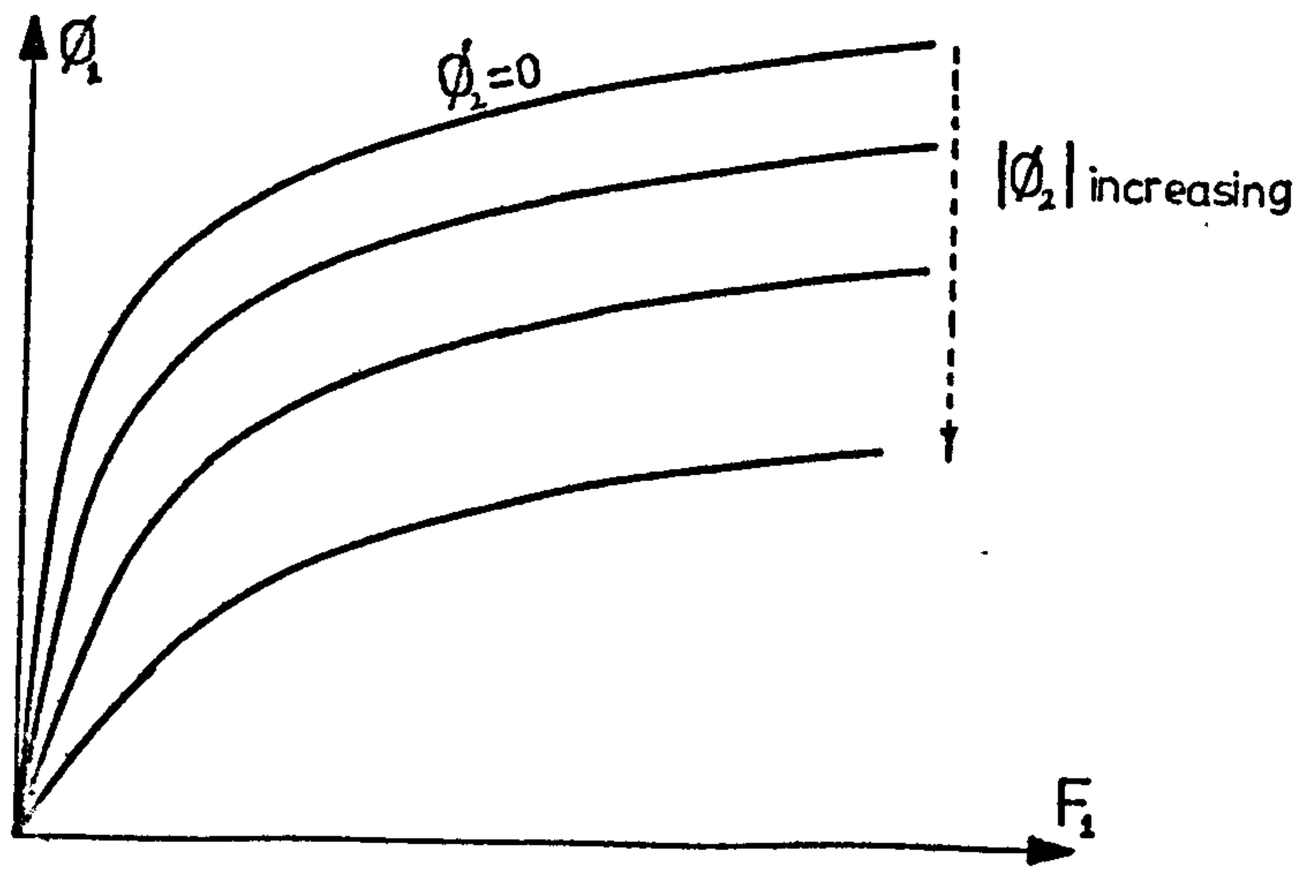

Figure 6.10 Primary magnetisation curves

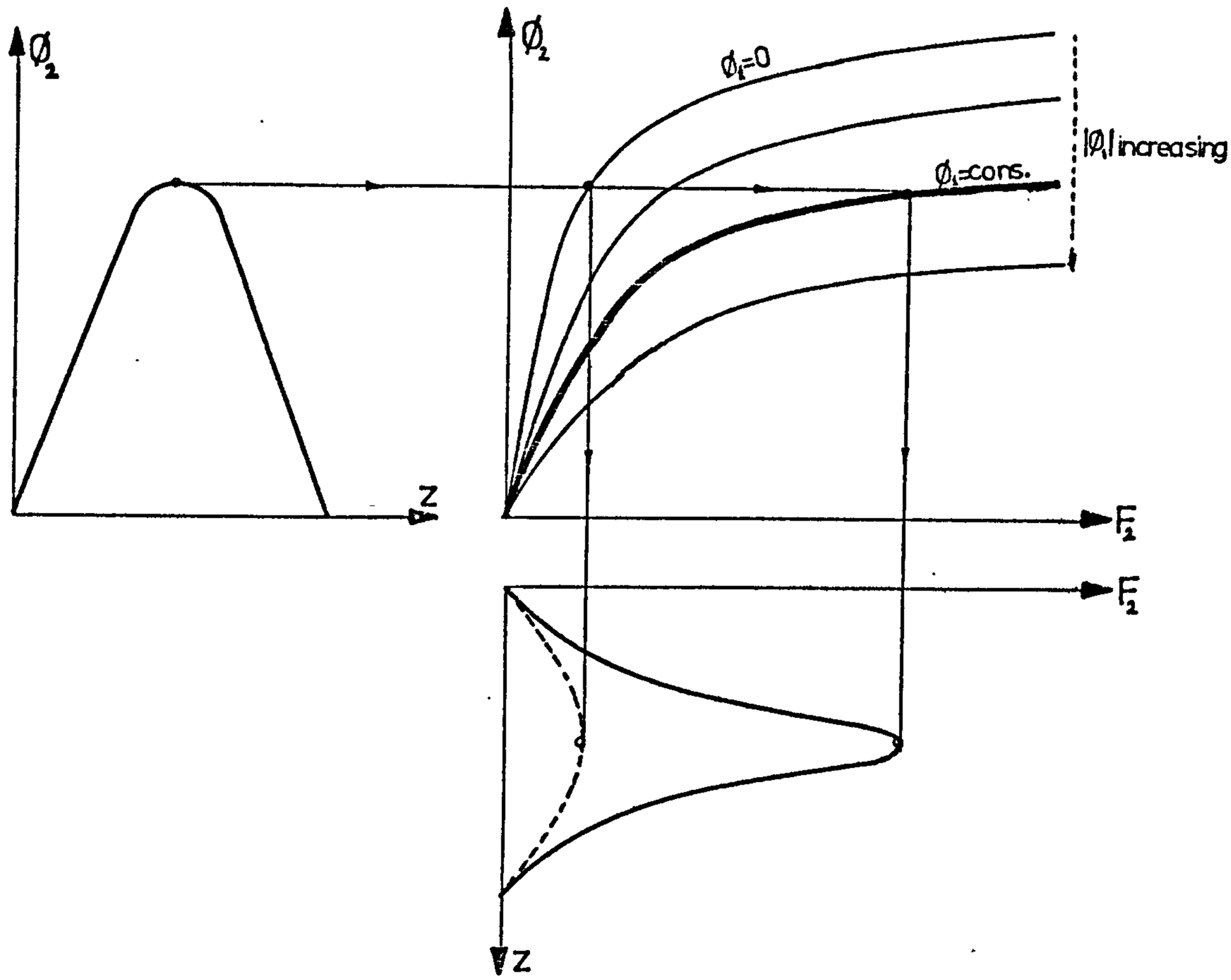

Figure 6.11 Secondary relative magnetisation curve when given ϕ_1 = constant

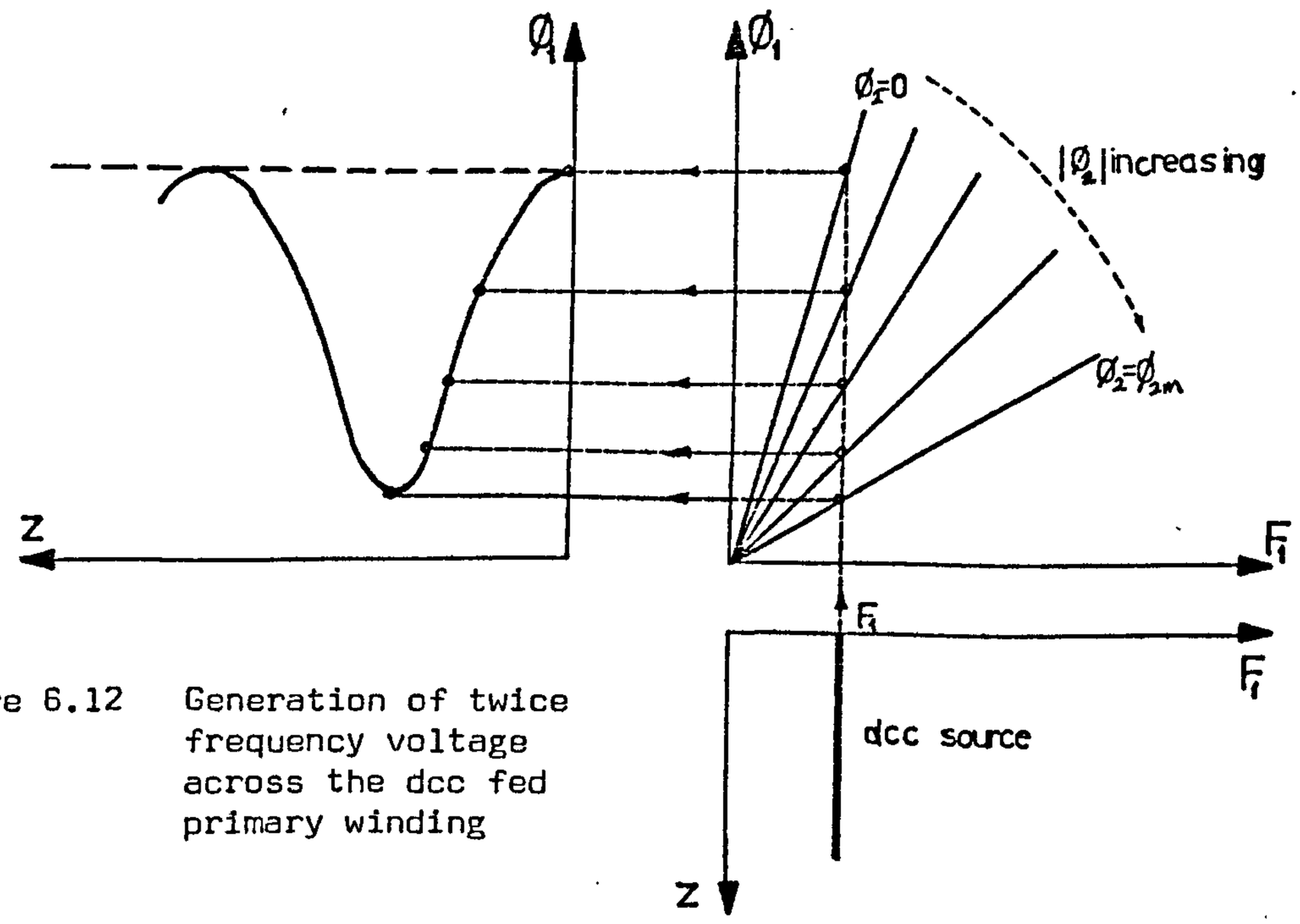

Figure 6.12 Generation of twice frequency voltage across the dcc fed primary winding

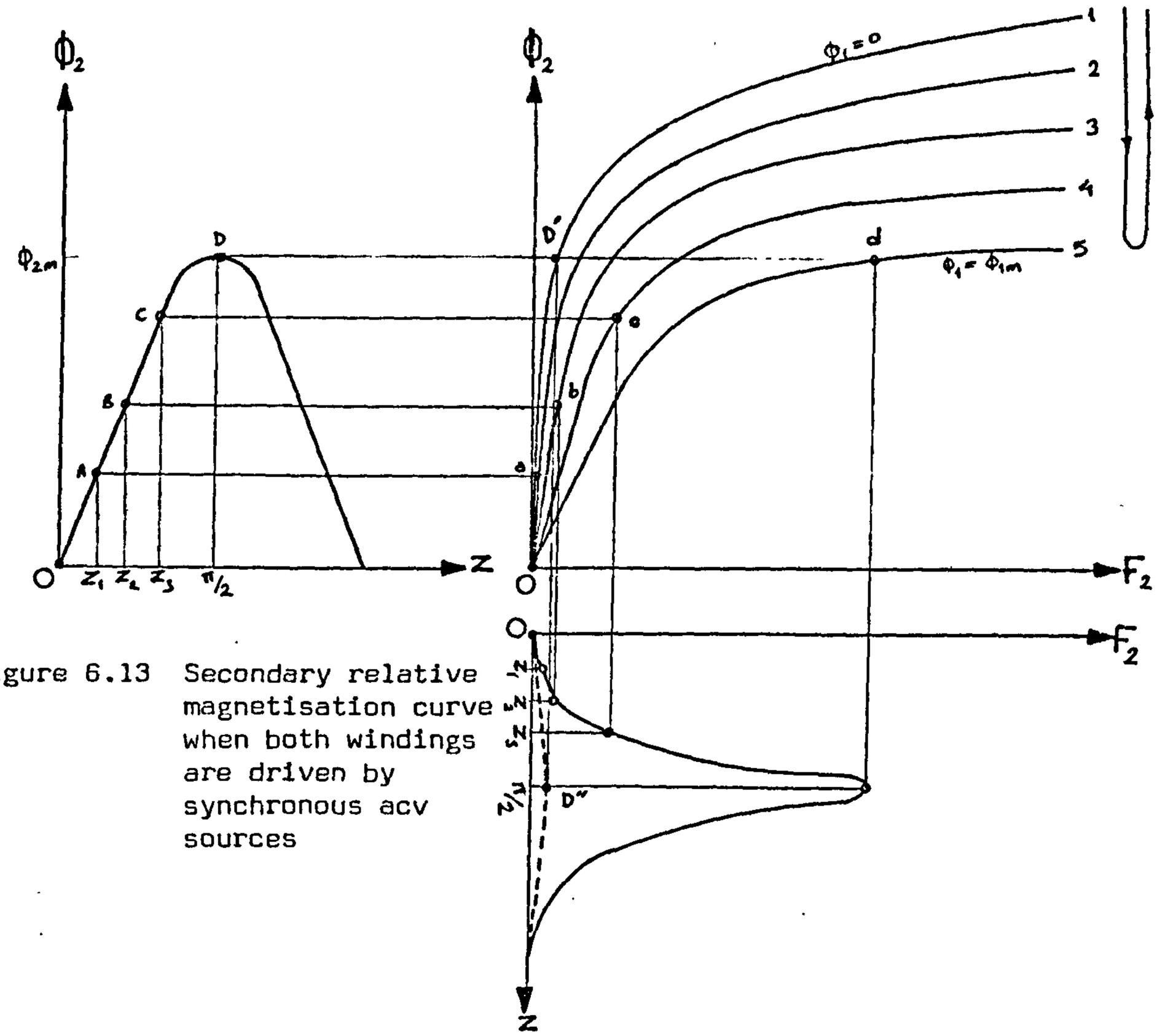

Figure 6.13 Secondary relative magnetisation curve when both windings are driven by synchronous acv sources

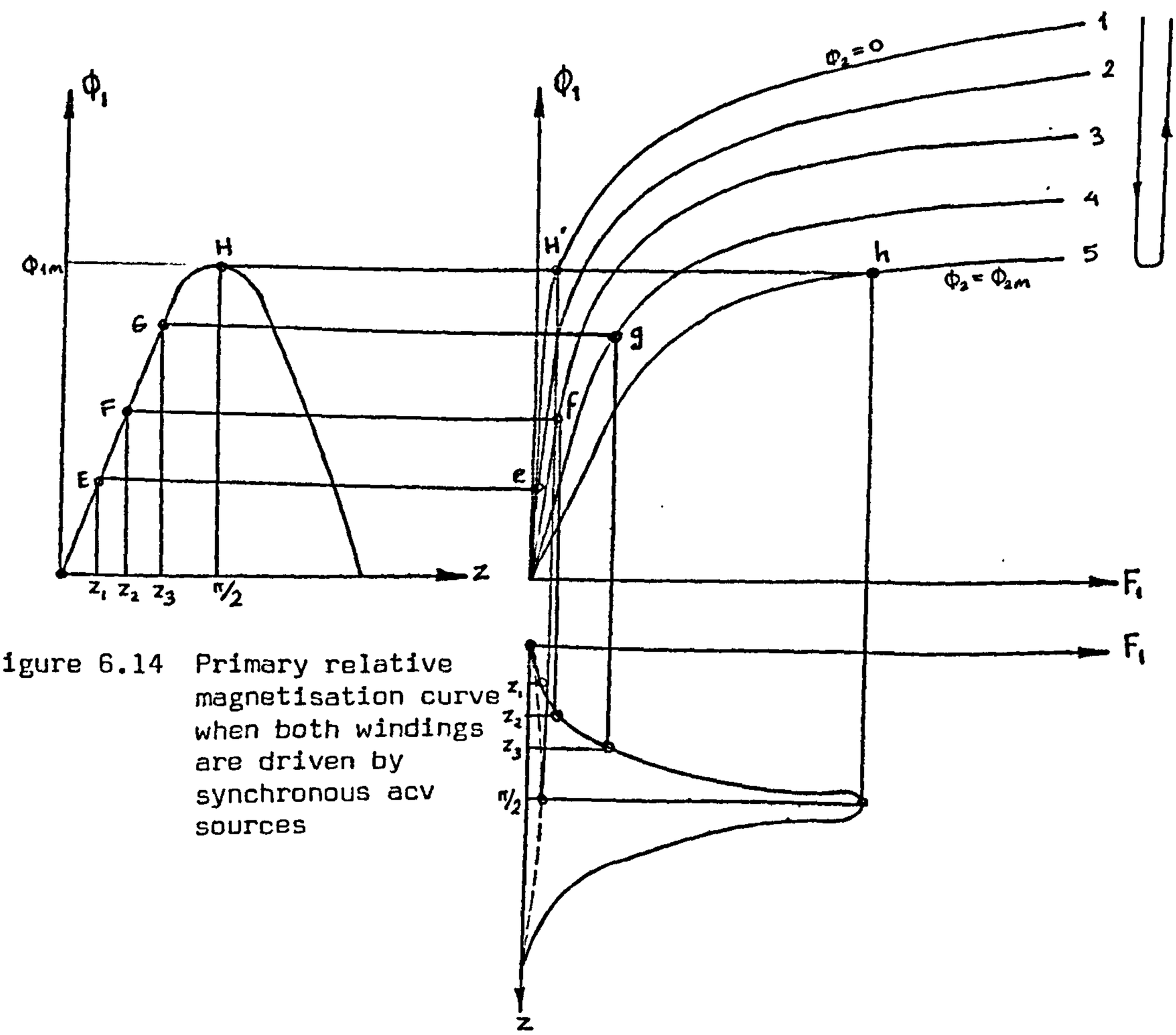

Figure 6.14 Primary relative magnetisation curve when both windings are driven by synchronous acv sources

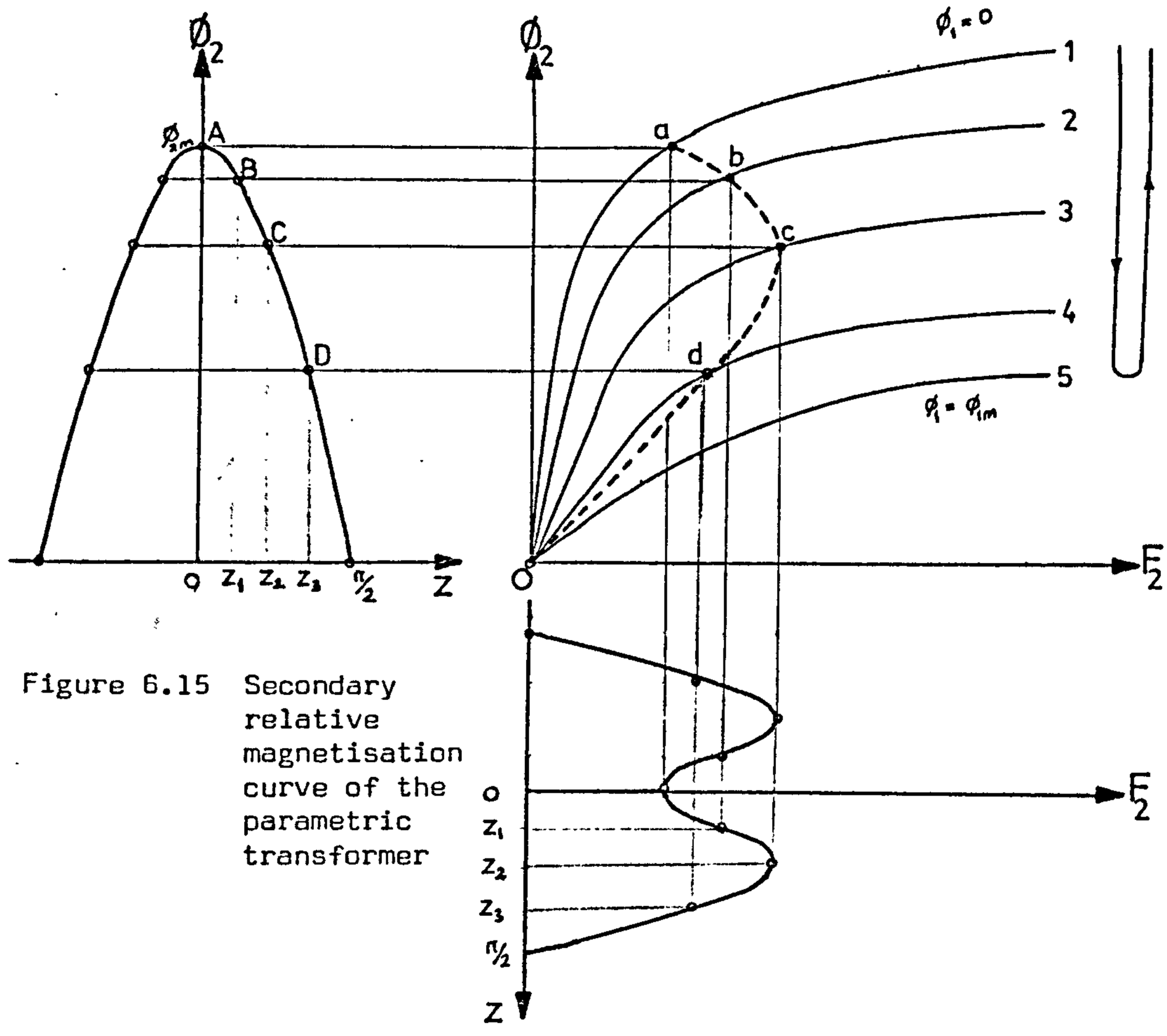

Figure 6.15 Secondary relative magnetisation curve of the parametric transformer

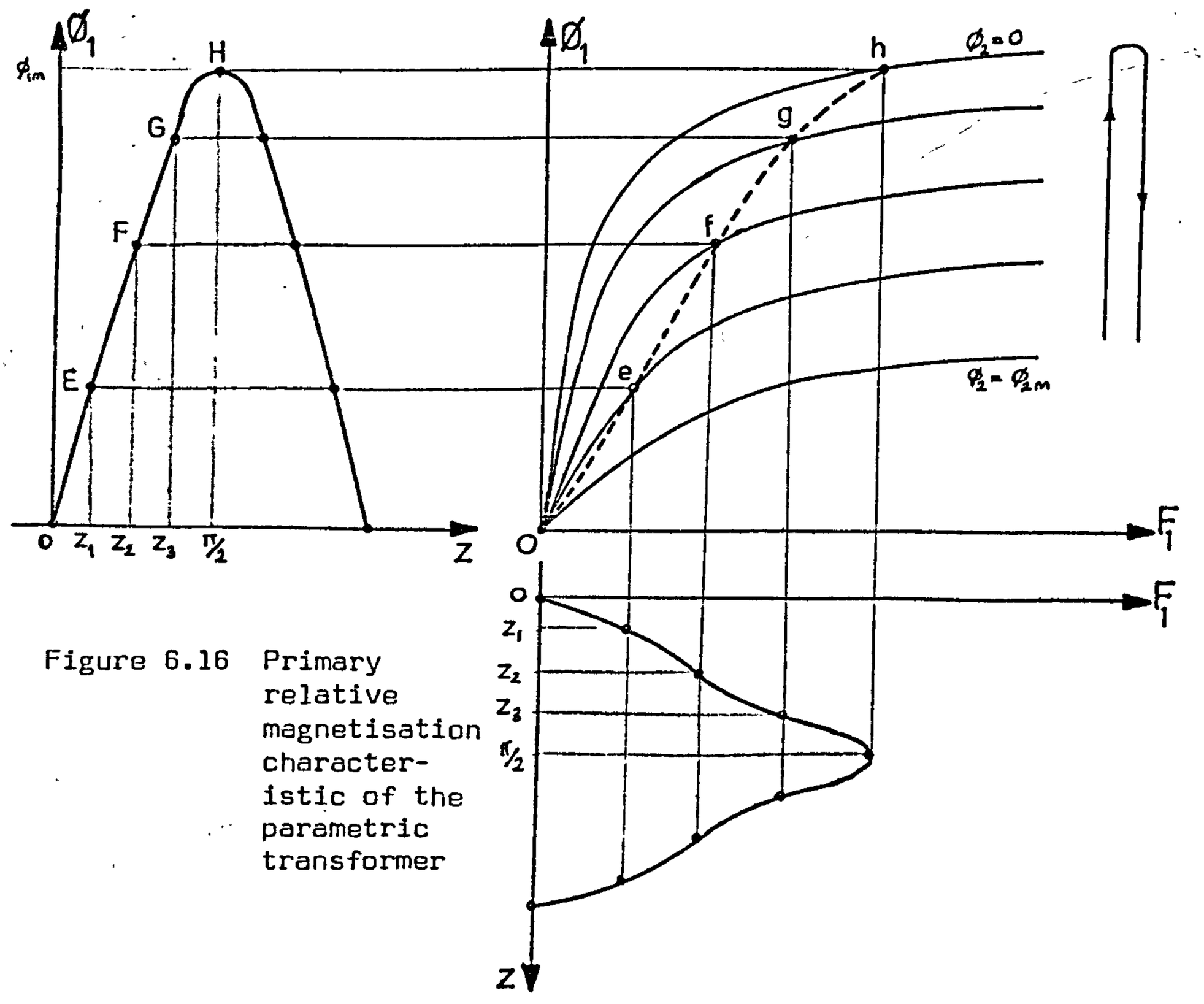

Figure 6.16 Primary relative magnetisation characteristic of the parametric transformer

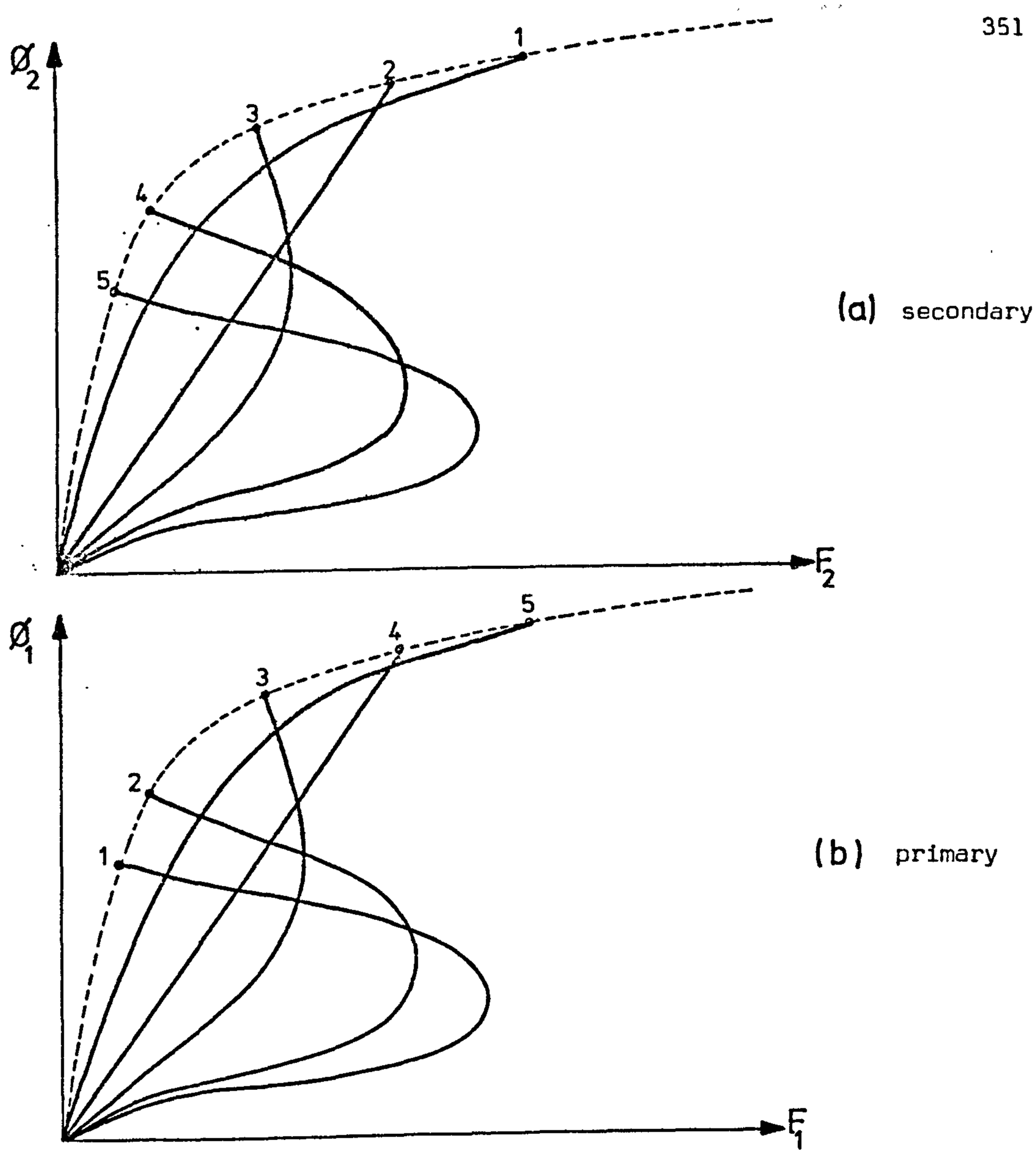

Figure 6.17 The primary and the secondary relative magnetisation characteristics for different values of ϕ_{1m}.

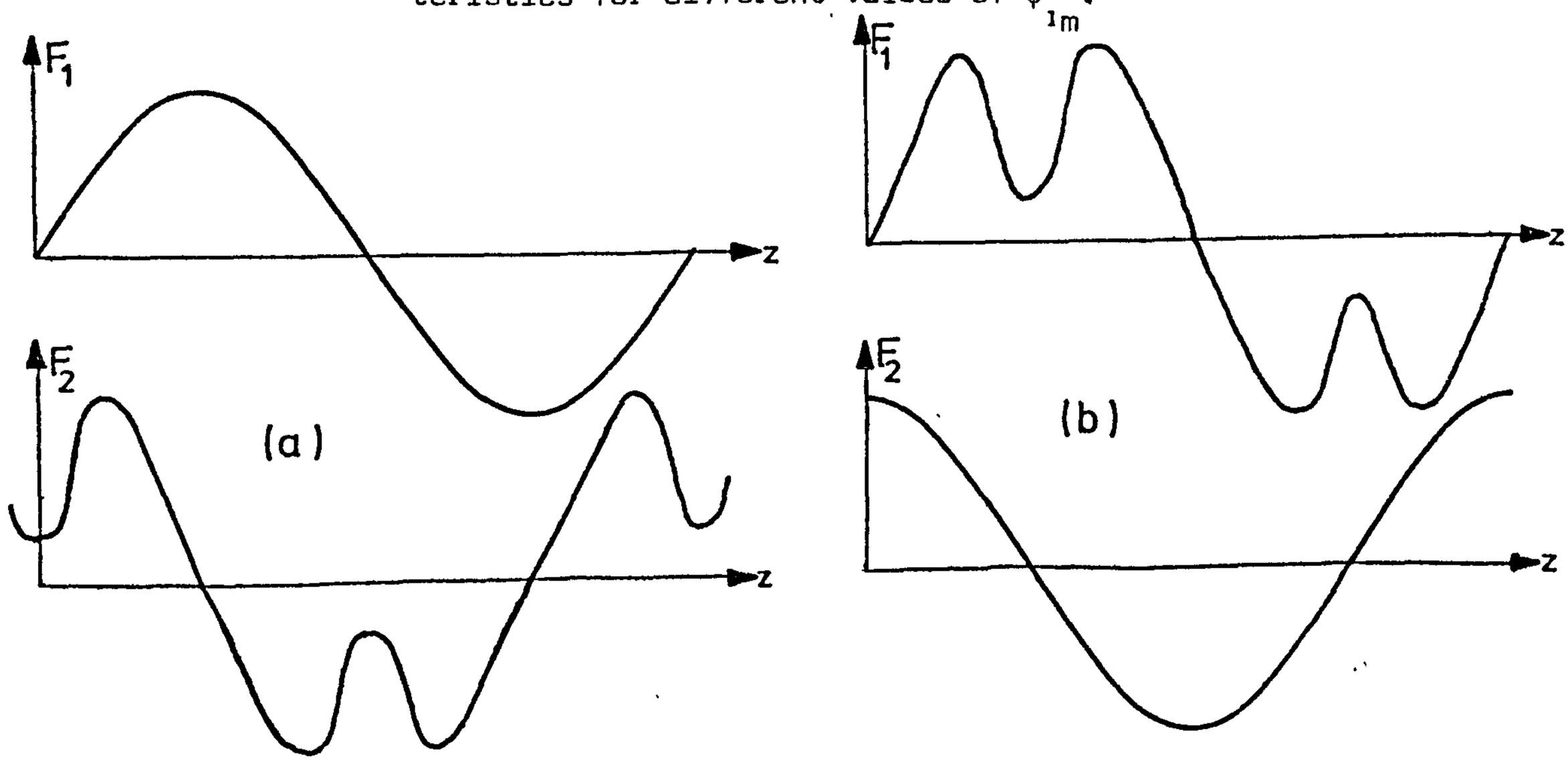

Figure 6.18 The primary and secondary current waveforms corresponding to the curves 2 and 4 in Figure 6.17

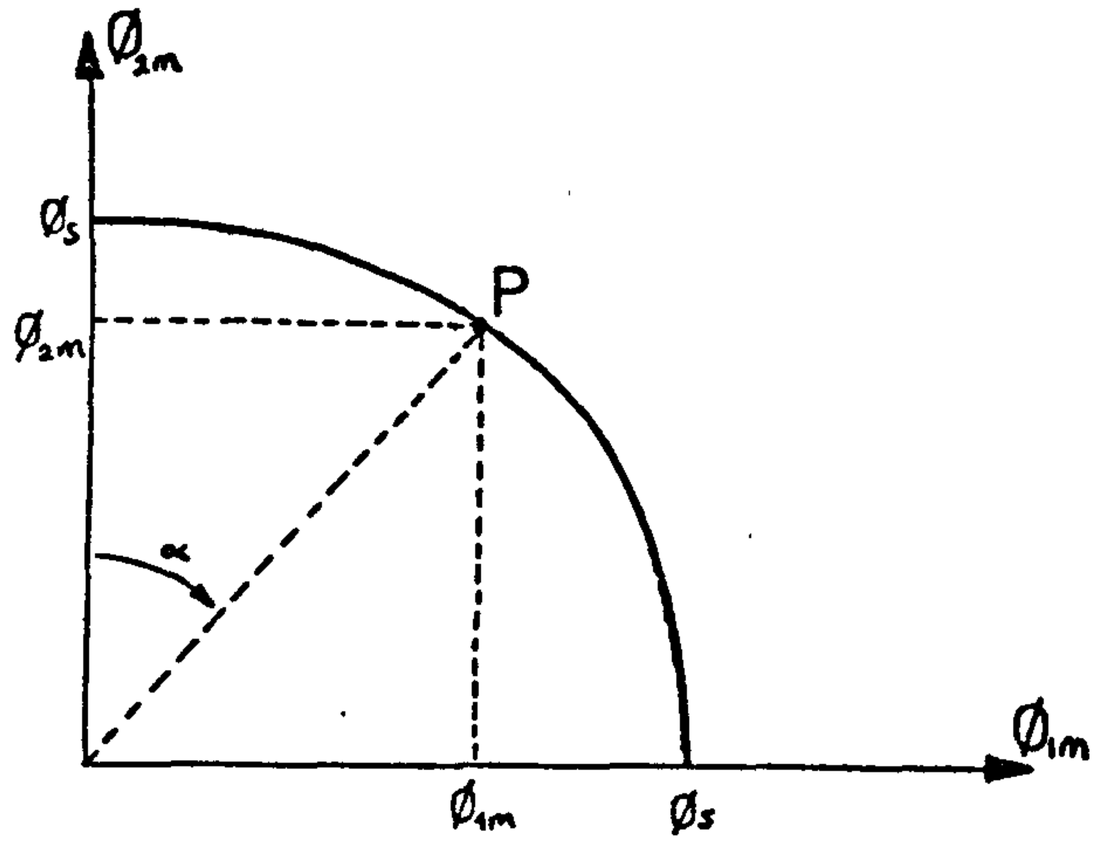

Figure 6.19 ϕ_{2m}/ϕ_{1m} characteristic for A = 1

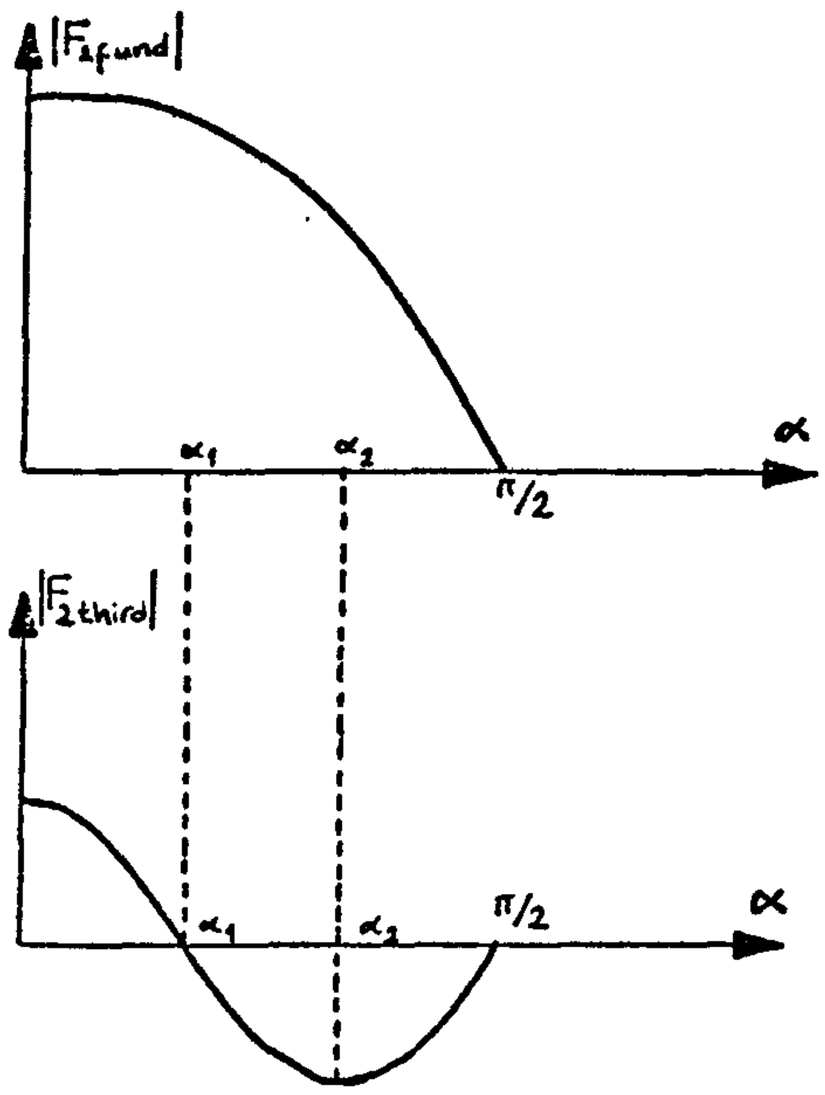

Figure 6.20 Amplitudes of the fundamental and the third harmonic in F_2 as a function of α

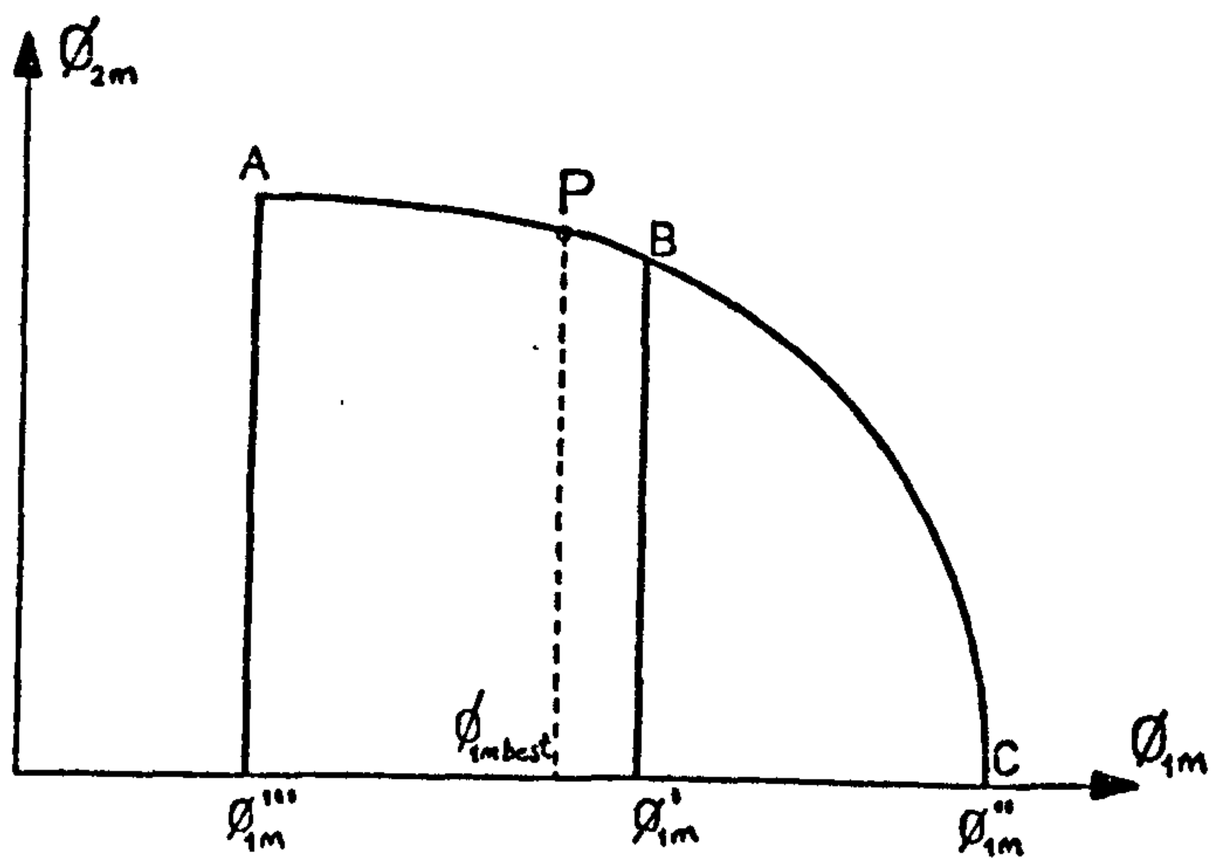

Figure 6.21 The value of ϕ_{1m} for the best condition of operation

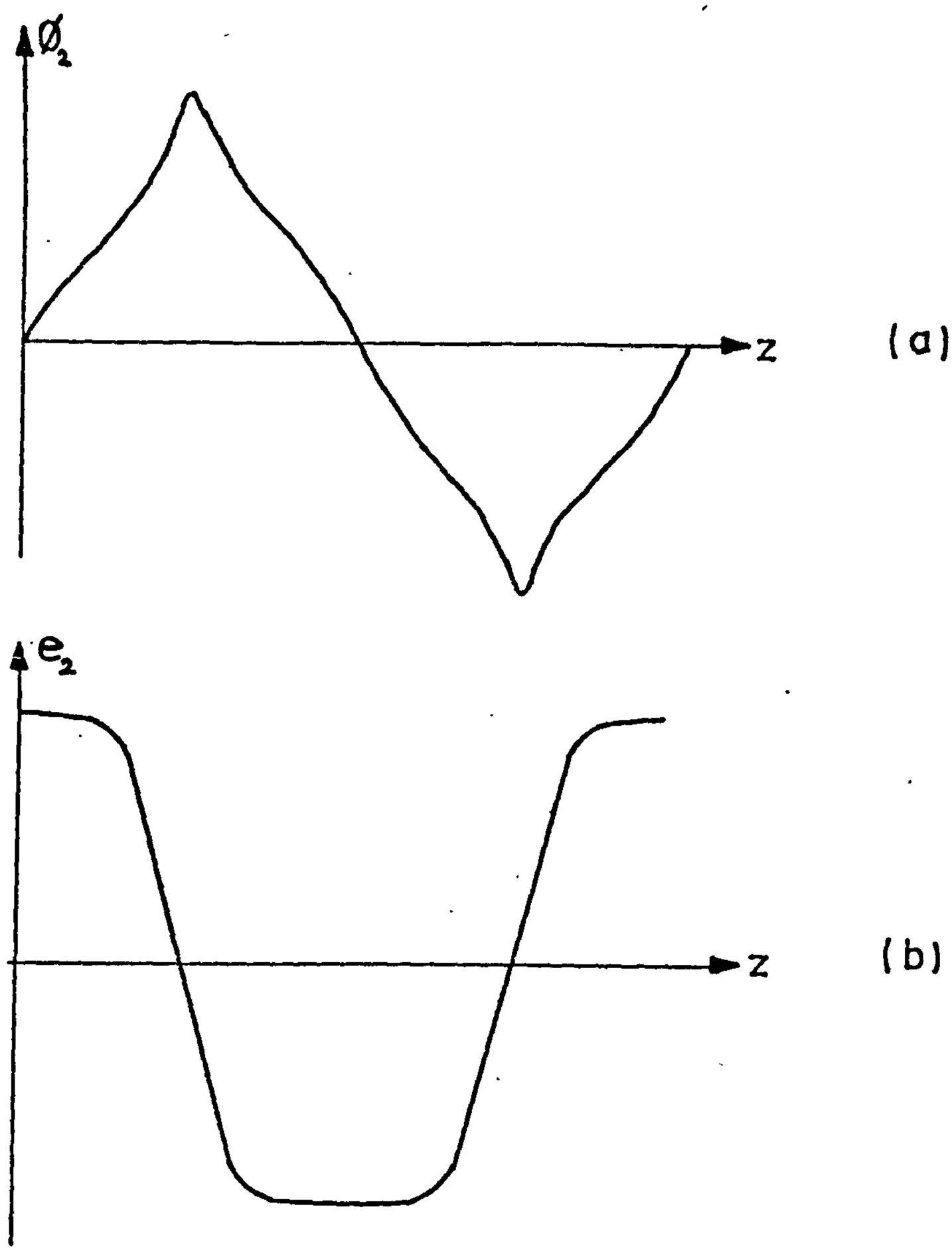

Figure 6.22 Secondary flux and output voltage waveforms when $\phi'''_{1m} < \phi_{1m} < \phi'_{1m}$

CHAPTER VII

APPLICATION OF ANALYTICAL APPROXIMATIONS OF THE B/H CURVE TO OBTAIN EXPLICIT EXPRESSIONS FOR THE $F_1(\phi_1, \phi_2)$ AND $F_2(\phi_1, \phi_2)$ FUNCTIONS

7.1 Analytical Representation of the B/H Curve

7.1.1 Requirements on the Form of Representation

A considerable amount of research has been devoted to finding the most suitable form of expression to represent the B/H curves of magnetic materials, and the use of digital computers has emphasized the need for a simple equation to represent magnetisation curves. The requirements are twofold. First, the form of representation should be usable in conjunction with other system equations to obtain an analytical solution for a particular problem. Secondly, and particularly for repetitive calculations in computers, the magnetisation curve should be accurately represented over the whole useful range by a single equation. Although the first requirement is a stringent one, the accuracy of representation is no less important.

In accordance with the needs of a particular problem, the magnetisation curve may be represented in two different forms, either as $H = f(B)$ or as $B = f(H)$, although the considerations here will be confined to only the first form since this is used in obtaining the functions $F_1(\phi_1, \phi_2)$ and $F_2(\phi_1, \phi_2)$ in Chapters IV and V. There has been many suggestions of approximate

representations, some of which can be used for either form of representation, but some of which can represent the magnetisation curve only for one direction of reading, i.e. B to be obtained from given values of H.

As the application of the function $H = f(B)$ in previous Chapters manifests, the requirements on the form of the representation to be used mean that the representation must be:

1. analytical (not numerical).
2. continuously differentiable.
3. a single expression (not different expressions for different subsections of the B scale).
4. valid for the entire range, i.e. $-\infty < B < +\infty$, $-\infty < H < +\infty$
5. odd-symmetrical in the first and the third quadrants of the H-B plane, and additionally,
6. must be an accurate approximation so that the errors are as small as possible.

The first two requirements were made clear in Section 6.1, where the functions $F_1(\phi_1, \phi_2)$ and $F_2(\phi_1, \phi_2)$ were obtained as analytical expressions, so that their derivative could be calculated. This condition, which is particularly important in many cases of finite element analysis of devices involving magnetic saturation[1], prohibits the use of numerical methods to represent the B/H curve, such as those due to Trutt, Erdelyi and Hopkins.[2] Although numerical methods based on linear interpolation represent the magnetisation curve most accurately, and

are very efficient for computer applications, they require a great number of data points to be stored in the memory, and this may be a disadvantage in some cases.[3] However, in our case, a numerical method can only be used if the derivatives of the functions $F_1(\phi_1, \phi_2)$ and $F_2(\phi_1, \phi_2)$ are not required, i.e. the mathematical model of the parametric transformer contains no winding resistances, no leakage inductances and no reactive loads.

The third requirement follows since the derivative of the function $H = f(B)$ must be continuous. It follows therefore that piece-wise linear methods, linear interpolation,[2], approximations by straight lines[4] etc., all of which require the magnetisation curve to be subdivided into a few or much more sections and each section to be approximated by a single straight line, cannot be used. Even if each subsection of the magnetisation curve is approximated by a polynomial or an exponential curve (as suggested in references 5 and 6), discontinuities will still occur in the derivatives of the $F_1(\phi_1, \phi_2)$ and $F_2(\phi_1, \phi_2)$ functions, and representation by different expressions for different subsections of the B scale is not applicable. Hence, our choice is restricted to a single function whose derivative is continuous over all the B range. This requirement is studied in detail elsewhere.[7]

It is not impossible to achieve continuity in the first derivative of the magnetisation curve,even when approximating with different functions to different subsections of the curve,

if these functions are carefully selected to satisfy boundary conditions. However, in the present situation, the representation must still be by a single expression valid for the entire range. When the B scale is subdivided into sections, each with a different approximate function, a process of decision-making is involved to find into which section the present value of B falls before the corresponding value of H can be calculated, and this requires B to be known at each instant. In the case of the parametric transformer, where oscillations are self-excited, the flux density in the core can only be known after the differential equations of the system are solved. In fact, the solution of these equations requires the $H = f(B)$ function to be given beforehand. The representation should therefore not involve such a decision-making process, and must be accomplished by a single expression.

Since the values of B and H cannot be known before the differential equations of the system are solved, it is not possible to put a limit beforehand on what maximum value they will achieve in either the positive or negative direction. The single equation to be used to represent the magnetisation curve should therefore be valid for the entire range $-\infty < B < +\infty$ and $-\infty < H < \infty$, and it should yield a curve odd-symmetrical in the first and the third quadrant of the B-H plane.

The last requirement on the accuracy of the representation will be dealt with in Chapter VIII, when curve fitting by computer is undertaken.

7.1.2 Some Forms of Analytical Representation by Single Explicit Expressions

From the foregoing discussion, it can immediately be seen that the inverse of the well-known Froelich's equation[2], i.e.

$$H = \frac{C_1 B}{1 - C_2 B} \qquad \ldots\ldots \qquad (7.1)$$

which gives an hyperbolic approximation, cannot be used since it does not satisfy either of the requirements 4 or 5. Using absolute values of B and H to make the approximation symmetrical about the origin is not allowable, as this would contradict the first requirement that the representation should be analytical.

By considering any given interval of the magnetisation curve to be part of a periodic curve subject to harmonic analysis, an approximation in the form of a Fourier series can be obtained[2]. The magnetic intensity can be expressed by

$$H = \sum_{n=1}^{n} C_n \sin n\,\alpha \qquad \ldots\ldots \qquad (7.2)$$

where $\alpha = \frac{B}{B_s} \cdot \frac{\pi}{2}$ and B_s is the maximum attainable value of B. However, a Fourier analysis approximation will not satisfy the fourth of the above requirements, and although it yields high levels of accuracy, it is not suitable for the purposes of this study.

Trigonometric functions may be used satisfactorily to represent magnetisation curves, particularly in the form $B = f(H)$. In the inverse form $H = f(B)$, the function

$$H = C_1 \tan (C_2 B) \qquad \ldots\ldots \qquad (7.3)$$

with $C_2 = \frac{\pi}{2} \frac{1}{B_s}$, satisfies all the requirements except for the B range being restricted to $-B_s < B < B_s$. However, the valid range for H is $-\infty < H < +\infty$ as $\lim_{B \to \mp B_s} H \to \mp \infty$, and it can therefore be used so long as $|B| < B_s$.

Several suggestions have been made for representing the magnetisation curve by transcendental functions, with varying degrees of accuracy over the whole range. These are extremely suitable, as many comply with all the requirements stated. However, some using exponentials, such as the simple function[2]

$$H = C_1 e^{C_2 B} \qquad \ldots\ldots \qquad (7.4)$$

or representation by a sum of exponentials[8], are not odd-symmerical and not valid for the entire range. The expression[9]

$$H = (C_1 e^{C_2 B^2} + C_3)B \qquad \ldots\ldots \qquad (7.5)$$

apart from conforming to all the requirements, appears to be quite easily fitted to the actual curve.

To achieve odd symmetry, absolute values of B cannot be used, because of the reason mentioned earlier, but with exponentials, various forms of hyperbolic functions may be utilized to yield a single expression valid for the entire range. Such an expression is

$$H = C_1 \sinh (C_2 B) \qquad \ldots\ldots \qquad (7.6)$$

which does not provide a very precise fit either in the knee region or in the saturated region. It is found that a better fit can be achieved by using the function

$$H = C_1 \sinh (C_2 B) + C_3 B \qquad \ldots\ldots \qquad (7.7)$$

where the first term approximates the knee and the saturated region, and the second term the linear region. Another hyperbolic function which may be used is

$$H = C_1 \tanh^{-1} (C_2 B) \qquad \ldots\ldots \qquad (7.8)$$

although the B range is here restricted to $\mp B_s$, as in the case of equation (7.3).

A different approach to the approximate representation of the magnetisation curve is to simulate the reluctivity function

$$r(B) = \frac{1}{\mu(B)}$$

by an analytical expression, which is then substituted in

$$H = f(B) = \frac{1}{\mu(B)} B = r(B)\ B \qquad \ldots\ldots \qquad (7.9)$$

The function r(B) should satisfy all the first four requirements, but for the fifth it must be even-symmetrical in the r(B)/B plane. This approach is followed in equation (7.5) where the reluctivity function r(B) is

$$r(B) = C_1\ e^{C_2\ B^2} + C_3$$

Similarly, the expression

$$H = C_1\ \cosh\ (C_2\ B).B \qquad \ldots\ldots \qquad (7.10)$$

may be used instead of equation (7.5). The rational-fraction approximation of Widger[3], which approximates the magnetisation curve by the equation

$$H = \frac{C_o + C_1\ B + C_2\ B^2 + \ldots. + C_n\ B^n}{1 + b_1\ B + b_2\ B^2 + \ldots. + b_n\ B^n}\ .B \ \ldots\ldots \qquad (7.11)$$

is a result of the same thought. However, if this equation is to be valid for both positive and negative B, special care must be taken to ensure that the ratio of the two polynomials yields an even-symmetrical curve. If only C_o and b_1 are non-zero, Widger's approximation reduces to the Froelich equation of equation (7.1).

The most straightforward approximation to the magnetisation curve is a power series in the general form

$$H = \sum_{i=0}^{\infty} C_{2i+1} B^{2i+1} \qquad \ldots\ldots \qquad (7.12)$$

offering a representation that is most directly related to the harmonic response of saturating devices. Only odd powers of B are taken in the series, to secure an odd-symmetrical curve. Although, theoretically, an infinite number of terms existsin the series, in practice only a finite number of terms is necessary for a sufficiently accurate representation. A power series approximation is more convenient to use in the form H = f(B) rather than B = f(H), since all the requirements are satisfied provided that C_1 and C_{2n+1} are positive constants. For the second form,powers smaller than one have to be used to provide a saturating characteristic, such as

$$B = C_1 H^n$$

where n<1. Alternatively, the correct saturating characteristic of the approximate curve may be obtained by properly choosing the signs of the coefficients C_i, such as

$$B = C_1 H - C_{2n+1} B^{2n+1}$$

where n is integral and C_1 and C_{2n+1} are positive constants. However, none of these expressions will be valid for the entire range.

An often-used and simpler form of power series approximation is the polynomial with two terms

$$H = C_1 B + C_{2n+1} B^{2n+1} \qquad (7.13)$$

in which any desired number of terms may be included to achieve the required accuracy. The choice of the parameter n depends on the curvature of the knee portion of the curve, and the C coefficients are easily determined by curve-fitting methods.

7.2 Application of Power Series Approximation to Two-C-Core Device

It is shown in Appendix IV that, when equation (7.12) is used as $H = f(B)$ function in equations (4.45) and (4.46), the $F_1(\phi_1, \phi_2)$ and $F_2(\phi_1, \phi_2)$ functions for the two-C-core device are obtained in the form

$$F_1(\phi_1, \phi_2) = R_g \phi_1 + \sum_{i=0}^{\infty} p_{2i+1} \phi_1^{2i+1} +$$

$$\sum_{i=0}^{\infty} \sum_{j=0}^{\infty} \phi_1^{2i+1} r_{2(i+j)+1} \binom{2(i+j)+1}{2i+1} \phi_2^{2j}$$

$$\ldots\ldots \qquad (7.14)$$

$$F_2(\phi_1, \phi_2) = R_g \phi_2 + \sum_{i=0}^{\infty} s_{2i+1} \phi_2^{2i+1} +$$

$$\sum_{i=0}^{\infty} \sum_{j=0}^{\infty} \phi_2^{2i+1} r_{2(i+j)+1} \binom{2(i+j)+1}{2i+1} \phi_1^{2j}$$

..... (7.15)

where

$$p_{2i+1} = \ell_1 \frac{C_{2i+1}}{(A_1)^{2i+1}}$$

$$s_{2i+1} = \ell_2 \frac{C_{2i+1}}{(A_2)^{2i+1}} \qquad (i=0,1,2,\ldots n)$$

..... (7.16)

$$r_{2i+1} = \ell_0 \frac{C_{2i+1}}{(2A_0)^{2i+1}}$$

Obviously, from the coefficients in equations (7.16), only those corresponding to $i = 0$, (i.e. p_1, s_1 and r_1) have reluctance dimension ($\frac{1}{C_1}$ is the magnetic permeability in the linear region of the B/H curve). When a finite number of terms (=n) is given in the power-series approximation of the B/H curve (equation (7.12)), the upper limits of the double summation in equations (7.14) and (7.15) are interrelated so that $2(i+j)+1 < n$ all the time.

During initiation of oscillations, the secondary circuit is considered linear, i.e. $F_2(\phi_1, \phi_2)$ is a linear function of ϕ_2 This is accomplished by setting i=o in equation (7.15) which

then becomes

$$F_2(\phi_1, \phi_2) = R_g \phi_2 + s_1 \phi_2 + \phi_2 \sum_{j=0}^{\infty} r_{2j+1} \binom{2j+1}{1} \phi_1^{2j}$$

..... (7.17)

The secondary reluctance is found in this case as

$$R_{m2}(\phi_1) = \frac{F_2(\phi_1, \phi_2)}{\phi_2} = R_g + s_1 + r_1 + \sum_{j=1}^{\infty} r_{2j+1} \binom{2j+1}{1} \phi_1^{2j}$$

..... (7.17)

which is the explicit expression for the trans-reluctance curve shown in Figure 2.2, Chapter II. With j=1 (only) in equation (7.17), the simplest expression for the dependence of the secondary reluctance on the primary flux is obtained as

$$R_{m2} = R_g + s_1 + r_1 + 3 r_3 \phi_1^2 \quad ..... \quad (7.18)$$

which is the same as equation (2.4), Chapter II. In Chapter II, the trans-reluctance curve and equation (2.4) were assumed on qualitative grounds, and most of the work in Chapter III, except where non-linearity was considered, was based on these assumptions. When equations (7.17) and (7.18) are obtained from the general expression for $F_2(\phi_1, \phi_2)$, these assumptions are fully justified, and the bridge between the theory of Chapter III and the physical considerations of Chapters IV to VII is established.

In order to refer to the work in Chapter III, it may be pointed out that equation (3.50), Section 3.1.2, which gave rise to the Hill equation, is the same as equation (7.17). The assumption made in equations (3.88) to (3.90) can be justified by considering only i=0 and j=0,1 in equation (7.14), which then gives

$$F_1(\phi_1, \phi_2) = (R_g + p_1 + r_1 + 3\, r_3\, \phi_2^2)\phi_1 \qquad (7.19)$$

and the primary reluctance $R_{m1} = F_1/\phi_1$ is obtained in the form of equation (3.88). To account for non-linearity in the secondary circuit, with only the terms corresponding to i=0, 1 and j=0 being considered in equation (7.15), the secondary mmf is obtained as

$$F_2 = (R_g + s_1 + r_1)\phi_2 + (s_3 + r_3)\phi_2^{\,3} \qquad (7.20)$$

which is the same as equation (3.99) under the assumption of equation (3.100). The influence of the primary flux on the mmf of the non-linear secondary circuit may be most simply expressed by taking i=0, 1 and j=0, 1 in equation (7.15) yielding

$$F_2(\phi_1, \phi_2) = (R_g + s_1 + r_1 + 3\, r_3\, \phi_1^{\,2})\, \phi_2 + (s_3 + r_3 + 10\, r_5\, \phi_1^{\,2})\phi_2^{\,3}$$

$$\ldots\ldots \qquad (7.21)$$

When the term involving $10\ r_5\ \phi_1^2$ in equation (7.21) is neglected, in accordance with the simplifying assumption in Section 3.2 that only the linear part of the secondary reluctance is modulated by the primary flux, equation (7.21) leads to the expression for the secondary reluctance given by equation (3.102). Finally, equation (3.205) is the same as equation (7.18), and equation (3.207) is a simpler form of equation (7.17), where j=0,1,2 and 3 only is considered.

The explicit expressions of the $F_1(\phi_1, \phi_2)$ and $F_2(\phi_1, \phi_2)$ functions for the saturable reactor of Figure 4.45 can be obtained in the same way as that followed in Appendix 4. They will then consist of only the third terms (double summation) in equations (7.14) and (7.15) but with r_{2i+1} computed by

$$r_{2i+1} = 2\,\ell\,\frac{C_{2i+1}}{A^{2i+1}} \qquad \ldots\ldots \qquad (7.22)$$

where ℓ and A are the mean flux-path length and the cross-sectional area of the cores.

7.2.1 Differentiation of the Function $F_2(\phi_1, \phi_2)$

The differential equation of the secondary circuit, equation (5.8) requires the first-order time derivative of the $F_2(\phi_1, \phi_2)$ function to be given in the form of equation (5.12). This can be achieved by determining the functions $f_1(\phi_1, \phi_2)$ and $f_2(\phi_1, \phi_2)$ defined in equations (5.13). For the expression in equation (7.15), these two functions (both partial derivatives of $F_2(\phi_1, \phi_2)$) are

$$f_1(\phi_1, \phi_2) = \frac{\partial F_2(\phi_1, \phi_2)}{\partial \phi_2} = R_g + \sum_{i=0}^{\infty} (2i+1)\, s_{2i+1}\, \phi_2^{2i} +$$

$$\sum_{i=0}^{\infty} \sum_{j=0}^{\infty} (2i+1)\, r_{2(i+j)+1} \binom{2(i+j)+1}{2i+1} \phi_1^{2j}\, \phi_2^{2i}$$

..... (7.23)

$$f_2(\phi_1, \phi_2) = \frac{\partial F_2(\phi_1, \phi_2)}{\partial \phi_1} = \sum_{i=0}^{\infty} \sum_{j=0}^{\infty} (2j)\, r_{2(i+j)+1} \binom{2(i+j)+1}{2i+1} \phi_1^{2j-1}\, \phi_2^{2i+1}$$

..... (7.24)

Throughout this work, reluctance has always been defined by

$$R_{m2} = \frac{F_2}{\phi_2} \qquad \text{.....} \qquad (7.25)$$

which may be termed a non-incremental reluctance. This is because, in all the circuit equations, the mmf is needed in the form

$$R_{m2}\, \phi_2 = F_2$$

In the literature, magnetic properties of materials are defined in various forms, due to the complications arising from non-linearity and hysteresis. The non-incremental permeability, or simply the permeability, is defined as[10]

$$\mu = \frac{B}{H}$$

which is characterized by the slope of the line OA in Figure 7.1. The differential permeability at any point on the B/H curve is defined as[11]

$$\mu = \frac{dB}{dH}$$

which is the slope of the tangent drawn to the curve at point A, as shown in Figure 7.1. The incremental permeability is used when the material is subjected to the excitation of superimposed dc and ac magnetic fields, and is defined as[11]

$$\mu = \frac{\Delta B}{\Delta H}$$

with the aid of minor hysteresis loops. The incremental permeability at point B in Figure 7.1 is given by the slope of the line CC'. Goral[12] defines an instantaneous permeability for use in parametrically excited circuits.

In accordance with these concepts, the quantity

$$R_{m2dif} = \left.\frac{\partial F_2(\phi_1, \phi_2)}{\partial \phi_2}\right|_{\substack{\phi_1 = \text{constant} \\ \phi_2 = \text{constant}}} = \left. f_1(\phi_1, \phi_2)\right|_{\substack{\phi_1 = \text{constant} \\ \phi_2 = \text{constant}}} \quad \ldots\ldots \quad (7.26)$$

can be defined as the differential reluctance of the secondary magnetic circuit which is different from the non-incremental reluctance

$$R_{m2} = \left.\frac{F_2(\phi_1, \phi_2)}{\phi_2}\right|_{\substack{\phi_1 = \text{constant} \\ \phi_2 = \text{constant}}} \quad \ldots\ldots \quad (7.27)$$

However, when both ϕ_1 and ϕ_2 are equal to zero, the differential and non-incremental values of reluctance become exactly the same, and equations (7.17) and (7.23) both give the minimum value of the secondary reluctance as

$$R_{m2min} = R_g + s_1 + r_1$$

which is the same as equation (4.51).

The function, obtained by taking ϕ_2 = constant in equation (7.24),

$$f_2(\phi_1) = f_2(\phi_1, \phi_2)\Big|_{\phi_2 = \text{constant}} = \frac{\partial F_2(\phi_1, \phi_2)}{\partial \phi_1}\Bigg|_{\phi_2 = \text{constant}} \quad \ldots\ldots \quad (7.28)$$

indicates how effectively the primary flux influences the secondary magnetic circuit, and is a measure of the generation of even harmonics in the secondary circuit when ϕ_2 = constant and ϕ_1 is alternating. Note that, when ϕ_2 = constant = 0, equation (7.28) or (7.24) has the value of zero, since the function $f_2(\phi_1, \phi_2)$ exist only when both ϕ_1 and ϕ_2 are simultaneously present in the magnetic core.

With $\frac{d\phi_1}{dz}$ eliminated and the terms rearranged, the second of equations (5.14) becomes

$$\frac{d^2\phi_2}{dz^2} + [b + c\, f_1(\phi_1, \phi_2)]\frac{d\phi_2}{dz} + [c\, f_2(\phi_1, \phi_2)\, e(z) - a\, c\, f_2(\phi_1, \phi_2)$$

$$F_1(\phi_1, \phi_2) + d\, F_2(\phi_1, \phi_2)] = 0 \quad \ldots\ldots \quad (7.29)$$

Substituting $f_1(\phi_1, \phi_2)$ from equation (7.23) and separating the terms corresponding to j = 0, the first derivative term in equation (7.29) which is responsible for losses, is obtained as

$$\{b + c\,[R_g + \sum_{i=o}^{\infty} (2i+1)\,(s_{2i+1} + r_{2i+1})\,\phi_2^{\,2i}]\}\,\frac{d\,\phi_2}{dz} +$$

$$c\{\sum_{i=o}^{\infty}\sum_{j=1}^{\infty} (2i+1)\,r_{2(i+j)+1}\binom{2(i+j)+1}{2i+1}\,\phi_1^{\,2j}\,\phi_2^{\,2i}\}\,\frac{d\,\phi_2}{dz}$$

..... (7.30)

The first term above expresses the autonomous losses caused by R_L, R_2 and the saturation non-linearity, while the second term gives the non-autonomous losses caused by the parametric interaction. In Section 3.3.1, only the terms from expression (7.30) corresponding to i=o and j=1 are taken into account, and in Section 3.3.2, only the terms corresponding to i=o,1 and j=1 are implicitly included in equation (3.148).

The extra reaction from the primary to the secondary circuit, represented by the terms involving $f_2(\phi_1, \phi_2)$ in equation (7.29), plays an important role in the parametric generation of energy in the secondary circuit, as mentioned in relation to equations (3.152) to (3.154) in Section 3.3.2. This reaction also affects the steady-state value of σ (the phase difference between the primary and the secondary fluxes) of equation (3.155), Section 3.3.2, by virtue of the additional term involving km. However, in Chapter III, the primary flux was assumed to be sinusoidal by neglecting the resistance of the primary winding. The term with a minus sign in equation

(7.29) did not enter into any differential equation in Chapter III, because the constant a defined in equations (5.13), becomes zero with $R_1 = 0$. In order to see the form of this reaction explicitly, the expressions for $f_2(\phi_1, \phi_2)$, $F_1(\phi_1, \phi_2)$ and $F_2(\phi_1, \phi_2)$, given by equations (7.24), (7.14), and (7.15) respectively, must be substituted into the third term in equation (7.29).

7.3 Application of Other Approximations of B/H Curve to the Two-C-Core Device

7.3.1 Hyperbolic Sine Function

When the approximation given by equation (7.6) is applied to equations (4.45) and (4.46), the primary and the secondary mmf in the two-C-core device are obtained as

$$F_1(\phi_1, \phi_2) = R_g \phi_1 + p_1 \sinh (p_2 \phi_1) + r_1 \cosh (r_2 \phi_2) \sinh (r_2 \phi_1) \quad \ldots\ldots \quad (7.31)$$

$$F_2(\phi_1, \phi_2) = R_g \phi_2 + s_1 \sinh (s_2 \phi_2) + r_1 \cosh (r_2 \phi_1) \sinh (r_2 \phi_2) \quad \ldots\ldots \quad (7.32)$$

where $p_1 = C_1 . \ell_1$

$p_2 = C_2 / A_1$

$r_1 = C_1 . \ell_0$

$r_2 = C_2 / 2A_0$ ..... (7.33)

$s_1 = C_1 . \ell_2$

$s_2 = C_2 / A_2$

and C_1 and C_2 are the coefficients of equation (7.6).

The partial derivatives of the $F_2(\phi_1, \phi_2)$ function takes the form

$$f_1(\phi_1, \phi_2) = \frac{\partial F_2}{\partial \phi_2} = R_g + s_1 . s_2 \cosh(s_2 \phi_2) + r_1 r_2 \cosh(r_2 \phi_1) \cosh(r_2 \phi_2)$$

..... (7.34)

$$f_2(\phi_1, \phi_2) = \frac{\partial F_2}{\partial \phi_1} = r_1 r_2 \sinh(r_2 \phi_1) \sinh(r_2 \phi_2) \qquad (7.35)$$

The minimum (constant) value of the secondary reluctance is calculated by

$$R_{m2min} = \left. \frac{\partial F_2}{\partial \phi_2} \right|_{\substack{\phi_1 = 0 \\ \phi_2 = 0}} = \left. \frac{F_2(\phi_1, \phi_2)}{\phi_2} \right|_{\substack{\phi_1 = 0 \\ \phi_2 = 0}} = R_g + s_1 . s_2 + r_1 . r_2$$

..... (7.36)

Substituting for s_1, s_2, r_1 and r_2 in equation (7.36), and noting that the product $C_1.C_2$ gives the initial reluctivity of the B/H curve, i.e.

$$C_1.C_2 = \frac{1}{\mu}$$

the minimum value of the secondary reluctance is obtained exactly as given by equation (4.51).

7.3.2 Tangent Function

Although the approximation in equation (7.3) does not satisfy all the requirements of Section 7.1.1, the form the $F_1(\phi_1, \phi_2)$ and $F_2(\phi_1, \phi_2)$ functions take when this approximation is employed gives an indication of the relationship between the physical structure of the core and the phase difference between the primary and secondary fluxes. The mmf functions are found to be

$$F_1(\phi_1, \phi_2) = R_g\,\phi_1 + p_1 \tan(p_2\,\phi_1) + r_1 \frac{[1 + \tan^2(r_2\,\phi_2)]\tan(r_2\,\phi_1)}{1 - \tan^2(r_2\,\phi_1).\tan^2(r_2\,\phi_2)} \quad \ldots\ldots \quad (7.37)$$

$$F_2(\phi_1, \phi_2) = R_g\,\phi_2 + s_1 \tan(s_2\,\phi_2) + r_1 \frac{[1 + \tan^2(r_2\,\phi_1)]\tan(r_2\,\phi_2)}{1 - \tan^2(r_1\,\phi_1).\tan^2(r_2\,\phi_2)} \qquad \ldots\ldots \quad (7.38)$$

where p_1, p_2, r_1, r_2, s_1 and s_2 are given in the same form as in equations (7.33), but where C_1 and C_2 are now the coefficients of equation (7.3). In fact, C_1 and C_2 are given by

$$C_1 = \frac{2}{\pi} B_s.S$$

$$C_2 = \frac{\pi}{2} \frac{1}{B_s} \qquad \ldots\ldots \quad (7.39)$$

where B_s is the saturation flux density and S is the initial slope of the magnetisation curve, as shown in Figure 7.2.

Since the flux density can never exceed B_s anywhere in the core, the following condition holds in the common magnetic region of the two-C-core device

$$\frac{\phi_1 \mp \phi_2}{2\,A_0} < B_s$$

This results in the condition that the denominator of equations

(7.37) and (7.38) should always be positive to ensure positive values of primary and secondary reluctances at all times, i.e.

$$|\tan (r_2 \phi_1).\tan (r_2 \phi_2)| < 1 \quad \ldots\ldots \qquad (7.40)$$

Assuming

$$\phi_1 = \phi_{1m} \sin z$$

$$\phi_2 = \phi_{2m} \sin(z - \sigma)$$

the condition (7.40) becomes

$$|\tan [\frac{\pi}{2} \frac{B_{1m}}{B_s} \sin z] .\tan[\frac{\pi}{2} \frac{B_{2m}}{B_s} \sin(z - \sigma)]| < 1 \text{ for all } z$$

$$\ldots\ldots \qquad (7.41)$$

where $B_{1m} = \frac{\phi_{1m}}{2A_0}$ and $B_{2m} = \frac{\phi_{2m}}{2A_0}$

In order for the condition (7.41) to hold for all z and for any given B_{1m} and B_{2m} (each $< B_s$), it follows that

$$\sigma = \mp \frac{\pi}{2}$$

which means that, during steady-state operation of the parametric

transformer, the phase difference between the primary and secondary fluxes is forced to be 90°. This situation has been qualitatively explained at the end of Section 3.2 in relation to Figures 3.19 and 3.20.

Some other analytical approximations for the B/H curve, such as equation (7.5), have also been applied and the explicit forms of the $F_1(\phi_1, \phi_2)$ and $F_2(\phi_1, \phi_2)$ functions obtained. However, they are not given here, since their forms have been found not to reveal any further information about the devices investigated, and since these functions, when evaluated numerically, will yield the same values whatever the form of the approximate expression for the B/H curve.

7.4 Application of Power-Series Approximation to Hollow Toroidal Core

In order to illustrate orthogonal flux interaction, the explicit expressions of the mmf functions for the hollow toroid core device will be given. Following a procedure similar to that of Appendix IV and with the approximation of equation (7.12) applied to equations (4.67) and (4.68), the mmf functions are obtained in the form

$$F_1(\phi_1, \phi_2) = \sum_{i=0}^{\infty} \sum_{j=0}^{\infty} p_{2(i+j)+1} \binom{i+j}{j} k^j \phi_2^{\,2j} \phi_1^{\,2i+1} \qquad \ldots\ldots \qquad (7.42)$$

$$F_2(\phi_1, \phi_2) = \sum_{i=0}^{\infty} \sum_{j=0}^{\infty} s_{2(i+j)+1} \binom{i+j}{j} \left(\frac{1}{k}\right)^j \phi_1^{\,2j} \phi_2^{\,2i+1} \qquad \ldots\ldots \quad (7.43)$$

where $k = \dfrac{A_1^{\,2}}{A_2^{\,2}}$

$$p_{2i+1} = \ell_1 \frac{C_{2i+1}}{A_1^{\,2i+1}} \qquad \ldots\ldots \quad (7.44)$$

$$s_{2i+1} = \ell_2 \frac{C_{2i+1}}{A_2^{\,2i+1}}$$

and $\binom{i+j}{i} = \dfrac{(i+j)!}{j!\ i!}$ (the binomial coefficients)

Comparing the form of equations (7.42) and (7.43) with the form of the third term in equations (7.14) and (7.15), it is seen that both parallel and orthogonal flux interaction result in similar mmf functions. However, a comparison of the coefficients of the product $\phi_1^{\,2j}.\phi_2^{\,2i+1}$ in equation (7.43) with those in equation (7.15) shows that parametric coupling is achieved more effectively in the case of parallel rather than orthogonal interaction of primary and secondary fluxes.

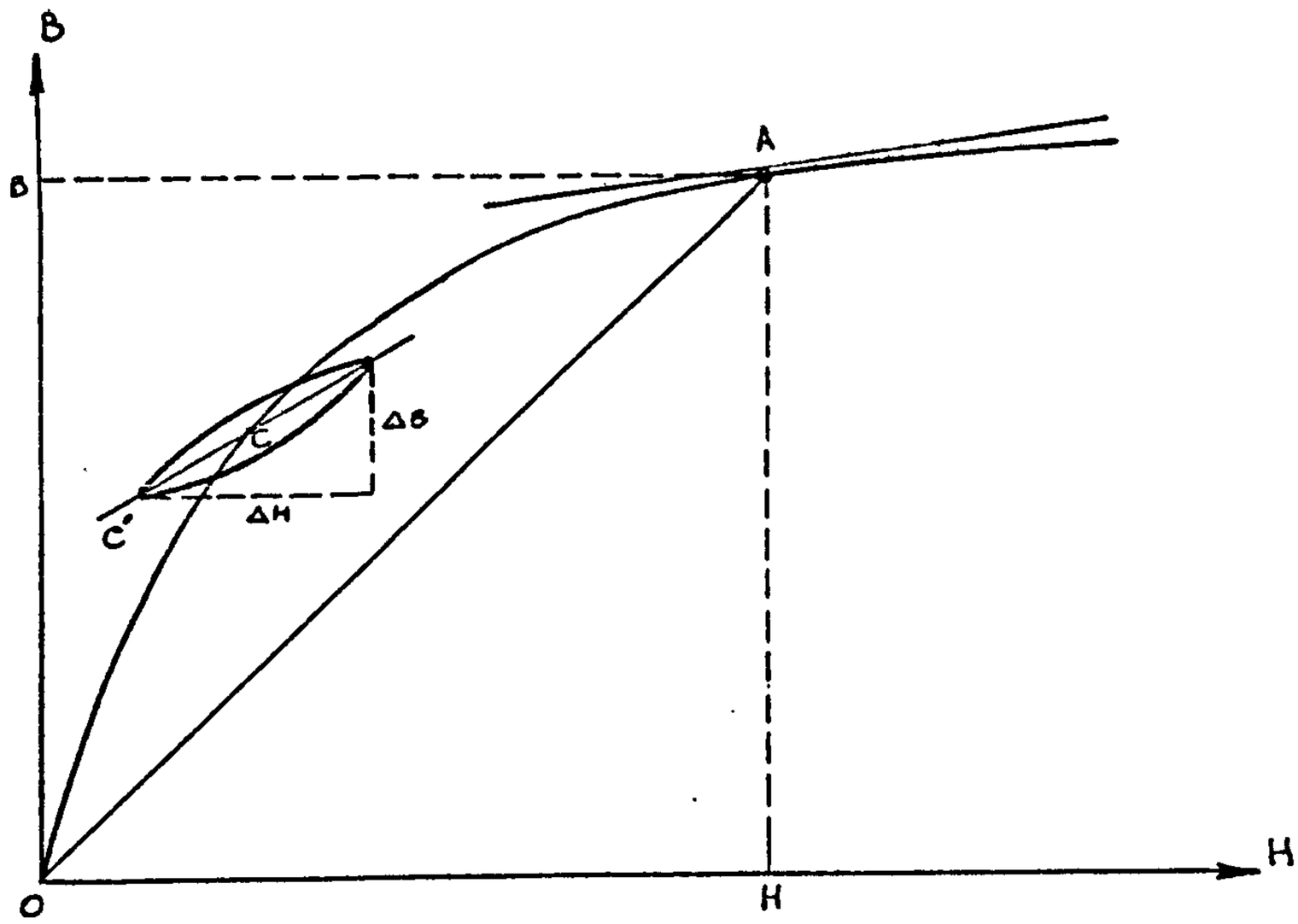

Figure 7.1 Illustrating definitions of non-incremental, differential and incremental permeability

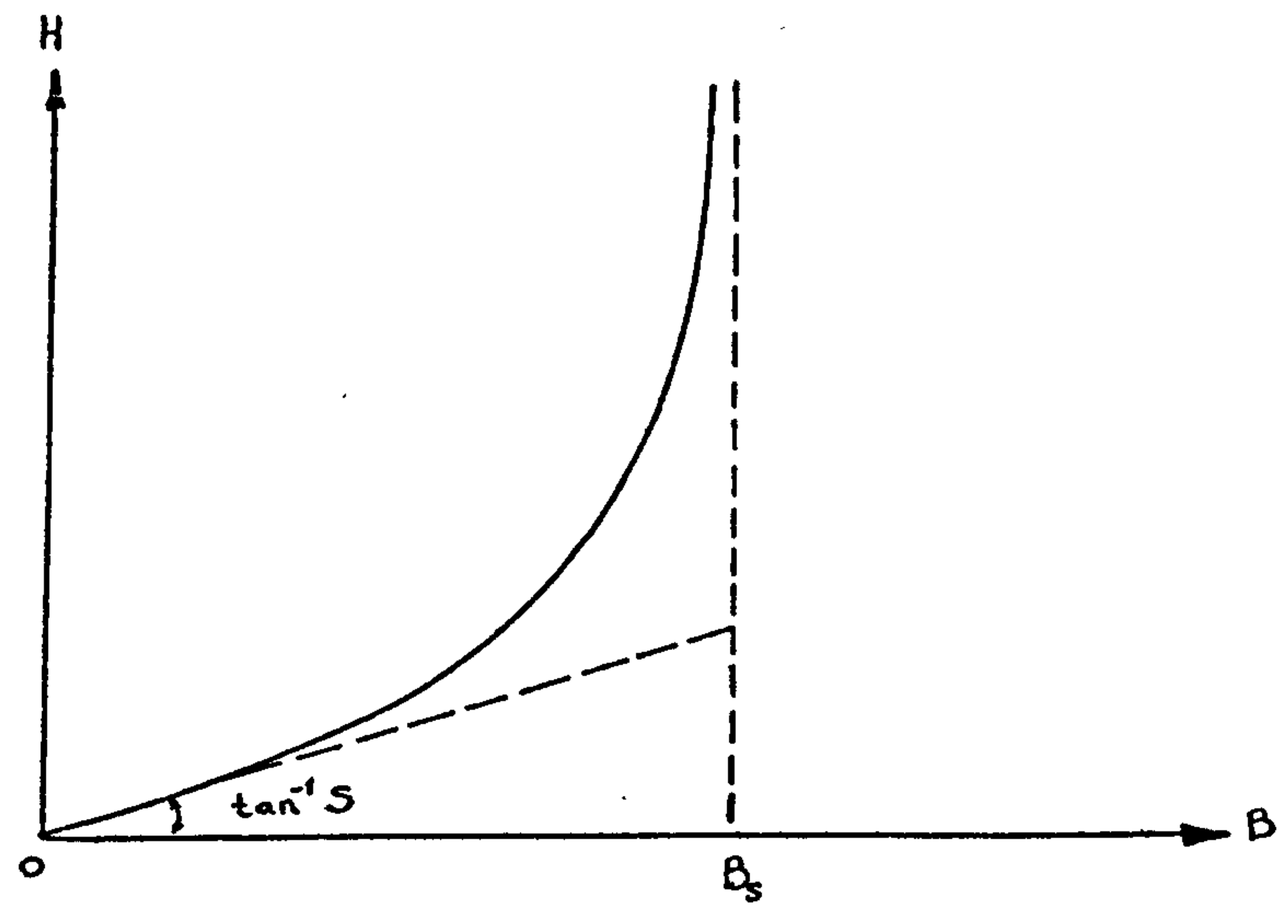

Figure 7.2 Tangent approximation, $H = \frac{2}{\pi} B_s . S . \tan\left(\frac{\pi}{2} \frac{B}{B_s}\right)$

CHAPTER VIII

DIGITAL COMPUTER SIMULATION

8.1 Curve Fitting to the Magnetisation Characteristic of the Core Material

When an approximate curve is fitted to the magnetisation characteristic of the core material, the overall accuracy of the approximation may be considered as satisfactory when the greatest error between the actual characteristic and the approximated characteristic is either:

a) below the accuracy of the metering with which the magnetisation characteristic is measured,

or

b) less than the variations that occur between samples of the same material.

In practice, it is not unusual to find that the magnetising force required to produce a given flux density varies by as much as 15% between samples of the same magnetic material. Because of this, (b) is the more stringent criterion for fitting an approximate equation to the magnetisation characteristic of the core material.

The material used in the C-cores of the parametric transformer is cold-rolled, grain-oriented silicon steel, with the data points for the magnetisation characteristic of such material obtained from reference 1, where the dc magnetisation curve and the hysteresis loops for ac excitation are given separately.

Since, in the parametric transformer, the cores are always ac excited, the magnetisation characteristic was taken as the curve passing through the tips of the hysteresis loops. When compared with the dc magnetisation curve, this provided slightly higher permeabilities below the knee of the curve and lower H values above the knee. The curvature around the origin was completely neglected, as none of the approximate equations to be used could take this into account.

Since the magnetisation characteristic is required in the form H=f(B), errors between the given data curve and the approximate curve are evaluated in the H sense, i.e. if for a given B, the magnetic field intensity is given as H by the data curve and as H' by the approximate curve, the absolute error is

$$\varepsilon = H' - H$$

as shown for two different points in Figure 8.1. Clearly, this absolute error may be quite large above the knee of the curve, although it is small for low values of B. If an approximate curve of the form of B=f(H) is fitted to the magnetisation characteristic, the absolute error in the B sense, (i.e. $\varepsilon = B' - B$) would not vary so much, and the curve fitting process would be easier.

In order to judge the quality of the approximation, a criterion has to be established. The two most often used are:

1) The vertical distance between the data curve and the approximate curve must be as small as possible at all points.

2) The net area between the two curves should be as small as possible.

For the second criterion, a merit figure[2] is defined as the ratio of the area between the two curves to the area under the data curve, and this merit figure is minimized to obtain a good approximation. For the first criterion three different definitions can be made:

a) The sum of the magnitudes of the errors between points of the data curve and corresponding points calculated by the approximate equation is minimised, i.e.

$$\sum_{i=1}^{n} |H_i' - H_i| \text{ is a minimum.}$$

b) The sum of the squares of the magnitudes of the same errors is minimised, i.e.

$$\sum_{i=1}^{n} (H_i' - H_i)^2 \text{ is a minimum.}$$

c) The maximum error is minimised, i.e.

$$\text{MAX } (H_i' - H_i) \text{ is a minimum.}$$

Of the three definitions (b) is chosen, because it is both the easiest to handle mathematically and provides a good compromise between (a) and (c). With this choice, the well-known least squares method[3-5] can be easily applied to the curve fitting problem. The error function to be minimised is

$$\varepsilon = \sum_{i=1}^{n} [f(B_i, c_1, c_2, \ldots, c_p) - H_i]^2 \quad \ldots. \quad (8.1)$$

where $f(B, c_1, c_2, \ldots c_p)$ is the approximate function with its coefficients as variables, and (B_i, H_i) are the coordinates of the ith data point. The minimum value of ε of equation (8.1) is found by equating the differentials $\frac{\partial\varepsilon}{\partial c_1}, \frac{\partial\varepsilon}{\partial c_2}, \ldots., \frac{\partial\varepsilon}{\partial c_p}$ to zero, and solving the resulting p equations for the p parameters $c_1, c_2, \ldots, c_p$. However, the equations obtained are non-linear, and are therefore not easily solved analytically. Numerical techniques such as the least squares method, are therefore applied to find the solution of a set of non-linear equations with variables $c_1, c_2, \ldots c_p$. Although the first-order derivatives of ε are normally required for the minimization process, numerical methods such as Peckham's[6] and Powell's[7], have been developed to find a least squares solution of a set of non-linear equations, without calculating the gradients.

8.1.1 The Method and Computer Program

For computer fitting of the magnetisation characteristic, Peckham's method was used to calculate the parameters of the approximate functions reviewed in Section 7.1.2. The power series approximation of equation (7.12), the hyperbolic sine approximation of equation (7.7), and the tangent approximation of equation (7.3), (although this has a valid range for B restricted to $\mp B_s$), were taken as suitable forms for the analytical representation of the B/H curve. The NAG (Numeric Algorithms Group) Library subroutine E04FAF, based on Peckham's method, was used to determine the parameters c, by non-linear regression starting from an externally supplied initial estimate of the minimum point.

E04FAF forms an approximation to a minimum of the sum of the squares of m residuals

$$F(\underline{X}) = \sum_{i=1}^{m} R_i(\underline{X})^2$$

where $\underline{X} = (x_1, x_2, \ldots, x_n)^T$ and $m \geqslant n$, by approximating the residuals $\underline{R}(\underline{X})$ (underlining denotes vectors) at the point $\underline{X}$ by a linear form $\underline{R} \simeq \underline{h} + J\,\underline{X}$, where $\underline{h}$ is a constant vector and J is the Jacobian matrix $J_{ig} = (\partial R_i/\partial X_g)$ calculated at X. Thus, an estimate of the minimum of the sum of squares was given by $\underline{Y}$, the solution of the equation

$$J^T J\,\underline{Y} = -J^T \underline{h} \qquad \cdots\cdots (8.2)$$

From the initial estimate of the minimum point, a set of at least n+1 points, $\underline{Xi}$ was generated and the corresponding residuals $\underline{Ri}$ were calculated. Considering the sum of the squares of the difference between the linear approximation and the actual residual values, formulae estimating the coefficients of the linear approximation (i.e. J and $\underline{h}$ in equation (8.2)) were obtained in terms of $\underline{Ri}$ and $\underline{Xi}$. These formulae were used in the matrix equation (8.2) to provide a set of functions $\underline{Y}$, in terms of the known quantities $\underline{Xi}$ and $\underline{Ri}$, which were then solved using orthogonal transformations. One iteration consisted of replacing that point of the current point set which had the largest sum of squares by the estimated solution of the previous iteration, and solving the set of equations derived from this new set to obtain a new estimate of the solution.

If $\underline{X}$ contained the best point obtained for one iteration and $\underline{Y}$ contained the best point for the following iteration, then the routine terminated with the current best point as the solution; that is the convergence criterion

$$|\underline{Xi} - \underline{Yi}| < \alpha$$

where α is a real scalar set initially for a required accuracy, was satisfied for two successive iterations.

From the final least squares estimate of the parameters X, the values of the approximate function $H_i' = f(B_i, \underline{X})$ and of the residuals $Ri = f(B_i, \underline{X}) - H_i$ were calculated at each data point.

The block diagram of the computing process is shown in Figure 8.2, and the listing of the program to fit the hyperbolic sine approximation to the magnetisation curve is given in Appendix V. The fitted curves of different approximations are plotted, together with the magnetisation characteristic of the core material, in Figures 8.3 to 8.10, where the explicit expressions and the values of the coefficients are also given. In all these figures, curves 1 are the actual magnetisation characteristic and curves 2 are the fitted curves produced by the approximate expression used.

8.1.2 Discussion of Results

The flexibility of the expression used to represent a given graphical form is an important factor in the curve-fitting process, since the range for which the approximation must be valid is $-\infty < H < +\infty$. Apart from the overall accuracy of the approximation, a main concern is the accurate representation of the characteristic features of the magnetisation curve, such as the initial slope around the origin, the saturation flux level etc. For this purpose, it is necessary to use the least squares method although this results in higher levels of absolute error at the data points above the knee of the curve. This is due both to the specific form of the magnetisation curve and to the ability of the approximate expression to represent this graphical form. Minimizing the maximum error, (definition C in Section 8.1) would yield a

better overall accuracy, but the characteristic features of the actual curve would not be preserved in the approximate curve fitted.

Minimizing the sum of the squares of the absolute errors, at each point, results in a better fit above the knee, since the errors here are much larger than those in the linear portion below the knee. Using, for the minimisation process, the relative error $\left(\frac{H_i' - H_i}{H_i}\right)$ at each point, rather than the absolute errors, yields a better accuracy at the linear portion but poor accuracy above the knee of the curve. This is obvious since the relative errors tend to increase as $H_i \to 0$. For these reasons, the weighted errors

$$[f(B_i) - H_i] \cdot W(B_i)$$

where $W(B_i)$ is the weighting function, are used to bring additional flexibility to the curve-fitting process. To accomplish this, a weighting factor which multiplies the absolute error at a particular data point, is assigned to each such point and the sum of the squares of the weighted errors is minimised.

To obtain a good overall fit and to be able to alter the weighting factors as required by the flexibility of the approximate expression used, the curve-fitting program had to be re-run several times for each expression, with the final estimates of the parameters obtained in one trial run taken as

the initial estimates in the following run. The final approximation attained therefore also depended on the choice of the weighting factors. Rather than obtaining the best approximation (i.e. the one with a minimum sum of the squares of the errors), these were chosen to provide an approximate curve which best displayed the specific features of the actual magnetisation characteristic, such as the initial slope and the saturation flux density.

The influence of the weighting factors on the shape of the approximate curve is illustrated in Figures 8.3 to 8.5, for the tangent approximation. Without any weighting factors, the process yields an approximate curve which fits precisely at the saturated region, but not at the linear region, as shown in Figure 8.3. Increasing the weighting for small values of B results in the curve shown in Figure 8.4, where the precise fit is now in the linear region. With a suitable choice of the weighting factors, the curve obtained after a few runs of the program and shown in Figure 8.5 established a good compromise between the previous curves.

It was also found that the hyperbolic-sine approximation of the form of equation (7.6) did not give a precise fit, if the actual characteristic had to be represented reasonably well in the linear region. Therefore, the expression in equation (7.7) was used, and the approximate curve obtained is shown in Figure 8.6..

With a limited number of terms in the power-series approximation, the problem was considered as fitting a polynomial to a given set of data points. For this purpose, numerical methods using orthogonal polynomials such as Forsythe's method[8], were developed, and the subroutines E02ABF, E02ACF, E02ADF etc. based on these methods are available in the NAG Library. However, they did not permit external control on the form of the polynomial to be fitted. Only the degree of the polynomial can be specified externally, and the polynomial contains both even and odd power terms. The magnetisation curve was approximated by using these algorithms, but the results were not suitable for accurate representation of the specific features of the curve, and the approximate curves were obtained in the form shown in Figure 8.11. This was due to the nature of the methods[4] using orthogonal polynomials such as Legendre polynomials, Chebyshev polynomials etc. which resulted in an oscillation property in the error function, similar to that encountered in the minimax type approximation.[3] Therefore, the least squares method employed in the subroutine E04FAF had to be used also for the power series approximation.

A polynomial including odd power terms only up to the 15th was first considered. It was found possible for the process to result in negative values of C_1 and C_{15} in

$$H = C_1 B + C_3 B^3 + \ldots + C_{15} B^{15} \quad \ldots\ldots \quad (8.3)$$

although the error function was still a minimum. Such an approximation is valid only within the interval in which the minimisation process is applied, and it therefore contradicts requirement 4 of Section 7.1.1. This led to the transformation of variables

$$C_1 = (X_1)^2$$

$$\ldots\ldots \qquad (8.4)$$

$$C_{15} = (X_{15})^2$$

and instead of C_1 .... C_{15}, X_1 to X_{15} were taken as the parameters to be determined by the minimisation process. The result is shown in Figure 8.7 which displays a precise overall fit between the two curves.

The repetitive use of a polynomial containing all the (odd) power terms up to a specified number would be too time-consuming when solving the system equations by computer, and a compromise has to be made between accuracy and computational time. Simple polynomials with only two or three terms were given consideration, but investigation was necessary to find which particular terms need to be included for a sufficiently accurate representation (especially of the curvature at the knee). The subroutine E04FAF was found to be unable to fit the polynomial

$$H = C_1 B + C_2 B^n \qquad \ldots\ldots \qquad (8.5)$$

when the power n was also taken as a parameter, since the set of non-linear equations first linearized and then solved by the algorithm became exponential, when the method became unapplicable. Consequently, the process was repeated with different (integer) values of n, and it was found that the approximate expression yielded the best representation for $n = 11$. The result is given in Figure 8.8. Greater values of n produced curves with a sharper knee, as shown for $n = 15$ in Figure 8.9. Another good approximation was obtained with the polynomial containing three terms,

$$H = C_1 B + C_3 B^3 + C_9 B^9 \qquad \ldots\ldots \qquad (8.6)$$

and the result is given in Figure 8.10.

Since solving the differential equations of the parametric transformer required the evaluation of the B/H curve many times for only a single step, the best yet the simplest approximation was required. The obvious choice was the polynomial

$$H = C_1 B + C_{11} B^{11} \qquad \ldots\ldots \qquad (8.7)$$

with the parameter values as given in Figure 8.8, and this expression was used in the rest of the computer simulation work, wherever the power-series approximation was applied.

8.2 Numerical Computation of Various System Functions

Since the analytical expression of the function $H = f(B)$ is now known, numerical evaluation of the $F_1(\phi_1, \phi_2)$ and $F_2(\phi_1, \phi_2)$ functions is possible if the values of A_1, ℓ_1, A_2, ℓ_2, A_0 and ℓ_0 are given. As will be seen in the next Chapter, an experimental parametric transformer was designed and constructed, on the basis of the bridged core being equivalent to the two-C-core construction. The physical dimensions and other data for the equivalent bridged core are given in Appendix VI.

With the analytical expression of the B/H curve given by equation (8.7), the explicit expressions for the $F_1(\phi_1, \phi_2)$ and $F_2(\phi_1, \phi_2)$ functions are

$$F_1(\phi_1, \phi_2) = (R_g + p_1 + r_1 + 11\, r_{11}\, \phi_2^{10})\, \phi_1 + 165\, r_{11}\, \phi_2^{8}\, \phi_1^{3} +$$

$$+ 462\, r_{11}\, \phi_2^{6}\, \phi_1^{5} + 330\, r_{11}\, \phi_2^{4}\, \phi_1^{7} + 55\, r_{11}\, \phi_2^{2}\, \phi_1^{9} +$$

$$+ (p_{11} + r_{11})\, \phi_1^{11} \qquad \ldots\ldots \quad (8.8)$$

$$F_2(\phi_1, \phi_2) = (R_g + s_1 + r_1 + 11\, r_{11}\, \phi_1^{10})\, \phi_2 + 165\, r_{11}\, \phi_1^{8}\, \phi_2^{3} +$$

$$+ 462\, r_{11} \phi_1^{6}\, \phi_2^{5} + 330\, r_{11}\, \phi_1^{4}\, \phi_2^{7} + 55\, r_{11}\, \phi_1^{2}\, \phi_2^{9} +$$

$$+ (s_{11} + r_{11})\, \phi_2^{11} \qquad \ldots\ldots \qquad (8.9)$$

where $p_1 = c_1 . \ell_1 / A_1$

$$p_{11} = c_{11} . \ell_1 / A_1^{11}$$

$$s_1 = c_1 . \ell_2 / A_2 \qquad \ldots\ldots \qquad (8.10)$$

$$s_{11} = c_{11} . \ell_2 / A_2^{11}$$

$$r_1 = c_1 . \ell_0 / 2A_0$$

and $r_{11} = c_{11} . \ell_0 / (2A_0)^{11}$

All the coefficients above are readily calculable from the data in Appendix VI, although the air-gap reluctance R_g $(= \ell_g / \mu_0 . A_0)$ in equations (8.8) and (8.9) is not yet known. Since the air gaps are unintentional and very small, the air-gap length ℓ_g cannot be measured from the physical device, although

an estimate can be made. Initially, the ratio of the air-gap length to the total length of the closed flux-path of the secondary magnetic circuit (or the primary magnetic circuit since $\ell_1 = \ell_2$ because of the symmetry), i.e.

$$\frac{\ell_g}{\ell_2 + \ell_0}$$

was estimated as approximately 0.02%.* The air-gap length was then calculated as $\ell_g = 5.10^{-5}$m.

In order to check the accuracy of this estimation, the experimental and the theoretical V/I characteristics of the secondary circuit (or the primary circuit because of complete symmetry) were compared. With the primary winding open-circuited the experimental V/I characteristic of the secondary winding was obtained as given by curve 1 in Figure 8.12. The theoretical characteristic was calculated by neglecting the winding resistance, when the acv source of effective value V_{2rms} creates a secondary flux

$$\phi_2 = \phi_{2m} \sin \omega t \qquad \ldots\ldots \quad (8.11)$$

This ratio can normally be taken as 0.01% when air-gaps are avoided. However, twice this value was taken because of the use of unmatched C cores, and their axes being in right angle.

where

$$\phi_{2m} = \frac{\sqrt{2}\ V_{2rms}}{N_2\ \omega} \qquad \ldots\ldots \qquad (8.13)$$

with $\phi_1 = 0$, the function $F_2(\phi_1, \phi_2)$ becomes

$$F_2 = F_2(\phi_2) \qquad \ldots\ldots \qquad (8.13)$$

It must be noted that equation (8.13) provides the relationship between the *instantaneous* values of the secondary flux and mmf. By increasing $z = \omega t$ in equation (8.11) at equal increments from 0 to π (since a half period is sufficient to calculate the rms values), instantaneous values of F_2 and $i_2 = F_2/N_2$ are calculated at each instant. Then, using numerical integration based on the rectangle rule, the rms value of the resulting secondary current waveform can be found. The computer program for this is given in Appendix VII, where Subroutine TEZ calculates the instantaneous values of the primary and the secondary mmf's, F_1 and F_2, for given values of the primary and the secondary fluxes (Z(1) and Z(2) in the program).

When determining the theoretical characteristic, leakage flux as well as winding resistance was neglected. Although the effects of the leakage flux could be accounted for in practice by some reduction in N_1 and N_2 from their actual values on the experimental unit, this has not been done, since the way N_1 and N_2

enter into the system equations is far less simple than in a conventional transformer.

It is seen from Figure 8.12 that the theoretical V/I characteristic gives higher values of the secondary current in the linear region but lower values in the saturated region. To fit the linear portions of the theoretical and experimental characteristics, the value of ℓ_g was re-chosen as $\ell_g = 3.10^{-5}$m which resulted in the precise fit shown in Figure 8.13. The differences between the two curves in the saturated region arise from the approximate B/H characteristic used in the calculations, since the magnetisation data of the core material was taken from reference 1 (as explained in Section 8.1) and was not actually measured from the experimental unit. To remove this difference, the value of the coefficient c_{11} in equation (8.7) was adjusted, and, when

$$c_{11} = 0.590113 \qquad \ldots\ldots \quad (8.14)$$

the theoretical and the experimental V/I characteristics fitted precisely in the range used, as shown in Figure 8.14.

Numerical values of all the constants in equations (8.8) and (8.9) are now known, and F_1 and F_2 can be calculated for given values of ϕ_1 and ϕ_2. Using Subroutine TEZ in a simple computer program, the function $F_1(\phi_1, \phi_2)$ was plotted in Figure 8.15, where ϕ_2, taken as a parameter, was incremented by $\Delta\phi_2 = 0.25.10^{-3}$ Wb to illustrate the dependence of F_1 on ϕ_2.

In this figure, curve 1 represents the function $F_1(\phi_1, \phi_2)\big|_{\phi_2=0}$, curve 2 the function $F_1(\phi_1, \phi_2)\big|_{\phi_2=\Delta\phi_2}$, ..., curve 9 the function $F_1(\phi_1, \phi_2)\big|_{\phi_2=8\Delta\phi_2}$ and so on. Similarly, the function $F_2(\phi_1, \phi_2)$ was plotted with the same increments of ϕ_1, and is given in Figure 8.16. These two figures are the exact numerical versions of Figures 6.3 and 6.4, but only in the first quadrant. Figure 8.17 shows in more detail the portions of the curves for $F_2(\phi_1, \phi_2)$ near the origin, and covers the area indicated in Figure 8.16. Corresponding to Figure 6.6a, this figure illustrates how the initial slope is affected by ϕ_1. It is clear that ϕ_1 must attain a value as high as $1.5\ 10^{-3}$ Wb for curve 7, before variations can occur in the initial slope.

Considering the non-incremental reluctance functions

$$R_{m1}(\phi_1, \phi_2) = \frac{F_1(\phi_1, \phi_2)}{\phi_1} \qquad \text{.....} \quad (8.15)$$

and

$$R_{m2}(\phi_1, \phi_2) = \frac{F_2(\phi_1, \phi_2)}{\phi_2}$$

as defined in Section 7.2.1., their graphical representations are given by Figures 8.18 and 8.19 respectively. The increments given to ϕ_1 or ϕ_2 when considered as a parameter were $0.25\ 10^{-3}$ Wb, as before, i.e. curve 1 in Figure 8.18 corresponds to $\phi_2 = 0$,

curve 2 to $\phi_2 = 0.25\ 10^{-3}$ Wb etc. The families of curves in these figures were first derived qualitatively in Section 6.1.1.

The trans-reluctance characteristic for the secondary circuit

$$R_{m2}(\phi_1) = \left.\frac{F_2(\phi_1, \phi_2)}{\phi_2}\right|_{\phi_2 \to 0}$$

is obtained from equation (8.9) as

$$R_{m2}(\phi_1) = R_g + s_1 + r_1 + 11\ r_{11}\ \phi_1^{10} \quad \ldots\ldots \quad (8.16)$$

and is plotted in Figure 8.20 together with the primary trans-reluctance characteristic

$$R_{m1}(\phi_2) = R_g + p_1 + r_1 + 11\ r_{11}\ \phi_2^{10} \quad \ldots\ldots \quad (8.17)$$

These two curves, assumed qualitatively in sections 2.1.1 and 3.1.5, play an important role in explaining parametric trans-former operation, especially with their constant part resulting in the under-voltage protection property.

The secondary inductance is calculated from

$$L_2 = \frac{N_2^{\ 2}}{R_{m2}} \quad \ldots\ldots \quad (8.18)$$

and when equation (8.16) is substituted for R_{m2}, the secondary inductance is obtained as a function of the primary flux

$$L_2 = L_2(\phi_1) \qquad \ldots\ldots \qquad (8.19)$$

Since the primary current can be calculated from

$$i_1 = \frac{F_1(\phi_1, \phi_2)}{N_1}\Big|_{\phi_2 = 0}$$

for given values of ϕ_1, changing the independent variable in equation (8.19) accordingly results in

$$L_2 = L_2(i_1) \qquad \ldots\ldots \qquad (8.20)$$

which gives the trans-inductance characteristic of the secondary circuit, in the sense used by Wanlass (see Section 2.1.1 and Figure 2.4). The function in equation (8.20) was plotted by computer as in Figure 8.21, where a constant portion is clearly seen before the secondary inductance falls to small values with increasing primary current.

To demonstrate the double-frequency variation in the secondary reluctance and to investigate the best sinusoidal waveform of this variation, the curves of Figure 8.22 were plotted. This figure corresponds to Figure 2.2 explaining the reluctance modulation. The supply voltage creates the primary

flux

$$\phi_1 = \frac{V_{1rms}\sqrt{2}}{N_1.\omega} \sin \omega t \qquad \ldots\ldots \quad (8.21)$$

and when equation (8.21) is substituted in equation (8.16), the waveform of the secondary reluctance variation can be obtained by varying $z = \omega t$ from 0 to 2π as in Figure 8.22, where curve 1 corresponds to V_{1rms} = 160 V, curve 2 to V_{1rms} = 180 V, curve 3 to V_{1rms} = 200 V and so on. Evidently, no variations occur in the secondary reluctance before the supply voltage reaches a certain amplitude. Figure 8.23 shows the variations in the secondary circuit inductance for the same values of V_{1rms}, and is obtained by calculating the inductance values at each instant from R_{m_2} and equation (8.18).

Finally, the relative magnetisation characteristics of the primary and secondary circuits were plotted as in Figures 8.24 and 8.25. The curve numbered 1 in Figure 8.24 is the same as curve 1 in Figure 8.15, and is the locus of the end-points of the primary relative magnetisation characteristics. The same is also true for curve 1 in Figure 8.25, which corresponds to curve 1 in Figure 8.16.

When deriving the relative magnetisation characteristics, the value of the primary flux at each instant was calculated from equation (8.21) for different values of V_{1rms}. The corresponding secondary flux value was found from equations (6.12) and

(6.13). Using Subroutine TEZ, the primary and the secondary mmf's were then determined for given instantaneous values of the primary and the secondary fluxes, by varying z from 0 to $\pi/2$. The same numbered curves in Figures 8.24 and 8.25 constitute pairs, corresponding to the same value of V_{1rms} so that the pair of curves numbered 2 are for V_{1rms} = 50 V, the pair numbered 3 for V_{1rms} = 100 V, and so on up to the pair numbered 7 which are for V_{1rms} = 300 V. It is noticeable from Figure 8.25 that the secondary relative magnetisation characteristic may be considered almost linear, when V_{1rms} is such that this characteristic is near curve 3 in the figure. It may also be deduced from Figure 8.24 that, for an almost linear primary relative magnetisation characteristic, the value of V_{1rms} must exceed that corresponding to curve 7 in the figure.

When calculating the secondary flux amplitude from equation (6.13), the saturation flux level ϕ_s was determined in the following manner: it was assumed that, in the bridge branches of the magnetic model (where the highest flux density occurs), the core material is fully saturated for a flux density of B_{0max} = 2.5 T. The maximum flux level in either of the magnetic circuits is then

$$\phi_s = 2 A_0 B_{0max} \qquad \text{.....} \quad (8.22)$$

Since there is no cubic term in equation (8.7), the $F_2(\phi_1, \phi_2)$ function in equation (8.9) does not contain the terms in s_3 and r_3, which were defined first by equations (6.17). However, A^2 $(= \frac{s_3 + r_3}{s_3})$ in equation (6.13) can still be calculated, as the coefficient c_3 from the power-series expansion of the B/H curve cancels out when the expressions for s_3 and r_3 are entered.

The relative magnetisation characteristics of Figures 8.24 and 8.25, although plotted by computer calculating exact numerical values, must be regarded in a qualitative basis for the reasons stated at the end of Section 6.3.

8.3 Numerical Solution of the Differential Equations

8.3.1 The Equations to be Solved

The explicit expressions of the differential equations to be solved by computer are obtained when equations (8.8) and (8.9) are substituted in equations (5.8) and (5.9). As required by the differential equation of the secondary circuit, the function in equation (8.9) is differentiated with respect to z, and the functions $f_1(\phi_1, \phi_2)$ and $f_2(\phi_1, \phi_2)$ as defined by equations (5.13), are obtained as

$$f_1(\phi_1, \phi_2) = \frac{\partial F_2}{\partial \phi_2} = (R_g + s_1 + r_1 + 11\, r_{11}\, \phi_1^{10}) + 3\, \phi_2^{2}\, (165\, r_{11}\, \phi_1^{8})$$

$$+ 5\, \phi_2^{4}\, (462\, r_{11}\, \phi_1^{6}) + 7\, \phi_2^{5}\, (330\, r_{11}\, \phi_1^{4}) + 9\, \phi_2^{8}\, (55\, r_{11}\, \phi_1^{2})$$

$$+ 11\, \phi_2^{10}\, (s_{11} + r_{11}) \qquad \ldots\ldots \quad (8.23)$$

$$f_2(\phi_1, \phi_2) = \frac{\partial F_2}{\partial \phi_1} = 10\, \phi_1^{9}\, (11\, r_{11}\, \phi_2) + 8\, \phi_1^{7}\, (165\, r_{11}\, \phi_2^{3}) + 6\, \phi_1^{5}$$

$$(462\, r_{11}\, \phi_2^{5}) + 4\, \phi_1^{3}\, (330\, r_{11}\, \phi_2^{7}) + 2\, \phi_1\, (55\, r_{11}\, \phi_2^{9})$$

$$\ldots\ldots \quad (8.24)$$

The differential equations may then be written in the normal form given by equation (5.17) and derived from the equivalent circuit of Figure 5.8, with leakage fluxes and core loss neglected and a load power factor of unity.

8.3.2 Review of Basic Numerical Methods

The purpose of a numerical method is to obtain an approximate solution of a differential equation. If a system of differential equations is given by

$$\frac{d\,y_i}{dx} = y_i' = f_i\,(x,\ y_1\,(x),\ y_2\,(x),\ \ldots,\ y_n\,(x)\,) \qquad (8.25)$$

$$(i = 1,\ 2\ \ldots.\ n)$$

with the initial conditions

$$y_i\,(x_0) = y_{i0} \qquad \ldots\ldots \qquad (8.26)$$

a numerical solution gives the values

$$y_i\,(x_0 + h)$$

where h is an arbitrary but usually small increment of the independent variable x.

Many numerical methods start by replacing the differential system by an approximate algebraic system. At a given step, a truncation error is introduced in the numerical integration process, usually by the replacement of an infinite process by an approximate series expansion with only a finite number of terms. This is known as the per-step truncation error. The cumulative error of the small per-step truncation errors and their magnification in calculating subsequent steps may lead to serious total errors in the final solution. The per-step truncation error is a function of the step size h, and obviously the only means of reducing this and its associated error is by reducing h.

Round off error or the error which results from replacing a number having more than n digits by a number of only n digits, arises because of the limited digital capacity of computers when fractions are transformed to non-terminating decimals. The per-step round off error is therefore independent of the step size, and when only a small number of equations are solved, the round off error is small and does not usually substantially affect the accuracy of the result. However, if many equations are solved simultaneously, the cumulative effect of round off errors may introduce relatively large errors. At the same time, when the method used is unstable and the integration therefore involves a large number of steps, the cumulative effect of round off errors and their magnification in calculating subsequent steps leads to serious total errors. Hence, a large

step length is desirable to minimise round off errors.

Stability of a numerical method is associated with the way in which the total errors introduced per step are propagated in later steps. A numerical solution is unstable when, as the computation progresses, the numerical values deviate more and more from the true solution. The instability of the numerical method is different from the instability of the differential system which produces unstable solutions growing in magnitude as a result of the nature of the system. The latter is called *inherent* instability and is analogous to ill-conditioning of the problem. Although the differential system may be quite well-behaved, the particular numerical method in use may be unstable and the deviation itself from the true solution becomes large. This is called *absolute* instability and, if the ratio of the deviation to the true solution becomes large, the numerical method is then said to be *relatively* unstable.

The differential equations may sometimes introduce spurious solutions, which although normally decreasing and tending to vanish as $h \to 0$, can, under some circumstances, increase faster than any solution of the differential equation. This is called *strong* instability and implies lack of convergence as well as lack of instability. If the solution converges but the asymptotic behaviour of the spurious solutions upsets the true solution, and causes instability, the phenomenon is called *weak* instability. These instabilities may be introduced at any step length and cannot be controlled by reducing the step length.

In some cases, the numerical method is stable only below some limiting value of step size. This is called *partial* instability and applies only for a particular combination of numerical method, differential equation and step-size.

Numerical methods to generate a unique solution over a range of x for a differential equation may be categorized into three groups:

i) Methods which use derivatives

The Taylor's series expansion of the function y(x) about a point $x = x_i$ provides a fundamental method of this type. The solution at the next point x_{i+1} is then given by

$$y_{i+1} = y\,(x_i + h) = y_i + h\,y_i' + \frac{h^2}{2!}\,y_i'' + \ldots \qquad (8.27)$$

and using the initial value y_i at $x = x_i$, the solution and its relevant derivatives at the next point $x_{i+1} = x_i + h$ are calculated. Taking this point as a new origin, the process is repeated until the whole range is covered.

Although this method is self-starting and, when enough derivatives are calculated, avoids truncation errors, it is of little practical value since the computation of higher derivatives is generally very difficult.

ii) Finite difference methods.

These basically use Adams-Bashforth predictor-corrector equations, with the solution effectively obtained by an iterative process. At the beginning of the computation, several early values are calculated by a Taylor series, since there are no differences available. Again, although this method attempts to avoid any truncation error, the necessity for extrapolation and subsequent correction, and also for differencing many values and the examination of these differences, make its practical use rather difficult.

iii) Lagrangian methods.

These are essentially variations of truncated versions of derivative and finite difference methods. Basically, they may be divided into two groups:

a) Runge-Kutta Methods (Euler, fourth order Runge-Kutta, etc).
   These are called one-step methods, as they use information only from the ith point to calculate the new values at the (i+1)th point.

b) Predictor-corrector methods (Milne, Hammings etc).
   These are called multi-step methods, as they use information from the ith, (i-1)th and (i-2)th points to calculate the new values at the (i+1)th point.

The advantages and disadvantages of each method may be summarized as follows:

Runge-Kutta Methods:

Advantages
a) Since they do not use information from previously calculated points, they are self-starting.
b) Being self-starting, they permit easy change of step-length.

Disadvantages
a) They require several evaluations of the system functions during each step, and are therefore slow and time consuming.
b) Generally, they provide no information about the local truncation error (although the Runge-Kutta-Merson method does).

Predictor-Corrector Methods:

Advantages
a) As they require fewer evaluations of the system functions per step, they are significantly faster.
b) The estimate of truncation error is obtained as a by product of the calculation.

Disadvantages
a) They are not self-starting and therefore require a starting method.
b) Changing the step-length is difficult and involves restarting using Runge-Kutta formula.

8.3.3 The Choice of Method

In order to choose the best method to solve the system of differential equations defined in Section 8.3.1, a number of factors have to be considered, including: (a) the accuracy required, (b) the ease with which the error at each step may be estimated, (c) the ease of starting the computation, (d) the ease of changing the interval between steps, (e) the speed with which the computation is performed.

Much consideration must be given to the stability of the method to be used, since the system of differential equations to be solved exhibits inherent instability due to the nature of the self-excited parametric oscillations. Any kind of instability due to the numerical method must be avoided, since it is not possible to predict the stability of the physical system without actually solving the differential equations. Obviously, it is absolutely necessary to know what causes any instability in the solution, in order to discriminate any inherent instability from those associated with error propagation, spurious solutions, partial instability etc.

For Runge-Kutta methods, it has been demonstrated that instability due to spurious solutions is not present. Apart from the inherent instability, the instability in these methods is due mainly to partial instability, which can be controlled by step-length variation. On the other hand, the predictor-corrector methods show strong instabilities through the introduction of spurious solutions. Considering all the factors

involved, it was decided that as a method of analysing the transient response of a system whose nature (i.e. the initial conditions, the values of parameters, the existence of self-excited oscillations etc) may be changing frequently, a Runge-Kutta method, although relatively slow, is the most suitable.

The fourth-order Runge-Kutta method is a popular one, and it has a truncation error proportional to h^5. Although the calculation of truncation error in this method is very difficult, formulae produced by Merson give an estimate of the local truncation error. The choice of step-size is also important to enable the method to be stable and to achieve high accuracy. Because of the relationship between the local round off and truncation errors and the step-size, the total error can be kept to a minimum only by maintaining the per-step truncation error within some appropriate bounds. The Runge-Kutta-Merson method achieves this by reducing the step-length if partial instability occurs and the accuracy departs from the defined limit.

8.3.4 The Computer Program

A computer subprogram (NAG Library subroutine D02ABF) which advanced the solution of a set of ordinary differential equations, equation (8.25), from x to x+h, using a number of steps of Merson's form of the Runge-Kutta method was used to solve the differential

equations described in Section 8.3.1. These equations were defined in the program by a subroutine "DERIV" which evaluated the derivatives G in terms of X (= ωt), Z(1) (= ϕ_1), Z(2) (= ϕ_2) and Z(3) (= $\frac{d\,Z(2)}{d\,X}$). The functions $F_1(\phi_1, \phi_2)$ (= MMF1), $F_2(\phi_1, \phi_2)$ (= MMF2), $f_1(\phi_1, \phi_2)$ (= FN1) and $f_2(\phi_1, \phi_2)$ (= FN2) were calculated for a given set of Z and X in the same subroutine, rather than in a different segment of the program, to minimise the execution time. Since this subroutine was called at least five times by the subroutine D02ABF, during each individual step of integration, the calculations in it were simplified as much as possible. The subroutine D02ABF obtained an estimate of the local truncation error at each step, and varied the step-size automatically to keep this estimate below an error bound specified earlier in the program. If the step length became less than 10^{-4} x (initial step length specified), the subroutine set an error marker and returned to the main program. The main program then printed out the instant at which partial instability had occurred, and the process was stopped.

The listing of the program for solving the differential equations defined in Section 8.3.1 is given in Appendix VIII, with a block diagram for the computing process shown in Figure 8.26. Having found the initial values (when ϕ_1 = 0) of the secondary reluctance and inductance, and of the corresponding resonating capacitance, the program proceeded to calculate the average value of the secondary reluctance, which normally required a numerical integration process. When expressions other than

polynomials were used for the H = f(B) function, this average value had to be calculated numerically by a NAG Library subroutine, such as D01ABF, which necessitated the variation of the secondary reluctance being defined by a separate function segment in the program. However, with polynomials, it was possible to calculate the average value of the secondary reluctance analytically.

The trans-reluctance characteristic for the secondary circuit is given by equation (8.16). If the primary flux is assumed sinusoidal, substitution of equation (8.21) into equation (8.16) and averaging over the interval $0 < z < \pi$ gives

$$R_{m2av} = R_g + s_1 + r_1 + 11\, r_{11}\, \phi_{1m}^{10}\, \frac{1}{\pi} \int_0^{\pi} (\sin z)^{10} dz \qquad \ldots\ldots \quad (8.28)$$

where the integral can be calculated analytically as 63/256.

When the sinusoidal primary flux is substituted in the $F_2(\phi_1, \phi_2)$ function and this function is expanded as

$$F(\phi_2, z) = (R_{m2av} + \text{periodic terms})\,\phi_2 + (\ldots)\,\phi_2^{\,3} + \ldots$$

the constant part of the coefficient of ϕ_2 in the fourth term of equation (5.8) becomes

$$\frac{1}{\omega^2 N_2^{\,2} C} \left(1 + \frac{R_2}{R_L}\right) . R_{m2av}$$

which corresponds to the characteristic number a of the Mathieu-Hill equation of Chapter III. Since a = 1 is the instability condition defining the parametric resonance, the value of the capacitor to tune the loaded secondary circuit to the input frequency is

$$C = \frac{R_{m2av}}{\omega^2 N_2^{\ 2}} \left(1 + \frac{R_2}{R_L}\right) \qquad \ldots\ldots \qquad (8.29)$$

which gives equation (3.167) for $R_L = \infty$. This value of the secondary capacitance was also calculated in the program, for comparison with the actual capacitor connected, and to see how much detuning was introduced into the secondary circuit.

The initial value of zero for the primary flux Z(1) in the program, assumed that no magnetic flux or electric charge existed in the primary circuit before the input voltage was applied. Since the total series resistance was very low, this could lead to high in-rush currents in the primary circuit, depending on the phase angle of the input voltage at X = 0. Because of the way the primary voltage is defined in the program, low in-rush currents are obtained with phase angles near $\frac{\pi}{2}$.

The initial conditions in the secondary circuit may be defined in two different ways. When only a remanent flux exists in the secondary magnetic circuit the initial conditions are Z(3) = 0 and Z(2) = 115 10^{-7} Wb, calculated by assuming a remanent flux density of 5.10^{-3} T in the secondary cross-sectional area of $A_2 = 23.10^{-4} m^2$. Although the remanent flux density in the iron core could in practice be preserved at higher

levels, depending on the past history of the secondary circuit, it was intentionally kept small to observe the parametric oscillations building up from very small amplitudes. Alternatively, a small initial oscillation could be assumed to exist in the secondary circuit, in which case both Z(2) and Z(3) take non-zero values. The amplitude of this initial oscillation was taken as corresponding to 5.10^{-3} T of initial flux density, and its phase at x = 0 could be varied, although in the program listing (see Appendix VIII) it is taken as $\frac{\pi}{4}$. It might be noted in advance that defining the initial conditions in the secondary circuit in these two different ways did not introduce any essential changes in the build-up process of the parametric oscillations.

In the program, the error bounds for the system variables were specified as $0.5\ 10^{-5}$. The same program was run with smaller error bounds, but this resulted in almost the same numerical values (up to the fifth decimal place) of the output variables E_1, I_1, E_2 and I_2. With the error bound of $0.5\ 10^{-5}$ the solution obtained by the Runge-Kutta-Merson method was therefore assumed to be the true solution, within an acceptable error.

Unless the step-length was reduced by the subroutine D02ABF when the error limits were exceeded, the integration of the differential equations was carried out by this subroutine in two equal steps of 0.05π over the range of 0.1π, between the two points for which numerical results were printed. At its

output, the subroutine produced the new values of F_1, F_2, ϕ_1 and ϕ_2 from which the instantaneous values e_2, i_1 and i_2 were calculated.

As previously explained, the starting operation of the parametric transformer needed the input voltage amplitude to be increased over a threshold, then to be reduced to a level where the best condition of operation was achieved. In order for an abrupt change in the primary voltage not to cause transient effects, V_{1eff} was reduced by a small amount at each increment of time between two pre-determined instants.

Since the instantaneous numerical values of e_1, e_2, i_1 and i_2 had already been calculated in the program, their effective values were found by numerical integration, using the rectangle rule over an interval of five cycles of the oscillation. The rectangle rule was considered to be of sufficient accuracy as the integration step was small. However, when the variations of e_2, i_1 and i_2 were quasi-periodic, or when they exhibited amplitude modulation, the effective values found were not reliable, since it was then necessary to perform the integration over much longer intervals.

The program was used to find the transient response of the parametric transformer under different conditions but over an interval of 50 periods (= 1 second), which, in most cases, was sufficient for the system to attain steady-state operation. The aim was to keep the job run time reasonably small, which otherwise would need to be increased in proportion to the interval of the investigation. For this reason, the gradual changes

of variables such as input voltage amplitude or load resistance (i.e. simulation of turning the knob of a variac or a rheostat in the physical system) had to be accomplished quite rapidly, in order to establish their effects in the rest of the interval. Since the time constants of the primary and the unloaded secondary circuits were quite large (because of high inductances but low resistances of the windings), the transient effects resulting from such changes sometimes took long time to settle.

The job time changed only slightly between the cases when normal oscillations were excited and when no oscillations occurred at all, but increased significantly when quasi-periodic oscillations were produced, because of the automatical reduction of the step length to maintain the required accuracy.

The waveforms of the input and output voltages and currents, resulting under various different operating conditions were plotted by computer and given in Figures 8.27 to 8.52.

8.4 Discussion of Results

The results obtained from the computer solution demonstrated all the characteristic features of parametric transformer operation. The secondary voltage amplitude reached values around 400 V as the oscillations built-up from very small values, as shown in Figure 8.27. As explained previously, the secondary voltage can attain its full amplitude at steady state, only after the primary voltage is reduced to levels corresponding to points between A and B in Figure 6.21. This is illustrated in Figure 8.28a, where the primary voltage was reduced in 1.2 V steps from 240 V at 0.1π intervals between $\omega t = 40\pi$ and 50π. It is seen for $\omega t < 40\pi$ that the secondary voltage reaches the steady state at a primary voltage between points B and C in Figure 6.21. The low secondary voltage exhibits a deep amplitude modulation. As the primary voltage is reduced when $40\pi < \omega t < 50\pi$ the secondary voltage increases accordingly and the amplitude modulation diminishes, with E_2 eventually reaching an almost constant amplitude. For $\omega t > 50\pi$, the depth of the modulation gradually decreases with time, as it is associated with the transient effects caused by the rapid reduction of V_{1rms}. However, if the primary voltage was maintained at its original amplitude, the secondary voltage would continue exhibiting the deep amplitude modulation. Briefly, the four different stages observed in the variation of E_2 in Figure 8.28a are:

i) $0 < \omega t < 20\pi$: initiation and growth of oscillations, ii) $20\pi < \omega t < 40\pi$: steady-state operation corresponding to $V_{1rms} = 240$ V, (iii) $40\pi < \omega t < 50\pi$: changes of V_{1rms} and V_{2rms} satisfying the operational characteristic of Figure 6.21 or 3.36 or 2.6, (iv) $\omega t > 50\pi$: steady-state operation corresponding to $V_{1rms} = 120$ V. The primary and the secondary current waveforms in this condition are given in Figure 8.28b. Figures 8.29a and b show the primary and secondary voltage and currents for $V_{1rms} = 260$ V which is then reduced by 120 V to 140 V. Figure 8.30a and b show the same quantities with V_{1rms} initially 280 V and then reduced to 160 V. Comparing the secondary voltage waveforms in these figures it is seen that as V_{1rms} is increased from 120 V to 160 V during the steady-state operation ($\omega t > 50\pi$), the secondary voltage amplitude starts to display a modulation similar to that occurring when $20\pi < \omega t < 40\pi$, with a depth increasing with V_{1rms}. In general, when working in region BC of Figure 6.21, the secondary voltage amplitude is modulated in addition to the waveform distortion explained in Section 3.6.2 with reference to Figure 3.38. (The distortion of the secondary voltage is best displayed in Figure 8.45, where the secondary voltage has a triangular waveform similar to Figure 3.38b). This phenomenon may be explained by the classical theory of the Mathieu-Hill equations, which demonstrates that the characteristic exponent μ, being a positive, real constant in an unstable region and zero on the boundary curves, can be considered as a complex constant in a stable region of the stability chart. When V_{1rms} is high, the parametric point at

the steady state, P' in Figure 3.16, rests higher on the boundary curve a_{c1}, from where it can easily be driven into the stable region between a_{c1} and a_{s2}. With μ having a small but imaginary value, the amplitude of the oscillations is then modulated accordingly. V_{1rms} must therefore be kept below the value corresponding to ϕ'_{1m}, so that the secondary voltage amplitude is determined only by the saturation flux level in the core.

It is now clear that the voltage regulation property of the parametric transformer exists because the peaks of the secondary voltage variation are limited by saturation. As long as V_{1rms} is within a certain range, the secondary voltage amplitude is always constant, although its rms value changes due to waveform distortion at different operational conditions. The voltage regulation property is demonstrated in Figure 8.31, where V_{1rms} is initially 240 V and is reduced by 180 V when $40\pi < \omega t < 50\pi$, and for $\omega t > 50\pi$, is multiplied by $[1 + 0.2 \sin (0.1\ \omega t)]$. The secondary voltage amplitude, having reached steady state by $\omega t = 50\pi$, is not substantially affected by the variations in V_{1rms}. (The slight variation in the secondary voltage amplitude is caused by the transient effects of the rapid reduction in V_{1rms}) Furthermore, the secondary voltage amplitude here is almost the same as in Figures 8.28a and 8.29a, illustrating another aspect of the voltage regulation property. Figure 8.32 shows the same waveforms obtained with V_{1rms} initially taken as 300 V. The variations in the secondary voltage amplitude for $\omega t > 50\pi$,

similar to those in Figures 8.30a, are independent of the variations of V_{1rms}, since the first is caused by operation in region BC of Figure 6.21, as the mean value of V_{1rms} is now sufficiently high.

The under- and over-voltage protection properties of the device were also established by the computer simulation. When V_{1rms} was given values below 200 V, the small initial oscillation in the secondary circuit was not excited and eventually died away, as shown in Figure 8.33. The other aspect of the under-voltage proptection property explained by equation (3.204) is illustrated in Figure 8.34, where V_{1rms} is reduced from 260 V to 110 V in the interval $30\pi < \omega t < 40\pi$, when the secondary voltage reaches the steady state with a constant amplitude. However, a further reduction of 70 V in V_{1rms}, accomplished when $60\pi < \omega t < 70\pi$, causes condition (3.204) to be satisfied, and the oscillations are no longer sustained but have an exponentially decaying amplitude. Since the secondary circuit is unloaded, it has a quite large time constant and the decrease occurs very slowly. However, if the under-voltage protection is exercised with a loaded secondary, the secondary voltage falls rapidly to zero, similar to that shown for over-load protection in Figure 8.50. Nevertheless, the large time constant of the secondary circuit ensures that the output voltage is unaffected by such irregularities in the primary voltage as an interruption lasting for a few cycles.

The over-voltage protection property is demonstrated in Figure 8.35, where V_{1rms} is reduced from 260 V to 80 V during $20\pi < \omega t < 40\pi$, and kept constant for $40\pi < \omega t < 50\pi$ to ensure that the secondary voltage reaches its full, constant amplitude. From $\omega t = 50\pi$ onwards, V_{1rms} is increased by 0.7 V at each step, reaching 360 V at $\omega t = 90\pi$. It is seen that the secondary voltage amplitude decreases as V_{1rms} is gradually increased, and finally becomes almost zero. From the relationship between the amplitudes of the primary and secondary voltages in this figure, the form of the characteristic in Figure 6.21 (or 3.36 or 2.6) can be readily deduced. The over-voltage protection feature is a result of the forced suppression of the secondary flux amplitude by the primary flux reaching high levels in the core. Since this suppression is achieved very rapidly in the computer simulation, some quasi-periodic oscillations are observed after V_{2rms} has become practically zero. This is due to the nature of the system and is true also for the physical device. In Figure 8.36, V_{1rms} is increased more rapidly, starting from 80 V at $\omega t = 50\pi$ and reaching 380 V at $\omega t = 80\pi$. The secondary voltage amplitude becomes very small just after the instant $\omega t = 70\pi$, when the over-voltage protection is achieved. However, with V_{1rms} already increasing further, the small oscillations after this instant are excited, and quasi-periodic oscillations of very high amplitudes and of mainly twice the frequency of the normal oscillations are obtained, as seen from the figure. These oscillations are not in a defined phase relationship with the primary voltage, but if V_{1rms} is subsequently

decreased, it is possible that they may become phase-locked with the primary voltage, in which case double frequency oscillations of very high amplitudes are obtained, as shown in Figure 8.37. This phenomenon has been explained in Section 3.4, with reference to Figure 3.28. Since the secondary circuit capacitance still has the value necessary for 50 Hz operation, the primary and secondary currents reach amplitudes in excess of 10A, which may be harmful for the actual device. This phenomenon is quite different from the normal frequency-doubling operation of the parametric transformer when the currents are of moderate amplitudes.

If the secondary capacitor is adjusted so that the condition a = 1 is always satisfied by equation (8.29), the secondary oscillations are excited and maintained with V_{1rms} higher than in operation with a constant capacitor. In Figures 8.38 and 8.39, the secondary capacitor is given such values, and V_{1rms} is reduced by 100 V from the initial value of 280 V in the first figure and 300 V in the second. Although these values of V_{1rms} are higher than in Figures 8.28a and 8.29a, the secondary voltage variation is just as good as in these figures.

It was found that the steady-state phase of the secondary voltage with respect to the primary voltage is determined by the instant when the process of build-up starts, rather than by the initial conditions specified in the program. This instant cannot be pre-determined as it depends on factors such as the initial phase of the primary voltage, the values of V_{1rms}, C, R_L

etc. as well as the initial conditions. Initiation of oscillations in the secondary circuit under different conditions is shown in Figures 8.40 to 8.46. In Figure 8.40, the phase of the primary voltage ALFA = 0.5π and the initial conditions are defined by assuming an initial oscillation in the secondary circuit of the form $\phi_2 = 11.5\ 10^{-6} \sin(\omega t + \frac{\pi}{4})$, when the final steady-state secondary voltage is obtained lagging in phase on the primary voltage by 90^0. Keeping the initial conditions in the secondary the same but changing ALFA to 1.5π to seek the second stable phase (90^0 leading) of the secondary voltage did not change the phase relationship between the primary and secondary voltages, as seen from Figure 8.41. In Figure 8.42, the same phase relationship (V_2 lagging v_1 by 90^0) was obtained with a different value for the phase of the initial oscillation. As can be seen from Figures 8.43 to 8.45 for different values of V_{1rms} and C, the secondary voltage leads the primary voltage by 90^0 at steady-state, proving the bistability of the phase. It was found equally likely for the secondary voltage to take either of the two stable phases, although which one will actually be taken cannot be predicted, since this depends in a very complex manner on all the system parameters and the circuit variables. However, one most important factor was found to be the phase of the in-rush currents occurring when the primary voltage was applied. Figure 8.46 shows the initial oscillation corresponding to an initial flux density of $2.5\ 10^{-2}$ T in the secondary circuit when the primary voltage is switched on with

ALFA slightly greater than 0.5π. It can also be observed in Figures 8.40 to 8.45 that, during build-up, the phase of the growing oscillations changes so that the phase difference between the primary and the secondary voltages becomes $\mp \pi/2$ at steady-state. This change of phase is shown in more detail in Figure 8.47.

In Figure 8.48, the secondary voltage has already attained the steady-state corresponding to $V_{1rms} = 180$ V, with the capacitor given the value of equation (8.29), when a load resistance of 1 kΩ is introduced into the system at $\omega t = 60\pi$. Since this value of R_L proved to be below the maximum acceptable load under these operating conditions, the secondary voltage fell to zero, illustrating the over-load protection property of the device. The same process is repeated in Figure 8.49, where the steady state is reached with $V_{1rms} = 200$ V. Introduction of the load resistance does not now switch off the secondary voltage, since the maximum acceptable load under these operating conditions is not exceeded. However, it is seen that the load resistance introduces a kind of ballast action, removing the modulation of the secondary voltage which existed previously. Figure 8.50 shows the same operation as Figure 8.48, but at $\omega t = 60\pi$ a load resistance of 2 kΩ is introduced and this is subsequently decreased by 6Ω at each step of integration until $\omega t = 85\pi$. It is seen that the secondary voltage amplitude is quite constant in the interval $60\pi < \omega t < 80\pi$, although the load resistance is monotonously decreasing, and this establishes the load regulating property of

the device. Just before $\omega t = 80\pi$, when R_L is decreased to below 1 kΩ, the over-load protection property comes into action and the secondary voltage starts to diminish.

As already observed in all the computer plotted figures, the secondary voltage is a very good sinusoid, although operation under many different conditions was considered. The waveforms of the primary and secondary currents for three different operation conditions are given in Figures 8.28b, 8.29b and 8.30b. It can be noticed from these that, when the primary voltage is high and the secondary voltage correspondingly low, the currents have waveforms similar to those in Figure 6.18a, and conversely that when the primary voltage is low but the secondary voltage is high, the current waveforms are similar to those in Figure 6.18b.

Apart from the secondary voltage being a good sinusoid, the filtering ability of the device is demonstrated by Figure 8.51, where the square waveform of the primary voltage is approximated by a Fourier series containing harmonics up to the 15th. The maximum value of the square wave is reduced from 380V to 140 V within the interval $20\pi < \omega t < 30\pi$. Since the primary voltage is quite high before $\omega t = 20\pi$, harmonic oscillations similar to those in Figure 8.36 are also observed. However, after the amplitude of the square-wave input voltage is reduced, it is clear that the secondary voltage has a quite good sinusoid waveform. As can be noticed from the diminishing depth of modulation in Figure 8.51, the variations in the secondary

voltage amplitude results from the rapid reduction of the input voltage in the interval $20\pi < \omega t < 30\pi$.

With the secondary capacitor given values to resonate the secondary circuit at 100 Hz, oscillations at twice the input frequency were obtained, as shown in Figure 8.52. Operation of the device as a frequency doubler was found to be much more sensitive to changes in the system variables and parameters than normal operation. It proved difficult to start the oscillations, and the amplitude of the initial oscillation in the secondary circuit was therefore taken as 10 times that for normal operation. The range of V_{1rms} for which the oscillations could be started and sustained was narrower in comparison with normal operation, as well as any slight changes in the circuit parameters C, R_L etc affecting the oscillations more critically.

As pointed out earlier, none of the approximate expressions used allows the reproduction of the curvature near the origin of the actual magnetisation characteristic. The initial (maximum) inductance of the secondary winding is calculated from equation (4.52) as 6.8H (see Figures 8.21 and 8.23). However, when this inductance was measured for the actual device by an impedance bridge type instrument, it was found to be about 0.6H. The value of the capacitor connected in the physical set-up is calculated from this measured value of the secondary inductance and it is therefore about 10 times higher than the value used in the computer simulation. The reason for the difference

between the two values of the secondary inductance (or of the primary inductance because of complete symmetry) is mainly because the slope of the B/H curve near the origin is assumed as high as in the linear region, which is untrue, although the experimental and theoretical V/I characteristics fit very precisely. Furthermore, the most important consequence of the increased capacitor value in the computer simulation was that the computer program yielded primary and secondary currents much lower than those measured during steady-state operation. The growth of oscillations in practice is accompanied by a large increase in the amplitude of the primary and secondary currents, and this was not demonstrated by the computer simulation, as can be seen from Figures 8.28b, 8.29b and 8.30b. The computer simulation produced secondary voltage amplitudes during steady-state which agreed well with the practical values, because the main factor determining this amplitude is the saturation flux level. In the actual device, the maximum electrostatic energy stored in the capacitor in the secondary tank circuit ($\frac{1}{2}$ C V_{2m}^2) is more than in the computer simulation, because of the higher value of the capacitor. A quarter period later, when this energy is totally converted to electromagnetic energy, the value of the secondary current in the simulation is therefore much lower than in the actual device. To account for these differences and to have a capacitor value in the simulation equal to the practical value, required the initial secondary inductance

to be made equal to the value measured for the actual device.

In the computer simulation, the difference between the calculated and measured secondary inductances could be removed simply by increasing the length of the air-gap. However, this would affect not only the portion near the origin but also the complete linear portion of the theoretical V/I characteristic in Figure 8.14. The precise fit seen in this figure would be totally upset resulting in the calculated secondary currents being much higher than those experimentally observed when no parametric oscillations occur. It was therefore necessary to take the curvature near the origin of the B/H curve into account. Having considered many possible solutions, it was found that the addition of a third term, so that equation (8.7) becomes

$$H = C_1 B + C_{11} B^{11} + k_1 \tanh (k_2 B) \qquad (8.30)$$

was the most suitable. With this expression taken as the H=f(B) function, the $F_1(\phi_1, \phi_2)$ and $F_2(\phi_1, \phi_2)$ functions were found to have the additional terms

$$F_1(\phi_1, \phi_2) = \text{terms of equation (8.8)} + u_1 \tanh (u_2 \phi_1)$$

$$+ \frac{1}{2} q_1 \{\tanh [q_2 (\phi_1 + \phi_2)] + \tanh [q_2 (\phi_1 - \phi_2)]\}$$

(8.31)

$$F_2(\phi_1, \phi_2) = \text{terms of equation (8.9)} + v_1 \tanh (v_2 \phi_2)$$

$$+ \frac{1}{2} q_1 \{\tanh [q_2 (\phi_1 + \phi_2)] - \tanh [q_2 (\phi_1 - \phi_2)]\}$$

(8.32)

and the partial derivatives of $F_2(\phi_1, \phi_2)$

$$f_1(\phi_1, \phi_2) = \text{terms of equation (8.23)} + v_1 v_2 \operatorname{sech}^2 (v_2 \phi_2)$$

$$+ \frac{q_1 q_2}{2} \{\operatorname{sech}^2 [q_2 (\phi_1 + \phi_2)] + \operatorname{sech}^2 [q_2 (\phi_1 - \phi_2)]\}$$

(8.33)

$$f_2(\phi_1, \phi_2) = \text{terms of equation (8.24)}$$

$$+ \frac{q_1 q_2}{2} \{\operatorname{sech}^2 [q_2 (\phi_1 + \phi_2)] - \operatorname{sech}^2 [q_2 (\phi_1 - \phi_2)]\}$$

(8.34)

where $u_1 = k_1 . \ell_1$

$$u_2 = k_2/A_1$$

$$v_1 = k_1 . \ell_2$$

$$v_2 = k_2/A_2 \qquad (8.35)$$

$$q_1 = k_1 . \ell_0$$

$$q_2 = k_2/(2A_0)$$

The transreluctance characteristic of the secondary is now

$$R_{m2}(\phi_1) = f_1(\phi_1, \phi_2)\Big|_{\phi_2=0} = R_g + s_1 + r_1 + 11\, r_{11}\, \phi_1^{10} +$$

$$+ v_1 v_2 + q_1 q_2 [1 - \tanh^2 (q_2 \phi_1)] \qquad (8.36)$$

The minimum constant value of the secondary reluctance is

$$R_{m2min} = f_1(\phi_1, \phi_2)\Big|_{\substack{\phi_2=0 \\ \phi_1=0}} = R_g + s_1 + r_1 + v_1 v_2 + q_1 q_2 \tag{8.37}$$

from which the initial value of the secondary inductance is calculated as

$$L_{2in} = \frac{N_2^2}{R_{m2min}} = \frac{N_2^2}{\frac{\ell_g}{\mu_0 A_0} + (\frac{\ell_2}{A_2} + \frac{\ell_0}{2A_0})(c_1 + k_1 k_2)} \tag{8.38}$$

The values of k_1 and k_2 were determined by equating the above expression (with all the other parameters unchanged) to the experimentally measured value of the secondary inductance. In order not to affect the precise fitting between the theoretical and experimental V/I characteristics, k_1 was assumed to be small and the corresponding value of k_2 was calculated. With k_1 = 10 and k_2 = 304.6 the secondary inductance became 0.6H and the value of C for the computer simulation was increased to near the values employed in the physical set-up, without the calculated V/I characteristic being substantially affected.

The computer program to solve the differential equations of the system was run many times for different operational conditions, with the new $F_1(\phi_1, \phi_2)$, $F_2(\phi_1, \phi_2)$, $f_1(\phi_1, \phi_2)$ and $f_2(\phi_1, \phi_2)$ functions, and many different combinations of parameter values were tried. However, all the attempts failed and no parametric oscillations in the secondary circuit could be achieved. With the magnetisation characteristic of equation (8.30) and the trans-reluctance characteristic of equation (8.36), Figure 2.2 becomes as Figure 8.53, where high peaks in the secondary reluctance variation are observed at the zero-crossing instants of the primary flux. During the growth of oscillations, the phase relationship between the primary and secondary fluxes is as in Figure 3.15. The relative positions of the initial oscillations and the high peaks of the reluctance variation are shown in Figure 3.54. Comparing this with Figure 3.10, in the light of Section 3.1.4, it can be concluded that the high peaks of reluctance withdraws rather than delivers energy to the secondary flux variation (since the value of the secondary flux at the instant of a negative-going edge of a peak is higher than that at a positive-going edge). The initial oscillation in the secondary circuit therefore diminishes rapidly by virtue of the parametric absorption of energy and no oscillations can be sustained.

Since the magnetisation curve is assumed a single-valued function, an operational point tracing this curve passes the sharp inflection near the origin once in each half cycle,

resulting in high peaks in the secondary reluctance variation. However, the practical situation is completely different and no such peaks occur, because of the existence of hysteresis. Although the dc magnetisation characteristic shows a curvature near the origin, the shape of the hysteresis loops under ac magnetisation conditions are not affected by this curvature. The phenomenon may be better understood by reference to Figure 8.55, where the portions of the B/H curve near the origin are shown for three different amplitudes of initial oscillation. Since the gradient of the axis of the hysteresis loops gradually increases as the amplitude of the initial oscillation grows, the secondary reluctance variation does not contain high peaks but exhibits a gradual decrease. The phenomenon of high peaks of secondary reluctance variation absorbing energy from the initial oscillation does not therefore occur in practice, and parametric excitation continues, although some detuning is introduced during the growth of oscillations by the fixed value of the capacitor corresponding to the low initial secondary inductances (line 1 of Figure 8.56). However, this detuning decreases as the steady-state operation is reached, when the effective secondary inductance decreases from that corresponding to line 2 to that corresponding to line 3 in Figure 8.55. Since parametric excitation is possible despite large detuning, and steady-state operation is reached within a few cycles, the practical device continues operating successfully although with a large increase in both the secondary and primary currents.

Finally, computer simulations were attempted of other approximations to the H=f(B) function, such as those in Section 7.3. Unfortunately, the transcendental forms of these expressions resulted in the execution time of the program to produce 50 cycles of oscillations proving too long for the LUT Computer Centre, and the facilities of the Regional Computer Centre at the University of Manchester were used. However, because of very long turn-round times, these attempts were later abandoned.

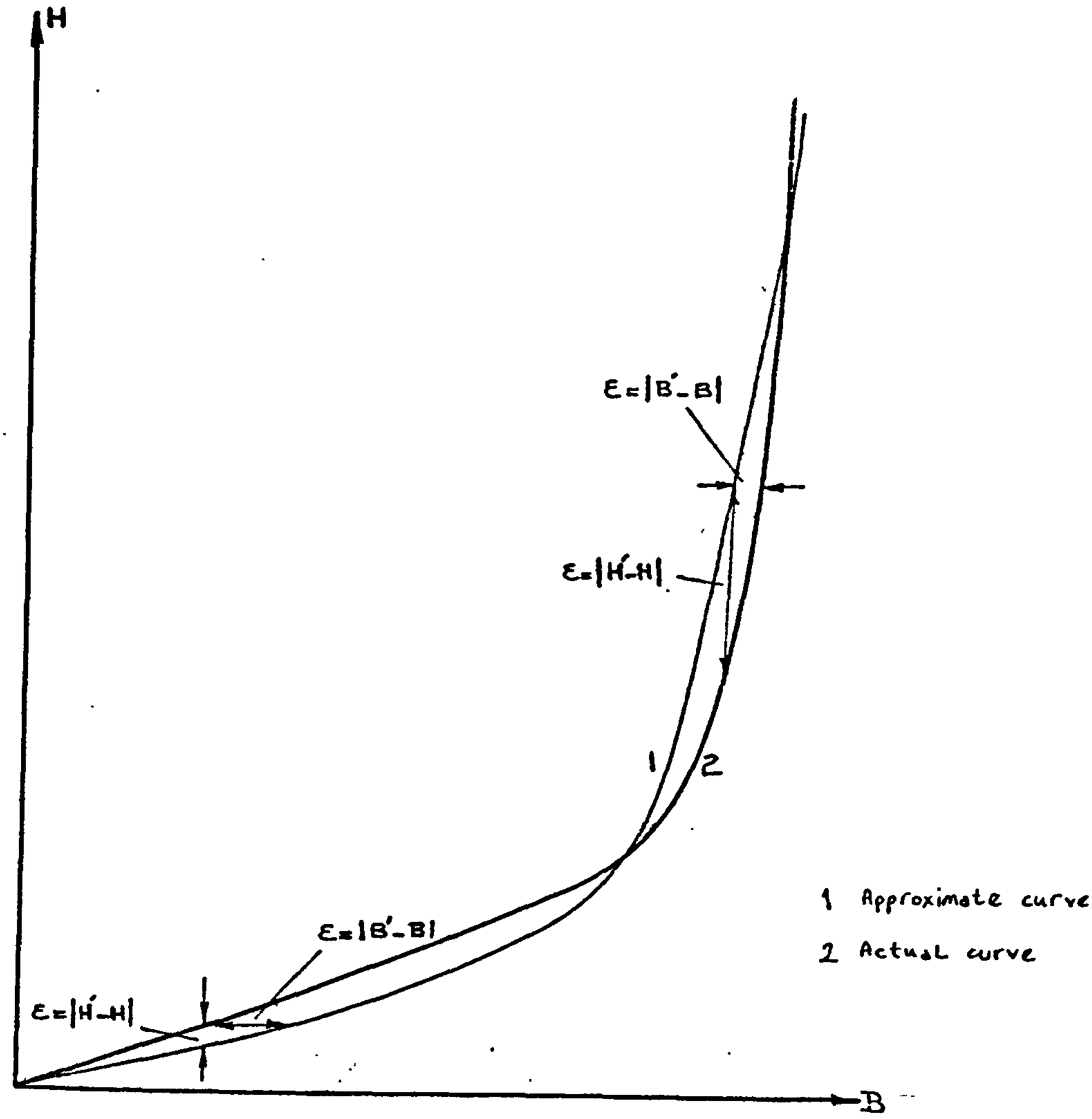

Figure 8.1 Errors in B and H sense

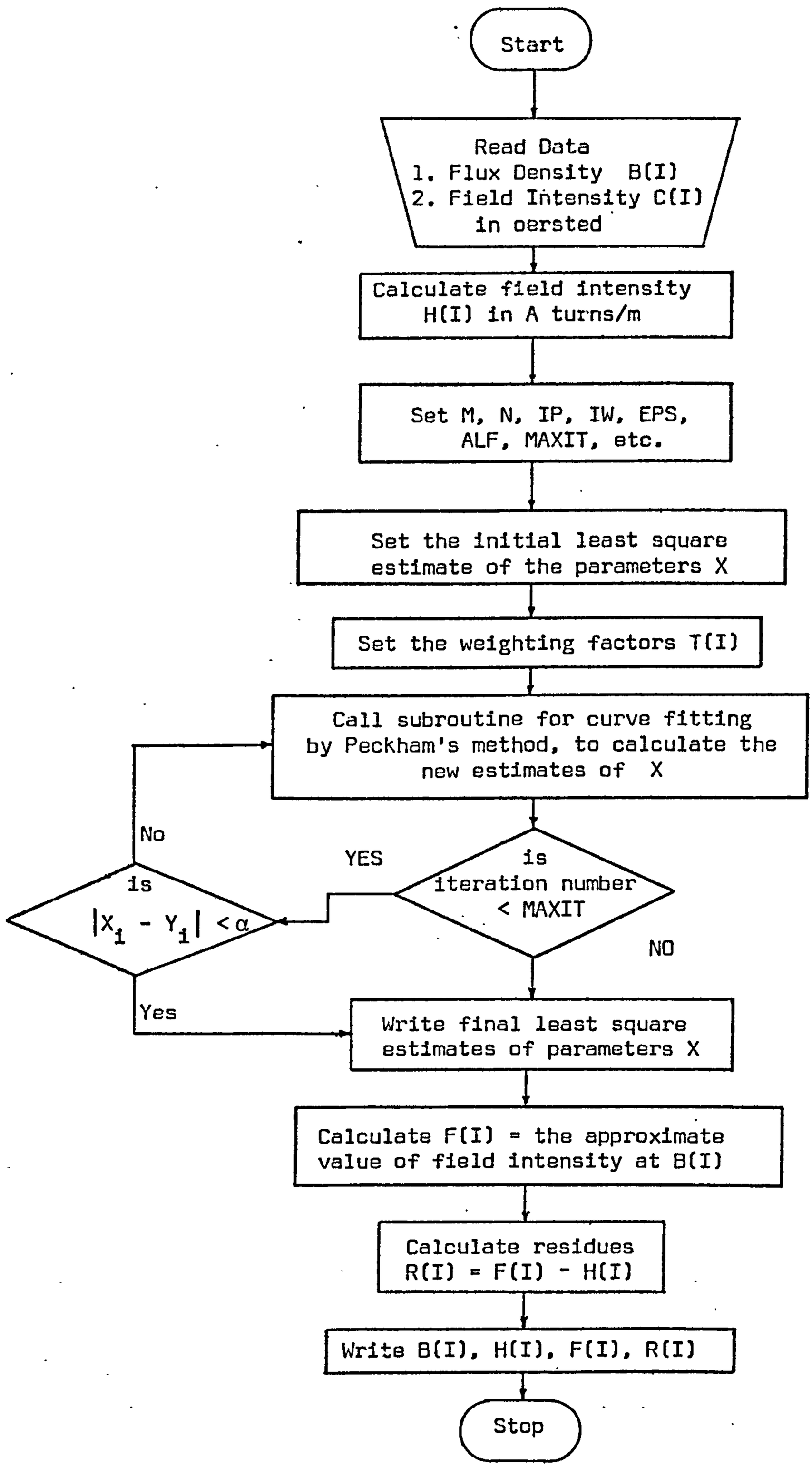

Figure 8.2 Block Diagram of the Curve-Fitting Process

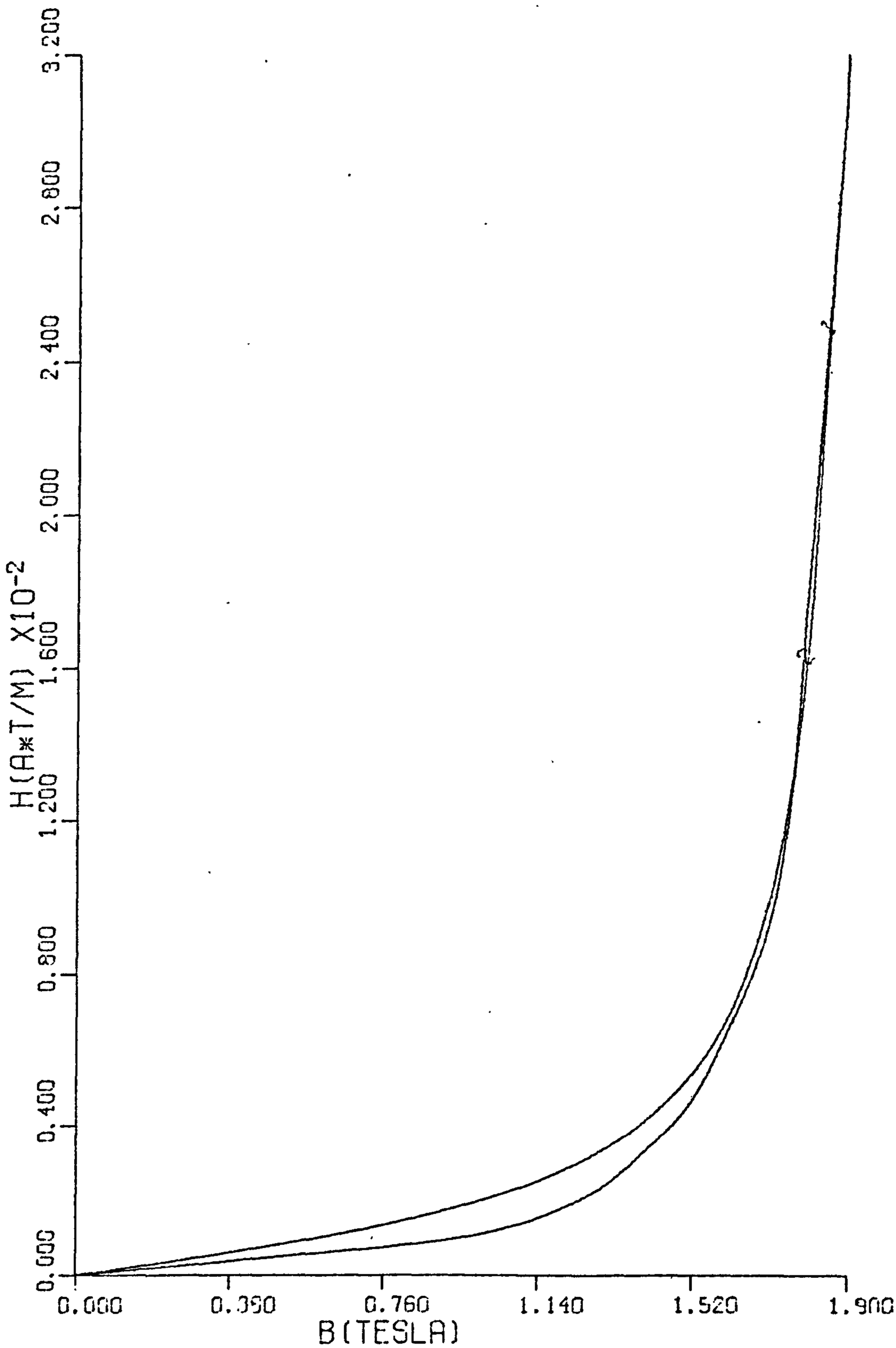

Figure 8.3 Tangent Approximation $H = \frac{2}{\pi} B_s . R \tan\left(\frac{\pi}{2} \frac{B}{B_s}\right)$

with $B_s = 1.9491705$

$R = 15.63937$

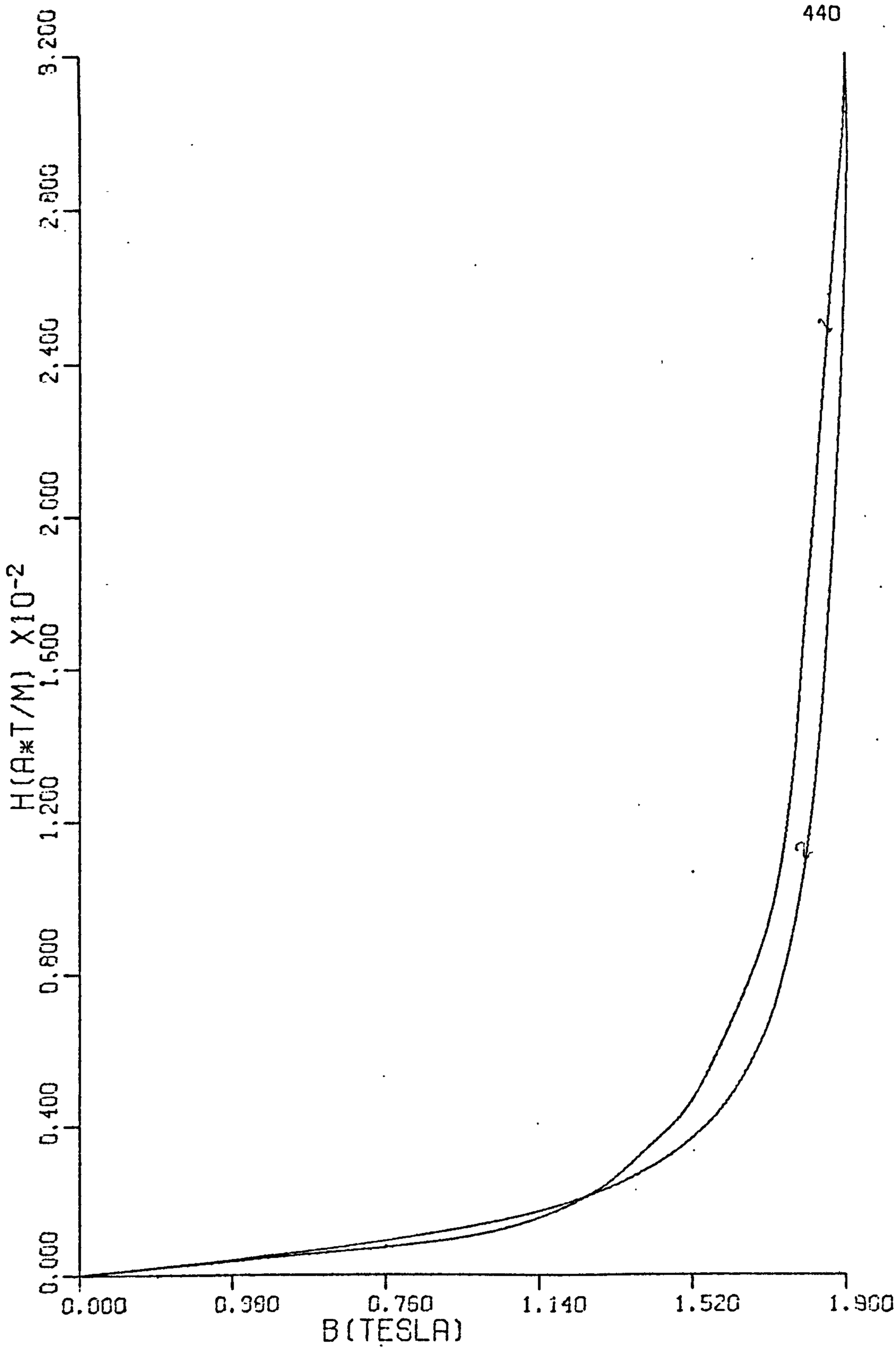

Figure 8.4 Tangent Approximation $H = \frac{2}{\pi} B_s R \tan\left(\frac{\pi}{2} \frac{B}{B_s}\right)$

with $B_s = 1.94917$

$R = 10.64613$

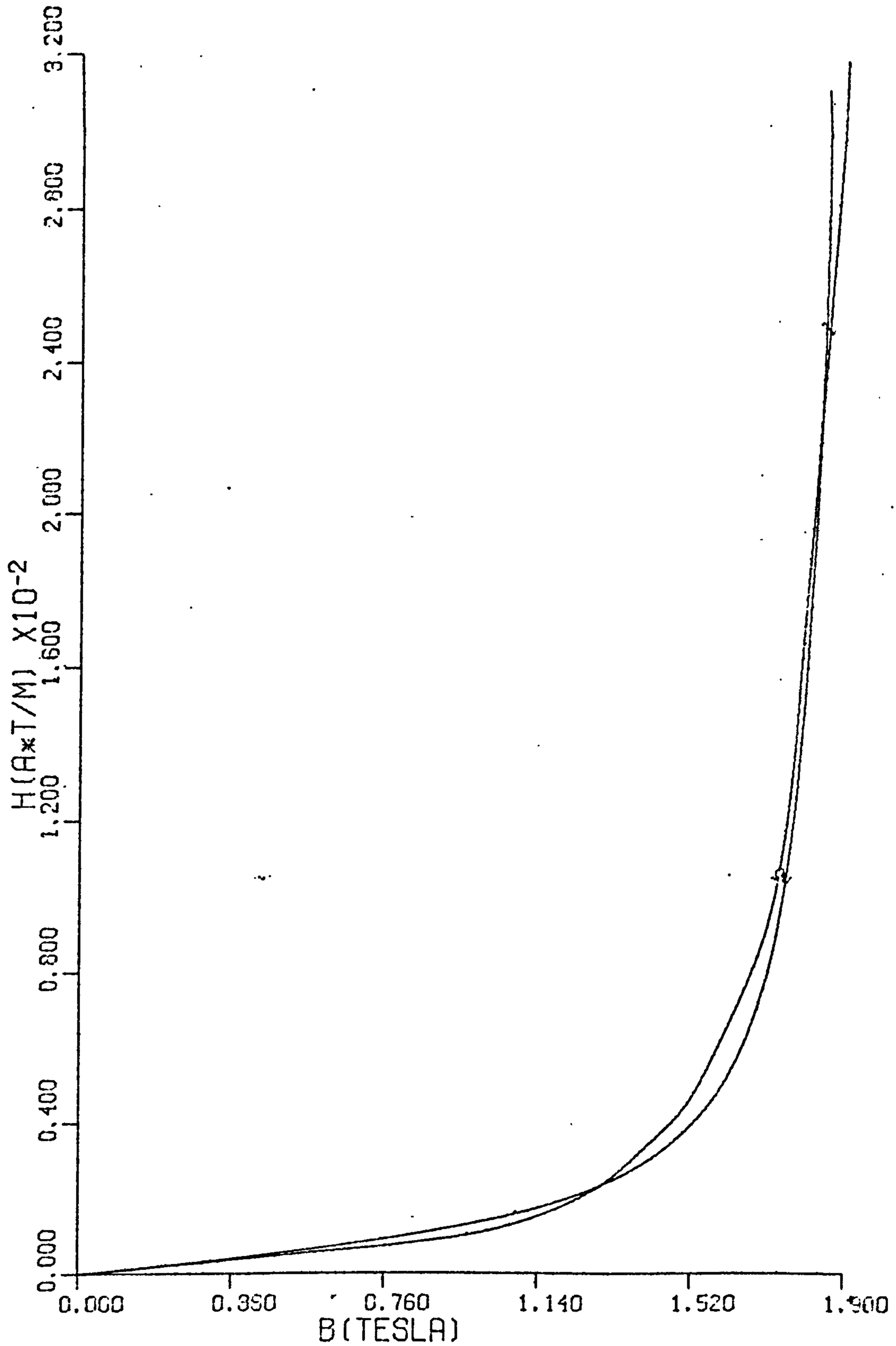

Figure 8.5 Tangent Approximation $H = \frac{2}{\pi} B_s R \tan\left(\frac{\pi}{2} \frac{B}{B_s}\right)$

with $B_s = 1.9018$

$R = 10.6389$

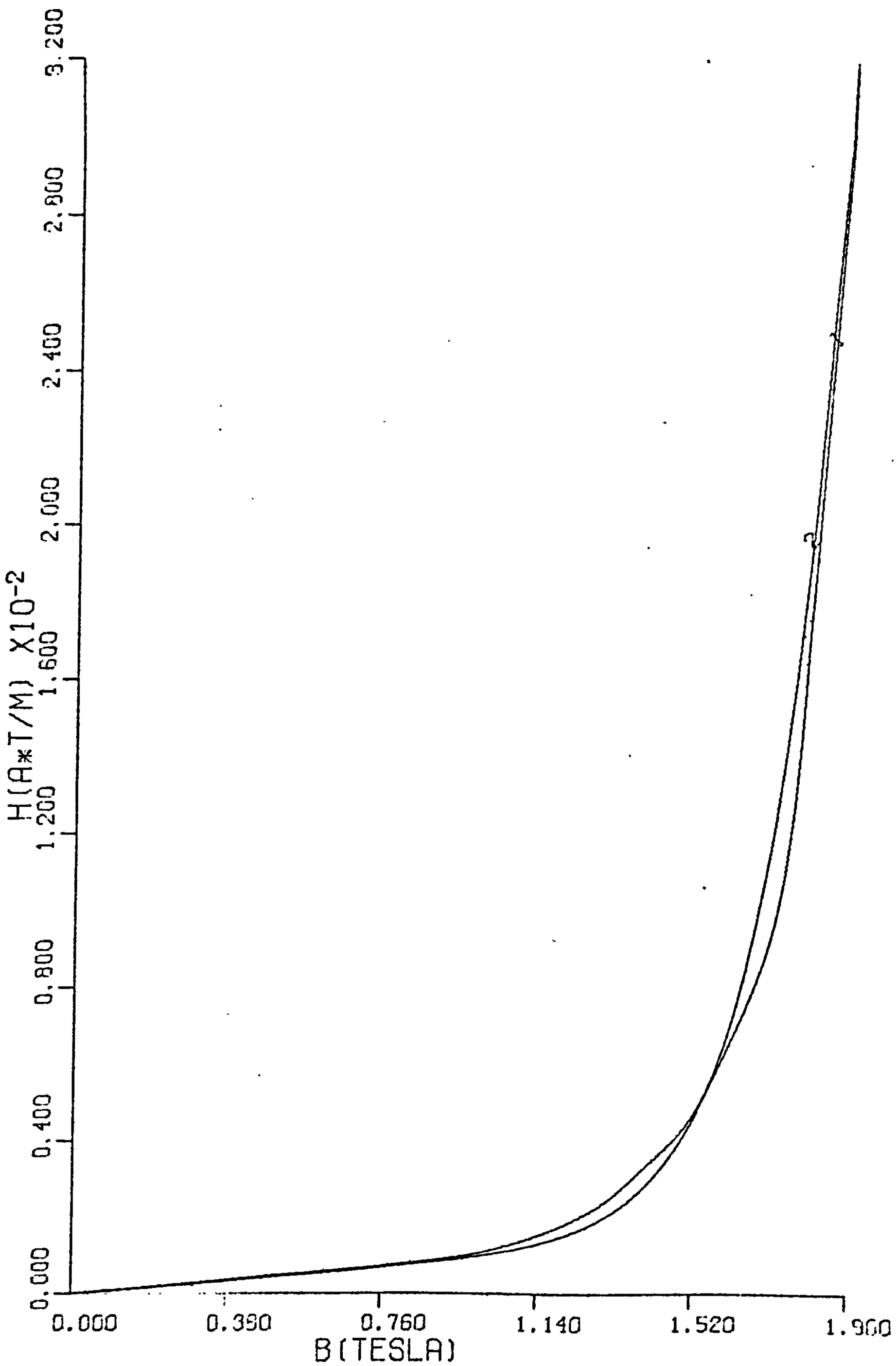

Figure 8.6 Hyperbolic-Sine Approximation $H = c_1 \sinh(c_2 B) + c_3 B$

with $c_1 = 0.00577256$

$c_2 = 6.1283431$

$c_3 = 9.0126331$

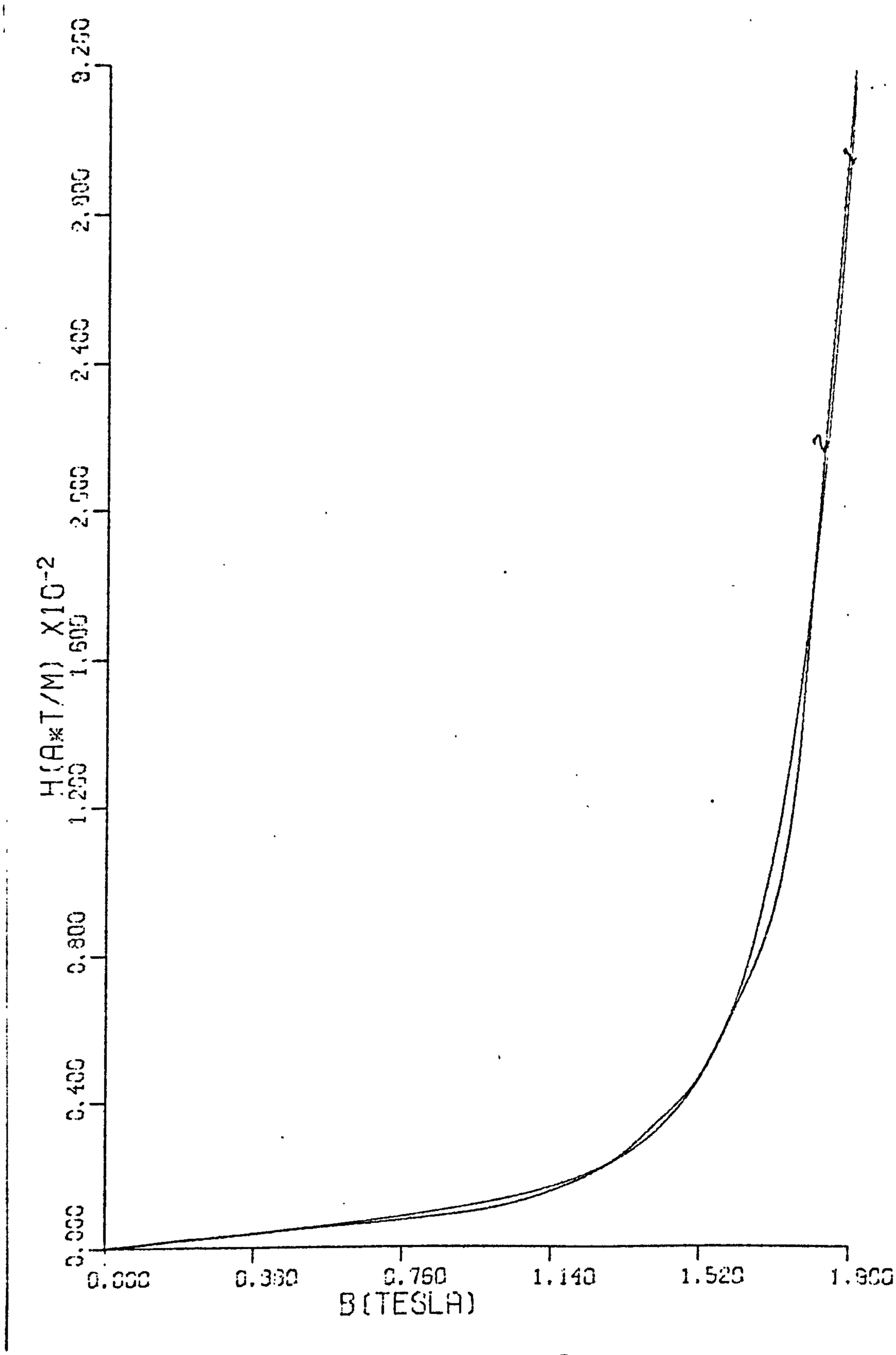

Figure 8.7 Power-Series Approximation $H = \sum_{i=1}^{7} c_{2i+1} B^{2i+1}$

with

$c_1 = 10.00014$ $c_3 = 1.478875$ $c_5 = 1.306037$

$c_7 = 0.039414$ $c_9 = 0.117981$ $c_{11} = 0.007954$

$c_{13} = 0.02025$ $c_{15} = 0.007714$

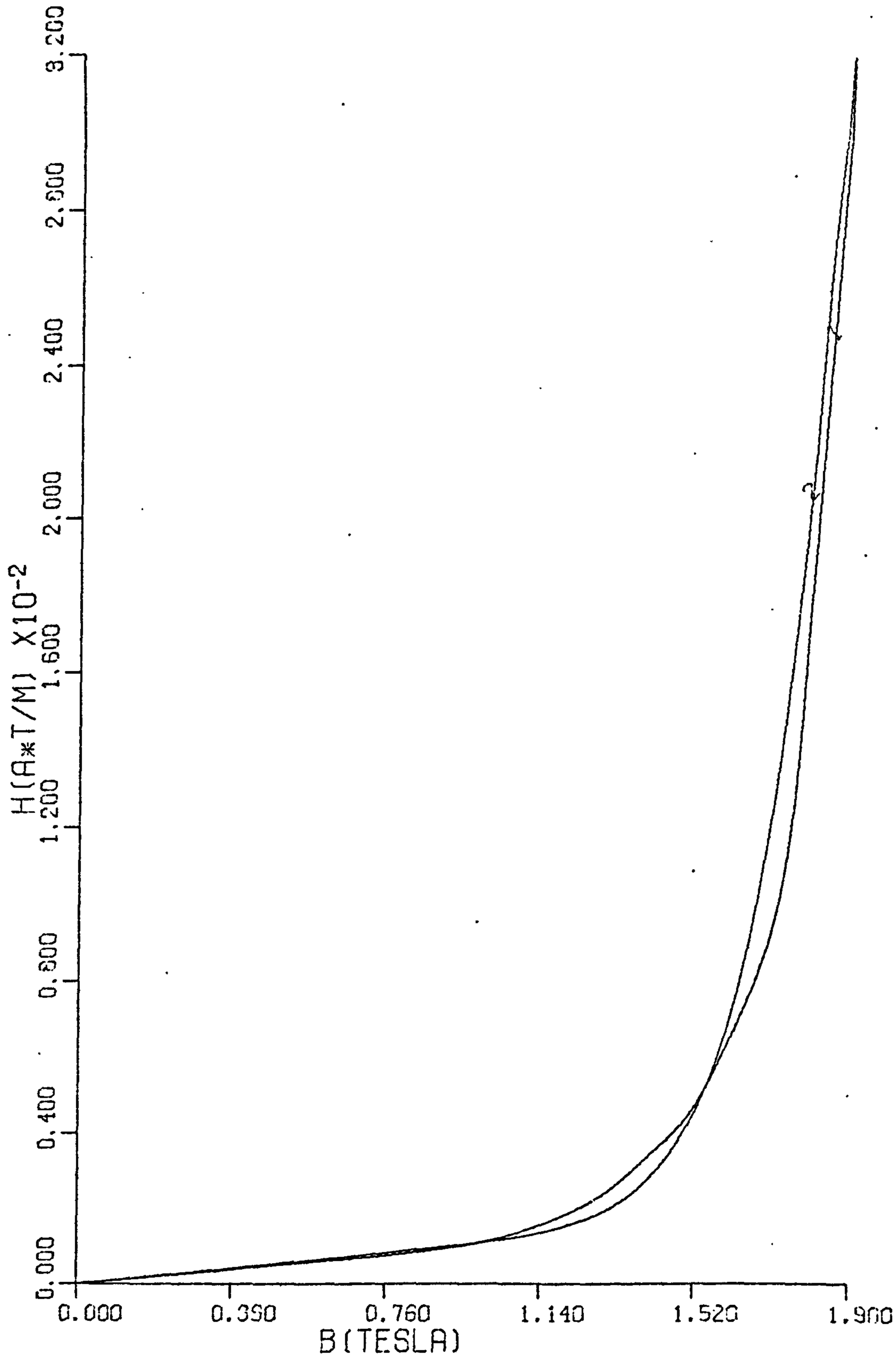

Figure 8.8 Polynomial Approximation $H = c_1 B + c_{11} B^{11}$

with $c_1 = 10.7975693$

$c_{11} = 0.2891732$

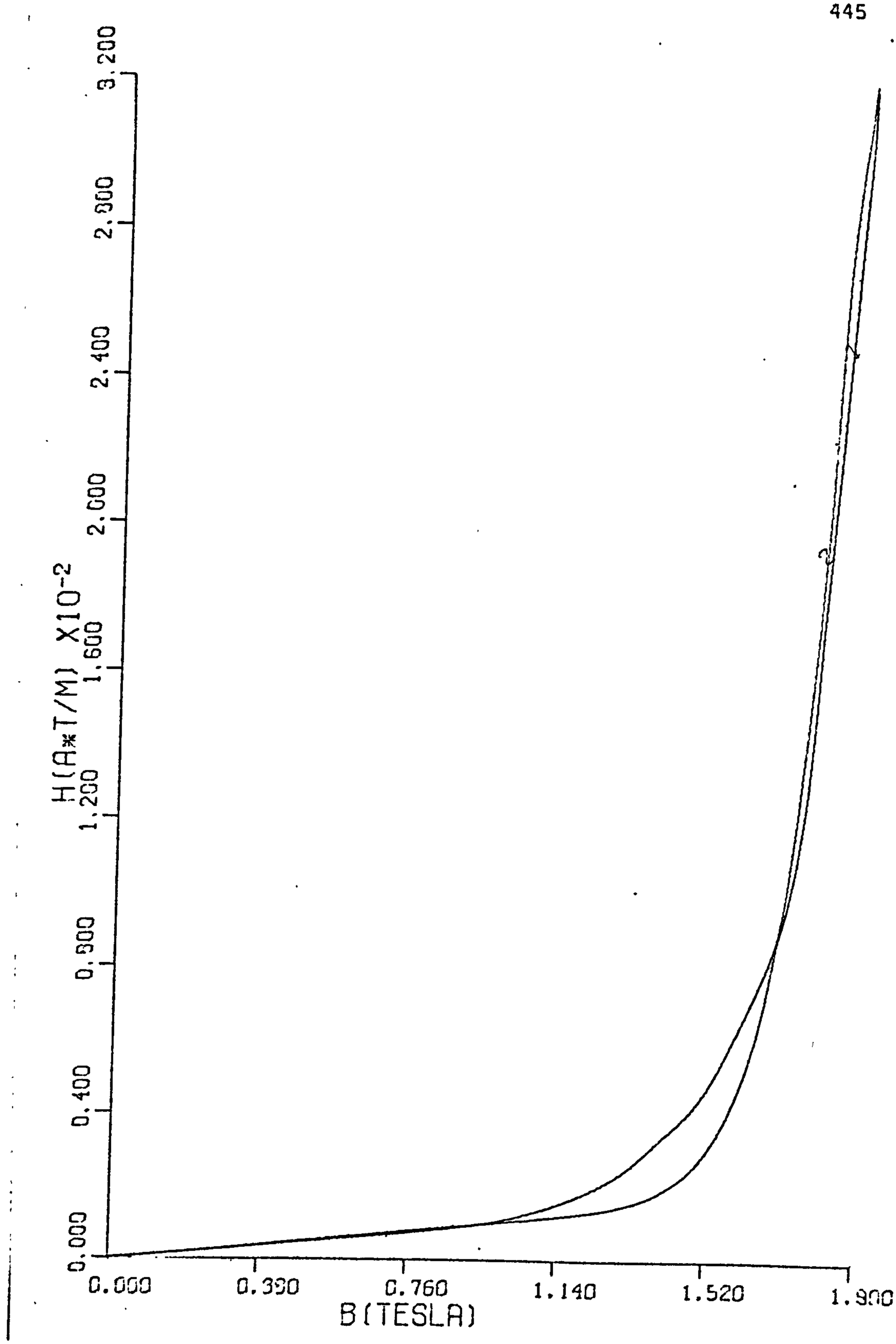

Figure 8.9 Polynomial Approximation $H = c_1 B + c_{15} B^{15}$

$c_1 = 10.628644$

$c_{15} = 0.0254539$

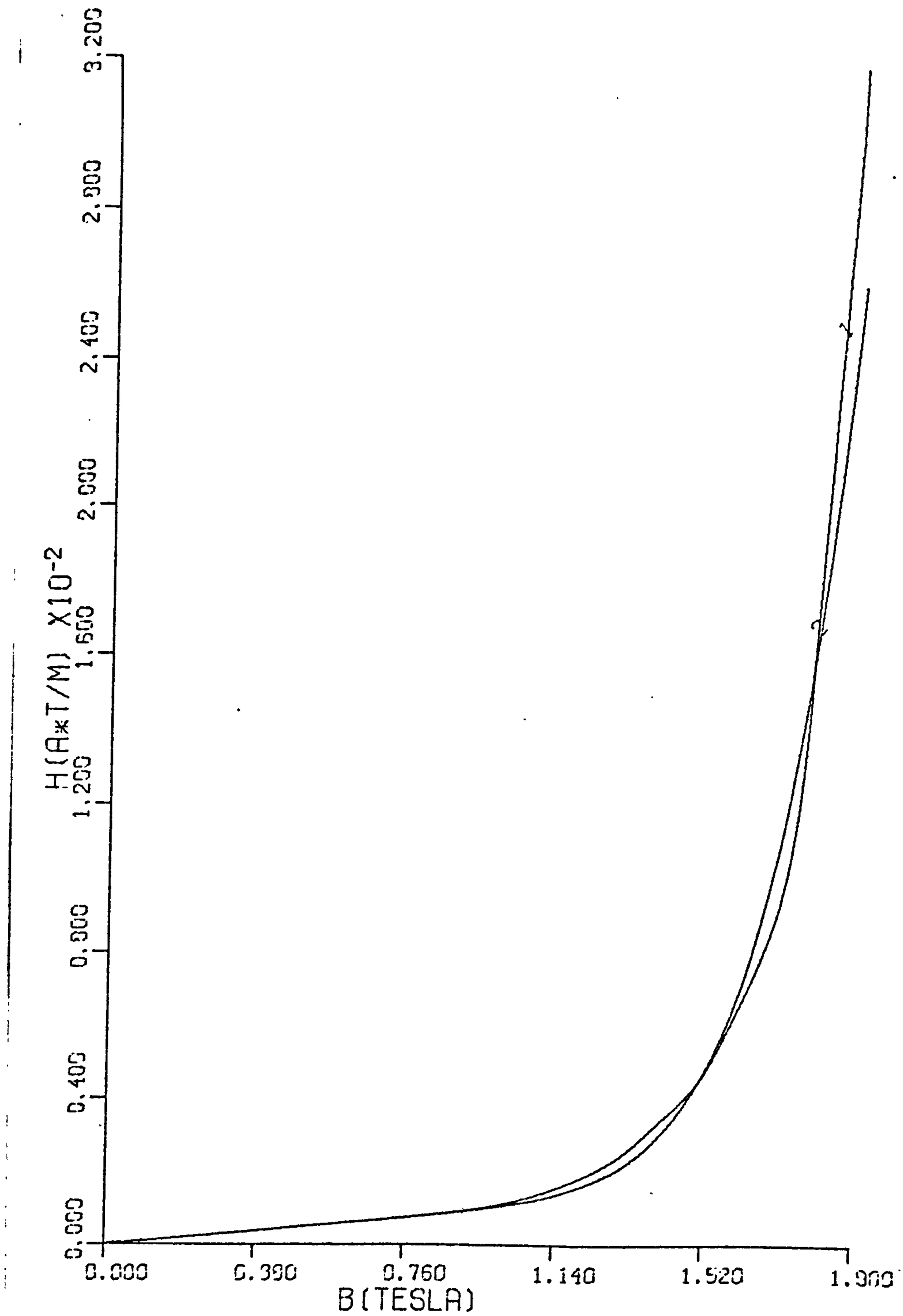

Figure 8.10 Polynominal Approximation $H = c_1 B + c_3 B^3 + c_9 B^9$

with $c_1 = 10.16103$

$c_3 = 0.04982$

$c_9 = 1.01314$

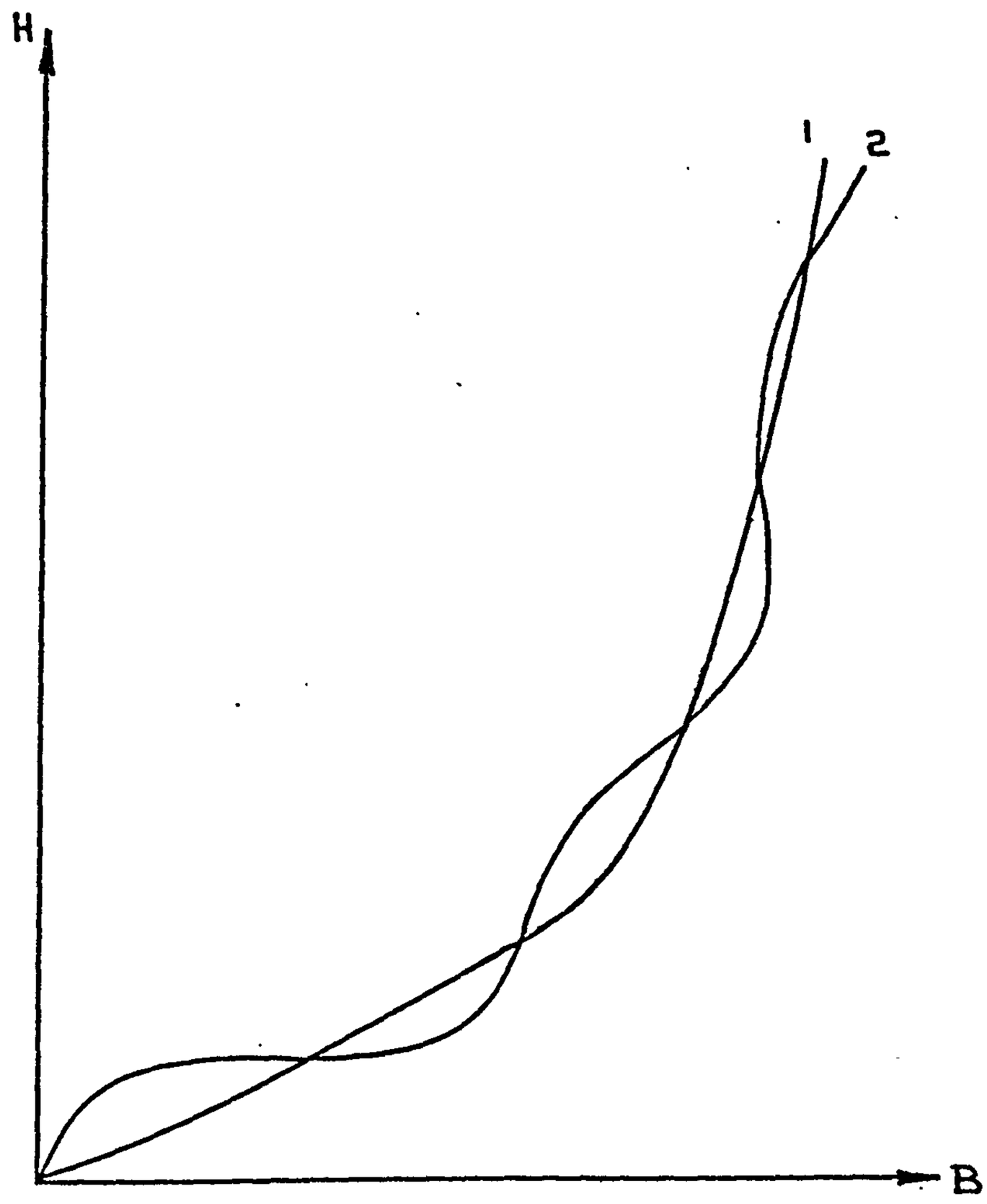

1. actual curve 2. approximate curve

Figure 8.11 Approximate curve exhibiting oscillation property in the error function

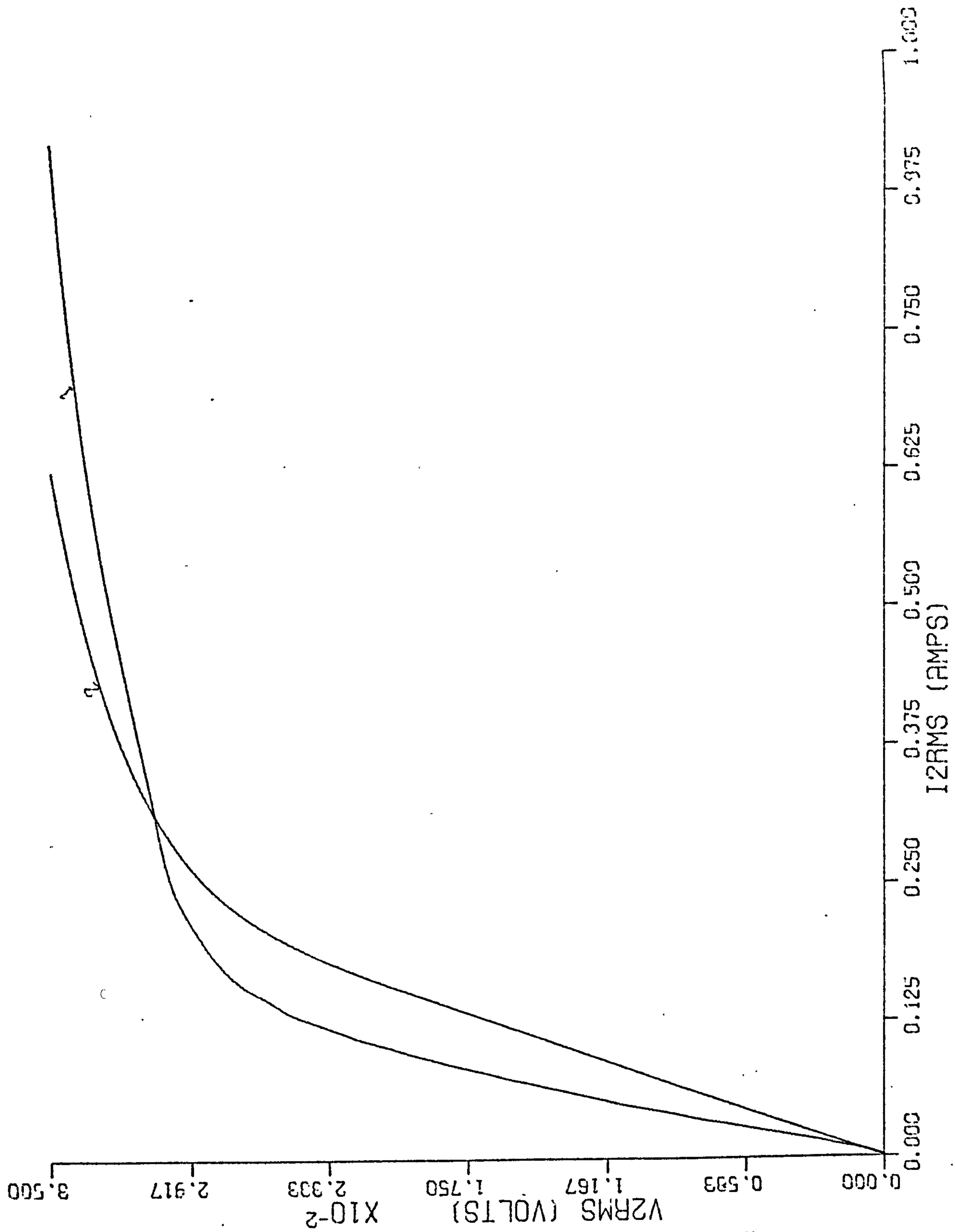

Figure 8.12 V/I Characteristics

1. Experimental
2. Theoretical, with $\ell g = 5.10^{-5}$m and $c_{11} = 0.2891732$

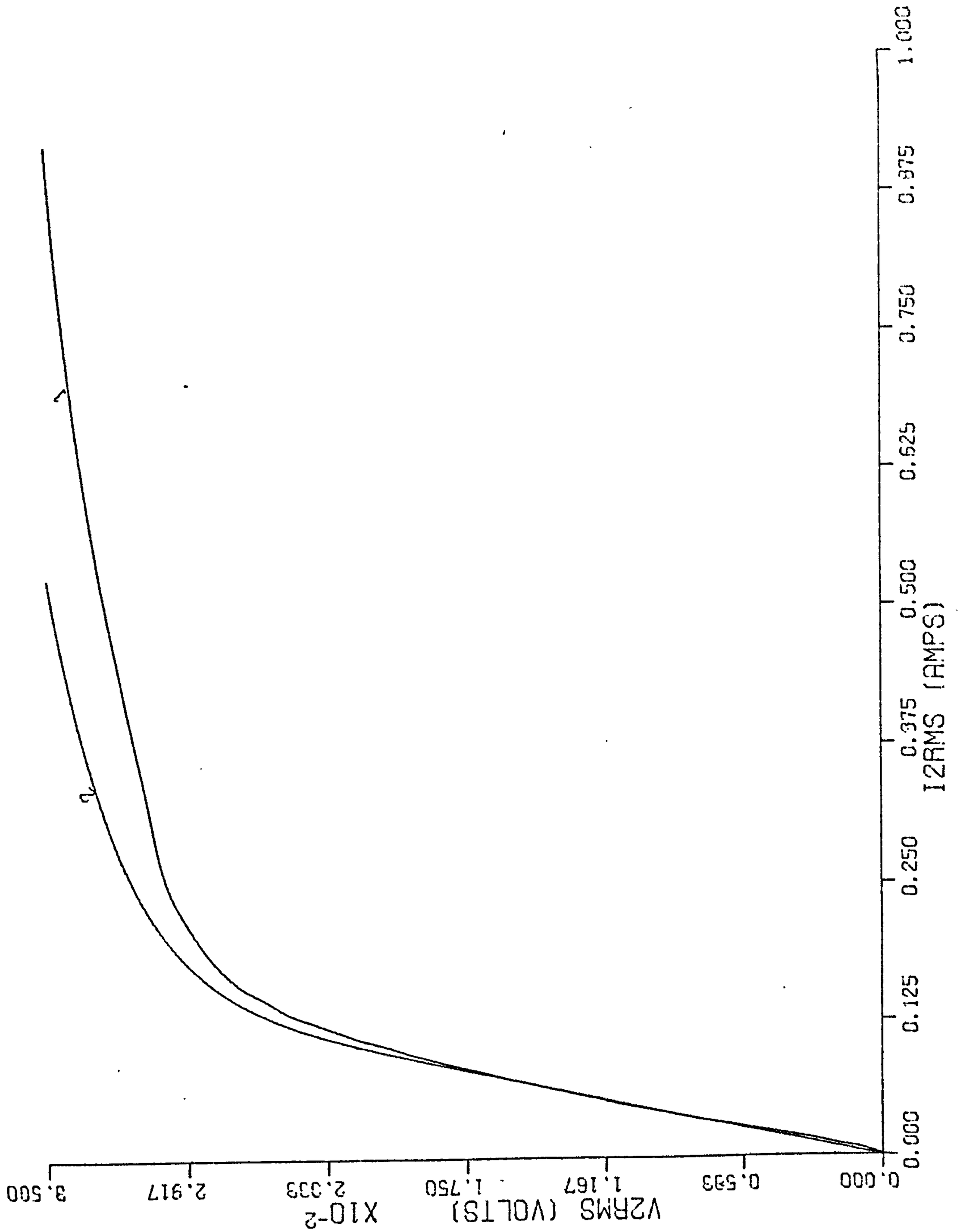

Figure 8.13 V/I Characteristics

1. Experimental
2. Theoretical, with $\ell g = 3.10^{-5}$m and $c_{11} = 0.2891732$

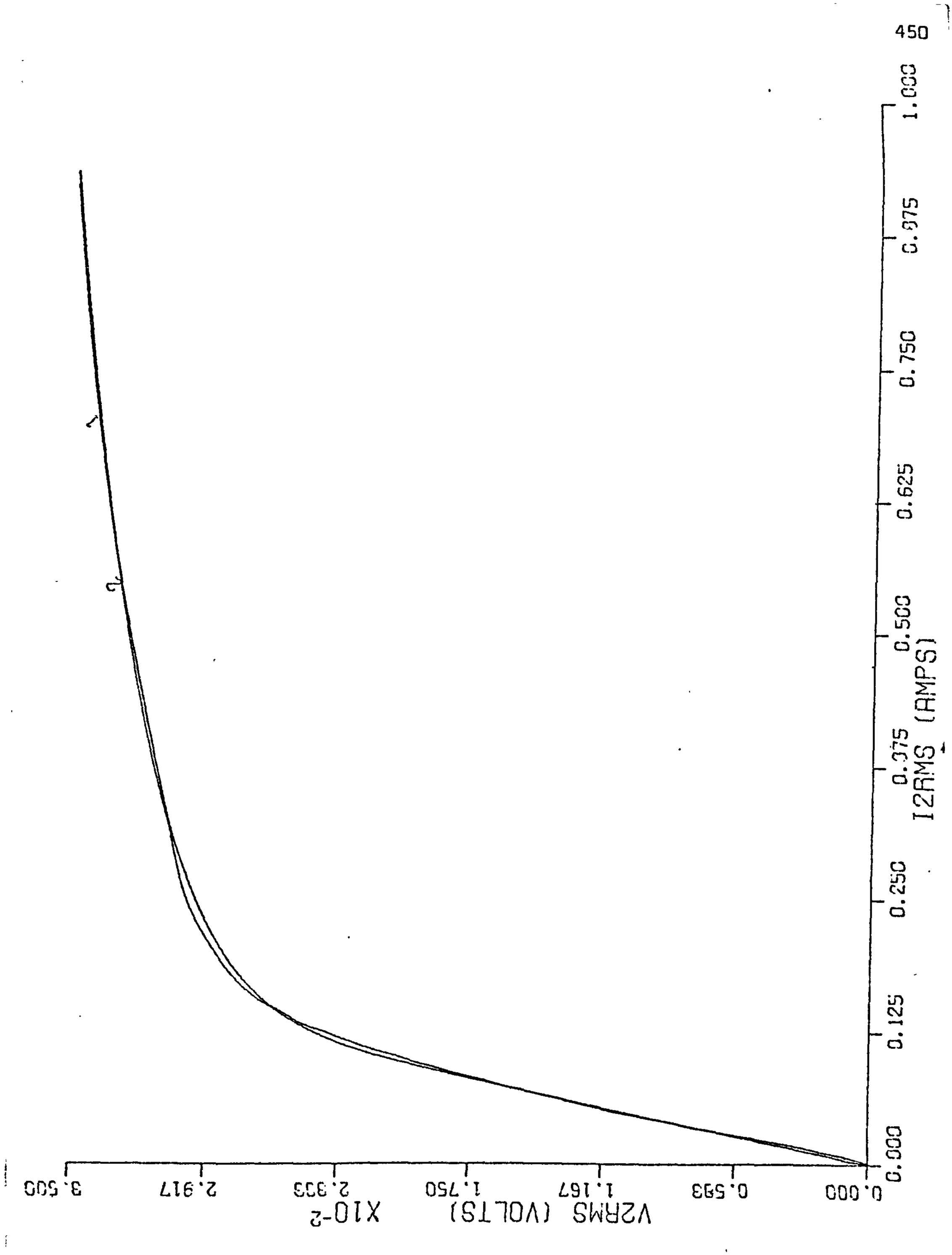

Figure 8.14 V/I Characteristics

1. Experimental.
2. Theoretical, with $\ell g = 3.10^{-5}$m and $c_{11} = 0.590113$

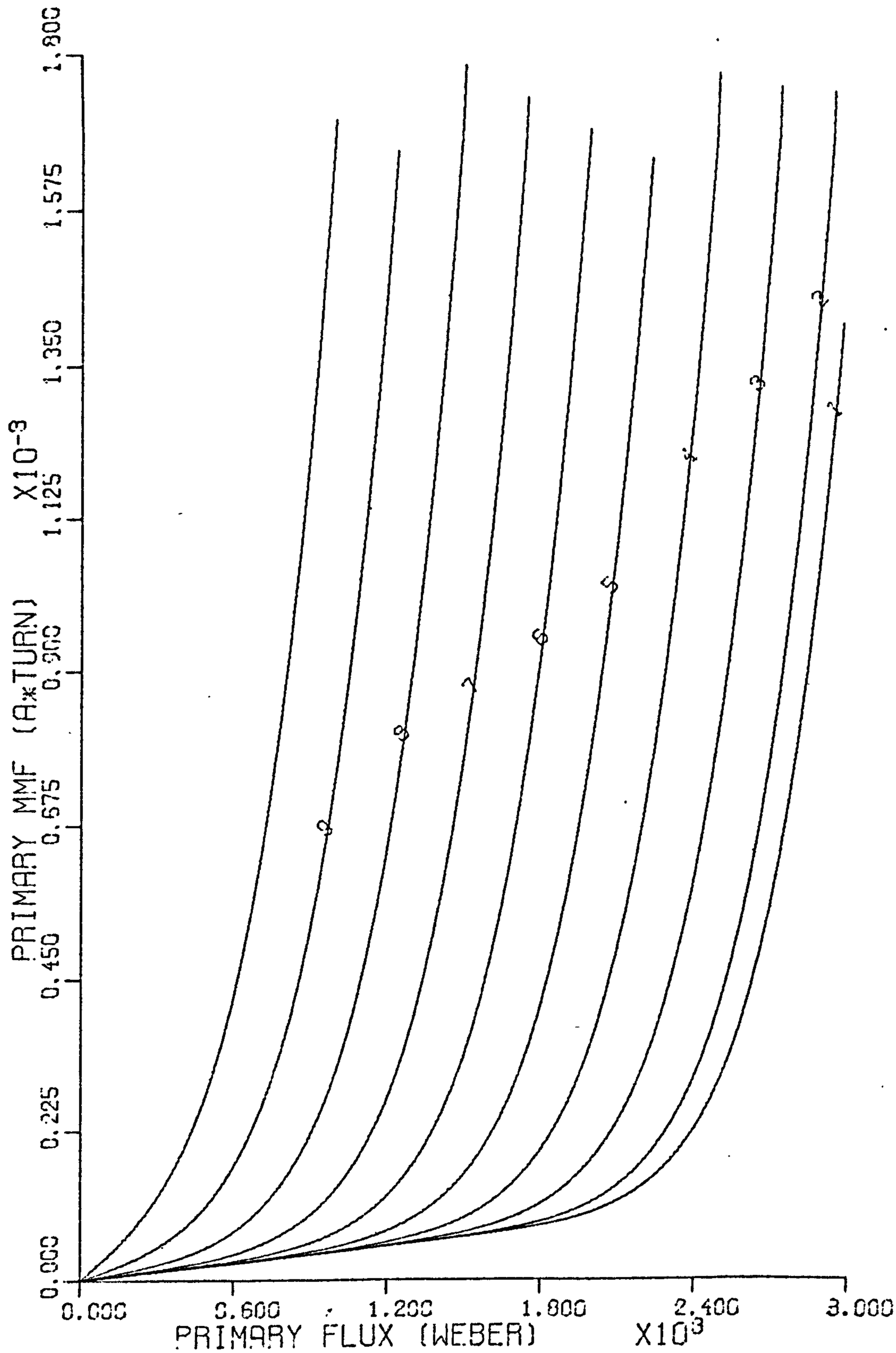

Figure 8.15 Family of Curves Representing the function $F_1(\phi_1, \phi_2)$

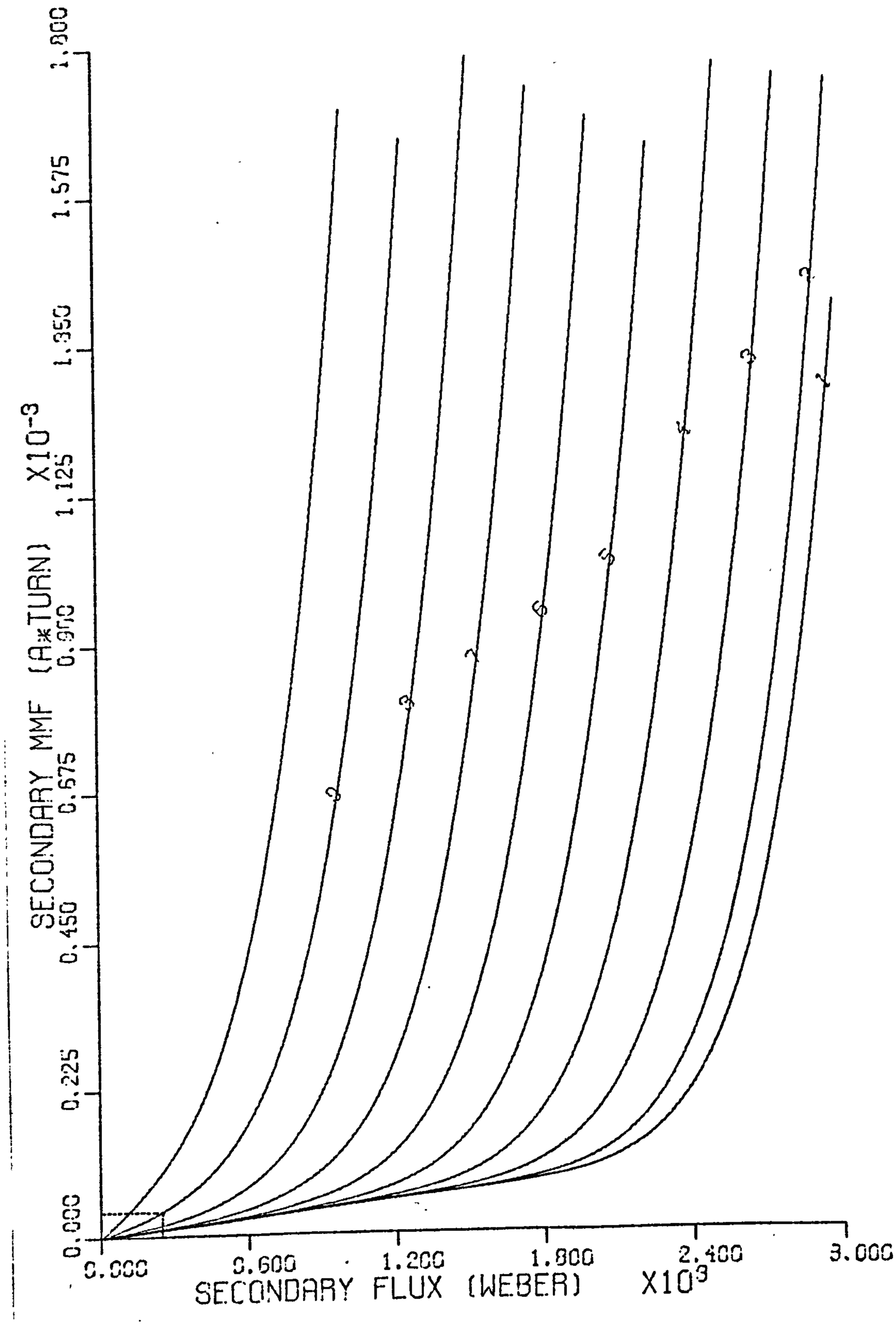

Figure 8.16 Family of Curves Representing the Function $F_2(\phi_1, \phi_2)$

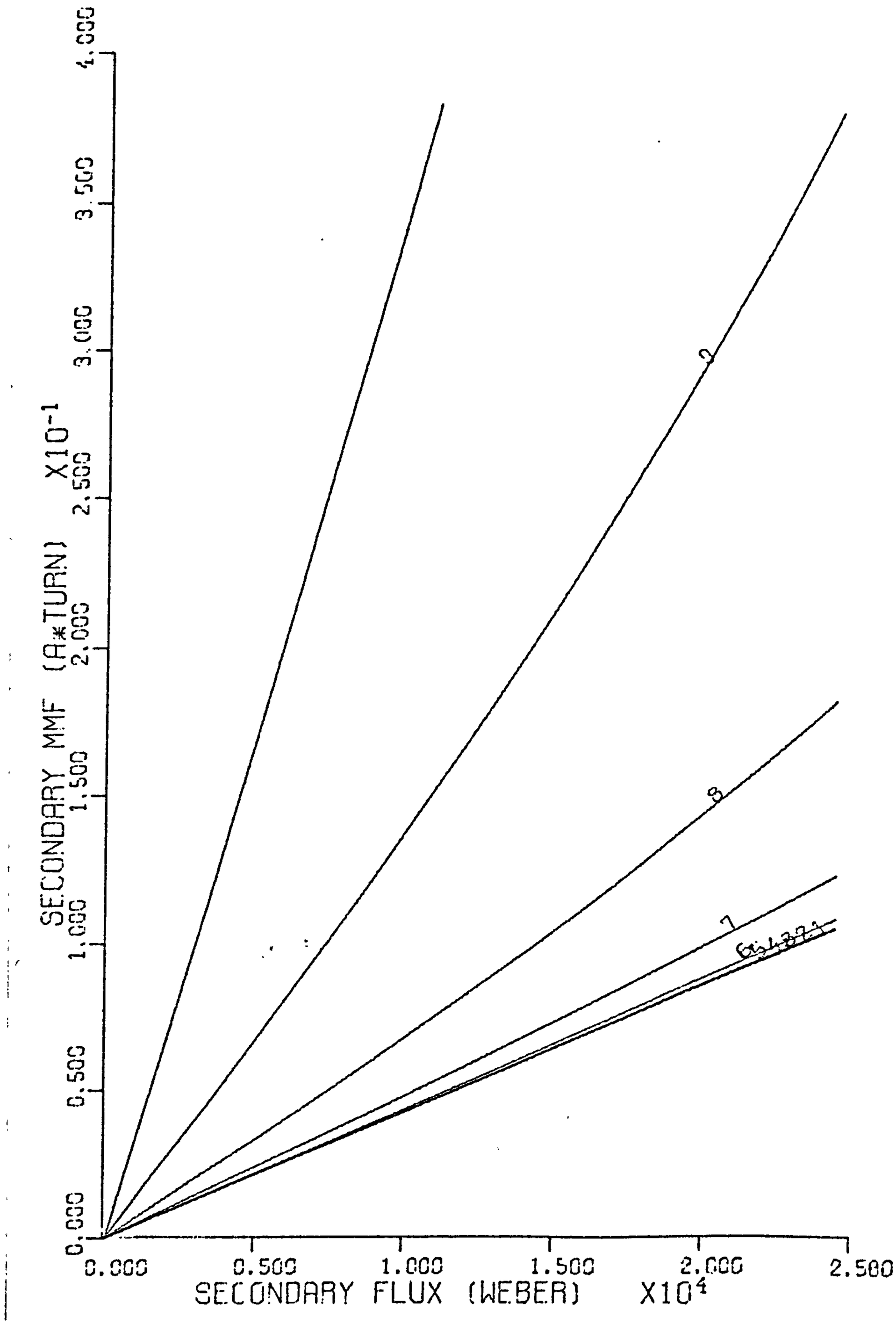

Figure 8.17 Portions of the Curves near the Origin

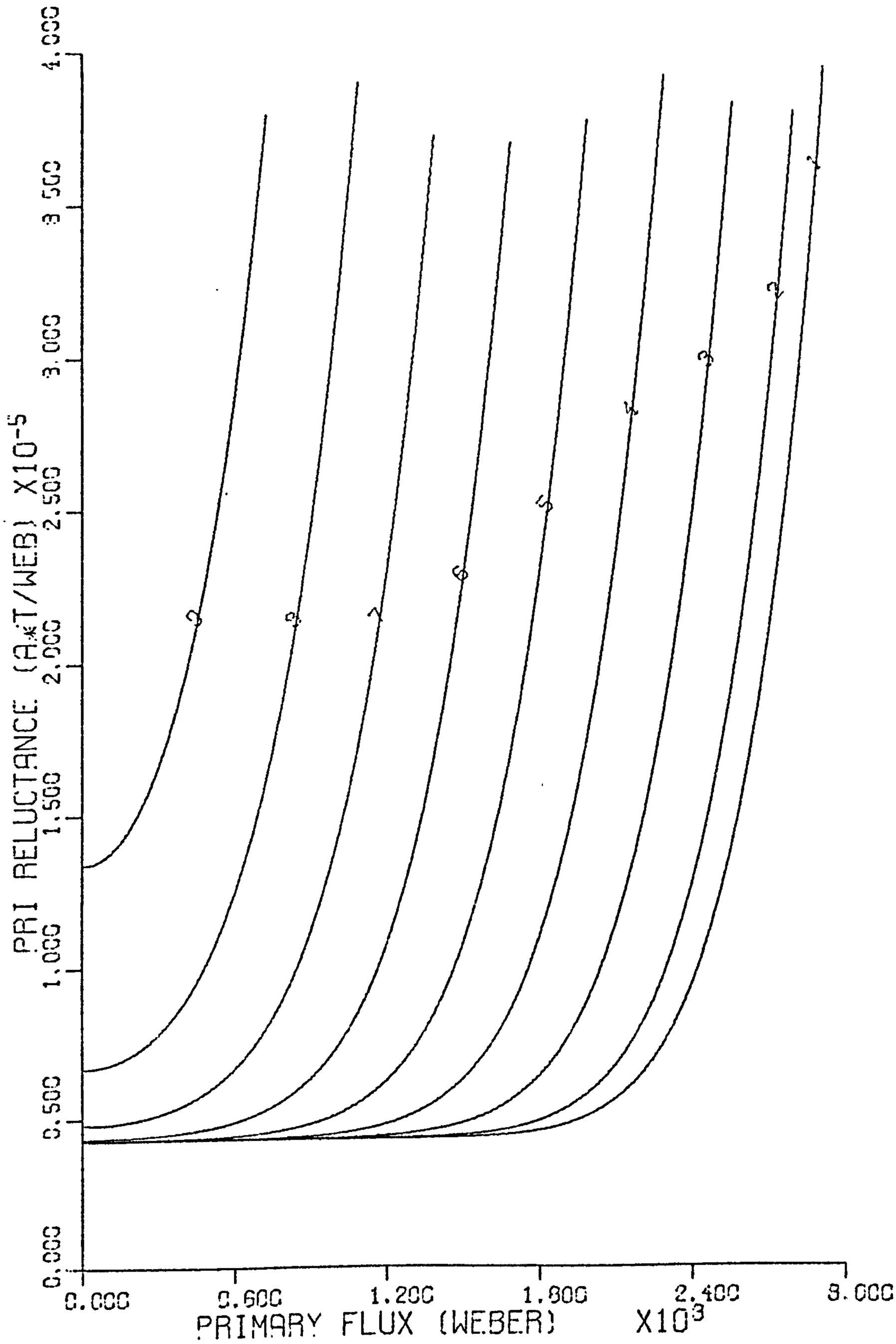

Figure 8.18 Family of Curves Representing the function R_{m1} (ϕ_1, ϕ_2)

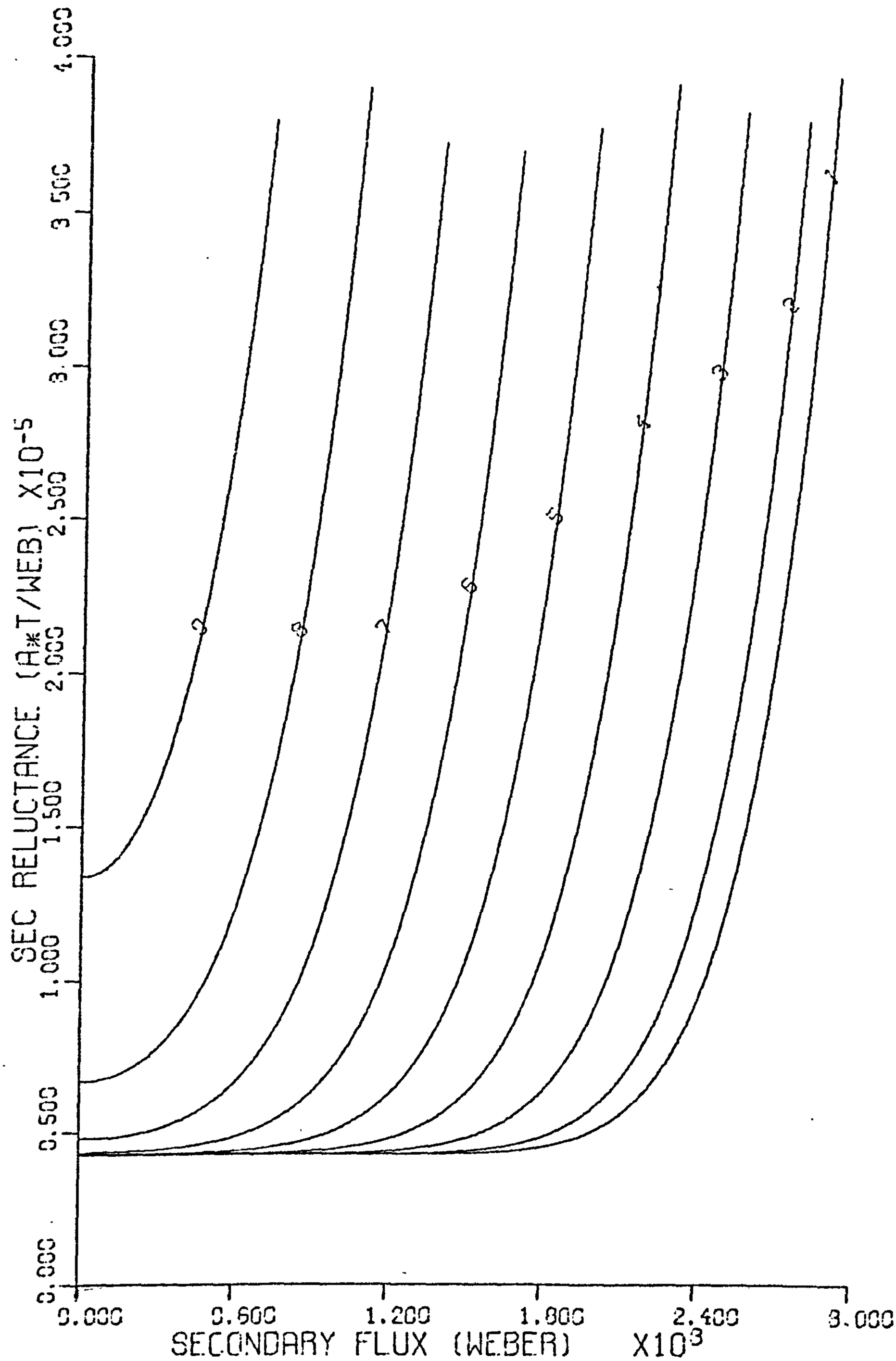

Figure 8.19 Family of Curves Representing the Function R_{m2} (ϕ_1, ϕ_2)

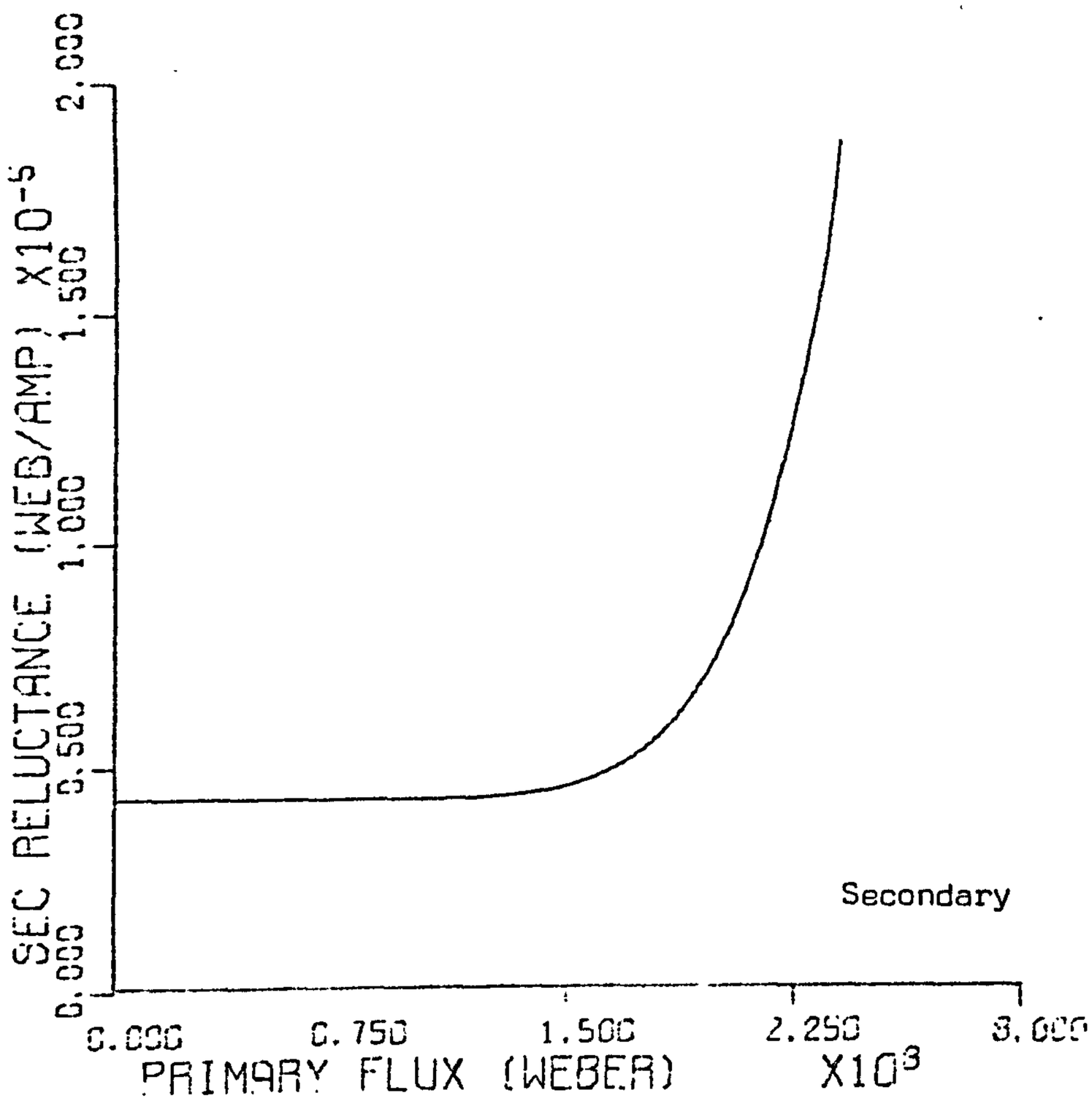

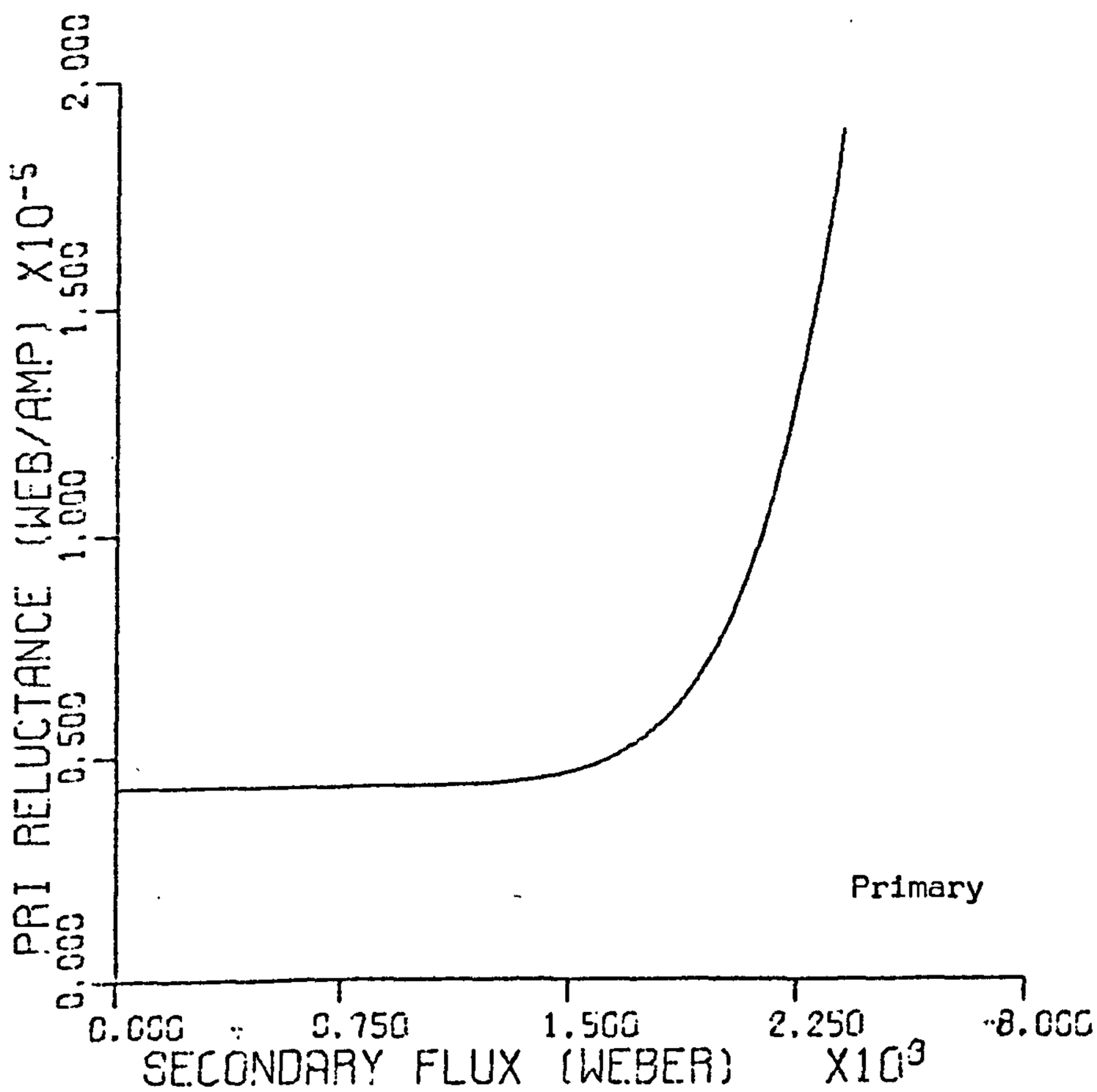

Figure 8.20 Primary and Secondary Trans-reluctance Characteristics

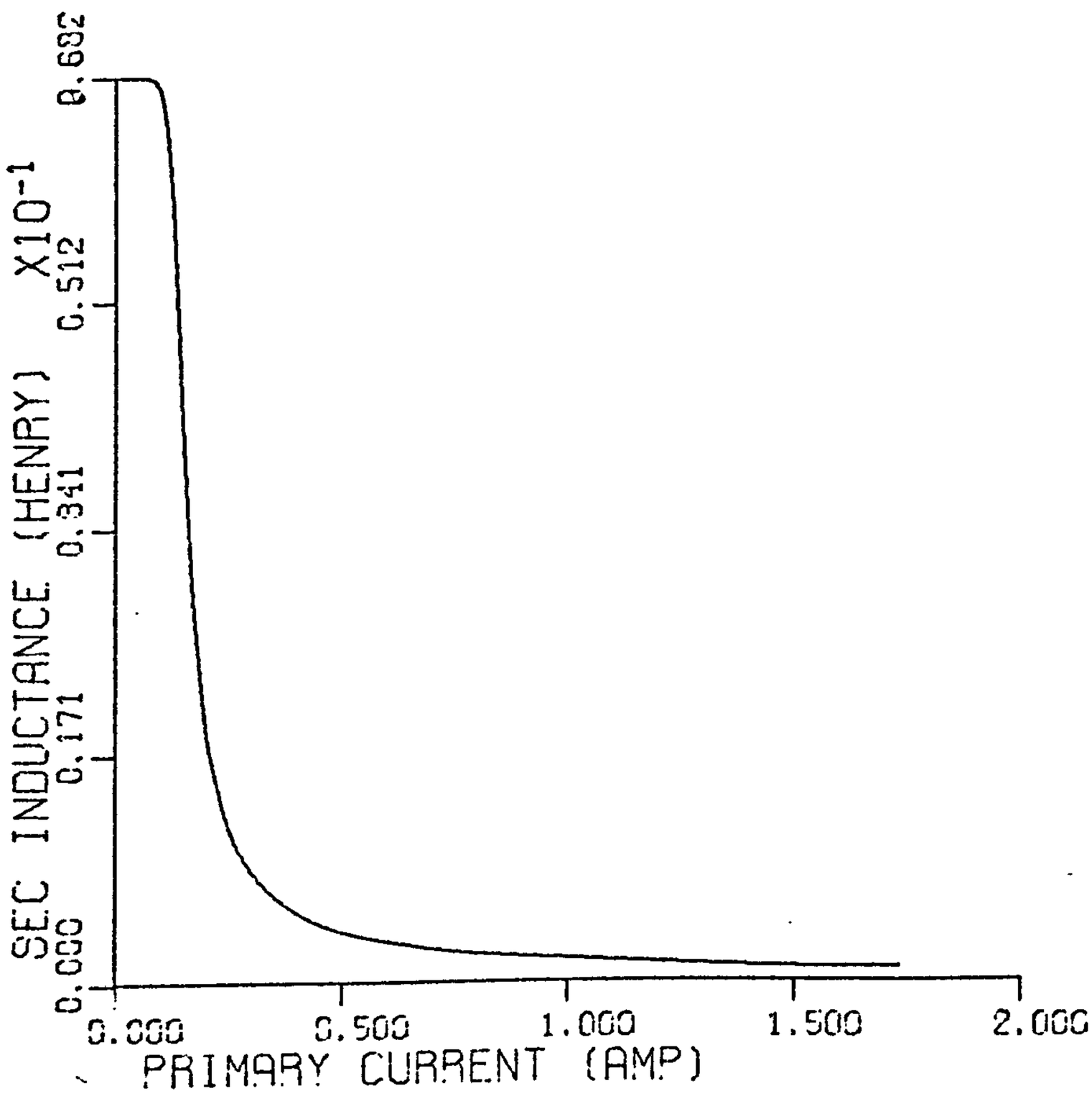

Figure 8.21 Secondary Trans-inductance Characteristic

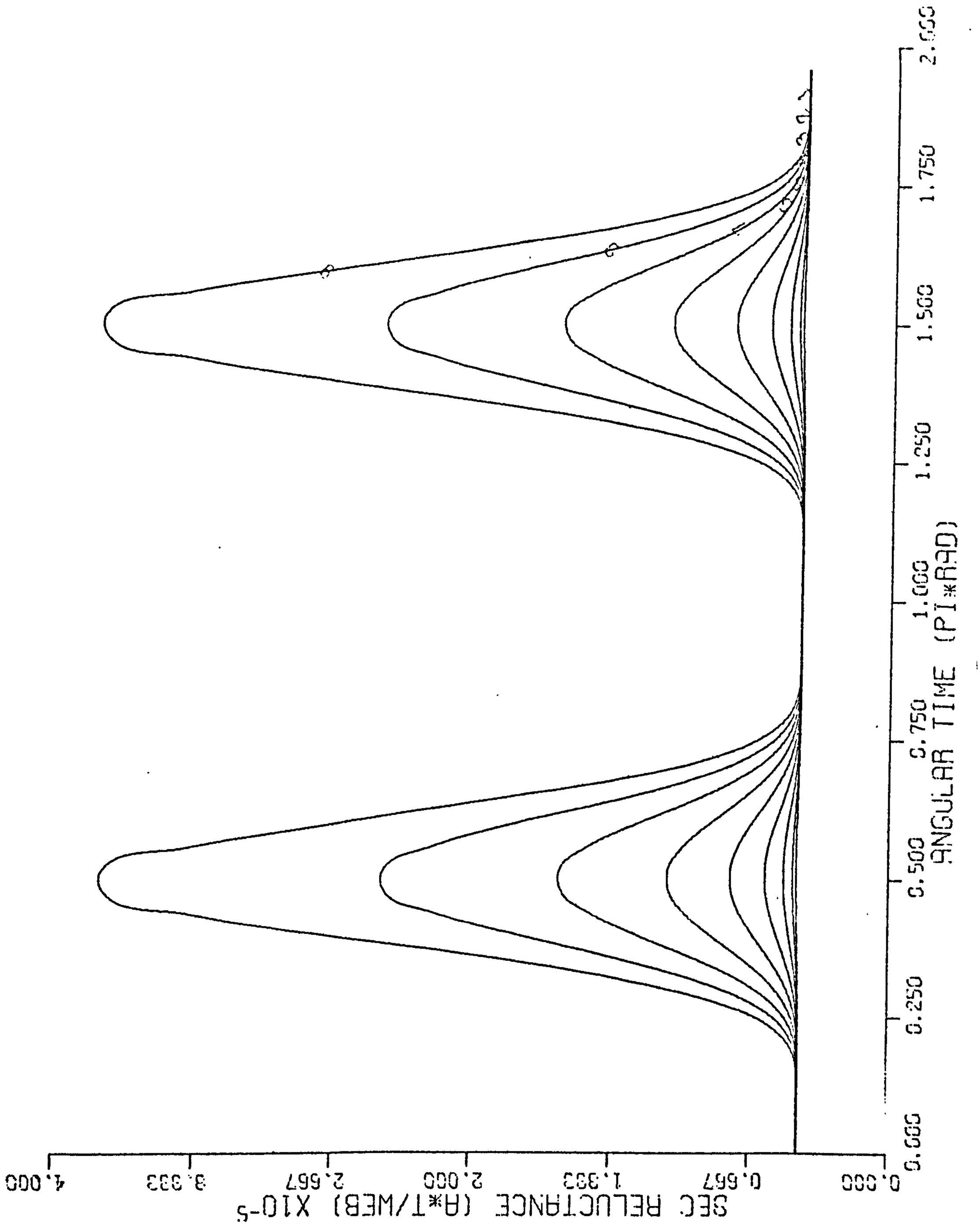

Figure 8.22 Variations in the Secondary Reluctance

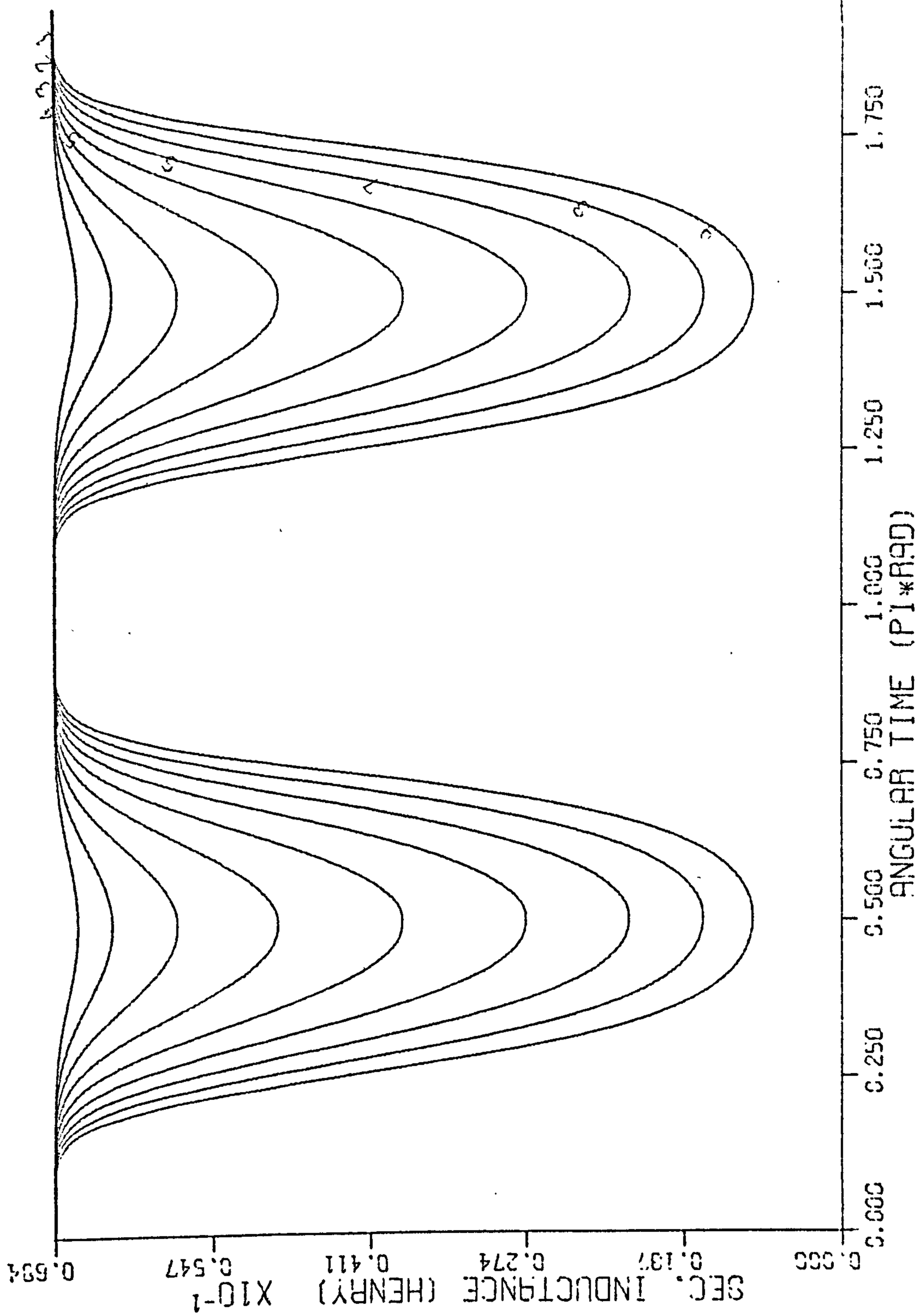

Figure 8.23 Variations in the Secondary Inductance

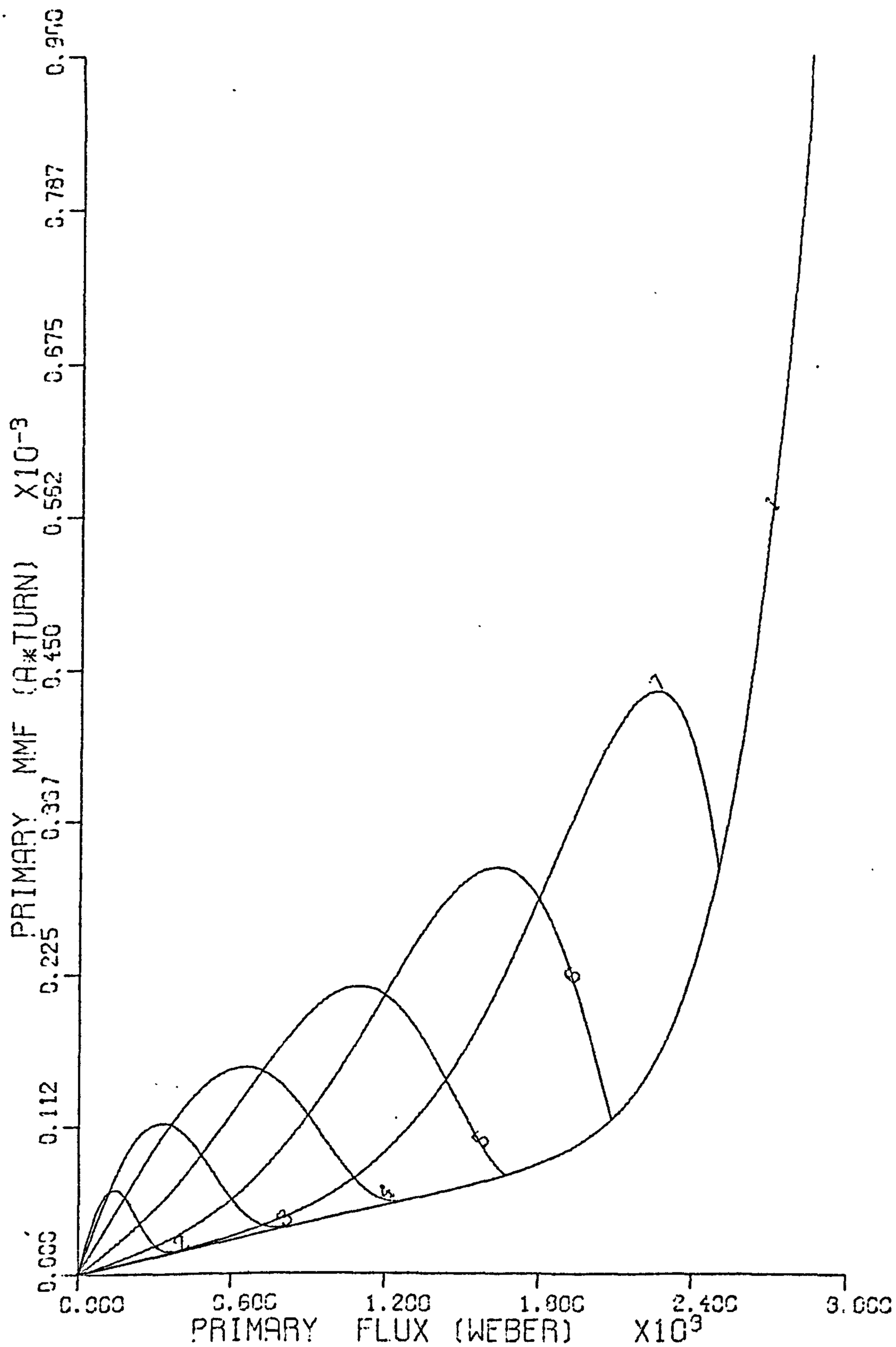

Figure 8.24 Primary Relative Magnetisation Characteristics

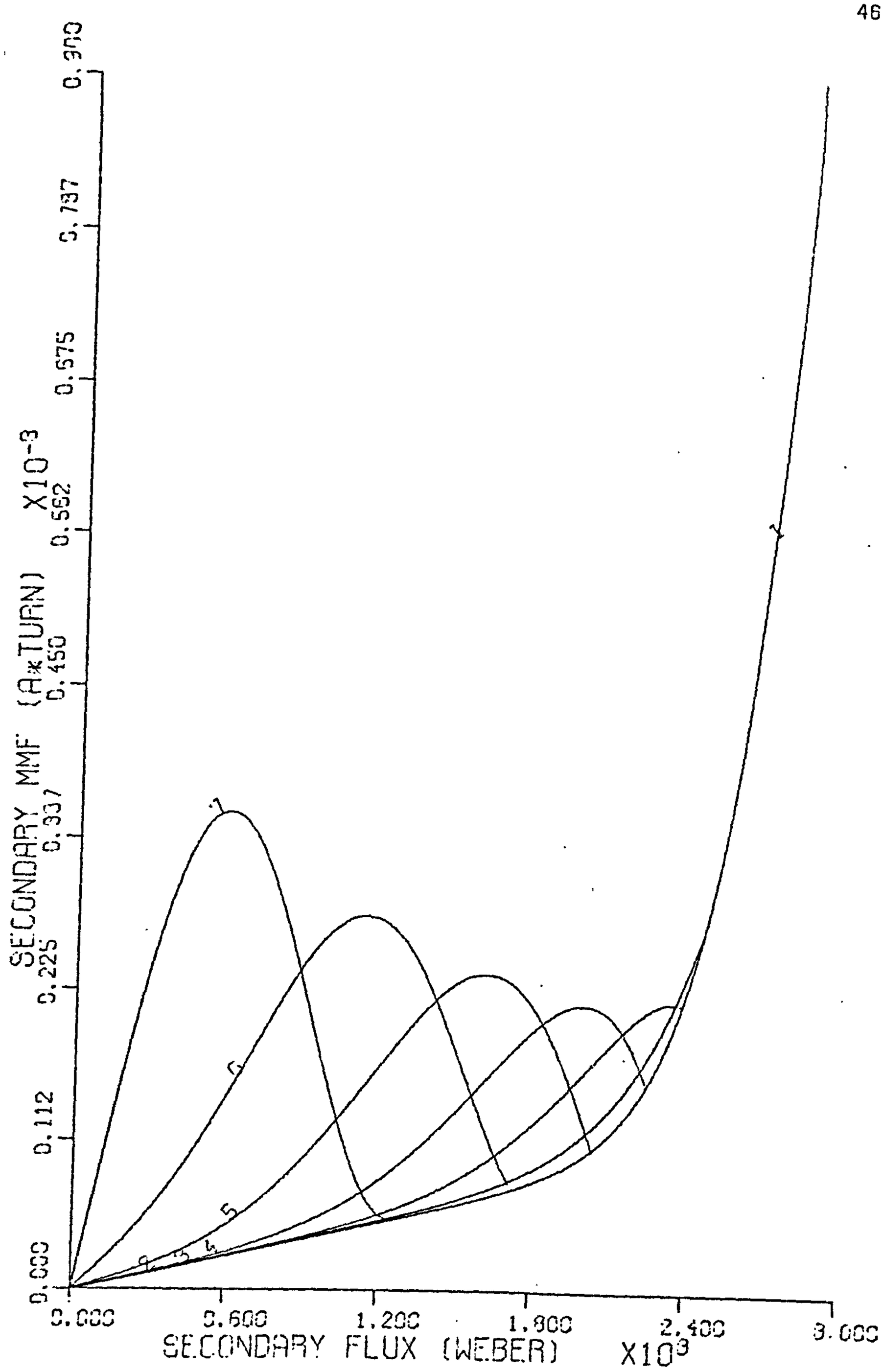

Figure 8.25 Secondary Relative Magnetisation Characteristics

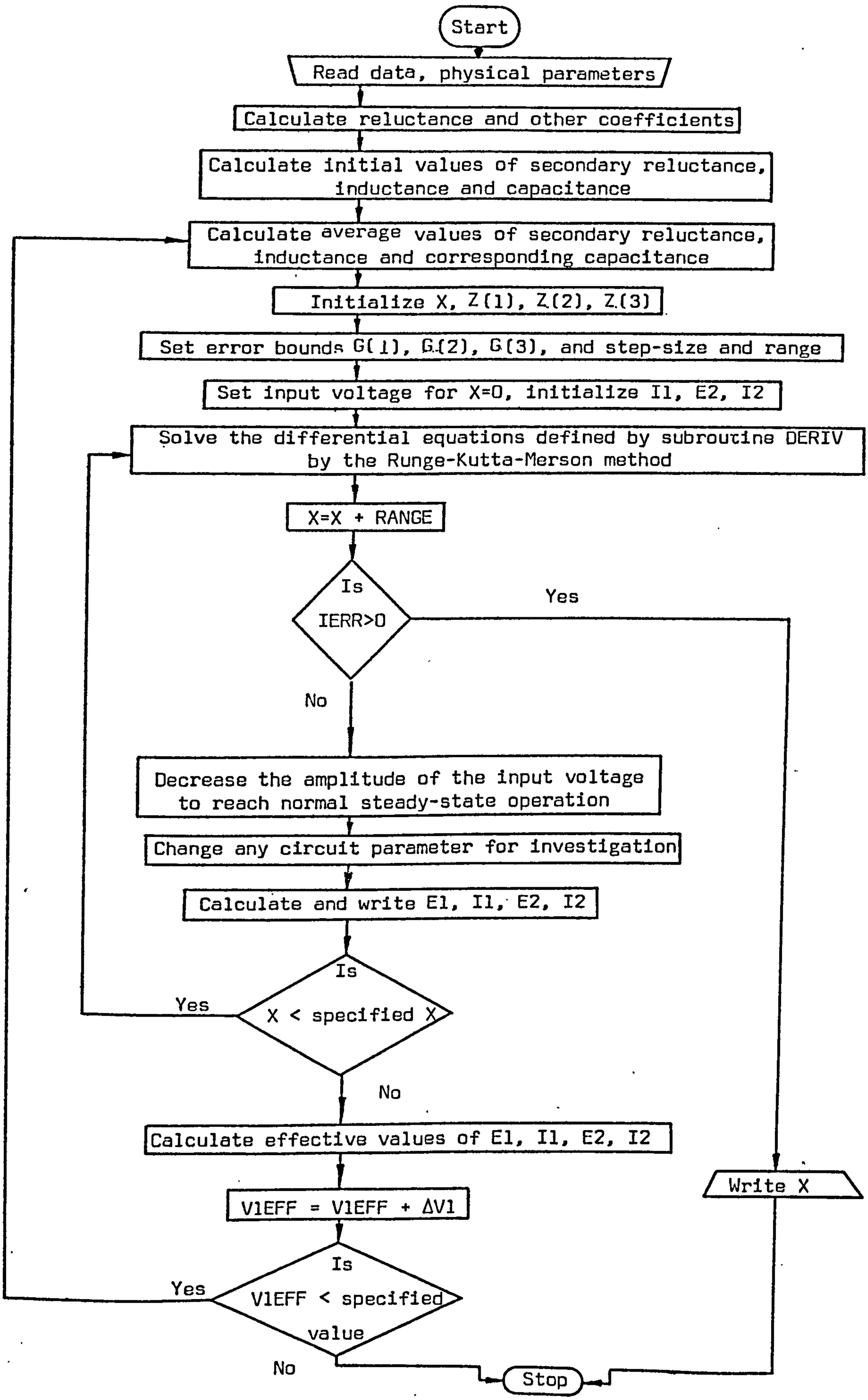

Figure 8.26 Block diagram for the process of solving the system equations

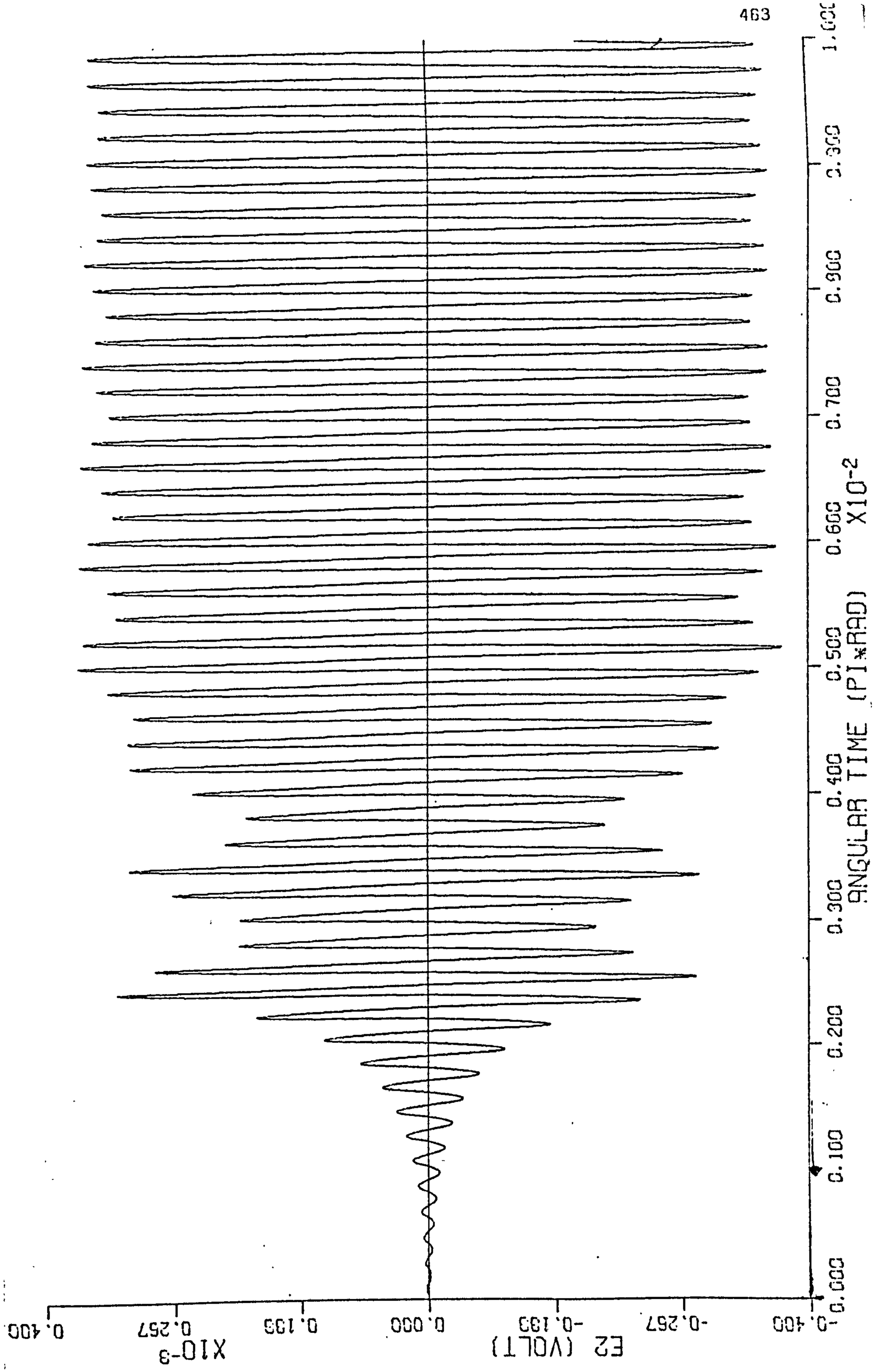

Figure 8.27 Build-up of oscillations

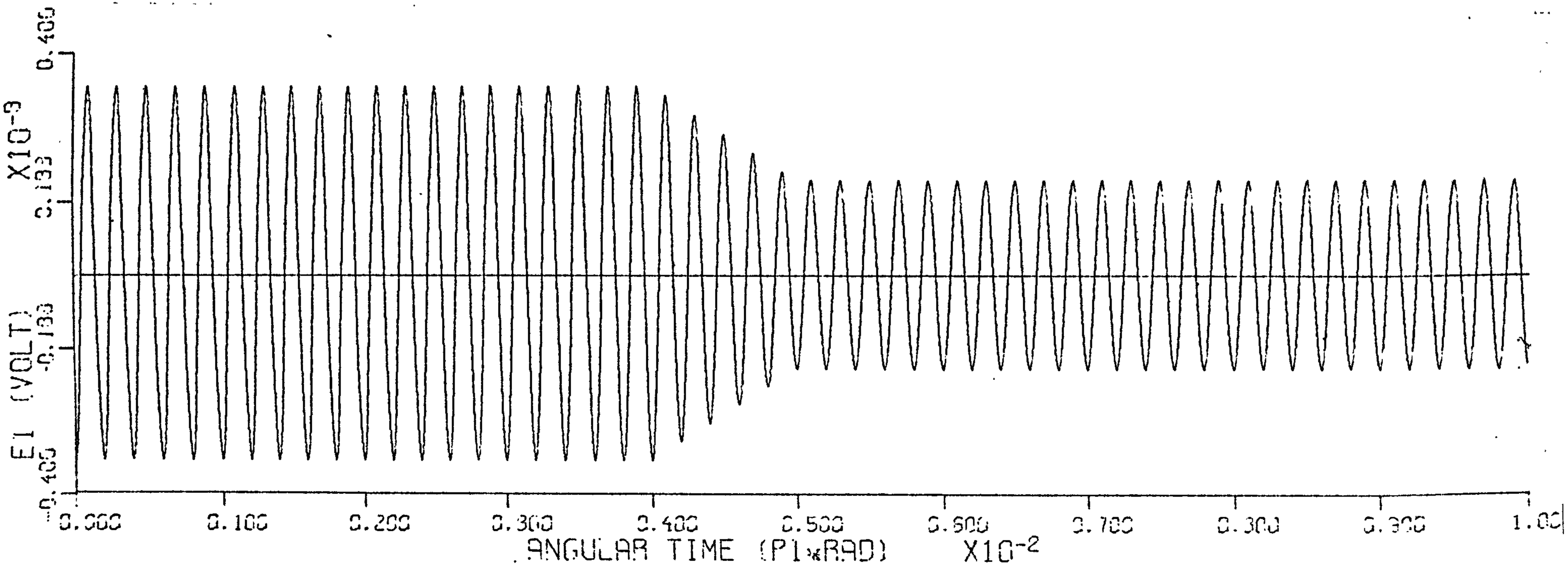
E1 (VOLT) X10-3
0.400
0.133
-0.133
-0.400
0.000
0.100
0.200
0.300
0.400
0.500
0.600
0.700
0.800
0.900
1.00
ANGULAR TIME (PI*RAD) X10-2

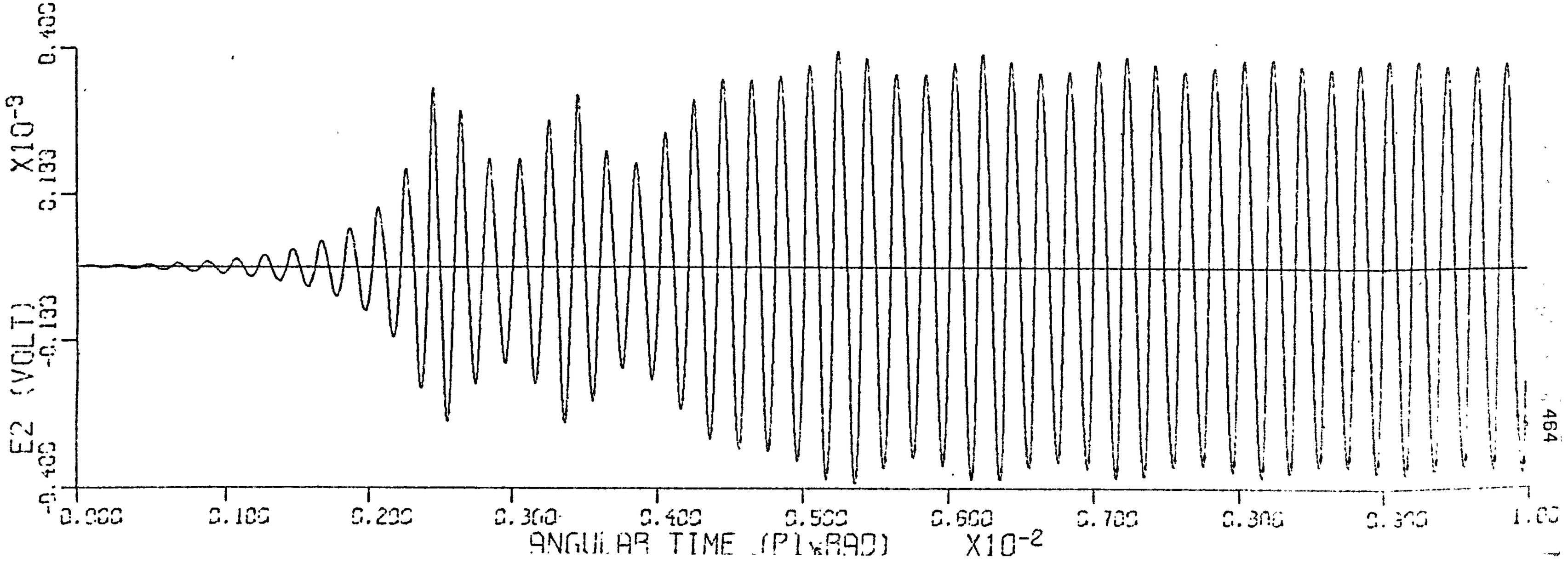
E2 (VOLT) X10-3
0.400
0.133
-0.133
-0.400
0.000
0.100
0.200
0.300
0.400
0.500
0.600
0.700
0.800
0.900
1.00
ANGULAR TIME (PI*RAD) X10-2

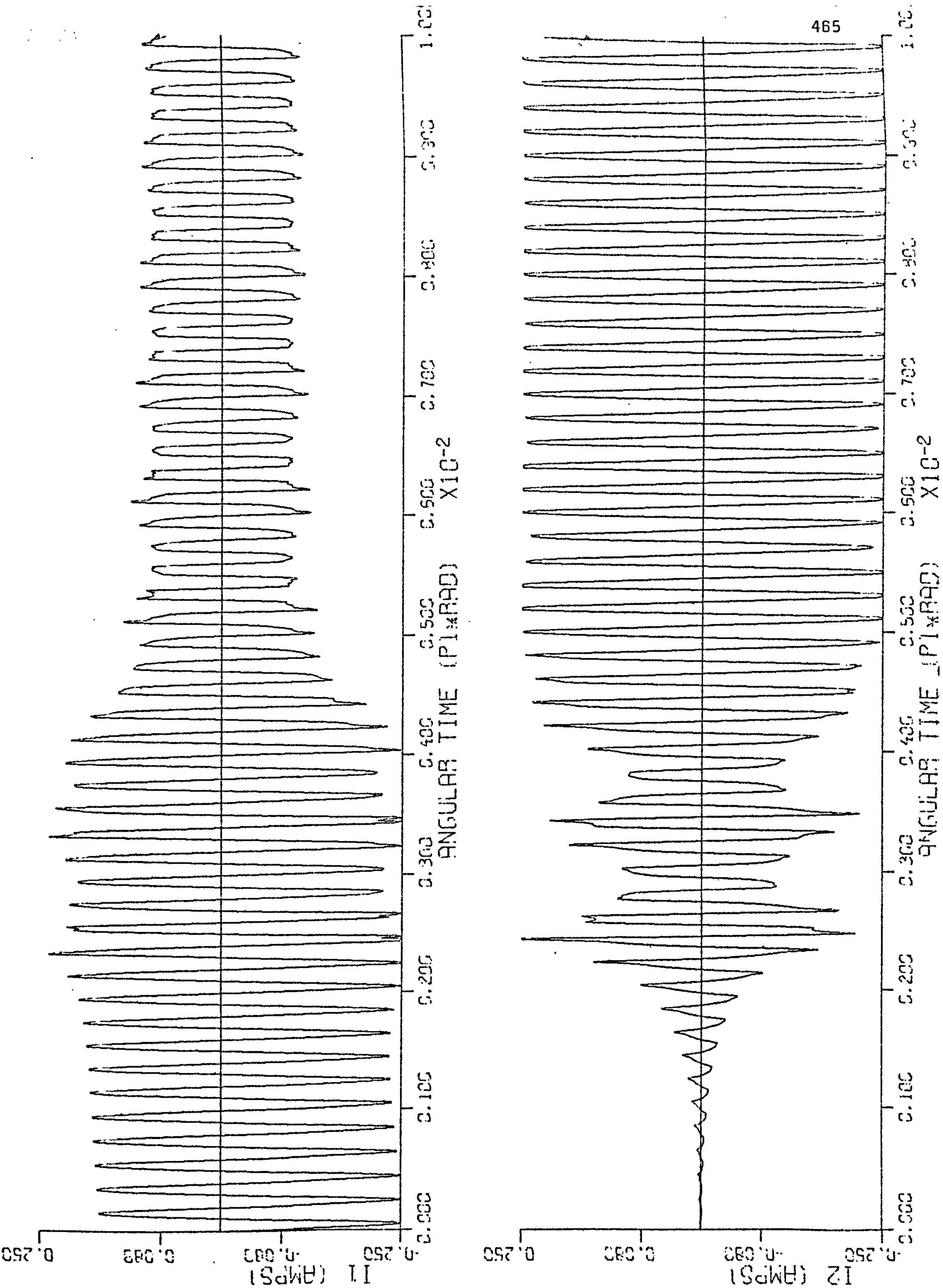

Figure 8.28b Current waveforms pertaining to Figure 8.28a

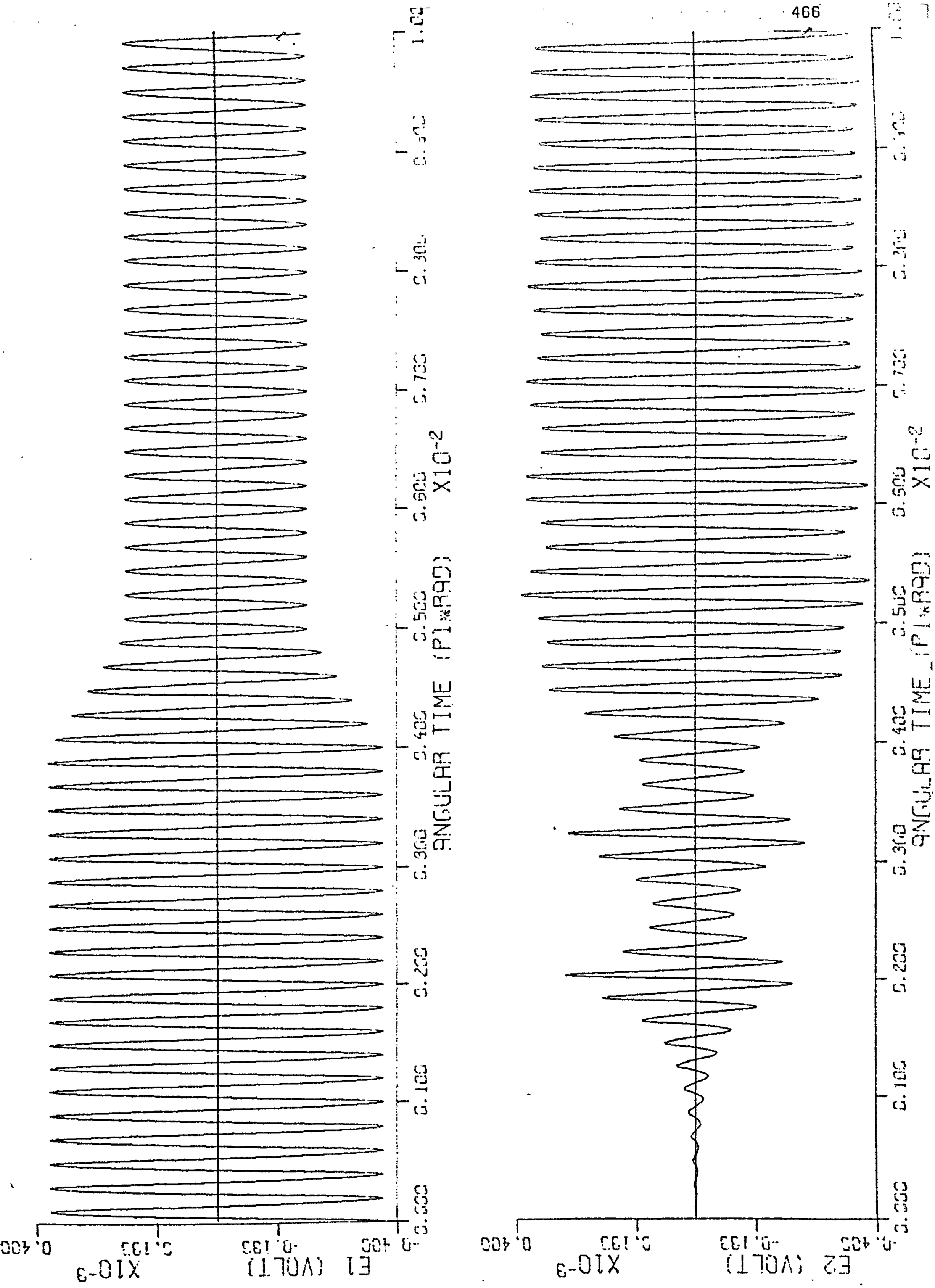

Figure 8.29a Operation at steady-state

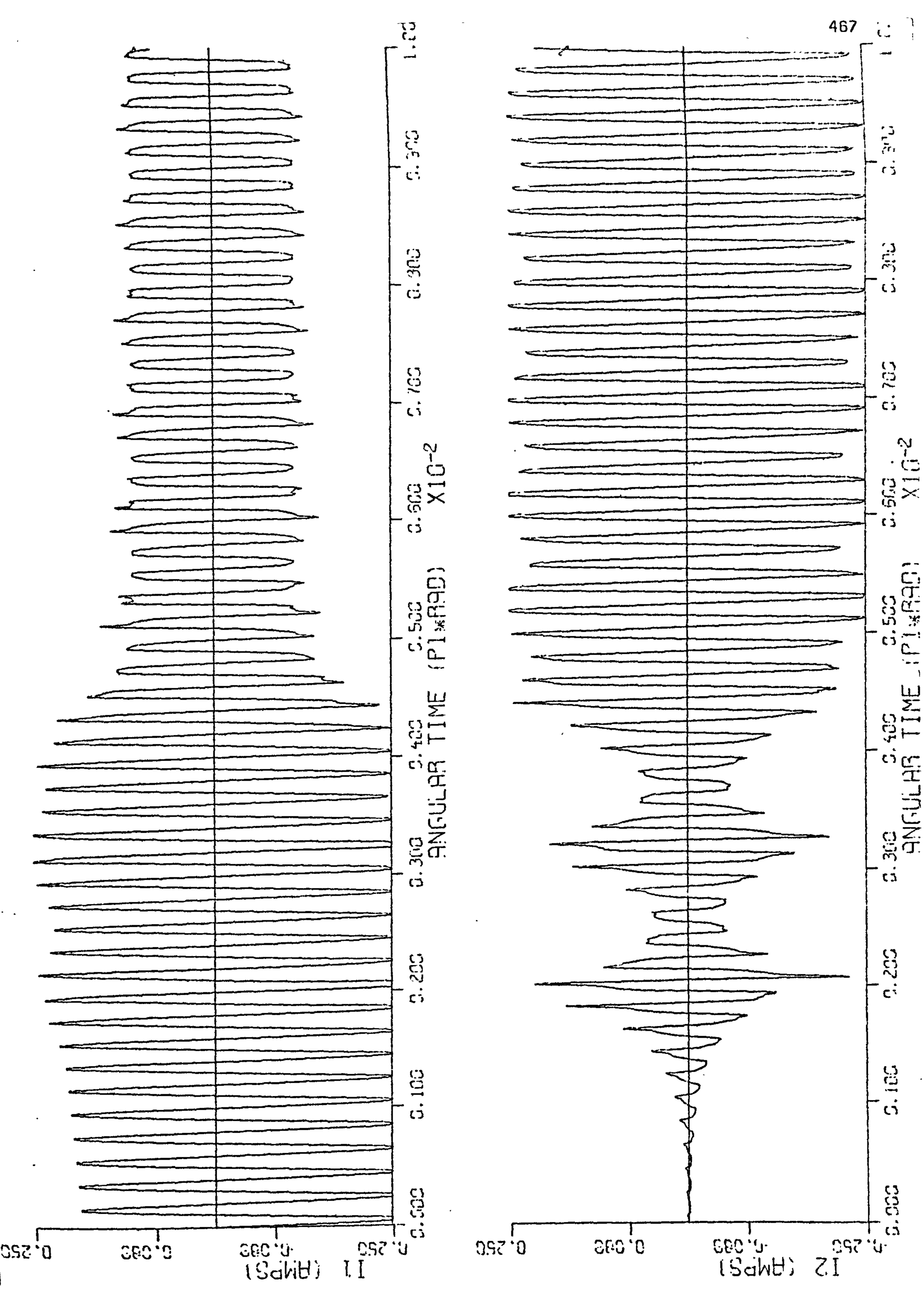

Figure 8.29b Current waveforms pertaining to Figure 8.29a

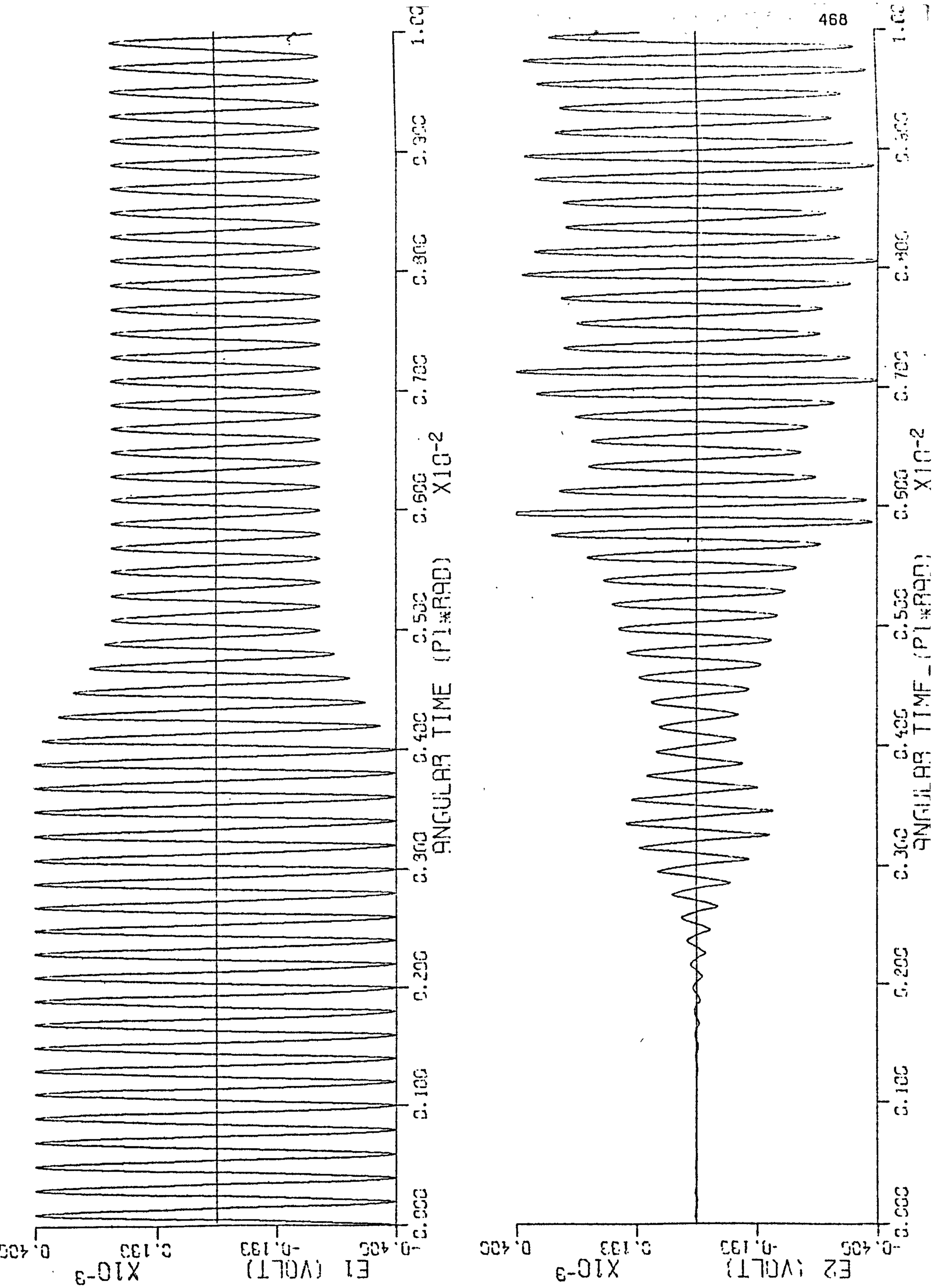

Figure 8.30a Operation at steady-state

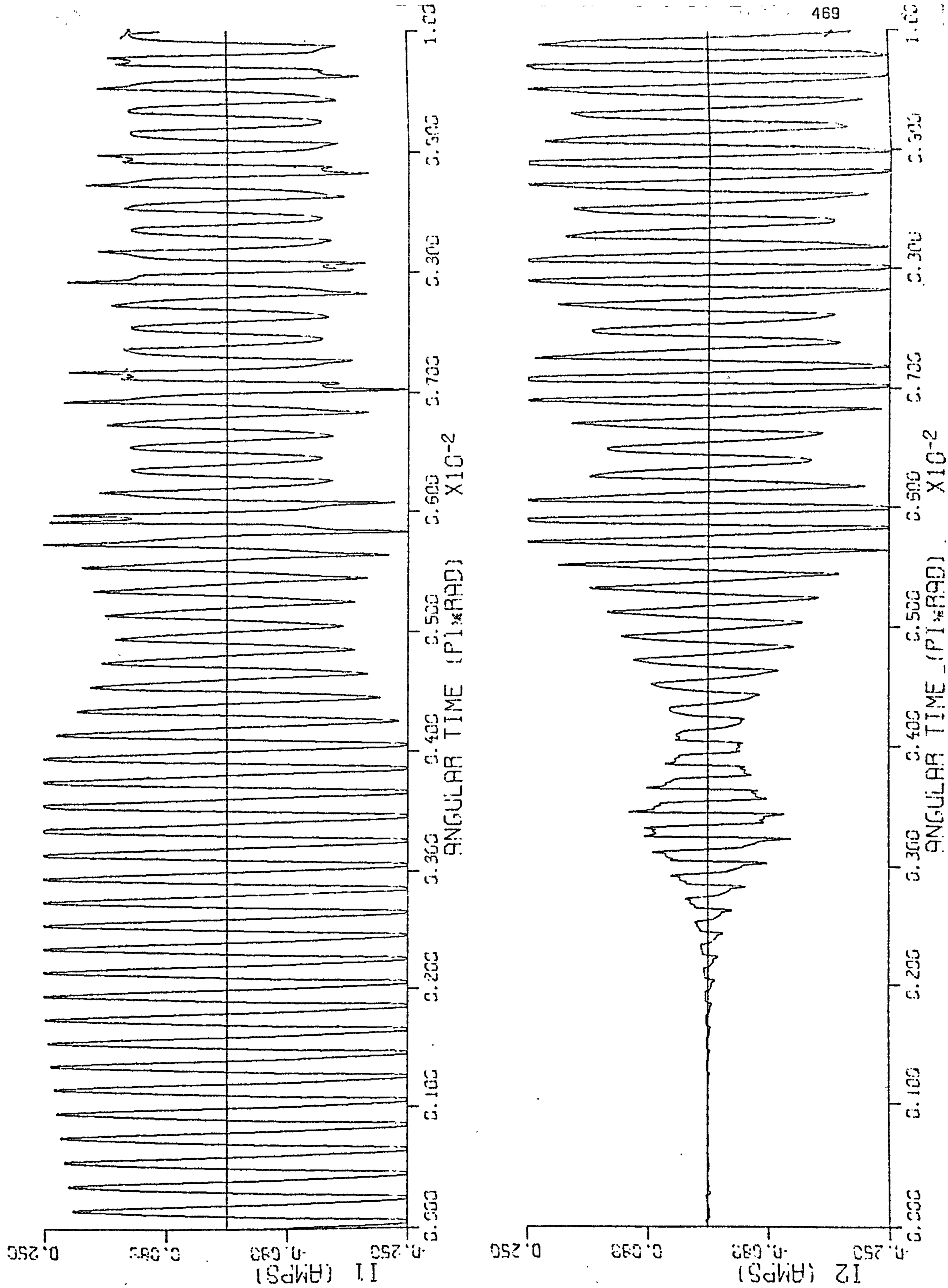

Figure 8.30b Current waveforms pertaining to Figure 8.30a

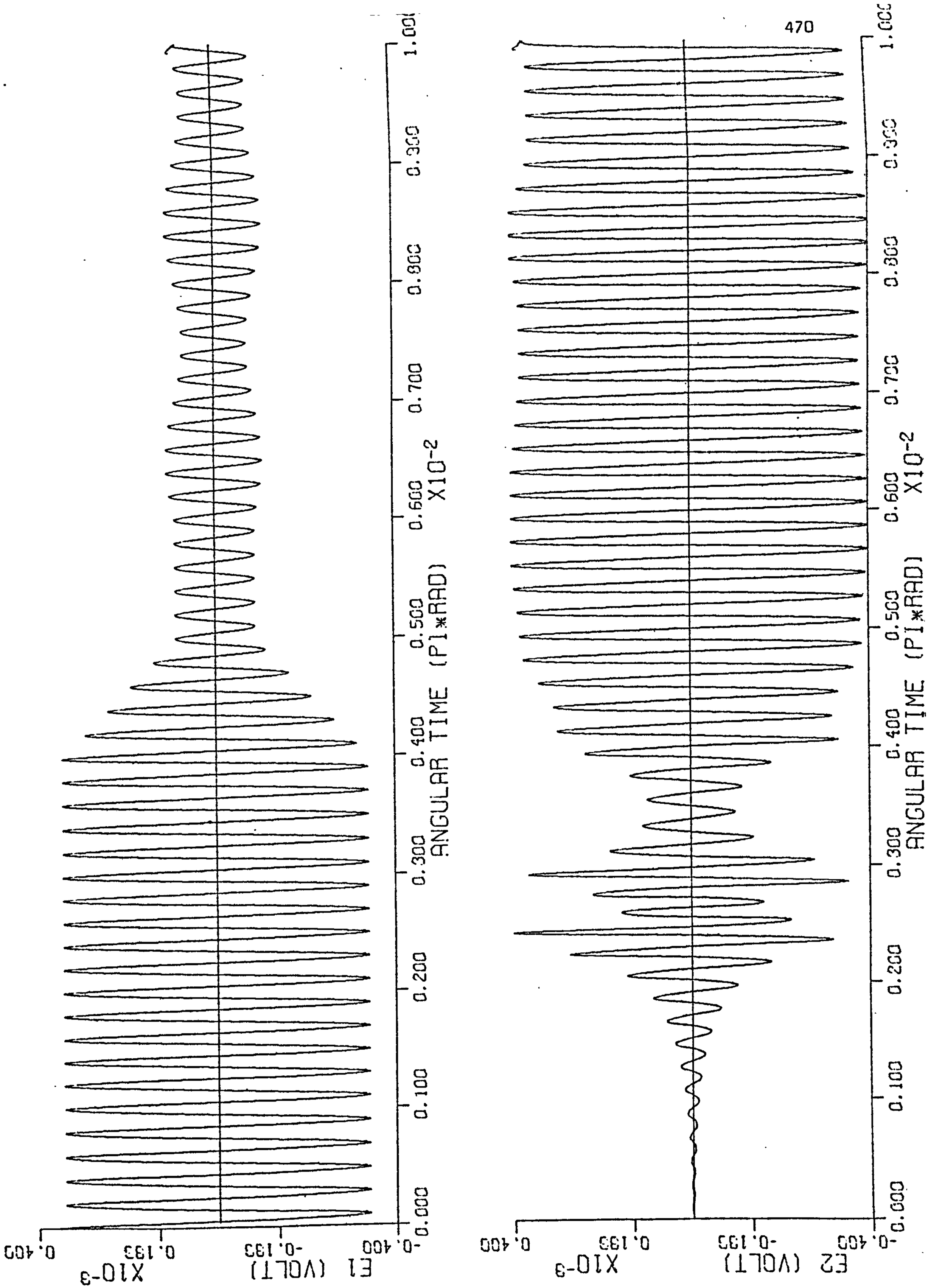

Figure 8.31 Voltage regulation

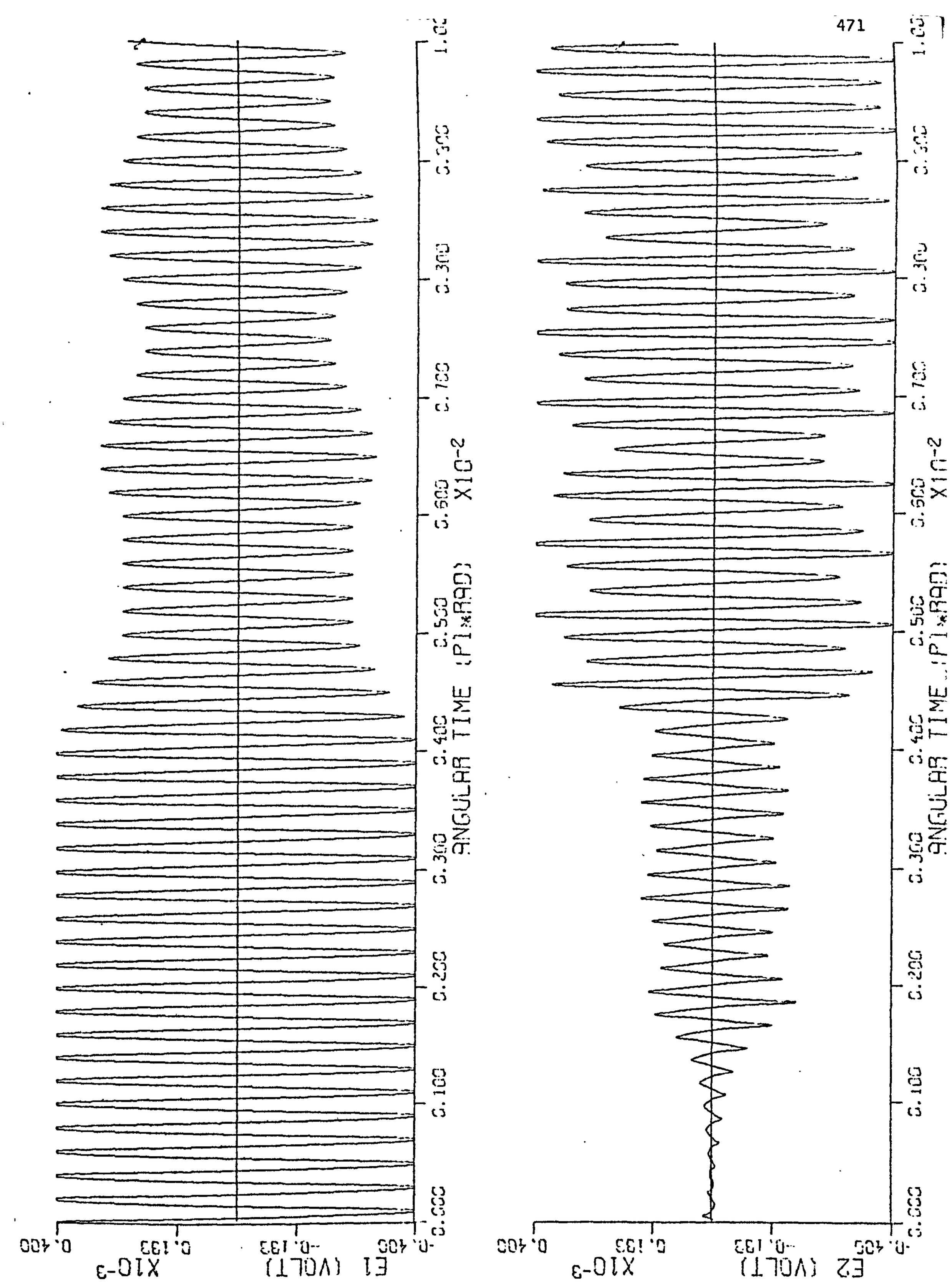

Figure 8.32 Voltage regulation

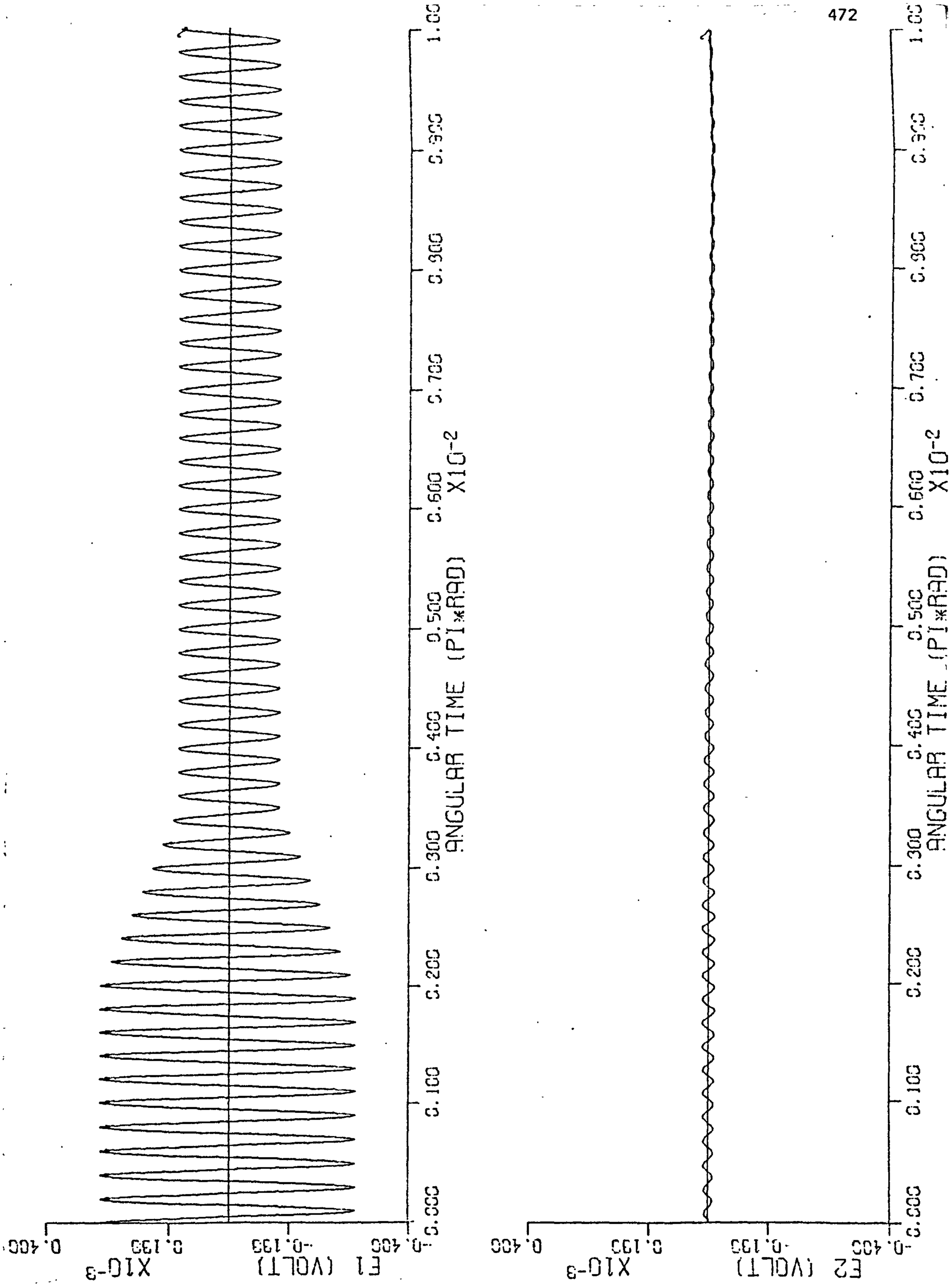

Figure 8.33 Under-voltage protection

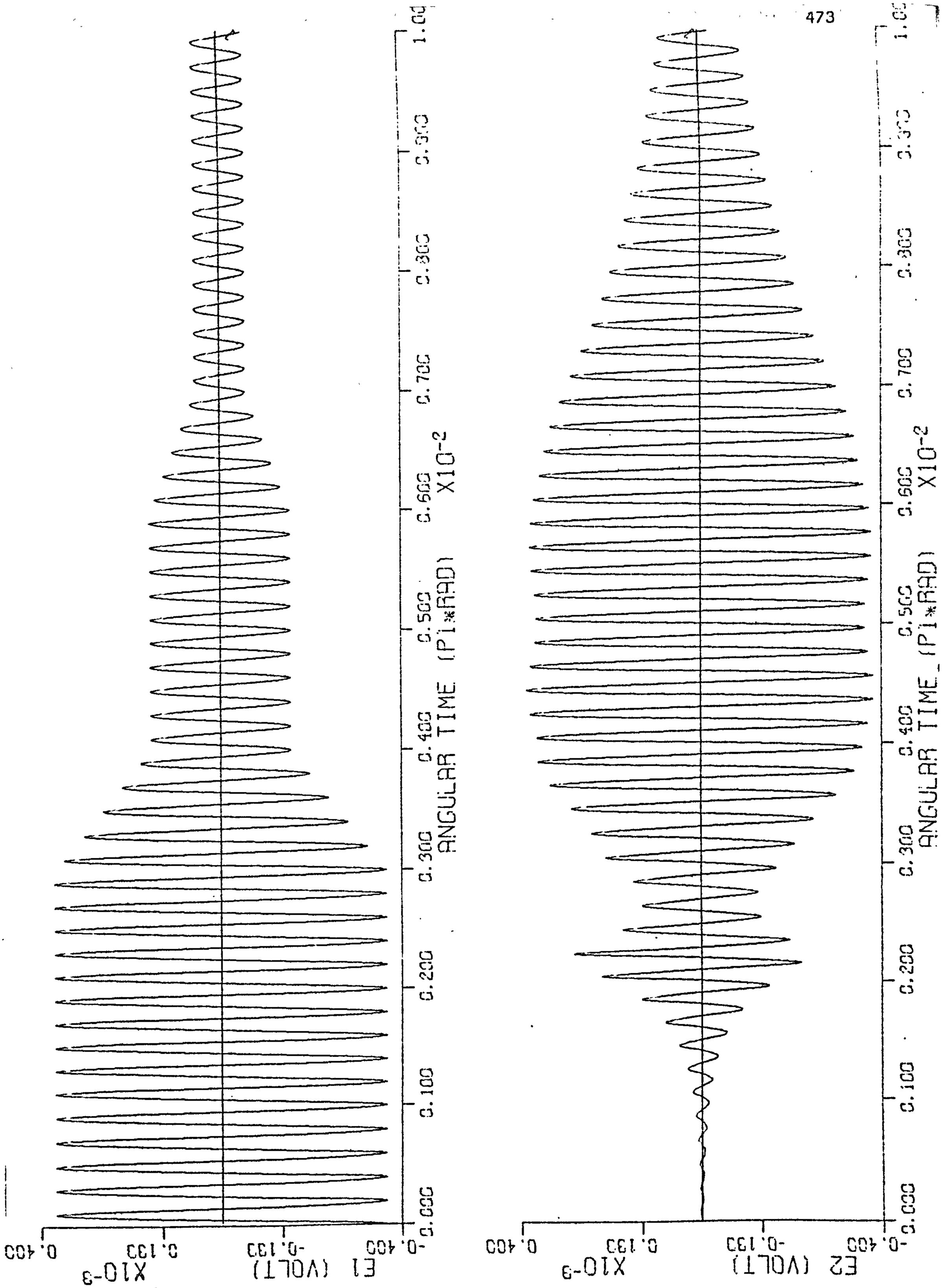

Figure 8.34 Under-voltage protection

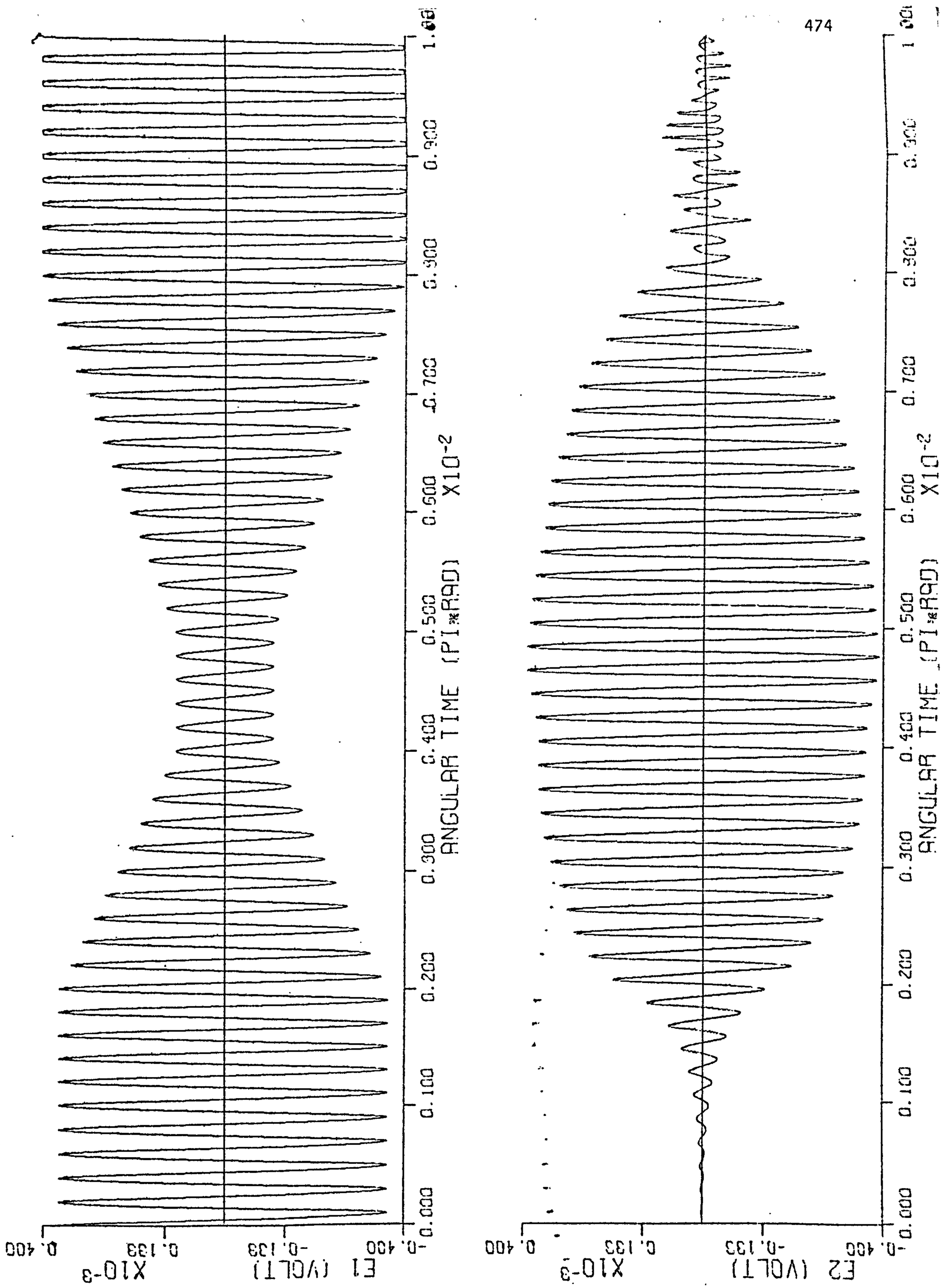

Figure 8.35 Over-voltage protection

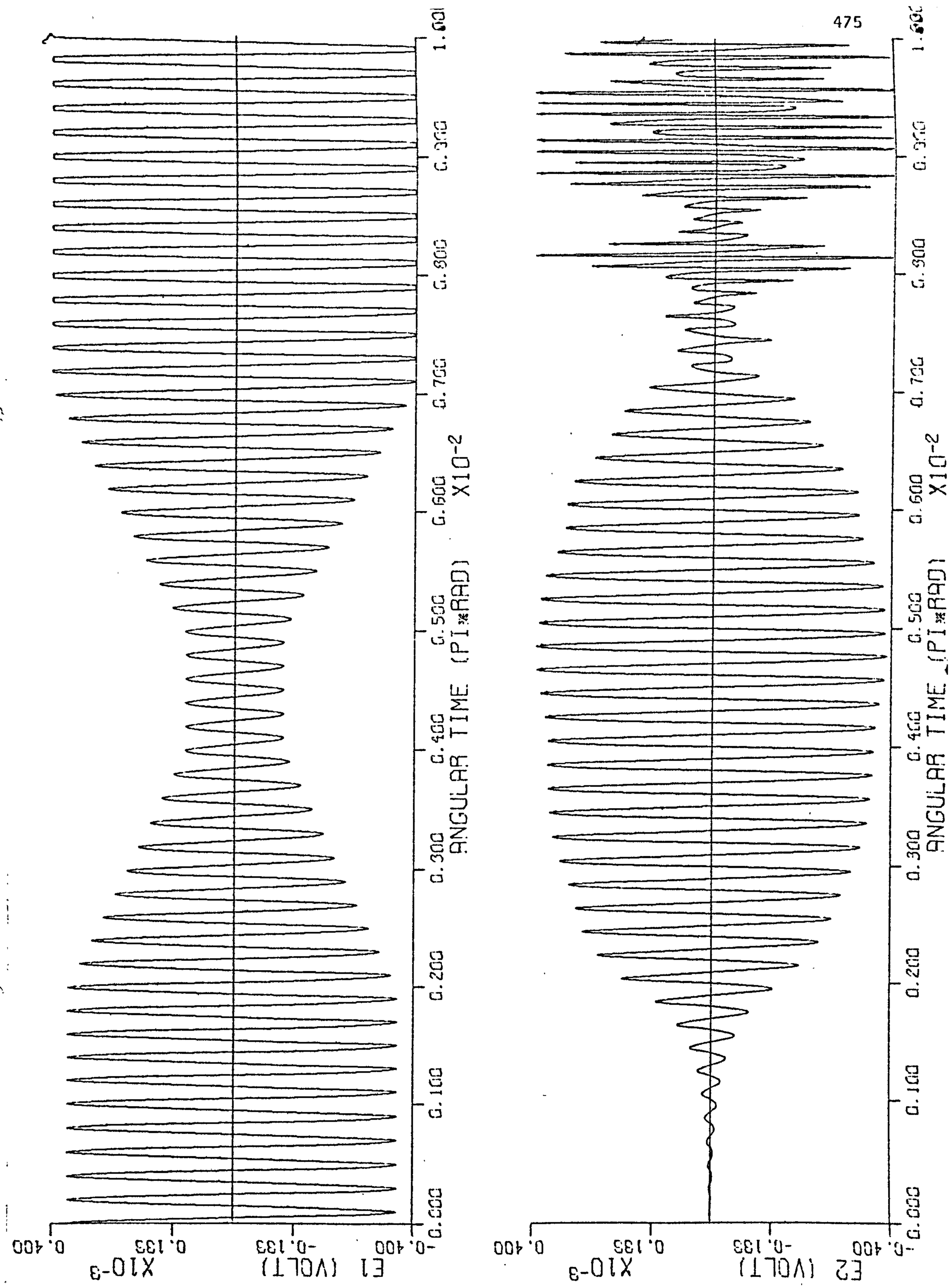

Figure 8.36 Over-voltage protection and quasi-periodic oscillations

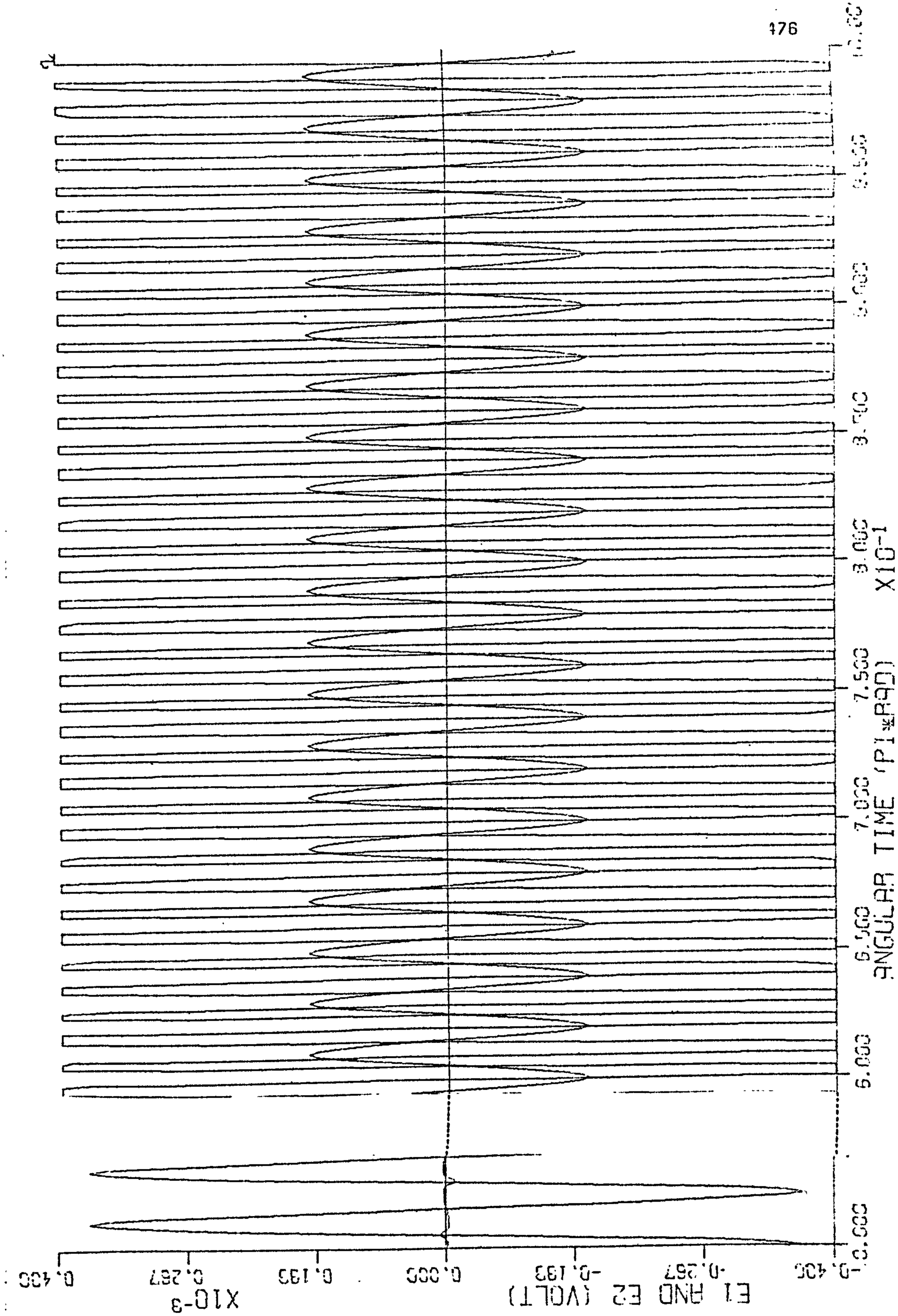

Figure 8.37 Double frequency oscillations of very high amplitude

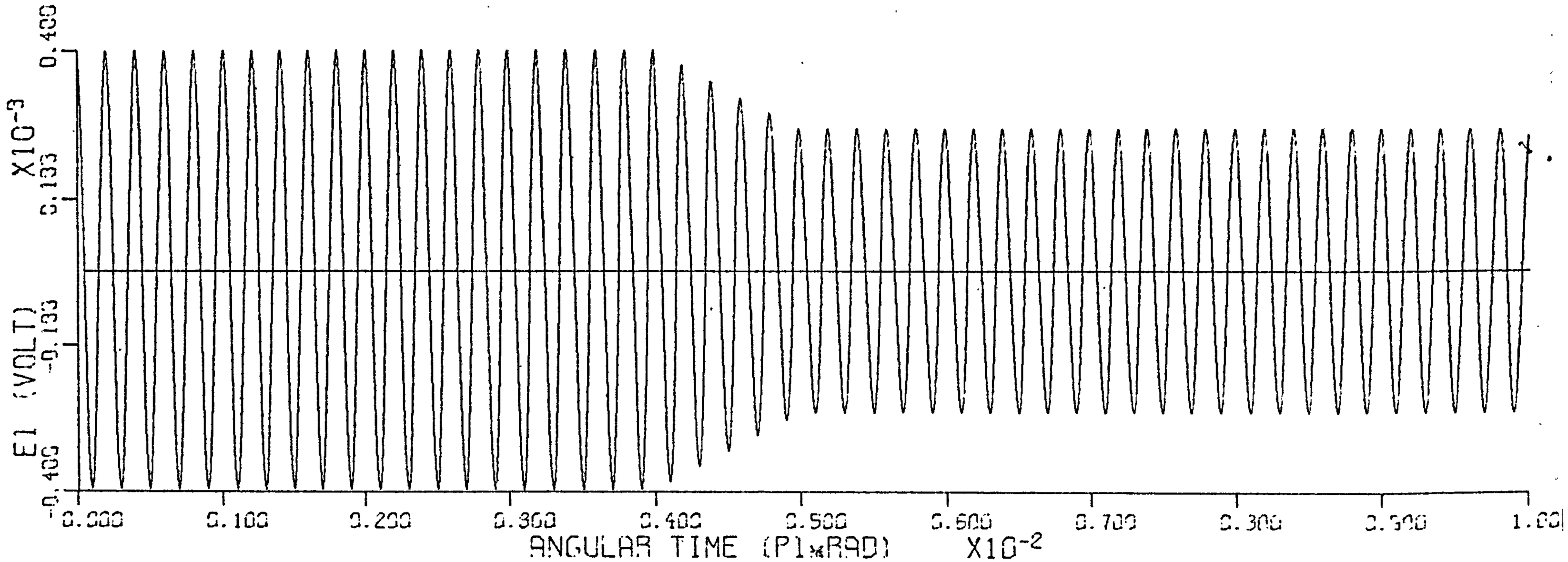

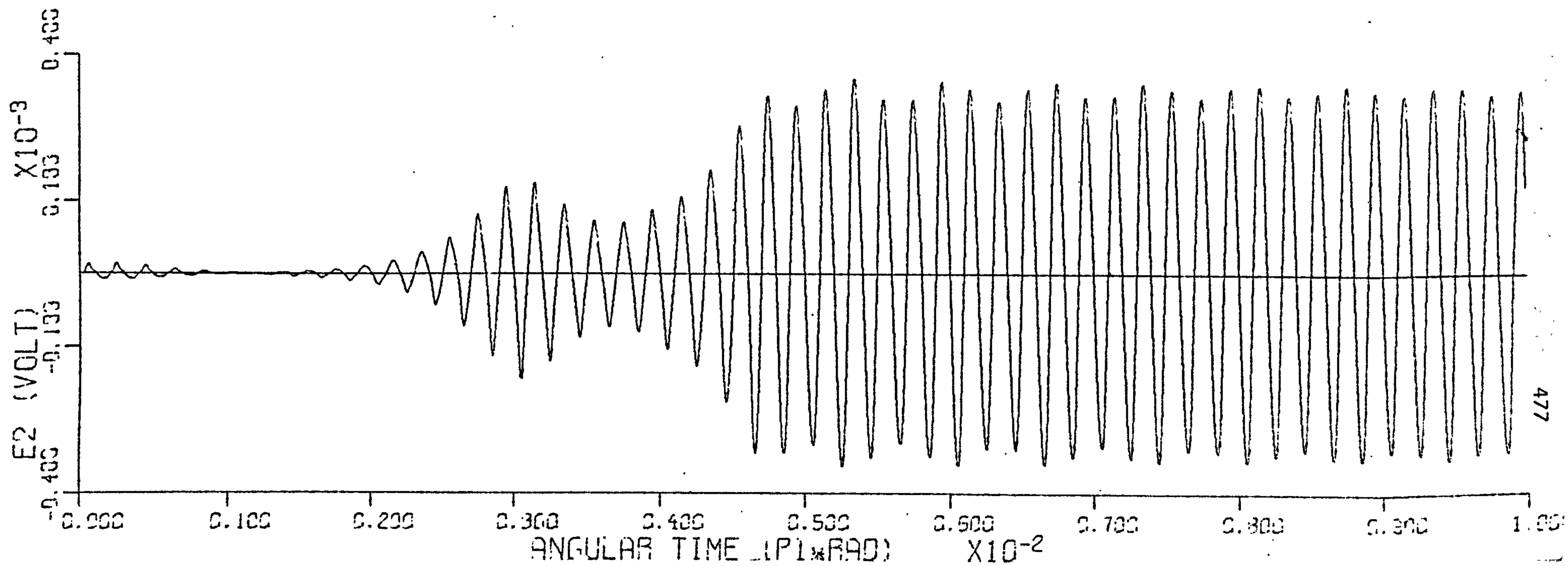

Figure 8.38 Operation with capacitor value satisfying a = 1

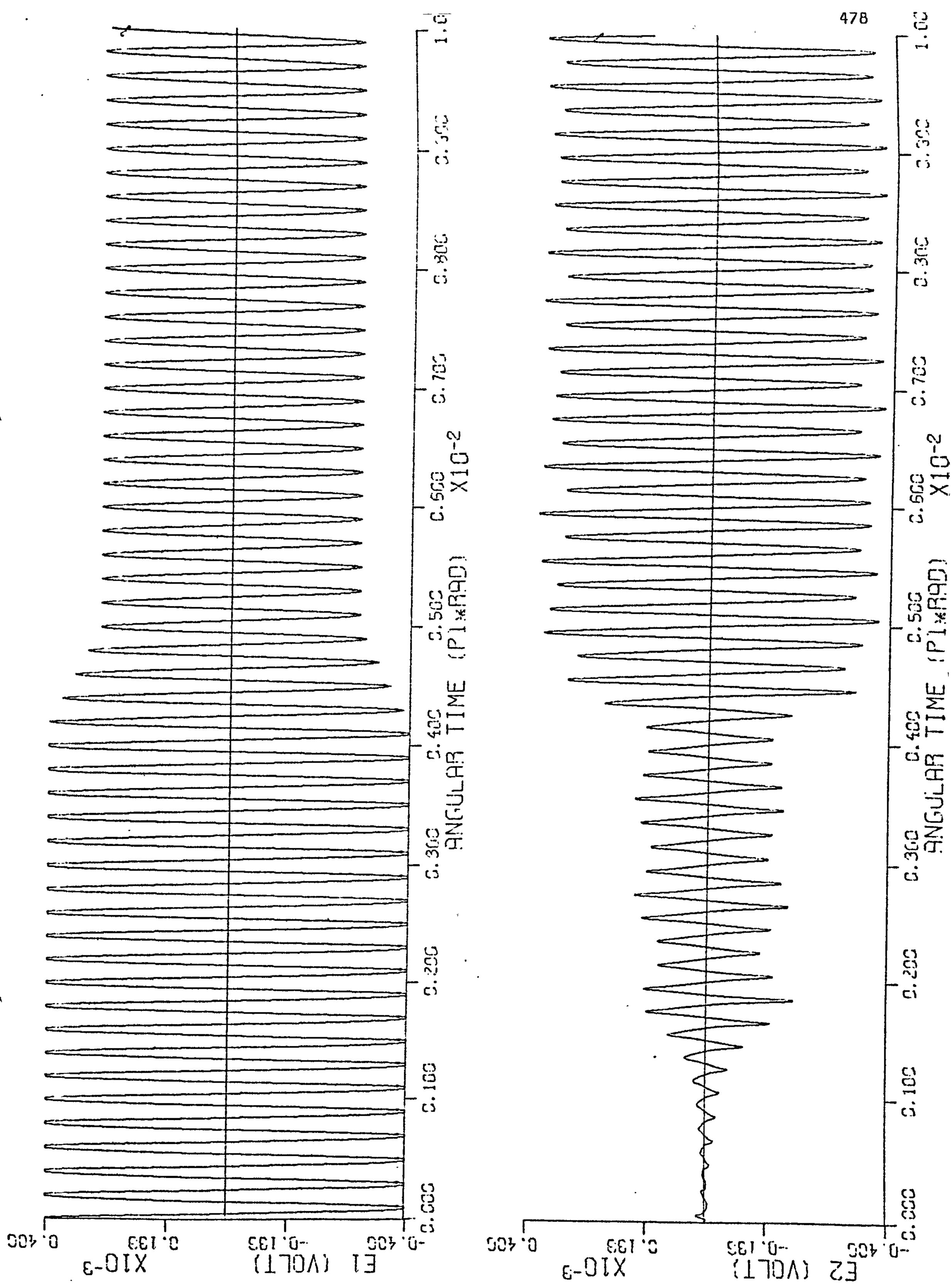

Figure 8.39 Operation with capacitor value satisfying a = 1

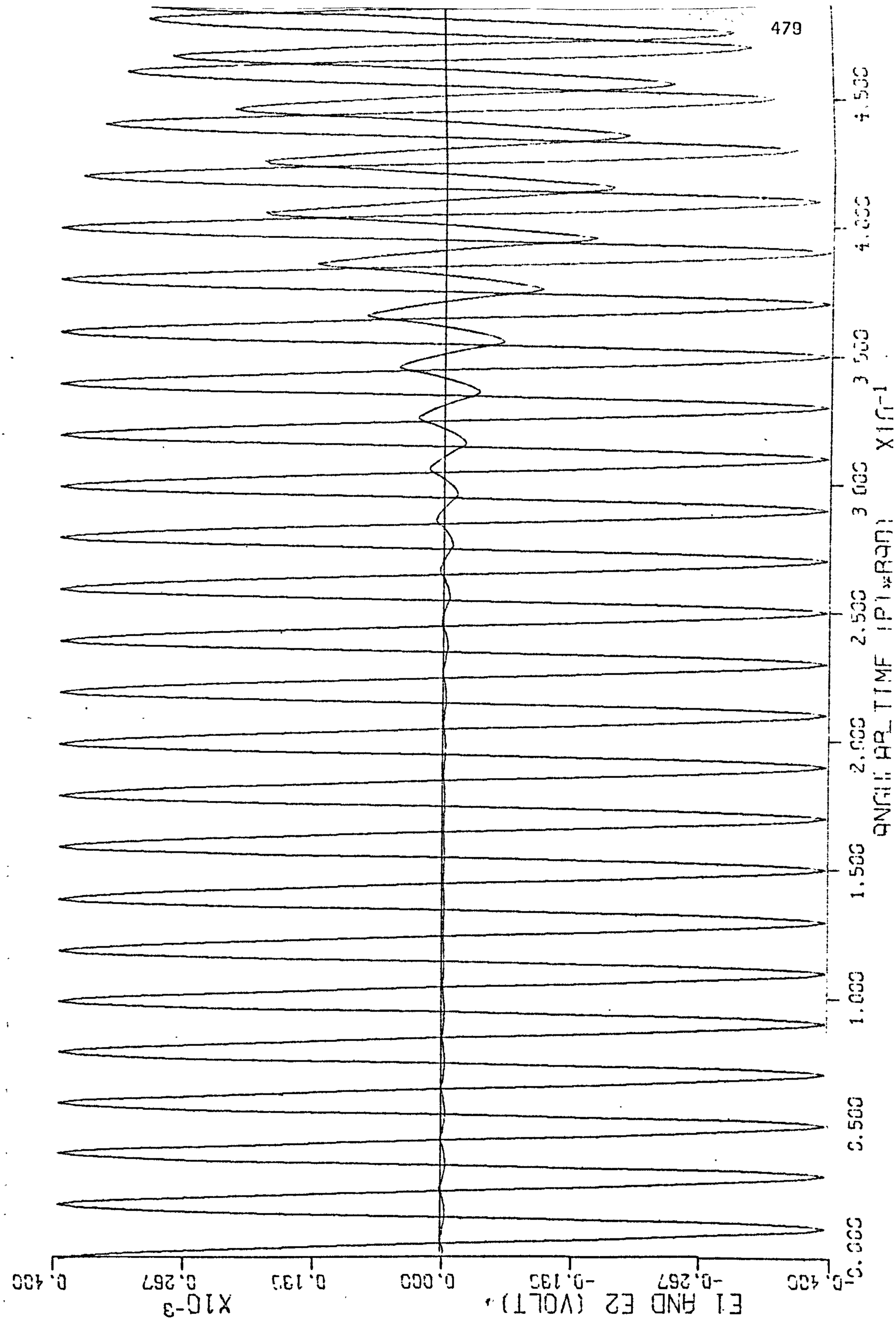

Figure 8.40 Initiation of oscillations, V_2 lagging V_1 by 90^0

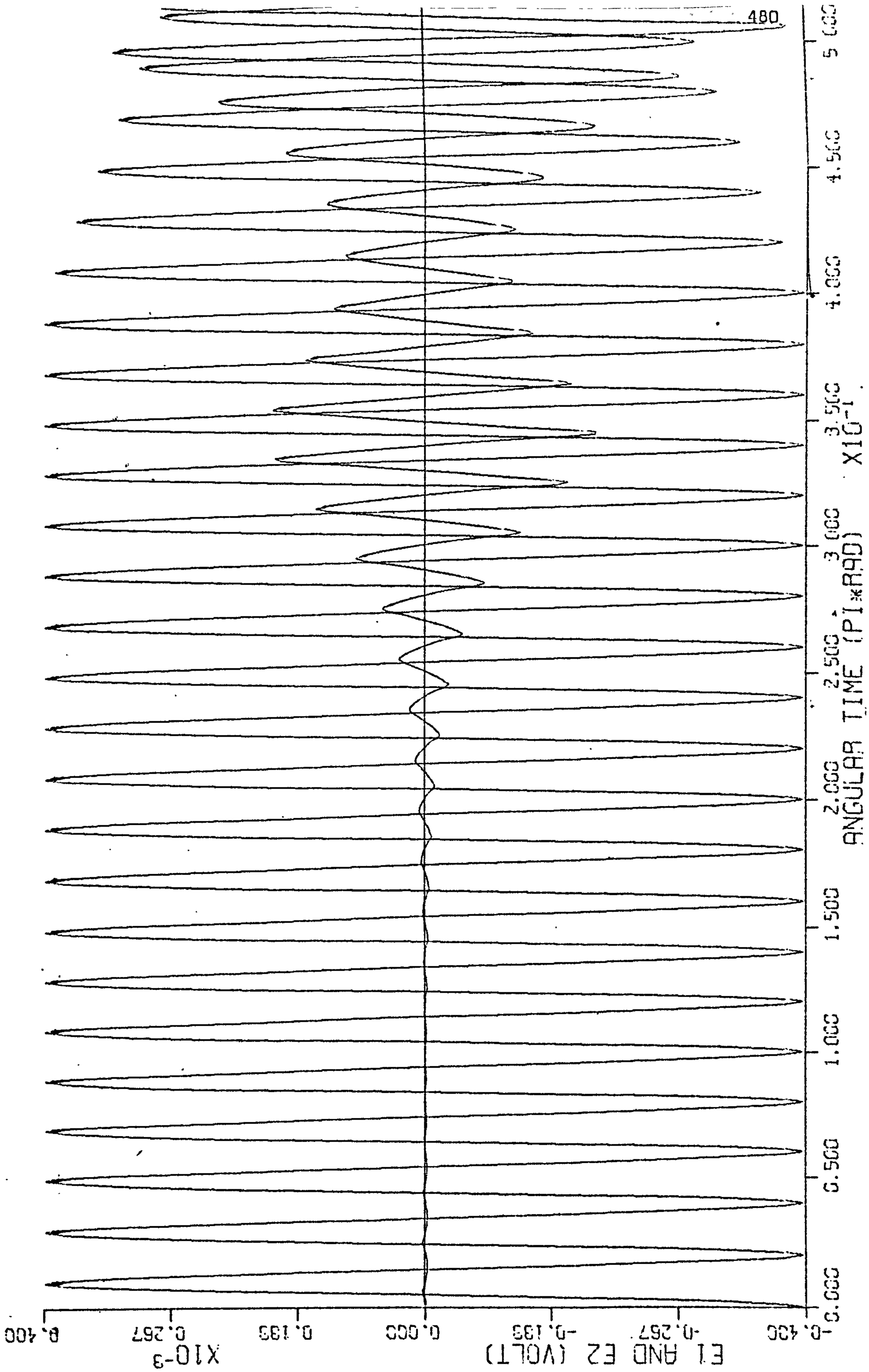

Figure 8.41 Initiation of oscillations, V_2 lagging V_1 by 90^0

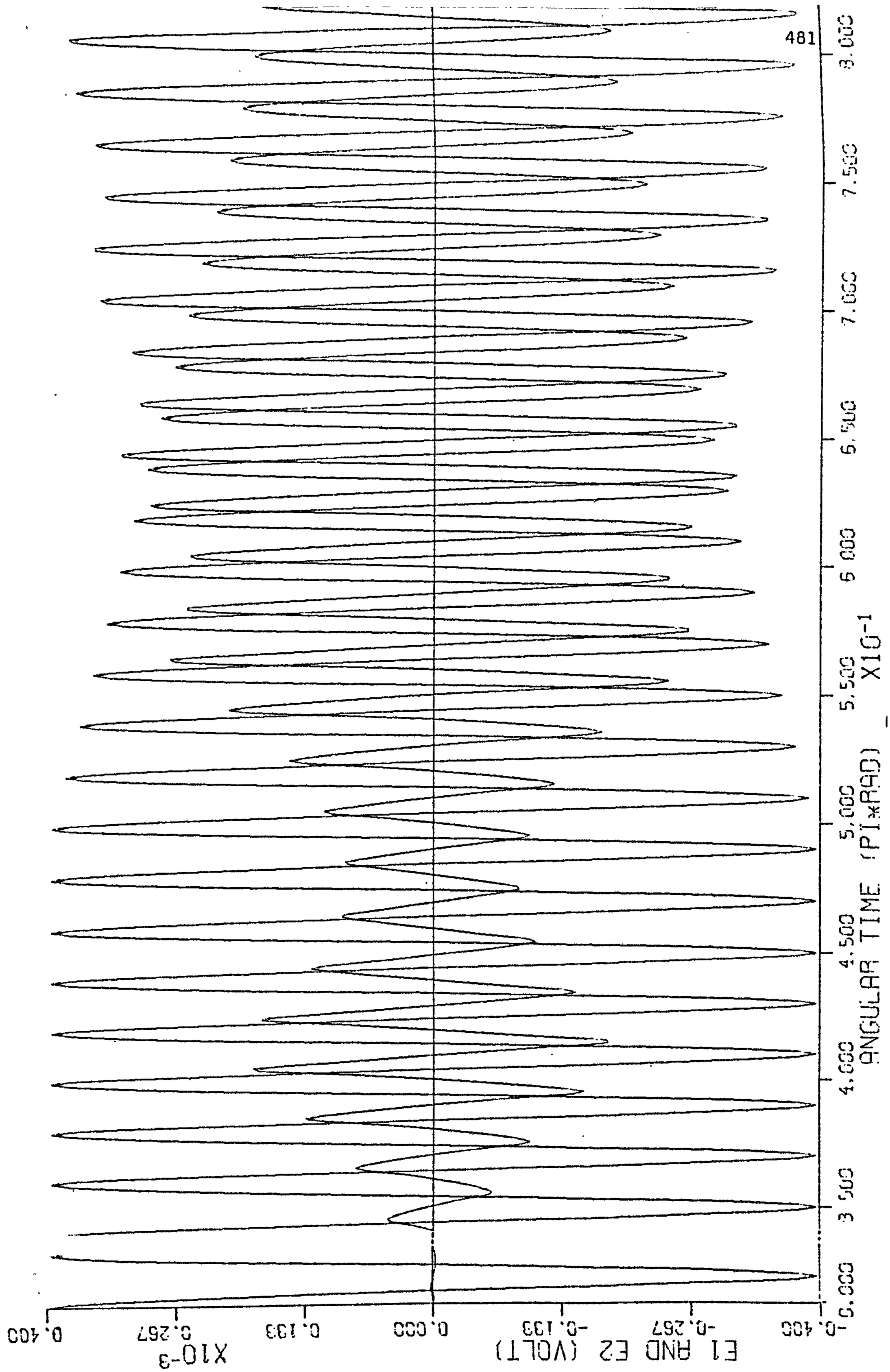

Figure 8.42 Initiation of oscillations, V_2 lagging V_1 by 90^0

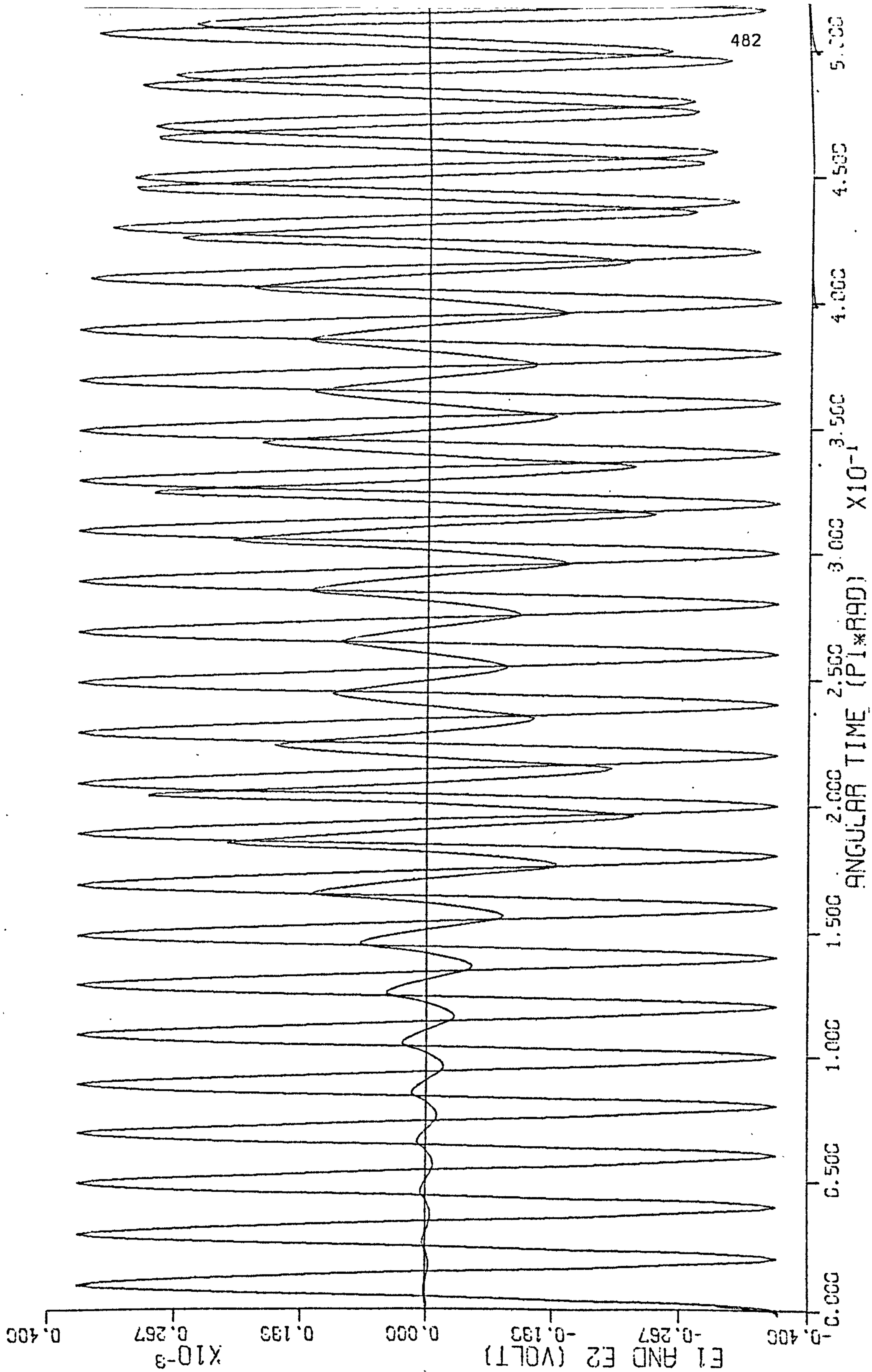

Figure 8.43 Initiation of oscillations. V_2 lagging V_1 by 90^0

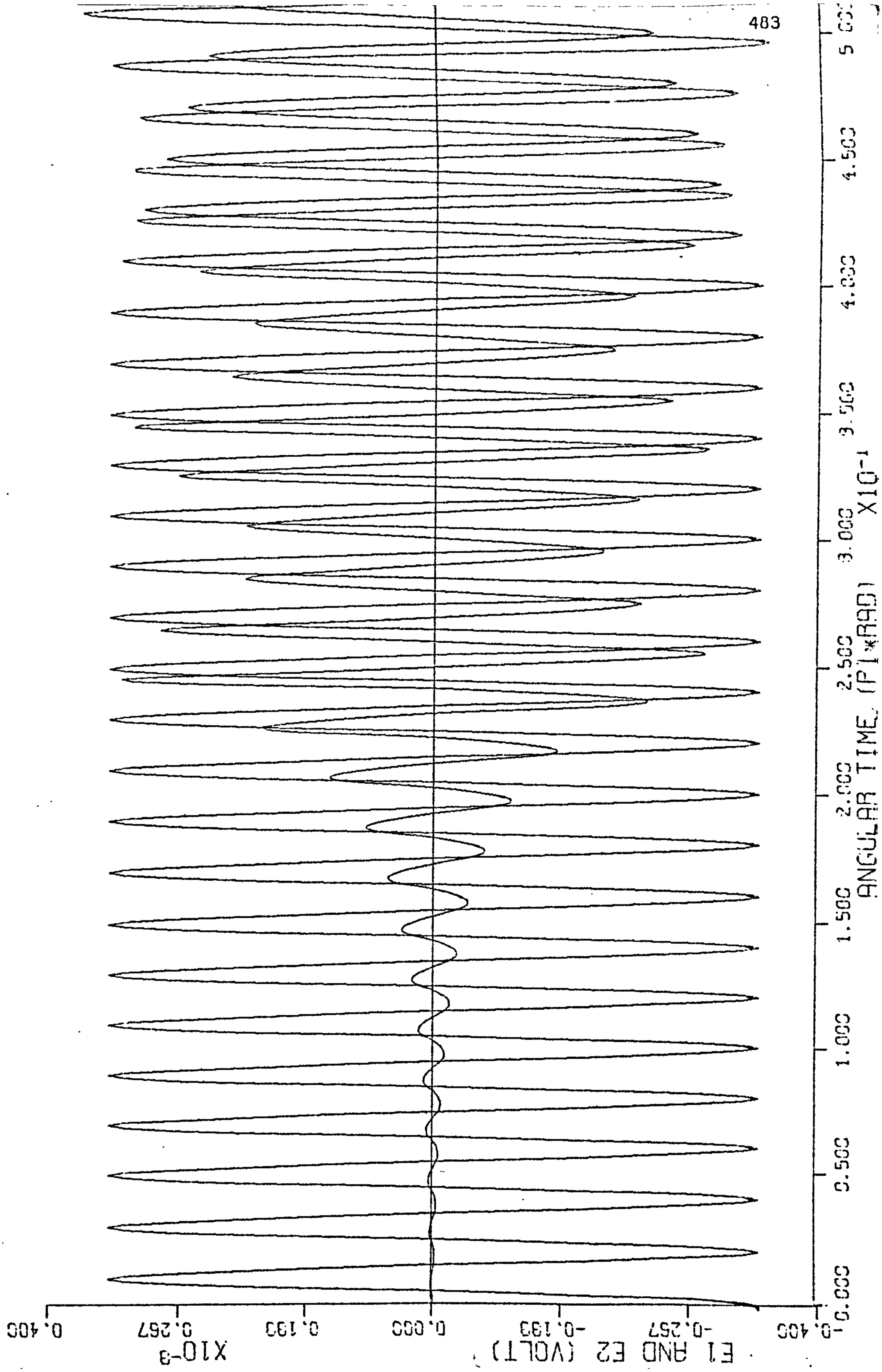

Figure 8.44 Initiation of oscillations, V_2 lagging V_1 by 90o

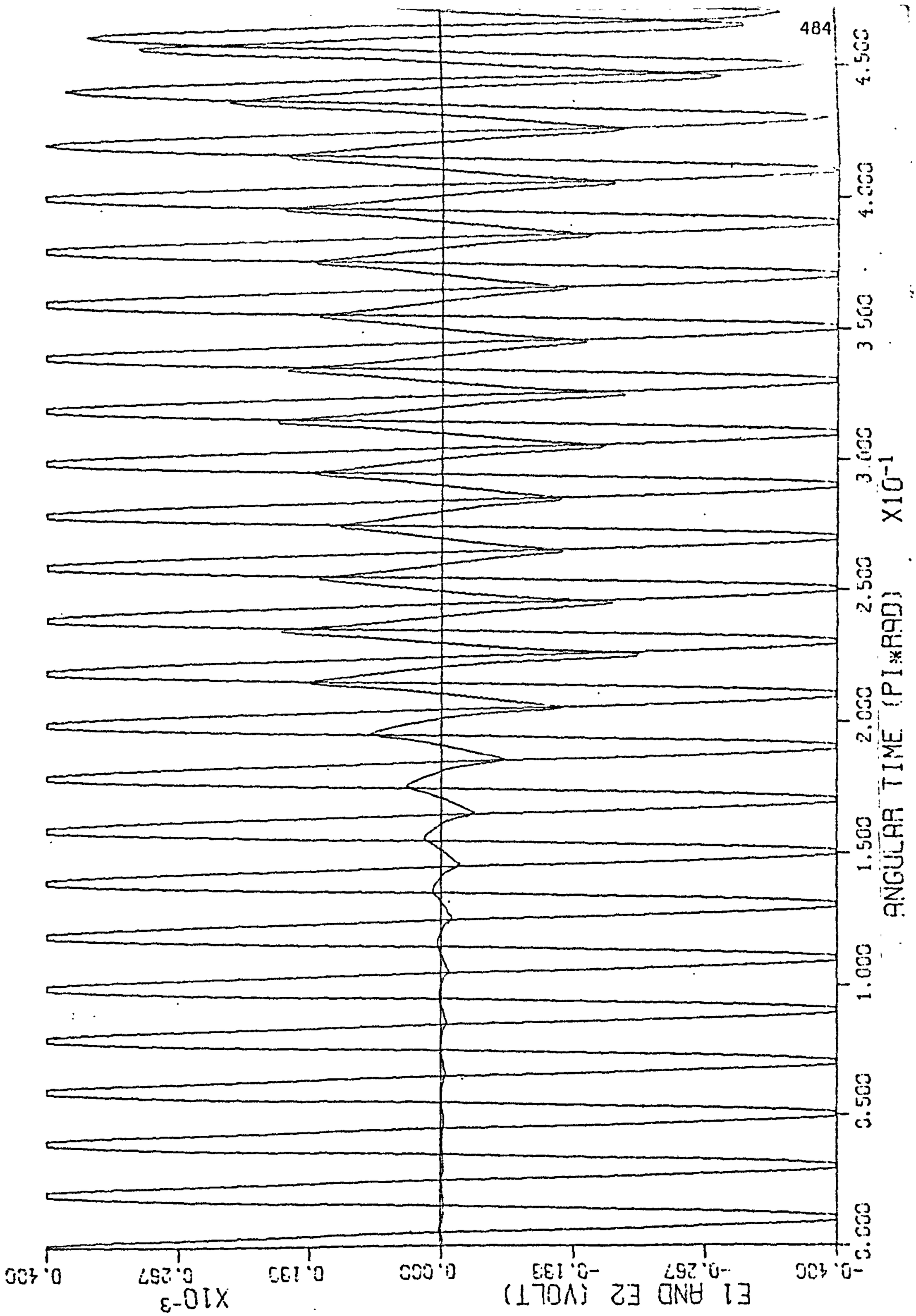

Figure 8.45 Initiation of oscillations, V_2 lagging V_1 by 90^0

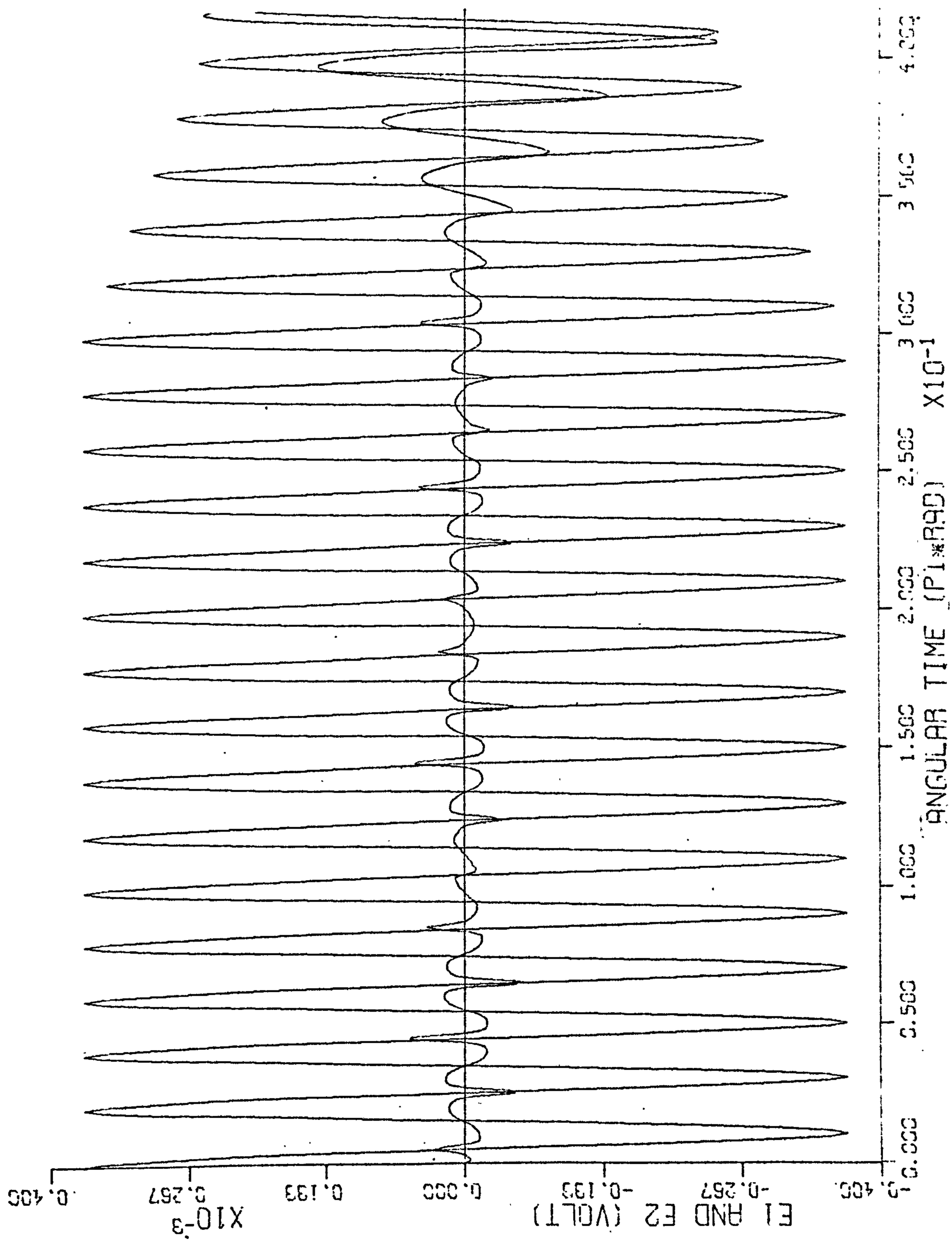

Figure 8.46 Effect of primary in-rush currents on initial oscillation in secondary

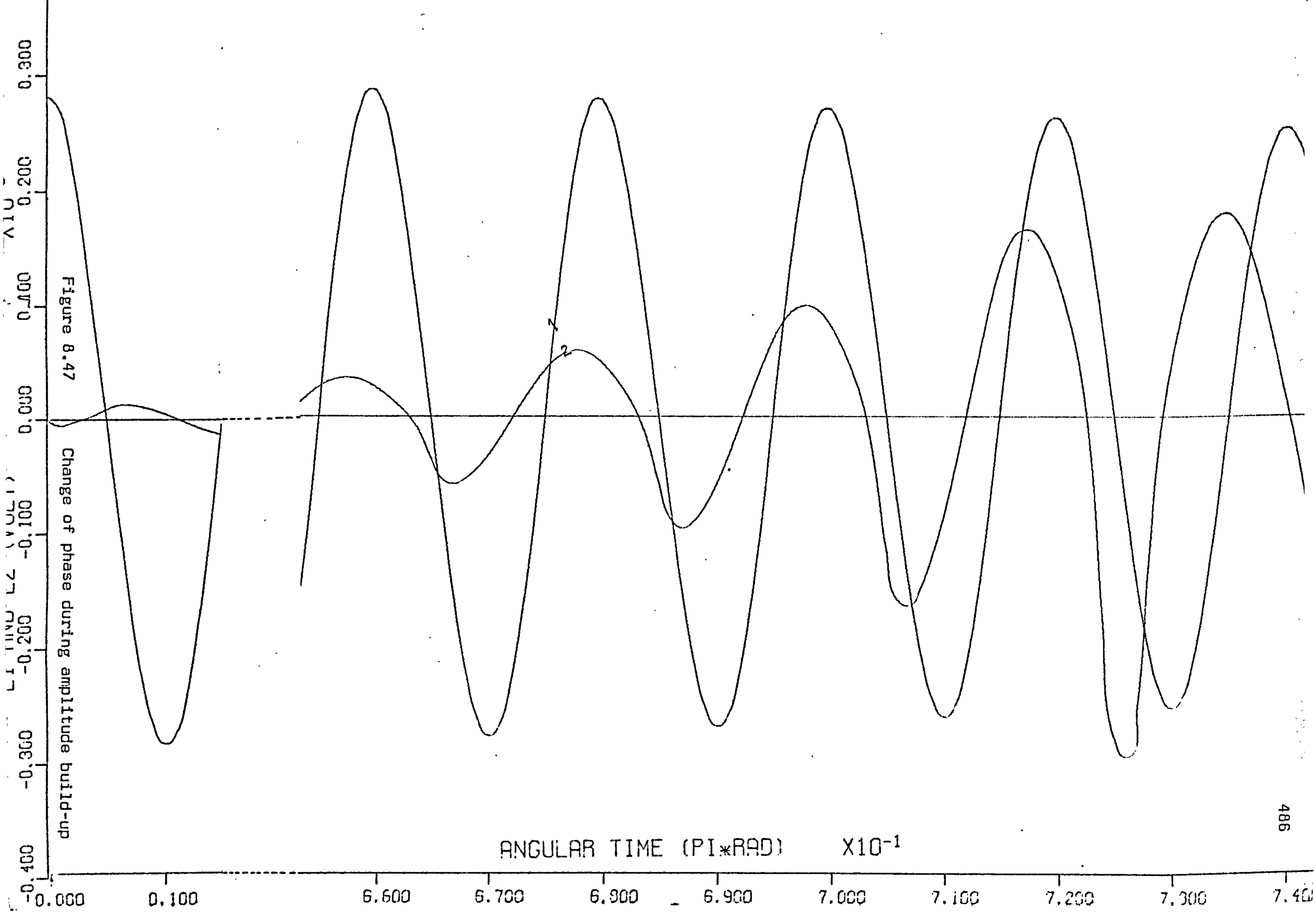

Figure 8.47

Change of phase during amplitude build-up

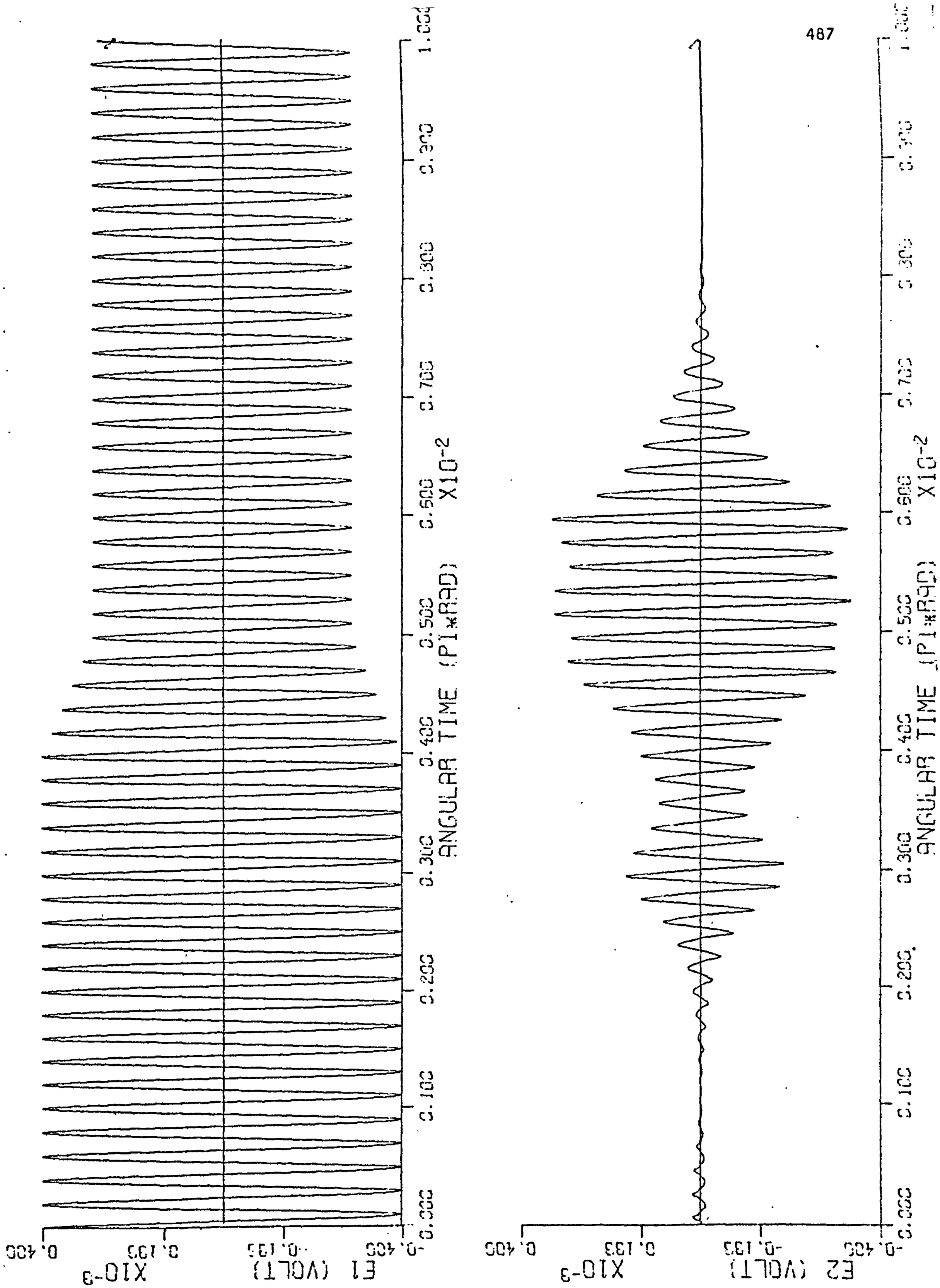

Figure 8.48 Over-load protection

Figure 8.48 Over-load protection

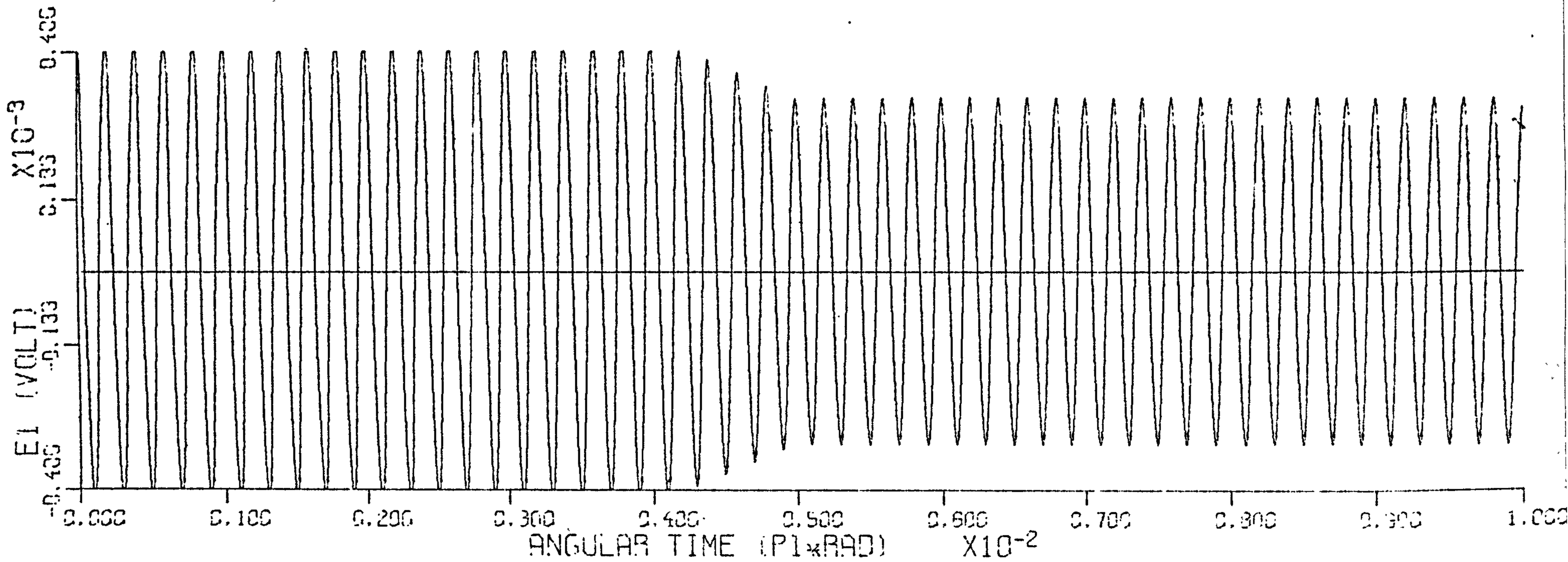

Figure 8.49 Load regulation

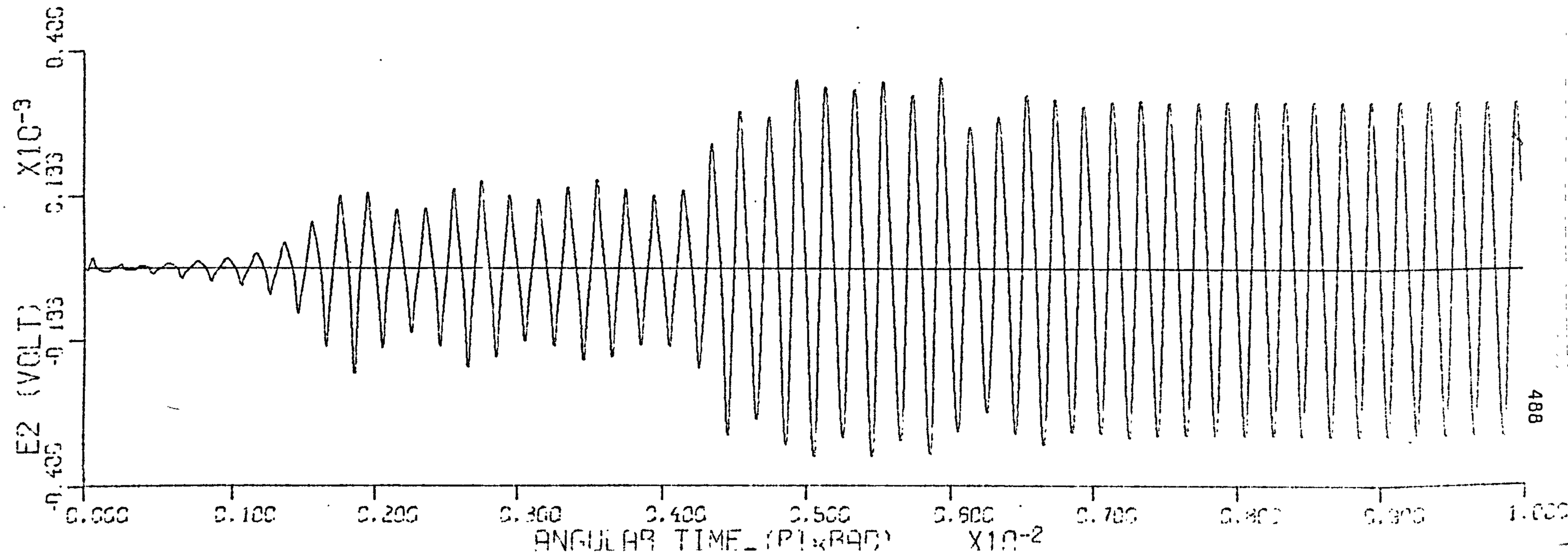

Figure 8.50 Overload motor action

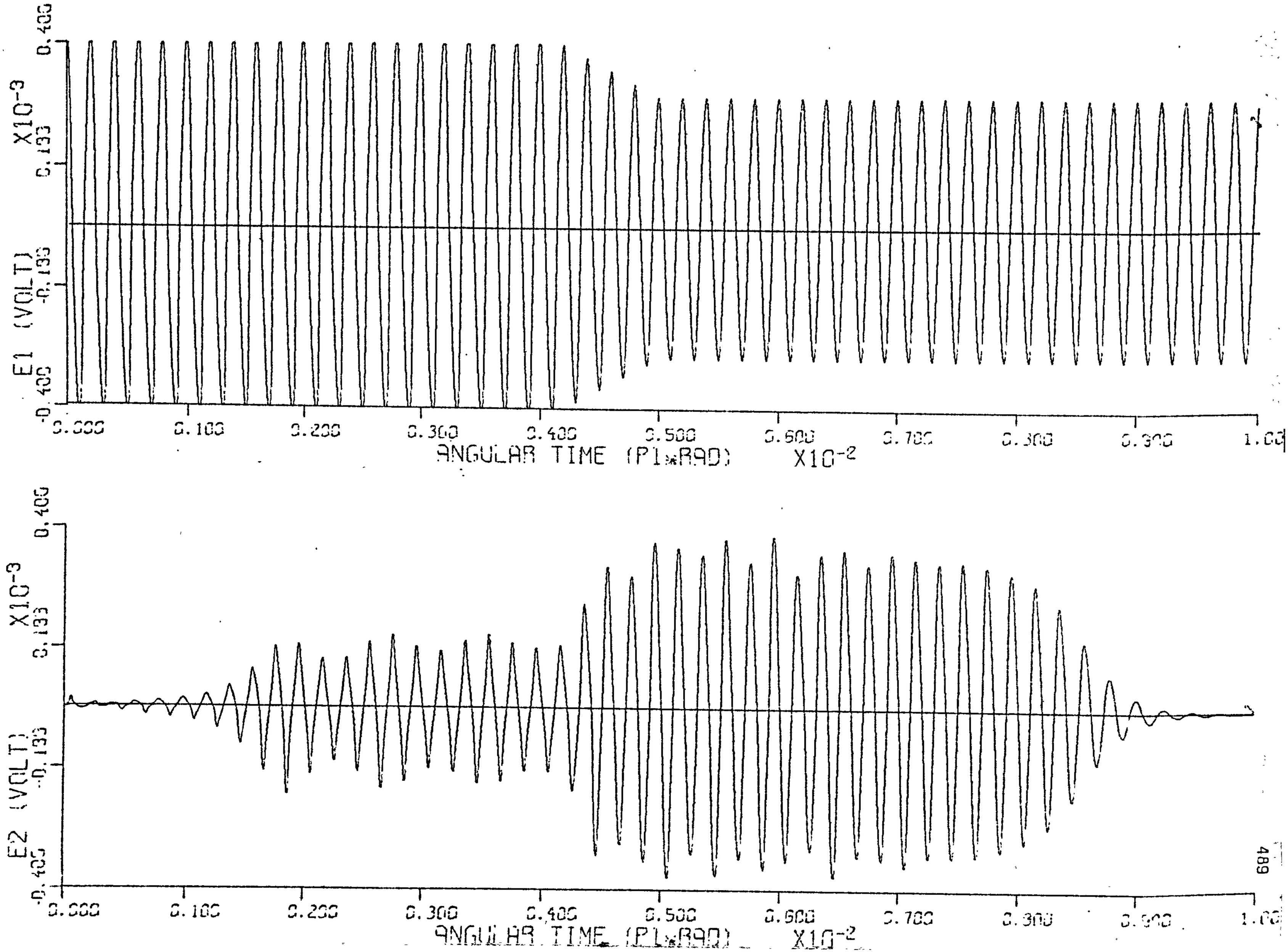

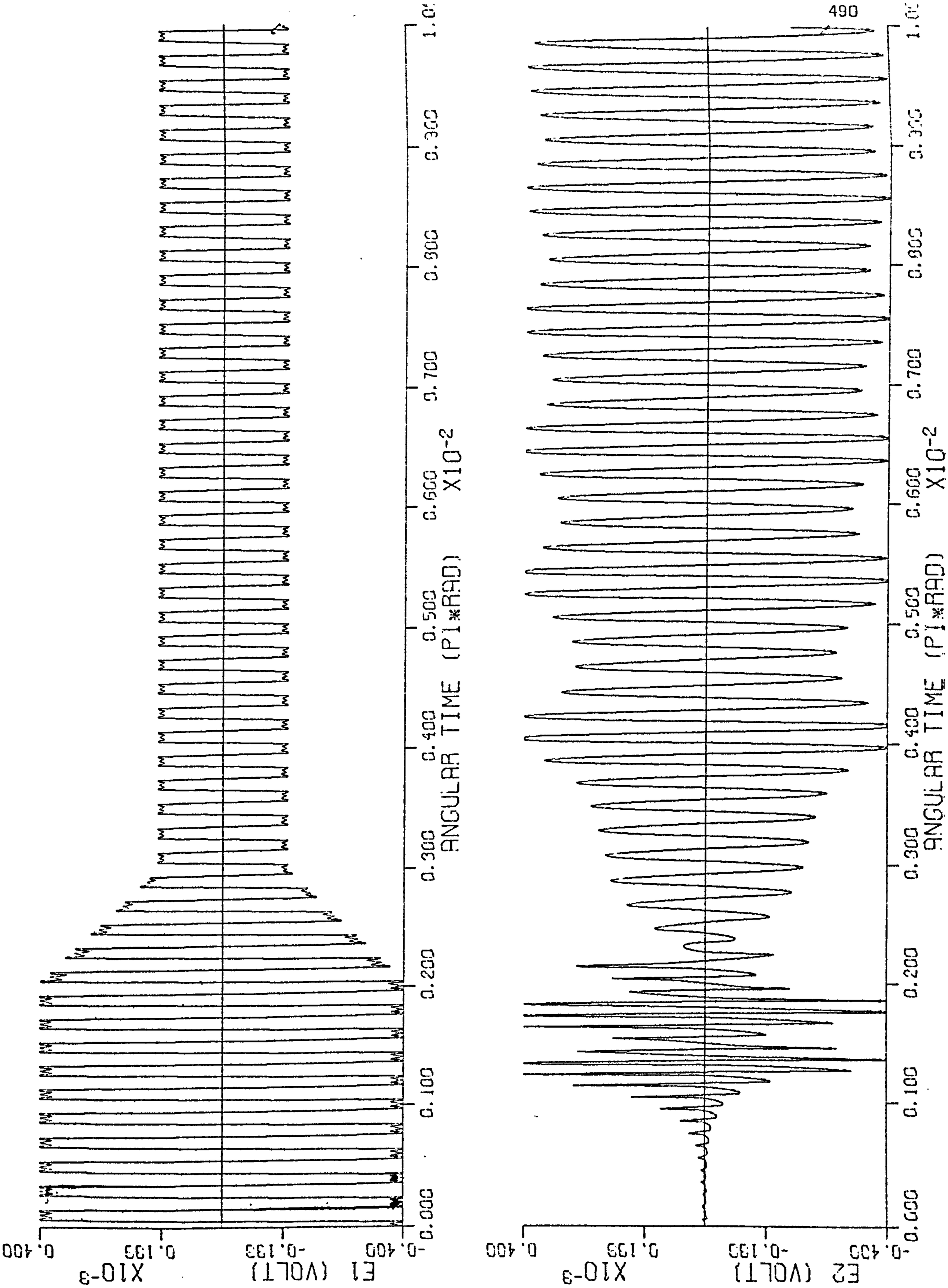

Figure 8.51 Filtering abiliti

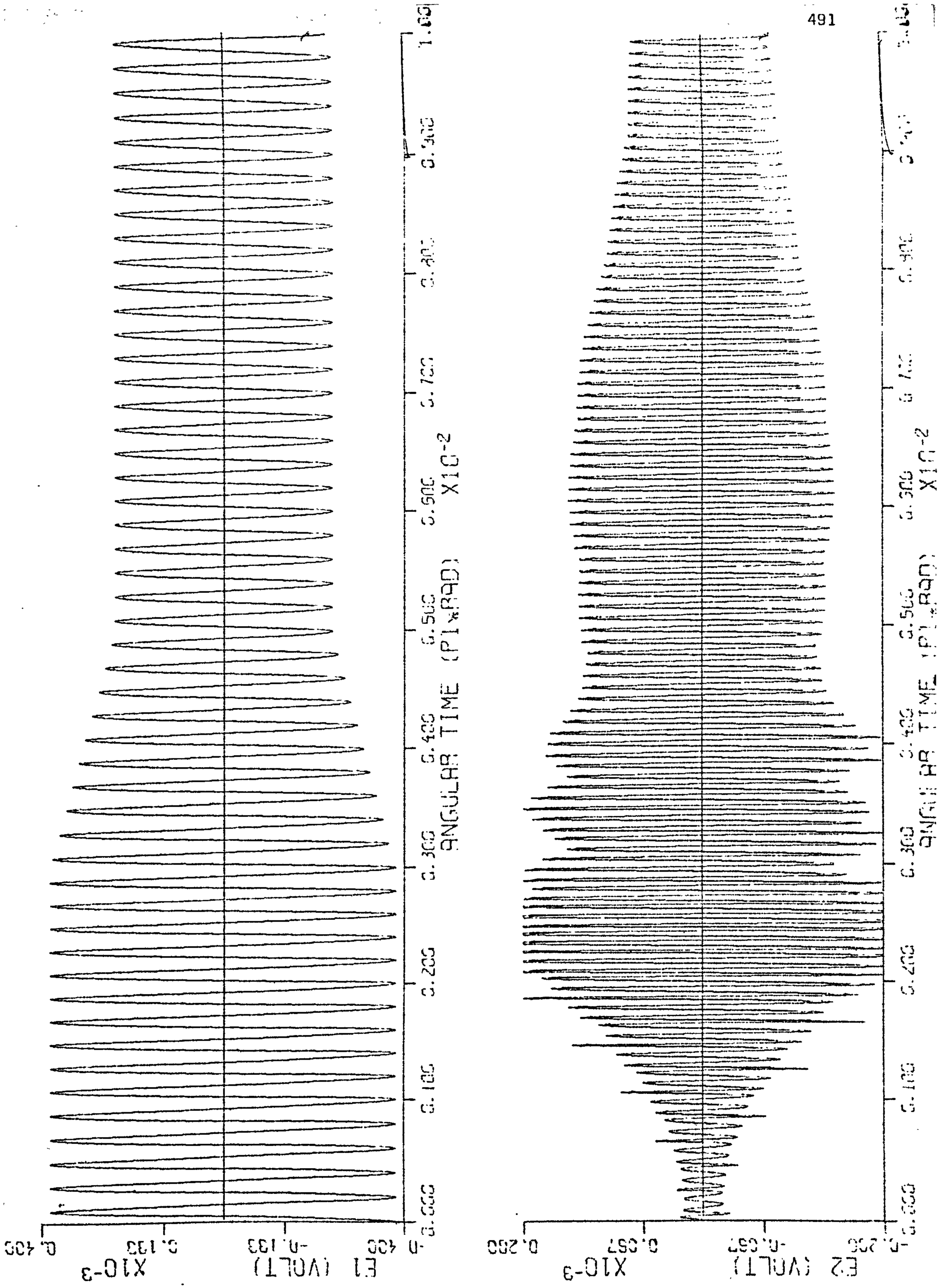

Figure 8.52 Operation as a frequency-doubler

Figure 8.52 Operation as a frequency-doubler

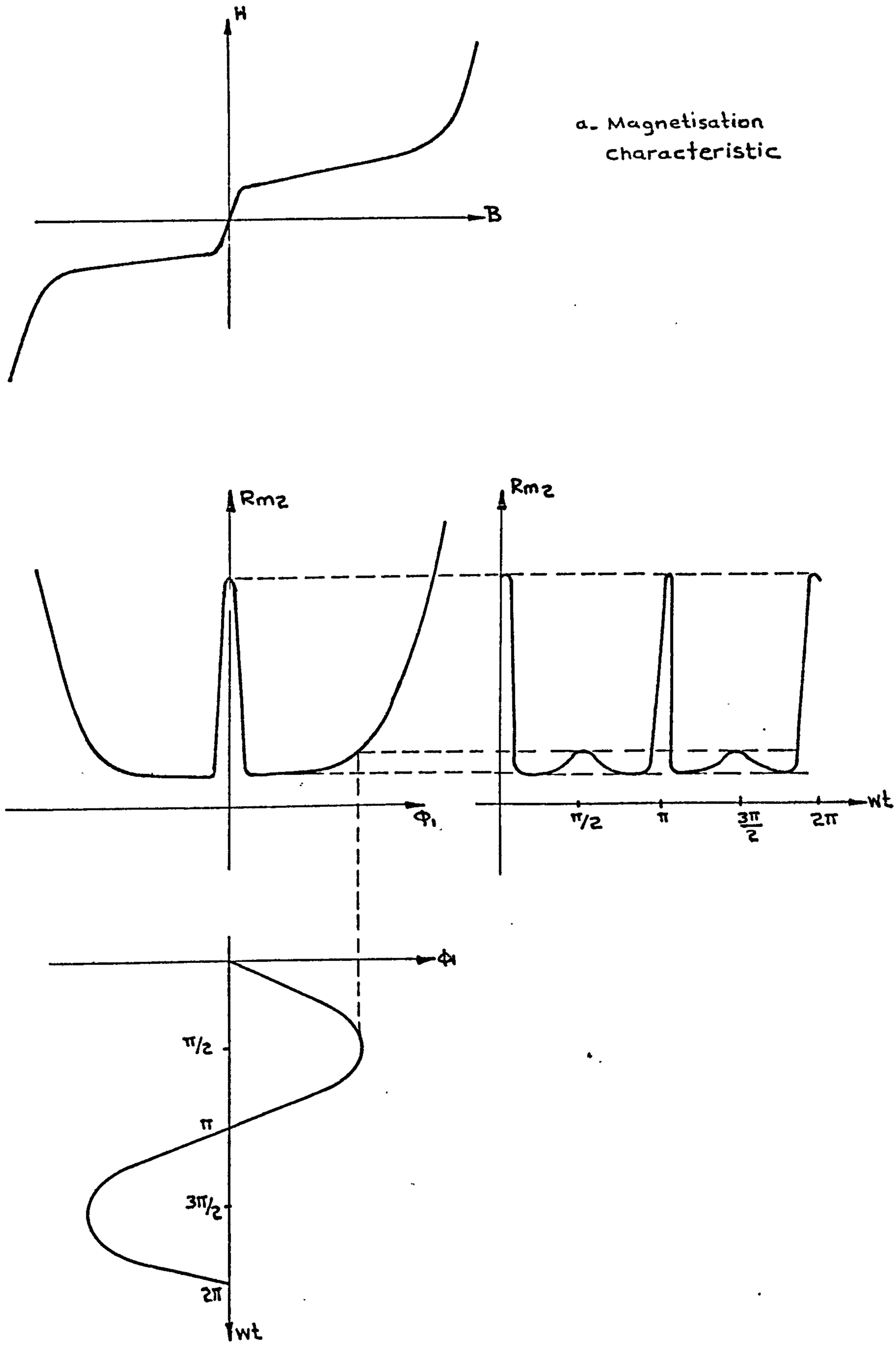

Figure 8.53 Reluctance Modulation with a B/H Curve having Inflection near the Origin

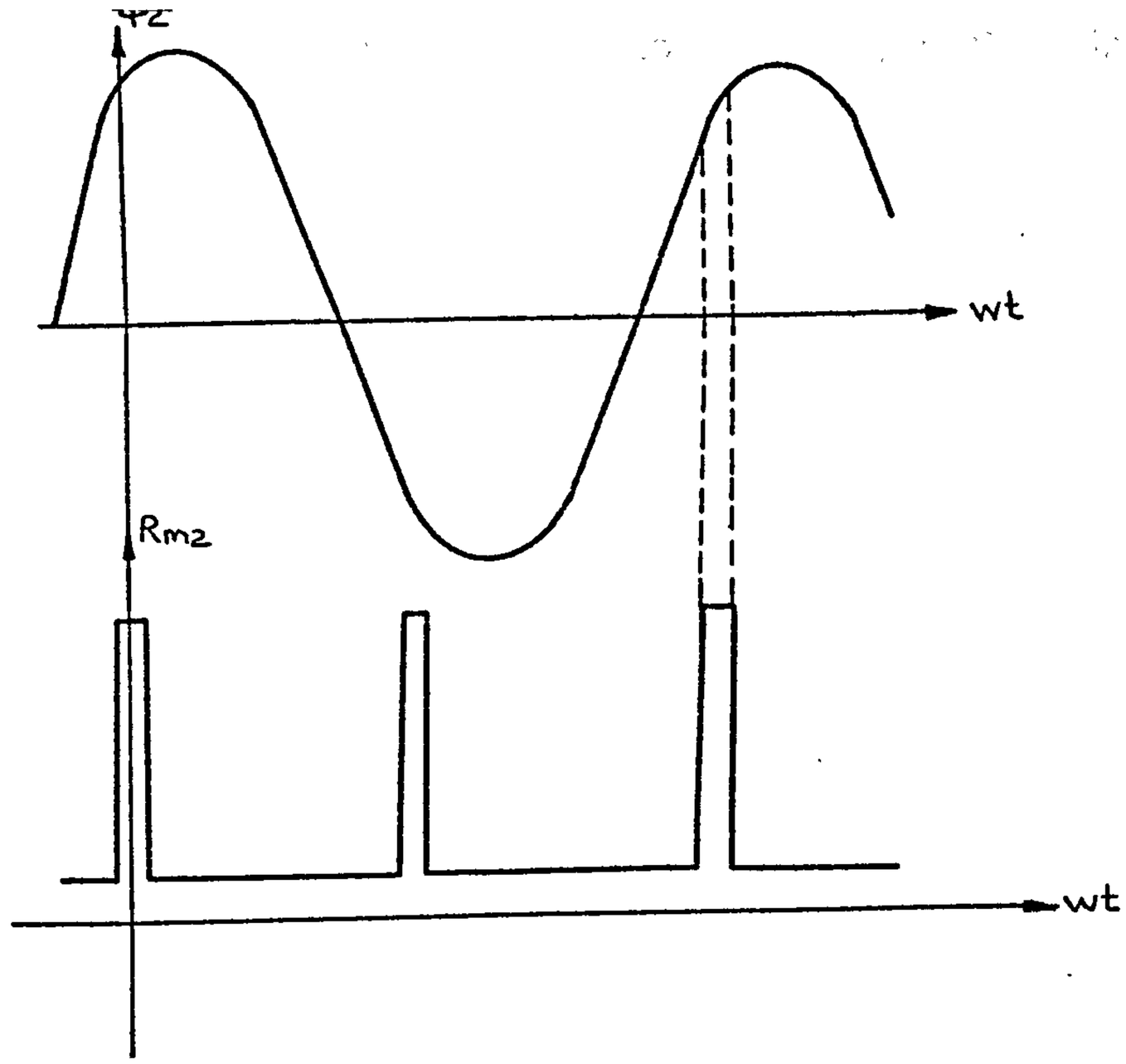

Figure 8.54 Relative Phases of Initial Oscillation and Reluctance Peaks

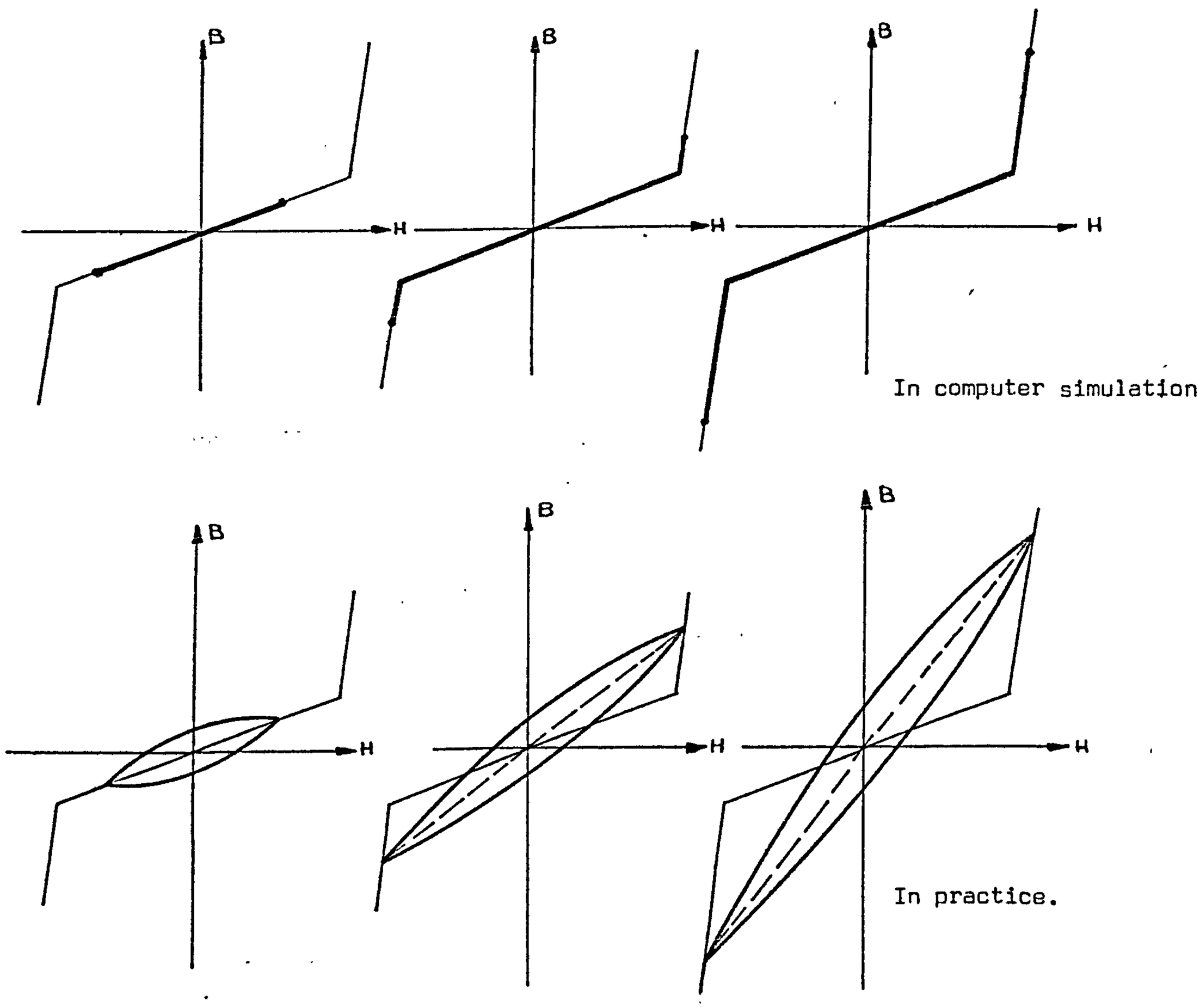

Figure 8.55 Effect of Hysteresis Causing Gradual Increase in Initial Reluctance

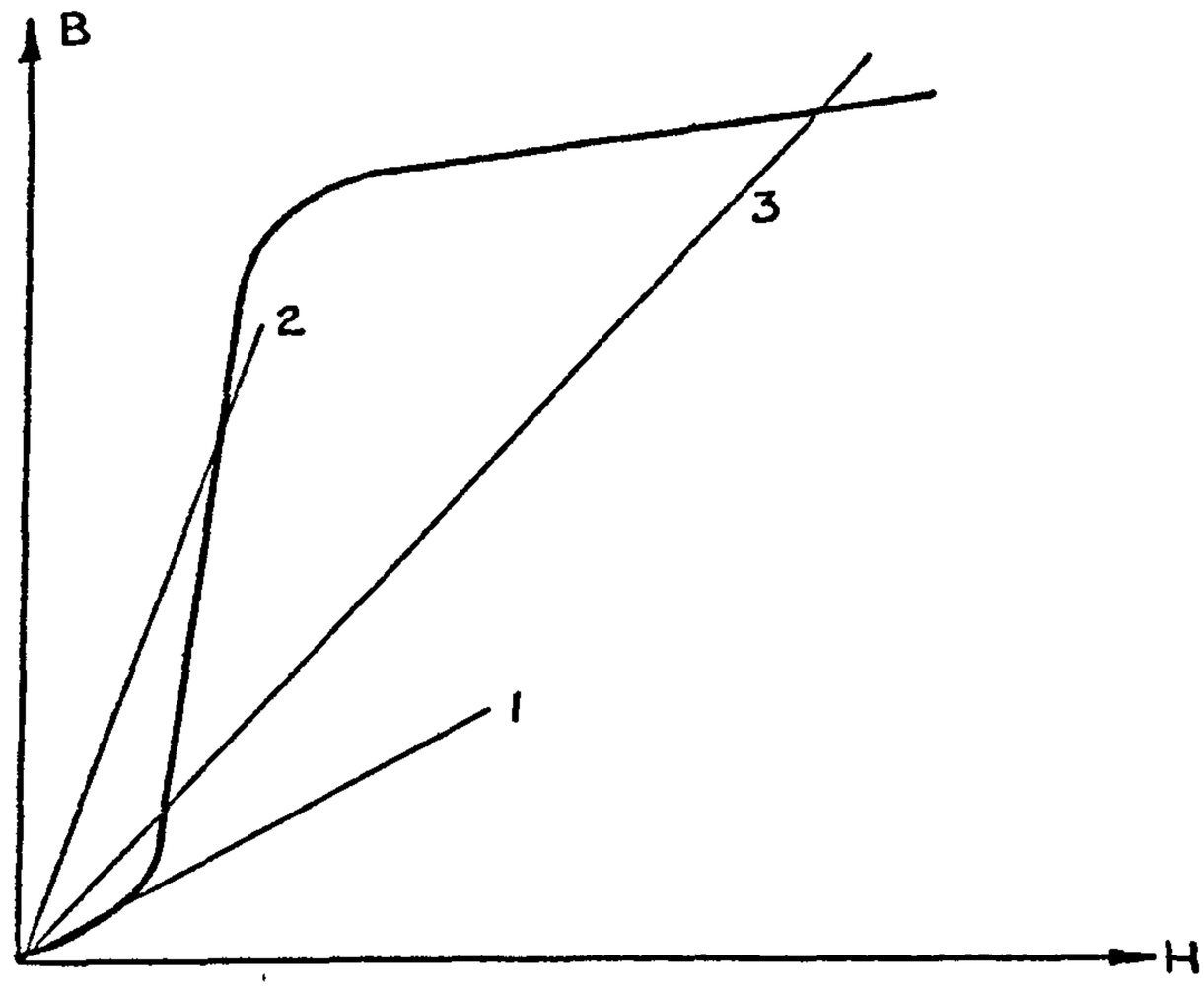

Figure 8.56 Change in Effective Inductance during Growth of Oscillations

CHAPTER IX

EXPERIMENTAL INVESTIGATION

9.1 Design

Construction of a two-C-core parametric transformer requires C cores of equal width and depth, because of the orthogonal positioning necessary. Although standard sizes of commercially available C cores provide only a limited choice, two parametric transformers using such cores were constructed. The first employed a single loop of HWR40/24 type C cores[1], while for the second, a construction with equal width and depth was produced by stacking three HWR110/20 type cores[1]. In both devices, the cores were of a 0.013" thickness strip, corresponding to an operational frequency of 50 Hz. The data on the physical dimensions of these cores, as obtained from reference 1, is given in Figure 9.1.

The main question in designing a two-C-core parametric transformer lies in deriving the dimensions of its bridged-core magnetic equivalent, and this was achieved in the following manner. The cross-sectional areas of the main branches of the bridged core, A_1 and A_2, were taken equal to the nett cross-sectional area (excluding inter-lamination insulation) of the C cores, and A_0 was taken as the nett area of one of the four portions of the core face in contact. The gross area for one such portion is E^2, where E is the dimension shown in

Figure 9.1. The nett area is k.E , where k, the stacking factor, is a constant (0.95 for 0.013" lamination thickness) which introduces the effect of the area of the inter-lamination insulation. However, A_0 was calculated as $k^2 E^2$, since the laminations of one core are perpendicular to those of the other at the faces in contact, and the effective nett area is therefore further reduced. Dimensions ℓ_1 and ℓ_2 were each taken as one-half of the mean flux path length for a loop of two C cores, and ℓ_0 was calculated as A-E. The dimensions A and E are shown in Figure 9.1.

The turn/volt ratio for the transformer is calculated from

$$n = \frac{N}{V} = \frac{\sqrt{2}}{\omega\ \phi_m} \qquad \ldots\ldots \qquad (9.1)$$

where $\omega = 2\pi f$ and f = 50 Hz, and ϕ_m is the maximum flux level in the core. The optimum condition of operation determined by point P in Figure 6.21 corresponds to an operational point slightly above the knee of the transreluctance characteristics of Figure 8.20, or in other words, to a maximum flux density level in the common region (or the bridge branches of the equivalent structure) slightly above the knee of the B/H curve. With the maximum flux density B_m in the bridge branches assumed as 1.7T, the maximum flux in the core is

$$\phi_m = B_m . 2\ A_0 \qquad \ldots\ldots \qquad (9.2)$$

and the turn per volt ratio from equation (9.1) is

$$n = 2.282 \qquad \ldots\ldots \qquad (9.3)$$

for the experimental unit employing 3 x HWR110/20 cores. For a nominal input voltage of 220V, the number of turns in the primary winding is

$$N_1 = n.V_1 = 502.2 \text{ turns} \qquad \ldots\ldots \qquad (9.4)$$

To allow for leakage flux and to obtain a number suitable for subdividing the winding for Scott-T connection, N_1 was increased by about 8% and the primary winding was wound with 540 turns. For complete symmetry, the secondary windings was given the same number of turns. Enamel insulated, SWG13 gauge wire was used for both windings.

Orthogonal positioning of the two halves of the cores presents difficulties in assembly, as standard clamping frames and bobbin carcasses cannot be used. Special care needs to be taken when the two cores are wrapped by banding with a metal strip, to prevent this acting as a short-circuited single-turn winding. The cores must be firmly in contact to avoid the introduction of large air-gaps, and cores with properly machined faces matching each other when orthogonally positioned should ideally be used. The effect of these unintentional air-gaps is quite different from those in conventional transformers, since

variation of their length causes a kind of reluctance modulation and affects the $F_1(\phi_1, \phi_2)$ and $F_2(\phi_1, \phi_2)$ functions, as explained in Section 4.4.3. A mechanical force is produced at double the supply frequency across the small air-gaps and since this may be quite high during parametric transformer operation, secure fixing is necessary to prevent the introduction of unwanted effects. Securing of the cores was achieved by a special clamp in the experimental device, a photograph of which is shown in Figure 9.2.

The inductance of the secondary winding was measured by a universal bridge as 0.588H, and the capacitance corresponding to this initial secondary inductance (when the primary circuit is non-energized) is

$$C = \frac{1}{\omega^2 L_2} = 17.23\ \mu F \qquad \ldots\ldots \qquad (9.5)$$

However, during parametric transformer operation, the secondary inductance is modulated and its average value is lower, and the capacitor needs to be given a somewhat higher value. The nominal value for the secondary capacitor was therefore taken as about 20 μF. The data for the experimental unit constructed with three HWR110/20 cores is given in Appendix VI.

In conventional transformer design, when operation frequency, primary and secondary voltages, and power rating are specified as initial requirements, the first step is to determine the size of cores suitable for the power rating

required. There are a number of factors involved in the determination of the size of a transformer other than the VA rating, such as (a) the permissible temperature rise, (b) the permissible voltage regulation, (c) the number of separate windings, (d) the individual winding voltages etc. Nevertheless, once the core size has been selected, the rest of the design is straightforward and presents little difficulty. However, the first condition to be met in selecting cores for a two-C-core parametric transformer, is that of equal depths and widths. Since standard cores were used, this determined their size and the design procedure thereafter became the reverse of that normally encountered with conventional transformers. A particularly important step in the design is the determination of the physical dimensions of the bridged core equivalent. The use of standard cores introduces the requirement of utilizing the whole available window area for a maximum power rating/core weight ratio. Since the number of turns in the windings is fixed by the nett cross-sectional area of the cores, the whole window area can be filled by conductor of lower gauge than necessary for nominal winding currents. This results in lower winding resistances and a consequent lower damping in the secondary resonant circuit, meaning that higher loads can be connected before overload protection occurs. Briefly, maximum power rating for the given cores is obtained when the available window area is fully used.

9.2 Operational Characteristics

The device was first tested as a saturable reactor. With mains voltage applied to the primary, the secondary voltage is only a few volts, and good isolation exists between the two windings due to absence of mutual flux coupling. With the primary driven by an alternating voltage source (instead of a dc source), the secondary voltage/current characteristics are shown in Figure 9.3, for different values of the alternating control voltage. These establish the controlling action explained by means of the relative magnetisation curves in Section 6.2.1.

With a capacitor of 19 μF connected across the secondary winding, the input voltage was varied from zero to over 400V and then reduced to zero, with the resulting input voltage/output voltage characteristic at no load, shown in Figure 9.4, clearly exhibiting over-voltage and under-voltage protection features. The different input voltages for switching-on and switching-off the oscillations, V_1' and V_1''', and the input voltage when the oscillations are suppressed by the over-voltage protection property, V_1'', are indicated in the figure. The changes in the primary and secondary currents as the input voltage is varied are shown in Figure 9.5, where the sudden increase and decrease in the currents on the initiation and cessation of oscillation is apparent. After over-voltage protection has occurred, the secondary current falls to a small

value, while the primary current continues increasing in accordance with the primary V/I characteristic .The slight peak in the secondary current variation in Figure 9.5 occurs when this current has the best sinusoidal waveform, i.e. the best condition of operation is achieved when V_1 is around 220V. The part of the curve between A and B in Figure 9.4 is not as constant as would be expected from a device exhibiting a very good voltage regulation, since this characteristic is derived from the effective values of the voltages, and the output voltage waveform and its rms value therefore changes with V_1, although its amplitude is quite constant.

To measure the effective values of voltages and currents, instruments indicating true rms values are required, since the waveforms of the output voltage and (especially) the primary and secondary currents are quite non-sinusoidal under different operational conditions. The currents were therefore measured with moving-iron ammeters with a frequency range 50-500 Hz, which was considered sufficient for a true rms indication as it included harmonics up to the 10th. Although moving-iron voltmeters were available with a frequency range 50-100 Hz, the effective values of the secondary voltage were measured using a Datron true rms converter. The results differed only slightly from those provided by moving-iron instruments, as the departure from sinusoidal is comparatively small and does not change much over the whole range.

Figure 9.6 shows V_2/V_1 characteristics of the unloaded device obtained in the same way, with different capacitors connected across the secondary winding. Within the region in which parametric excitation is possible, the output voltage is obtained at the fixed frequency 50 Hz, although the capacitor value is almost doubled between the two extremes. As seen from the figure, higher capacitor values result in higher output voltages. Since the output voltage is phase-locked with the input voltage and its frequency is therefore fixed, the higher capacitance causes higher secondary currents to flow, as the maximum energy oscillating in the secondary circuit is now higher.

When a variable resistive load was connected across the capacitor, the load regulation characteristic obtained was as shown in Figure 9.7, for V_1 = 220V and C = 19 μF. The load regulation property of the device is evident, as the output voltage initially changes only slightly with increasing load current. When the load resistance is decreased beyond a certain value the output voltage decreases more rapidly, and then suddently falls to zero, together with the load current, when over-load protection occurs. The load regulation characteristic for different input voltages and secondary capacitor values are shown in Figures 9.8 to 9.11. From these, it follows that the higher the input voltage the lower is the output voltage, but that a higher maximum load current is obtainable. In Figure 9.12, characteristics are drawn for a fixed input voltage but different capacitor values, and a similar conclusion may be drawn

from this figure for the effect of the capacitor value on the load characteristic. Although the device was designed for nominal values of V_1 = 220V and C = 20 μF, it is evident that higher load currents can be supplied if V_1 and C are increased, but at the expense of higher secondary currents and consequently, higher currents from the mains supply.

9.3 Voltage and Current Waveforms

The voltage and current waveforms at different operational conditions as recorded by an UV recorder are given in Figures 9.13 to 9.46. The good sinusoidal output voltage waveform at no-load operation with V_1 = 220V and C = 21 μF is apparent in Figure 9.13, where it is also seen that V_2 leads V_1 by 90°. The other stable phase, with V_2 lagging V_1 by 90°, is shown in Figure 9.15, obtained for the same operational conditions, and Figures 9.14 and 9.16 show the primary and secondary current waveforms corresponding respectively to Figures 9.13 and 9.15. Since the input voltage is at the best operational condition, the secondary current I_2 is almost sinusoidal but the primary current I_1 is quite distorted. These waveforms are the same as those given previously in Figure 6.18b, justifying the concept of relative magnetisation characteristics developed in Chapter VI. Using the sign convention of Figure 5.8, the relative phases of V_1, V_2, I_1 and I_2 are shown in Figure 9.17 for the two different stable conditions,

with the phasor I_1 determined from the zero-crossing instants of the primary current. The current waveforms in Figures 9.14 and 9.16 are repeated in Figures 9.18 and 9.19, from which the phase relationship in Figure 9.17 can be more readily deduced. Similarly, the relative phases of V_1 and I_1, and V_2 and I_2 can be seen in Figures 9.20 and 9.21. The primary current always lags the input voltage by 90°, as inductive energy is drawn from the supply. The secondary current always leads the output voltage by 90°, independently of the phase relationship between V_1 and V_2.

With the same capacitor value and no secondary load, the waveforms obtained for V_1 and I_1 at the reduced input voltage of 100V are shown in Figure 9.22. The corresponding secondary voltage and current waveforms are given in Figure 9.23, from which it is seen that the waveform of the secondary voltage is now somewhat flattened (the slight fluctuations on the peaks in Figure 9.23 are due to the transient response of the galvanometer in the UV recorder). This rather square-shaped waveform was predicted previously in Figure 6.22 by the relative magnetisation characteristics. Comparing Figure 9.22 with 9.20, shows that the height of one of the two peaks within a half period of the primary current is now smaller. Reducing V_1 to nearer V_1''' results in a diminution of the smaller of these peaks until finally, when $V_1 = V_1''' = 80V$ and just before under-voltage protection occurs, the primary current waveform becomes as in Figure 9.24. (The variation of the primary current waveform as V_1 is reduced can be better seen in Figure 9.32).

If the secondary voltage had taken the other stable phase (V_2 lagging V_1 by 90°), the currents appearing in opposite phase in Figure 9.24 would be in the same phase. The voltage V_1''', satisfying condition (3.204) or (3.199), is determined by the level at which the shrinking peak in the primary current completely disappears, and no more real power can be drawn from the mains supply.

Figure 9.25 shows the input and output voltage waveforms at no-load operation, with the capacitor unchanged but with V_1 = 380V. Corresponding to operation with $V_1' < V_1 < V_1''$, the output voltage waveform is now rather triangular in shape, as explained in Section 3.6.2 and shown in Figure 3.38. The primary and secondary current waveforms in Figure 9.26, are the same as in Figure 6.18a, for operation with the primary and secondary relative magnetisation curves as given by the pair numbered 4 in Figure 6.17. Similarly, the current waveforms in Figure 9.14 or 9.16 correspond to the pair of relative magnetisation characteristics numbered 2 in this figure. The variation of the primary and secondary current waveforms between these two cases as V_1 is increased can be better seen in Figure 9.34.

The secondary voltage and current take the waveforms in Figure 9.27, when operating with V_1 = 220V and C = 21 μF, and a load current I_L = 450 mA is drawn by a resistive load connected across the capacitor. The corresponding primary voltage and current waveforms are in Figure 9.28. The peaks of the secondary voltage are slightly affected by loading, but otherwise it

may still be considered a good sinusoid. The effect of the load on the secondary voltage waveform becomes more apparent in Figure 9.29, for which the load current is I_L = 700 mA, an effect explained in Section 3.6.2 by reference to Figure 3.40. The primary voltage and current waveforms for operation at a load current I_L = 700 mA, just below the value at which over-load protection occurs, are shown in Figure 9.30. The primary current waveform of Figure 9.28 and 9.30 are similar to those of Figures 9.22 and 9.24, respectively. The effect of the increasing load on the primary current waveform thus resembles the effect of reducing the input voltage during no-load operation. Just before oscillations are switched off, due to over-load protection at I_L = 705 mA, the shrinking peak of the primary current completely flattens, as in the case of under-voltage protection (see I_1 in Figure 9.32).

With loads of lagging power factor, the behaviour of the transformer was inferior to that for unity power factor load, in respect of waveform distortion of the output voltage, load regulation, and load power. However, for leading power factor loads a better load regulation characteristic and a higher maximum load power were achieved. Such a load increases the effective capacitance in the secondary circuit, and its effect on the load regulation characteristic may be deduced from Figure 9.12.

In Figure 9.31, the primary and secondary voltages are recorded for no-load operation, with C = 21 μF and V_1 gradually decreased from 220V. The corresponding current waveforms are in Figure 9.32, where their variations with V_1 can be clearly observed. When the input voltage falls below a certain level (around 85V), the output voltage drops suddenly to zero, as under-voltage protection occurs. Above this level the amplitude of V_2 can be seen to remain constant, although V_1 is changing considerably, thereby establishing the voltage regulation property of the device. However, the rms value of V_2 is not constant but varies slightly, in accordance with the operational characteristics of Figure 9,6, due to the waveform variation noticeable in Figure 9.31. After under-voltage protection causes the parametric excitation to cease, the oscillations die away exponentially,with the secondary voltage no longer phase-locked with the primary voltage. The period of the decaying oscillations becomes greater than that of the supply frequency, since, with the high capacitor value used, the resonant frequency of the secondary is less than this frequency.

The over-voltage protection feature of the transformer is exhibited in Figure 9.33, obtained by gradually increasing the input voltage from 220V to over 400V. The amplitude of V_2 remains constant, until V_1 is sufficient for relationship (3.201) to become effective and the amplitude of V_2 decreases accordingly. After the secondary voltage amplitude is suppressed by the overwhelming input voltage, oscillations in the secondary continue

at very small amplitude: in contradistinction to under-voltage protection (or over-load protection), the oscillations are now not switched off but only suppressed. If the input voltage is decreased to normal amplitude, the secondary voltage is restored to its full amplitude. The variation of the secondary voltage waveform as V_1 is increased is noticeable in Figure 9.33. At high input voltage levels, but before over-voltage protection occurs, the secondary voltage waveform becomes distorted to a triangular shape, and its rms value therefore decreases more rapidly than its amplitude, as given by the operational characteristics of Figure 9.6. The corresponding current waveforms are shown in Figure 9.34, in which the transformation of the waveforms from those in Figure 6.18b to those in Figure 6.18a can be readily observed.

Figure 9.35 shows the output voltage and the load current, with I_L varied from 400 mA up to 710 mA, and the load regulation property is shown by the amplitude of V_2 remaining constant throughout. When the load resistance becomes lower than a certain value, both the output voltage and the load current fall immediately to zero, establishing the over-load protection feature of the device. Since V_1 is not greater than V_1', oscillations are now switched off and the output voltage will not be restored after removal of the excessive load.

The oscillations in the secondary are self-excited only when $V_1' < V_1 < V_1''$. The initiation of the oscillations may be seen in Figure 9.36, where V_1 is initially 280V, slightly less than

V_1' in no-load operation with C = 21 μF (see Figure 9.6). The small oscillations existing prior to the start of parametric excitation arise through some very small mutual flux coupling through stray leakage flux.With a slight increase of V_1, so that $V_1 > V_1'$, the secondary voltage amplitude builds up rapidly, as the threshold condition (3.144) is satisfied. However, the secondary voltage now exhibits a deep amplitude modulation, the depth of which reduces as V_1 is decreased towards its nominal value,just as in the case of the computer plotted figures provided by the computer simulation in the previous Chapter. This amplitude modulation is accompanied by a waveform distortion similar to that in Figure 9.25, since V_1 is higher than the best condition of operation. When V_1 is decreased to near 220V, the secondary voltage waveform becomes a good sinusoid, as well as maintaining a constant amplitude.

For input voltages below the threshold V_1', the oscillations in the secondary can still be started by instantaneous application of the input voltage to the primary winding. Depending on the instant at which the input voltage is applied, high in-rush currents occur in the primary winding, and these create an mmf sufficient for the threshold condition to be momentarily satisfied. The build-up of the secondary voltage under such circumstances is shown in Figures 9.37 and 9.38 for two different instances. In the first of these, the secondary voltage, after an interval of aperiodic oscillations,

finally settles to the steady state, with its phase leading V_1 by 90°. Modulation of the amplitude, similar to that in Figure 9.36, is also present. In the latter, a rather larger interval of aperiodic oscillations exists before the secondary voltage settles in the steady state, with its phase lagging V_1 by 90°. As can be seen from the variations of V_2, which of the two stable phases is actually taken by the secondary voltage cannot be predetermined until the steady state is reached. The primary and secondary current waveforms when the input voltage is instantaneously switched on at another instant are shown in Figure 9.39, where the high primary in-rush currents and the build-up of the secondary current can be observed.

It was found in practice that it was not equally likely for the secondary voltage to take either of the two stable phases, and that the secondary voltage more often took the phase leading V_1 by 90°. This is due to the reaction occurring between the primary and secondary circuits because of the existence of winding resistances, with the second term in the third of equations (5.17) being responsible for the losses in the secondary winding resistance. These losses take slightly different values depending on whether V_2 is leading or lagging V_1, and the losses are less and the initiation of oscillations becomes easier if the secondary voltage takes the stable phase 90° ahead of the primary voltage. Furthermore, the maximum power delivered to the load under this condition is slightly higher than that when the secondary voltage takes the lagging phase.

Operation of the device as a frequency doubler was also investigated. The primary and secondary voltage waveforms, obtained with a 8 μF capacitor connected across the secondary and 275V applied at the primary winding, are shown in Figure 9.40. The secondary voltage, phase-locked with the primary voltage, is at twice supply frequency and has a good sinusoidal waveform, and the primary and secondary current waveforms corresponding to this operation are in Figure 9.41. Frequency-doubler operation exhibited the same characteristic features, i.e. under- and over-voltage protection, over-load protection etc., as in the normal operation. However, the range of the input voltage and capacitor values for which oscillations could be started and maintained was narrower. The maximum load current that could be drawn under this condition was I_L = 150 mA, when the 100 Hz output voltage was about 650V.

When an input voltage exceeding 400V, i.e. $V_1 > V_1''$, was suddenly switched on, with a secondary capacitor corresponding to normal operation (21 μF), another mode of oscillations was produced in the unloaded secondary circuit. These oscillations were either quasi-periodic or sometimes of double frequency, but they were always of very large amplitude. Since the ensuing primary and secondary currents are far greater than 10A, they could not be permitted to flow for more than a very short time and no UV recordings could be obtained. This phenomenon was predicted by the computer simulation, and an explanation was given in Section 3.4, with reference to Figure 3.28.

9.4 Single-to-Three Phase Conversion

During normal operation, the transformer output voltage is in quadrature with the input voltage, and this property makes it possible to convert from a single phase input to a polyphase output, or vice versa, merely by a suitable winding combination. Scott-T type connection[2] is a well-known method of obtaining a 3-phase supply from a 2-phase one. Considering the input and output voltages of a parametric transformer as together forming a 2-phase supply, the necessary connection is achieved by the winding arrangement shown in Figure 9.42. With $N_1 = N_2 = 540$, the number of turns for various sections of the windings are calculated as

$$N_{LK} = \frac{1}{\sqrt{3}} N_1 = 312$$

$$N_{RS} = \frac{\sqrt{3}}{2} . N_1 = 468 \qquad \ldots\ldots \qquad (9.6)$$

$$N_{nS} = \frac{1}{3} N_{RS} = 156$$

The windings of the experimental device were wound in sections of 2 x (72 + 84 + 114) turns, to permit the required combination above to be realised.

With a single-phase input of 110V applied at terminals LK, and a capacitor of 19 μF connected as shown in Figure 9.42, the voltages at terminals R, B and Y with respect to the neutral point n were simultaneously recorded, as in Figure 9.43. These voltage and capacitor values selected give phase voltages of equal amplitude and with the most sinusoidal waveforms. In regard to the operational characteristics, such as under- and over-voltage protection, over-load protection etc. the behaviour of the device in phase converter operation differs from that in normal parametric transformer operation, because the phase voltages V_R, V_B and V_Y are obtained by combining portions of the input and output voltages. Before parametric oscillations are excited, voltages are induced at terminals R, B and Y, with respect to the neutral point n, due to mutual flux coupling between the relevant winding sections, and Figure 9.44 shows the phase voltages under these conditions when V_1 = 90V. If the input voltage is decreased after parametric excitation has begun and the waveforms in Figure 9.43 have been achieved, the waveforms of the phase voltages become distorted with flattened peaks and their phase relationship changes. The waveforms of the phase voltages at V_1 = 40V, just before the under-voltage protection occurs and parametric oscillations cease, are shown in Figure 9.45, and with the cessation of parametric oscillations, the phase voltages resume the waveforms of Figure 9.44 at a corresponding amplitude. Increasing the input voltage to a higher level, when the device is already operating as in Figure 9.43, causes

over-voltage protection and the parametric oscillations are suppressed. However, only one of the phase voltages is suppressed in amplitude and the other two remain at a high amplitude. Figure 9.46 shows the phase voltage when V_1 is increased to 260V and the over-voltage protection level of the device has already been reached, and the phase relationship between the phase voltages is now similar to that in Figure 9.44.

Although the phase differences between each voltage in Figure 9.43 are not exactly 120^0, they may be considered practically to constitute a symmetrical 3-phase system. This is valid only for a specific input voltage V_1, because with different values of V_1 the phase symmetry between the voltages V_R, V_B and V_Y is lost, as well as their amplitudes becoming different. In conventional transformers converting a 2-phase to a 3-phase supply, the phases of the 2-phase supply are independent in respect of amplitude, waveform and phase variation, but with a parametric transformer this property is lost and the waveform and the rms value of V_2 changes with V_1. If a parametric transformer is designed for use as a phase converter, the level of V_1 at which the phase voltages form the best symmetrical 3-phase system must therefore be a major consideration in the design procedure.

9.5 Power and Efficiency Considerations

The efficiency of a power conversion device is defined as

$$E = \frac{\text{the power delivered to the load}}{\text{the power drawn from the supply}} \tag{9.7}$$

which is normally a constant expressed in percentage. In practice, as much as possible of the power drawn from the supply should be delivered to the load, when the losses are small and the efficiency approaches 100%. Furthermore, when no load is connected, the power drawn from the supply must be as small as possible.

In the case of the parametric transformer the situation is different, since the device draws a high apparent power from the supply even during no-load operation. Before parametric oscillations start, the device acts as a single iron-cored inductor, when the apparent power drawn from the supply with $V_1 < V_1'$ is therefore almost wholly reactive. The real power drawn at this stage is very small, since both the primary current and the total losses are correspondingly small. In the experimental device, the real power amounted to about 7-8W, before initiation of parametric oscillations for $V_1 < V_1'$. However, with the initiation of parametric excitation, the rms value of the primary and the secondary currents jumps to about 2A, as seen in Figure 9.5, when the power drawn from the supply suddenly increases, as determined by the increased primary

current with the waveform and phase shown in Figure 9.20. The primary current always lags the input voltage by about 90° during parametric transformer operation, and the input power is always inductive. The complex power drawn from the supply at this no-load operation with C = 21 μF is $P_1 = V_{1rms} \cdot I_{1rms} = 220 \times 2.1 = 462$ VA. Since the primary and the secondary currents are now high, the losses in the transformer are high and 85W is drawn from the supply. This quantity remains almost constant for different values of V_1, so long as parametric oscillations exist. With a resistive load connected across the secondary capacitor, the real input power was measured for different load currents. The relationship between the load power P_L and the real input power P_{1r} is shown in Figure 9.47, where the intermittent line corresponds to a power efficiency of 100%. The distance between the two lines in this figure is almost constant, and is equal to the total losses at no-load operation. At point A, the maximum achievable power of 251W is delivered to the load, when I_L = 652 mA and the output voltage V_2 = 368V. The load power cannot be further increased as over-load protection immediately occurs and both V_2 and I_L become zero. The efficiency in the real power sense is

$$E = \frac{P_L}{P_{1r}} \simeq \frac{P_L}{P_o + P_L} \qquad \ldots\ldots \qquad (9.8)$$

where P_o is the real power drawn from the supply at no-load operation and is constant (= 85W). The efficiency defined by equation (9.8) is not a constant but is a function of P_L and therefore varies with the load current, i.e. maximum efficiency occurs only when maximum power is delivered to the load. The maximum real power efficiency at this operation is thus calculated at point A of Figure 9.47 as

$$E_{max} = \frac{251(W)}{322(W)} = 78\% \qquad \ldots\ldots \qquad (9.9)$$

When operating with different values of V_1 and C, the characteristic in Figure 9.47 remains basically the same, although its length varies as the maximum load current is different at different operational conditions. For example, with V_1 = 200V, the maximum load current is I_L = 572 mA, when V_2 = 379V and the real input power is 302W. The maximum efficiency is then found as 72%.

The efficiency considered above is based on real power considerations. However, in parametric transformer operation, a high apparent power (462 VA) is drawn from the supply even on no load, and a useful conceptual efficiency is defined as the ratio of the load power to the total apparent input power. With 251W delivered to the load, the primary rms current was I_1 = 2.52A, and the total complex input power 220 x 2.52 = 554 VA. On this new definition, the overall maximum efficiency is therefore

$$E_{max} = \frac{P_{Lmax}}{P_1} = \frac{251(W)}{554(VA)} \approx 46\% \qquad \ldots\ldots \qquad (9.10)$$

The efficiency defined this way will vary with the load power, with the maximum occurring when maximum power is delivered to the load since, as the load is decreased, the complex input power falls from 554 VA to 462 VA at no load.

With the transformer operating with increased values of V_1 and C, higher maximum load currents can be supplied, but it was found that the maximum efficiency did not change substantially and remained within 43 - 47%. It should be noted that this efficiency was achieved by the experimental device in which the window area available for the secondary winding was not fully used. Since the condition for overload protection, equation (3.199), determines the maximum load current, and this depends on the damping in the secondary circuit, the maximum achievable load power and the power efficiency can therefore be increased by minimising the secondary damping. Apart from minimisation of the iron losses, this requiresthe secondary capacitor to have a very small internal leakage conductance and the secondary winding a minimum winding resistance. The latter is accomplished by filling the whole window area with the secondary winding, unlike the experimental device which used only about 65% of this area. Under this condition, the maximum load power that could be supplied by the experimental device might be expected to increase by 30%, with the corresponding efficiency becoming raised

to about 60%. For the commercially available parametric transformers, a power efficiency of 65% is typically claimed.[3]

Since the parametric transformer draws lagging reactive power from the supply at a low power factor, power factor correction may be necessary by a suitably chosen capacitor connected across the primary winding. The non-sinusoidal primary current, and the change in the waveform with load, present difficulties in resolving the apparent input power into its real and reactive components, and the apparent power factor therefore varies with load. The capacitance value necessary for a 100% correction of the input power factor may be determined rather more satisfactorily by experimentation under the normal operational conditions.

The size of the resonating capacitor connected across the secondary winding of the parametric transformer is determined mainly by the necessary VA rating. With the output voltage between 375 - 400V, the capacitor has to carry about 2.5A during parametric transformer operation, so that its VA rating must be at least 1000 VA. Since the maximum power that could be delivered to the load, is 250 VA, the ratio of the capacitor VA rating to the transformer VA rating is clearly an important factor when the weight of the total device is considered.

Excluding the capacitor, most of the weight of the device arises from the iron core. The weight of a single loop of HWR110/20 size C cores is 2.29 kg, as given in Figure 9.1, with a VA rating when used in a conventional transformer[1] of 350 VA.

The maximum power output expected from the experimental parametric transformer using three of these loops and with the full window area used is about 325 VA, so that 250 VA may be taken as the nominal power rating. Taking the weight of the copper into account, it is then found that the parametric transformer is some 2.8 times heavier than a conventional 2-winding transformer of the same VA rating. Inclusion of the weight of the capacitor will obviously worsen this ratio.

The maximum power rating of the experimental unit operating as a frequency-doubler was about 100 VA, or 2.5 times less than in normal operation. Furthermore, the efficiency (the load power to apparent input power) was also very much less, since the apparent input power was about three times that in normal operation and was in fact about 10%. Although an improved design could improve this figure slightly, it is doubtful if any major increase could be achieved.

9.6 Relation Between Relative Magnetisation Characteristics, Current Waveforms and Real Input Power

A close relationship exists between the primary current waveform, the primary relative magnetisation characteristic and the real power drawn from the supply. With nominal input voltage, the primary and the secondary relative magnetisation characteristics are as given by the pair of curves numbered 2

in Figure 6.17 and the current waveforms by Figure 6.18b. In obtaining these, losses are neglected and the primary current, despite its unusual waveform, is therefore fully reactive, as can be seen in Figure 9.20. However, the current waveform obtained in practice differs from that in Figure 6.18b, in particular with respect to the different heights of the two peaks within a half cycle. If the variation of the apparent power input is obtained from Figure 9.20, by calculating the product $v_1.i_1$ at each instant and integrating this over a supply period, it is seen that an average (real) power exists due to the difference between the peak heights of the primary current. This average power drawn from the supply provides the losses existing in the device at no-load operation.

From the observation above, it may be concluded that the primary relative magnetisation characteristic is not the unique curve of Figure 6.17, but is as shown in Figure 9.48a. The two different sections of the curve in this figure are traced as indicated, within a half cycle of the primary flux variation. The section of the curve traced as ϕ_1 increases from zero to its maximum is different from that traced when ϕ_1 decreases from the maximum to zero, and this results in the difference between the heights of the peaks in Figure 9.20. The area indicated in Figure 9.48a corresponds to the energy supplied within a half period, to counteract the existing losses. In other words, with a flux/mmf

characteristic as in this figure, the primary winding as an inductor becomes a non-conservative element[4] absorbing energy from the supply.

It is now evident that the primary winding acts as a parametric energy absorber. However, it should be noted that if the closed path of the relative magnetisation characteristic in Figure 9.48a was followed in an anti-clockwise direction, the situation would be reversed, with the inductive element becoming a parametric generator, which is the case for the secondary. Note also that, in this case, the first peak within the half period of the current waveform becomes lower than the second (see I_2 in Figure 9.34), with the difference being a measure of the energy produced in a half cycle.

When the input voltage on no load is decreased towards V_1''', the multi-valued primary relative magnetisation characteristic in Figure 9.48a undergoes the change in shape illustrated, so that the area between the two curve sections remains almost constant. This is clearly because the real power drawn from the supply at no-load (measured as 85W in the experimental device with C = 21 μF) does not change substantially when $V_1''' < V_1 < V_1'$. The change in the shape of the curve section traced when ϕ_1 is decreasing fully explains the variation of the primary current waveform in Figure 9.32, with one of its peaks decreasing as V_1 is decreased. This change of shape continues, until when the curve section traced as ϕ_1 is decreasing falls on the intermittent curve in Figure 9.48d , and the

decreasing peak thus completely disappears. Figure 9.48d therefore illustrates the condition for under-voltage protection. Because the shaded area in this figure representing the energy drawn from the supply in a half cycle is equal to the total energy losses and a further decrease in V_1 makes this area smaller than the total loss, the oscillations in the secondary can no longer be sustained.

The effect of the load on the current waveforms can be demonstrated in a similar manner. The area encircled by the primary magnetisation characteristic in Figure 9.49a is equal to the total no load loss. With a fixed input voltage, a moderate secondary load causes this characteristic to change to that in Figure 9.49b, from which the primary current waveform in Figure 9.28 can be readily obtained. The area encircled is now larger as more energy is drawn from the supply. In terms of power, the shaded portion of this area corresponds to the real power delivered to the load, while the unshaded portion corresponding to the losses remains almost constant, in accordance with Figure 9.47. The load can be increased until the changing curve section fully coincides with the intermittent curve, as shown in Figure 9.49c, when the primary current takes the waveform in Figure 9.30, and the decreasing peak completely disappears. The unshaded area corresponding to the losses is unchanged but the area corresponding to the real power delivered to the load is now a maximum, and the figure determines the condition for over-load protection. For a fixed V_1 and C, the total area encircled by the primary relative

magnetisation characteristic cannot be increased further than that in Figure 9.49c. If an attempt is made to further increase the load, the maximum real power that can be drawn is unsufficient to supply both the losses and the required load power. The parametric oscillations can no longer be sustained and over-load protection occurs. The shaded area in Figure 9.49c therefore determines the maximum power that can be delivered to the load, under the existing operational conditions.

Finally, it should be noted that the considerations of an increased efficiency of the experimental device were based on minimising the unshaded area in Figure 9.49c so that the maximum achievable load power (the shaded area) is increased.

Telmag/Strip Wound Cores

Telmag 'C' type cores: British Standard Range

Code No. HWR	Nominal Dimensions (inches)						Nett Area (sq. ins.)		Flux Path (ins.)	Weight per Loop (lbs.)		Int. Service Cat. No.	
	A	B	D	E	F	G	·004″	·012/4″		·004″	·012/4″	·004″	·012/4″
3/ 4	$\frac{3}{4}$	$1\frac{1}{16}$	$\frac{1}{4}$	$\frac{1}{4}$	$\frac{1}{4}$	$\frac{9}{16}$	·058	—	2·36	·037	—	Z 371030	—
4/ 5	$\frac{15}{16}$	$1\frac{5}{16}$	$\frac{5}{16}$	$\frac{5}{16}$	$\frac{5}{16}$	$\frac{11}{16}$	·090	—	2·93	·071	—	Z 371031	—
5/ 6	$1\frac{1}{8}$	$1\frac{5}{8}$	$\frac{3}{8}$	$\frac{3}{8}$	$\frac{3}{8}$	$\frac{7}{8}$	·129	—	3·63	·126	—	Z 371032	—
7/ 6	$1\frac{3}{16}$	$1\frac{7}{8}$	$\frac{3}{8}$	$\frac{3}{8}$	$\frac{7}{16}$	$1\frac{1}{8}$	·129	—	4·26	·149	—	Z 371033	—
10/ 8	$1\frac{1}{8}$	$2\frac{1}{8}$	$\frac{1}{2}$	$\frac{5}{16}$	$\frac{1}{2}$	$1\frac{1}{2}$	·144	·148	4·87	·193	·199	Z 371018	Z 371038
10/12	$1\frac{1}{8}$	$2\frac{1}{8}$	$\frac{3}{4}$	$\frac{5}{16}$	$\frac{1}{2}$	$1\frac{1}{2}$	·216	·223	4·87	·289	·298	Z 371019	Z 371000
10/16	$1\frac{1}{8}$	$2\frac{1}{8}$	1	$\frac{5}{16}$	$\frac{1}{2}$	$1\frac{1}{2}$	·288	·297	4·87	·385	·396	Z 371020	Z 371001
10/24	$1\frac{1}{8}$	$2\frac{1}{8}$	$1\frac{1}{2}$	$\frac{5}{16}$	$\frac{1}{2}$	$1\frac{1}{2}$	·431	·445	4·87	·578	·596	Z 371034	Z 371002
30/ 8	$1\frac{3}{8}$	$2\frac{3}{4}$	$\frac{1}{2}$	$\frac{3}{8}$	$\frac{5}{8}$	2	·172	·178	6·34	·300	·310	Z 371021	Z 371039
30/12	$1\frac{3}{8}$	$2\frac{3}{4}$	$\frac{3}{4}$	$\frac{3}{8}$	$\frac{5}{8}$	2	·259	·267	6·34	·449	·466	Z 371022	Z 371003
30/16	$1\frac{3}{8}$	$2\frac{3}{4}$	1	$\frac{3}{8}$	$\frac{5}{8}$	2	·345	·356	6·34	·601	·622	Z 371023	Z 371004
30/20	$1\frac{3}{8}$	$2\frac{3}{4}$	$1\frac{1}{4}$	$\frac{3}{8}$	$\frac{5}{8}$	2	·431	·445	6·34	·752	·776	Z 371035	Z 371005
40/12	$1\frac{1}{2}$	3	$\frac{3}{4}$	$\frac{3}{8}$	$\frac{3}{4}$	$2\frac{1}{4}$	·259	·267	6·96	·495	·512	Z 371024	Z 371040
40/16	$1\frac{1}{2}$	3	1	$\frac{3}{8}$	$\frac{3}{4}$	$2\frac{1}{4}$	·345	·356	6·96	·660	·683	Z 371025	Z 371006
40/20	$1\frac{1}{2}$	3	$1\frac{1}{4}$	$\frac{3}{8}$	$\frac{3}{4}$	$2\frac{1}{4}$	·431	·445	6·96	·825	·853	Z 371026	Z 371007
40/24	$1\frac{1}{2}$	3	$1\frac{1}{2}$	$\frac{3}{8}$	$\frac{3}{4}$	$2\frac{1}{4}$	·517	·534	6·96	·990	1·023	Z 371036	Z 371008
50/14	$1\frac{7}{8}$	$3\frac{1}{2}$	$\frac{7}{8}$	$\frac{1}{2}$	$\frac{7}{8}$	$2\frac{1}{2}$	·402	·416	8·12	·898	·927	Z 371027	Z 371041
50/18	$1\frac{7}{8}$	$3\frac{1}{2}$	$1\frac{1}{8}$	$\frac{1}{2}$	$\frac{7}{8}$	$2\frac{1}{2}$	·517	·534	8·12	1·151	1·192	Z 371028	Z 371009
50/24	$1\frac{7}{8}$	$3\frac{1}{2}$	$1\frac{1}{2}$	$\frac{1}{2}$	$\frac{7}{8}$	$2\frac{1}{2}$	·690	·712	8·12	1·539	1·590	Z 371029	Z 371010
50/32	$1\frac{7}{8}$	$3\frac{1}{2}$	2	$\frac{1}{2}$	$\frac{7}{8}$	$2\frac{1}{2}$	·920	·950	8·12	2·058	2·120	Z 371037	Z 371011
70/12	$2\frac{3}{8}$	$4\frac{1}{4}$	$\frac{3}{4}$	$\frac{5}{8}$	$1\frac{1}{8}$	3	·431	·445	10·00	1·187	1·223	—	Z 371042
70/18	$2\frac{3}{8}$	$4\frac{1}{4}$	$1\frac{1}{8}$	$\frac{5}{8}$	$1\frac{1}{8}$	3	·647	·668	10·00	1·778	1·834	—	Z 371012
70/24	$2\frac{3}{8}$	$4\frac{1}{4}$	$1\frac{1}{2}$	$\frac{5}{8}$	$1\frac{1}{8}$	3	·862	·891	10·00	2·415	2·446	—	Z 371013
70/32	$2\frac{3}{8}$	$4\frac{1}{4}$	2	$\frac{5}{8}$	$1\frac{1}{8}$	3	1·150	1·187	10·00	3·159	3·261	—	Z 371014
90/16	$2\frac{7}{8}$	5	1	$\frac{3}{4}$	$1\frac{3}{8}$	$3\frac{1}{2}$	·690	·712	11·90	2·262	2·334	—	Z 371043
90/24	$2\frac{7}{8}$	5	$1\frac{1}{2}$	$\frac{3}{4}$	$1\frac{3}{8}$	$3\frac{1}{2}$	1·035	1·069	11·90	3·383	3·495	—	Z 371015
90/32	$2\frac{7}{8}$	5	2	$\frac{3}{4}$	$1\frac{3}{8}$	$3\frac{1}{2}$	1·380	1·425	11·90	4·514	4·657	—	Z 371016
90/44	$2\frac{7}{8}$	5	$2\frac{3}{4}$	$\frac{3}{4}$	$1\frac{3}{8}$	$3\frac{1}{2}$	1·897	1·959	11·90	6·196	6·399	—	Z 371017
110/20	$3\frac{3}{4}$	$6\frac{1}{2}$	$1\frac{1}{4}$	1	$1\frac{3}{4}$	$4\frac{1}{2}$	1·150	1·187	15·42	4·891	5·054	—	Z 371044
110/32	$3\frac{3}{4}$	$6\frac{1}{2}$	2	1	$1\frac{3}{4}$	$4\frac{1}{2}$	1·840	1·900	15·42	7·846	8·101	—	Z 371045

Limits of Tolerance and Basis for Weight Calculation

Dimensions (inches)	For ·013″, ·004″ and ·002″ ribbon Dimensions in inches
A	$-0+\frac{5}{64}$
B	$-0+\frac{3}{32}$ if $B \leq 2\frac{1}{2}$
B	$-0+\frac{1}{8}$ if $B > 2\frac{1}{2}$ and $E \leq \frac{3}{4}$
B	$-0+\frac{3}{16}$ if $B > 2\frac{1}{2}$ and $E > \frac{3}{4}$
E	$-0+\frac{1}{32}$
F and G	Not less than nominal
D	$-0+\frac{1}{32}$ if $D \leq 2$
D	$-0+\frac{1}{16}$ if $D > 2$
R	$\frac{1}{32}$ for Types HWR 3–7 inclusive $\frac{1}{16}$ for Types HWR 10–30 inclusive $\frac{1}{8}$ for Types HWR 40 and up

Weight = (D × E × L × K × 0·275) Lbs.
Where: L = Mean Length of Flux Path Ins.
For ·002″ strip K = 0·88
For ·004″ strip K = 0·92
For ·013″ strip K = 0·95

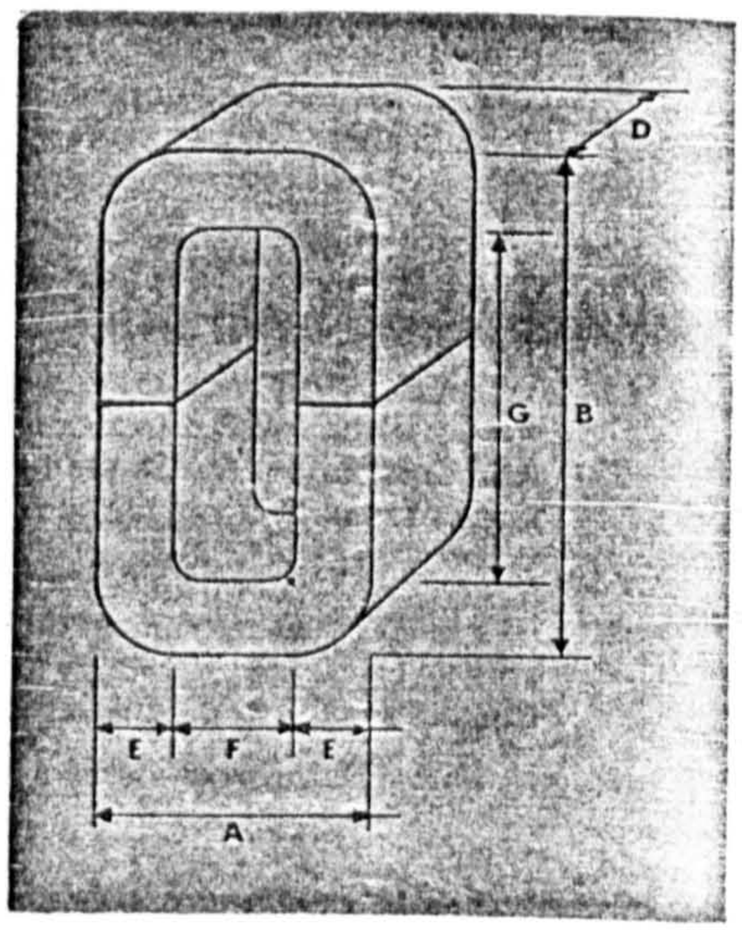

Chapelhall Airdrie Lanarkshire Scotland

Figure 9.1 Data on the Cores Used

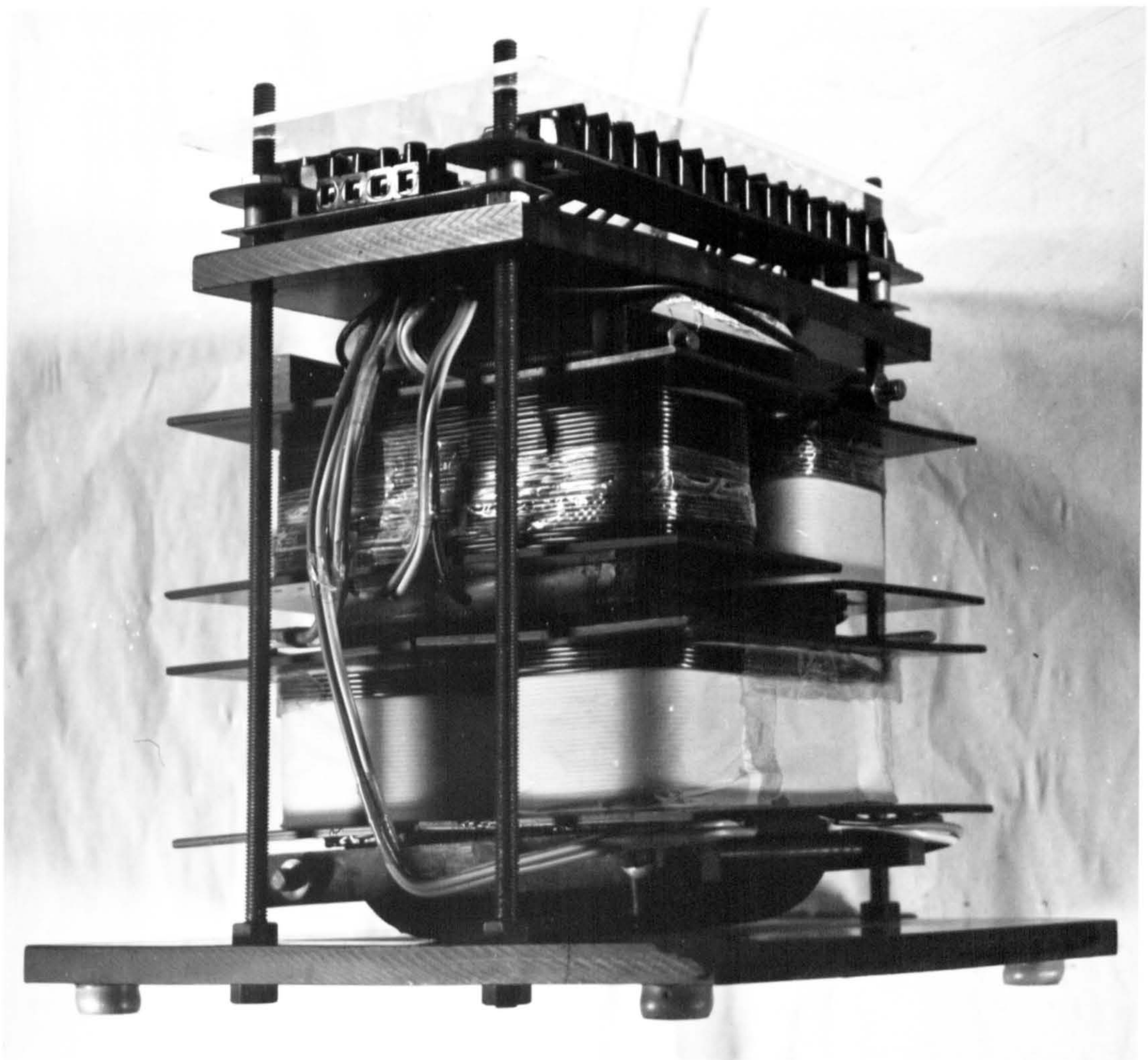

Figure 9.2 Experimental Device constructed with 3 x HWR 110/20 Cores

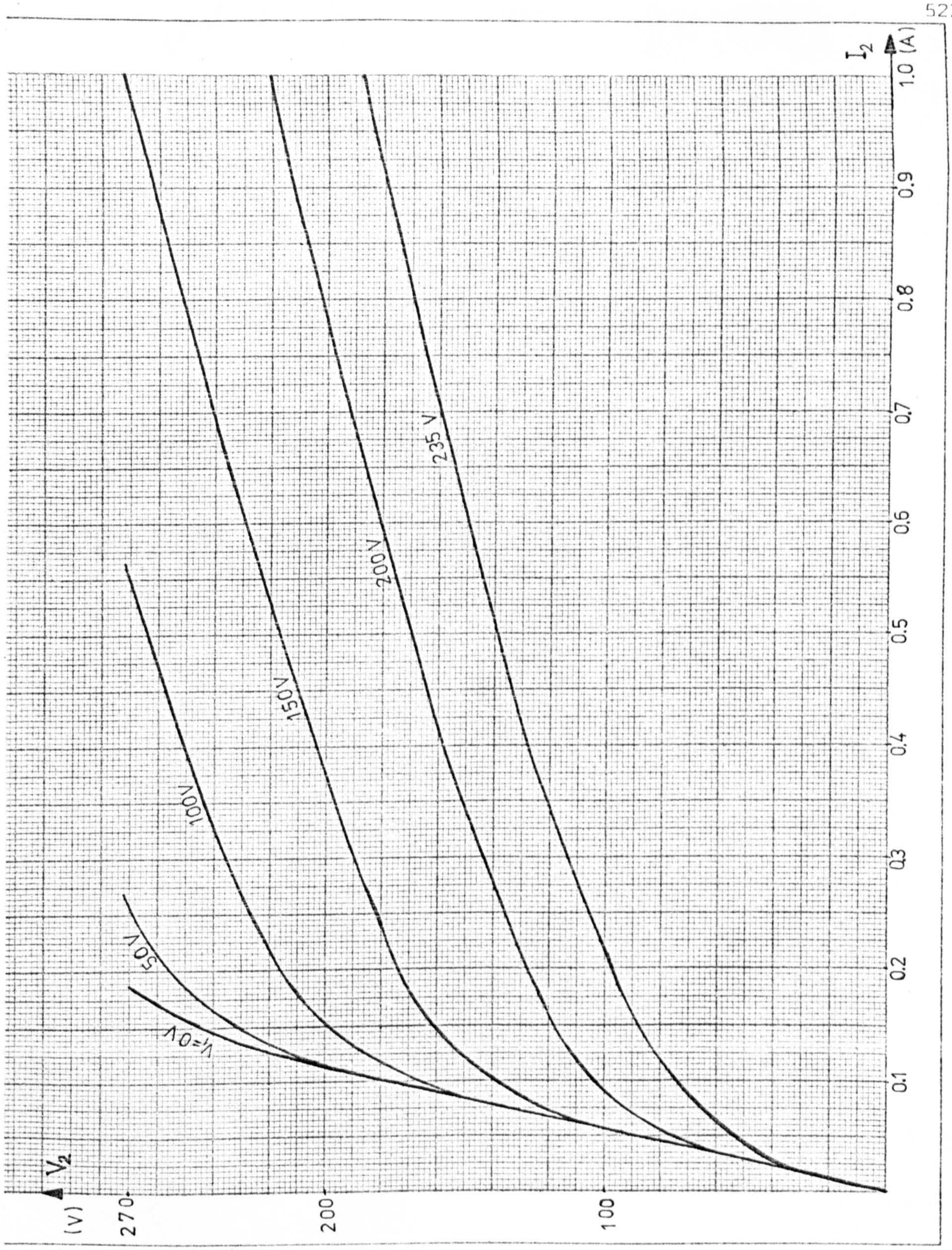

Figure 9.3 V_2/I_2 characteristics at operation as saturable reactor with control winding driven by acv source

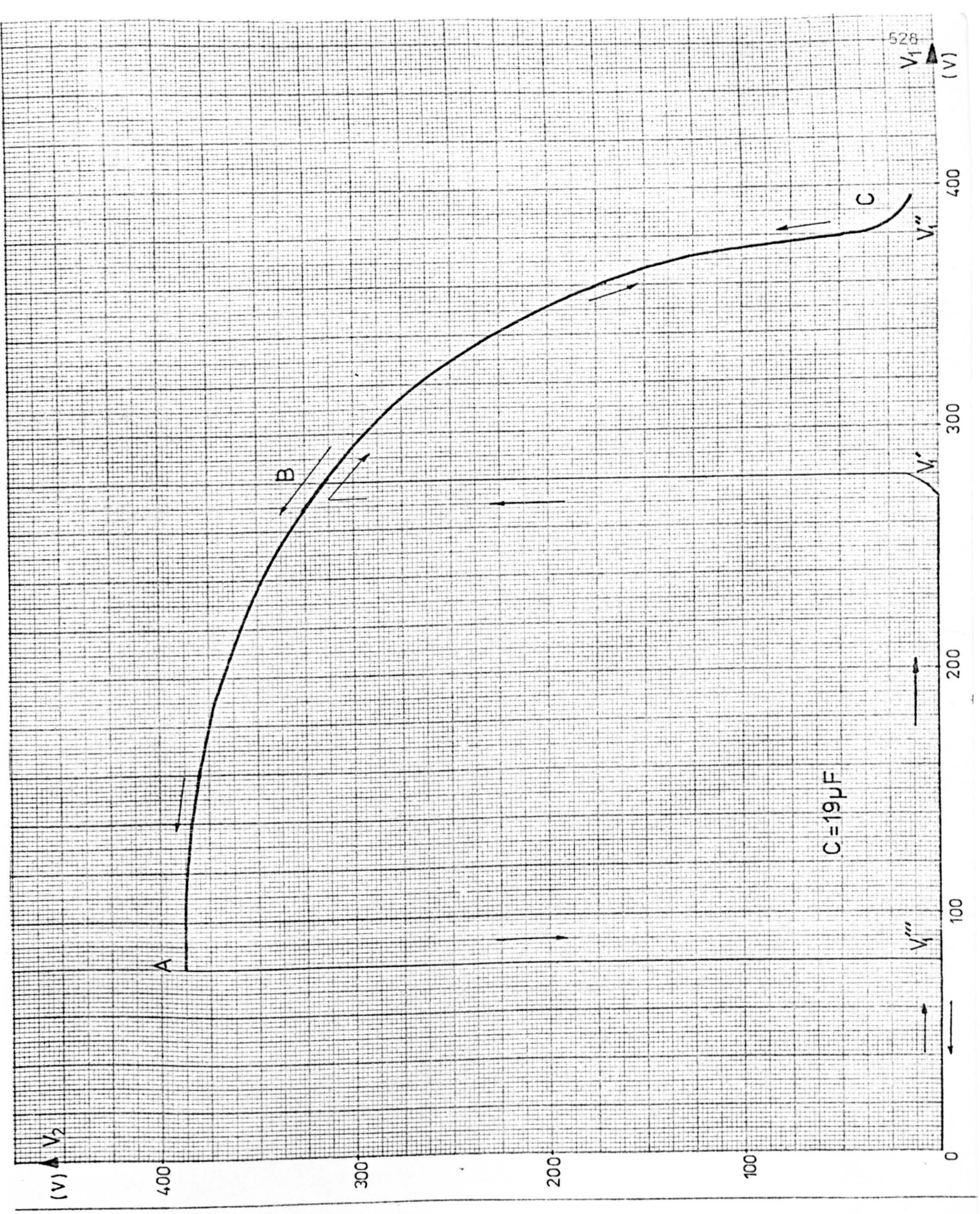

Figure 9.4 V_2/V_1 Characteristic at No-Load Operation

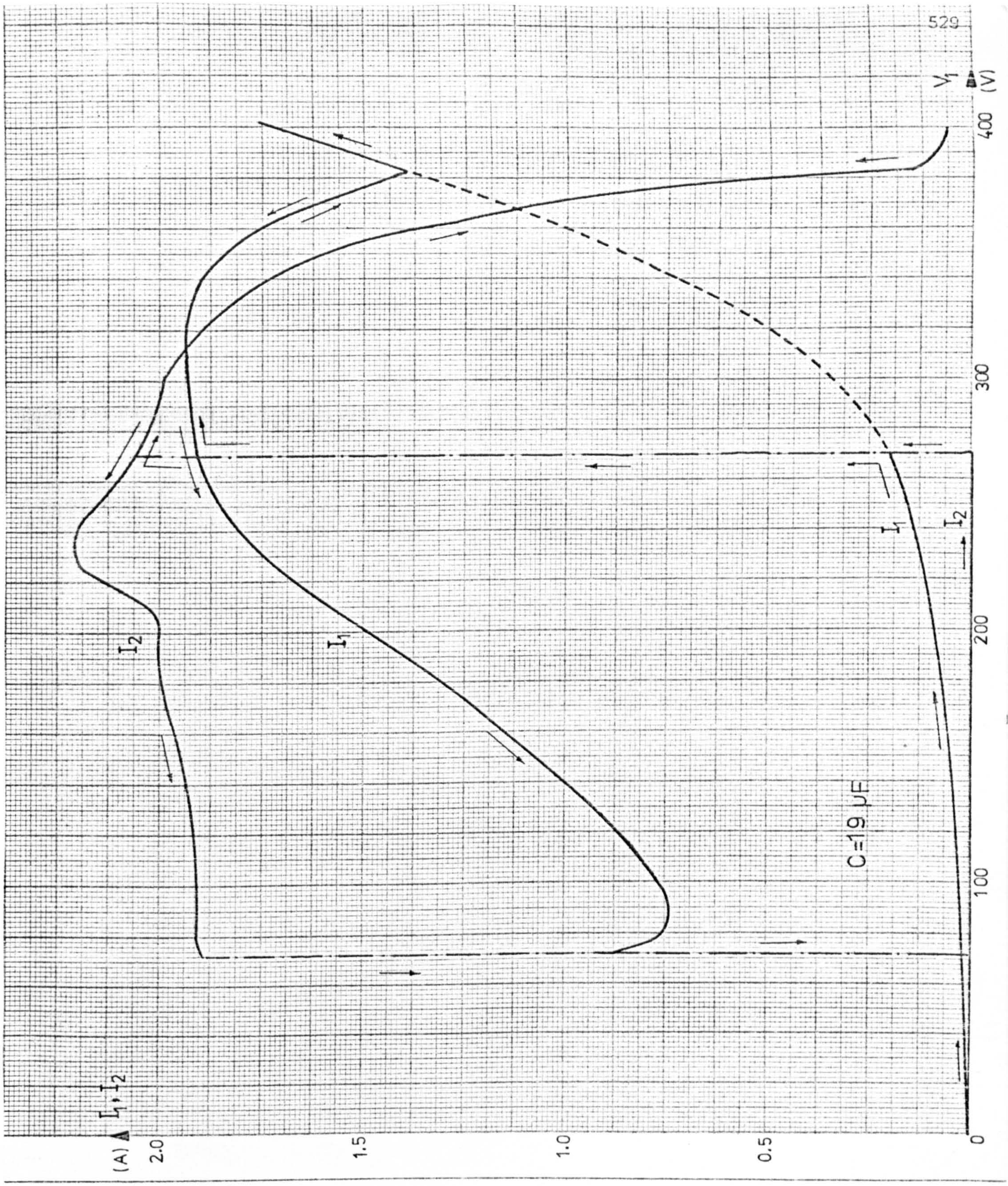

Figure 9.5 Variation of I_1 and I_2 with V_1, No-load Operation

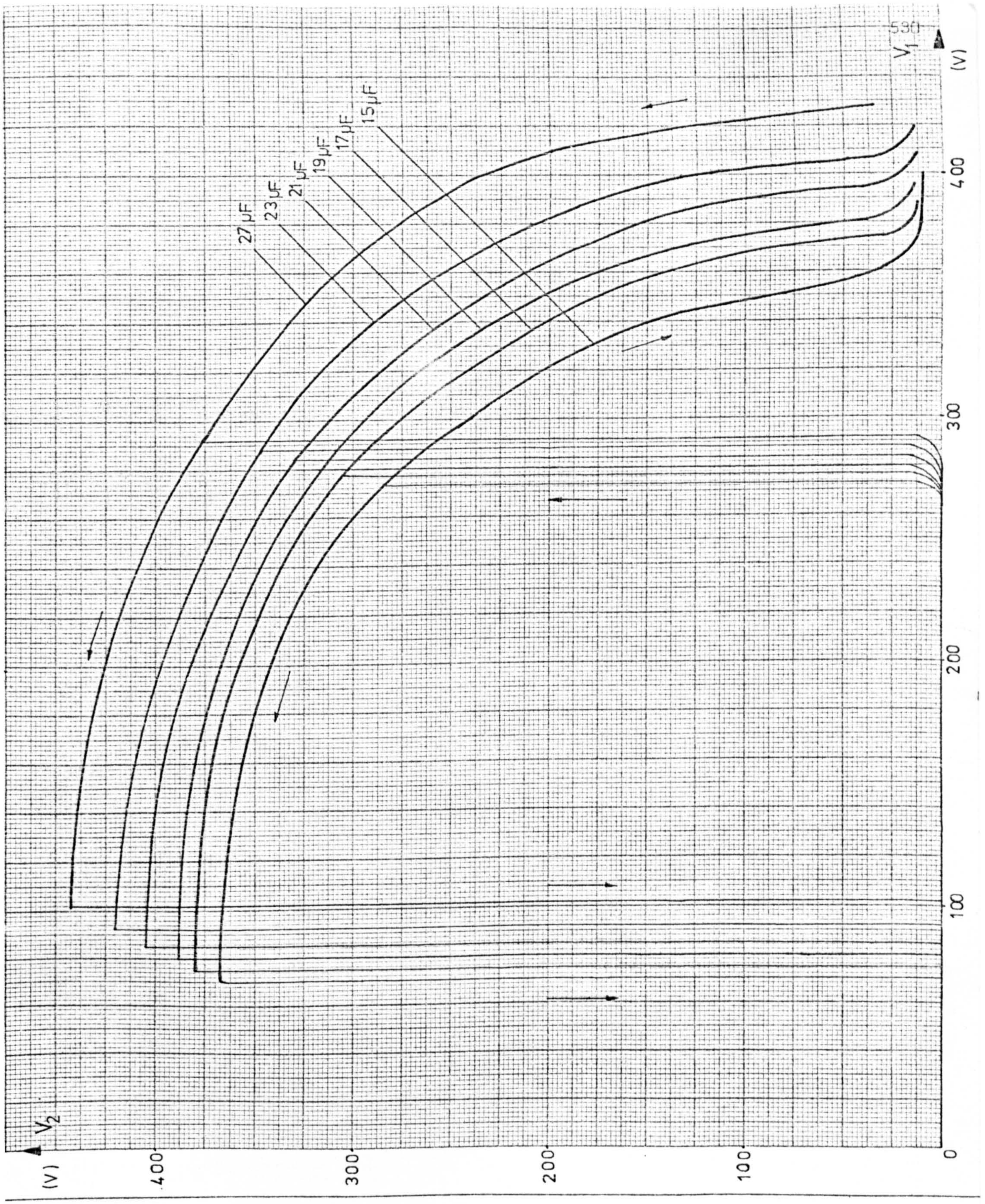

Figure 9.6 V_2/V_1 Characteristics for Different Values of C, at No-load Operation

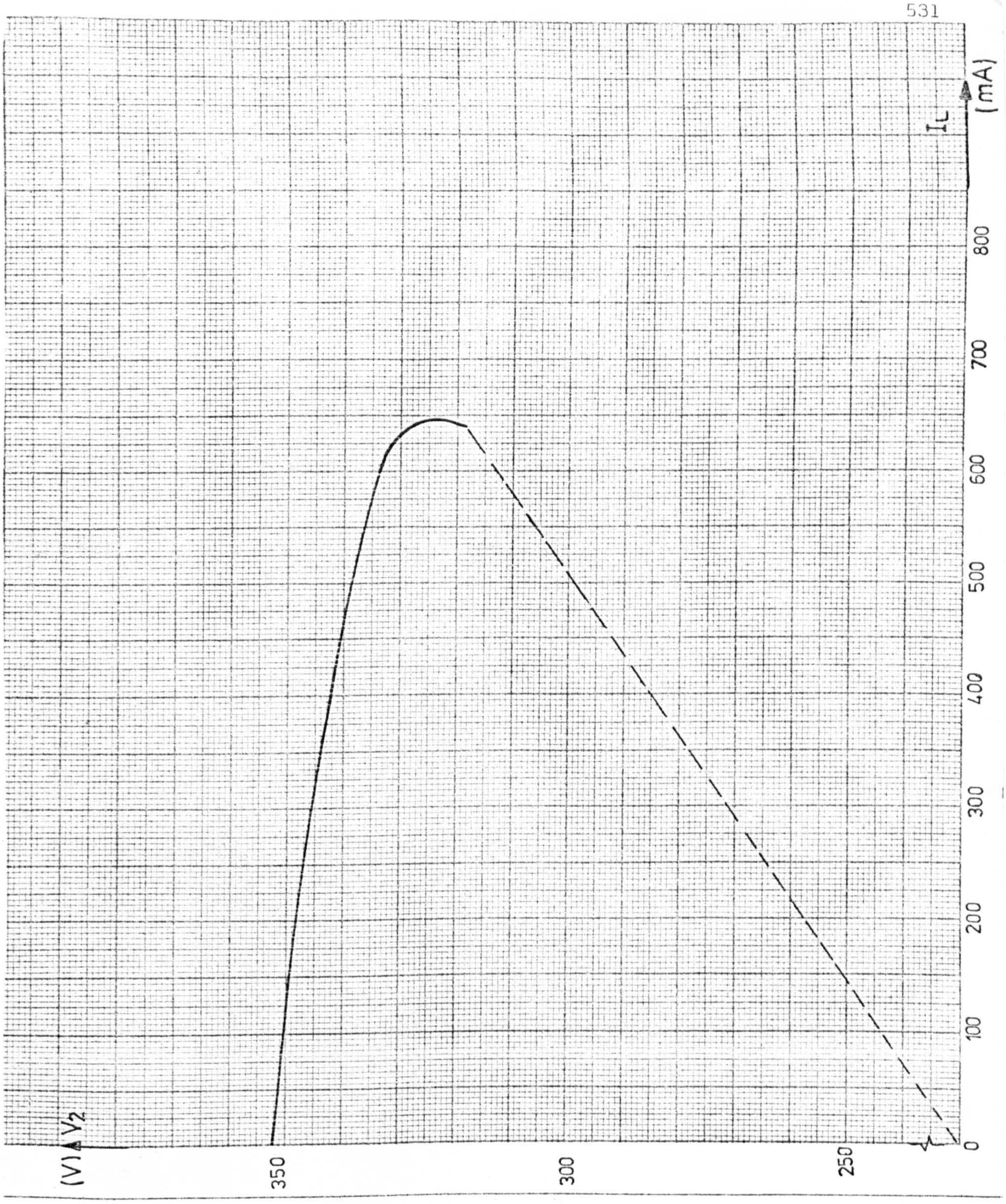

Figure 9.7 Load Characteristic, for V_1 = 220V and C = 19 μF.

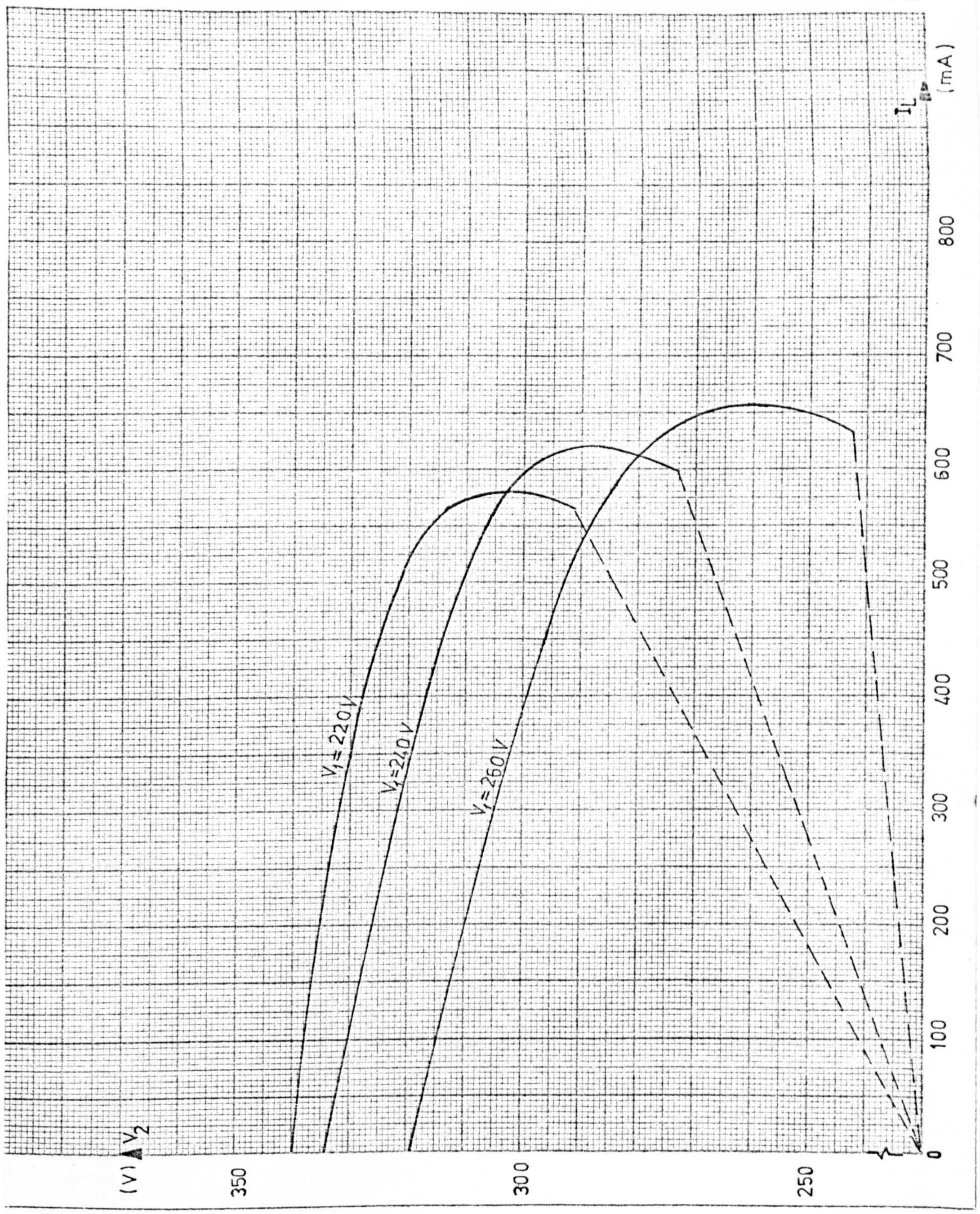

Figure 9.8 Load Characteristics, C = 17 μF.

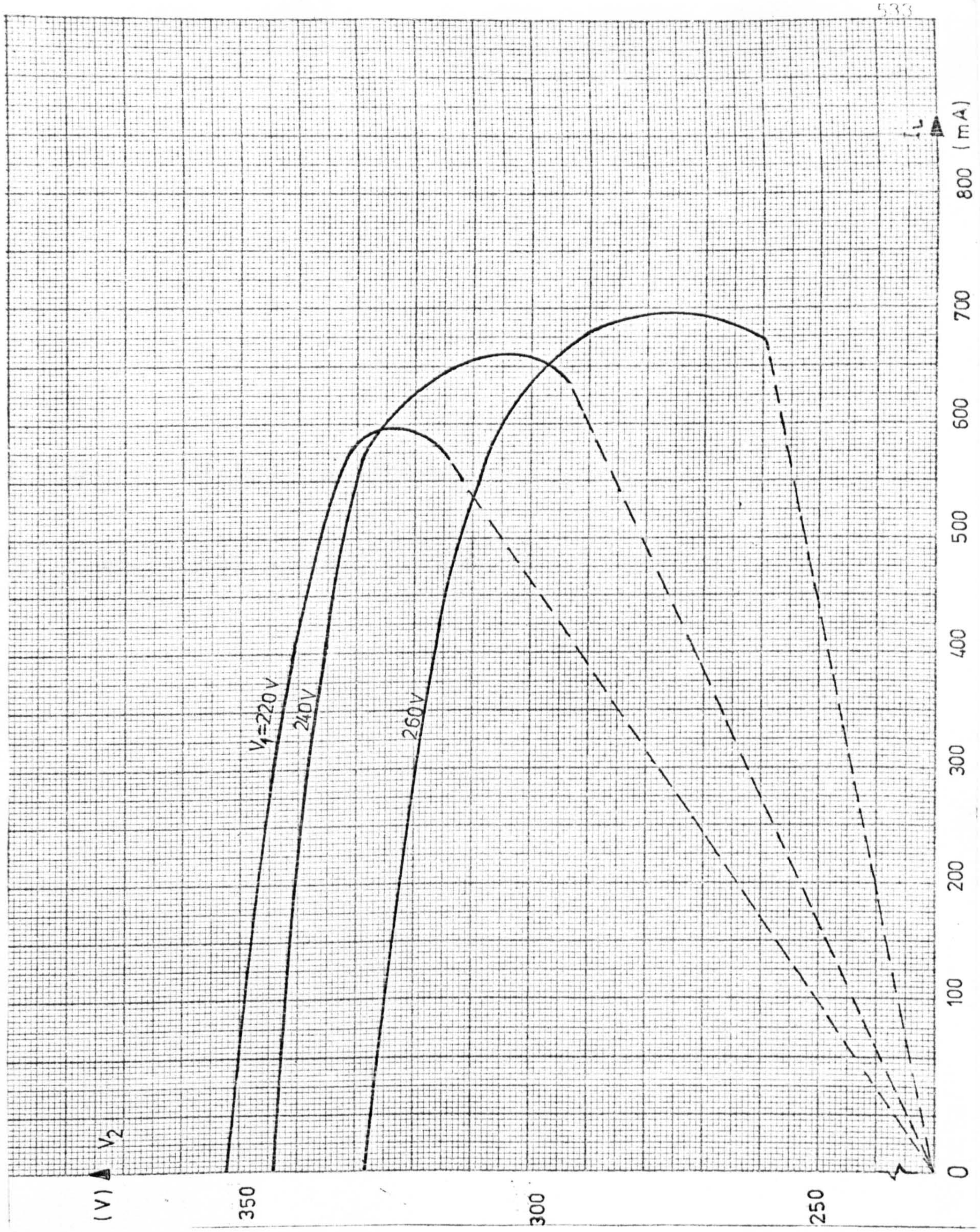

Figure 9.9 Load Characteristics, C = 19 μF.

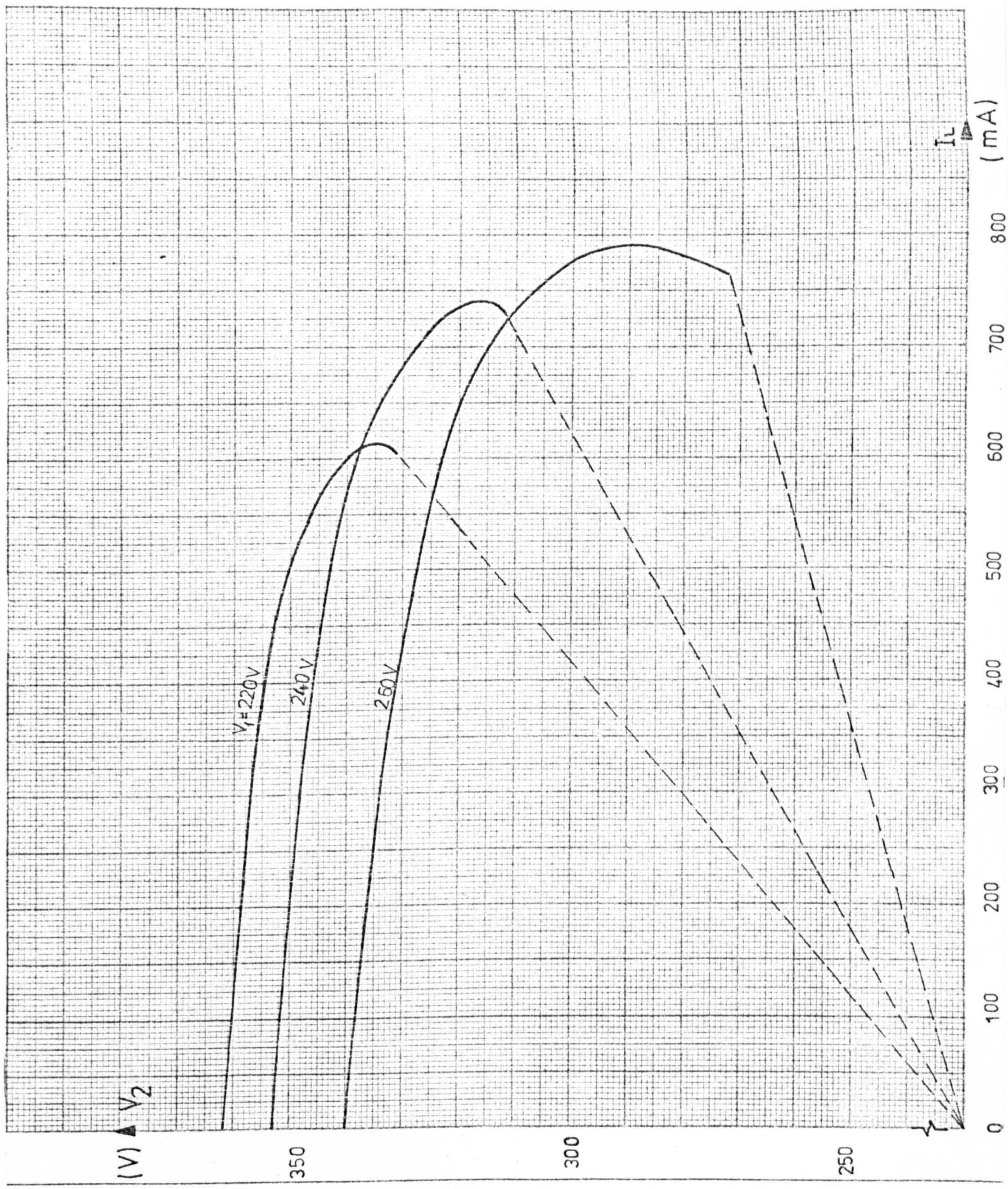

Figure 9.10 Load Characteristics C = 21 μF.

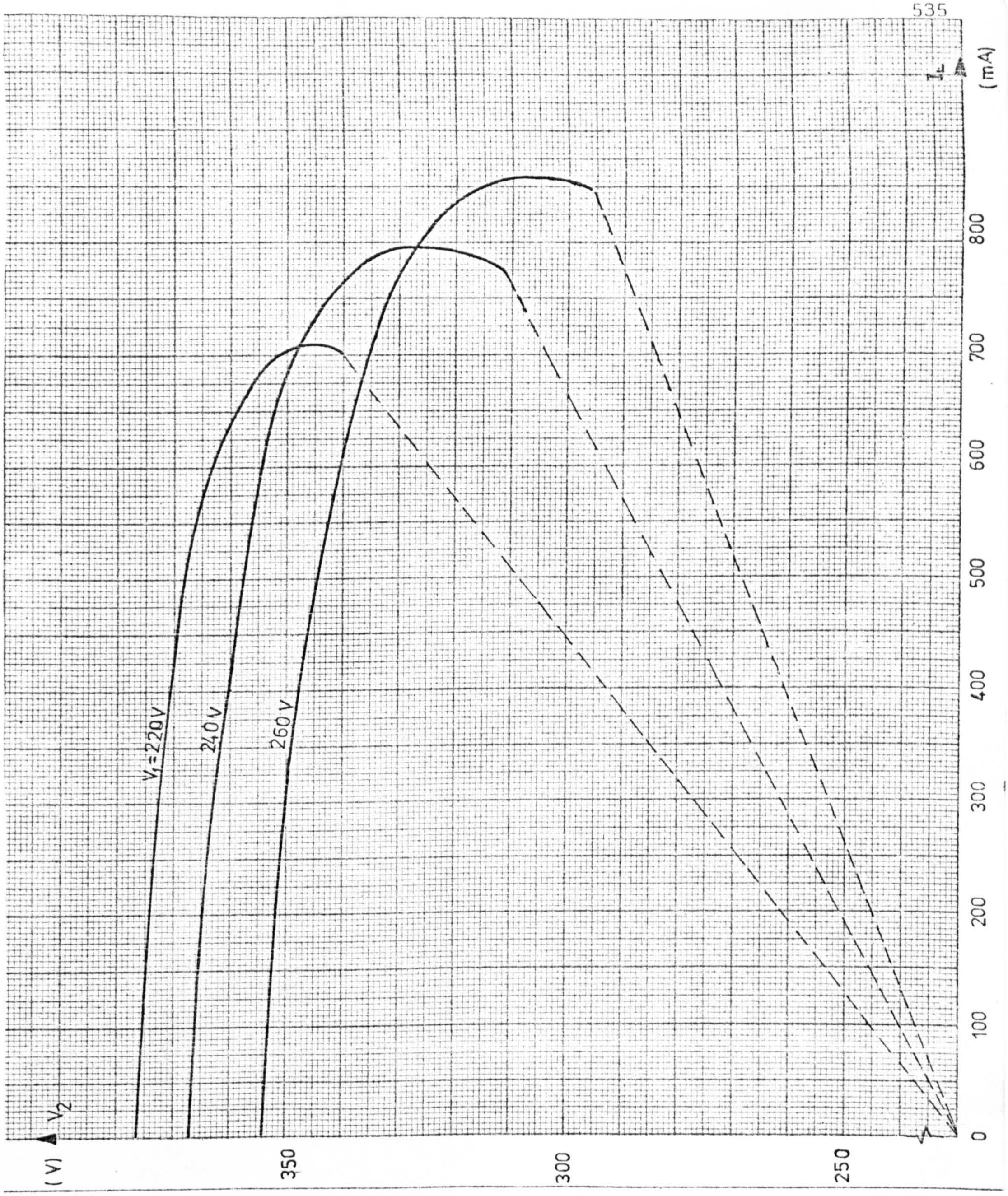

Figure 9.11 Load Characteristics, C = 23 μF.

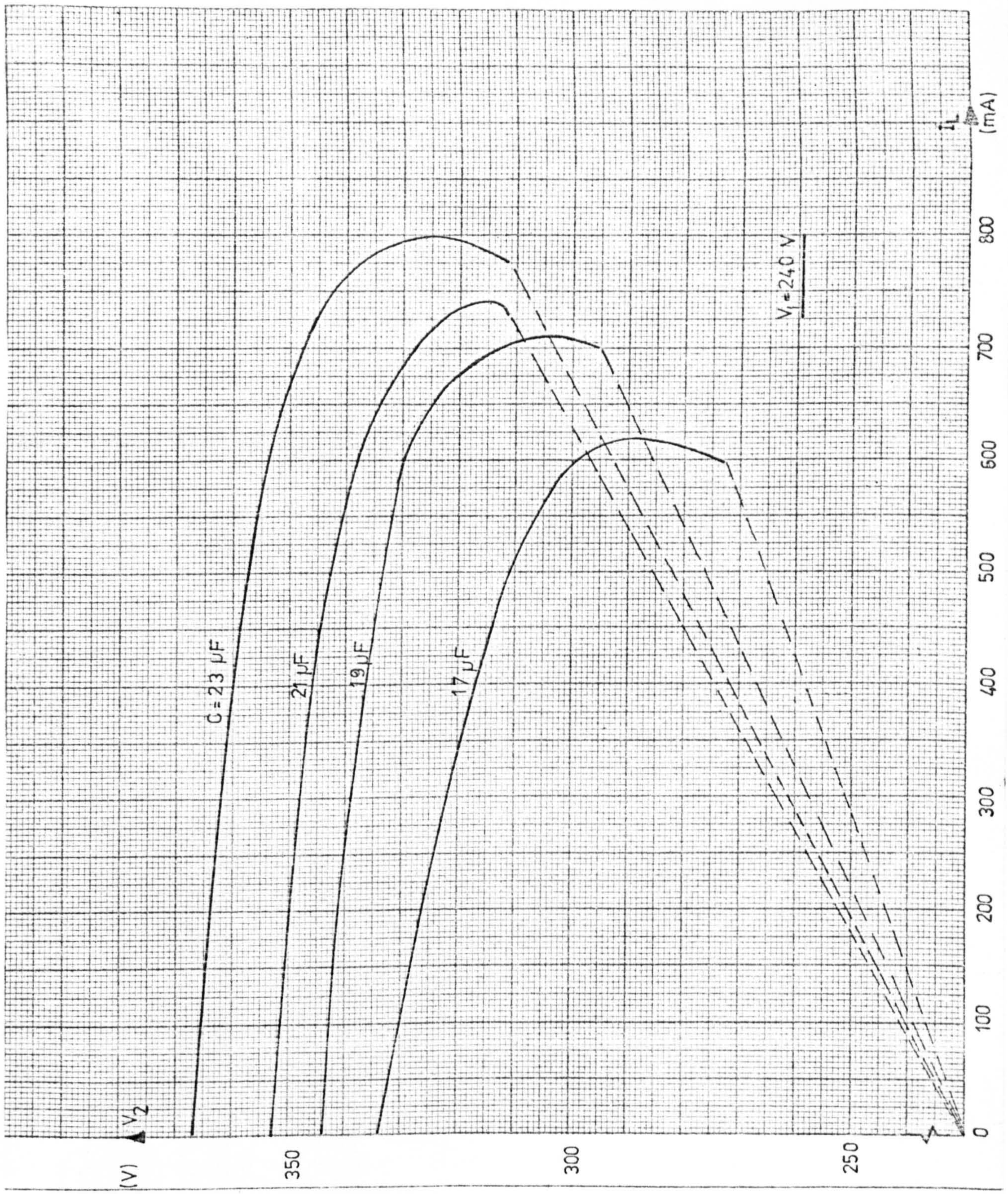

Figure 9.12 Load Characteristics for Different Capacitor Values

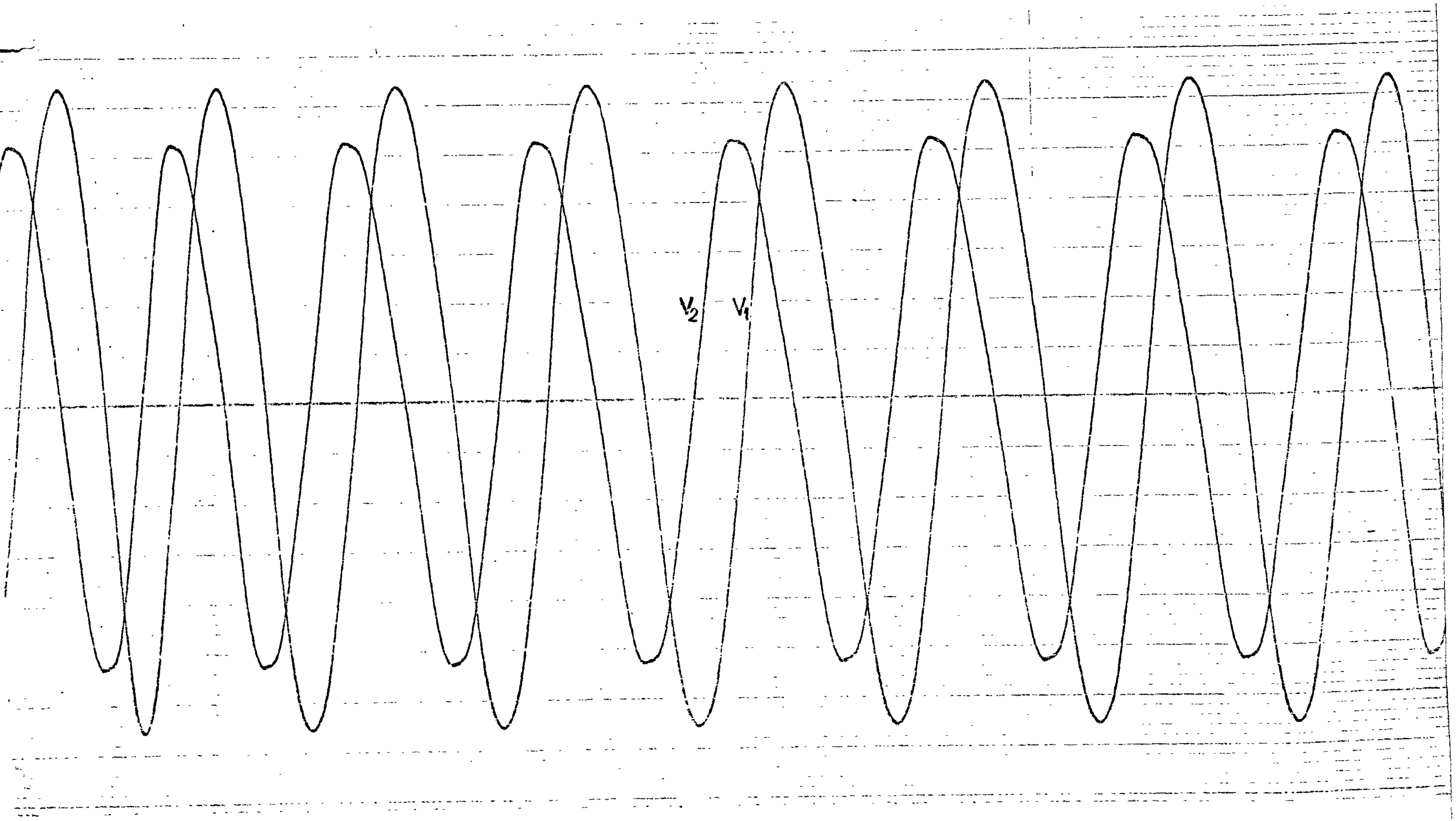

Figure 9.13 Input and Output Voltage Waveforms, V_2 leading V_1 by 90°. Scaling V_1: 50V/cm, V_2 = 100V/cm

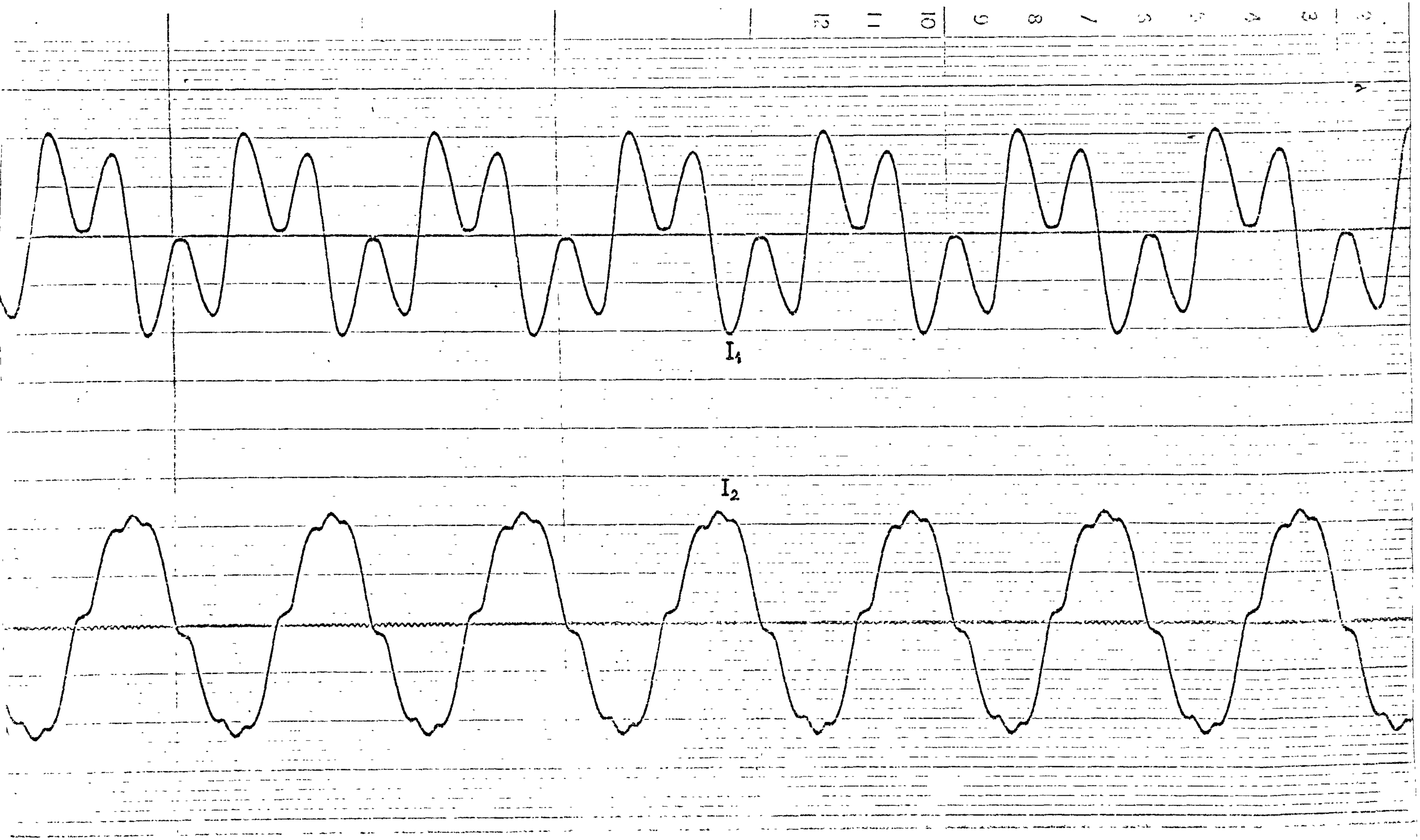

Figure 9.14 Primary & Secondary Current Waveforms Pertaining to Fig.9.13 Scaling: I_1: 2A/cm I_2: 2A/cm

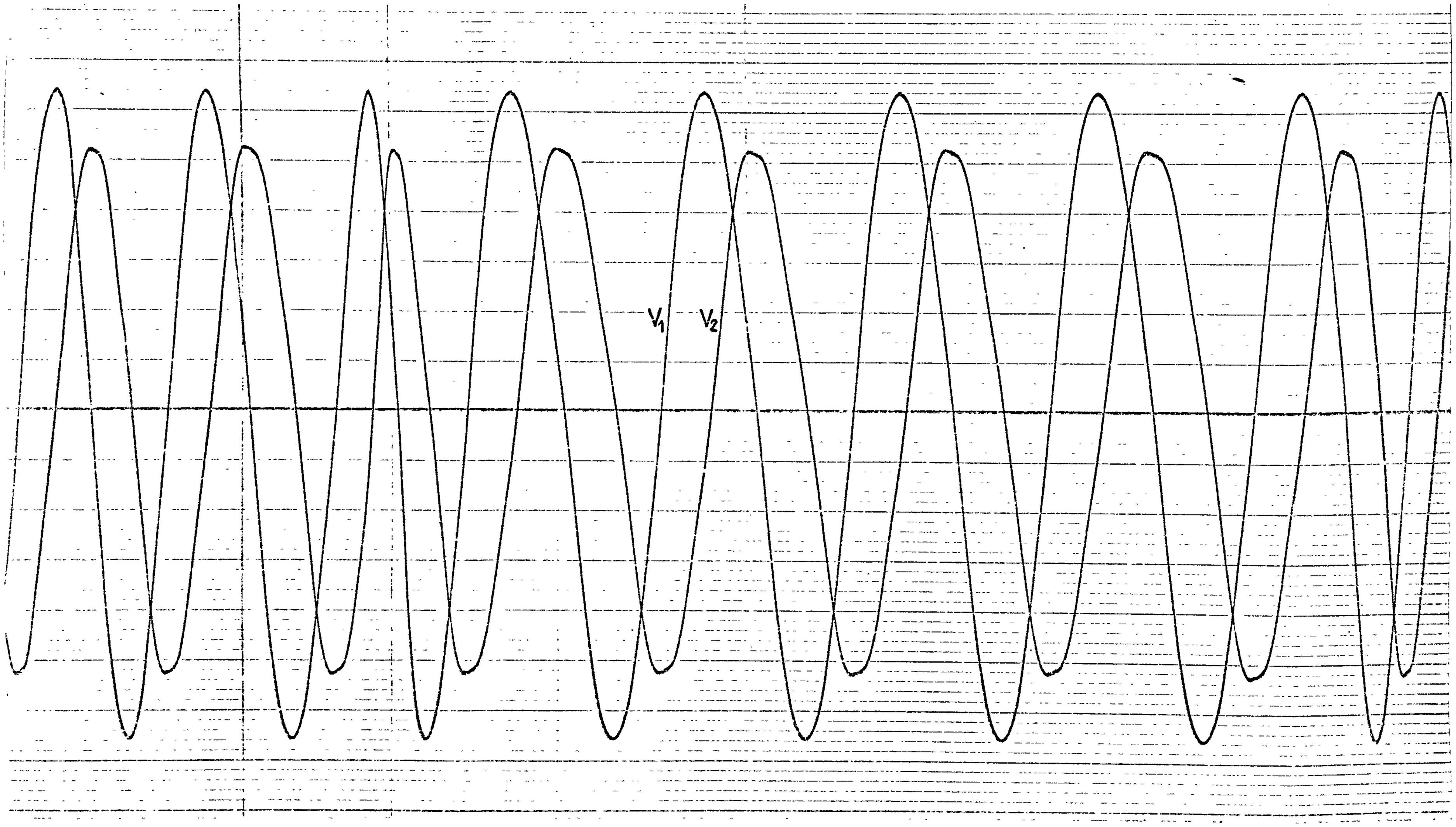

Figure 9.15 Input and Output Voltage Waveforms, V_2 lagging V_1 by 90^0 Scaling: V_1: 50 V/cm V_2 : 100 V/cm

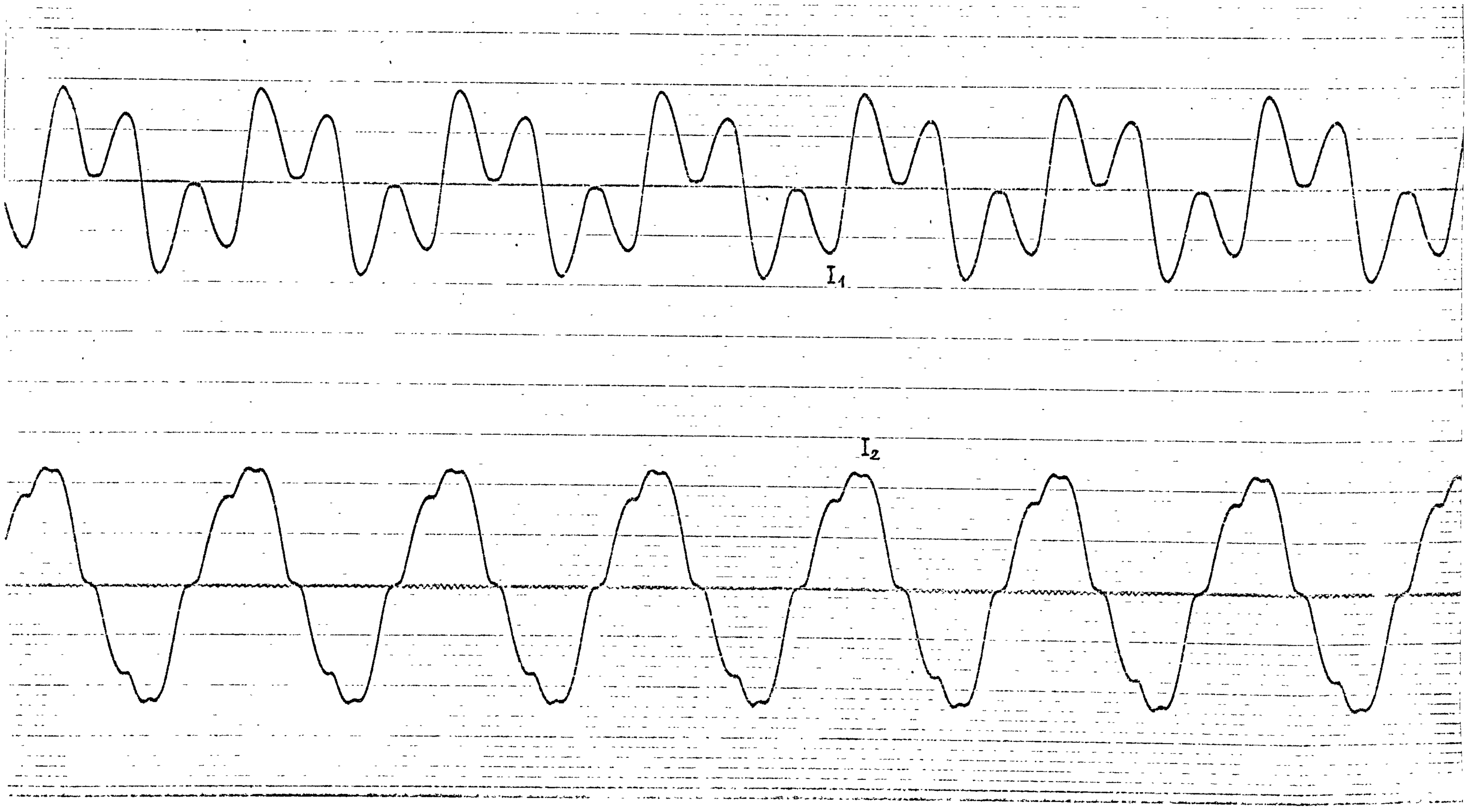

Figure 9.16 Primary and Secondary Current Waveforms Pertaining to Fig. 9.15 Scaling I_1 : 2A/cm I_2: 2A/cm

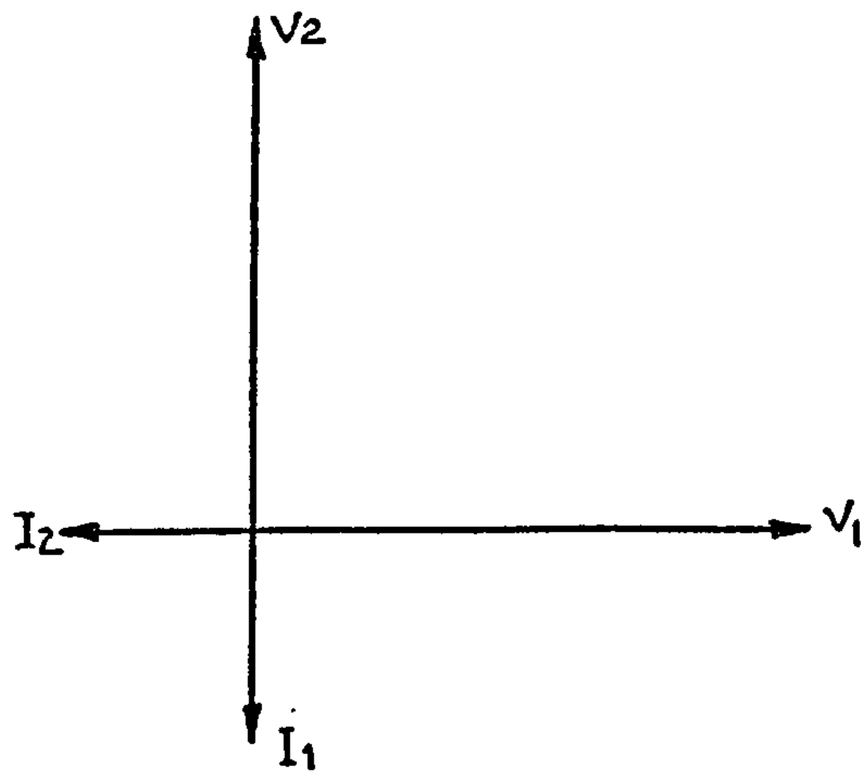

(a) V_2 leading V_1

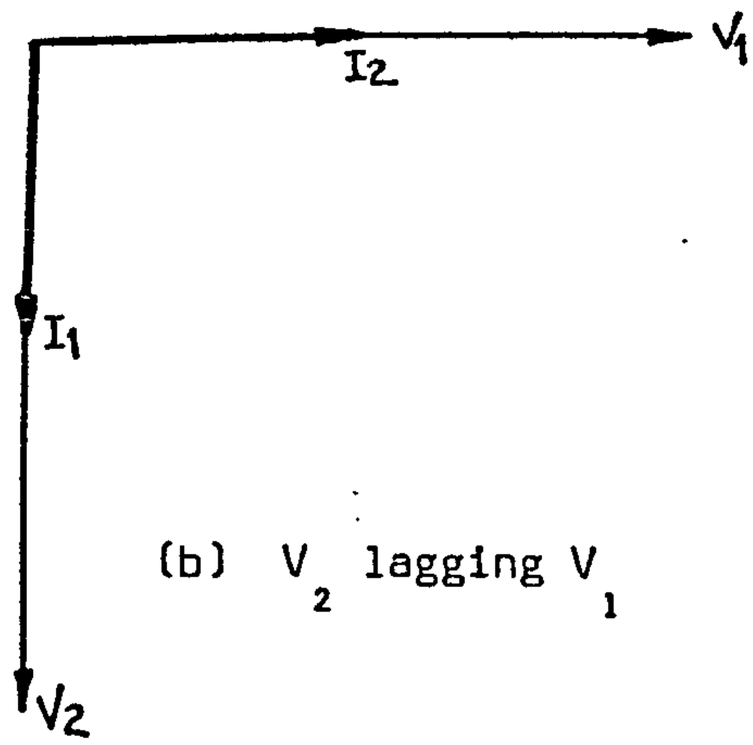

(b) V_2 lagging V_1

Figure 9.17 Relative Phases of Input and Output Variables

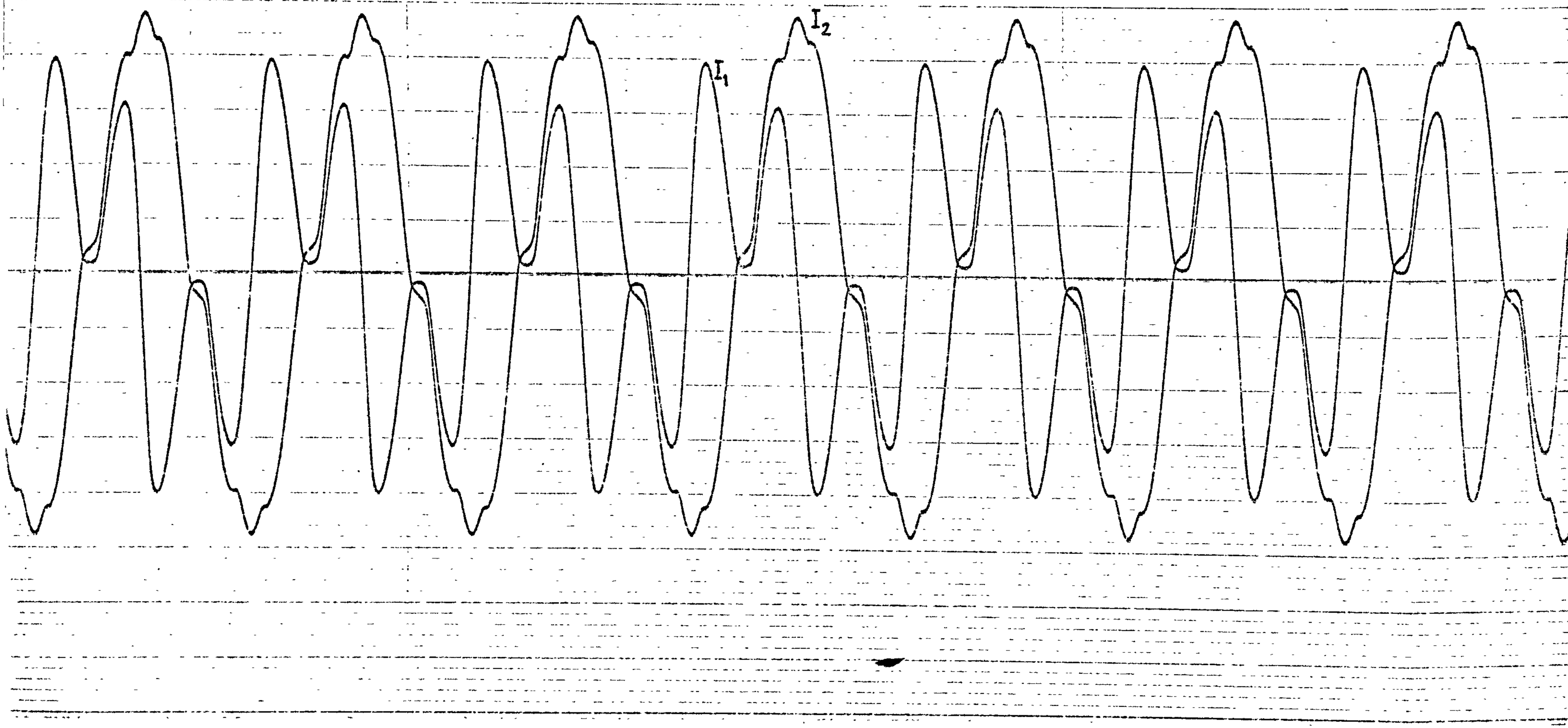

Figure 9.18 Relative Phases of I_1 and I_2 when V_2 leads V_1 by 90o Scaling: I_1 : 1A/cm I_2: 1A/cm

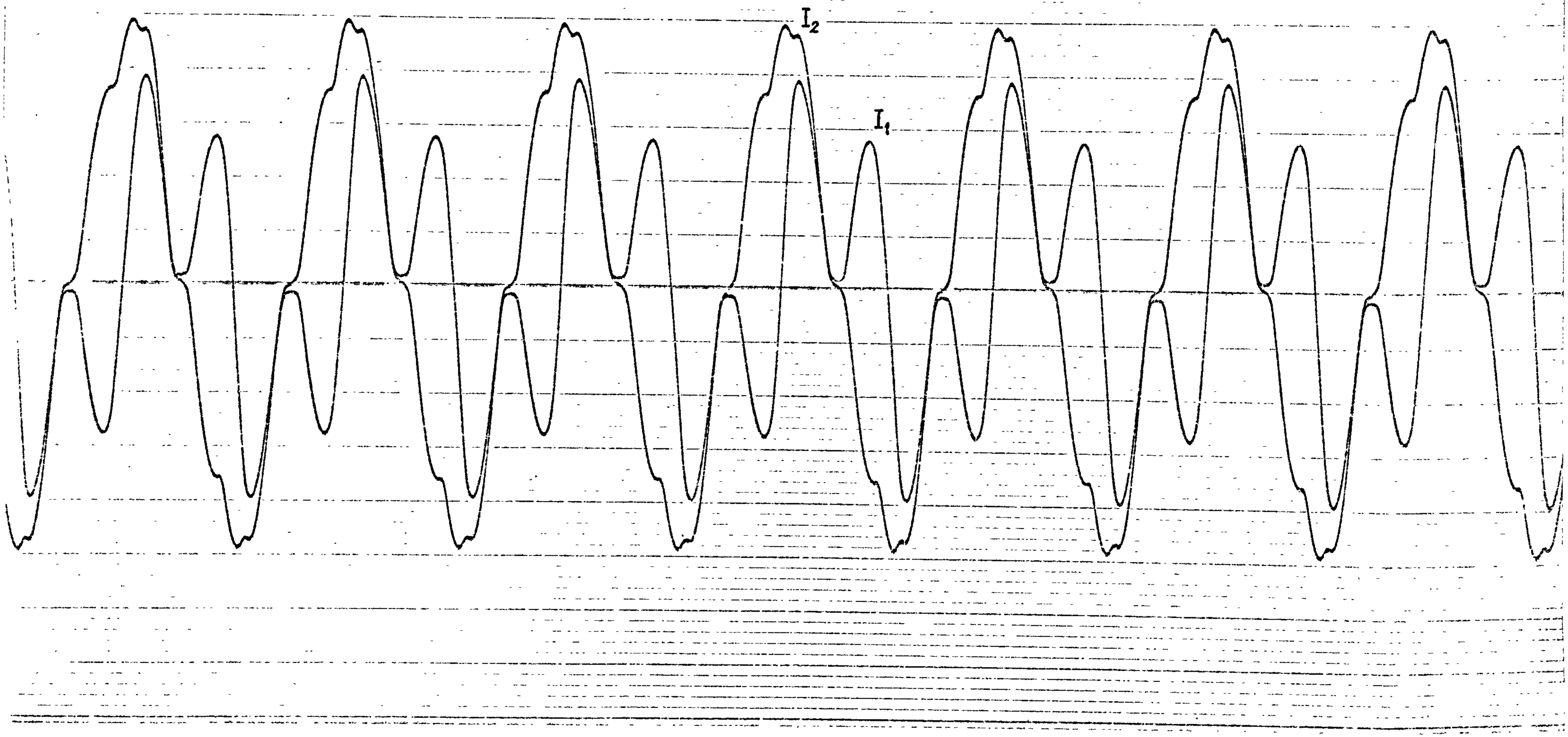

Figure 9.19 Relative Phases of I_1 and I_2 when V_2 lags V_1 by 90^0

Scaling: I_1: 1A/cm I_2: 1A/cm

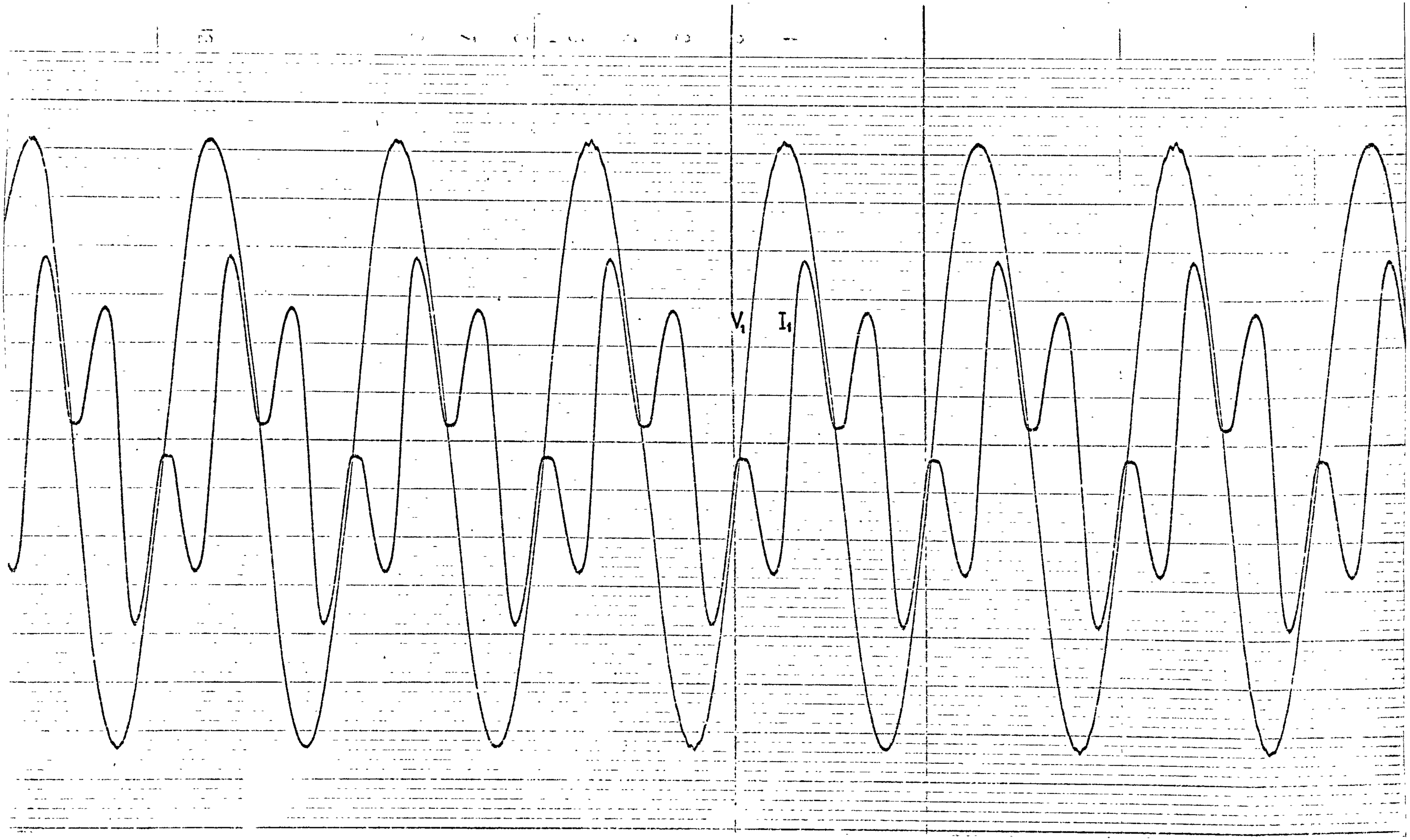

Figure 9.20 Relative Phases of V_1 and I_1 Scaling: V_1 = 50V/cm I_1: 1 A/cm

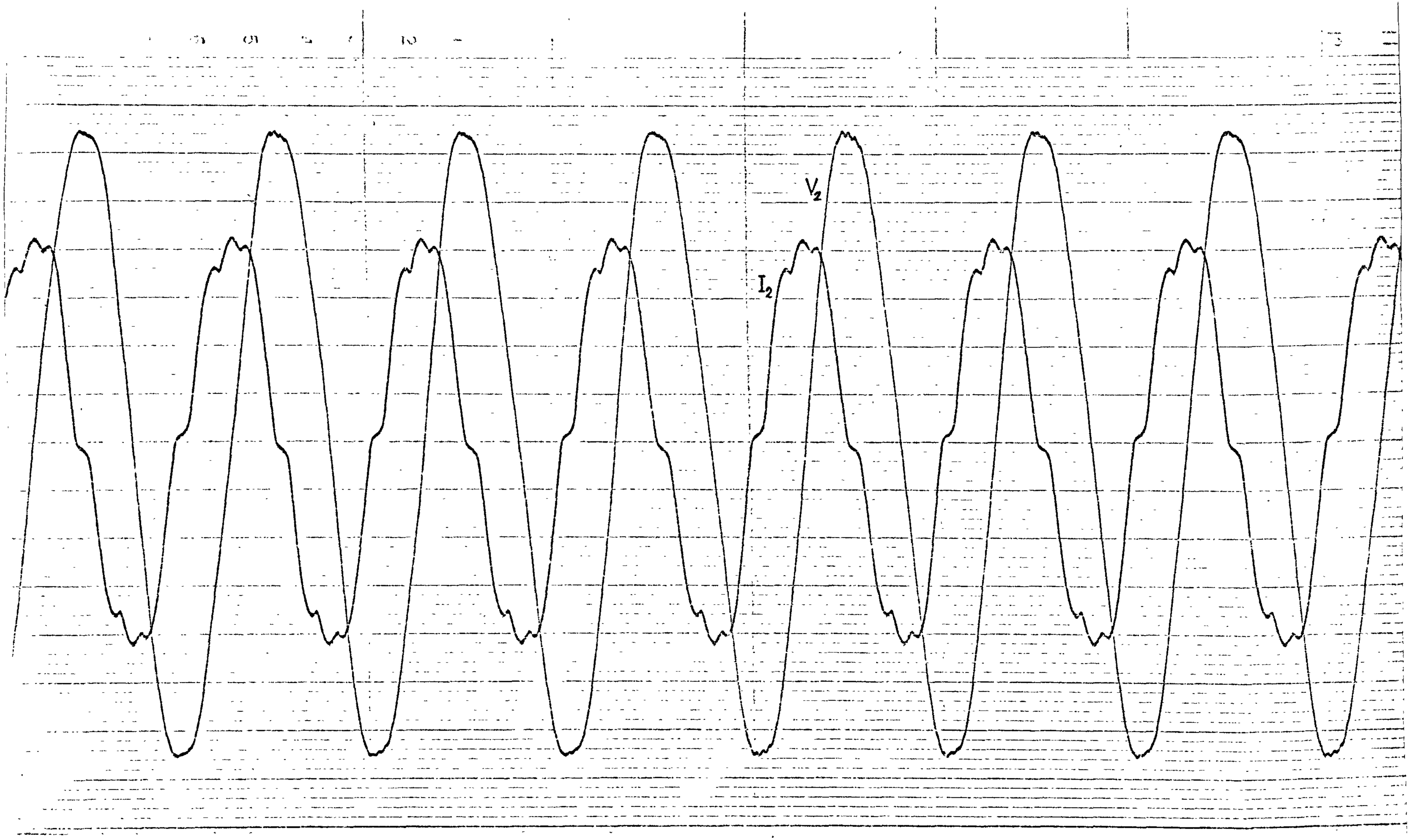

Figure 9.21 Relative Phases of V_2 and I_2 Scaling: V_2: 83.3 V/cm I_2: 1A/cm

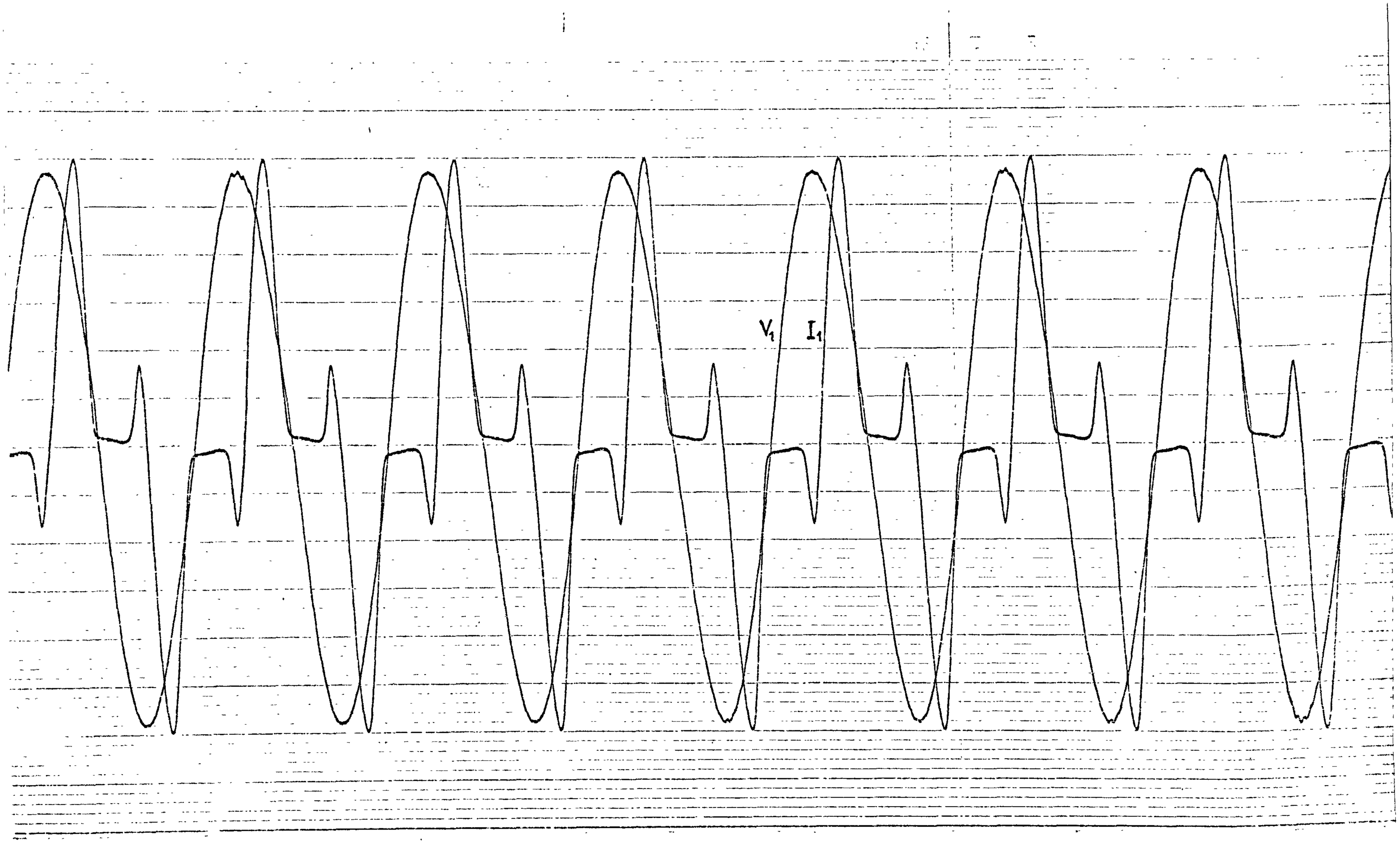

Figure 9.22 Primary Voltage & Current Waveforms for V_1 = 100V Scaling: V_1 : 25 V/cm I_1: 0.5 A/cm

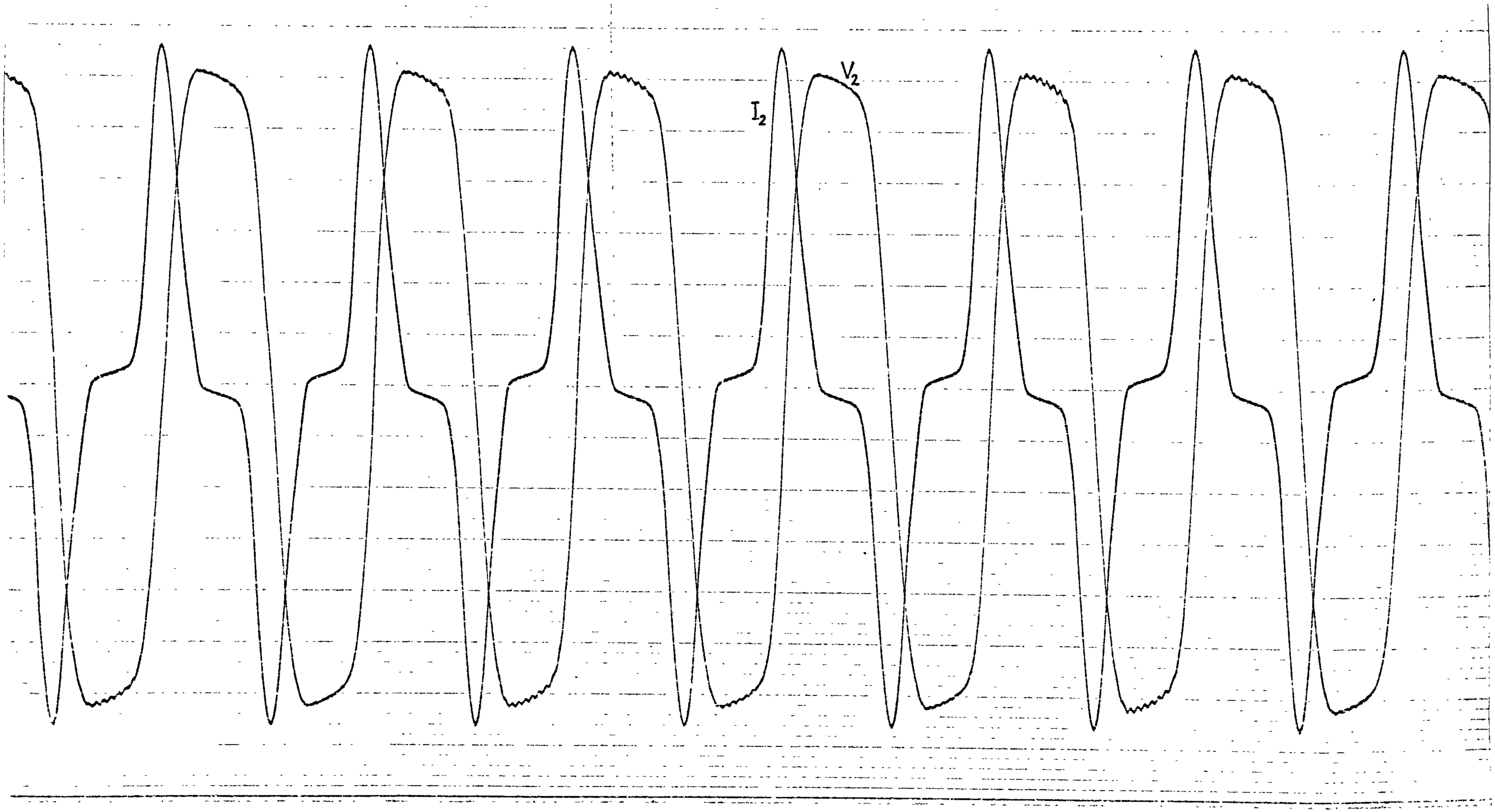

Figure 9.23 Secondary Voltage & Current Waveforms for V_1 = 100V Scaling: V_2: 83.3 V/cm I_2: 1A/cm

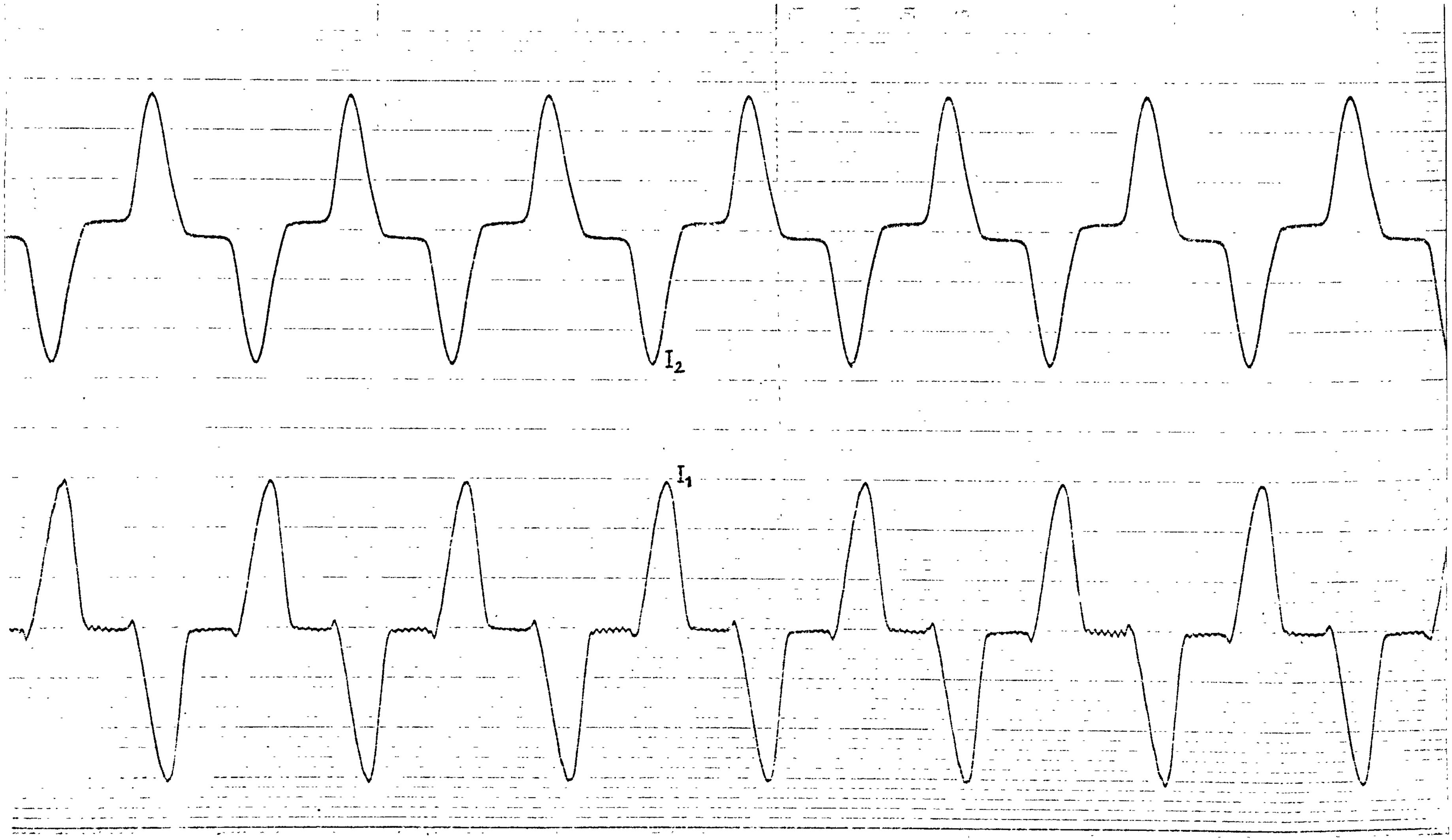

Figure 9.24 Primary & Secondary Current Waveforms for V_1 = 80V (V_2 leading V_1 by 90^0)

Scaling: I_1: 1A/cm I_2: 2.5A/cm

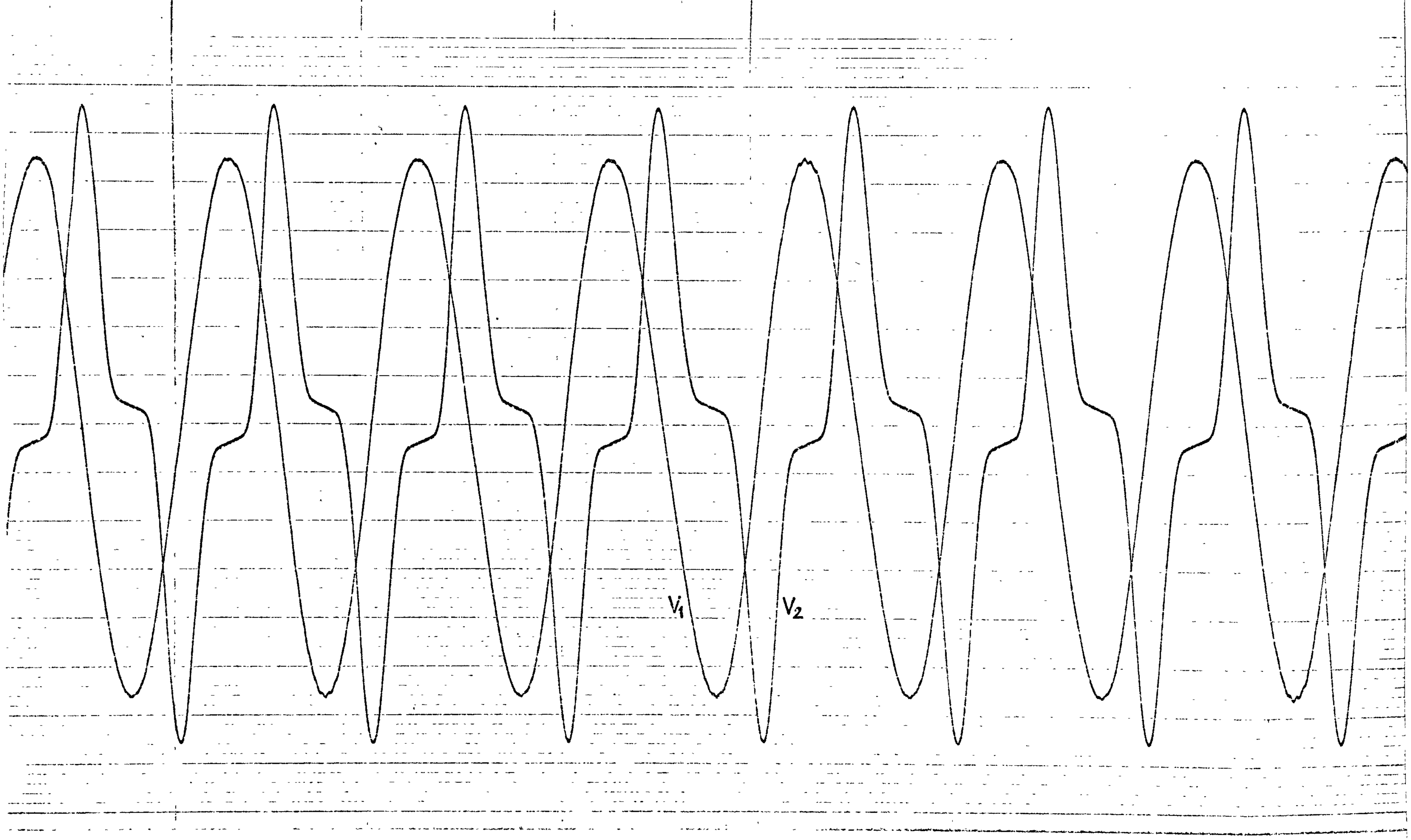

Figure 9.25 Input and Output Voltage Waveforms for V_1 = 360V Scaling: V_1: 100 V/cm V_2: 50 V/cm

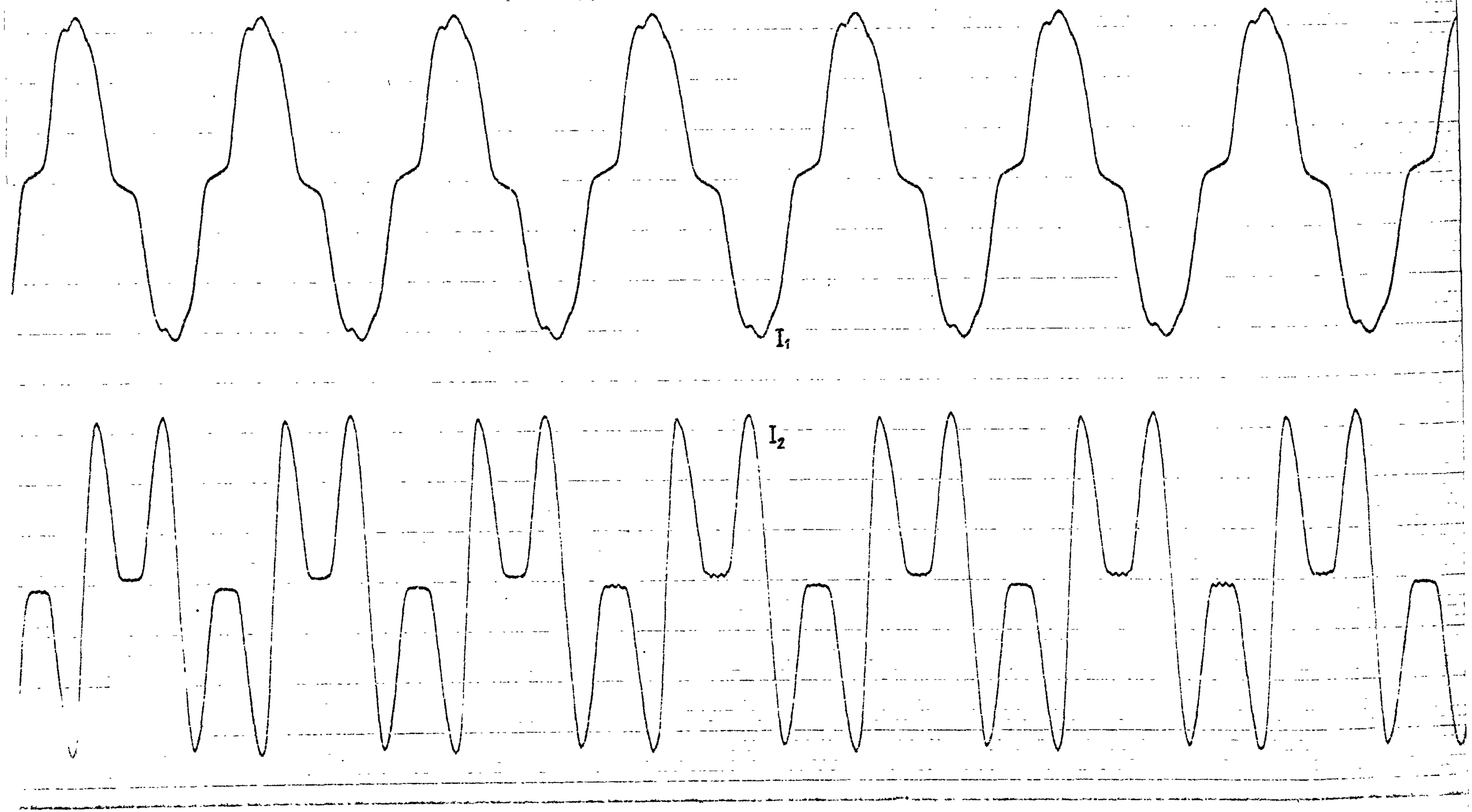

Figure 9.26 Primary & Secondary Current Waveforms for V_1 = 380V Scaling: I_1 : 2.5A/cm I_2 : 1A/cm

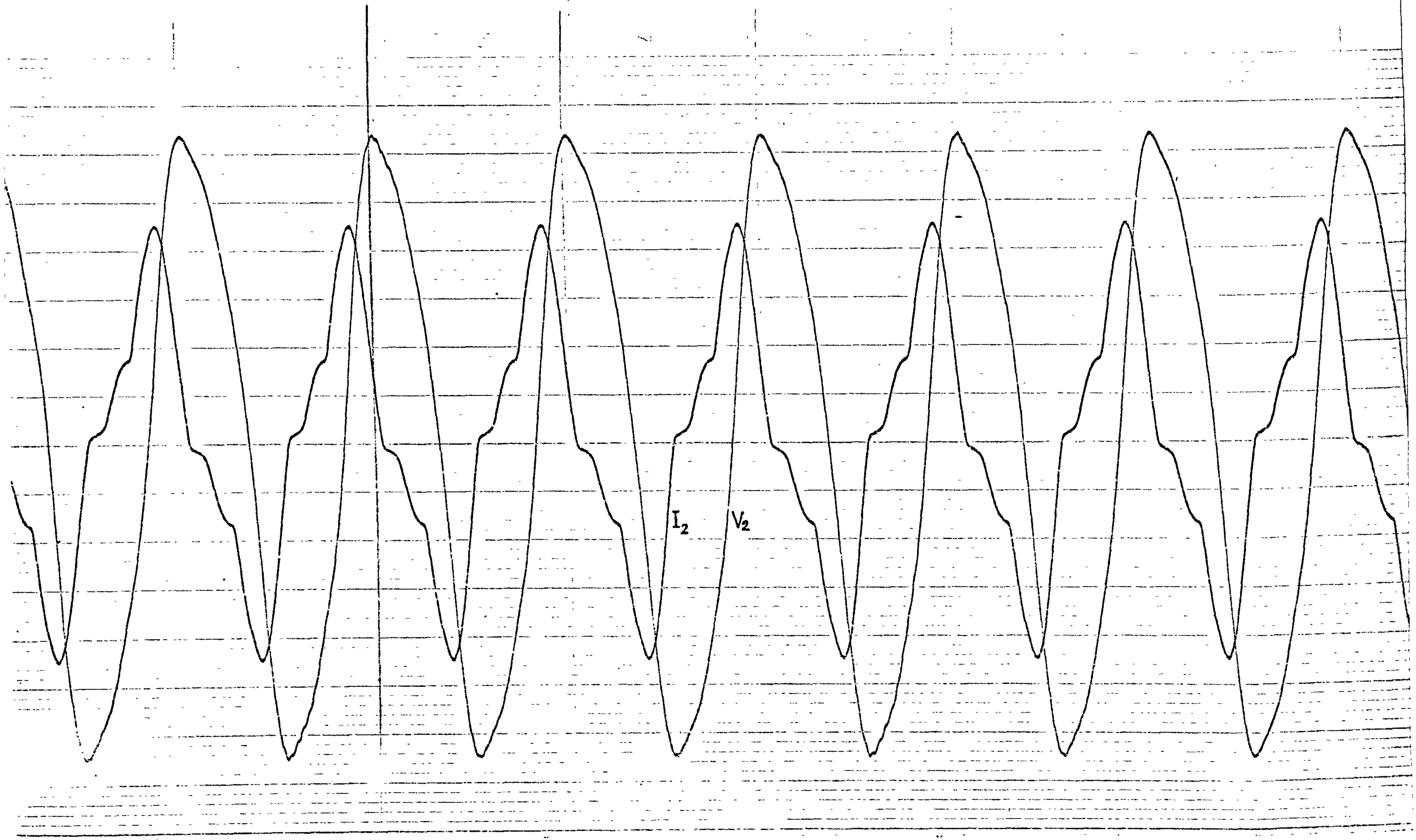

Figure 9.27 Secondary Voltage & Current Waveforms, with I_L = 450 mA Scaling: V_2: 83.3 V/cm I_2: 1A/cm

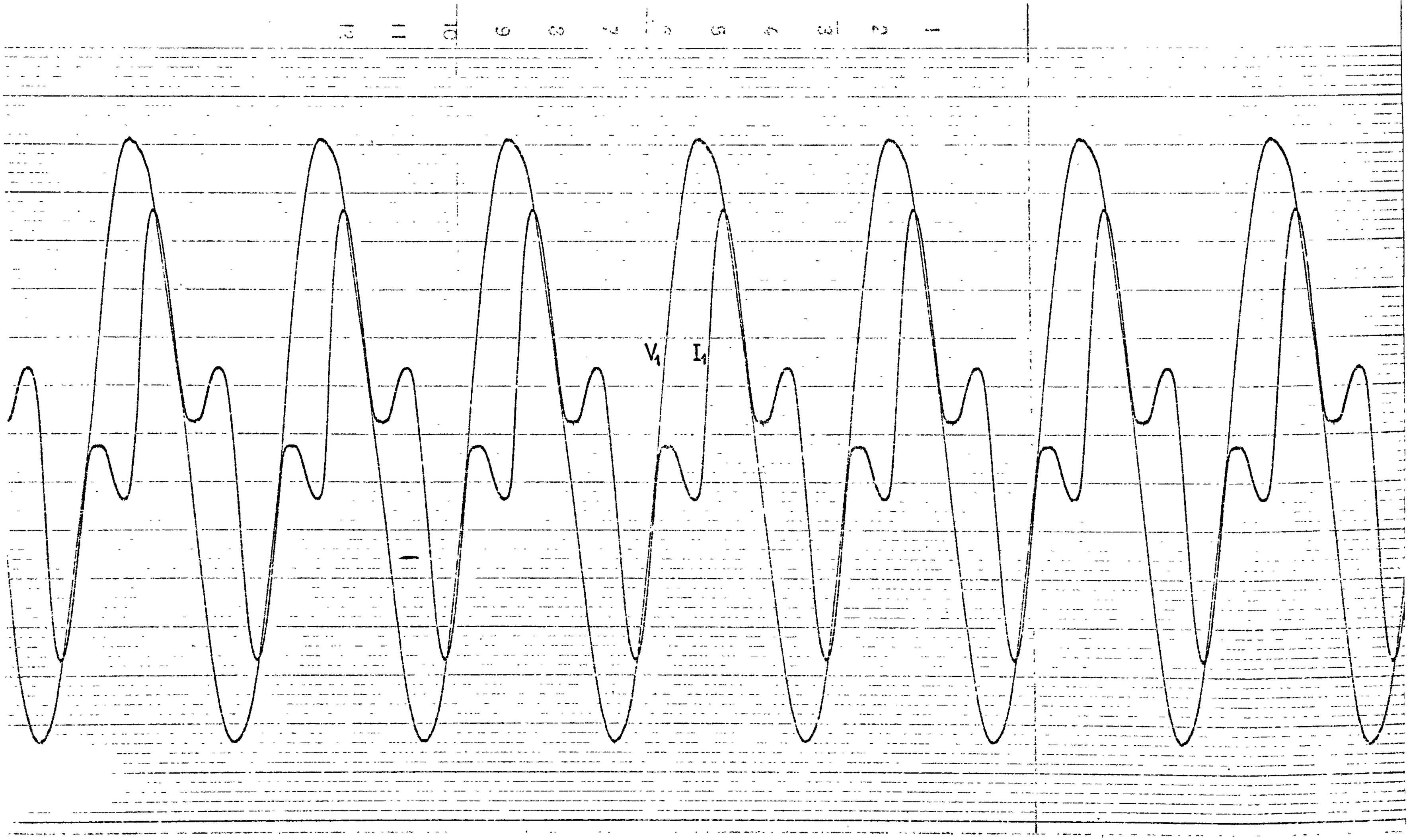

Figure 9.20 Primary Voltage and Current Waveforms, with I_L = 450 mA Scaling: V_1: 50 V/cm I_1: 1A/cm

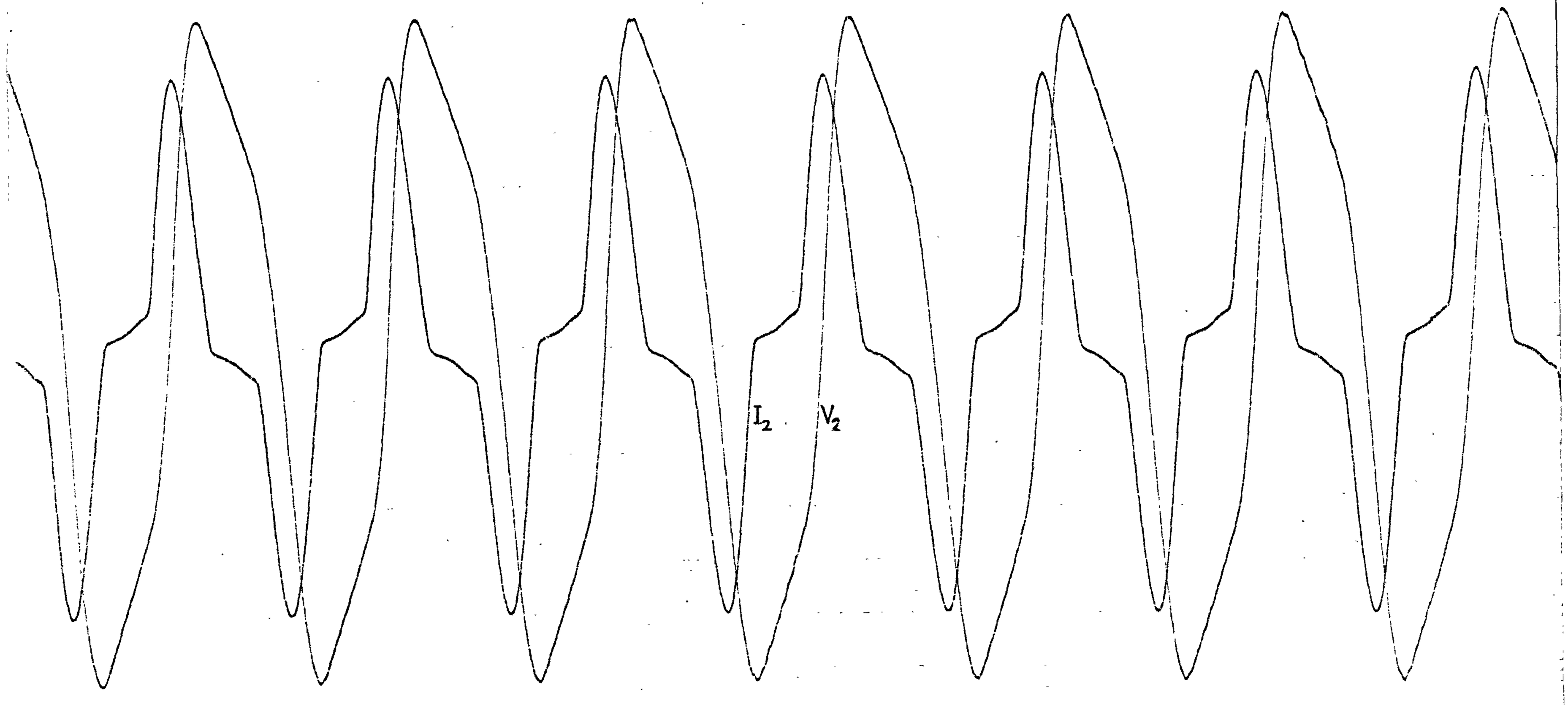

Figure 9.29 Secondary Voltage & Current Waveforms with I_L = 700 mA Scaling : V_2: 83.3 V/cm I_2: 1A/cm

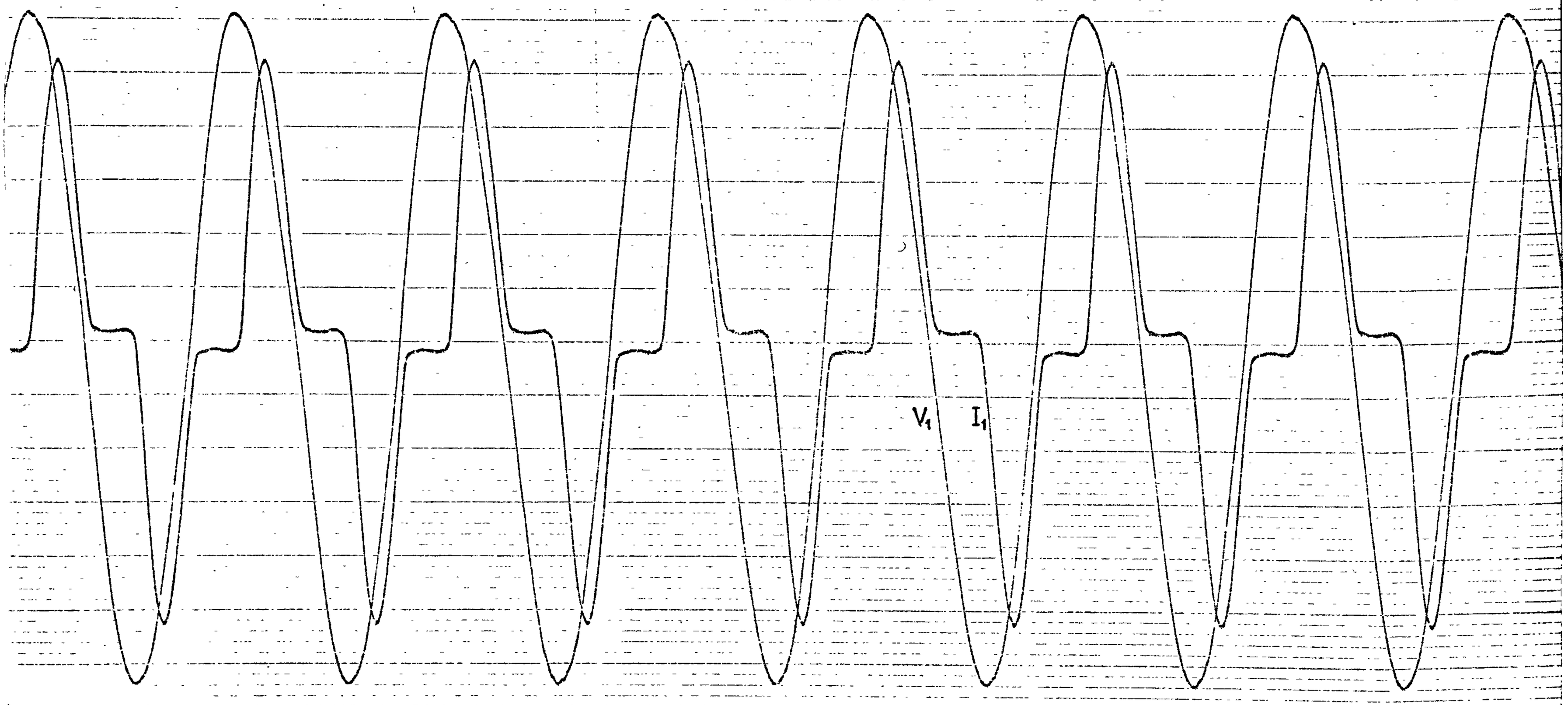

Figure 9.30 Primary Voltage and Current Waveforms, with $I_L = I_{Lmax} = 700$ mA Scaling: V_1: 50 V/cm I_1: 1A/cm

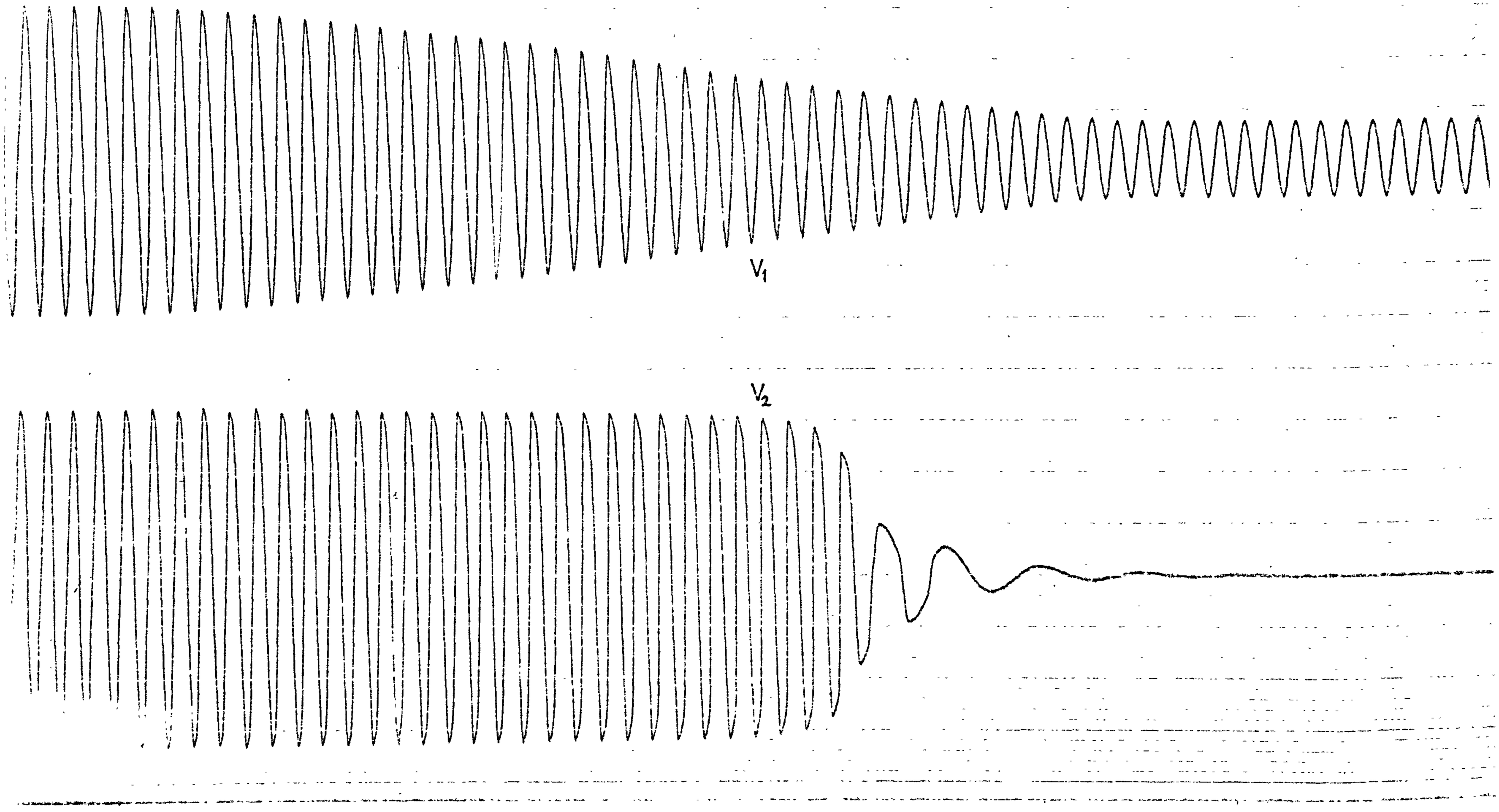

Figure 9.31 Under-voltage Protection and Voltage Regulation Scaling: V_1: 100 V/cm V_2: 166.6 V/cm

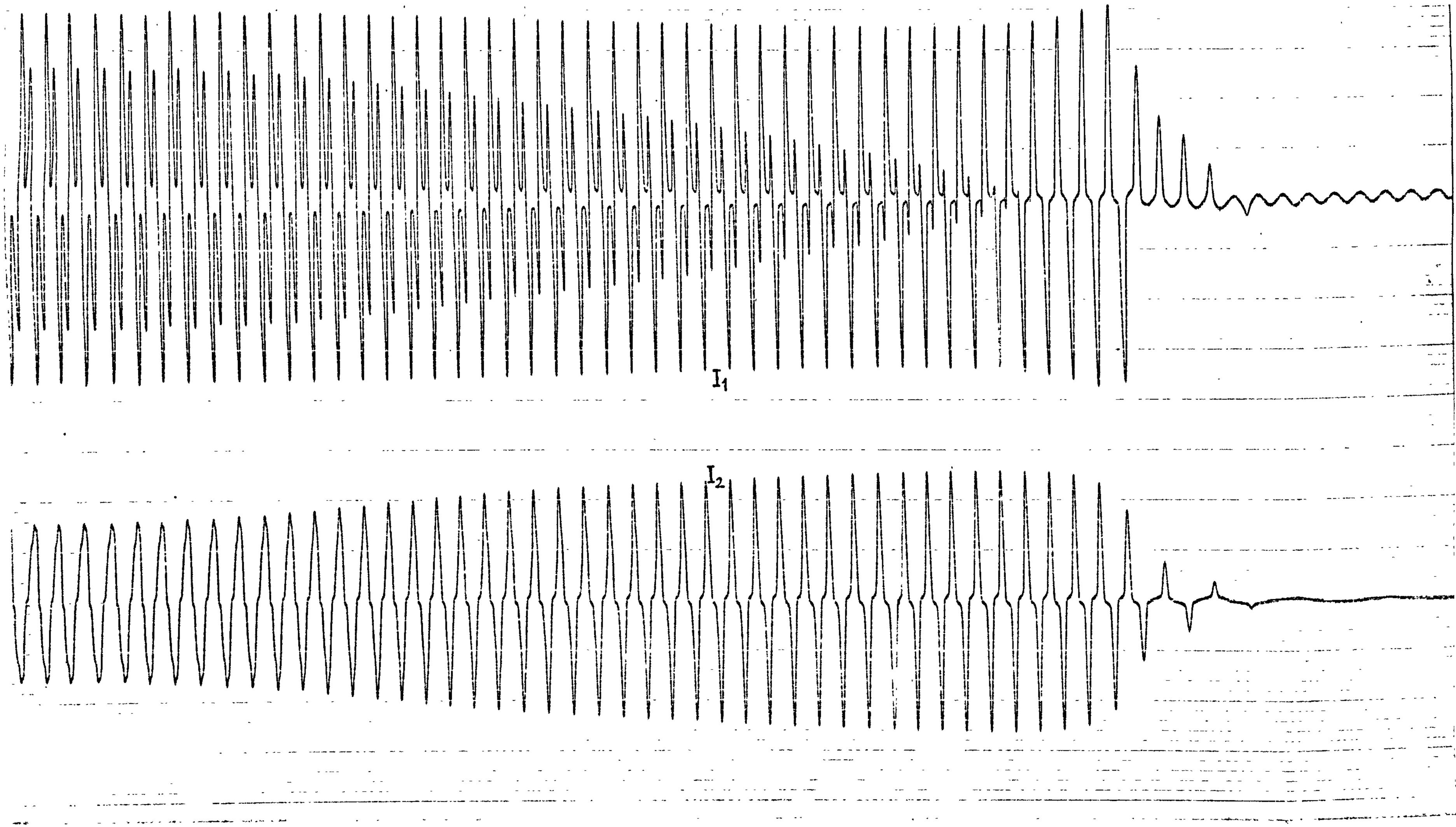

Figure 9.32 Primary and Secondary Current Waveforms Pertaining to Fig. 9.31 Scaling I_1: 1A/cm I_2: 2.5 A/cm

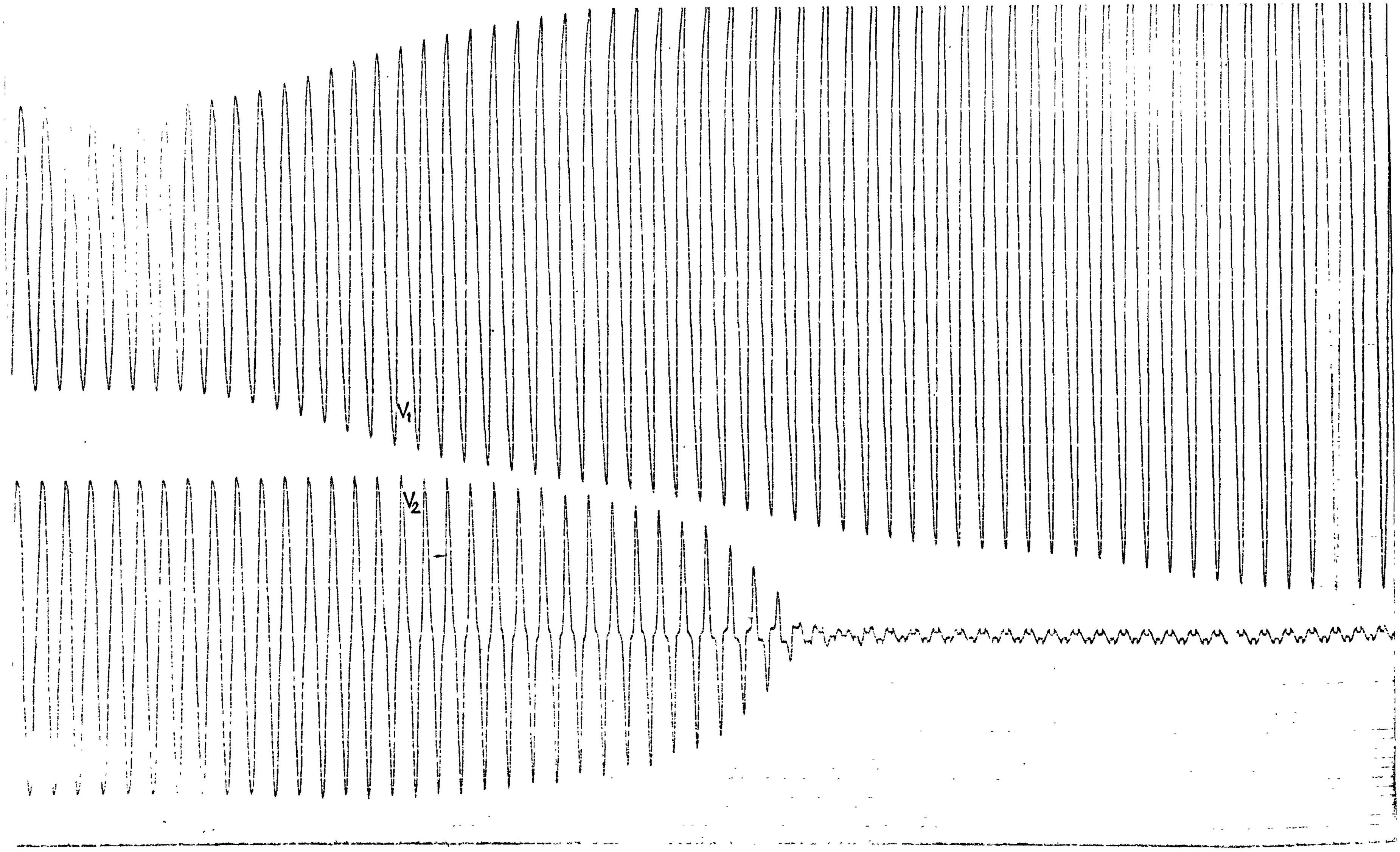

Figure 9.33 Over-voltage Protection and Voltage Regulation Scaling: V_1: 100 V/cm V_2: 166.6 V/cm

Figure 9.34 Primary & Secondary Current Waveforms Pertaining to Fig 9.33 Scaling: I_1: 2.5A/cm I_2: 1A/cm

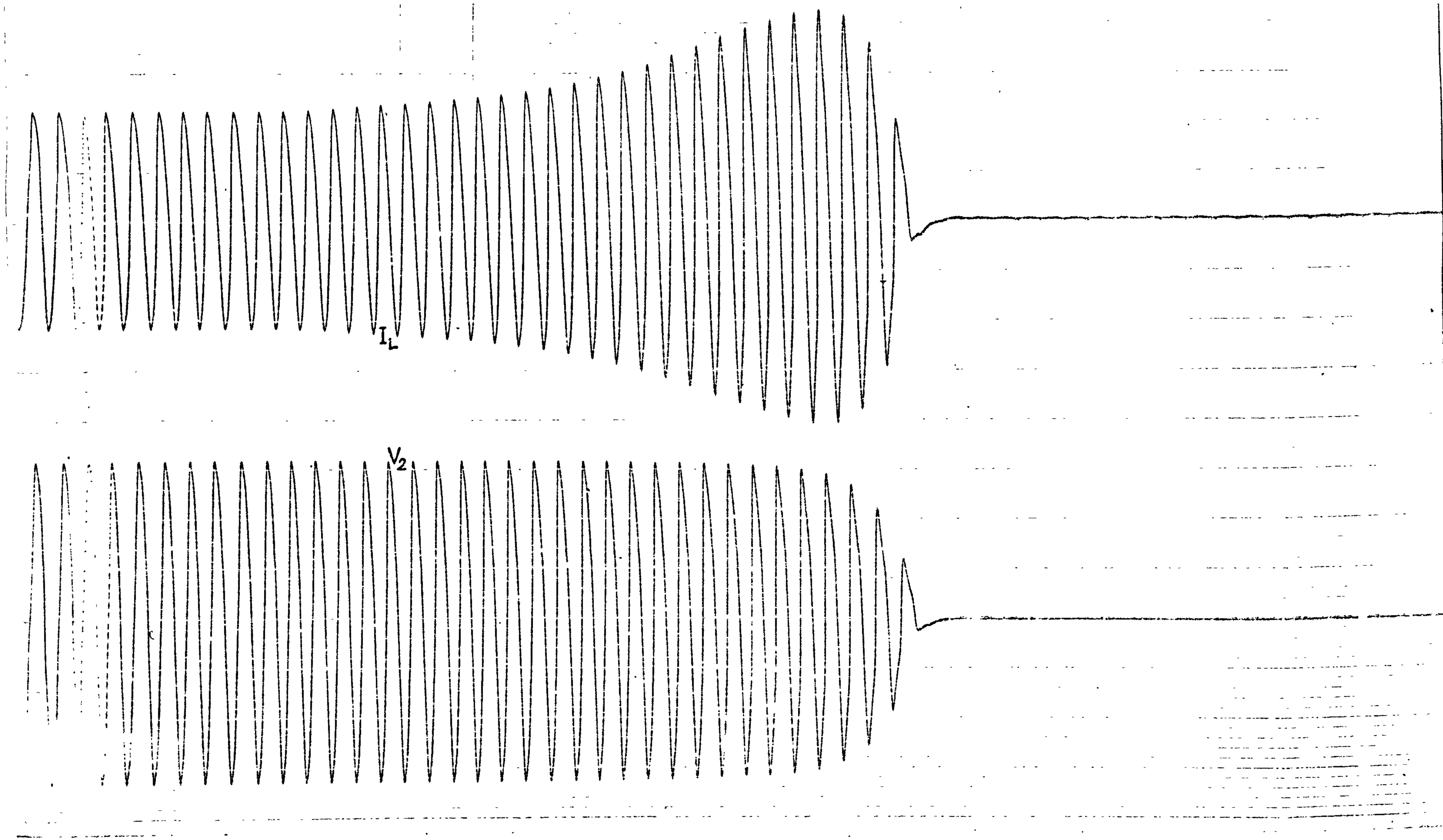

Figure 9.35 Over-load Protection and Load Regulation

Scaling: I_L : 0.25 A/cm V_2 : 166.6 V/cm

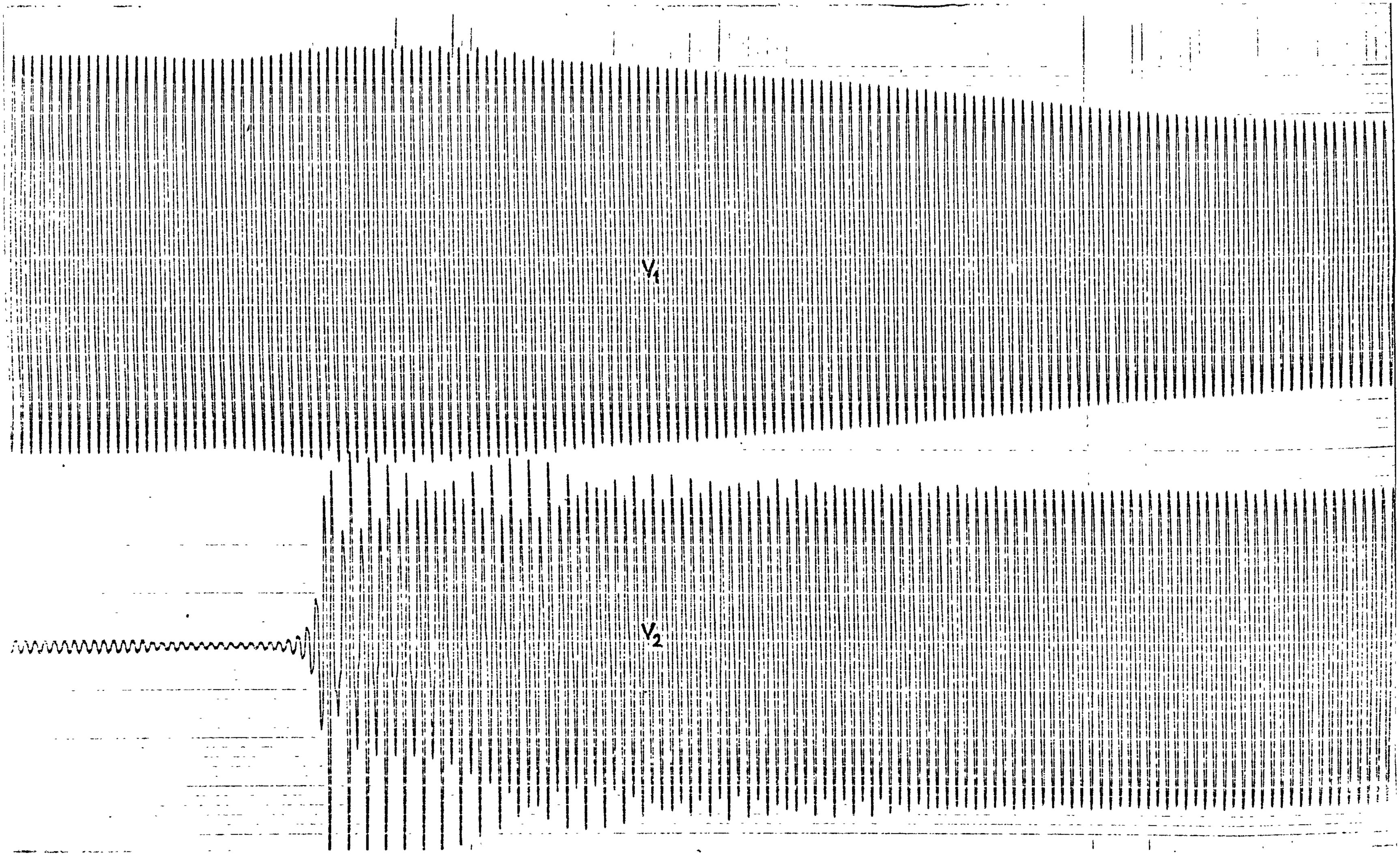

Figure 9.36 Initiation of Oscillations with $V_1 > V_1'$ Scaling: V_1: 100V/cm V_2: 166.6 V/cm

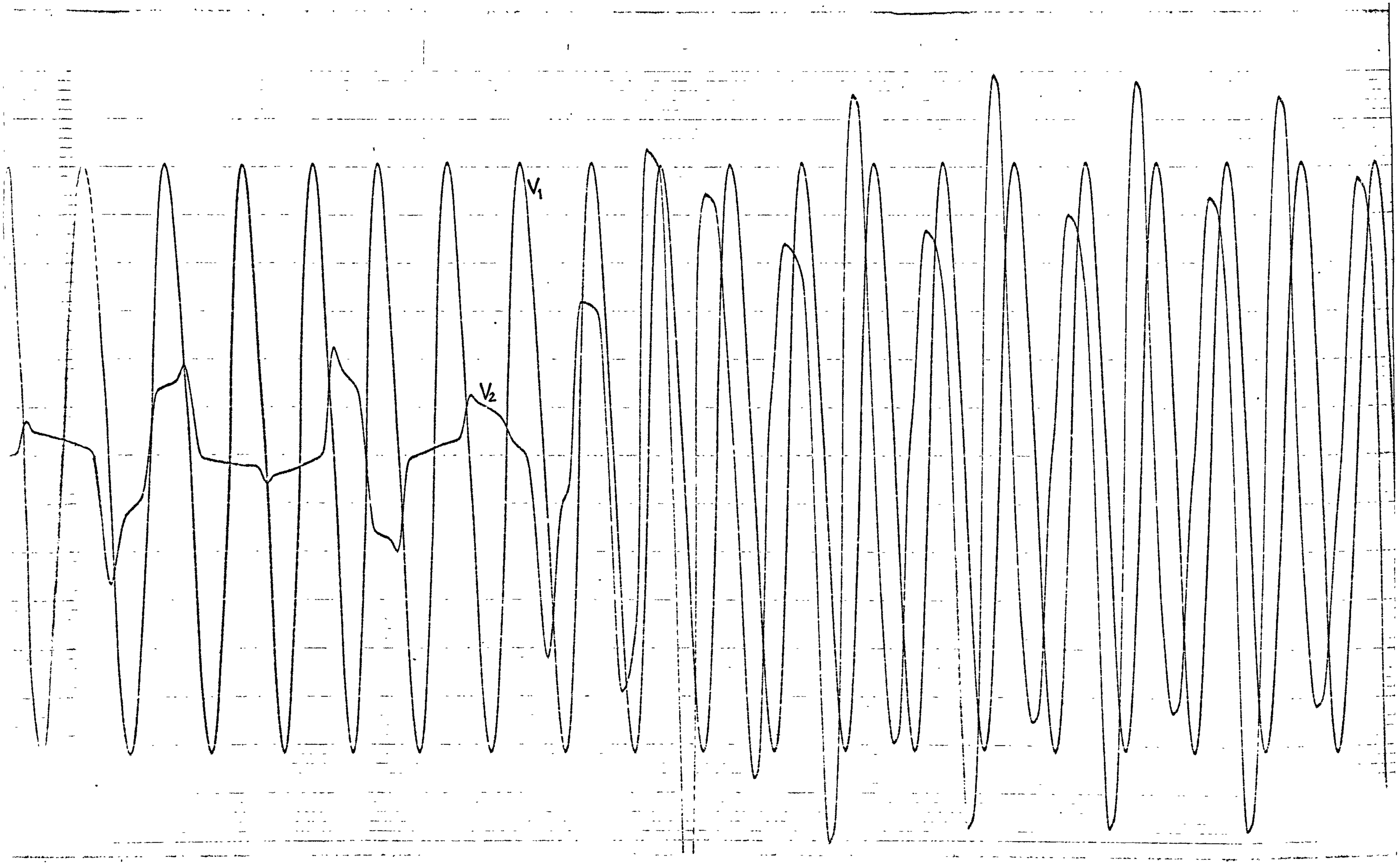

Figure 9.37 Initiation of oscillations when V_1 (< V_1') Instaneously Switched on Scaling: V_1: 50V/cm V_2: 83.3 V/cm

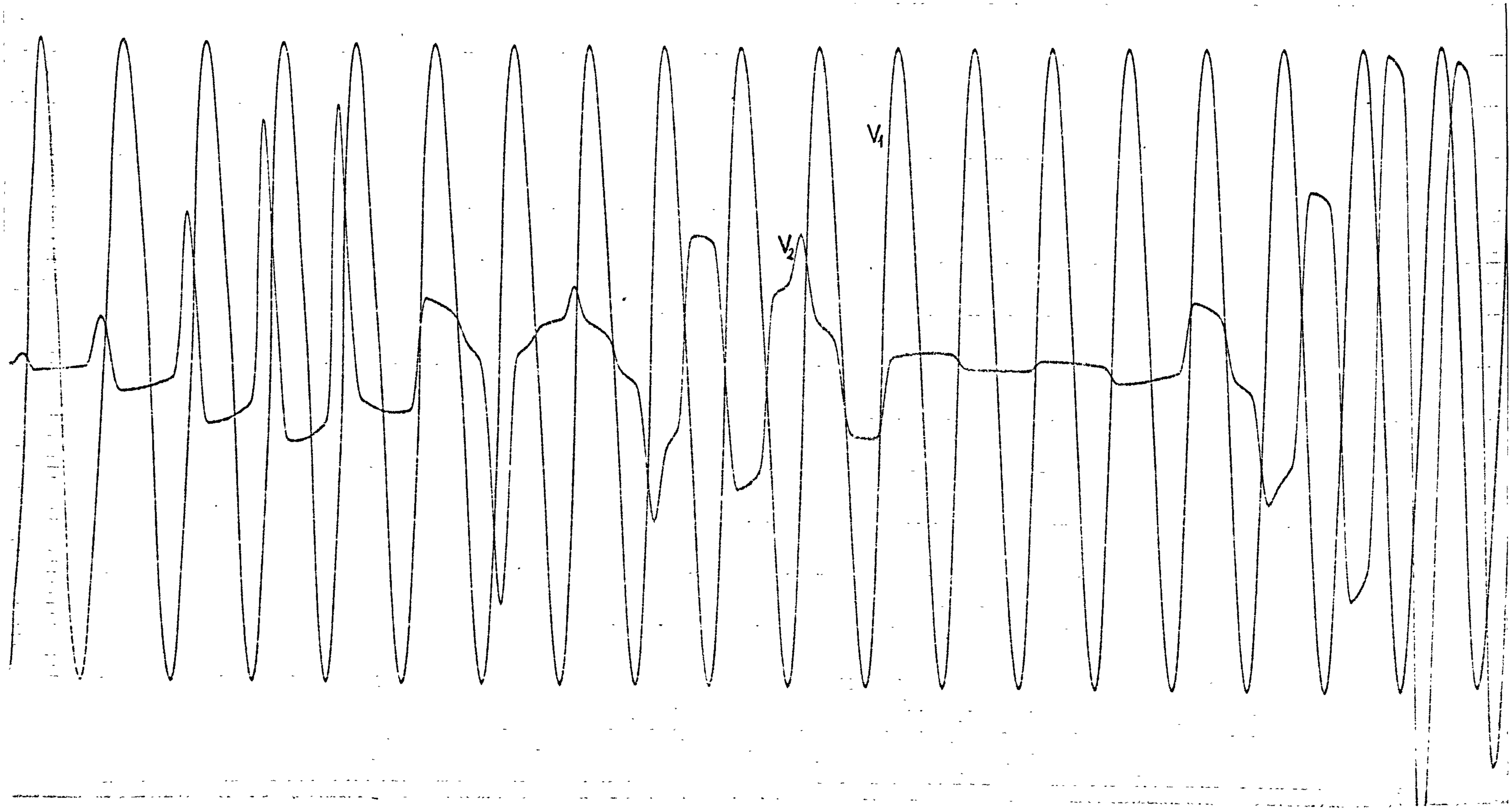

Figure 9.38 Initiation of Oscillations when $V_1 (< V_1^*)$ Instantaneously Switched on Scaling: V_1: 50V/cm V_2: 83.3 V/cm

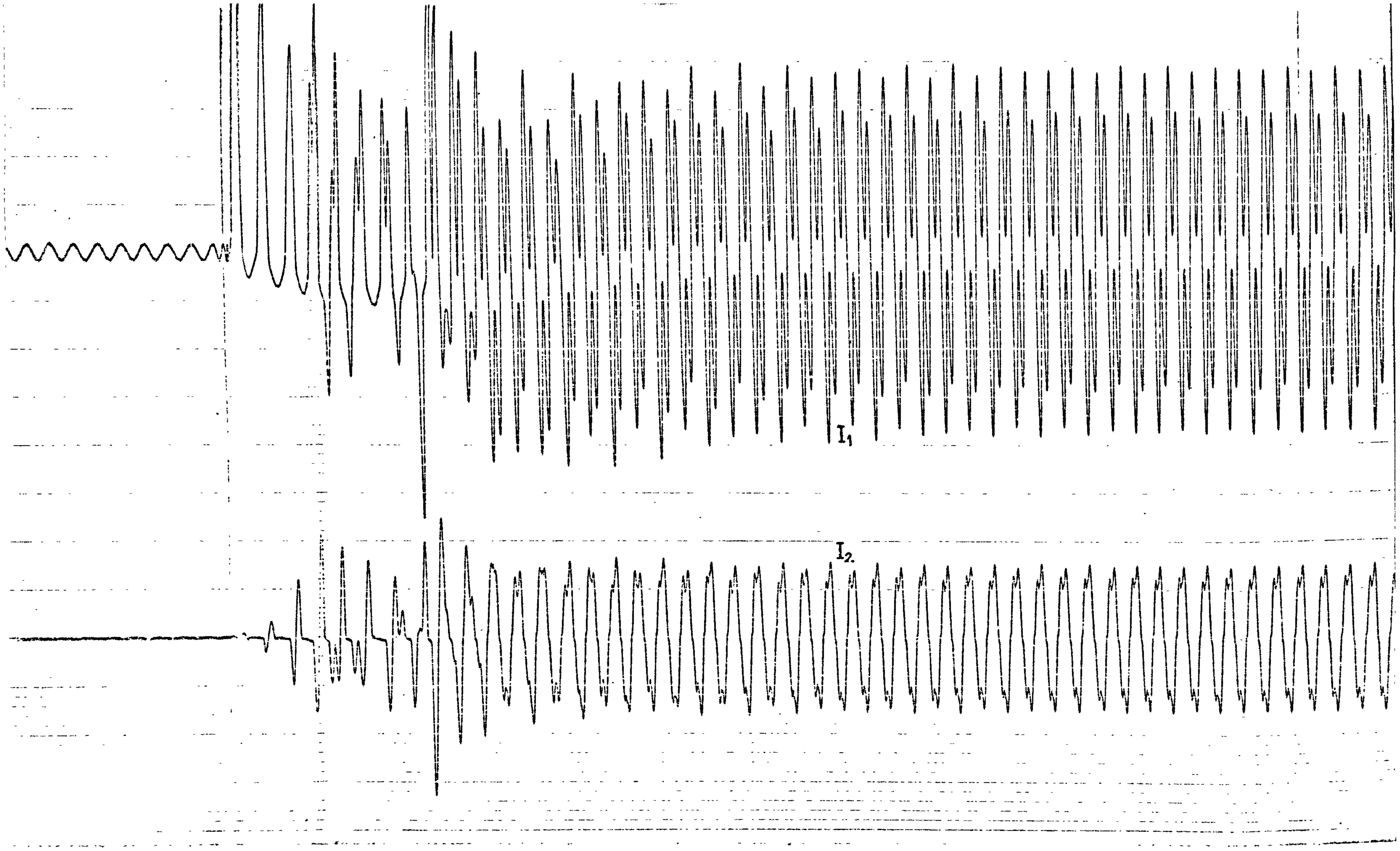

Figure 9.39 Current Waveforms when Input Voltage is Applied Instantaneously Scaling: I_1: 1A/cm I_2: 2.5A/cm

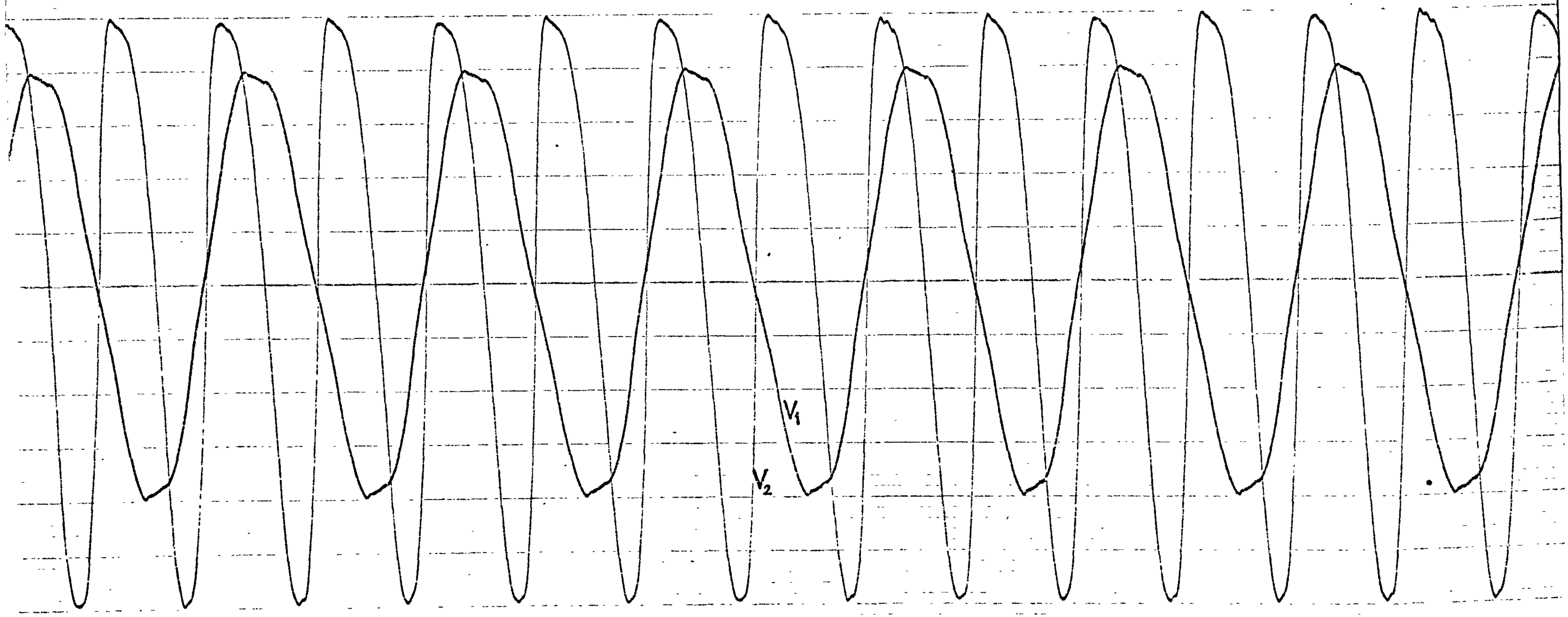

Figure 9.40 Operation as a Frequency Doubler

Scaling: V_1 : 100V/cm V_2 : 166.6 V/cm

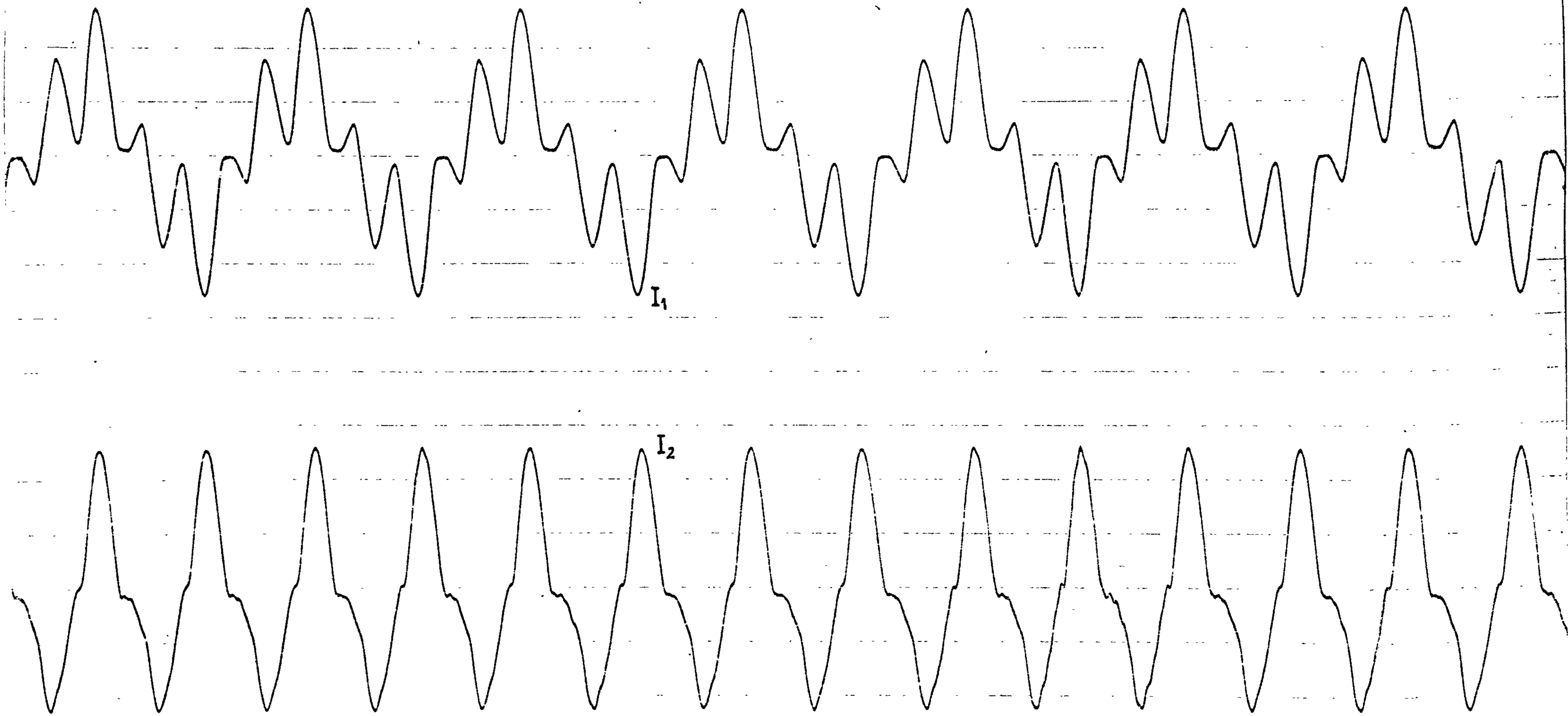

Figure 9.41 Current Waveforms Pertaining to Fig. 9.40 Scaling: I_1: 5A/cm I_2: 2.5A/cm

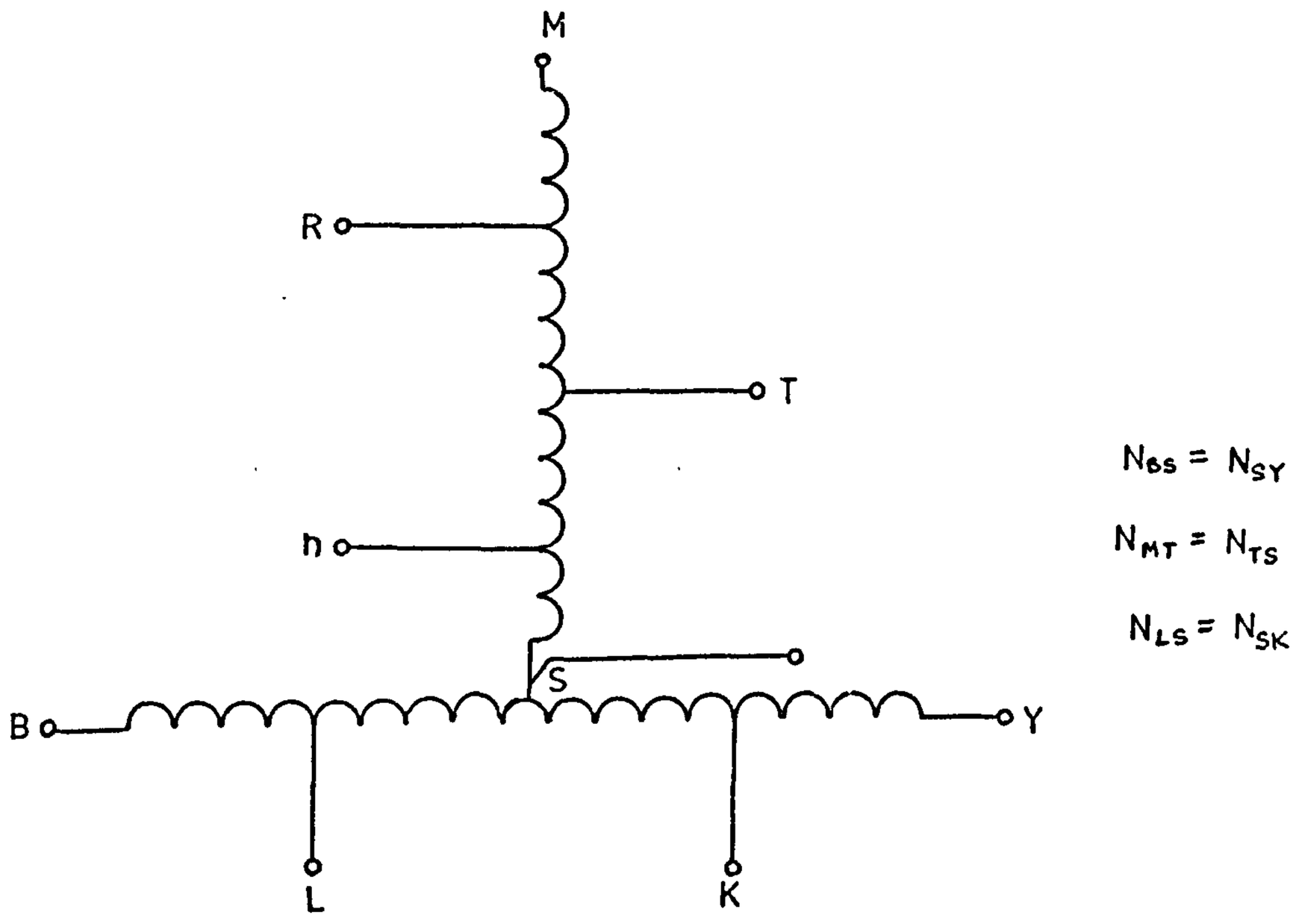

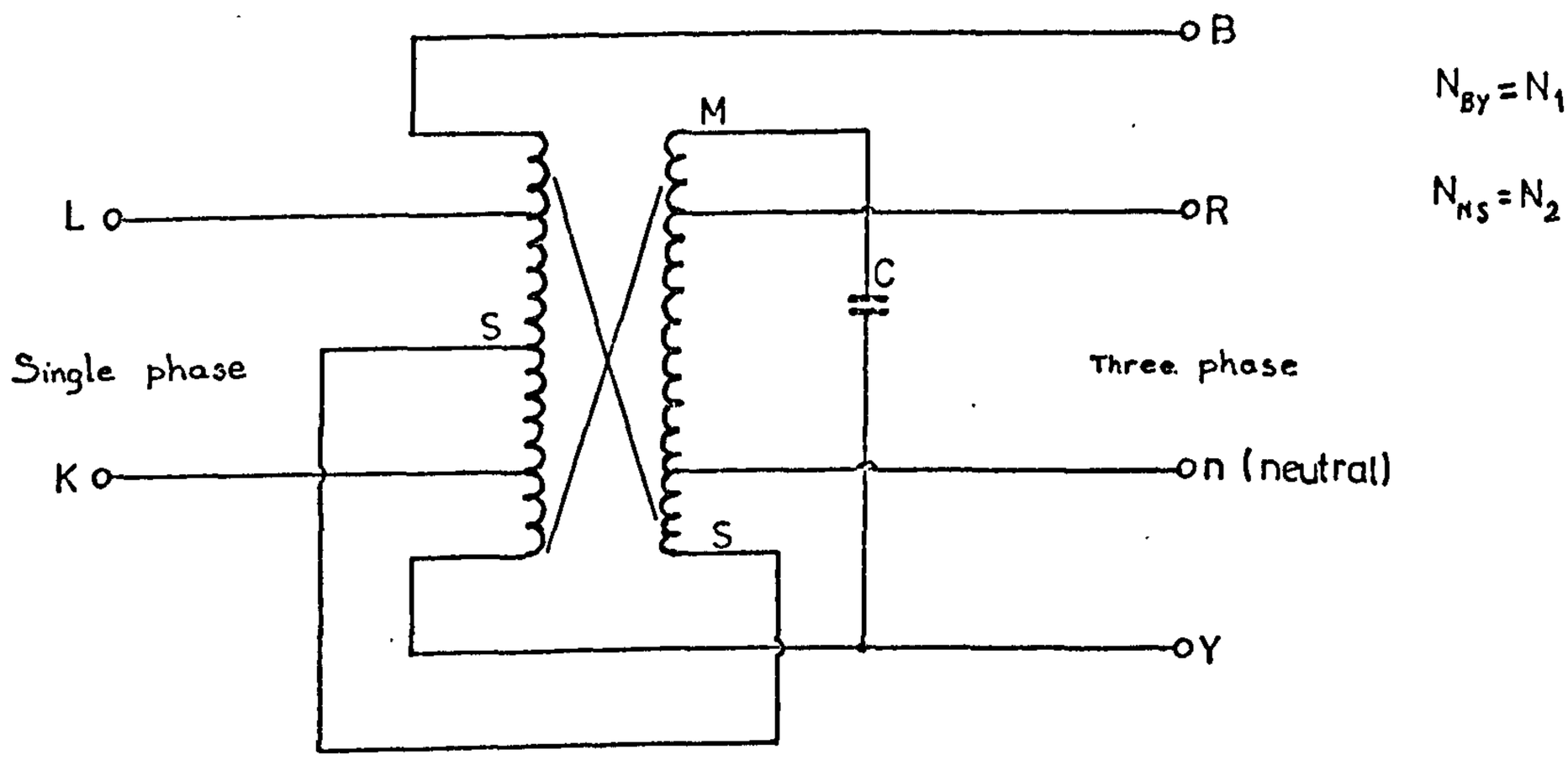

Figure 9.42 Scott-T Connection and its Application to Parametric Transformer

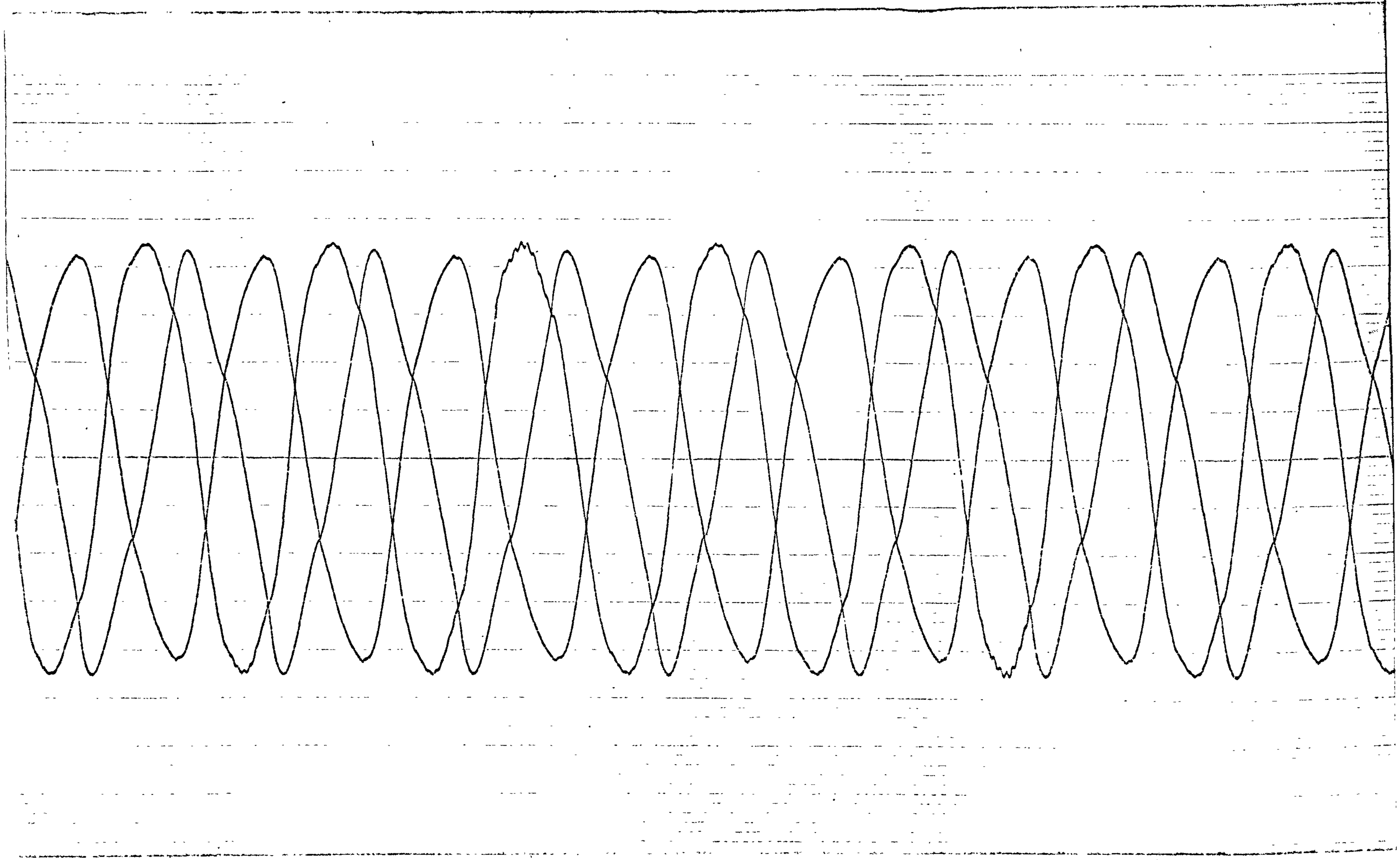

Figure 9.43 Operation as a Single-to-Three Phase Converter Scaling: 50V/cm foreach phase

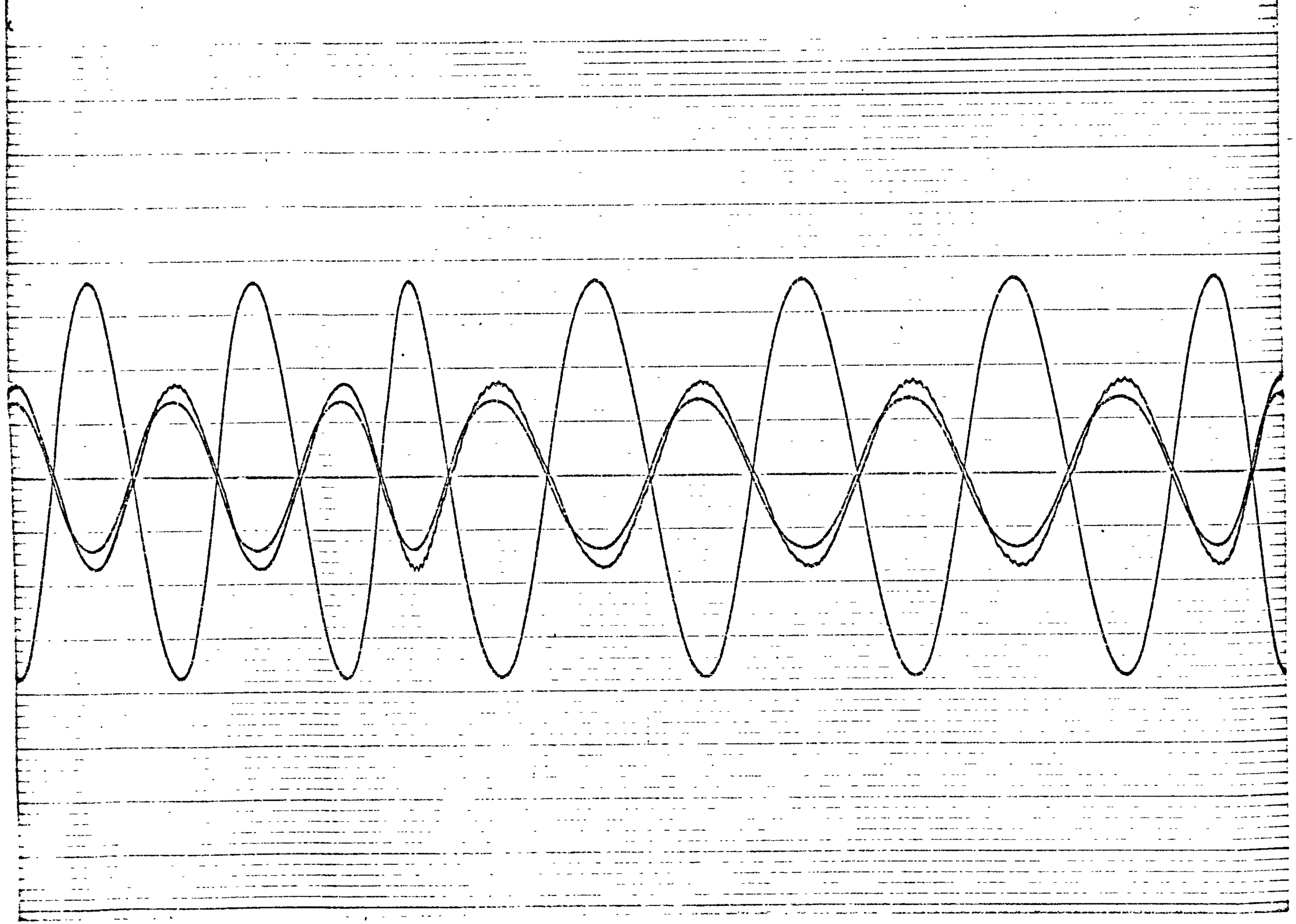

Figure 9.44 Phase Voltages for V_1 = 90V, before Parametric Excitation. Scaling: 50V/cm for each phase

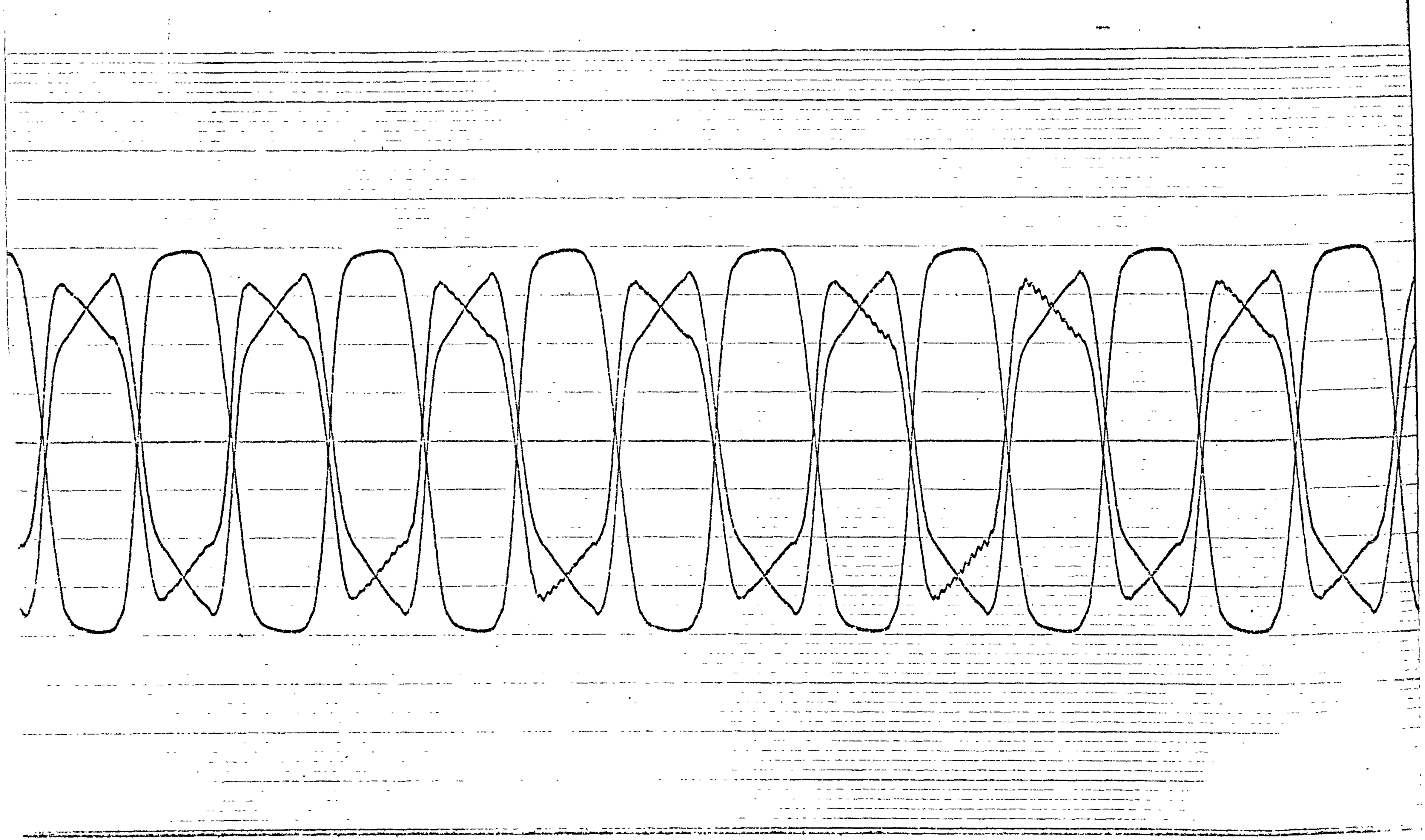

Figure 9.45 Phase Voltages Before Under-Voltage Protection Occurs, V_1 = 40V Scaling: 50V/cm for each phase

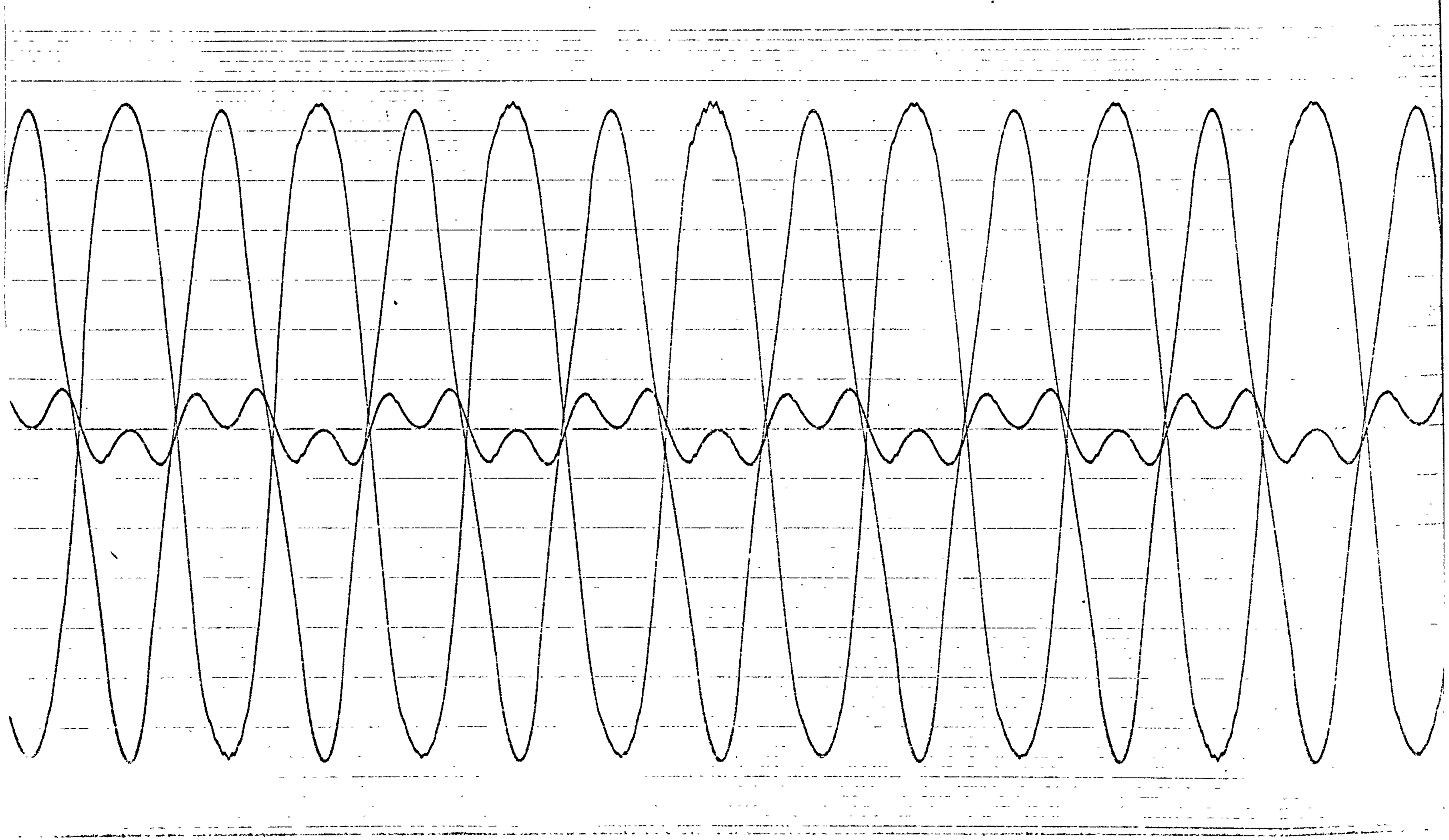

Figure 9.46 Phase Voltages After Over-voltage Protection has occurred, V_1 = 260V Scaling: 50 V/cm for each phase

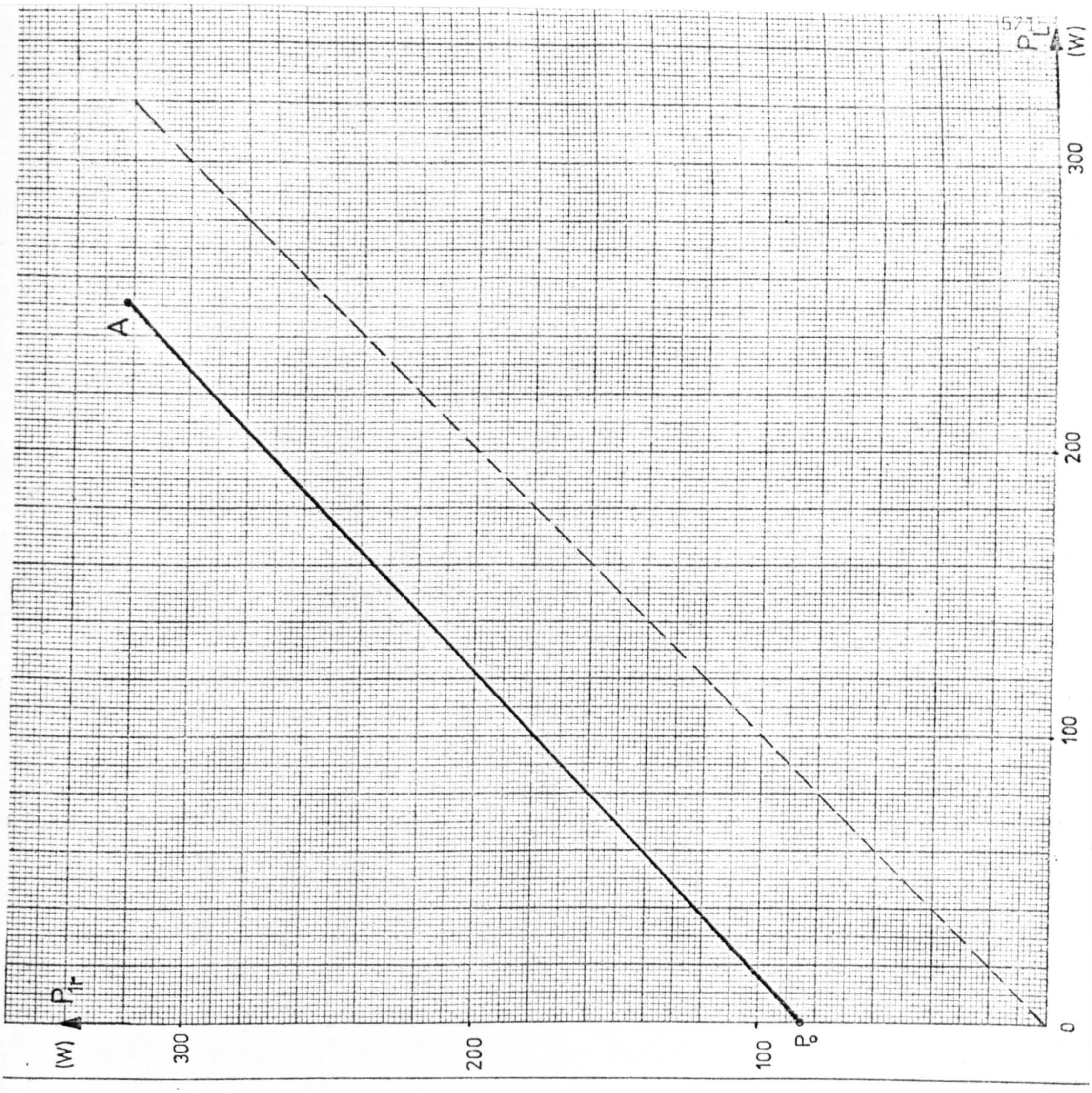

Figure 9.47 Real Input Power/Load Power Characteristic

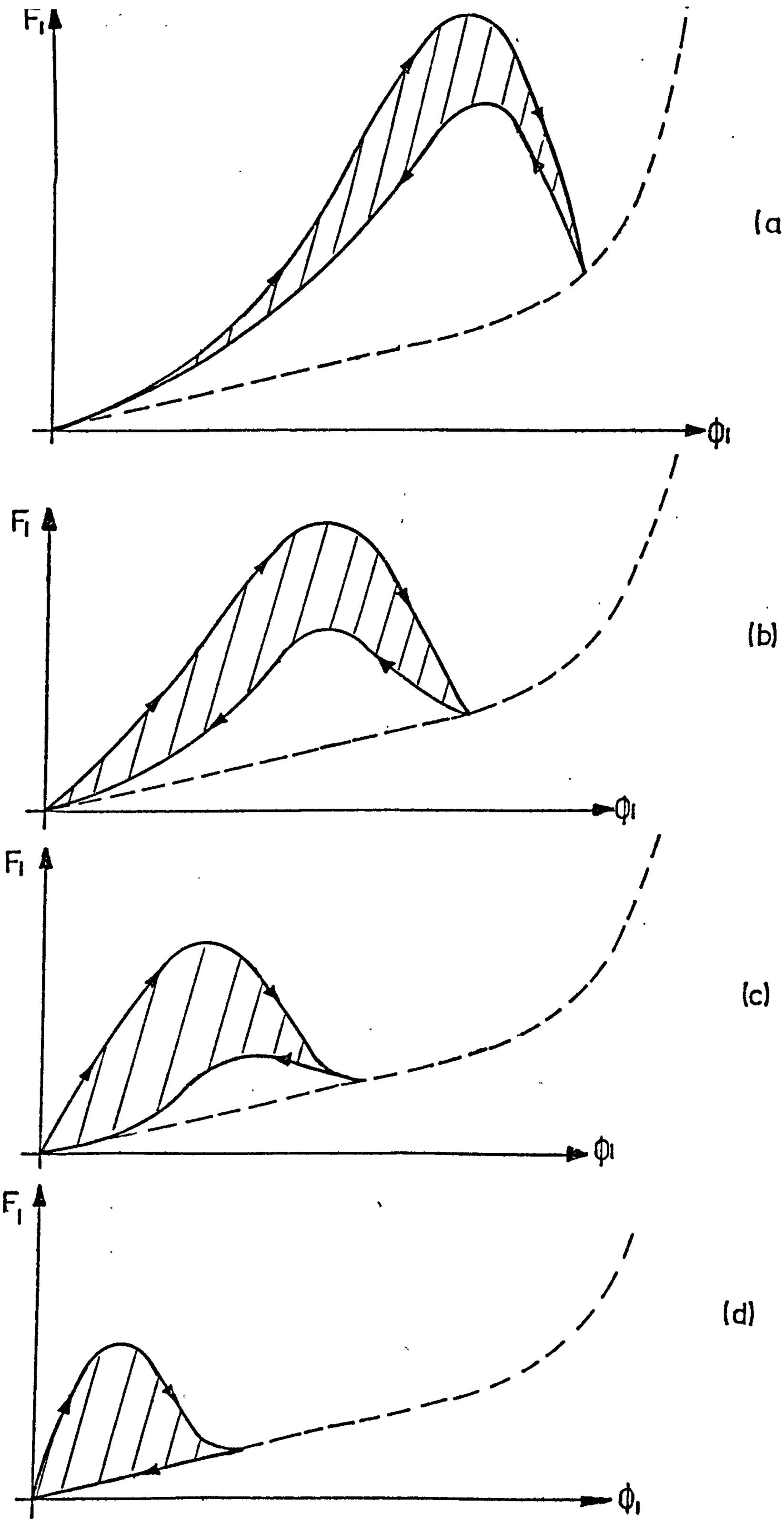

Figure 9.48 Effect of Losses on Primary Relative Magnetisation Characteristic at No-load Operation, with V_1 decreasing to V_1'''

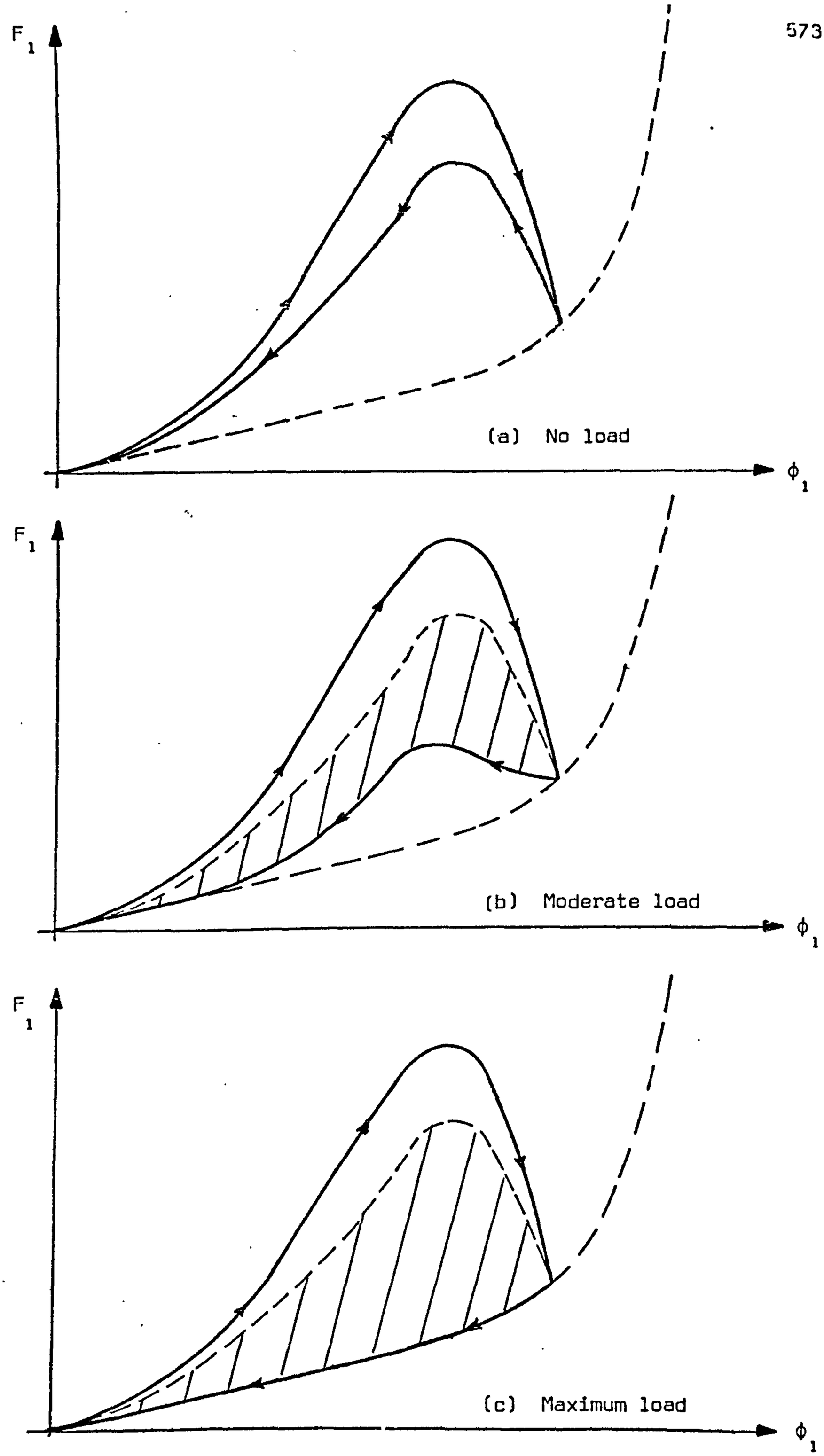

Figure 9.49 Effect of Increasing Load on Primary Relative Magnetisation Characteristics

CHAPTER X

APPLICATIONS OF THE PARAMETRIC TRANSFORMER

10.1 Applications as a Saturable Reactor

The two-C-core structure employed in commercially available parametric transformers, or any of the other equivalent structures shown in Figure 4.31, may be used for saturable reactors, wherever such applications arise. These range from simple ac power controllers to magnetic modulators and magnetic amplifiers[1], and although the progress in semiconductor technology has reduced the importance of magnetic devices in many areas of control engineering, application still exists when reliability, robustness and maintenance-free operation are of prime importance.

Although the devices of Figure 4.31 are simply saturable reactors, they have a major advantage over conventional saturable reactors (e.g. Figures 4.3 and 4.5) in that good isolation exists between the load and control circuits. Rather than cancelling the effects of flux coupling, its existence is removed (through method 3b of Section 4.1.1), and large alternating voltages are not induced in the control winding,even when the functions of the windings are reversed. This is clearly valuable in many applications, but since flux interaction is restricted to only part of the core, these devices are bulkier than conventional reactors for the same range of control.

Although a number of applications have been proposed[2,3] for the two-C-core saturable reactor, possibly the most important one is for voltage regulation.[4] A block diagram of this application is shown in Figure 10.1. After comparing the line voltage with a reference voltage, the resulting error signal is amplified and fed to the control winding of the saturable reactor, the load winding of which is in series with the line. If the amplitude of the line voltage varies, the amplified error signal changes accordingly, so that voltage regulation is provided by the varying impedance offered to the supply. In a practical device, the dc error signal is not directly amplified, but is used to pulse-width modulate the output of a generator producing one pulse per supply half cycle. The pulses are amplified and fed to the control winding of the saturable reactor, where they are integrated by the high winding inductance to result in a dc voltage with an average value proportional to the mark/space ratio of the pulses. If the error signal changes, the mark/space ratio and consequently the dc control voltage change to provide the necessary regulating action.

When saturable reactors are viewed as variable inductors, it should always be borne in mind that parametric coupling exists mutually between the load and control windings. Since the parametric coupling is mutual, even harmonic voltages are induced in the dc control circuit from the alternating source energising the load winding. Figure 4.28 or 4.29, which assumes parametric

coupling to exist in one direction only (i.e. from the control to the load winding), may therefore be misleading in some cases. For instance, in the two-C-core saturable reactor proposed in reference 2 for amplification purposes, and shown in Figure 10.2, it is claimed that the alternating input signal varies the dc flux already linking the load winding and established by a direct voltage source. The corresponding variations in the load winding inductance then induce an alternating voltage in the load winding, with the result that the voltage across the resistor is an amplified version of the input signal. However, this is unfortunately not true, since:

1. If the input signal is from a voltage source of frequency f, the load winding inductance is varied at 2f, and even harmonic currents circulate in the load winding. The voltage across the resistor has the same waveform as the current in the load winding, and is similar to that shown in Figure 4.25a or Figure 4.27e. The output voltage waveform, apart from being at twice the input frequency, does not therefore bear a direct relationship to the waveform of the input signal, and in this mode of operation the device cannot be considered as an amplifier.

2. Since the alternating flux and mmf in the core must be sufficiently high to take advantage of the non-linearity of the magnetisation characteristic, the input power necessary to create variations in the load winding inductance is also quite high. The device cannot therefore be

considered as a power or even a voltage amplifier, since the voltage across the resistor is much lower than the alternating input voltage which must be about that corresponding to ϕ_s in Figure 2.2b.

Both points are true, regardless of the form of saturable reactor employed and the manner of flux interaction in the core. The fallacy arises because Wanlass[2] assumes a trans-inductance characteristic of the form of Figure 2.4, although the actual shape of this curve is as Figure 8.21.

10.2 Applications of the Parametric Transformer

The operational characteristics of the parametric transformer are very suitable for many power conversion and conditioning applications. In fact, each of these characteristics can be exploited separately in different applications, with the other characteristics remaining as extra advantages. In the following sections, possible applications are viewed according to which characteristic is primarily utilized in obtaining the required function.

10.2.1 Power Conditioning (Voltage Regulator-Filters)

The need for regulating and filtering mains voltage to provide a transient-free, constant-amplitude, sinusoidal alternating voltage, especially for electronic equipment employing

integrated circuitry, is obvious. With its inherent voltage regulating and filtering properties, the parametric transformer can provide an optimum solution, providing also under- and over-voltage and overload protection. As the output voltage waveform of the parametric transformer is determined solely by the position of the operational point on the V_2/V_1 characteristic, a correct positioning provides both good voltage regulation and a good sinusoidal output waveform, although necessitating a restarting action whenever oscillations are switched off. The almost total isolation between the primary and secondary circuits prevents any disturbances in the mains voltage from being transferred to the load, and any load voltage irregularities from being reflected back to the mains supply. A noise attenuation factor of 50 dB is claimed commercially for parametric transformers[4,5], and for voltage regulation, a regulation factor within $\mp$ 0.5% and $\mp$ 1%. However the finding of an extremely good regulation of the rms voltages[6] conflicts with the findings of this project that, although the amplitude is extremely well regulated, the rms value is not, because of the change in the output waveform.

Although in this project, the parametric transformer was investigated with a load connected across the secondary capacitor, it is more practical to have the load supplied by another winding coupled to the main winding, as shown in Figure 10.3, and this allows the level of the output voltage to be chosen more freely. The essential advantage of this arrangement is that

the secondary resonant circuit can be wound with a large number of fine turns, to obtain a high inductance and so keep small the required value of the resonating capacitor. A high voltage is developed across the capacitor and a small current flows in the resonant circuit, conditions under which a capacitor operates more efficiently.

10.2.2 Power Conversion Applications

10.2.2.1 AC to DC Inverters (DC Power Supplies)

With the parametric transformer used as a mains regulator-filter, its noise-free output voltage may be rectified to provide a regulated dc power supply, as shown in Figure 10.4. Although the regulation property is provided by the parametric transformer, filtering of the ripples on the dc output is achieved by the filter shown in the figure. The principal advantages of this arrangement obviously include again mains over and under voltage protection, intrinsic overload protection and high noise immunity to mains voltage irregularities. Since the parametric transformer regulates the amplitude of the mains voltage, good regulation after filtering can be achieved, although the ac ripple in the output will obviously depend on the effectiveness of the filter employed.

10.2.2.2 DC to AC Inverters

The remarkable filtering ability of the parametric transformer is particularly well-suited to this type of application. Even with a square-wave input, the parametric transformer produces

a good sinusoidal output and this makes it particularly useful for switching mode power supplies. In conventional techniques (Figure 10.5a), the dc source is first commutated to obtain an alternating square-wave voltage, which is then filtered to remove unwanted harmonic frequencies and noise spikes introduced by the thyristors in the commutation process. However the parametric transformer can successfully replace the filter, as in Figure 10.5b, simply by tuning the output resonant circuit to the frequency of the square-wave voltage. In addition to providing an inherent overload protection, the employment of the parametric transformer ensures that the regulated output is always sinusoidal and spike-free. With the isolation between the output and the chopping circuits, the output voltage level can be transformed and multiple outputs provided.

The frequency of the chopper and that to which the output resonant circuit is tuned must be high (e.g. 20 kHz), to reduce the size of the core and the number of turns of the windings. At these frequencies, switching transistors can be used for the commutation process more effectively than thyristors.

The parametric transformer in Figure 10.5b replaces only the filter of Figure 10.5a, and chopping of the dc input voltage is performed by a separate circuit generally using both electrical and magnetic components. However, if the primary winding of the parametric transformer is used appropriately in the chopper circuit, the need for coupling the chopper to the parametric transformer is eliminated, as well as one extra step in the conversion process. This type of application, illustrated in Figure 10.5c,

has been investigated[8] with a chopper circuit due to Royer[9]. The dc to ac converter circuit is shown in Figure 10.6, where the sections of the primary winding of the parametric transformer are used in the chopper circuit with two alternately operating transistors. In the original circuit, the magnetic coupling between the bases and collectors of the transistors was achieved by windings on a toroidal magnetic core[9], but this is now replaced by the (primary) magnetic circuit of one of the two C-cores of the parametric transformer.

10.2.2.3 DC to DC Converters

With the filtering ability of the parametric transformer used beneficially in dc to ac inverters to supply a stepped-up ac output voltage, it is apparent that the parametric transformer can also be used in dc to dc conversion while retaining the extra advantages mentioned above. The conventional dc to dc conversion process is shown in Figure 10.7a, and with the filter and the step-up transformer replaced by the parametric transformer, the arrangement becomes modified as in Figure 10.7b. Prior to the final stage of rectification and filtering at the output of this figure, the process is the same as in Figure 10.5, and the parametric transformer may also be employed here with the configuration of Figure 10.5c. A high chopping frequency for both the chopper and the parametric transformer is again desirable to reduce the overall size.

The variation of the output voltage of the parametric transformer with the resonant frequency of the secondary circuit has already been demonstrated (see Figures 9.6 and 9.12). The same effect can also be created by varying the input frequency, when the secondary resonant frequency is fixed. In this way, it is possible to adjust or to regulate the output voltage of the parametric transformer, although the output voltage, being phase-locked with the input, will also have the same varying frequency. However in dc to dc conversion, this does not introduce any problems, and its use has been proposed[7] for a regulated dc power supply. As shown in Figure 10.8, the forward path required is the same as in Figure 10.7b, with the addition of a rectifier filter at the input. The dc output voltage is compared with a reference voltage in the sensing circuit, with the error signal being used to vary the frequency of a voltage-controlled oscillator so that the chopping frequency is varied in response to variations in the dc output voltage. As the input frequency to the parametric transformer is altered, its output voltage changes to provide a voltage regulation additional to that inherent in the parametric transformer. However, the circuitry required in the feedback path in Figure 10.8 is quite complicated[7], and the application may therefore be impractical. Nevertheless, using the configuration of Figure 10.6 for the forward path of Figure 10.8 may well prove valuable, since the frequency of this circuit is easily controllable as it is proportional to the dc level of the input to be chopped.[9]

10.2.2.4 Frequency Converters

The use of the parametric transformer in dc to ac power conversion makes possible conversion of the frequency of an alternating source. A block diagram for this is shown in Figure 10.9, where the alternating input voltage of f_1 is first rectified and filtered before being chopped to an independent frequency f_2. The parametric transformer operating at frequency f_2 converts the alternating square-wave input to a good sinusoidal output. In this mode of operation, any desired frequency conversion ratio can be achieved, since the chopper frequency can be independently chosen and the secondary tank circuit of the parametric transformer is easily tuned to this frequency.

10.2.3 Frequency Multiplier/Dividers

The frequency multiplying/dividing property of the parametric transformer can be utilized in many applications requiring static frequency changing. As distinct from the previous section, the output voltage in this application can be obtained only at multiples or submultiples of the input frequency, and the frequency conversion is achieved by inherent parametric transformer operation in the second (or third, etc) unstable region.

Early interest was shown in static frequency changing by non-linear magnetic devices[10], and many such devices developed early in the century were in fact a form of parametric transformer.[11] Although these devices are now of little importance,there may still

be a need in special applications such as the generation of a low frequency ringing current in telecommunication equipment. The essential drawback of the frequency-changing operation of the parametric transformer is its low power efficiency, which makes the device unsuitable for power level applications. However, it may still be of value where power efficiency is not of prime importance, since the frequency changing is achieved quite simply without the need for complex circuitry.

10.2.4 Parametric Filters

The excellent filtering ability of the parametric transformer has led to a proposal[12] for its use in analysing the frequency spectrum of complex waveforms. The proposal requires a number of parametric transformers, each tuned to a different frequency and with their primary windings connected in parallel (see Figure 10.10) to form the input to the frequency analyzer. Each different frequency component of the input will drive a separate transformer, tuned to a different harmonic frequency to operate in the first unstable region. A voltage is thus parametrically produced at the output of each transformer for which a component is present in the input, and the main advantage of the proposal is claimed as the need for only a single input amplifier.

Although the filtering network of Figure 10.10 may be considered theoretically as operational, it is not possible to realize it practically, since

1. The parametric transformer exhibits under-voltage protection even if the damping is practically zero (Section 3.6.1),

2. The input voltage to create the necessary reluctance variations is high (Section 2.1.1.),

3. The harmonic amplitudes in a complex waveform are usually much smaller than that of the fundamental.

It is clear therefore that the threshold effect in the parametric transformer will not permit its use as a conventional filter. Furthermore, if the input frequency varies, the output frequency also varies, and parametric excitation is possible within a quite wide frequency band (see equation (3.179)). Like all non-linear resonant circuits the output voltage/input frequency characteristic exhibits hysteresis,which also makes it different from a conventional linear and passive filter.

10.2.5 Phase Conversion

The phase quadrature between the input and output voltage of a parametric transformer may be used for single-to-three phase conversion, as explained in Section 9.4. Applications have been suggested in rapid transit railroads[13], but the 3-phase output which can be obtained may be found unsatisfactory, since the changing phase symmetry and relative amplitude of each phase with the input voltage may not meet the stringent requirements involved. However, conversion from a single phase to a 3-phase supply by a simple device is an outstanding feature, and parametric transformers carefully designed for this purpose may offer major advantages in

some applications. Their employment for 3-phase to single phase conversion is also a possibility, which can be of value when a single-phase load is to be fed from a 3-phase supply without introducing any phase imbalance.

With a parametric transformer as in Figure 4.11, the quadrature phase between the primary and secondary fluxes gives rise to another application of the basic concept. During steady-state operation, the common region where the two core loops join is subjected to a rotating magnetic field, arising from the 90° phase difference between two orthogonally-spaced fluxes. By placing a rotor in this common region, a parametric 2-phase motor driven by a single phase supply is obtained,[14] which may provide better performance characteristics than a single-phase induction motor. Obviously, the resulting performance will be influenced by the type of the rotor used in the motor, e.g. squirrel-cage, hysteresis, reluctance type etc.

10.3 Advantages and Disadvantages of the Parametric Transformer

In the light of the experimental and theoretical investigation described, the main advantages and disadvantages of a parametric transformer may be summarized as:

Advantages

1. Operational characteristics: Each of the inherent properties of the parametric transformer (filtering ability, voltage

regulation, 90° phase difference etc) can be used to special advantage in different situations.

2. Simultaneous furnishment of all characteristics: The parametric transformer in its normal mode of operation exhibits all the basic characteristics. Thus, while one of the characteristics (e.g. voltage regulation) is used in a particular application, the others (e.g. filtering, overload protection etc) remain as extra advantages.

3. Simplicity: All the beneficial properties are provided in a simple device, without the need for any additional circuitry. That will be quite complex even if at least one of the operational characteristics inherent in the parametric transformer is to be otherwise achieved.

4. Reliability: This common feature of all magnetic control devices is shared by the parametric transformer. Components sensitive to changes in environmental conditions or with a short life-time are not employed, and operation of the parametric transformer is essentially maintenance-free. The inherent overload and over-voltage protection also serve to enhance the reliability, and the robust construction is an advantage where mechanical stresses are likely.

Disadvantages

1. Low power efficiency: The low efficiency of 60-65% is the greatest drawback of the parametric transformer, restricting its potential use for power conversion and conditioning

applications, although the parametric transformer offers unique characteristics valuable in such areas of application.

2. Large size and weight: As a result of the low power efficiency and a construction in which the core is not efficiently used, the parametric transformer is about 3 times heavier and more costly than a conventional transformer of the same power rating. The need for a large highly-rated capacitor further increases the overall size, weight and cost, and restricts its use in portable equipments where limited space is available. However, these increases will be counterbalanced in some applications by the beneficial utilization of the operational characteristics.

3. Difficulty in constructing large power units: As the size and weight of a parametric transformer increase, the realization of the device becomes more and more impractical. Although saturable reactors to control hundreds of kilowatts are constructed, the maximum power output in parametric transformer operation is much less than this. Another limiting factor at high power levels is obviously the much higher power rating required by the capacitor. The largest commercially available parametric transformer has a power rating of 2.5 KVA, with outputs of 5 KVA obtained by parallel connection[4].

4. Low input power factor: Since the input current drawn from the supply is largely reactive, a capacitor may be necessary

to correct the corresponding low input power factor, and this will yet further increase the overall size, weight and cost. If this is not done, the parametric transformer may adversely affect the output of the driving circuits, and difficulties of coupling may arise.

5. Poor behaviour on lagging power factor loads: In industry, lagging power factor loads are the most frequently encountered, and the poor behaviour of the parametric transformer under these conditions is somewhat of a disadvantage.

6. Need for manual re-start: Whenever the parametric transformer provides overload or under-voltage protection, oscillations are switched off and a manual re-start is necessary. In commercial devices, a push-button switch is used for injecting a small voltage to initiate oscillations in the secondary winding after normal conditions are restored. However, this clearly presents a problem in remote or unattended locations.

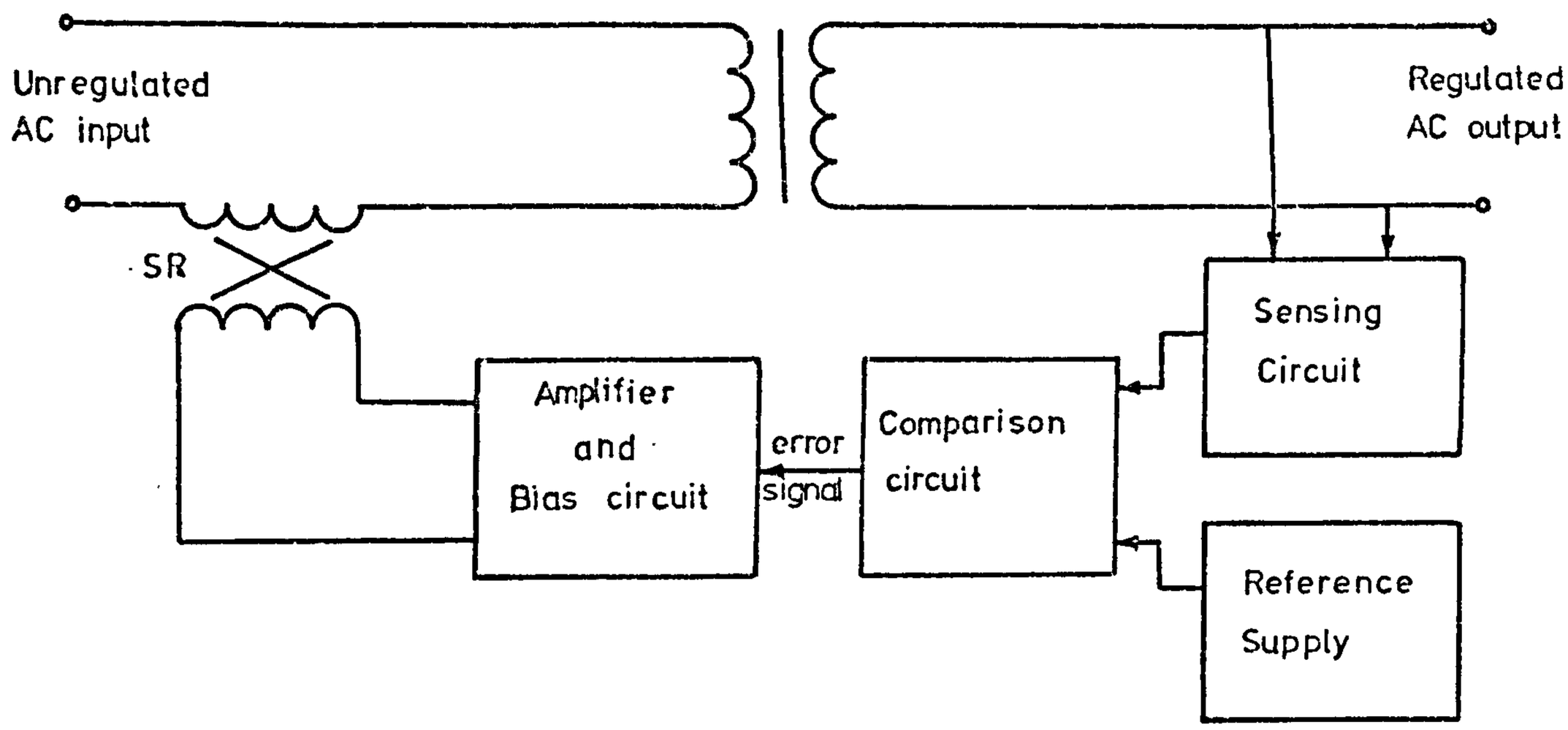

Figure 10.1 Block diagram for voltage regulator (Varax)

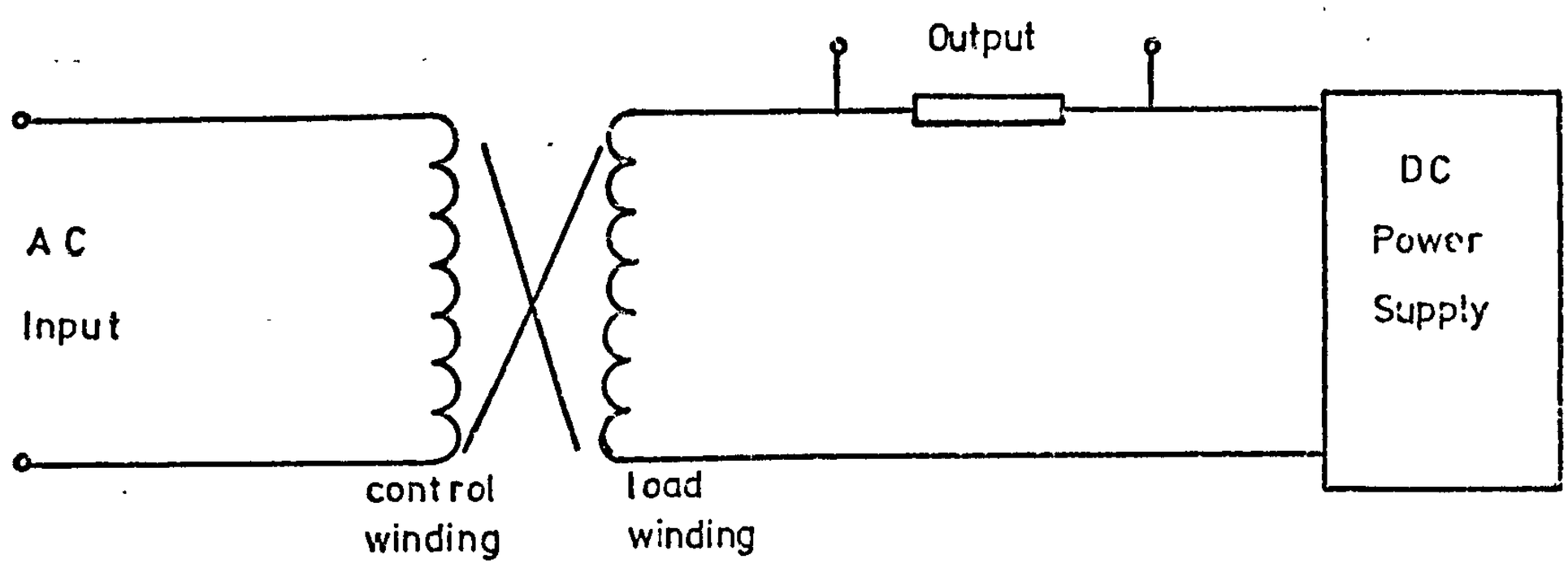

Figure 10.2 The amplifier proposed by Wanlass

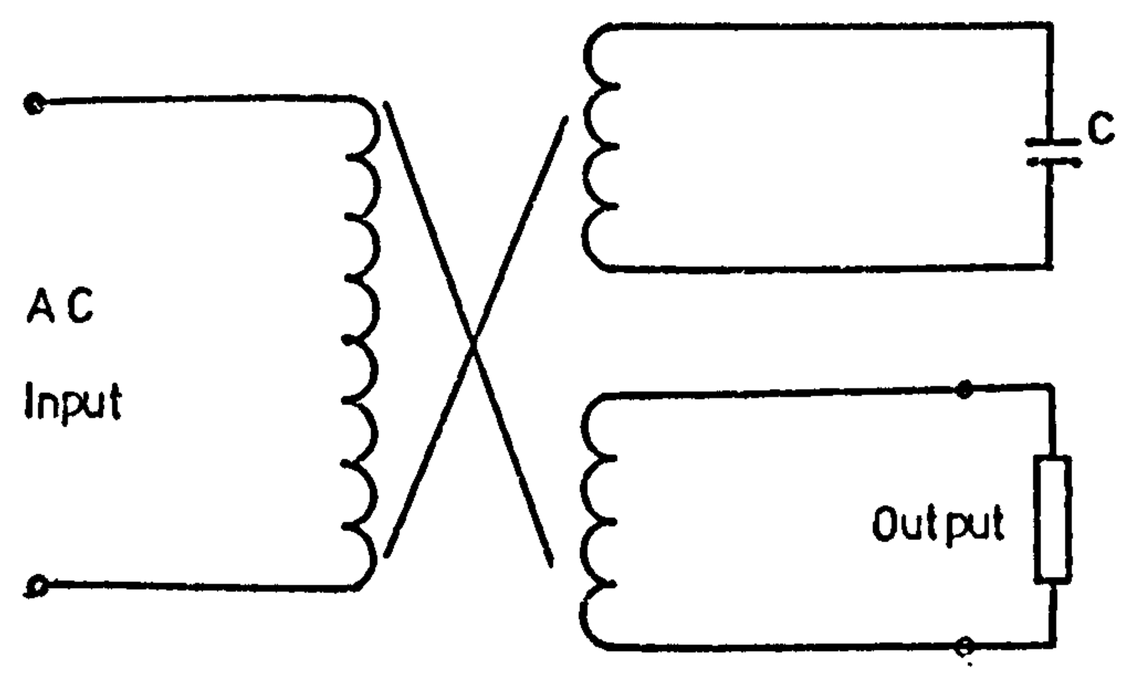

Figure 10.3 Separate output windings

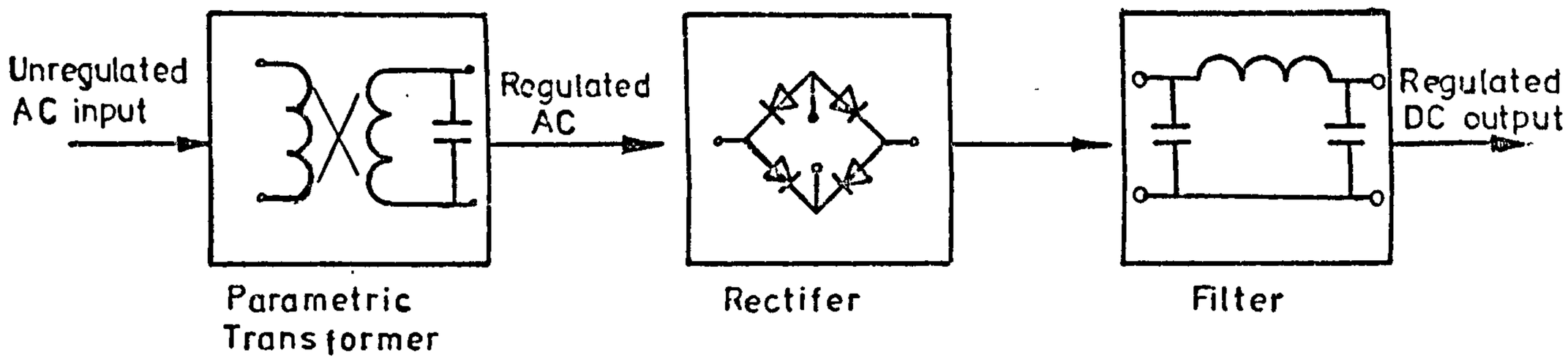

Figure 10.4 DC Power supply employing parametric transformer

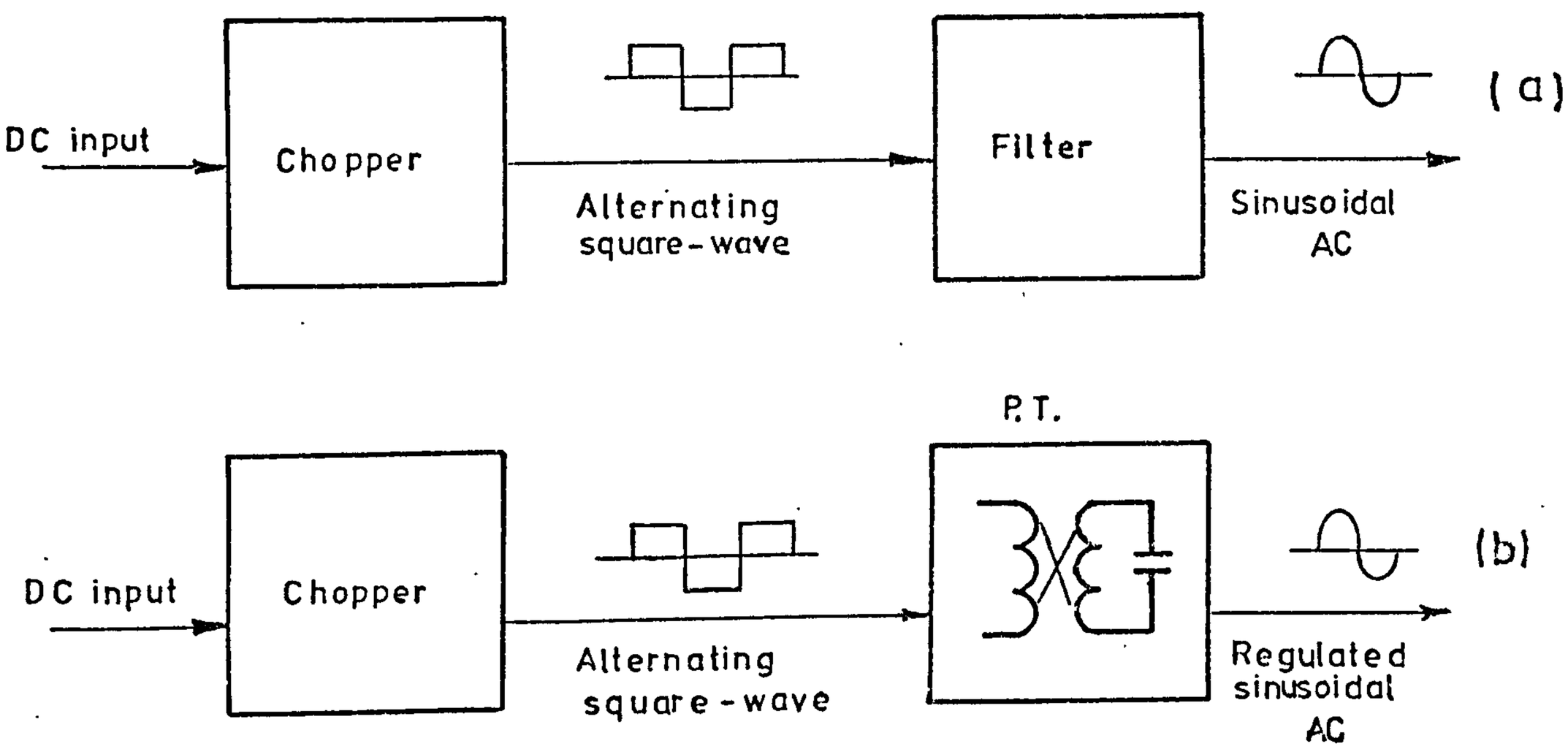

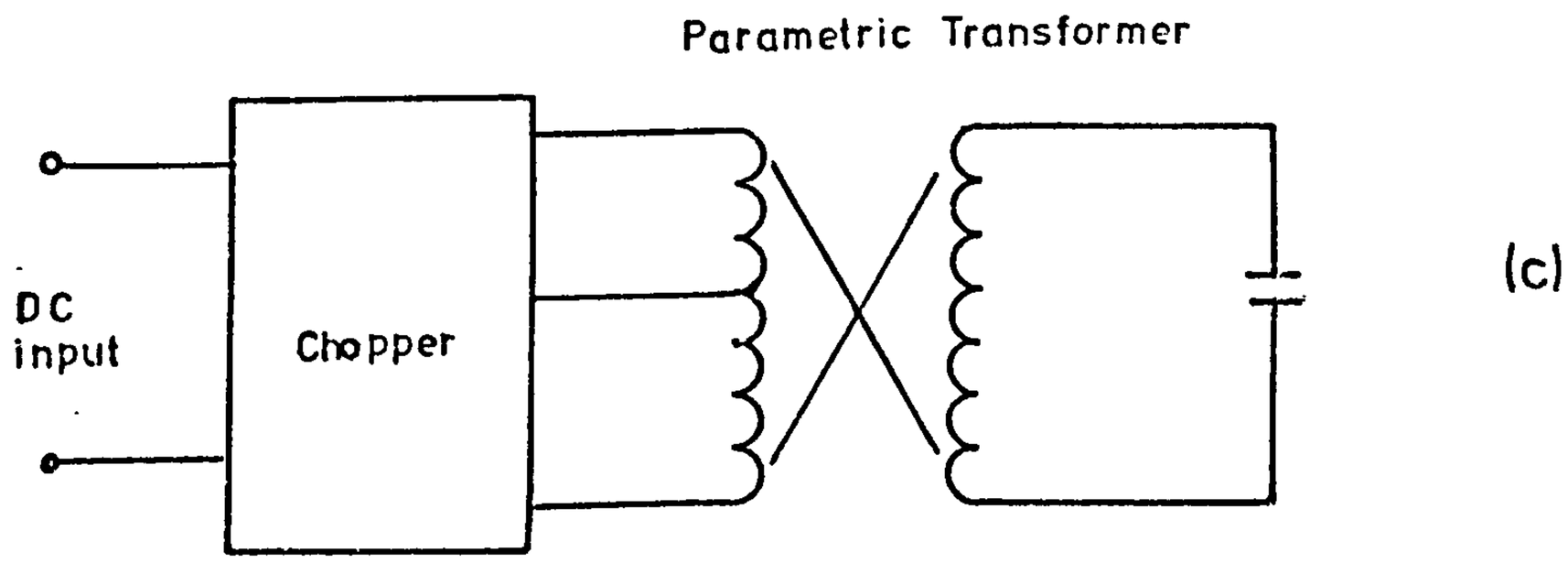

Figure 10.5 DC to AC Conversion (a) Conventional
(b) Employing parametric transformer
(c) With primary winding utilized in the chopper

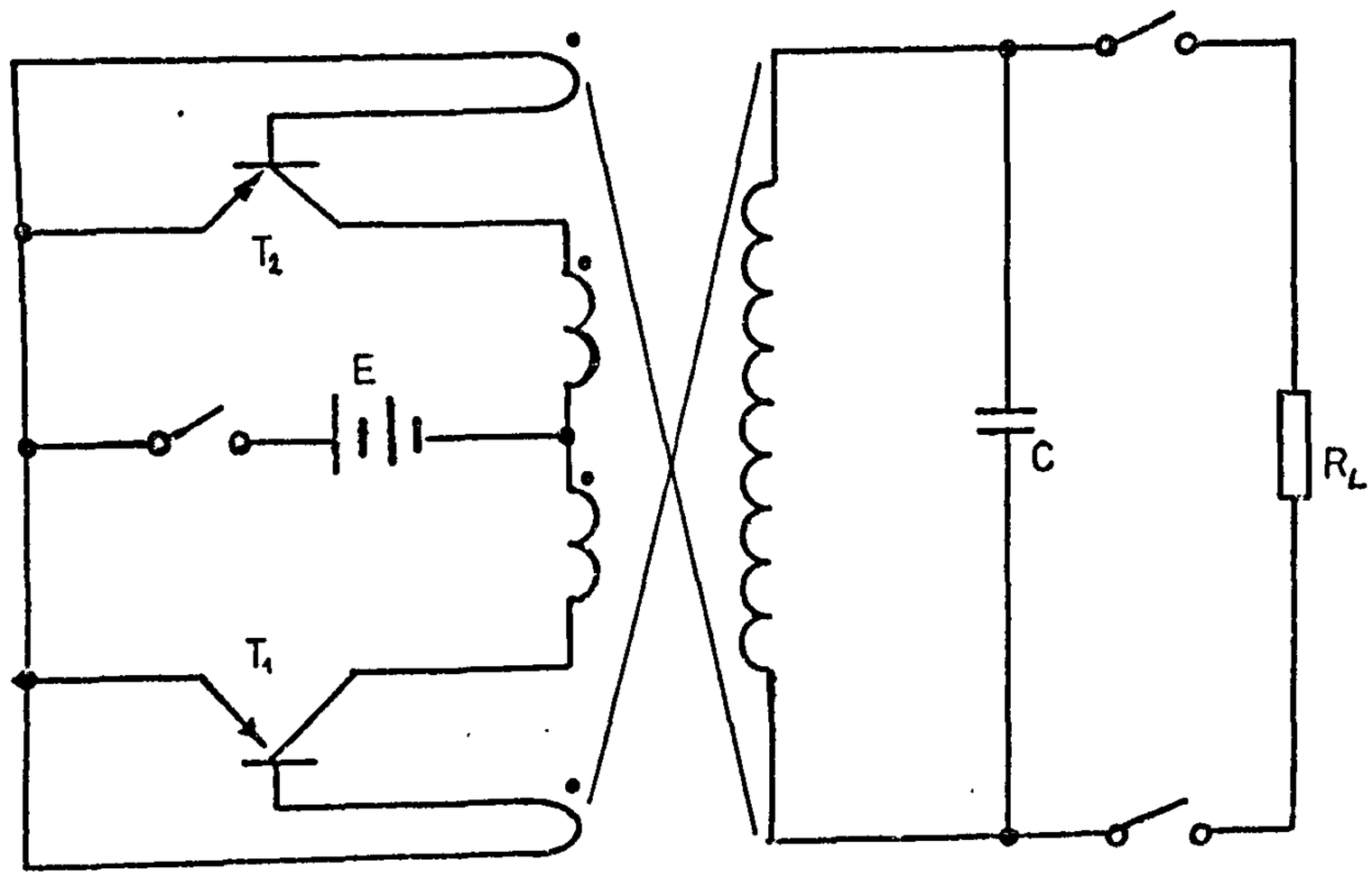

Figure 10.6 Chopper circuit directly coupled to parametric transformer

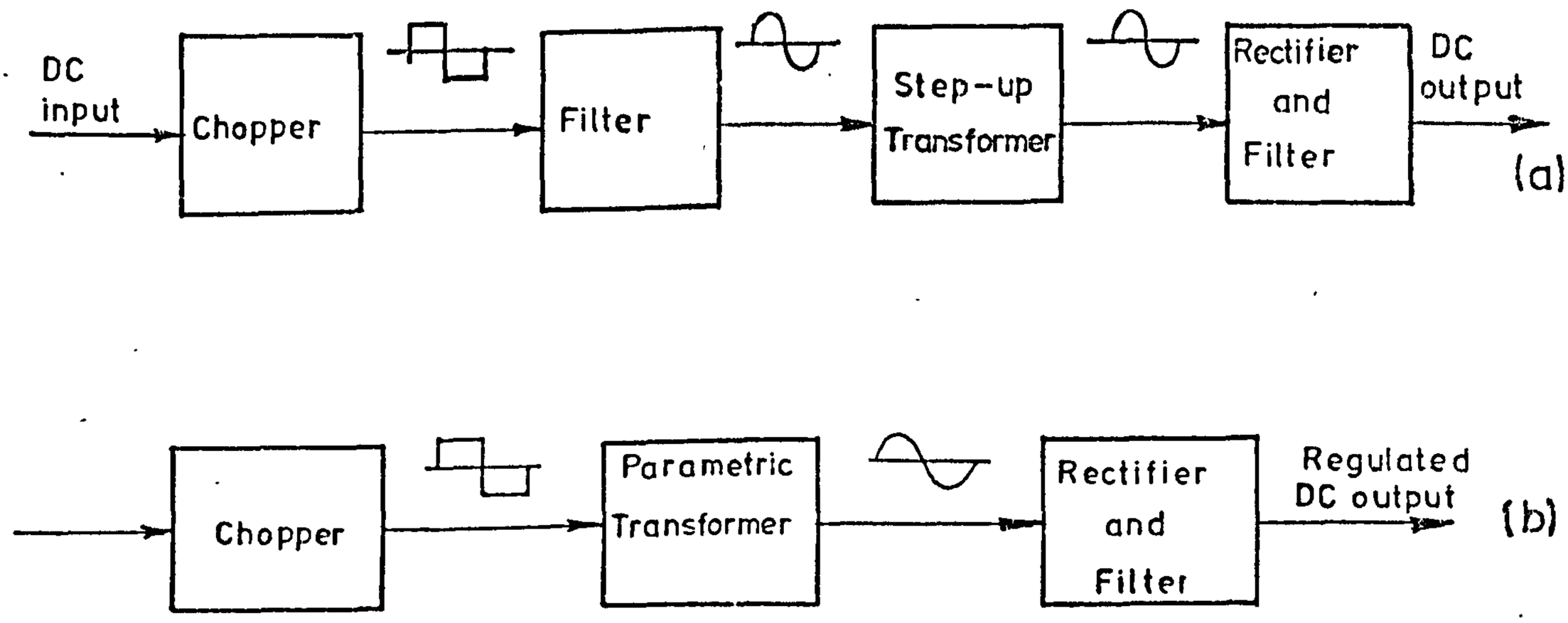

Figure 10.7 DC to DC Conversion (a) Conventional
(b) Employing parametric transformer

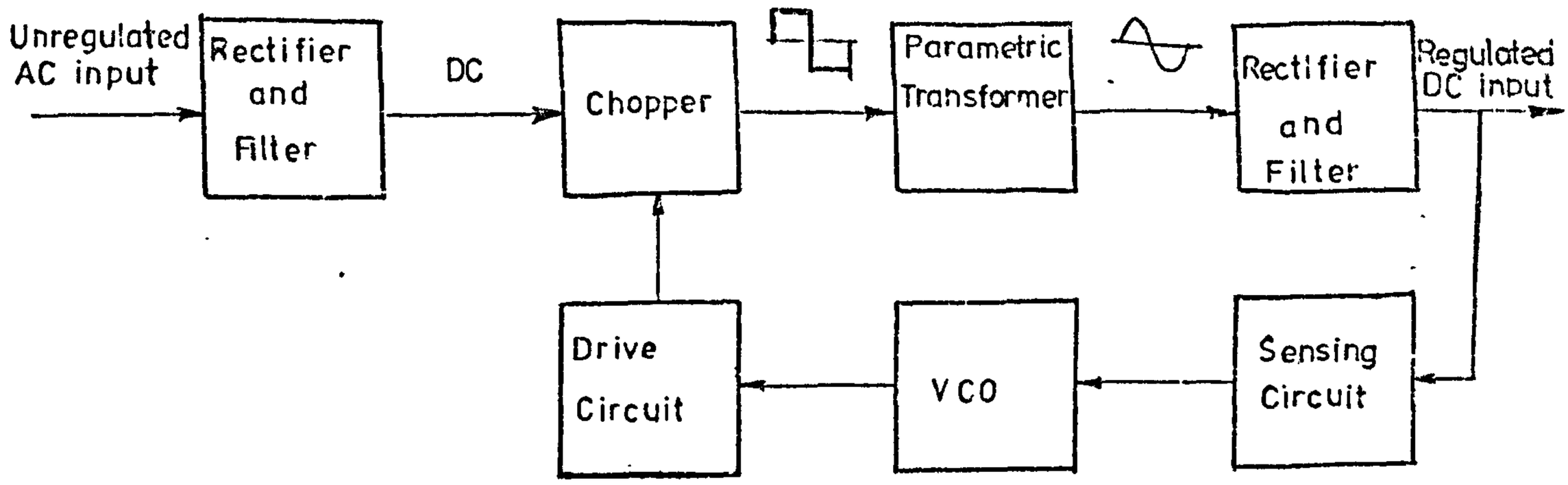

Figure 10.8 Voltage regulation by varying the chopper frequency

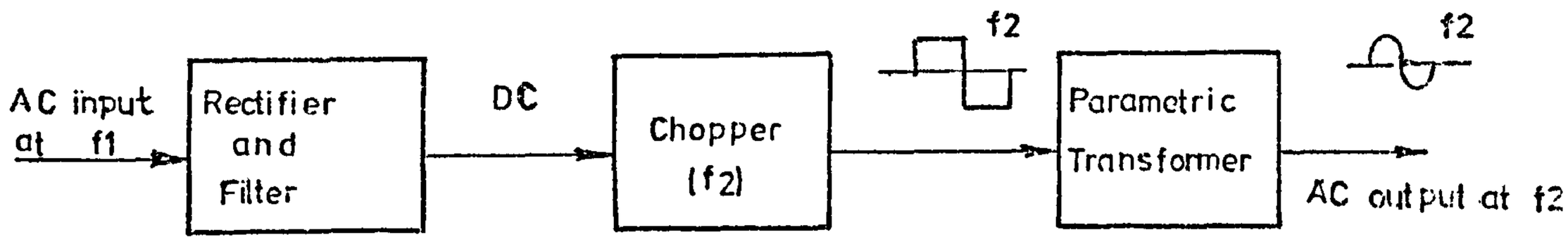

Figure 10.9 Frequency conversion

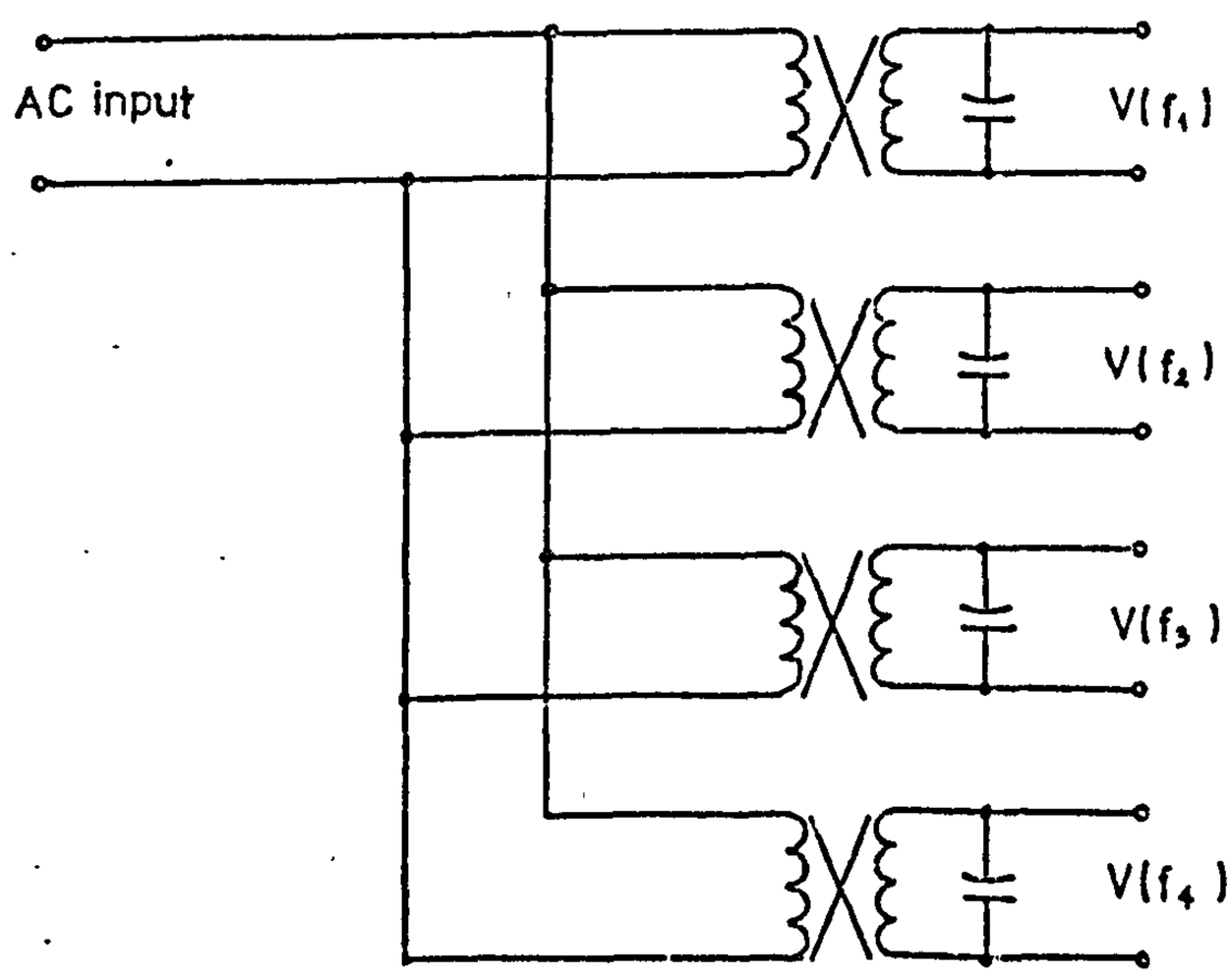

Figure 10.10 Parametric Filter

CHAPTER XI

CONCLUSIONS

The conclusions arising from the project, together with suggestions for future extension of the work, may be summarised as

1. Difficulties in the mathematical analysis of the secondary circuit of the parametric transformer arise, since no complete theory exists for non-linear systems with time-varying parameters. The method employed in Chapter III permitted to a limited extent the derivation of relationships between the operational characteristics and the differential equation of the secondary circuit. However, alternative analytical techniques, such as the phase-pulse method, may prove useful, by providing additional knowledge for the establishing of these relationships, and to obtain better means of manipulation leading to improvements in the operational characteristics of the device.

2. The theory developed using mmf functions in the circuit differential equations is applicable to any parametric transformer, employing any form of saturable reactor in its magnetic construction. The overall complexity of the system equations, which can be solved only by a computer, still requires simplifying assumptions during their derivation from the physical system. However, it is believed that this is the first appropriate mathematical representation of the problem,

making possible the direct use of computer evaluation of a particular physical construction. Since this is a real-time analysis providing instantaneous values of the system variables, the derivation of the performance characteristics is only possible by repetitive solution of the system equations.

3. The results produced by the computer simulation of the two-C-core parametric transformer agreed well with the experimental observations in most respects, except for the necessary value for the secondary capacitor and, consequently, the amplitudes of the secondary and primary currents. The assumption of a single-valued B/H curve did not allow introduction of initial curvature near the origin into the computer simulation; since such a B/H curve produces not a gradual increase in the average reluctance but high peaks in its time variation. Because of this assumption, neither can the computer show the effect of hysteresis and eddy current losses in distorting the waveforms of the circuit variables. No possible solution has yet been found for the complete and simultaneous representation of all the properties of an actual magnetisation characteristic.

4. Since the parametric transformer offers characteristics very advantageous in many applications, future studies must concentrate on eliminating the disadvantages viewed in Section 10.3, most importantly on increasing the power efficiency and reducing the size of the device.

5. It may be concluded, both from the experimental and computer investigation in this thesis, that an important factor creating many disadvantages is the need for a high resonating capacitor to initiate parametric oscillation. Theoretically, with a material not exhibiting the magnetisation characteristic phenomenon of Figure 8.55, the value of the capacitor employed becomes small, resulting in smaller currents in both the secondary and the primary windings. The consequences of smaller currents would include:

a) higher efficiencyin the real power sense, since the total losses (mostly the iron losses) at no load would significantly decrease,

b) higher input power factor, since the reactive component of the primary current would be much smaller,

c) higher overall efficiency (load power/apparent input power) since the apparent power drawn from the supply would be greatly reduced,

and d) smaller size and weight, since the power rating of the capacitor and gauge of wire in the transformer could be much smaller.

However, all magnetic materials used for transformer cores normally possess an initial curvature in their B/H characteristics, and the high circulating currents and low efficiency are therefore inevitable.

6. The investigation of flux interaction and parametric coupling in various saturable reactors shows that in an ideal saturable reactor device

   a) mutual flux coupling must be eliminated (not cancelled) by a proper magnetic configuration, with two separate magnetic paths for the primary and the secondary fluxes,

   b) flux interaction must take place in the whole core and not merely in a part of this,

   c) flux interaction must occur in a parallel manner.

   The power efficiency and size of a parametric transformer mainly depend on how effectively parametric coupling is achieved between the windings. Investigations on increasing the power efficiency and the power rating/weight or the power rating/volume ratio of parametric transformers must therefore be directed towards the physical realization of a saturable reactor device possessing all these three properties simultaneously.

7. For a given magnetic structure, improvements can be obtained in the power efficiency and weight of a parametric transformer by keeping the total losses as small as possible, and by modifying the magnetic construction appropriately. For example, a parametric transformer can be constructed on a magnetic arrangement formed by the 90° rotation of one half of a conventional transformer using two-C-core loops with a square cross-section overall. This will obviously reduce the leakage fluxes and increase the volume in which flux interaction occurs.

However, the possibility of unintentional air gaps and the difficulty in securing the assembly are clearly increased. Furthermore, in two-C-core parametric transformers, the flux density in a large portion of one of the C cores is quite low, indicating ineffective utilization of the core material. It appears therefore that a configuration with a smaller A_2/A_0 ratio (of the equivalent bridged core) is more desirable.

8. Further experimental work on multi-valued relative magnetisation characteristics may lead to a criterion to be used for minimising the total losses and increasing the power efficiency, by observing the effects of various system parameters on the shape of these characteristics.

9. Together with efforts to reduce the disadvantages of the parametric transformers, further theoretical and experimental investigations must be performed in various areas of application. Applications requiring switched mode operation in conjunction with semiconductor devices deserve special interest. Finally, the possibility of obtaining characteristics similar to those of parametric transformers makes bridge-connected reactor circuits an area to which special attention should be devoted.

REFERENCES FOR CHAPTER I

1. M. Faraday, *"On a Peculiar Class of Acoustical Figures; and on certain forms assumed by a Group of Particles Upon Vibrating Elastic Surfaces"*, Phil. Trans. Roy. Soc., London, Vol. 121, pp. 299-318; May 1831.

2. F. Melde, *"Uber errerung stehender Wellen eines fadenformeigen korpers"*, Ann. der Physik und Chemie, Scr. 2., Vol. 109, pp. 193-215, 1859.

3. E. Mathieu, *"Memoire sur le mouvement vibratoire d'une membrane de forme elliptique"*, Jour. de Math. Pures et Apliquees (Jour. de Liouville), Vol. 13, p. 137, 1868.

4. G.W. Hill, *"Mean motion of the Lunar Perigee"*, Acta. Math., Vol. 8, p.1, 1886.

5. Lord Rayleigh, J.W. Strutt, *"On the Maintenance of Vibrations by Forces of Double Frequency, and Propagation of Waves Through a Medium with a Periodic Structure"*, Phil. Mag. Ser. 5., Vol. 24, Issue 147, pp. 145-149, Aug. 1887.

6. G. Floquet, *"Sur les equations differentielles lineaires"*, Ann. de l'Ecole Normale Superieure, Vol. 12, p. 47, 1883.

7. E.T. Whittaker, *"General Solution of Mathieu's Equation"*, Proc. Edinburg Math. Soc., Vol. 32, p.75, 1914.

8. E.L. Ince, *"General Solution of Hill's Equation"*, Monthly Notices of Roy. Astron. Soc., Vo. 75, p.436, 1915.

9. E. Heisner, *"Uber Schuttelschwingungen in Systemen mit Periodisch veranderlicher Elastizitat"*, Schweizer Bauzeitung, Vol. 72, pp. 95-98, 1918.

10. M.J.O. Strutt, *"Der charakteristische Exponent der Hillschen Differentialgleichung"* Mathematische Annalen, Vol. 101, p.559, 1929.

11. N.W. McLachlan, *"Theory and Application of Mathieu Functions"*, Oxford University Press, London, 1947. See Chapter I: Historical Introduction.

12. See Section 7.422 in the book *"Ordinary Non-linear Differential Equations in Engineering and Physical Sciences"*, by N.W. McLachlan, Second Edition, Oxford University Press, 1956.

13. J. Bethenod, Comptes Rendus des Seances de L'Academie de Sciences, Paris, Vol. 207, 1937; also p. 495 in the book *"Non-linear Oscillations"* by N. Minorsky, D. Van Nostrad Co., 1962.

14. C.A. Ludeke, *"Resonance"*, Journal of Applied Physics, Vol. 13, p.418, 1942, and *"The Generation and Extinction of Subharmonics"*, presented at the Symp. of Non-linear Circuits, Polytech.Inst. Brooklyn, April 1953.

15. See Section 7.30 in Op. cit, reference 12.

16. L. Brillouin, *"Theorie d'un alternateur auto-excitateur"*, Eclairage Electrique, Vol. 11, pp.49-59, April 1897.

17. H. Poincare, *"Sur quelques theoremes generaux de l'electrothecnique"*, ibid, vol. 50, pp.293-301, March 1907.

18. L. Kuhn, *"Uber ein neves radiotelephonische system"*, Jahr. fur dracht. Teleg. und. Telephone, vol. 9, pp.502-534, June 1915.

19. J. Zenneck, *"A Contribution to the Theory of Magnetic Frequency Doublers"*, presented at IRE meeting, New York, Sept. 1915.

20. E.F.W. Alexenderson, *"A Magnetic Amplifier for Radiotelephony"*, Proc. IRE, Vol. 4, pp.101-149, April 1916.

21. R.V.L. Hartley, U.S. Patent No. 1,287,982.

22. E. Peterson, *"Magnetic Wave Amplifying Repeater"*, U.S. Patent, 1,884,844, issued October 25, 1932.

23. M.W. Mumford, *"Some Notes on the History of Parametric Transducers"*, Proc. IRE, pp.848-852, May 1960.

24. K. Heegner, *"Uber Systeme mit gestorter Superposition"*, Zeitschrift fur Physik, Vol. 30, pp.85-112, 1925.

25. Guenther-Winter, Zeitschrift fur Hochfrequenztechnik, Vol.34, pp.41-49, 1929.

26. Guenther-Winter, ibid, Vol. 35, p.132, 1931, and Jahr. fur dr. Tel. und. Tel, Vol. 37, p.172, 1931.

27. Y. Watanabe, T. Saito and K. Kaito, *"Building-up of a Self-Oscillation in an Oscillation Circuit including a Periodically Varying Inductance"*, Journal of Inst. of El. Eng. of Japan, Vol. 53, Part 5, pp.201-205, 1933.

28. L. Mandelstam, N. Papalexi, A. Andronov, S. Chaikin and A. Witt, *"Expose des recherces recentes sur les oscillations non-lineaires"*, Journal of Technical Physics of the USSR, Vol. 2, pp.81-134, 1935. This is a report made to the Radiophysics Section of the General Assembly of the International Scientific Radio Union (ISRU), London, 12-18 September 1934. English translation by NASA, TTF-12, 678, Washington DC, Nov. 1969.

29. L. Mandelstam and N. Papalexi, Zhurnal Teknicheskoi Fiziki, p.5, 1931.

30. L. Mandelstam and N. Papalexi, Journal of Technical Physics (USSR), V, p.8, 1934 and IV, p.1141, 1935.

31. A. Tscharakhtschian, *"On the Harmonic Effects in a System of Two Parametrically-Coupled Stages"*, (in Russian), Journal of Technical Physics (USSR), Vol. VI, part 7, pp.1230-1241, 1936.

32. W.L. Barrow et al, *"A Further Study of Oscillatory Circuits having Periodically Varying Parameters"*, Journal of Franklin Institute, Vol. 221, pp.403-529, March-April, 1936.

33. N. Minorsky, *"Parametric Excitation"*, Journal of Applied Physics, Vol. 22, No. 1, pp.49-54, Jan. 1951.

34. N. Minorsky, *"Sur l'oscillateur non lineaire de Mathieu"*, Comptes Rendus, Faculty of Science, Paris, Vol. 232, pp.2179-2180, June 1950, and many other articles on parametric excitation published in the same periodical.

35. E.I. Hawthorne, *"Sinusoidal Variation of Inductance in a Linear Series RLC Circuit"*, Proc. IRE, pp.78-81, January 1951.

36. J. Von Neuman, *"Non-linear Capacitance or Inductance Switching, Amplifying and Memory Organs"*, U.S. Patent No. 2,815,488, filed April 28, 1954, issued Dec. 3, 1957.

37. E. Goto, *"The Parametron, a Digital Computing Element which Utilizes Parametric Oscillation"*, Proc. IRE, pp.1304-1316, August 1959.

38. S. Muroga, *"Elementary Principle of Parametron and its Application to Computers"*, Datamation Res. & Eng., pp.31-34, Sept/Oct. 1958.

39. *"Sola Standart Sinusoidal Constant Voltage Transformers"*, Bulletin No. CVS-3631, Sola Electric Co., Chicago, Ill., February 1961. A considerable literature exists for ferroresonant transformers, e.g. see Chapter III, reference 5 cited for Chapter IV.

40. S.D. Wanlass et al, *"The Paraformer, A New Passive Power Conversion Device"*, IEEE, Wescon Technical Papers, Vol. 12, No. 2, p.17/2, 1968.

41. L.K. Wanlass, *"Parametric Device"*, British Patent No. 1,206,279, filed 24 Oct. 1967.

42. L.K. Wanlass, *"Improvements in or relating to Variable Inductor Devices"*, British Patent No. 1,153,901, filed 13 May, 1966.

43. L.K. Wanlass, *"Electrical Energy Translating Devices and Regulators Using the Same"*, U.S. Patent No. 3,403,323, filed May 14, 1965, issued Sept. 24, 1968.

44. W.H.T. Holden, *"Electrical Systems for Rapid Transit Railroads"*, IEEE Trans. on Ind. and Gen. App., Vol. IGA-7, No. 5, pp.580-587, Sept/Oct. 1972.

45. K. Burian, *"Theory and Analysis of a Parametrically Excited Passive Power Converter"*, IEEE Trans. on Ind. App., Vol. IA-8, No. 3, pp.278-282, May/June 1972.

46. W.Z. Fam and R.P. Verma, *"Theory and Performance of Parametric Transformers"*, IEEE Trans. on Power App. and Sys. Vol. PAS-91, pp.2494-2503, Nov./Dec. 1972.

47. B.K. Jones, *"Parametric Oscillators and Amplifiers"*, Physics Education, Vol. 8, pp.310-214 (Part I), 374-376 (Part II), 1973.

48. I.R. Smith and E.S. Tez, *"Der Parametrische Transformator, Prinzipien und Eigenshaften eines interressanten Bauelements"*, Elektrotechnik, Vol. 57, No. 1/2, pp.10/12, 23 January 1975.

49. Z.H. Meiksin, *"Comparison of Orthogonal and Parallel-Flux Variable Inductors"*, IEEE Trans. on Ind. App., Vol. IA-10, No. 3, pp.417-423, May/June 1974.

50. Z.H. Meiksin, *"Orthogonal Flux Parametric Voltage Regulator"*, ibid pp.424-427.

51. Z.H. Meiksin, *"Parallel-Flux Parametric Voltage Regulator and Comparison with Orthogonal-Flux Parametric Voltage Regulator"*, ibid. pp.428-430.

52. W.Z. Fam and G.K. Bahl, *"Two Related Types of Parametric Transformers"*, IEEE Trans. on Magnetics, Vol. Mag-10, No. 3, pp.690-693, Sept. 1974.

53. K. Bessho, F. Matsumura and M. Suzuki, *"Some Experiments and Considerations on Behaviour of the Power Converter with Bridge-Connected Reactor Circuit"*, IEEE Trans. on Magnetics, Vol. Mag-10, No. 3, pp.965-968, Sept.1974.

54. K. Bessho, F. Matsumura, Y. Aoki and M. Suzuki, *"Theory and Analysis of a New Power Converter with Centre-Tap Reactor Circuit"*, IEEE Trans. on Magnetics, Vol. Mag-11, No. 5, pp. 1558-1560, Sept. 1975.

55. H.M. Power, *"Analysis of a Passive Power Converter as a Non-linear Feedback System"*, IEEE Trans. on Ind. App., Vol. IA-11, No. 5, pp.556-559, Sept/Oct. 1975.

REFERENCES FOR CHAPTER II

1. See references 41-43 cited for Chapter I.

2. See reference 12 cited for Chapter X.

3. See references 37,38 cited for Chapter I.

REFERENCES FOR CHAPTER III

1. See reference 11, cited for Chapter I.

2. See reference 6, cited for Chapter I.

3. W.J. Cunningham, *"Introduction to Non-linear Analysis"*, McGraw-Hill, N.Y. 1958, Section 9.4b, pp.265-267.

4. See Section 2.17, op.cit. reference 1.

5. See Sections 2.13 and 2.14, op.cit, reference 1.

6. See reference 7, cited for Chapter I.

7. See Section 4.30, op. cit, reference 1.

8. C. Hayashi, *"Non-linear Oscillations in Physical Systems,"* McGraw Hill, 1964.

9. See reference 9, cited for Chapter 1.

10. N. Minorsky, *"On Parametric Excitation"*, Journal of Franklin Institute, Vol. 240, pp.25-46, 1945.

11. N. Minorsky, *"Non-linear Oscillations"*, D. Van Nostrad Co., 1962, p.505.

12. See Section 4.11, op. cit, reference 1.

13. See Section 9.4a, pp.261-265, op. cit, reference 3.

14. See Section 4, Chapter 20, pp.495-498, op. cit, reference 11.

15. See Section 7, Chapter 20, pp. 506-509, op. cit, reference 11.

16. T. Stern, *"Theory of Non-linear Networks and Systems"*, Addison-Wesley, Mass., 1965, and many text books on the theory of non-linear differential equations, such as those cited in references 3, 8 and 11.

17. This method was first applied by Van der Pol in *"Forced Oscillations in a Circuit with Non-linear Resistance"*, Phi. Mag, Ser. 7, No. 3, pp. 65-80, 1927, and was subsequently used by many authors such as Andronow and Witt, reference 28, cited for Chapter I and Hayashi, op-cit, reference 8.

18. N.. Bogoliubov and J. Mitropolsky, *"Asymptotic Methods in the Theory of Non-linear Oscillations"*, Russian edition: Moscow, 1958; English Edition: Delhi, Hindustan Publishing Corp., 1961.

19. J. Mitropolsky, *"Problems of the Asymptotic Theory of Non-stationary Vibrations"*, Russian Edition: Moscow 1964; English Edition: Jerusalem, Israel Program for Scientific Translations Ltd., 1965.

20. See Section 11.3, pp. 496-518, op. cit, reference 16.

21. See Chapter 16, op. cit, reference 11.

22. See reference 37, cited for Chapter I.

23. See Section 11.3.2, op. cit, reference 16.

24. R.A. Willoughby, *"An Analysis of the Bistability of the Parametron"*, Int. Symp. on Nonlin. Dif. Eq. and Nonlin. Mech., J.P. Salle and S. Lefschetz, N.Y. Academic Press, 1963.

25. See Section 8, Chapter 20, op. cit, reference 11.

26. J.M. Manley and H.E. Rowe, *"Some General Properties of Non-linear Elements I, General Energy Relations"*, Proc. IRE, Vol. 44, pp. 904-913, 1956.

27. H.E. Rowe, *"Some General Properties of Non-linear Elements II, Small Signal Theory"*, Proc. IRE, Vol. 46, pp. 850-860, 1958.

28. J.M. Manley, *"Some Properties of Time-Varying Networks"*, IRE, Trans. on Circuit Theory, Vol. CT-7, pp. 69-78, 1960.

29. P. Penfield, *"Frequency-Power Formulas"*, Cambridge, Mass., M.I.T. Press, 1960.

30. S. Oshima, H. Enomoto and S. Watanabe, *"Analysis of Parametrically Excited Circuits - Parametron and Magnetic Amplifiers"*, Journal of Inst. El. Comm. Eng. of Japan, Vol. 41, pp. 971-978, 1958.

31. K.A. Samoilo, *"The Development of Phase-Pulse Method for Near to Conservative Second-Order Systems with Non-Linear Reactance"*, IZV. VUZ Radioteknika, Vol. 7, No. 5, pp. 545-555, 1964.

32. K.A. Samoilo, *"Synchronization of Harmonic Oscillations, Generators, and Parametric Oscillators and Amplifiers"*, MIREA, Moscow, 1967.

33. K.A. Samoilo, T.S. Fedosova and A.Y. Spasov, *"Generalization of the Phase-Pulse Method for Second-Order Systems with Non-linear Reactance for Non-autonomous Systems"*, Proc. MEI, Elektroteknika, pp. 142-153, 1965.

34. A.Y. Spasov, *"Free Oscillations in Non-linear Oscillating Circuit"*, Electronics Letters, Vol. 3, No.6, pp. 259-261, June 1967.

35. A.Y. Spasov, *"Parametric Resonance in an Oscillating Circuit Utilising Non-linear Capacitance"*, Electronics Letters, Vol. 4, No. 13, pp. 264-265, June 1968.

36. A.Y. Spasov, *"Forced Oscillations in an Oscillating Circuit Utilising Non-linear Capacitance"*, Electronics Letters, Vol. 4, No. 17, August 1968.

37. A.Y. Spasov, *"Oscillating Circuit Using Non-linear Inductance"*, Electronics Letters, Vol. 5, No. 11, pp. 241-243, May 1969.

38. A.Y. Spasov and I. Angelov, *"Forced Oscillations and Parametric Resonance in an Oscillatory Circuit with Non-linear Inductance"*, Bulletin of the Inst. of Electronics, Bulgarian Academy of Sciences, Vol. 6, pp. 105-111, 1972.

39. J.J. Stoker, *"Non-linear Vibrations in Mechanical and Electrical Systems"*, Interscience Publishers, N.Y., 1950, and many other text books such as references 3, 8, 11 and 16.

40. W.T. Clary, Jr., *"Non-linear Resonant Circuit Devices"*, U.S. Patent, No. 2,838,687, issued June 10, 1958.

REFERENCES FOR CHAPTER IV

1. A. Mandelstam, N. Paplexi, et al, *"Expose Des Decherces Recentes Sur les Oscillations NonLineaires"*, Tech.Pys. USSR, Leningrad, Vol. 2, pp.81-134, 1935.

2. H.F. Storm, *"Magnetic Amplifiers"*, p.62, John Wiley & Sons, New York, 1955.

3. See, for example, *"Tranduktor Technik"*, AEG Mitteilungen, Vol. 49, No. 8/9, pp.329-352, 1959.

4. See *"The International Dictionary of Physics and Electronics"*, p.32, D. Van Nostrad Co., Inc., Princeton, N.Y. 1956.

5. W.A. Geyger, *"NonLinear Magnetic Control Devices"*, p.30, McGraw Hill Book Co. Inc., New York, 1969.

6. C.F. Burgess and B. Frankenfield, *"Regulation of Electric Circuits"*, U.S. Patent 720,884, issued February 17, 1903.

7. C.F. Burgess and B. Frankenfield, *"Means for Regulating Self-Inductance in Electric Circuits"*, U.S. Patent 743,444, issued November, 1903.

8. Storm, op. cit, reference 2.

9. A.G. Milnes, *Transductors and Magnetic Amplifiers"*, St. Martins Press, New York, 1957.

10. E.H. Frost-Smith, *"The Theory and Design of Magnetic Amplifiers"*, John Wiley and Sons, New York, 1958.

11. L.K. Wanlass, *"Improvements in or Relating to Variable Inductor Devices"*, British Patent 1,153,301, Complete Specification published June 4, 1969.

12. L.K. Wanlass, *"Parametric Device"*, British Patent 1,206,279, Complete specification published September 23, 1970.

13. See Figure 3, C.F. Burgess and B. Frankenfield, op. cit, reference 6.

14. See Figure 6, C.F. Burgess and B. Frankenfield, op. cit, reference 6.

15. R.J. Spreadbury, *"A New Parametric Device for Filtering and Voltage Stabilization"*, Westinghouse Engineering, Vol. 31, No. 2, pp.42-45, March 1971.

16. R.J. Spreadbury, *"A Parametric Device for Filtering and Voltage Stabilization"*, Electronics and Instrumentation, December 1971, pp.17-21.

17. See Figure 5, C.F. Burgess and B. Frankenfield, op. cit, reference 6.

18. A.A. Jaecklin, *"A Multiaperture Magnetic Control Device"*, IEEE Trans. on Magnetics, Vol. Mag-2, No. 3, pp.356-359, September 1966.

19. S. Tominaga, *" Magnetic Modulators"*, U.S. Patent No. 2,990,521, issued June 27, 1961.

20. M.K. Haynes, et al, *"Magnetic Shift Register"*, U.S. Patent 3,106,702, issued October 8, 1963.

21. E.L. Woods, *"Magnetic Memory Device"*, U.S. Patent 3,056,118, issued September 25, 1962.

22. J.A. Rajchman et al, *"Magnetic Systems"*, U.S. Patent 3,093,817, issued June 11, 1963.

23. R.A. Hertz and H. Buelteman, Jr., *"The Application of Perpendicularly Superposed Magnetic Fields"*, AIEE Transactions, Vol. 74, Part I, pp.655-660, November 1955.

24. D.W. Boensel, *"Theory and Operation of a Cross-Field Magnetic Modulator"*, Spec. Tech. Conf. on Non-linear Magnetics and Mag. Amps., AIEE & IRE, Aug. 1958, pp.370-387.

25. D.A. Buck and W.I. Frank, *"Nondestructive Sensing of Magnetic Cores"*, AIEE Transactions, Vol. 72, Part I, pp.822-832, January 1954.

26. W. McMurray, *"Analog Division Circuit"*, Spec.Tech.Conf. on Non-linear Magnetics & Mag. Amps., AIEE &IRE, Aug.1958, pp.113-129.

27. A.H. Bobeck, *"Magnetic Translating Circuit"*, U.S. Patent 2,985,768, issued May 23, 1961.

28. C.L. Wanlass, *"Logis System Gating Circuit"*, U.S. Patent 3,060,410, issued October 23, 1962.

29. C.L. Wanlass, *"Magnetic Memory Device with Orthogonal Intersecting Flux Paths"*, U.S. Patent 3,134,964, issued May 26, 1964.

30. R.H. Cornerly, et al, *"Magnetic Memory Employing Anisotropy"*, U.S. Patent 3,259,888, issued July 5, 1966.

31. D.S. Shull, Jr., and L.A. Finzi, *"An Investigation of the Quasi-static Magnetisation Process in Cross-Magnetized Multipath Ferrite Structures"*, IEEE Transactions on Magnetics, Vol. Mag-2, No. 1, pp.47-54, March 1966.

32. C.L. Wanlass, *"Flip-Flop Circuit"*, U.S. Patent 2,983,829, issued May 9, 1961.

33. C.L. Wanlass, *"Gating Circuit"*, U.S. Patent 3,061,820, issued October 30, 1962.

34. C.L. Wanlass, *"Impedance Gate"*, U.S. Patent 3,088,039, issued April 30, 1963.

35. C.L. Wanlass, *"Gating Circuit"*, U.S. Patent 3,097,305, issued July 9, 1963.

36. C.L. Wanlass, *"Magnetic Memory Core"*, U.S. Patent 3,124,785, issued March 10, 1964.

37. E.L. Woods, *"Magnetic Device"*, U.S. Patent 3,060,321, issued October 23, 1962.

38. E.L. Woods, *"Multiaperture Core Memory System"*, U.S. Patent 3,238,517 issued March 1, 1966.

39. H.J. McCreary, *"The Magnetic Cross-Valve and its Application to Sub-frequency Power Generation"*, Proceeding of the National Electronics Conference, Vol. 5, pp.450-466, October 1949.

40. H.J. McCreary, *"The Magnetic Cross Valve"*, AIEE Transactions, Vol. 70, Part II, pp.1868-1875, October 1951.

41. H.J. McCreary, *"Magnetic Frequency Changer"*, U.S. Patent No. 2,445,857, issued July 27, 1948.

42. H.J. McCreary, *"Frequency Changer"*, U.S. Patent No. 2,455,078, issued November 30, 1948.

43. H.J. McCreary, *"Magnetic Frequency Reducer"*, U.S. Patent No. 2,461,992, issued February 15, 1949.

44. H.J. McCreary, *"Magnetic Frequency Changer having Partial Gaps"*, U.S. Patent No. 2,567,116, issued September 4, 1951.

45. H.J. McCreary, *"Magnetic Frequency Divider"*, U.S. Patent No. 2,602,153, issued July, 1 1952.

46. H.J. McCreary, *"Frequency Generator Employing a Magnetic Double Cross Valve"*, U.S. Patent No. 2,611,119, issued September 16, 1952.

47. H.J. McCreary, *"Magnetic Cross Valve Having Self-starting Characteristics"*, U.S. Patent No. 2,611,120, issued September 16, 1952.

48. H.J. McCreary, *"Voltage Regulating System"*, U.S. Patent No. 2,623,205, issued December 23, 1952.

49. H.J. McCreary, *"Magnetic Cross Valve Circuits"*, U.S. Patent No. 2,703,388, issued March 1, 1955.

50. W.H. Higa, *"Theory of Magnetic Cross Valves"*, AIEE, Transactions, Vol. 74, Part I, pp.204-208, March 1955.

51. See Figure 7, C.F. Burgess and B. Frankenfield, op. cit, reference 6.

52. See references 45, 46, 49 and 55 cited for Chapter I. It is understood that orthogonality in the physical construction of the devices has given to the authors such impression that they consider the commercial paraformers as orthogonal flux systems.

53. L.K. Wanlass, *"Electrical Energy Translating Devices and Regulators Using the Same"*, U.S. Patent No. 3,403,323, issued September 24, 1968.

REFERENCES FOR CHAPTER V

1. See, for example, reference 16, cited for Chapter III.

2. See textbooks such as *"Electromechanics and Machines"*, by R.E. Steven, Chapman and Hall, 1970.

3. J. Hindmarsh, *"Large de machine performance and design"*, series of articles in Electrical Times, Vols. 134-135, 1958-59.

4. Bean, Chackan, Moore and Wentz, *"Transformers for the Electric Power Industry"*, McGraw Hill, 1959.

5. K.A. Mcfadyen, *"Small Transformers and Inductors"*, Chapman and Hall, London, 1953.

6. A.S. Jackson, *"Analog Computation"*, McGraw Hill, 1960, Section 4.5.

7. A.S. Charlesworth and J.R. Fletcher, *"Systematic Analogue Computer Programming"*, Isaac Pitman and Bath Univ. Press, 1970, Section 12.3.

8. See Section 11.4, op. cit, reference 7.

REFERENCES FOR CHAPTER VI

1. See, for example, references 8-10 cited for Chapter IV.

2. Graphical treatment for analysing saturable reactors dates back to the beginning of the century. A concise treatment is given by W.C. Johnson, et al, *"Universal Curves for DC Controllable Reactors"*, AIEE Transactions, Vol. 68, pp.31-40, 1949.

REFERENCES FOR CHAPTER VII

1. P. Silvester, H.S. Cabayan, and B.T. Browne, *"Efficient Techniques for Finite Element Analysis of Electric Machines"*, IEEE Trans. on Power Apparatus and Systems, Vol. PAS-92, No. 4, pp.1274-1281, July/August 1973.

2. F.C. Trutt, E.A. Erdelyi, and R.E. Hopkins, *"Representation of the Magnetisation Characteristic of DC Machines for Computer Use"*, IEEE Trans. on Power App. and Systems, Vol. PAS-87, No. 3, pp.665-669, March 1968.

3. G.F.T. Widger, *"Representation of Magnetisation Curves over Extensice Range by Rational-Fraction Approximations"*, Proc. IEE, Vol. 116, No. 1, pp.156-160, January 1969.

4. R.J. Kavanagh, *"An Approximation to the Harmonic Response of Saturating Devices"*, Proc. IEE, Vol. 107C, pp.127-133, 1960.

5. M. Kosicka, *"Research of Dynamic Performance of ac Machine Excitation with a Parabolic Approximation of the Magnetisation Curve"*, Prague Instytut Electrotechniki, Vol. 18, No. 65, pp.37-48, 1970.

6. S. Lehman, *"Analytical Representation of Magnetisation Characteristics for Digital Computation"*, Elektronische Datenverarbeitung, Vol. 6, pp.165-172, August 1964.

7. S. Masters, *"Contribution a la determination des reptes dans les toles ferromagnetiques"*, PhD Thesis, Faculte Polytechnique de Mons, Belgium, 1968.

8. M.K. El-Sherbing, *"Representation of the Magnetisation Characterstic by a Sum of Exponentials"*, IEEE Trans. on Magnetics, Vol. MA6-9, No. 1, pp.60-61, March 1973.

9. J.R. Brauer, *"Simple Equations for the Magnetisation and Reluctivity Curves of Steel"*, Electronic Letters, No. 11, p.81, 1974.

10. R. Langman, *Measurement of Reverse Permeability Using Solid Specimens"*, Proc. IEE, Vol. 117, No. 9, September 1970.

11. T. Spooner, *"Permeability"*, Trans. AIEE, Vol. 13, pp.1887-90, February 1923.

12. A.B. Goral, *"Characterization of Ferromagnetics as Working in the Parametrically Excited Circuits"*, IEEE Trans. on Magnetics, Vol. MAG-2, No. 3, pp.543-6, September 1966.

REFERENCES FOR CHAPTER VIII

1. *"English Electric C Cores, a Handbook for Designers of Transformers for the Electronic Industry"*, Publication TF/229B, third edition, The English Electric Co. Ltd., Liverpool.

2. See reference 2, cited for Chapter VII.

3. L. Fox and D.F. Mayers, *"Computing Methods for Scientists and Engineers"*, Clarendon Press, Oxford, 1968.

4. P.W. Williams, *"Numerical Computation"*, T. Nelsons and Sons Ltd., 1972.

5. D. McCracken and W.S. Dorn, *"Numerical Methods and Fortran Programming"*, John Wiley and Sons, Inc., 1966.

6. G. Peckham, *"A New Method for Minimising a Sum of Squares without Calculating Gradients"*, Computer J., Vol. 13, pp. 418-420, 1970.

7. M.J.D. Powell, *"A Fortran Subroutine for Solving Systems of Non-linear Algebraic Equations"*, Harwell Report, AERE-R5947, H.M. Stationery Office, 1968.

8. G.E. Forsythe, *"Generation and Use of Orthogonal Polynomials for Data-Fitting with a Digital Computer"*, S.I.A.M. Journal, No. 5, 1957.

REFERENCES FOR CHAPTER IX

1. *"Telmag Strip Wound C-type Cores in Grain Oriented Silicon-Iron"*, Publication Ref. No. TC.1/8/14, Telcon Magnetic Cores Ltd., Airdrie, Lanarks., Also, *"Handbook for Designers of Transformers for the Electronic Industry"*, 3rd Edition, Publication Ref. No. TF/229B, The English Electric Co. Ltd., Liverpool 10.

2. Many books on Electrical Technology, e.g. H. Cotton, *"Advanced Electrical Technology"*, Sir Isaac Pitman, London, 1967.

3. *"Line Conditioners and Regulators"*, Publication Ref. No. 203, Tele-dynamics/Wanlass, Division of Ambac Ind. Inc., Fort Washington, PA 19034.

4. See page 27 of reference 16 cited for Chapter III, for a discussion on non-conservative non-linear inductors.

REFERENCES FOR CHAPTER X

1. See reference 5 cited for Chapter IV.

2. See reference 42 cited for Chapter I.

3. See reference 43 cited for Chapter I.

4. See reference 3 cited for Chapter IX.

5. *"Power Supplies and Line Conditioners"*, Publication Ref. No. 301, Teledynamics/Wanlass, Division of Ambac. Ind. Inc., Fort Washington. PA 19034.

6. See reference 40 cited for Chapter I.

7. Wanlass Electric Co., *"High Frequency Parametric Voltage Regulator"*, British Patent No. 1,287,133, filed 30 Oct. 1969.

8. K. Murakami and E. Miyazawa, *"A new DC-AC converter by a combination of Royer's circuit and parametric excitation"*, IEEE Trans. on Magnetics, Vol. MAG-10, No. 4, pp.1129-1132, Dec. 1974.

9. G.H. Royer, *"A Switching Transistor DC to AC Converter having an Output Frequency Proportional to the DC Input Voltage"*, Trans. AIEE (Comm. and Elect), Vol.74, pp.322-326, July 1955.

10. See Chapters 1 and 10, op. cit, reference 1.

11. See references 24, 31 cited for Chapter I and references 39-49 cited for Chapter IV.

12. L.K. Wanlass, *"Parametric Device"*, British Patent No. 1,301,123, filed 5 May 1970, complete spec. published 29 Dec. 1972.

13. See reference 44 cited for Chapter I.

14. W.F. Zam, *"Parametric Motor"*, U.S.Patent No. 3,716,734 filed Oct. 18. 1971. issued Feb. 13. 1973.

APPENDIX I

THE AMPLITUDE OF THE FUNDAMENTAL FREQUENCY COMPONENT[1]

Using the method of harmonic balance, a solution assumed as

$$\phi_2 = A \cos z + B \cos 3z \qquad \ldots\ldots \qquad (1)$$

is introduced into the differential equation

$$\frac{d^2 \phi_2}{dz^2} + (a - 2q \cos 2z)\, \phi_2 + g\, \phi_2^{\,3} = 0 \qquad (2)$$

When only the fundamental and the third harmonic are considered, and the coefficients of $\cos z$ and $\cos 3z$ are equated to zero, the equations obtained are

$$A(a - 1 - q) - Bq + \frac{g}{4}(3A^3 + 3A^2B + 6B^2) = 0 \qquad (3)$$

and

$$(a - 9)\, B - Aq + \frac{g}{4}(A^3 + 6A^2B + 3B^3) = 0 \qquad (4)$$

which may be solved for A and B.

Firstly, assuming $B \simeq 0$ and neglecting therefore terms in B in equation (3) yields

$$A(a - 1 - q) + \frac{3}{4}\, g\, A^3 = 0 \qquad \ldots\ldots \qquad (5)$$

giving a zero-order approximation for the amplitude of the secondary flux as

$$A^2 \simeq \frac{4}{3g}\,(1 - a + q) \qquad \ldots\ldots \qquad (6)$$

which is the same as equation (3.113) in Chapter III, evaluated only for the fundamental term. To obtain a better approximation, although with B still considered small, terms of the order of $\frac{B}{A}$ are not neglected, although $\left|\frac{B}{A}\right| < 1$. On neglecting B^2 term in equation (3), and dividing both sides by A, it follows that

$$a - 1 - q - \frac{B}{A}\,q + \frac{3}{4}\,g\,A^2\,(1 + \frac{B}{A}) = 0 \qquad (7)$$

from which A^2 is obtained as

$$A^2 = \frac{4}{3g}\,\{[1 - a + q\,(1 + \frac{B}{A})]\,\frac{1}{(1 + \frac{B}{A})}\} \qquad (8)$$

By expanding the rational fraction $\frac{1}{1+\frac{B}{A}}$ into a power series and neglecting all but the first two terms,

$$\frac{1}{1 + \frac{B}{A}} \simeq 1 - \frac{B}{A} \qquad \ldots\ldots \qquad (9)$$

On substituting equation (9) into equation (8), and neglecting the term in $\frac{B^2}{A^2}$, equation (8) takes the form

$$A^2 \simeq \frac{3}{4g}\,[1 + q - a + (a - 1)\,\frac{B}{A}] \qquad \ldots\ldots \qquad (10)$$

Neglecting B^3 term in equation (4) and dividing both sides by A^3, it follows that

$$(a - g)\frac{B}{A^3} - \frac{q}{A^2} + \frac{g}{4}\left(1 + 6\frac{B}{A}\right) = 0 \qquad \ldots\ldots \qquad (11)$$

To calculate $\frac{B}{A}$ from this equation, the zero-order approximation for A^2 in equation (6) is substituted into equation (11), giving

$$\frac{B}{A} \simeq \frac{2q + a - 1}{3(2q - a - 7)} \qquad \ldots\ldots \qquad (12)$$

Substituting from equation (12) for $\frac{B}{A}$ in equation (10) gives the amplitude of the fundamental frequency component in the secondary flux as

$$A^2 \simeq \frac{4}{3g}\left[1 + q - a + (a - 1)\frac{2q + a - 1}{3(2q - a - 7)}\right] \qquad (13)$$

which is a better approximation then equation (6).

1. See section 7.230 in reference 12 cited for Chapter I.

APPENDIX II

HARMONIC DISTORTION IN THE SECONDARY FLUX WITH A SQUARE-WAVE INPUT VOLTAGE

When the resistance of the primary circuit is neglected, a square-wave input voltage results in a triangular waveform of primary flux, which may be expressed in a Fourier series as

$$\phi_1 = \phi_{1m} \frac{8}{\pi^2} (\sin z + \frac{1}{9} \sin 3z + \frac{1}{25} \sin 5z + \ldots) \qquad (1)$$

Since, normally, $\phi_{1m} < \phi_s$ (saturation flux level), it is sufficient to take the trans-reluctance characteristic as

$$R_{m2} = R_{m2min} + \Gamma_1 \phi_1^2 \qquad \ldots\ldots \qquad (2)$$

which leads to a Hill equation, in which the θ coefficients are

$$\theta_0 = \frac{1}{\omega^2 N_2^2 C} [R_{m2min} + \frac{41}{81} \Gamma_1 (\frac{8 \phi_{1m}}{\pi^2})^2]$$

$$\theta_1 = \frac{1}{2\omega^2 N_2^2 C} [- \frac{7}{18} \Gamma_1 (\frac{8 \phi_{1m}}{\pi^2})^2]$$

(3)

$$\theta_2 = \frac{1}{2\omega^2 N_2^2 C} [- \frac{1}{9} \Gamma_1 (\frac{8 \phi_{1m}}{\pi^2})^2]$$

and $$\theta_3 = \frac{1}{2\omega^2 N_2^2 C} [- \frac{1}{162} \Gamma_1 (\frac{8 \phi_{1m}}{\pi^2})^2]$$

when only first two terms in equation (1) are taken into account.

The amplitude of the third harmonic in equation (3.206) may be taken as, approximately,

$$A = \frac{1}{8} (\theta_1 + \theta_2) \qquad \ldots\ldots \qquad (4)$$

since $\theta_1 < 1$ and $\theta_2 < 1$. On substituting for θ_1 and θ_2, equation (4) becomes

$$A = -\frac{1}{32} \frac{1}{\omega^2 N_2^{\,2} C} \Gamma_1 \left(\frac{8 \phi_{1m}}{\pi^2} \right)^2 \qquad \ldots\ldots \qquad (5)$$

If θ_0 is equated to unity, by proper adjustment of the secondary resonant circuit, the ratio of the amplitude of the fundamental to that of the third harmonic in the secondary flux is

$$\frac{1}{|A|} = \frac{\theta_0}{|A|} = \frac{R_{m2min} + \frac{41}{81} \Gamma_1 \left(\frac{8 \phi_{1m}}{\pi^2} \right)^2}{\frac{1}{32} \Gamma_1 \left(\frac{8 \phi_{1m}}{\pi^2} \right)^2} \simeq \frac{\pi^4}{2} \frac{R_{m2min}}{\Gamma_1 \phi_{1m}^{\,2}} + 16$$

$$\ldots\ldots \qquad (6)$$

The ratio $\frac{R_{m2min}}{\Gamma_1 \phi_{1m}^{\,2}}$ is a measure of the modulation depth in the secondary reluctance variations, as the modulation index from equation (2.8) (Chapter 2) is

$$m = \frac{\frac{\Gamma_1}{2} \phi_{1m}^{\,2}}{R_{m2min} + \frac{\Gamma_1}{2} \phi_{1m}^{\,2}} \qquad \ldots\ldots \qquad (7)$$

In normal operation, $\phi_{1m} < \phi_s$ and m is small. However, even with a modulation depth value of 25%, equation (6) gives

$$\frac{1}{|A|} \simeq 79$$

or, inversely, the ratio of the amplitudes of the third harmonic to the fundamental is of the order of $\frac{1}{80} = 1.25\%$, which establishes the filtering ability of the parametric transformer. Obviously, the greater the modulation depth becomes as ϕ_{1m} is increased, the more distorted becomes the output waveform, indicating that this is dependent on the primary flux amplitude rather than the waveform of the primary flux.

APPENDIX III

NON-UNIFORM FLUX DISTRIBUTION IN THE HOLLOW TOROID CORE

When the secondary winding only is driven by a voltage source, the secondary flux created is distributed in the toroidal core of Figure 4.46, with the flux density varying as

$$B_2(\alpha) = \frac{\phi_2}{A_2(\alpha)} \qquad (1)$$

where $$A_2(\alpha) = a - b\cos\alpha \qquad (2)$$

and $$a = 2\pi R\,(R_2 - R_1) \qquad (3)$$

$$b = \pi\,(R_2^{\,2} - R_1^{\,2}) \qquad (4)$$

as given in equation (4.63). If the magnetisation characteristic of the core material is given by

$$H - f(B) = c_1 B + c_3 B^3 + c_5 B^5 + \ldots.$$

then, $$H_2 = H_2(\alpha) = f\left(\frac{\phi_2}{A_2(\alpha)}\right) = c_1 \frac{\phi_2}{(a - b\cos\alpha)} + c_3 \frac{\phi_2^{\,3}}{(a - b\cos\alpha)^3} + c_5 \frac{\phi_2^{\,5}}{(a - b\cos\alpha)^5} + \ldots. \qquad (5)$$

Applying the circuital law of magnetism to the secondary magnetic circuit, the secondary mmf is

$$F_2 = \oint H_2 \, d\ell$$

$$= \int_0^{2\pi} H_2(\alpha) \, r d\alpha = r \int_0^{2\pi} H_2(\alpha) \, d\alpha \qquad (6)$$

by the change of variable $d\ell = r \, d\alpha$, where $r = \frac{R_2 + R_1}{2}$.

Substituting for $H_2(\alpha)$, the integral becomes

$$F_2(\phi_2) = \frac{R_2 + R_1}{2} \left[c_1 \cdot \phi_2 \int_0^{2\pi} \frac{d\alpha}{a - b \cos\alpha} + c_3 \, \phi_2^3 \int_0^{2\pi} \frac{d\alpha}{(a - b \cos\alpha)^3} \right.$$

$$\left. + c_5 \, \phi_2^5 \int_0^{2\pi} \frac{d\alpha}{(a - b \cos\alpha)^5} + \ldots \right] \qquad (7)$$

Upon integration, α vanishes from the expression, and the function $F_2(\phi_2)$ is obtained in the form

$$F(\phi_2) = S_1 \, \phi_2 + S_3 \, \phi_2^3 + S_5 \, \phi_2^5 + \ldots$$

where the coefficients S_1, S_3, S_5, ... are functions of both the physical dimensions R, R_2, R_1 and the coefficients of the magnetisation characteristic. The dependence of the S on R, R_1 and R_2 is quite complex and very tedious to derive, as would be expected from the form of the integral. Even the simplest integral in equation (7), in its indefinite form, gives*

---

* See page 78, "Mathematical Handbook," by M.R. Spiegel, Schaum's Outline Series, McGraw Hill, 1968.

$$\int \frac{d\alpha}{a - b\cos\alpha} = \frac{1}{\sqrt{b^2 - a^2}} \ln \left(\frac{\tan\frac{\alpha}{2} + \sqrt{(b-a)/(a+b)}}{\tan\frac{\alpha}{2} - \sqrt{(b-a)/(a+b)}} \right)$$

where a and b are functions of R, R_1 and R_2, as given by equations (3) and (4). This illustrates the complexity of the form of the function $F_2(\phi_2)$ which is even much more difficult to obtain in the form $F_2(\phi_1, \phi_2)$ when ϕ_1 is also present and orthogonal flux interaction occurs.

If it is assumed that $R \gg R_1$ and R_2, b may be taken as zero, and the constant (mean) value of A_2 is $A_2 = a$. Equation (7) then becomes

$$F_2(\phi_2) = \frac{R_2 + R_1}{2} \left[\frac{c_1 \phi_2}{a} \int_0^{2\pi} d\alpha + \frac{c_3 \phi_2^{\,3}}{a^3} \int_0^{2\pi} d\alpha + \frac{c_5 \phi_2^{\,5}}{a^5} \int_0^{2\pi} d\alpha + \ldots\ldots \right]$$

$$= \ell_2 \left(\frac{c_1}{A_2} \phi_2 + \frac{c_3}{A_2^{\,3}} \phi_2^{\,3} + \frac{c_5}{A_2^{\,5}} \phi_2^{\,5} + \ldots\ldots \right)$$

where $\ell_2 = \pi(R_2 + R_1)$ is the mean flux-path length, and A_2 is the mean orthogonal area for the secondary flux.

APPENDIX IV

APPLICATION OF POWER SERIES APPROXIMATION TO TWO-C-CORE DEVICE

The power series approximation of the B/H characteristic is

$$H = f(B) = \sum_{i=o}^{n} C_{2i+1} B^{2i+1} \qquad (1)$$

as given by equation (7.12). The $F_1(\phi_1, \phi_2)$ and $F_2(\phi_1, \phi_2)$ functions for the two-C-core device are

$$F_1(\phi_1, \phi_2) = R_g \phi_1 + \ell_1 . f(\frac{\phi_1}{A_1}) + \frac{1}{2} \ell_0 \left[f(\frac{\phi_1 + \phi_2}{2A_0}) + f(\frac{\phi_1 - \phi_2}{2A_0}) \right] \qquad (2)$$

$$F_2(\phi_1, \phi_2) = R_g \phi_2 + \ell_2 . f(\frac{\phi_2}{A_2}) + \frac{1}{2} \ell_0 \left[f(\frac{\phi_1 + \phi_2}{2A_0}) - f(\frac{\phi_1 - \phi_2}{2A_0}) \right] \qquad (3)$$

as given by equations (4.45) and (4.46). Introducing equation (1) into equation (2) gives

$$F_1(\phi_1, \phi_2) = R_g \phi_1 + \sum_{i=o}^{n} p_{2i+1} \phi_1^{2i+1}$$

$$+ \frac{1}{2} \left[\sum_{i=o}^{n} r_{2i+1} (\phi_1 + \phi_2)^{2i+1} + \sum_{i=o}^{n} r_{2i+1} (\phi_1 - \phi_2)^{2i+1} \right] \qquad (4)$$

where $$p_{2i+1} = \ell_1 \frac{C_{2i+1}}{(A_1)^{2i+1}} \quad (i=0,1,2....n) \qquad (5)$$

$$r_{2i+1} = \ell_0 \frac{C_{2i+1}}{(2A_0)^{2i+1}} \quad (i=0,1,2....n) \qquad (6)$$

Denoting the third term in equation (4) as F_a, its expansion gives

$$F_a = \frac{1}{2}\,[r_1(\phi_1 + \phi_2) + r_3(\phi_1 + \phi_2)^3 + r_5(\phi_1 + \phi_2)^5 + ...+r_{2n+1}(\phi_1 + \phi_2)^{2n+1}] +$$

$$\frac{1}{2}\,[r_1(\phi_1 - \phi_2) + r_3(\phi_1 - \phi_2)^3 + r_3(\phi_1 - \phi_2)^5 + ...+r_{2n+1}(\phi_1 - \phi_2)^{2n+1}]$$

(7)

Using the binomial formula to expand each term in equation (7) and making all possible cancellations, F_a becomes

$$F_a = \phi_1(r_1 + 3r_3\phi_2^{\,2} + 5\,r_5\,\phi_2^{\,4} + 7\,r_7\,\phi_2^{\,7} + ...) + \phi_1^{\,3}(r_3 + 10\,r_5\phi_2^{\,2} + 35\,r_7\,\phi_2^{\,4} +)$$

$$+ \phi_1^{\,5}\,(r_5 + 21\,r_7\,\phi_2^{\,2} + ...) + \phi_1^{\,7}\,(r_7 + ...) + ...$$

(8)

With a careful examination of Pascal's triangle shown on the next page, it is seen that F_a includes only those terms which correspond

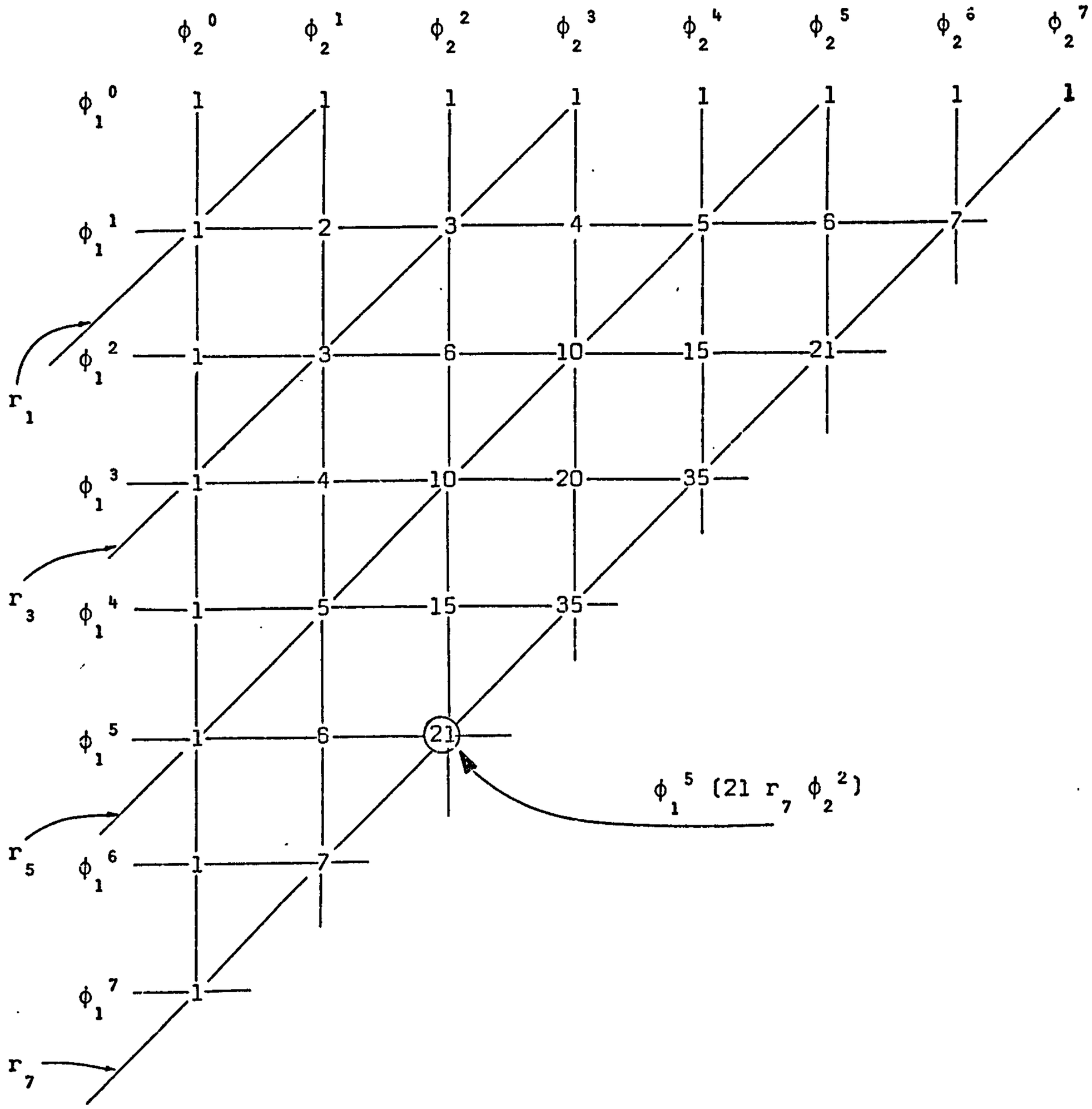

Pascal's Triangle

to those locations in the triangle where three different lines simultaneously intersect. (To illustrate this, one particular term corresponding to the location indicated is also shown). Equation (8) can thus be written in the form

$$F_a = \phi_1 \sum_{i=0}^{n} r_{2i+1} \binom{2i+1}{1} \phi_2^{2i} + \phi_1^3 \sum_{i=1}^{n} r_{2i+1} \binom{2i+1}{3} \phi_1^{2i-2} +$$

$$\phi_1^5 \sum_{i=2}^{n} r_{2i+1} \binom{2i+1}{5} \phi_2^{2i-4} + \phi_1^7 \sum_{i=3}^{n} r_{2i+1} \binom{2i+1}{7} \phi^{2i-6} + \ldots \tag{9}$$

where the binomial coefficients are given by

$$\binom{k}{\ell} = \frac{k!}{\ell!\,(k-\ell)!} \tag{10}$$

Changing i in equation (9) so that each sum starts from $i=0$, we obtain

$$F_a = \phi_1 \sum_{i=0}^{n} r_{2i+1} \binom{2i+1}{1} \phi_2^{2i} \quad \phi_1^3 \sum_{i=0}^{n-1} r_{2i+3} \binom{2i+3}{3} \phi_2^{2i} +$$

$$\phi_1^5 \sum_{i=0}^{n-2} r_{2i+5} \binom{2i+5}{5} \phi_2^{2i} + \phi_1^7 \sum_{i=0}^{n-3} r_{2i+7} \binom{2i+7}{7} \phi_2^{2i} + \ldots \tag{11}$$

which can be written as

$$F_a = \sum_{j=o}^{n} \phi_1^{2j+1} \cdot \sum_{i=o}^{n-j} r_{2(i+j)+1} \binom{2(i+j)+1}{2j+1} \phi_2^{2i} \qquad (12)$$

The whole function giving the primary mmf in terms of ϕ_1 and ϕ_2, is

$$F_1(\phi_1, \phi_2) = R_g \phi_1 + \sum_{i=o}^{n} p_{2i+1} \phi_1^{2i+1} + \sum_{i=o}^{n} \sum_{j=o}^{n-i} \phi_1^{2i+1} r_{2(i+j)+1} \binom{2(i+j)+1}{2i+1} \phi_2^{2j} \qquad (13)$$

Through the same procedure, the explicit expression for the secondary mmf is obtained as

$$F_2(\phi_1, \phi_2) = R_g \phi_2 + \sum_{i=o}^{n} s_{2i+1} \phi_2^{2i+1} + \sum_{i=o}^{n} \sum_{j=o}^{n-i} \phi_2^{2i+1} r_{2(i+j)+1} \binom{2(i+j)+1}{2i+1} \phi_1^{2j} \qquad (14)$$

where $$s_{2i+1} = \ell_2 \frac{C_{2i+1}}{(A_2)^{2i+1}}. \qquad (15)$$

APPENDIX V: PROGRAM LISTING, CURVE-FITTING

```
      MASTER MAIN
C
C     CURVE FITTING PROGRAM TO CALCULATE THE CONSTANTS X(1) AND X(2)
C     OF THE EQUATION
C     H=X(2)*SINH(X(1)*B)
C
      LOGICAL SING,LIM
      EXTERNAL FUNCT,MONIT
      DIMENSION R(15),H(15),B(15),C(15),X(2),V(2),W(800),F(15),RES(15),
     UT(15)
      COMMON H,B,T
C
C     DATA POINTS TAKEN FROM REFERENCE 1,CHAPTER VIII
C
      READ(1,10)B,C
 10   FORMAT(30G0.0)
C
C     CONVERSION OF FIELD INTENSITY UNIT FROM OERSTED TO A*TURN/M
C
      DO 20 I=1,M
      H(I)=C(I)*1000./(4.*PI)
 20   CONTINUE
C
C     SPECIFYING VARIOUS PARAMETERS
C
      N=2
      M=15
      IP=M+3+N/3
      IW=2*M+4*N+M*N+(N*N+N)/2+IP*(M*2+2*N)
      PI=4.*ATAN(1.)
      IFAIL=1
      IPRINT=2
      EPS=1.0E-8
      ALF=1.0E-5
      MAXIT=309
C
C     INITIAL VALUES OF PARAMETERS
C
      X(1)=5.7276454
      X(2)=0.014193963
      V(1)=2.0
      V(2)=1.0
      WRITE(2,50)X
 50   FORMAT(////32H0INITIAL ESTIMATES OF PARAMETERS,5X,
     15HX(1)=,E12.6,10X,5HX(2)=,E12.6/)
      WRITE(2,60)V
 60   FORMAT(/16H0VALUES OF V ARE//2F15.1/)
C
C     WEIGHTING FACTORS
C
```

```
      T(1),T(2),T(3),T(4),T(5),T(6),T(7)=1.0
      T(8),T(9),T(10),T(11),T(12),T(13)=10.0
      T(14),T(15)=2.0
C
C     CALL SUBROUTINE FOR CURVE FITTING
C
      CALL EU4FAF(M,N,X,R,S,EPS,ALF,V,W,IW,FUNCT,MONIT,IPRINT,
     1MAXIT,IFAIL)
C
C     FINAL ESTIMATES OF PARAMETERS
C
      WRITE(2,70)
 70   FORMAT(43H0FINAL LEAST SQUARE ESTIMATES OF PARAMETERS)
      WRITE(2,80)X
 80   FORMAT(/5X,5HX(1)=,E14.8,5X,5HX(2)=,E14.8//)
      WRITE(2,90)IFAIL
 90   FORMAT(9H0IFAIL = ,I1)
      WRITE(2,100)EPS
 100  FORMAT(7H0EPS = ,F4.0///)
C
C     DETERMINING APPROXIMATE CURVE AND COMPARING IT WITH ACTUAL CURVE
C
      WRITE(2,200)
 200  FORMAT(/8X,1HB,9X,1HC,12X,1HH,12X,3HFIT,12X,3HRES/)
      DO 1 I=1,M
      F(I)=X(2)*SINH(X(1)*B(I))
      RES(I)=F(I)-H(I)
 1    WRITE(2,300)B(I),C(I),H(I),F(I),RES(I)
 300  FORMAT(5X,F6.2,5X,F6.3,3F15.5)
      STOP
      END


      SUBROUTINE FUNCT(M,N,X,R)
      DIMENSION X(N),R(M),H(15),B(15),T(15)
      COMMON H,B,T
      DO 10 I=1,M
      R(I)=X(2)*SINH(X(1)*B(I))-H(I)
      R(I)=R(I)*T(I)
10    CONTINUE
      RETURN
      END


      SUBROUTINE MONIT(M,N,X,S,ITERC,SING,LIM)
      LOGICAL SING,LIM
      DIMENSION X(N)
      WRITE(2,10)ITERC
 10   FORMAT(11H0ITERATION ,I3)
      WRITE(2,20)S
 20   FORMAT(16H SUM OF SQUARES=,E14.6)
      WRITE(2,30)X
 30   FORMAT(20HVALUES OF PARAMETERS,5X,2E16.6)
      IF(SING)WRITE(2,40)
 40   FORMAT(9H SINGULAR)
      IF(LIM)WRITE(2,50)
 50   FORMAT(8H LIMITED)
      RETURN
      END
      FINISH
****
```

APPENDIX VI

DATA ON THE EXPERIMENTAL DEVICE

The physical dimensions of the bridged core equivalent (see Figure 4.39) of the parametric transformer constructed with three HWR110/20 cores were derived from the data in Figure 9.1 as

Primary main branch	Secondary main branch	Bridge branches
$A_1 = 0.0023\ m^2$	$A_2 = 0.0023\ m^2$	$A_0 = 0.00058\ m^2$
$\ell_1 = 0.196\ m$	$\ell_2 = 0.196\ m$	$\ell_0 = 0.07\ m$

The number of turns in each winding are:

$N_1 = 540$ $\qquad$ $N_2 = 540$

of SWG 13 gauge wire.

The inductance and resistance of each winding was measured as

$$L_1 \simeq L_2 = 0.588H$$

$$R_1 \simeq R_2 = 2.85\Omega$$

The nominal value of the secondary capacitor is

$$C = 20\ \mu F$$

and the nominal input and output voltages are

$V_1 = 220V$ $V_2 = 350V$

The power rating of the device is 250 VA.

APPENDIX VII: PROGRAM LISTING, VOLTAGE/CURRENT CHARACTERISTIC

```
      MASTERMAIN
C
C     PROGRAM TO DETERMINE THEORETICAL VOLTAGE/CURRENT CHARACTERISTIC
C     OF SECONDARY WINDING
C
      REAL L1,L2,L0,N1,N2,MMF1,MMF2,MU0,LG,I2,I2RMS
      DIMENSION Z(2),XI2RMS(35),XV2EFF(35),EXPI2(35)
      COMMON A1,L1,N1,A2,L2,N2,A0,L0,C1,C11,RG
C
C     READ PHYSICAL QUANTITIES AND EXPERIMENTAL DATA
C
      READ(1,1)A1,L1,N1,A2,L2,N2,A0,L0,C1,C11,LG,EXPI2
1     FORMAT(46G0.0)
C
C     APPROXIMATE EXPRESSION FOR THE MAGNETISATION CHARACTERISTIC IS
C     H(B)=C1*B+C11*B**11
C
C     WRITE ALL PARAMETERS
C
100   WRITE(2,10)
 10   FORMAT(/////5X,35HCOEFFICIENTS OF THE FUNCTION H=F(B)//)
      WRITE(2,20)C1,C11
 20   FORMAT(///5X,3HC1=,E14.9,5X,4HC11=,E14.9)
      WRITE(2,11)
 11   FORMAT(///5X,23HOTHER SYSTEM PARAMETERS///)
      WRITE(2,3)A1,L1,N1,R1,A2,L2,N2,R2,A0,L0
 3    FORMAT(5X,8HA1(SQM)=,E10.4,5X,6HL1(H)=,E10.4,5X,10HN1(TURNS)=,
     1E10.4,
     15X,9HR1(OHMS)=,E10.4///5X,8HA2(SQM)=,E10.4,5X,6HL2(H)=,E10.4,5X,
     110HN2(TURNS)=,E10.4,5X,9HR2(OHMS)=,E10.4///5X,8HA0(SQM)=,E10.4,5X,
     16HL0(H)=,E10.4///)
66    WRITE(2,25)LG
25    FORMAT(///5X,8HAIR GAP=,E8.2,4H (M)//)
C
C     AIR GAP RELUCTANCE
C
      PI=4.*ATAN(1.)
      W=100.*PI
      MU0=4.*PI*1.0E-07
      RG=LG/(MU0*A0)
C
C     DETERMINATION OF THEORETICAL V/I CHARACTERISTIC AND PLOTTING
C
      CALL UTPOP
      WRITE(2,27)
27    FORMAT(//////5X,12HV2EFF(VOLTS),10X,11HI2RMS(AMPS),10X,
     112HB0MAX(TESLA)/)
      CALL UTP4A(0.0,1.0,0.0,350.0,8.0,6.0,12HI2RMS (AMPS),2,13HV2RMS (V
     COLTS),2)
      V2EFF=10.
```

```
      DO 200 I=1,35
      F2M=V2EFF*SQRT(2.)/(N2*W)
      BOMAX=F2M/(2.*A0)
      SUM,X=0.0
      DO 300 J=1,20
      Z(2)=F2M*SIN(X)
      CALL TEZ(Z,MMF1,MMF2)
      I2=MMF2/N2
      SQI2=I2*I2
      SUM=SUM+SQI2
      X=X+PI/20.
300   CONTINUE
      I2RMS=SQRT(0.05*SUM)
      WRITE(2,28)V2EFF,I2RMS,BOMAX
28    FORMAT(8X,F7.1,12X,E12.6,12X,E12.6)
      XI2RMS(I)=I2RMS
      XV2EFF(I)=V2EFF
      V2EFF=V2EFF+10.
200   CONTINUE
      CALL UTP4B(EXPI2,XV2EFF,35,0)
      CALL UTP4B(XI2RMS,XV2EFF,35,0)
      CALL UTPCL
      STOP
      END


      SUBROUTINE TEZ(Z,MMF1,MMF2)
C
C     THIS SUBROUTINE CALCULATES PRIMARY AND SECONDARY MMF'S,MMF1 AND
C     MMF2,FROM GIVEN VALUES OF PRIMARY AND SECONDARY FLUXES,Z(1) AND
C     Z(2)
C
      REAL L1,L2,L0,N1,N2,MMF1,MMF2
      DIMENSION Z(2)
      COMMON A1,L1,N1,A2,L2,N2,A0,L0,C1,C11,RG
      F(B)=C1*B+C11*B**11
      H1=F(Z(1)/A1)
      H2=F(Z(2)/A2)
      HA=F((Z(1)+Z(2))/(2.*A0))
      HB=F((Z(1)-Z(2))/(2.*A0))
      MMF1=H1*L1+(HA+HB)*L0/2.+RG*Z(1)
      MMF2=H2*L2+(HA-HB)*L0/2.+RG*Z(2)
      RETURN
      END
      FINISH
****
```

APPENDIX VIII: PROGRAM LISTING, SOLUTION OF DIFFERENTIAL EQUATIONS OF PARAMETRIC TRANSFORMER

```
      MASTER MAIN
C
C     PROGRAM TO SOLVE DIFFERENTIAL EQUATIONS SIMULATING PARAMETRIC
C     TRANSFORMER
C
      EXTERNAL DERIV
      REAL L1,L2,L0,N1,N2,MMF1,MMF2,I1,I2,LG,MU0,IND2IN,IND2AV
      REAL I1RMS,I2RMS
      DIMENSION Z(3),G(3),Y0(3),E(3),A(3),B(3),C(3),D(3),
     I  XT(1000),XE1(1000),XE2(1000),XI1(1000),XI2(1000)
      DIMENSION XE1SQ(1000),XE2SQ(1000),XI1SQ(1000),XI2SQ(1000)
      COMMON EMF1,AA,BB,CC,DD,MMF1,MMF2,REL1IN,REL2IN,D0,D1,D2,D3,D4,D5,
     UD6,D7,D8,D9,D10,D11,D12,D13,D14,D15,D16
C
C     READ AND WRITE PHYSICAL DATA
C
      READ(1,1)  C1,C11,LG,A1,L1,N1,R1,A2,L2,N2,R2,A0,L0,F,CAP,V1EFF,RL
1     FORMAT(16G0.0,E0.0)
      WRITE(2,10)
 10   FORMAT(/////5X,35HCOEFFICIENTS OF THE FUNCTION H=F(B)//)
      WRITE(2,20)C1,C11
20    FORMAT(///5X,3HC1=,E12.6,5X,4HC11=,E12.6/)
      WRITE(2,25)LG
25    FORMAT(///5X,8HAIR GAP=,E8.2,4H (M)//)
      WRITE(2,11)
 11   FORMAT(///5X,23HOTHER SYSTEM PARAMETERS///)
      WRITE(2,3)A1,L1,N1,R1,A2,L2,N2,R2,A0,L0,RL,CAP,F,V1EFF
 3    FORMAT(5X,8HA1(SQM)=,E10.4,5X,6HL1(M)=,E10.4,5X,10HN1(TURNS)=,
     1E10.4,
     I5X,9HR1(OHMS)=,E10.4///5X,8HA2(SQM)=,E10.4,5X,6HL2(M)=,E10.4,5X,
     I10HN2(TURNS)=,E10.4,5X,9HR2(OHMS)=,E10.4///5X,8HA0(SQM)=,E10.4,5X,
     I6HL0(M)=,E10.4///5X,9HRL(OHMS)=,E10.4,5X,9HCAP(FRD)=,E10.4,5X,
     I6HF(HZ)=,E10.4,5X,13HV1EFF(VOLTS)=,E10.4///)
C
C     RELUCTANCE AND OTHER COEFFICIENTS
C
      PI=4.*ATAN(1.)
      W=2.*PI*F
      MU0=4.*PI*1.0E-07
      RG=LG/(MU0*A0)
      ALFA=0.5
      WRITE(2,40)ALFA
40    FORMAT(/5X,39HPRIMARY VOLTAGE SWITCH-ON PHASE   ALFA=,F4.2,
     U5H (PI)/)
      ALFA=ALFA*PI
      S1=C1*L2/A2
      P1=C1*L1/A1
      RR1=C1*L0/(2.*A0)
      S11=C11*L2/(A2**11)
      P11=C11*L1/(A1**11)
```

```
      RR11=C11*L0/((2.*A0)**11)
      D0=11.*RR11
      D1=165.*RR11
      D2=462.*RR11
      D3=330.*RR11
      D4=55.*RR11
      D5=P11+RR11
      D6=S11+RR11
      D7=3.*D1
      D8=5.*D2
      D9=7.*D3
      D10=9.*D4
      D11=11.*D5
      D12=10.*D0
      D13=8.*D1
      D14=6.*D2
      D15=4.*D3
      D16=2.*D4
C
C     INITIAL VALUES OF SECONDARY RELUCTANCE,INDUCTANCE AND CAPACITANCE
C
103   REL2IN=RG+S1+RR1
      REL1IN=RG+P1+RR1
      IND2IN=N2*N2/REL2IN
      WRITE(2,26)REL2IN,IND2IN
 26   FORMAT(//5X,19HINITIAL RELUCTANCE=,E12.6,12H (A*T/WEBER),10X,
     U19HINITIAL INDUCTANCE=,E12.6,8H (HENRY)///)
      CAPIN=1.0/(IND2IN*W*W)
      WRITE(2,21)CAPIN
 21   FORMAT(/5X,36HCAPACITANCE TO RESONATE WITH IND2IN=,E12.6,
     U8H (FARAD)/)
C
C     CALCULATION OF AVERAGE SECONDARY RELUCTANCE ASSUMING SECONDARY
C     FLUX SINUSOIDAL
C
      F1M=V1EFF*SQRT(2.)/(N1*W)
      REL2AV=REL2IN+(252./1024.)*11.*RR11*F1M**10/PI
      WRITE(2,27)REL2AV
 27   FORMAT(///5X,7HREL2AV=,E12.6,12H (A*T/WEBER)/)
      IND2AV=N2*N2/REL2AV
      WRITE(2,29)IND2AV
 29   FORMAT(//5X,7HIND2AV=,E12.6,8H (HENRY)//)
      CAPR=1.0/(IND2AV*W*W)
      WRITE(2,28)CAPR
 28   FORMAT(//5X,36HCAPACITANCE TO RESONATE WITH IND2AV=,E12.6,
     U8H (FARAD)/)
      CAP=REL2AV*(1.+R2/RL)/(W**2*N2**2)
      WRITE(2,60)CAP
 60   FORMAT(//5X,40HRESONANCE CAPACITANCE IN LOADED CIRCUIT=,E12.6,
     U8H (FARAD)/)
```

```
      WRITE(2,66)CAP
 66   FORMAT(//5X,20HCONNECTED CAPACITOR=,E16.7)
C
C     CONSTANTS IN DIFFERENTIAL EQUATIONS AND TUNING
C
      AA=R1/(W*N1**2)
      BB=1./(W*RL*CAP)
      CC=R2/(W*N2**2)
      DD=(1.+R2/RL)/(W**2*N2**2*CAP)
      WRITE(2,80)
 80   FORMAT(////5X,38HCOEFFICIENTS IN DIFFERENTIAL EQUATIONS)
      WRITE(2,70)AA,BB,CC,DD
 70   FORMAT(//5X,4E18.7////)
      TI=SQRT(REL2AV*DD)
      F0=TI*W/(2.*PI)
      WRITE(2,101)TI,F0
101   FORMAT(//5X,7HTUNING=,F5.3,10X,20HRESONANCE FREQUENCY=,F8.5,
     U8H (HERTZ)/)
C
C     INITIALIZE THE VARIABLES X AND Z
C
      X=0.0
      Z(1)=0.0
C     INITIAL VALUE OF Z(2) CORRESPONDS TO INITIAL SECONDARY FLUX
C     DENSITY OF 5.0E-03 WB
C     INITIAL OSCILLATION IN THE FORM Z(2)=0.0000115*SIN(X+PI/4.)
      Z(2)=0.0000115*SIN(+PI/4.)
      Z(3)=0.0000115*COS(+PI/4.)
C
C     ERROR BOUNDS
C
      G(1),G(2),G(3)=0.000005
      STEP=0.05*PI
      IT=1
      NO=3
      IERR=1
      RANGE=0.1*PI
C
C     INITIAL VALUES OF INPUT AND OUTPUT VOLTAGES AND CURRENTS
C
      E1=V1EFF*SQRT(2.)*SIN(X+ALFA)
      EMF1=E1/(N1*W)
      I1,I2,E2=0.0
      T=X/PI
      XT(1)=T
      XE1(1)=E1
      XE2(1),XI1(1),XI2(1)=0.0
      WRITE(2,4)
 4    FORMAT(5X,4HTIME,8X,15HPRIMARY VOLTAGE,8X,17HSECONDARY VOLTAGE,
     18X,15HPRIMARY CURRENT,8X,17HSECONDARY CURRENT//5X,4H(PI),12X,
```

```
      17H(VOLTS),17X,7H(VOLTS),17X,6H(AMPS),18X,6H(AMPS))
       WRITE(2,5)T,E1,E2,I1,I2
  5    FORMAT(3X,F7.2,3X,F15.6,8X,F17.6,8X,F15.6,8X,F17.6)
C      - - - - - - - - - - - - - - - - - - - - - - - - - - - - - - - - - - -
C      CALL SUBROUTINE TO INTEGRATE EQUATIONS OVER THE RANGE
C
       II=0
  7    CALL DU2ABF(X,Z,G,IT,NO,IERR,RANGE,STEP,DERIV,YO,E,A,B,C,D)
       T=X/PI
       IF(IERR.GT.0)GO TO 6
       I1=MMF1/N1
       I2=MMF2/N2
       E2=-N2*W*Z(3)-R2*I2
C
C      DECREASING V1EFF GRADUALLY,TO  ATTAIN NORMAL STEADY-STATE
C      OPERATION
C
       IF(T.GT.70.)GO TO 201
       IF(T.GT.30.)V1EFF=V1EFF-0.35
201    E1=V1EFF*SQRT(2.)*SIN(X+ALFA)
       EMF1=E1/(N1*W)
       I=II+2
       XT(I)=T
       XE1(I)=E1
       XE2(I)=E2
       XI1(I)=I1
       XI2(I)=I2
       WRITE(2,5)T,E1,E2,I1,I2
       II=II+1
       IF(II.LE.998) GO TO 7
C      - - - - - - - - - - - - - - - - - - - - - - - - - - - - - - - - - - -
C      RMS VALUES FOUND BY NUMERICAL INTEGRATION USING RECTANGULAR RULE
C      BETWEEN  896 AND 995
       SUM1,SUM2,SUM3,SUM4=0.0
       DO 106 I=896,995
       XE1SQ(I)=XE1(I)**2
       XE2SQ(I)=XE2(I)**2
       XI1SQ(I)=XI1(I)**2
       XI2SQ(I)=XI2(I)**2
       SUM1=SUM1+XE1SQ(I)
       SUM2=SUM2+XE2SQ(I)
       SUM3=SUM3+XI1SQ(I)
       SUM4=SUM4+XI2SQ(I)
106    CONTINUE
       V1RMS=SQRT(0.010*SUM1)
       V2RMS=SQRT(0.010*SUM2)
       I1RMS=SQRT(0.010*SUM3)
       I2RMS=SQRT(0.010*SUM4)
       WRITE(2,107)
107    FORMAT(/////5X,35HRMS VALUES OF VOLTAGES AND CURRENTS//)
```

```
      WRITE(2,108)V1RMS,V2RMS,I1RMS,I2RMS
108   FORMAT(/5X,6HV1RMS=,F9.4,5X,6HV2RMS=,F9.4,5X,6HI1RMS=,F9.4,5X,
     16HI2RMS=,F9.4/)
C
C     PLOTTING VARIATIONS OF INPUT AND OUTPUT VOLTAGES AND CURRENTS
C
      CALL UTPOP
      XMIN=0.0
      XMAX=100.0
      YMAX=400.0
      YMIN=-YMAX
      XINS=20.
      YINS=6.0
      CALL UTP4A(XMIN,XMAX,YMIN,YMAX,XINS,YINS,
     U21HANGULAR TIME (PI*RAD),3,16HE1 AND E2 (VOLT),4)
      CALL UTP2(0.0,0.5*YINS,1)
      CALL UTP2(XINS,0.5*YINS,2)
      CALL UTP4B(XT,XE1,1000,2)
      CALL UTP4B(XT,XE2,1000,2)
      V1EFF=V1EFF+160.
      WRITE(2,102)V1EFF
102   FORMAT(////////////5X,22HPRIMARY VOLTAGE V1EFF=,F5.1,8H (VOLTS)/)
      IF(V1EFF.LE.261.)GO TO 103
      CALL UTPCL
      STOP
6     WRITE(2,8) T
8     FORMAT(27H INTEGRATION FAILED AT T = ,F8.4)
      STOP
      END


      SUBROUTINE DERIV(G,Z,X)
C
C     THIS SUBROUTINE CALCULATES MMF1 AND MMF2 FROM GIVEN Z(1) AND Z(2)
C     AND DEFINES DIFFERENTIAL EQUATIONS SIMULATING PARAMETRIC
C     TRANSFORMER
C
      REAL MMF1,MMF2
      DIMENSION G(3),Z(3)
      COMMON EMF1,AA,BB,CC,DD,MMF1,MMF2,REL1IN,REL2IN,D0,D1,D2,D3,D4,D5,
     UD6,D7,D8,D9,D10,D11,D12,D13,D14,D15,D16
      F1E2=Z(1)*Z(1)
      F1E3=F1E2*Z(1)
      F1E4=F1E3*Z(1)
      F1E5=F1E4*Z(1)
      F1E6=F1E5*Z(1)
      F1E7=F1E6*Z(1)
      F1E8=F1E7*Z(1)
      F1E9=F1E8*Z(1)
      F1E10=F1E9*Z(1)
      F1E11=F1E10*Z(1)
      F2E2=Z(2)*Z(2)
```

```
      F2E3=F2E2*Z(2)
      F2E4=F2E3*Z(2)
      F2E5=F2E4*Z(2)
      F2E6=F2E5*Z(2)
      F2E7=F2E6*Z(2)
      F2E8=F2E7*Z(2)
      F2E9=F2E8*Z(2)
      F2E10=F2E9*Z(2)
      F2E11=F2E10*Z(2)
      MMF1=Z(1)*(REL1IN+D0*F2E10)+F1E3*D1*F2E8+F1E5*D2*F2E6+F1E7*D3*F2E4
     U+F1E9*D4*F2E2+F1E11*D5
      MMF2=Z(2)*(REL2IN+D0*F1E10)+F2E3*D1*F1E8+F2E5*D2*F1E6+F2E7*D3*F1E4
     U+F2E9*D4*F1E2+F2E11*D6
      FN1=REL2IN+D0*F1E10+F2E2*D7*F1E8+F2E4*D8*F1E6+F2E6*D9*F1E4+
     UF2E8*D10*F1E2+F2E10*D11
      FN2=Z(2)*D12*F1E9+F2E3*D13*F1E7+F2E5*D14*F1E5+F2E7*D15*F1E3+
     UF2E9*D16*Z(1)
      G(1)=EMF1-AA*MMF1
      G(2)=Z(3)
      G(3)=-BB*Z(3)-CC*(FN1*Z(3)+FN2*(EMF1-AA*MMF1))-DD*MMF2
      RETURN
      END
      FINISH
****
```